C

C- and F-Processes Model and Dynamic Thermoelasticity

Kumar K. Tamma, Xiangmin Zhou and
Christianne V. D. R. Anderson
Department of Mechanical Engineering,
University of Minnesota, Minneapolis, MN, USA

Overview

Emanating from the Boltzmann transport equation, a newly developed C- and F-processes heat conduction constitutive model and the associated dynamic thermoelasticity are described. The model acknowledges the notion of the simultaneous coexistence of both the slow Cattaneo-type C-processes and fast Fourier-type F-processes in the mechanisms of heat conduction. The formulation leads to a generalization of the macroscale in space one temperature theory for heat conduction in solids of the Jeffreys-type model, Cattaneo model, and the Fourier model for heat conduction in solids. This is unlike the Jeffreys-type phenomenological model which cannot reduce to the classical Fourier model (but only to a Fourier-like representation with relaxation), and the Jeffreys-type model cannot explain the underlying physics associated the C- and F-processes model. A generalized thermoelastic theory is described to study the dynamic thermoelastic behavior of solids with special features which can explain the classical and nonclassical dynamic thermoelastic theories.

Introduction

The basis of heat conduction and transport relies heavily upon the underlying heat flux constitutive models, and the fusion of the mechanisms associated with heat conduction to those of elasticity lead to the fundamental description of the thermoelastic behavior of solids. Among the various currently available heat flux constitutive models, the Fourier model [1] which is based upon steady-state assumptions has long been widely accepted for a variety of practical engineering situations. With the Fourier model, the resulting transient temperature equations are of the parabolic type. Under certain special heating durations and scales (regime maps) of applications and temperature regimes, the Fourier model not only fails to predict the temperature propagation speed [2, 3] but also suffers from certain anomalies. To account for the temperature propagation speed and to account for the anomalies associated with the Fourier model, the Cattaneo model [4] was introduced. With the Cattaneo model, the resulting temperature equations are of the hyperbolic type. Joseph and Preziosi [5] independently note (based on analogies of viscoelastic flows) a phenomenological model formalized as the so-called Jeffreys' type for heat conduction. The Cattaneo model and a Fourier-like diffusive model are sub-cases which can be degenerated from this generalized constitutive model. A point of clarification is important regarding the Jeffreys-type model. Although it can be degenerated to the Cattaneo model, it

R.B. Hetnarski (ed.), *Encyclopedia of Thermal Stresses*, DOI 10.1007/978-94-007-2739-7,

does not exactly degenerate to the classical Fourier model; the resulting mathematical representation is a Fourier-like diffusive model but with relaxation term involved. Here, a new C- and F-processes heat conduction constitutive model is overviewed from physical principles emanating from the Boltzmann transport equation (BTE). A nondimensional heat conduction model number is introduced in the process of the development of the formulations. A new generalized dynamic thermoelastic theory employing the C- and F-processes heat conduction constitutive model is also described.

The C-Processes and F-Processes Model for Heat Conduction

Assuming that simultaneously Fourier-type fast processes (F-processes) which have infinite speed of propagation and Cattaneo-type slow processes (C-processes) which have finite speed of propagation independently coexist in the heat conduction process, a C- and F-processes heat conduction model with a physical interpretation and the notion of a linear combination of the total heat flux as the sum of the F-processes and C-processes is described as

$$\mathbf{q}_F = -k_F \nabla T = -F_T k \nabla T \tag{1}$$

$$\mathbf{q}_C + \tau \frac{\partial \mathbf{q}_C}{\partial t} = -k_C \nabla T = -(1 - F_T) k \nabla T \tag{2}$$

$$\mathbf{q} = \mathbf{q}_F + \mathbf{q}_C \tag{3}$$

In the above, $\mathbf{q}$ is the total heat flux due to the mechanism of heat conduction (which is comprised of that associated with each of the Fourier-type fast and Cattaneo-type slow processes) and k is the total conductivity which is the sum of the Fourier (effective) conductivity k_F and the Cattaneo (elastic) conductivity k_C. Thus, $k = k_F + k_C$. It is to be noted that the subscripts F and C pertain to the F-processes and C-processes, and the model acknowledges the coexistence of both finite and infinite speed of propagation of the thermal disturbances. Also note that when $F_T \in (0, 1)$ the combined representation of the C- and F-processes model leads to the Jeffreys-type model, when $(F_T = 0)$ the C- and F-processes model naturally reduces to the Cattaneo model, and when $(F_T = 1)$ the C- and F-processes model naturally reduces to the Fourier model. At very early in the transient, the Cattaneo-type slow processes dominate, and subsequently with evolution of time the Fourier-type fast processes dominate.

We define the F-processes associated with the Fourier-type heat flux law from (1) as

$$\mathbf{q}_F := -F_T k \nabla T \tag{4}$$

We rewrite (2) of the C-processes associated with the Cattaneo-type heat flux law in integral form [6] as

$$\mathbf{q}_C := -\frac{(1 - F_T)k}{\tau} \int_{-\infty}^{t} e^{-\frac{t-s}{\tau}} \nabla T(\mathbf{x}, s) ds \tag{5}$$

Now substituting (4) and (5) into (3) leads to the total heat flux given as

$$\mathbf{q} = \mathbf{q}_F + \mathbf{q}_c = -F_T k \nabla T(\mathbf{x}, t) - \frac{(1 - F_T)k}{\tau} \int_{-\infty}^{t} e^{-\frac{t-s}{\tau}} \nabla T(\mathbf{x}, s) ds \tag{6}$$

On the other hand, we next write the Jeffreys-type heat flux model in integral form [5, 7] as

$$\mathbf{q} = -F_T k \nabla T(\mathbf{x}, t) - \frac{(1 - F_T)k}{\tau} \int_{-\infty}^{t} e^{-\frac{t-s}{\tau}} \nabla T(\mathbf{x}, s) ds \tag{7}$$

Therefore, the C- and F-processes model leads to and is identical with the Jeffreys-type phenomenological model as

$$\mathbf{q} + \tau \frac{\partial \mathbf{q}}{\partial t} = -k \left[\nabla T + \tau F_T \frac{\partial (\nabla T)}{\partial t} \right] \tag{8}$$

Note that we introduced a *macroscale heat conduction model number*, F_T, defined as follows:

$$F_T := \frac{\text{Conductivity}(k_F)\text{due to F-processes}}{\text{Conductivity}(k_F)\text{due to F-processes} + \text{conductivity}(k_C)\text{due to C-processes}} \tag{9}$$

The evolution of F_T with time starting from zero and leading to unity bridges the constitutive models associated with C-processes and the F-processes.

Derivation of the C- and F-Processes Model Via the Boltzmann Transport Equation

The Boltzmann transport equation (BTE) is given as

$$\frac{\partial f}{\partial t} + v \cdot \nabla f + a \cdot \frac{\partial f}{\partial v} = \left(\frac{\partial f}{\partial t}\right)_{scatt} \tag{10}$$

where $f(\mathbf{x}, T, E(\omega))$ is the nonequilibrium thermodynamic distribution function (Maxwell-Boltzmann distribution for identical but distinguishable particles (such as ideal gas), Bose-Einstein distribution for boson particles (such as photons and phonons), and Fermi-Dirac distribution for fermion particles (such as electrons)), $v(\omega)$ is the heat carrier velocity which is the speed of the first sound of the medium, $a(v)$ is the particle acceleration, T is absolute temperature, ω is the frequency, and $E(\omega)$ is energy state. The first term in (10) represents the net rate of particles over time, the second term is the convective inflow of particles in physical space, the third term is the net convective inflow due to acceleration in velocity space, and the term on the right-hand side is the net rate of change of particles inside a control volume due to collisions. Assuming the heat carrier velocity is constant over a large frequency range, $\frac{\partial f}{\partial v}$ can be neglected [8, 9]. Both energy and temperature gradient tend to disturb the distribution function f; this tendency is opposed by processes that restore equilibrium. Therefore, the scattering term is linearly approximated under the relaxation-time approximation which simplifies the equation as

$$\left(\frac{\partial f}{\partial t}\right)_{scatt} = \frac{\partial (f - f^0)}{\partial t} = \frac{f^0 - f}{\tau} \tag{11}$$

where $f^0(\mathbf{x}, T, E(\omega))$ is the thermodynamic distribution at equilibrium, $\frac{\partial f^0}{\partial t} = 0$, and $\tau(\omega, v)$ is the rate of return to equilibrium and called as the relaxation time.

Fourier Model: Derivation

For a steady-state one-dimensional case, (10) describes the particle diffusion and reduces to

$$v_x \frac{\partial f}{\partial x} = \frac{f^0 - f}{\tau} \tag{12}$$

The kinetic theory is derived under the premise of *local thermal dynamic equilibrium* (LTE). LTE is implied and $\frac{\partial f}{\partial x} \sim \frac{\partial f^0}{\partial x}$ and the $\frac{\partial f}{\partial x}$ term can be approximated as (see [10])

$$\frac{\partial f}{\partial x} = \frac{df^0}{dT}\frac{dT}{dx} \tag{13}$$

Multiplying (12) by $v_x \hbar\omega D(\omega)$ and integrating over all frequency, we obtain the following expression:

$$\int_0^{\omega_D} v_x^2 \hbar\omega \frac{df^0}{dT}\frac{dT}{dx} D(\omega)\, d\omega = \int_0^{\omega_D} v_x \hbar\omega D(\omega) \frac{f^0 - f}{\tau}\, d\omega \tag{14}$$

where $\hbar$ is the Planck's number divided by 2π, $D(\omega)$ is the density of states, and ω_D is the Debye cutoff angular frequency. The first term in the right-hand side is zero (v_x is an odd function and f^0 is an even function of v_x). Thus, the net particle conduction heat flux vanishes for the equilibrium function f^0.

The flux due to heat conduction of particles is given by

$$q(x) = \int_0^{\omega_D} v_x f(x) \hbar\omega D(\omega)\, d\omega \tag{15}$$

Using the particle flux definition in (15), we can reduce (14) to

$$q(x) = -\frac{dT}{dx}\int_0^{\omega_D} v_x^2 \tau \frac{df^0}{dT}\hbar\omega D(\omega)\, d\omega \tag{16}$$

The specific heat is given as

$$c = \int_0^{\omega_D} \frac{df^0}{dT}\hbar\omega D(\omega)\, d\omega \tag{17}$$

and based on kinetic theory, the thermal conductivity is related to the specific heat as

$$k = \int_0^{\omega_D} v_x^2 \tau \frac{df^0}{dT}\hbar\omega D(\omega)\, d\omega = \frac{1}{3} c v \lambda \tag{18}$$

where $k(T)$ is the total thermal conductivity, $c(T)$ is the total specific heat per unit volume, v is the average speed of the heat carriers ($v_x^2 = \frac{1}{3}v$), and λ is the mean free path ($\lambda = v\tau$).

Substituting (17) and (18) into (16), the Fourier model is derived as (see also [9])

$$q(x) = -k\frac{dT}{dx} \tag{19}$$

Note that from this derivation the obtained thermal conductivity is the total conductivity with the assumption that the velocity and relaxation time are independent of frequency. Hence, this yields

$$k = v_x^2 \tau \int_0^{\omega_D} \frac{df^0}{dT}\hbar\omega D(\omega)\, d\omega \tag{20}$$

Cattaneo Model: Derivation

The transient one-dimensional BTE equation under the relaxation-time approximation and the temperature gradient approximation yields

$$\frac{\partial f}{\partial t} + v_x \frac{df^0}{dT}\frac{dT}{dx} = \frac{f^0 - f}{\tau} \tag{21}$$

As with the Fourier model, (21) is multiplied by $v_x \hbar\omega D(\omega)$ and integrated over all frequency range to yield

$$\int_0^{\omega_D} v_x \hbar\omega D(\omega)\left(\frac{\partial f}{\partial t} + v_x \frac{df^0}{dT}\frac{dT}{dx} - \frac{f^0 - f}{\tau}\right) d\omega = 0 \tag{22}$$

Applying similar definitions from (15), (17), (18), and (20), the Cattaneo model is readily derived as (see also [11])

$$q + \tau\frac{dq}{dt} = -k\frac{dT}{dx} \tag{23}$$

The C- and F-Processes Model: Derivation

The difference between the Fourier model and the Cattaneo model is in the presence of the term $\frac{\partial f}{\partial t}$. For a given location, temperature, and time, the three possible distribution functions existing are given as

Maxwell-Boltzmann distribution function:

$$f(E(\omega)) = f_{MB}(E(\omega)) := \frac{1}{Ae^{\frac{E(\omega)}{T\kappa_B}}} \tag{24}$$

Bose-Einstein distribution function:

$$f(E(\omega)) = f_{BE}(E(\omega)) := \frac{1}{Ae^{\frac{E(\omega)}{T\kappa_B}} - 1} \tag{25}$$

Fermi-Dirac distribution function:

$$f(E(\omega)) = f_{FD}(E(\omega)) := \frac{1}{Ae^{\frac{(E(\omega)-E_F)}{T\kappa_B}} + 1} \tag{26}$$

where A is a normalized constant, κ_B is the Boltzmann's constant, and E_F is the Fermi energy.

If the frequency ω is large enough, in the above distribution functions, we have

$$f(E(\omega)) \approx 0, \qquad \forall\omega \in [\omega_T, \omega_D] \tag{27}$$

Therefore, we have

$$\frac{\partial f(E(\omega))}{\partial t} \approx 0, \qquad \forall\omega \in [\omega_T, \omega_D] \tag{28}$$

We now define the total heat flux as

$$q = \int_0^{\omega_T} v_x f \hbar\omega D(\omega)\, d\omega + \int_{\omega_T}^{\omega_D} v_x f \hbar\omega D(\omega)\, d\omega = q_C + q_F \tag{29}$$

where the postulation made here is that the integral up to a threshold frequency ω_T involves the slow C-processes and termed q_C and that the integral from the threshold to infinity involves the fast F-processes and termed q_F.

Multiplying the BTE by $v_x \hbar\omega D(\omega)$ and integrating over the entire frequency range yields

$$\begin{aligned}&\int_0^{\omega_T} v_x \hbar\omega D(\omega)\frac{\partial f}{\partial t}\, d\omega + \int_0^{\omega_T} v_x^2 \hbar\omega D(\omega)\frac{\partial f}{\partial x}\, d\omega \\ &\quad + \int_{\omega_T}^{\omega_D} v_x^2 \hbar\omega D(\omega)\frac{\partial f}{\partial x}\, d\omega \\ &= \int_0^{\omega_T} v_x \hbar\omega D(\omega)\left(\frac{f^0 - f}{\tau}\right) d\omega \\ &\quad + \int_{\omega_T}^{\omega_D} v_x \hbar\omega D(\omega)\left(\frac{f^0 - f}{\tau}\right) d\omega\end{aligned} \tag{30}$$

Note that the $\int_{\omega_T}^{\omega_D} v_x \hbar\omega D(\omega)\frac{\partial f}{\partial t} d\omega = 0$ (not shown above) due to the observation that the distribution function is constant over time for high frequency; therefore, $\frac{df}{dt} = 0$.

Instead of dealing directly with (30) which describes the total heat conduction process, we next independently derive from the BTE the following two equations which are associated with the C-processes and the F-processes:

$$\begin{aligned}&\int_0^{\omega_T} v_x \hbar\omega D(\omega)\frac{\partial f}{\partial t}\, d\omega + \int_0^{\omega_T} v_x^2 \hbar\omega D(\omega)\frac{\partial f}{\partial x}\, d\omega \\ &= \int_0^{\omega_T} v_x \hbar\omega D(\omega)\left(\frac{f^0 - f}{\tau}\right) d\omega\end{aligned} \tag{31}$$

and

$$\begin{aligned}&\int_{\omega_T}^{\omega_D} v_x^2 \hbar\omega D(\omega)\frac{\partial f}{\partial x}\, d\omega \\ &= \int_{\omega_T}^{\omega_D} v_x \hbar\omega D(\omega)\left(\frac{f^0 - f}{\tau}\right) d\omega\end{aligned} \tag{32}$$

Note that (31) and (32) can indeed explain and lead to (30); however, the converse is not true. We further define

$$k = \int_0^{\omega_T} v_x^2 \tau \frac{df^0}{dT} \hbar\omega D(\omega)\, d\omega + \int_{\omega_T}^{\omega_D} v_x^2 \tau \frac{df^0}{dT} \hbar\omega D(\omega)\, d\omega = k_C + k_F \tag{33}$$

and introducing the nondimensional *heat conduction model number* as the following ratio:

$$F_T = \frac{\int_{\omega_T}^{\omega_D} v_x^2 \tau \frac{df^0}{dT} \hbar\omega D(\omega)\, d\omega}{\int_0^{\omega_D} v_x^2 \tau \frac{df^0}{dT} \hbar\omega D(\omega)\, d\omega} \tag{34}$$

then (29), (31), and (32) finally yield the C- and F-processes heat conduction model as

$$q_F = -F_T k \frac{dT}{dx} \tag{35}$$

$$q_C + \tau \frac{dq_C}{dt} = -(1 - F_T) k \frac{dT}{dx} \tag{36}$$

$$q = q_F + q_C \tag{37}$$

In general, we now readily have

$$\mathbf{q}_F = -k_F \nabla T = -F_T k \nabla T \tag{38}$$

$$\mathbf{q}_C + \tau \frac{\partial \mathbf{q}_C}{\partial t} = -k_C \nabla T = -(1 - F_T) k \nabla T \tag{39}$$

$$\mathbf{q} = \mathbf{q}_F + \mathbf{q}_C \tag{40}$$

which explains the derivation based on fundamental physical principles emanating from the Boltzmann transport equation.

One Temperature Equation for Heat Conduction in Solids

When (1)–(3) for the C- and F-processes model are coupled with the energy equation, this results in a generalized heat conduction temperature equation of the Jeffreys' type which is

macroscopic in space and microscopic in time and termed here as the generalized one-step [GOS] formulation associated with the one temperature theory given by

$$\frac{1}{c_T^2}\frac{\partial^2 T}{\partial t^2}+\frac{1}{\alpha}\frac{\partial T}{\partial t}=\nabla^2 T+\tau F_T\frac{\partial}{\partial t}\left(\nabla^2 T\right)+\frac{1}{k}\left(S+\tau\frac{\partial S}{\partial t}\right) \tag{41}$$

where $F_T \in [0,1]$

Remarks. The differences contrasting the C- and F-processes model [12] and the Jeffreys-type model formulations are the following:

1. When the *macroscale heat conduction model number* $F_T \in (0,1)$, the combined representation of the C- and F-processes constitutive model, (6), leads to the Jeffreys-type model, which in conjunction with the energy equation leads to the GOS temperature (41) which is of the Jeffreys' type. It is strictly parabolic in nature with the discontinuities being smoothed by diffusion effects associated with the effective thermal conductivity k_F. Consequently, even for very small values of F_T, although the diffusive response is wavelike, nonetheless the transmission of information is felt everywhere.
2. When the *macroscale heat conduction model number* $F_T = 0$, the C- and F-processes constitutive model, (1)–(3), pertains to the Cattaneo model and in conjunction with the energy equation yields (42) below which is the hyperbolic one-step [HOS] equation of the Cattaneo type which is propagative, where heat is now transmitted as waves with finite speeds dictated by c_T:

$$\frac{1}{c_T^2}\frac{\partial^2 T}{\partial t^2}+\frac{1}{\alpha}\frac{\partial T}{\partial t}=\nabla^2 T+\frac{1}{k}\left(S+\tau\frac{\partial S}{\partial t}\right) \tag{42}$$

3. When the *macroscale heat conduction model number* $F_T = 1$, the C- and F-processes constitutive model, (1)–(3), pertains to the classical Fourier model which in conjunction with the energy equation yields (43) below which is the classical parabolic one-step [POS] temperature equation which is diffusive (i.e., the transmission of information is felt everywhere) and is given by

$$\frac{1}{\alpha}\frac{\partial T}{\partial t}=\nabla^2 T+S \tag{43}$$

Note that the Jeffreys-type constitutive model, for the selection of the retardation time equal to the relaxation time, only yields a Fourier-like diffusive model with relaxation which in conjunction with the energy equation yields the following diffusive temperature equation:

$$\frac{1}{c_T^2}\frac{\partial^2 T}{\partial t^2}+\frac{1}{\alpha}\frac{\partial T}{\partial t}=\nabla^2 T+\tau\frac{\partial}{\partial t}\left(\nabla^2 T\right)+\frac{1}{k}\left(S+\tau\frac{\partial S}{\partial t}\right) \tag{44}$$

The C- and F-Processes-Based Generalized Dynamic Thermoelasticity

Consider the Lagrangian finite strain measure of the Green-St. Venant strain tensor at time t with respect to the Lagrangian configuration at time t_α as $\mathbf{E}_{t\alpha} \in \Re^3 \times \Re^3$ and defined as

$$\mathbf{E}_{t_\alpha} := \frac{1}{2}\left(\mathbf{C}_{t_\alpha}-\mathbf{I}\right) \tag{45}$$

where $\mathbf{I}$ is the second-order identity tensor and $\mathbf{C}_{t_\alpha}$ is the right Cauchy-Green deformation tensor which is defined in terms of the deformation gradient tensor $\mathbf{F}_{t_\alpha} \in \Re^3 \times \Re^3$ as

$$\mathbf{C}_{t_\alpha} := \mathbf{F}_{t_\alpha}^T\mathbf{F}_{t_\alpha} \tag{46}$$

The deformation gradient tensor is a two-point tensor defined by the change of a material particle of a deformable body of the Eulerian description $\mathbf{x} = (x, y, z)$ with respect to the Lagrangian description $\mathbf{X} = (X, Y, Z)$ as

$$\mathbf{F}_{t_\alpha} := \frac{\partial \mathbf{x}}{\partial \mathbf{X}} \tag{47}$$

We have the following constitutive model in Lagrangian configuration

$$\mathbf{S}_{t_\alpha} = \mathcal{C}_{t_\alpha} : \mathbf{E}_{t_\alpha} + a_6 \mathbf{I}\theta \tag{48}$$

$$\rho_0 s = -2a_6\theta - a_5 \mathbf{E}_{t_\alpha} \tag{49}$$

where

$$\mathcal{C}_{t_\alpha} := \lambda \mathbf{I} \otimes \mathbf{I} + 2\mu\mathcal{I} \tag{50}$$

and $\mathcal{I}$ is the fourth-order identity tensor and defined as

$$\mathcal{I}_{ijkl} := \delta_{ik}\delta_{jl} \tag{51}$$

and δ_{ij} is the Kronecker delta.

Considering the C- and F-processes model described previously,

$$\mathbf{q}_F = -F_T k \nabla T \tag{52}$$

$$\mathbf{q}_C + \tau \frac{\partial \mathbf{q}_C}{\partial t} = -(1 - F_T) k \nabla T \tag{53}$$

$$\mathbf{q} = \mathbf{q}_F + \mathbf{q}_C \tag{54}$$

Finally, we have the C- and F-processes generalized dynamic thermoelasticity model of the Lagrangian configuration in the form

$$\nabla \cdot \mathbf{q}_F = -F_T k \nabla^2 T \tag{55}$$

$$\left(1 + \tau \frac{\partial}{\partial t}\right)(\nabla \cdot \mathbf{q}_C) = -(1 - F_T) k \nabla^2 T \tag{56}$$

$$2T_0 a_6 \dot{\theta} + T_0 a_5 \frac{\partial}{\partial t}(\nabla \mathbf{u}) + \rho r = \nabla \cdot (\mathbf{q}_C + \mathbf{q}_F) \tag{57}$$

$$\mathcal{C}_{t_\alpha} : \mathbf{E}_{t_\alpha} + a_5 \mathbf{I}\theta + \rho \mathbf{b} = \rho \frac{\partial^2 \mathbf{u}}{\partial t^2} \tag{58}$$

For $F_T = 1$, the C- and F-processes thermoelasticity model reduces to the classical linear thermoelasticity model in Lagrangian configuration

$$2T_0 a_6 \dot{\theta} + T_0 a_5 \frac{\partial}{\partial t}(\nabla \mathbf{u}) + \rho r = -k \nabla^2 T \tag{59}$$

$$\mathcal{C}_{t_\alpha} : \mathbf{E}_{t_\alpha} + a_5 \mathbf{I}\theta + \rho \mathbf{b} = \rho \frac{\partial^2 \mathbf{u}}{\partial t^2} \tag{60}$$

For $F_T = 0$, the C- and F-processes thermoelasticity model reduces to the Lord and Shulman model [13] in Lagrangian configuration:

$$\left(1 + \tau \frac{\partial}{\partial t}\right)\left[2T_0 a_6 \dot{\theta} + T_0 a_5 \frac{\partial}{\partial t}(\nabla \mathbf{u}) + \rho r\right] = -k \nabla^2 T \tag{61}$$

$$\mathcal{C}_{t_\alpha} : \mathbf{E}_{t_\alpha} + a_5 \mathbf{I}\theta + \rho \mathbf{b} = \rho \frac{\partial^2 \mathbf{u}}{\partial t^2} \tag{62}$$

Example. The illustrative numerical test example described here concerns dynamic thermoelastic wave propagation in an elastic half-space ($x > 0$) due to second sound effects. The bounding plane $x = 0$ is subjected to loading situations; a sudden step change in temperature (Model 1) (following the original work of Danilovskaya [14, 15] where the classical thermoelastic model was employed). The bounding plane at $x = 0$ is assumed to be traction free at all times and the half-space is constrained so that there is only uniaxial motion. Hence, we have

$$\begin{aligned} u_x &= u(x,t) \\ u_y &= 0 \\ u_z &= 0 \end{aligned} \tag{63}$$

The initial and boundary conditions are given as

$$\begin{aligned} u_x(x,0) = \dot{u}_x(x,0) &= 0 \\ T(x,0) &= T_i \\ \dot{T}(x,0) &= \dot{T}_i \\ \sigma_x(x,0) &= 0 \end{aligned} \tag{64}$$

This test case concerns the dynamic thermoelastic response due to second sound effects when a sudden change in temperature is applied on the plane $x = 0$. The data employed for the computations is representative of stainless steel. First the analysis was performed for equal speeds of thermal and structural model

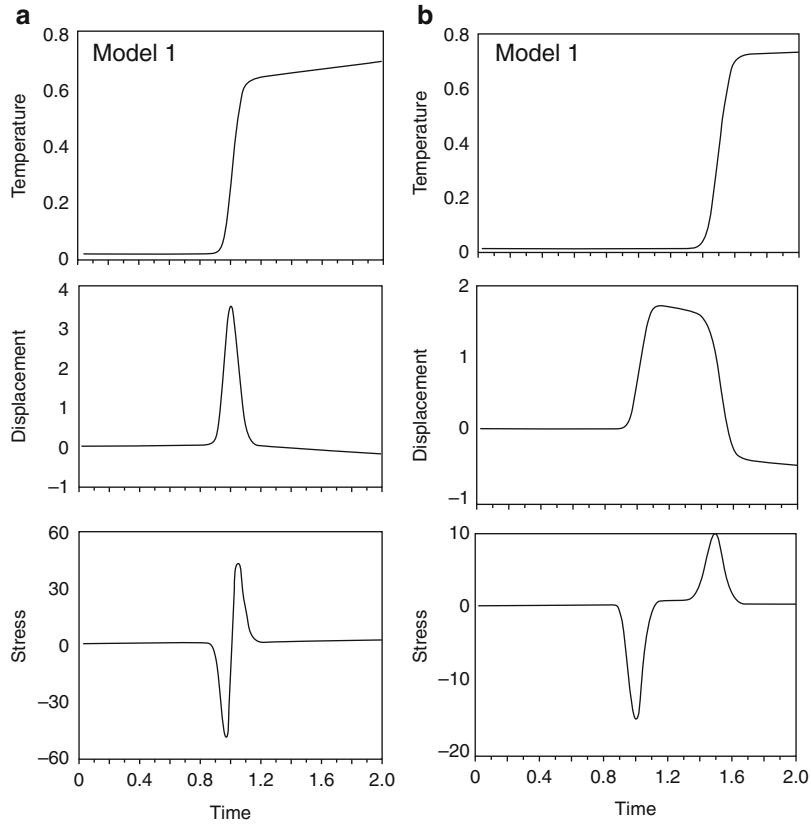

C- and F-Processes Model and Dynamic Thermoelasticity, Fig. 1 Representative temperature, displacement and stress histories for (**a**) $C_s = C_T$ and (**b**) $C_s = \frac{2}{3}C_T$

($C_T = C_s$). A nondimensional characteristic length ($l = 4$) and a mesh having 501 degrees of freedom were used. The time step employed for the computation was $\Delta t = 0.001$. Figure 1a shows the temperature, displacement, and stress histories obtained (after smoothing) via the present formulations. However, employing a further refined mesh of 501 degrees of freedom, the resulting response is significantly higher. This may be attributed to the fact that the presence of jump in stress is caused because of the presence of sharp front which occurs in the displacement and temperature profiles for non-Fourier models at the nondimensional location ($\xi = 1.0$). The dynamic thermoelastic response for the case of unequal speeds ($C_T = \frac{2}{3}C_s$) is shown in Fig. 1b. Note that the thermal wave front is at a different location and the displacement and stress histories are not sharp. Furthermore, the magnitude of the stress is comparatively less than that for the case of equal speeds. The results presented here depict the representative response and are accurate to within the framework of the mesh refinement. Nonetheless, in comparison to the assumption of infinite speed of thermal wave propagation (see Danilovskaya [14, 15]), the results are significantly different and indicate the important effect due to second sound.

Concluding Remarks

The new C- and F-processes heat conduction constitutive model which emanates from the physics of the Boltzmann transport equation and the associated generalized dynamic thermoelastic theory for studying the thermomechanical

behavior of solids acknowledges the notion of the simultaneous coexistence of both slow Cattaneo-type C-processes and fast Fourier-type F-processes in the process of heat conduction. The new C- and F-processes-based generalized dynamic thermoelastic theory readily encompasses the classical and nonclassical dynamic thermoelasticity theories.

Acknowledgments Support in form of computer grants from the Minnesota Supercomputer Institute (MSI), Minneapolis, Minnesota, is also gratefully acknowledged.

References

1. Fourier JBJ (1822) Théorie analytique de la chaleur. Firmin Didot pére et fils, Paris
2. Tisza L (1938) Sur la supraconductibilité thermique de l'helium II liquide et la statistique de Bose-Einstein. C R Acad Sci 207(22):1035
3. Baumeister KJ, Hamill TD (1969) Hyperbolic heat conduction equation – a solution for the semi-infinite body problem. J Heat Transf 91:543
4. Carlo Cattaneo M (1948) Sulla conduzione de calor. Atti Semin Mat Fis Della Univ Modena 3:3
5. Joseph DD, Preziosi L (1989) Heat waves. Rev Mod Phys 171:289
6. Gurtin ME, Pipkin AC (1968) A general theory of heat conduction with finite wave speed. Arch Ration Mech Anal 31:113
7. Nunziato JW (1971) On heat conduction in materials with memory. Q Appl Math 29:187–204
8. Ziman JM (1960) Electrons and phonons. Oxford University Press, London
9. Kittel C (1986) Introduction to solid state physics, 6th edn. Wiley, New York
10. Callaway J (1959) Model for lattic thermal conductivity at low temperatures. Phys Rev 113(4): 1046–1051
11. Qiu TQ, Tien CL (1993) Heat transfer mechanism during short-pulse laser heating of metals. J Heat Transf 115:835
12. Anderson CVDR, Tamma KK (2006) Novel heat conduction model for bridging different space and time scales. Phys Rev Lett 96(18):184301
13. Lord HW, Shulman Y (1967) Generalized dynamic theory of thermoelasticity. J Mech Phys Solids 15:299
14. Danilovskaya VI (1950) Thermal stress in elastic half-space arising after a sudden heating of its boundary. Prikl Mat Mekh 14:316
15. Danilovskaya VI (1952) Dynamical problem of thermoelasticity. Prikl Mat Mekh 16:341

C- and F-Processes Model: A Generalized Approach to Solving Transient Diffusive, Wavelike and Ballistic Solid State Heat Conduction Problems

V. M. Wheeler and Kumar K. Tamma
Department of Mechanical Engineering, University of Minnesota, Minneapolis, MN, USA

Overview

The classical description of solid state heat transfer, described by Fourier law, holds up for many or most of the systems encountered in engineering design. However, this diffusive description of energy transport breaks down under certain conditions, many of which are interesting for the development of novel engineering systems. Using the particle description of solids, particles such as electrons, phonons, and molecules act as energy carriers. Within this framework three types of thermal transport mechanisms have been identified. For purposes of illustration, consider a block of solid material divided into many tiny (differential) volumes.

- Diffusive Transport: All energy carriers are constantly scattering. Any differential volume of the solid has numerous collisions taking place at any time. Diffusion is a local effect – energy in one differential volume is carried only to the volumes around it. Any change in temperature in the solid is felt everywhere in the solid instantaneously. This is the so-called heat conduction paradox. Allowing for this paradox is, however, a reasonable approximation for most systems under consideration in everyday engineering applications.
- Wavelike Transport: The wave description of heat conduction is also local and energy carriers are considered to be constantly scattering. However, the instantaneous nature of the Fourier description is removed by introduction of a finite propagation speed as

described by Cattaneo [1]. This effect has been studied since the early to mid-twentieth century in very low-temperature environments which, in general, only exist in an extreme lab setting. Recently, however, wavelike transport has been found at more commonly encountered temperatures during studies of pulsed laser heating of metals [2] and in porous materials [3].

- Ballistic Transport: Energy carriers may not scatter. This phenomenon is nonlocal since an energy carrier in one differential volume of our imaginary solid could travel and deposit its energy into any other volume within the solid. First proposed in 1938 [4], a recent push to understand this process has led to numerous mathematical models [5–7] and proposed applications [8]. Since the times and spatial scales associated with ballistic transport are so small, no experimental measurement of temperature profile (or widely accepted definition of temperature!) exists to date.

Numerous physical descriptions and equations governing these processes exist. While many models give the same predictions at steady state, it is the transient response predicted by these models that are significantly different. All models (to the author's knowledge) are either first- or second-order in time. One model that has arisen with particular promise to make prediction for diffusive, wavelike, and ballistic behavior is the C- and F- (C-F) model [9]. Since this mathematical model can lead to a first- *or* second-order system in time depending on a physically based parameter, we will use it to demonstrate how to numerically solve a general class of problems arising in heat conduction.

To integrate in time the semi-discretized systems resulting from spatial finite elements, we will use the newly established isochronous integration or *i*Integration framework. This framework unifies two existing families of algorithms and features powerful numerical and order-preserving attributes. Of note is the second-order accuracy regardless of the order of the system or the amount of controllable numerical dissipation applied. The advantage emanating from such an integrated framework is the practicality and convenience of using the same computational framework and numerical implementation when solving first- and/or second-order systems without having to resort to separately switching from one individual framework to another.

We will proceed as follows: Section "Model Development" gives a physical description of the C-F model: the governing heat transport equations and the corresponding boundary conditions. Section "Numerical Formulation in Space" gives a brief summary of the spatial discretization of the resulting model. Section "Numerical Formulation in Time: The *i*Integration Framework" presents the unified time integration framework. Section "Numerical Results" presents several illustrative examples. In Section "Concluding Remarks", we conclude with final remarks.

Model Development

The C-F model, like many models of heat conduction, has been derived from the Boltzmann transport equation. The foundational assumption made in deriving the C-F model is that we can split up the particles into high and low energy carriers. This leads to the simultaneous coexistence of heat carriers that behave "Fourier-like" and "Cattaneo-like" – hence the model's name. The result is a thermal conductivity associated with each process such that

$$K = K_C + K_F \tag{1}$$

The idea of a dimensionless heat conduction model number can be introduced:

$$F_T = \frac{K_F}{K_C + K_F} \tag{2}$$

For a full derivation of the C-F model, see Anderson and Tamma [9]. For illustration, we consider the heat conduction across a thin film of thickness, L. We assume the film to be dielectric, so the dominant energy carriers are acoustic waves which, in a crystalline film, are

quantized and can be treated as particles called phonons. Our problem can now be approximated as one-dimensional with the governing equation

$$C\tau\frac{\partial^2 T}{\partial t^2}+C\frac{\partial T}{\partial t}=K\frac{\partial^2 T}{\partial x^2}+\tau F_T K\frac{\partial}{\partial t}\left[\frac{\partial^2 T}{\partial x^2}\right]+S+\tau\frac{\partial S}{\partial t},\quad \text{for } F_T<1 \tag{3}$$

$$C\frac{\partial T}{\partial t}=K\frac{\partial^2 T}{\partial x^2}+S,\quad \text{for } F_T=1 \tag{4}$$

where T is the temperature, t is time, x is location, C is the volumetric heat capacity, τ is the relaxation time of the heat carrier (average time traveled before scattering), and S is a volumetric source within the film. Note that for $F_T=0$, the hyperbolic heat equation is recovered from (3) and for $F_T=1$, the parabolic heat equation is exactly recovered. Thus, by the choice of F_T, our model can represent a fully diffusive description of heat conduction or a fully wavelike description along with any behavior in between.

Boundary conditions of three different types are considered for the thin film problem:

- *Type 1 or Dirichlet* – This boundary condition corresponds to a given temperature on a surface of the film. Type 1 conditions are typical in all presentations of phonon heat transfer models and exact solutions exist for parabolic and hyperbolic heat conduction problems. Complications arise when considering reports of so-called temperature "jumps" at the boundaries of the films due to the nonlocal nature of ballistic transport. Type 1 conditions are given by

$$T=T_{\infty 1}\quad \text{at } x=0 \tag{5}$$

$$T=T_{\infty 2}\quad \text{at } x=L \tag{6}$$

- *Type 2 or Neumann* – The heat flux is given at the boundary of the film. It permits jumps at the boundaries and is given by the following:

If $F_T<1$,

$$-K\frac{\partial T}{\partial x}-K\tau F_T\frac{\partial^2 T}{\partial x\partial t}=\text{constant}\quad \text{at } x=0 \tag{7}$$

$$K\frac{\partial T}{\partial x}+K\tau F_T\frac{\partial^2 T}{\partial x\partial t}=\text{constant}\quad \text{at } x=L \tag{8}$$

If $F_T=1$

$$-K\frac{\partial T}{\partial x}=\text{constant}\quad \text{at } x=0 \tag{9}$$

$$K\frac{\partial T}{\partial x}=\text{constant}\quad \text{at } x=L \tag{10}$$

- *Type 3 or Robin* – This form of boundary condition is the kind often found in classical heat conduction problems with convection on the surface of the solid. It is argued that type 3 conditions can recover the boundary slip result found using models like the equation of phonon radiative transport [10] and can be considered a "microscale boundary condition" resulting in a description of ballistic transport. An example is given in section "Case 2". Drawing upon the work of Klitsner [11], we use the following form:

If $F_T<1$,

$$-K\frac{\partial T}{\partial x}-K\tau F_T\frac{\partial^2 T}{\partial x\partial t}=\beta(T_{\infty 1}-T)+\beta\tau\left(\dot{T}_{\infty 1}-\dot{T}\right)\quad \text{at } x=0 \tag{11}$$

$$K\frac{\partial T}{\partial x}+K\tau F_T\frac{\partial^2 T}{\partial x\partial t}=\beta(T_{\infty 2}-T)+\beta\tau\left(\dot{T}_{\infty 2}-\dot{T}\right)\quad \text{at } x=L \tag{12}$$

If $F_T=1$

$$-K\frac{\partial T}{\partial x}=\beta(T_{\infty 1}-T)\quad \text{at } x=0 \tag{13}$$

$$K\frac{\partial T}{\partial x}=\beta(T_{\infty 2}-T)\quad \text{at } x=L \tag{14}$$

Here the parameter β is a "microscale coefficient." This parameter has been found to be a sufficient parameter to fit a multitude of experimental thermal conductivity data.

Before proceeding with the numerical discretization, we introduce $\theta = \frac{T-T_{\infty 2}}{T_{\infty 1}-T_{\infty 2}}$, $\eta = \frac{x}{L}$, and $\xi = \frac{t}{\tau}$ to nondimensionalize the C-F model. If we assume the classic kinetic theory result, $K = \frac{1}{3}Cv\lambda$, this allows us to express (3), with no source, in terms of only the Knudsen number, $K_n = \frac{\lambda}{L}$, and the heat conduction model number. λ is the mean free path of the energy carriers. For $F_T \in [0, 1)$,

$$\frac{\partial^2\theta}{\partial\xi^2} + \frac{\partial\theta}{\partial\xi} = \frac{K_n^2}{3}\frac{\partial^2\theta}{\partial\eta^2} + \frac{K_n^2}{3}F_T\frac{\partial}{\partial t}\left[\frac{\partial^2\theta}{\partial\eta^2}\right] \tag{15}$$

and for $F_T = 1$,

$$\frac{\partial\theta}{\partial\xi} = \frac{K_n^2}{3}\frac{\partial^2\theta}{\partial\eta^2} \tag{16}$$

Note that in nondimensionalizing (11)–(14), we have introduced a dimensionless microscale coefficient, $\gamma = \frac{\beta}{Cv}$. We now have a mathematical model which we would like to solve that is either a first- or second-order partial differential equation in time.

Numerical Formulation in Space

We proceed to fully discretize (15) in space and time. Because of the flexibility of the *i*Integration framework, this formulation also adapts to (16) as will be shown in a later section. For spatial discretization we choose the Galerkin finite element method with linear shape functions. For (15) this yields the semi-discrete equations as

$$[M]\{\ddot{\theta}\} + ([C_1] + [C_2])\{\dot{\theta}\} + [K_1]\{\theta\} = \{q_1\} \tag{17}$$

where for a particular element, e,

$$\begin{aligned}
[M] &= \int_0^h \lfloor N\rfloor^T \lfloor N\rfloor d\eta \\
[C_1] &= \int_0^h \lfloor N\rfloor^T \lfloor N\rfloor d\eta \\
[K_1] &= \frac{K_n^2}{3}\int_0^h \lfloor B\rfloor^T \lfloor B\rfloor d\eta \\
[C_2] &= \frac{K_n^2}{3}F_T\int_0^h \lfloor B\rfloor^T \lfloor B\rfloor d\eta
\end{aligned} \tag{18}$$

where h is the element length, $\lfloor N\rfloor = \left[1 - \frac{\eta}{h}\ \frac{\eta}{h}\right]$, and $\lfloor B\rfloor = \frac{d}{d\eta}\lfloor N\rfloor$. Additional terms due to Neumann- and Robin-type boundary conditions (denoted by a subscript N or R, respectively) result in a final semi-discretized system

$$[M]\{\ddot{\theta}\} + [C]\{\dot{\theta}\} + [K]\{\theta\} = \{q\} \tag{19}$$

where

$$\begin{aligned}
&[C] = [C_1] + [C_2] + [C_R] \qquad [K] = [K_1] + [K_R] \\
&\{q\} = \{q_1\} + \{q_{R/N}\}
\end{aligned} \tag{20}$$

Similarly for the first-order case, (16), we get

$$[C]\{\dot{\theta}\} + [K]\{\theta\} = \{q_1\} \tag{21}$$

where $[C_2] = 0$. So for $F_T = 1$, (20) becomes

$$\begin{aligned}
&[C] = [C_1] + [C_R] \quad [K] = [K_1] + [K_R] \\
&\{q\} = \{q_1\} + \{q_{R/N}\}
\end{aligned} \tag{22}$$

Numerical Formulation in Time: The *i*Integration Framework

The generalized single-step single-solve (GS4-2) computational framework has been recently developed to yield a family of second-order accurate, implicit, unconditionally stable algorithms with controllable numerical dissipation on the zeroth-, first-, and second-order time derivatives as well as zero-order overshooting behavior [12]. While originally designed for time integration of structural dynamics which are second-order in time, the more recent works extend to the so-called GS4-1 framework dealing with time marching of first-order systems [13]. These algorithms have the same desirable features as their second-order counterparts.

The essence of the framework and the underlying algorithms by design is as follows: using a generalized method of time-weighted residuals, the various unknowns to be solved for and the consequent update variables are chosen to be approximated by general asymptotic series

expansions. This allows for a general algorithm architecture or rather a whole family of infinitely many algorithms, which are expressed in terms of the coefficients of the expansion terms. By imposing a "wish list" (a set of algorithmic properties), the authors were able to reduce these coefficients down to a set of parameters all described in terms of the eigenvalues of the amplification matrix. These parameters, known as $\left(\rho_\infty^{\min}, \rho_\infty^{\max}, \rho_\infty^{s}\right)$, allow the user to choose between virtually any known (to date, in the context of LMS methods) implicit algorithm for second-order systems in time. It also includes new and optimal designs of algorithms within this framework.

Because of their common roots, it has been suspected that there is a connection between GS4-1 and GS4-2. Indeed, it has been shown that the first-order algorithms can be recovered from the second-order algorithms by a shift in variables and parameters [14]. The resulting general set of algorithms can recover most implicit time integration algorithms for first- *or* second-order systems in time. The framework also includes new and optimal designs of algorithms with useful features that preserve the problem physics. The complete details and derivation of this *i*Integration framework can be found in Masuri et al. [14].

We obtain a fully discretized system by applying the GS4 framework to (19) along with the initial conditions

$$\{\theta\}(0) = \theta_0 \tag{23}$$

$$\{\dot{\theta}\}(0) = \dot{\theta}_0 \tag{24}$$

The result is the following system:

$$[M]\{\widetilde{\ddot{\theta}}\} + [C]\{\widetilde{\dot{\theta}}\} + [K]\{\widetilde{\theta}\} = \{\widetilde{q}\} \tag{25}$$

where

$$\{\widetilde{\ddot{\theta}}\} = \{\ddot{\theta}\}_n + \Lambda_6 W_1 \left(\{\ddot{\theta}\}_{n+1} - \{\ddot{\theta}\}_n\right) \tag{26}$$

$$\{\widetilde{\dot{\theta}}\} = \{\dot{\theta}\}_n + \Lambda_4 W_1 \Delta t \{\ddot{\theta}\}_n + \Lambda_5 W_2 \Delta t \times \left(\{\ddot{\theta}\}_{n+1} - \{\ddot{\theta}\}_n\right) \tag{27}$$

$$\{\widetilde{\theta}\} = \{\theta\}_n + \Lambda_1 W_1 \Delta t \{\dot{\theta}\}_n + \Lambda_2 W_2 \Delta t^2 \{\ddot{\theta}\}_n + \Lambda_3 W_3 \Delta t^2 \left(\{\ddot{\theta}\}_{n+1} - \{\ddot{\theta}\}_n\right) \tag{28}$$

$$\{\tilde{q}\} = (1 - W_1)\{q\}_n + W_1 \{q\}_{n+1} \tag{29}$$

and the subscript n indicates the timestep. Substituting these into (25), we can solve for $\{\Delta\ddot{\theta}\} = \{\ddot{\theta}\}_{n+1} - \{\ddot{\theta}\}_n$ from

$$\begin{aligned}(\Lambda_6 W_1 [M] + \Lambda_5 W_2 \Delta t [C] + \Lambda_3 W_3 \Delta t^2 [K])\{\Delta\ddot{\theta}\} \\ = -[M]\{\ddot{\theta}\}_n - [C](\{\dot{\theta}\}_n + \Lambda_4 W_1 \Delta t \{\ddot{\theta}\}_n) \\ - [K](\{\theta\}_n + \Lambda_1 W_1 \Delta t \{\dot{\theta}\}_n + \Lambda_2 W_2 \Delta t^2 \{\ddot{\theta}\}_n) \\ + (1 - W_1)\{q\}_n + W_1 \{q\}_{n+1}\end{aligned} \tag{30}$$

Once we have $\{\Delta\ddot{\theta}\}$ we can solve for dimensionless temperature and its first- and second-order derivatives in time, at time $t = n + 1$, using

$$\{\ddot{\theta}\}_{n+1} = \{\ddot{\theta}\}_n + \{\Delta\ddot{\theta}\} \tag{31}$$

$$\{\dot{\theta}\}_{n+1} = \{\dot{\theta}\}_n + \lambda_4 \Delta t \{\ddot{\theta}\}_n + \lambda_5 \Delta t \{\Delta\ddot{\theta}\} \tag{32}$$

$$\{\theta\}_{n+1} = \{\theta\}_n + \lambda_1 \Delta t \{\dot{\theta}\}_n + \lambda_2 \Delta t^2 \{\ddot{\theta}\}_n + \lambda_3 \Delta t^2 \{\Delta\ddot{\theta}\} \tag{33}$$

where

$$\Lambda_1 W_1 = \frac{3 + \rho_\infty^{\min} + \rho_\infty^{\max} - \rho_\infty^{\min}\rho_\infty^{\max}}{2(1 + \rho_\infty^{\min})(1 + \rho_\infty^{\max})}$$

$$\Lambda_2 W_2 = \frac{1}{(1 + \rho_\infty^{\min})(1 + \rho_\infty^{\max})}$$

$$\Lambda_3 W_3 = \frac{1}{(1 + \rho_\infty^{\min})(1 + \rho_\infty^{\max})(1 + \rho_\infty^{s})}$$

$$\Lambda_4 W_1 = \frac{3 + \rho_\infty^{\min} + \rho_\infty^{\max} - \rho_\infty^{\min}\rho_\infty^{\max}}{2(1 + \rho_\infty^{\min})(1 + \rho_\infty^{\max})}$$

$$\Lambda_5 W_2 = \frac{2}{(1 + \rho_\infty^{\min})(1 + \rho_\infty^{\max})(1 + \rho_\infty^{s})}$$

$$\Lambda_6 W_1 = \frac{2 + \rho_\infty^{\min} + \rho_\infty^{\max} + \rho_\infty^{s} - \rho_\infty^{\min}\rho_\infty^{\max}\rho_\infty^{s}}{(1 + \rho_\infty^{\min})(1 + \rho_\infty^{\max})(1 + \rho_\infty^{s})}$$

$$W_1 = \frac{3 + \rho_\infty^{\min} + \rho_\infty^{\max} - \rho_\infty^{\min}\rho_\infty^{\max}}{2(1 + \rho_\infty^{\min})(1 + \rho_\infty^{\max})}$$

$$\lambda_1 = 1, \quad \lambda_2 = 1/2,$$
$$\lambda_4 = 1\lambda_3 = \frac{1}{2(1+\rho_\infty^s)}, \tag{34}$$
$$\lambda_5 = \frac{1}{1+\rho_\infty^s}$$

are the algorithmic parameters which can be controlled via a set of user-defined parameters $\left(\rho_\infty^{\min}, \rho_\infty^{\max}, \rho_\infty^s\right)$ associated with the high-frequency damping of the variables ($\{\theta\}$, $\{\dot{\theta}\}$, $\{\ddot{\theta}\}$), respectively. These parameters must satisfy the relation

$$1 \geq \rho_\infty^{\max} \geq \rho_\infty^{\min} \geq \rho_\infty^s \geq 0 \tag{35}$$

Note that the algorithm given by (34) corresponds to the so-called $V0$ family of algorithms of GS4-2. There also exists a family of $U0$ algorithms. Details can be found in Zhou and Tamma [15].

This entirely describes the spatial and temporal discretization of (15). To adapt the above framework for (16), one must perform the following procedure:

1. $[M] := [C]$
2. $[C] := [K]$
3. $[K] := [0]$ (Note that because of this assignment, $\{\theta\}$ no longer participates in the solution)
4. Treat $\{\ddot{\theta}\}$ as $\{\dot{\theta}\}$
5. Treat $\{\dot{\theta}\}$ as $\{\theta\}$
6. $\rho_\infty^{\max} = 1$
7. Treat $\rho_\infty^{\min}$ as ρ_∞
8. Disregard (24)

where $:=$ is the assignment operation (i.e., assign the value of $[C]$ to $[M]$). We have essentially interpreted the $(n+1)$st order derivative and its corresponding coefficient matrix as the nth order derivative and its corresponding coefficient matrix. This set of operations yields the GS4-1 family of algorithms *exactly* as given in Masuri et al. [13]. We now have an integrated computational framework in which general first- and second-order systems can be solved using the same code.

It should be pointed out that the parameters $\left(\rho_\infty^{\min}, \rho_\infty^{\max}, \rho_\infty^s\right)$ serve to control the numerical dissipation on the zeroth-, first-, and second-order derivative of the dependent variable for a second-order system, respectively. When GS4 is shifted to handle first-order systems, $\rho_\infty^{\max} = 1$, $\left(\rho_\infty, \rho_\infty^s\right)$ now control the numerical dissipation on the zeroth- and first-order derivatives, respectively. From (35), the family of first-order algorithms must now satisfy the relation

$$1 \geq \rho_\infty \geq \rho_\infty^s \geq 0 \tag{36}$$

Numerical Results

In this section we consider three different values of the heat conduction model number, F_T, and Knudsen numbers, K_n. Using these three different values for F_T and K_n, we can demonstrate the ability of the GS4 computational framework to handle both first-order parabolic $(F_T = 1)$ and second-order hyperbolic $(F_T = 0)$ systems. We also present the use of type 1, 2, and 3 boundary conditions. We follow these results with the corresponding convergence plots which show the second-order time accuracy of the algorithm regardless of the values for $\left(\rho_\infty^{\min}, \rho_\infty^{\max}, \rho_\infty^s\right)$. The examples given for these are separated into three cases which span large length scales and varying strengths of wavelike transport.

A film starts at temperature $\theta = 0$ when suddenly:

1. $F_T = 1, K_n = 1$. A constant heat flux, (9) with constant $= 0.2$ is enforced at $\eta = 0$ and a Robin condition with $\gamma = 1$ is applied at $\eta = 1$ for $\xi > 0$.
2. $F_T = 0.5, K_n = 10$. Both boundaries are given a type 3 conditions, (11)–(12) with $\gamma = 1$ for $\xi > 0$.
3. $F_T = \frac{1}{2}, K_n = 0.1$. A Dirichlet condition, (5) is applied to $\eta = 0$ while a Robin condition with $\gamma = 1$ is enforced at $\eta = 1$ for $\xi > 0$.

A brief description of the model resulting from our choice of the heat conduction model number is included in each of the following subsections. Numerical issues, as they arise, are also highlighted. Note that the use of "exact solution" in Figs. 1–3 is not literal. These curves should be

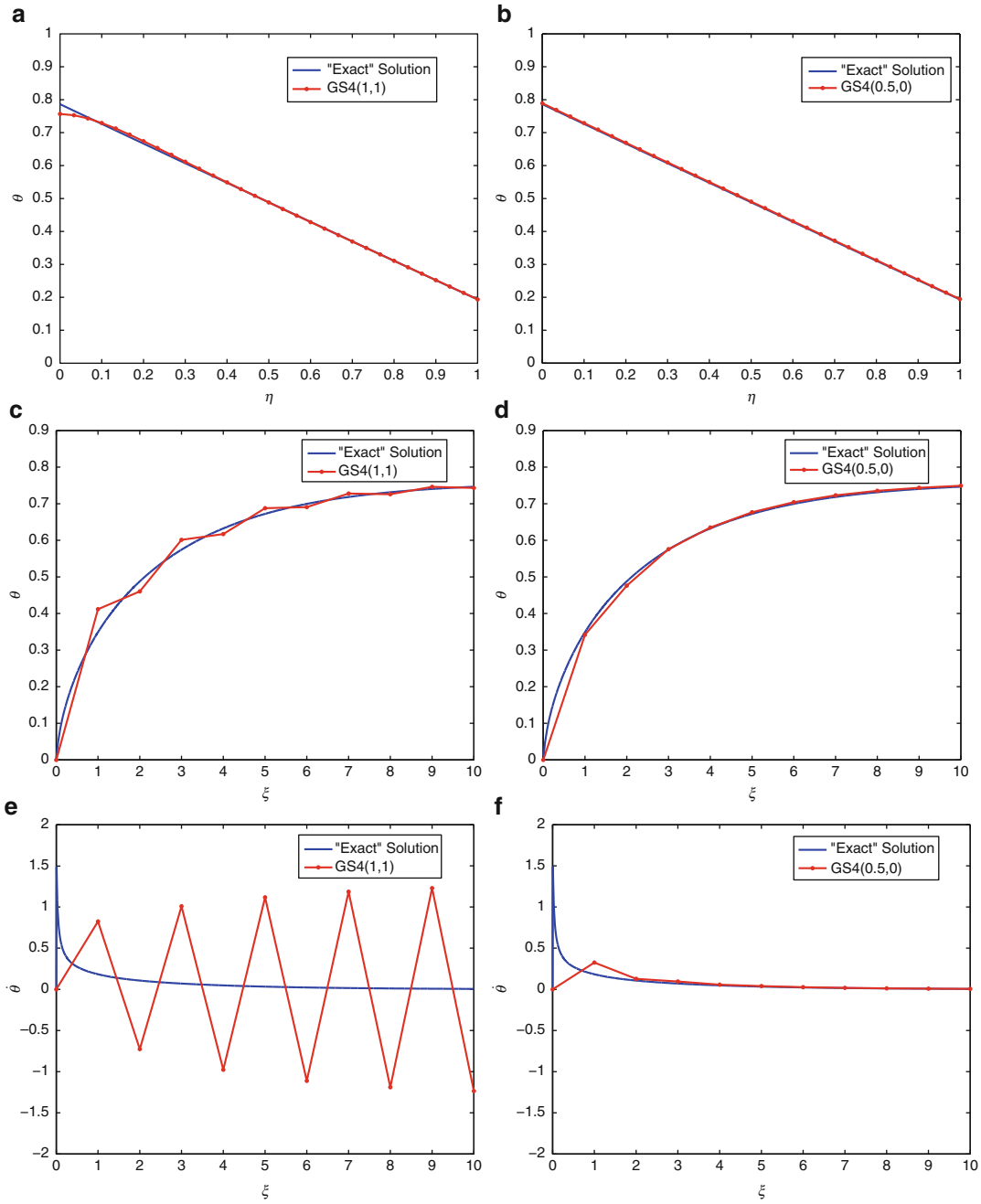

C- and F-Processes Model: A Generalized Approach to Solving Transient Diffusive, Wavelike and Ballistic Solid State Heat Conduction Problems, Fig. 1 Results for Case 1: $F_T = 1$, $K_n = 1$. Plots on the *left-hand side* correspond to $\left(\rho_\infty, \rho_\infty^s\right) = (1, 1)$ and plots on the *right-hand side* correspond to $\left(\rho_\infty, \rho_\infty^s\right) = (0.5, 0)$. (**a**, **b**) A snapshot in time of the temperature profile. (**c**, **d**) Nodal time history of nondimensional temperature. (**e**, **f**) Nodal time history of time derivative of nondimensional temperature

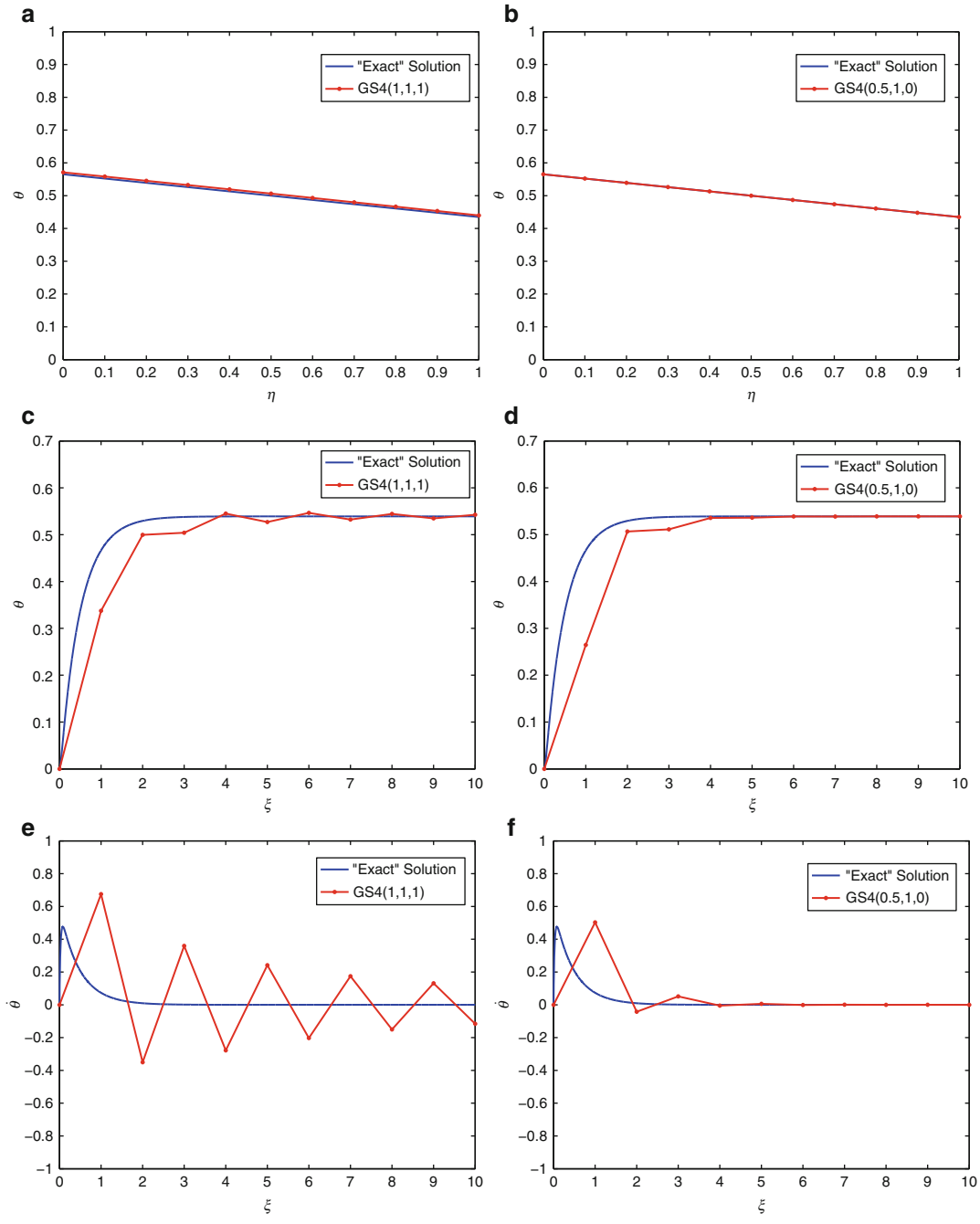

C- and F-Processes Model: A Generalized Approach to Solving Transient Diffusive, Wavelike and Ballistic Solid State Heat Conduction Problems, Fig. 2 Results for Case 2: $F_T = 0.5$, $K_n = 10$. Plots on the *left-hand side* correspond to $\left(\rho_\infty^{\min}, \rho_\infty^{\max}, \rho_\infty^s\right) = (1, 1, 1)$ and plots on the *right-hand side* correspond to $\left(\rho_\infty^{\min}, \rho_\infty^{\max}, \rho_\infty^s\right) = \left(\frac{1}{2}, 1, 0\right)$. (**a**, **b**) A snapshot in time of the temperature profile. (**c**, **d**) Nodal time history of nondimensional temperature. (**e**, **f**) Nodal time history of time derivative of nondimensional temperature

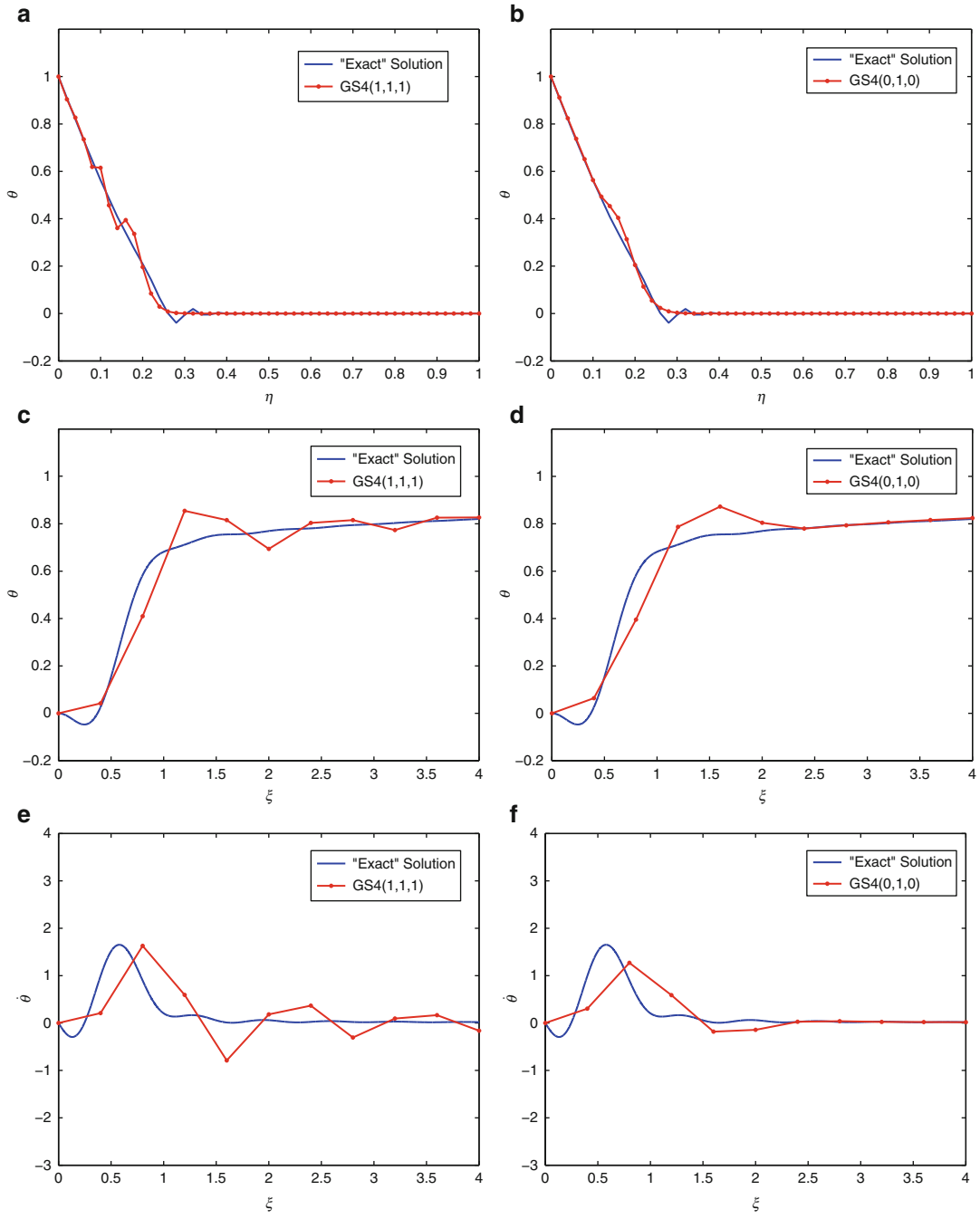

C- and F-Processes Model: A Generalized Approach to Solving Transient Diffusive, Wavelike and Ballistic Solid State Heat Conduction Problems, Fig. 3 Results for Case 3: $F_T = 1$, $K_n = 1$. Plots on the *left-hand side* correspond to $\left(\rho_\infty^{\min}, \rho_\infty^{\max}, \rho_\infty^{s}\right) = (1, 1, 1)$ and plots on the *right-hand side* correspond to $\left(\rho_\infty^{\min}, \rho_\infty^{\max}, \rho_\infty^{s}\right) = (0, 1, 0)$. (**a**, **b**) A snapshot in time of the temperature profile. (**c**, **d**) Nodal time history of nondimensional temperature. (**e**, **f**) Nodal time history of time derivative of nondimensional temperature

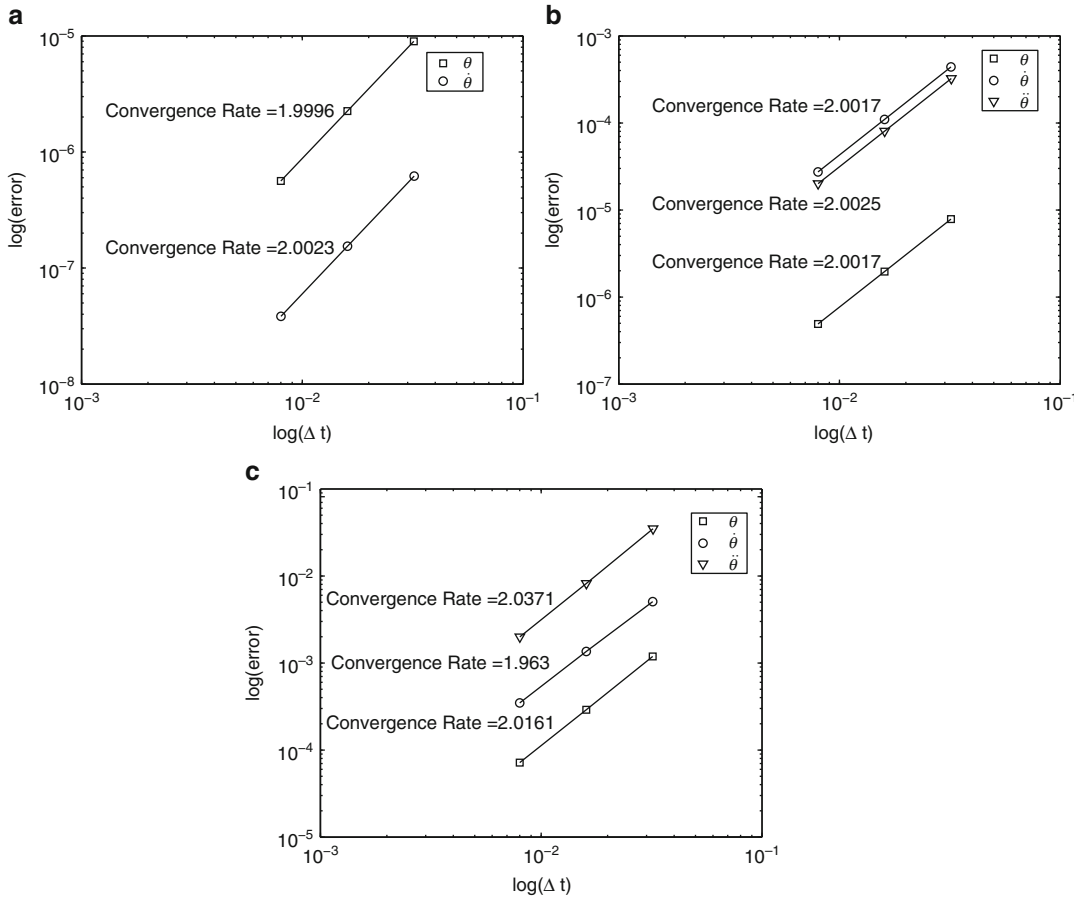

C- and F-Processes Model: A Generalized Approach to Solving Transient Diffusive, Wavelike and Ballistic Solid State Heat Conduction Problems, Fig. 4 Convergence plots for all three cases showing second-order time accuracy in the zeroth-, first-, and second-order derivatives. These plots correspond to and reflect the convergence behavior after numerical dissipation has been applied to the solution. (**a**) Case 1, $\left(\rho_\infty, \rho_\infty^s\right) = (0, 0)$. (**b**) Case 2, $\left(\rho_\infty^{\min}, \rho_\infty^{\max}, \rho_\infty^s\right) = \left(\frac{1}{2}, 1, 0\right)$ (**c**) Case 3, $\left(\rho_\infty^{\min}, \rho_\infty^{\max}, \rho_\infty^s\right) = (0, 1, 0)$

taken as a reference solution which solves the same problem with the same number of elements and a very large number of timesteps, 10,000.

Case 1

In this case, our choice of $F_T = 1$ recovers classical Fourier-type heat conduction. The choice of $K_n = 1$ is the transition region for ballistic transport. Solving this transient system shows the ability of the *i*Integration framework to shift seamlessly between first- and second-order systems. Note that the *i*Integration framework allows for selective control of numerical dissipation on θ and $\dot{\theta}$. Less numerical dissipation results in a more accurate solution at the risk of having numerical oscillations present as seen in Fig. 1. The algorithm chosen to remove numerical oscillations in Case 1, $\left(\rho_\infty, \rho_\infty^s\right) = (0.5, 0)$, shows successful damping of oscillatory behavior.

Case 2

The general C-F model given by (15) with $F_T \in (0, 1)$ takes on the same form as an existing heat conduction model which is known as Jeffreys model. An excellent overview of wavelike heat propagation as well as a discussion and derivation of Jeffreys model can be found in the work of Joseph and Preziosi [16]. $K_n = 10$ indicates

a very thin film where ballistic transport is the dominant energy transfer mechanism. The use of type 3 boundary conditions is of particular importance as the ability to change $\gamma = \frac{\beta}{Cv}$ has been shown to be important in fitting thermal conductivity experiments where ballistic transport is important. A characteristic feature of ballistic transport, a temperature jump at the boundaries, is evident in the solution given in Fig. 2a, b.

Significant oscillations can be seen in the time derivative of the dependent variable which is controlled by the $\rho_{\infty}^{\max}$ parameter. The GS4 framework has the unique ability to provide control of numerical damping of this variable independently of θ. In heat transfer applications, the time derivative of temperature can be of fundamental importance when modeling, for example, plumes in turbulent convection [17] or crystallization of materials [18]. These results can be seen in Fig. 2.

Case 3

For the case of the C-F model with $F_T = 0$, the so-called hyperbolic heat equation (also known as the Cattaneo-Vernotte equation and the telegraph equation) is recovered. The hyperbolic nature of this equation causes its solution to be wavelike. This brings about unphysical oscillatory behavior in numerical solution schemes, and various efforts have been put forth to combat these difficulties. The choice of $K_n = 0.1$ is generally considered the diffusive or macroscale limit.

The GS4 framework, with its tunable numerical dissipation, easily controls this phenomenon. Nodal oscillations over time of the temperature and its time derivative are controlled to permit more physically realistic results as shown in Fig. 3.

Convergence plots for all three cases presented above can be found in Fig. 4a–c. These plots demonstrate the second-order accuracy of the *i*Integration framework after the application of numerical dissipation.

Concluding Remarks

We have presented the unified isochronous integration (i) computational framework for integrating first- and second-order transient systems arising in the study of thermal transport in solids. Numerical oscillations for a class of problems have been shown to be more easily treated while retaining the second-order in time accuracy of the selected algorithm within this integrated framework. A theoretical model of solid state heat transfer, the C-F model, has been used for illustration. This model represents all heat conduction mechanisms – diffusive, wavelike, and ballistic transport as was shown through various examples. Application of the described approach allows for an efficient and effective solution to any transient problem of heat conduction in solids.

References

1. Cattaneo C (1958) A form of heat conduction equation which eliminates the paradox of instantaneous propagation. Compte Rendus 247(4):431–433
2. Qiu TQ, Tien CL (1993) Heat transfer mechanisms during short-pulse laser heating of metals. J Heat Transf (Trans ASME (Am Soc Mech Eng), Ser C) 115(4):835–841
3. Nnanna AGA, Haji-Sheikh A, Harris KT (2005) Experimental study of non-Fourier thermal response in porous media. J Porous Media 8(1):31–44
4. Casimir HBG (1938) Note on the conduction of heat in crystals. Physica 5:495–500
5. Naqvi KR, Waldenstrøm S (2005) Brownian motion description of heat conduction by phonons. Phys Rev Lett 95(6):65901
6. Alvarez FX, Jou D (2009) Memory and nonlocal effects in heat transport: from diffusive to ballistic regimes. Appl Phys Lett 90(8):083109
7. Chen G (2001) Ballistic-diffusive heat-conduction equations. Phys Rev Lett 86(11):2297–2300
8. Cahill DG, Ford WK, Goodson KE, Mahan GD, Majumdar A, Maris HJ, Merlin R, Phillpot SR (2003) Nanoscale thermal transport. J Appl Phys 93:793
9. Anderson CVDR, Tamma KK (2006) Novel heat conduction model for bridging different space and time scales. Phys Rev Lett 96(18):184301
10. Majumdar A (1993) Microscale heat conduction in dielectric thin films. ASME Trans J Heat Transf 115:7–16
11. Klitsner T, VanCleve JE, Fischer HE, Pohl RO (1988) Phonon radiative heat transfer and surface scattering. Phys Rev B 38(11):7576–7594
12. Zhou X, Tamma KK (2006) Algorithms by design with illustrations to solid and structural me-chanics/dynamics. Int J Numer Method Eng 66(11):1738–1790
13. Masuri S, Sellier M, Zhou X, Tamma KK (2011) Design of order-preserving algorithms for transient first-order systems with controllable

numerical dissipation. Int J Numer Method Eng. doi:10.1002/nme.3228
14. Masuri S, Tamma KK, Zhou X. Integrators: an isochronous unified order preserving framework for integrating first/second order parabolic/hyperbolic systems (in preparation)
15. Zhou X, Tamma KK (2004) Design, analysis, and synthesis of generalized single step single solve and optimal algorithms for structural dynamics. Int J Numer Method Eng 59(5):597–668
16. Joseph DD, Preziosi L (1989) Heat waves. Rev Mod Phys 61(1):41
17. Belmonte A, Libchaber A (1996) Thermal signature of plumes in turbulent convection: the skewness of the derivative. Phys Rev E 53(5):4893
18. Schroers J, Masuhr A, Johnson WL, Busch R (1999) Pronounced asymmetry in the crystalliza-tion behavior during constant heating and cooling of a bulk metallic glass-forming liquid. Phys Rev B 60(17):11855

Calculated Temperature Profile

▶ Refined and Advanced Governing Equations for the Thermomechanical Analysis of Shells
▶ Temperature Profiles in Composite and Sandwich Shells
▶ Temperature Profiles in One-Layered and Multilayered Isotropic Shells
▶ Thermal Stress Analysis of Functionally Graded Material Plates
▶ Thermomechanical Bending in Functionally Graded Material Shells

Canonical Formulation of "Nondissipative Thermoelasticity" (with Application to Thermoelastic Fracture)

Gerard A. Maugin
Institut Jean Le Rond d'Alembert, Unité mixte de recherche 7190, Universite Pierre et Marie Curie, Paris, France

Overview

Classical linear thermoelasticity with Fourier's law of heat conduction leads to a propagation of thermal disturbances at infinite speed (cf. [6]), what is contrary to the existence of a limiting speed for physical processes. Furthermore, the *canonical* writing of such a theory provides a nonhomogeneous system of conservation laws of momentum and energy (cf. [3]), what has for direct consequence to provide path-dependent integrals in fracture (cf. [5]). Several approaches have been proposed to remedy the first deficiency. Among these, one is the theory of Green and Naghdi [1] that exploits the notion of *thermal displacement* or "thermacy" (introduced by van Dantzig in the 1920s). The idea is to give to the temperature the status of a velocity (time derivative of a scalar). As a result, it is possible to construct a thermoelasticity with no apparent dissipation (we have at hand a "dissipation-free" theory of thermoelastic conductors; almost an oxymoron!), yielding a finite speed of propagation (i.e., the mathematical system under study becomes hyperbolic). It is also possible to construct path-independent integrals in the resulting theory of fracture (cf. Dascalu and Maugin [2]). This works out just like a magician trick notwithstanding the lack of deep physics. Both basic formulation involving a modified material Eshelby stress and the accompanying revisited version of the thermoelastic fracture problem involving path-independent integrals are given.

Field Equations and Conservation Equations

Thus, we introduce a scalar variable γ such that the thermodynamic temperature is given by

$$\theta(\mathbf{X}, t) = \frac{\partial}{\partial t}\gamma(\mathbf{X}, t) \equiv \dot{\gamma} \quad \text{or} \quad \gamma = \int_0^{\mathrm{t}} \theta(\mathbf{X}, \mathrm{t}')\, \mathrm{dt}' \tag{1}$$

A variational formulation based on a direct-motion description will consider a Lagrangian density per unit reference volume in the form

$$L^{th} = \bar{L}^{th}\left(\mathbf{v} = \dot{\bar{\mathbf{x}}},\ \mathbf{F} = \nabla_R \bar{\mathbf{x}},\ \dot{\gamma},\ \nabla_R \gamma\right) = \frac{1}{2}\rho_0 \mathbf{v}^2 - \overline{W}(\mathbf{F}, \dot{\gamma}, \nabla_R \gamma) \tag{2}$$

where no inertia term is isolated for the field γ which, just like $\mathbf{x}$ or the usual displacement $\mathbf{u} = \mathbf{X} - \mathbf{x}$, does not appear just by itself (Galilean invariance; but $\mathbf{X}$ would be present in both ρ_0 and $\overline{W}$ in the presence of true material inhomogeneities). Here, the potential (Helmholtz) energy depends on temperature and the *past history* of the temperature gradient since

$$\nabla_R \gamma = \int_0^t \left(\nabla_R \theta(\mathbf{X}, t')\right) dt'$$

Skipping details of the derivation [3], the Euler-Lagrange field equations for $\mathbf{x}$ and γ valid at regular material points $\mathbf{X}$ are readily obtained as the linear (physical) momentum equation

$$\frac{\partial \mathbf{p}}{\partial t} - div_R \mathbf{T} = \mathbf{0}, \quad \mathbf{p} := \rho_0 \mathbf{v}, \quad \mathbf{T} = \partial \overline{W}/\partial \mathbf{F} \tag{3}$$

and the entropy equation in the form

$$\frac{\partial S}{\partial t} + \nabla_R . \mathbf{S} = 0, \quad S = -\frac{\partial \overline{W}}{\partial \dot{\gamma}} = -\frac{\partial \overline{W}}{\partial \theta}, \quad \mathbf{S} = -\frac{\partial \overline{W}}{\partial (\nabla_R \gamma)} \tag{4}$$

The first of (4) has no source term although S is obviously identified as the entropy density. That is the reason why this theory is called a theory of thermoelasticity "without dissipation." Application of Noether's theorem to the present variational formulation for space-time translations in material space yields the canonical equations of (material) momentum and energy in the form (compare [5])

$$\left.\frac{\partial \mathbf{P}^{th}}{\partial t}\right|_X - div_R \mathbf{b}^{th} = \mathbf{0}, \quad \left.\frac{\partial H^{th}}{\partial t}\right|_X - \nabla_R . \mathbf{Q}^{th} = 0 \tag{5}$$

where

$$\mathbf{P} = \mathbf{P}^{mech} - S\, \nabla_R \gamma, \quad \mathbf{P}^{mech} := -\mathbf{p}.\mathbf{F} \tag{6}$$

$$\mathbf{b}^{th} = -\left(L^{th} + \mathbf{T}.\mathbf{F} - \mathbf{S} \otimes \nabla_R \gamma\right) \tag{7}$$

$$H^{th} = \frac{1}{2}\, \rho_0 \mathbf{v}^2 + E, \quad E = \overline{W} + S\theta, \quad \mathbf{Q}^{th} = \mathbf{T}.\mathbf{v} - \theta \mathbf{S} \tag{8}$$

Thus, the energy equation given by the second of (5) is in a standard form if one accepts the identifications considered in (5), and $\overline{W}$ as the free energy, and we set the material heat flux $\mathbf{Q} = \theta \mathbf{S}$. What is new here are the additional contributions due to $\nabla_R \gamma$ in the expressions of the canonical linear momentum $\mathbf{P}$ and of the new Eshelby material stress tensor $\mathbf{b}^{th}$. Thus, both $(3)_1$ and $(5)_1$ are in their classical form while $(4)_1$ and $(5)_1$ contain no source terms.

We could have started with a variational formulation based on the consideration of the inverse motion, for which the initial Lagrangian density is taken per unit actual volume of mass density $\rho(\mathbf{x}, t)$ as [4]

$$J_F^{-1} L = \frac{1}{2}\, \rho\, \mathbf{V}.\mathbf{C}.\mathbf{V} - \overline{w}\left(\mathbf{F}^{-1}(\mathbf{x}, t),\ \partial \gamma(\mathbf{x}, t)/\partial t,\ \nabla \gamma = \partial \gamma / \partial \mathbf{x}\right) \tag{9}$$

where

$$\mathbf{C} = \mathbf{F}^T \mathbf{F}, \quad \mathbf{V} = -\mathbf{F}^{-1}.\mathbf{v} \tag{10}$$

In this case, the Euler-Lagrange equations are directly the equation of canonical material momentum $(5)_1$ and the entropy $(4)_1$, while the standard linear momentum $(3)_1$ and the energy $(5)_2$ are obtained by application of Noether's theorem.

The Problem of Thermoelastic Fracture Revisited

This was considered by Dascalu and Maugin [2]. There is no need to duplicate the arguments followed in [5]. We simply note that with the requirements that

$$\mathbf{N}.\mathbf{T}^{\pm} = \mathbf{0}, \quad \mathbf{N}.\mathbf{Q}^{\pm} = 0 \tag{11}$$

along the faces of the crack, equations similar to (12) and (13) of [7] will be obtained but with quantities noted with superscript *th* (here in quasi-statics),

$$\mathbf{F}^{th}_{crack} = lim \int_{\Gamma} \left(\mathbf{P}^{th}(\overline{\nabla}.\mathbf{N}) + \mathbf{N}.\mathbf{b}^{th}\right) d\Gamma \ \ as\ \Gamma \rightarrow\ 0 \tag{12}$$

$$G_{crack} = lim \int_{\Gamma} \left(H^{th}(\overline{\nabla}.\mathbf{N}) + \mathbf{N}.(\mathbf{T}.\mathbf{v} - \mathbf{Q})\right) d\Gamma \ as\ \Gamma \rightarrow 0 \tag{13}$$

These two are compatible, yielding the local statement of the second law of thermodynamics

$$G_{crack} = \overline{\nabla}.\mathbf{F}^{th}_{crack} \geq 0 \tag{14}$$

when we have the following asymptotic behavior of the fields at the crack tip

$$\dot{\gamma}(\mathbf{X}, t) \approx -\left(\overline{\nabla}.\nabla_R\right)\gamma(\mathbf{X}, t) \tag{15}$$

$$\theta \approx -\overline{\nabla}.\nabla_R\gamma, \quad \mathbf{v} \approx -\overline{\nabla}.\mathbf{F}^T$$

while

$$S\overline{\nabla}.\nabla_R\gamma \approx -S\theta, \quad \overline{\nabla}.\mathbf{P}^{mech} \approx \rho_0\mathbf{v}^2 \tag{16}$$

Note that the result (14) is general, being in fact independent of the considered thermoelasticity theory. An equivalent form of (13) is obtained as

$$G_{crack} = \int_{\Lambda} \left(\mathbf{N}.\left(\mathbf{b}^{th} + \left(\overline{\nabla}.\mathbf{P}^{th}\right)\mathbf{1}_R\right).\overline{\nabla}\right)ds - \frac{d}{dt}\int_A \overline{\nabla}.\mathbf{P}^{th}dA \tag{17}$$

where Λ is another contour encircling the domain A which contains the crack tip and moves together with it. In quasi-statics, this reduces to

$$G_{crack} = \int_{\Lambda} \mathbf{N}.\mathbf{b}^{th}.\overline{\nabla}ds \tag{18}$$

where the kinetic energy is no longer involved in the Eshelby stress $\mathbf{b}^{th}$. This is compatible with (14).

Recovery of Classical Thermoelasticity

We are obviously aware of the amount of artificiality in the Green and Naghdi [1] construct. All is based on the assumptions made regarding the free energy functional dependence. An approximation yielding the classical theory of thermoelasticity has, therefore, to be obtained from an approximation of that energy. With $\beta = \nabla_R\gamma$, we can write a Taylor series expansion with respect to that material vector about its zero value. Thus,

$$W(\mathbf{F},\ \theta = \dot{\gamma},\ \beta = \nabla_R\gamma) = \hat{W}(\mathbf{F},\ \theta,\ \beta = \mathbf{0}) + \frac{\partial W}{\partial \beta}(\beta = \mathbf{0}) : \beta + 0\left(\beta^2\right) \tag{19}$$

We let the reader evaluate all the derivatives of W needed in the theory, with

$$\hat{S} = -\frac{\partial \hat{W}}{\partial \theta}, \hat{\mathbf{S}} = -\frac{\partial W}{\partial \beta}(\beta = \mathbf{0}), \hat{\mathbf{Q}} = \theta\hat{\mathbf{S}} \tag{20}$$

It is checked that $(3)_1$, $(4)_1$, and (5) yield the equations [3] (Section 6 in that reference)

$$\frac{\partial \mathbf{p}}{\partial t} - div_R\hat{\mathbf{T}} = \mathbf{0} \tag{21}$$

$$\frac{\partial \hat{S}}{\partial t} + \nabla_R.\hat{\mathbf{S}} = -\theta\,\hat{\mathbf{S}}.\ \nabla_R\theta = -\hat{\mathbf{Q}}.\nabla_R\theta \tag{22}$$

$$\frac{\partial \mathbf{P}^{mech}}{\partial t} - div_R\hat{\mathbf{b}} = \hat{\mathbf{f}}^{th} = \hat{S}\nabla_R\theta \tag{23}$$

$$\frac{\partial \hat{H}}{\partial t} - \nabla_R.\left(\hat{\mathbf{T}}.\mathbf{v} - \hat{\mathbf{Q}}\right) = 0 \tag{24}$$

where all symbols with a superimposed caret are indeed those of the classical theory, e.g., in $\hat{H}$, $\hat{E} = \hat{W} + \hat{S}\theta$, and $\mathbf{P}^{mech}$ is none other than the

classical purely mechanical term. In the fracture problem, one has to focus attention on the additional terms that were involved in the Eshelby stress of the Green-Naghdi theory. In this limit, a source term will appear in the expression of the driving force. This will be none other than the bulk integral of the material thermal force present in the right-hand side of (23). Thus, in (20) through (24), one simply has to forget about the way the entropy flux was introduced (the second of (20)) and then construct a constitutive equation for it or for $\hat{\mathbf{Q}}$ as is usually done [5].

References

1. Green AE, Naghdi PM (1993) Thermoelasticity without energy dissipation. J Elast 31:189–202
2. Dascalu C, Maugin GA (1995) The thermoelastic material-momentum equation. J Elast 39:201–212
3. Kalpakides VK, Maugin GA (2004) Canonical formulation and conservation laws of thermoelasticity "without dissipation". Rep Math Phys 53:371–391
4. Maugin GA, Kalpakides VK (2002) A Hamiltonian formulation for elasticity and thermoelasticity. J Phys A MathGen 35:10775–10788
5. Maugin GA (2011) Configurational forces. CRC/Chapman & Hall/Taylor and Francis, Boca Raton, pp 245–249, Chapter 8
6. Maugin GA (2013a) Article in the ETS: Thermomechanics of continua
7. Maugin GA (2013b) Article in the ETS: Thermoelastic fracture in terms of configurational forces

Canonical Formulation of Thermoelasticity

Gerard A. Maugin
Institut Jean Le Rond d'Alembert, Unité mixte de recherche 7190, Universite Pierre et Marie Curie, Paris, France

Overview

Traditionally, the basic equations of balance of continuum mechanics and thermodynamics are first presented in the framework designed by *Cauchy* and other scientists in the nineteenth century, i.e., at actual time t and per unit volume or surface in the so-called actual, or physical, configuration, K_t. Speaking of finitely deformable solids, with *Piola* and *Kirchhoff*, another format was introduced which still considers equations of motion in the actual framework but per unit volume or surface of a reference configurations K_R. More recent works dealing with the theory of material inhomogeneities and the progress of material defects require a full projection of these equations onto the *material manifold* itself as this is the true arena of these phenomena. This may be related to the insightful works of *J.D. Eshelby* (1916–1981). But this new format may also be called *canonical* as it no longer deals with the actual configuration. This format is particularly enlightening in thermoelasticity. It emphasizes the role played by the conservation law of so-called (canonical) material momentum with the appearance of the material Eshelby stress and the accompanying form of the local energy equation. Here we are concerned with equations valid at any regular material point $\mathbf{X}$ in a thermoelastic body B. But the formulation demonstrates its full power in rationally introducing the driving forces acting on field singularities (discontinuity surfaces, cracks, etc.; see the corresponding entries in the ETS).

Cauchy Format of the Basic Equations of Thermoelasticity in Finite Strains

At time t and actual placement $\mathbf{x}$ resulting from a finite deformation $\mathbf{x} = \overline{\mathbf{x}}(\mathbf{X}, \mathbf{t})$ between a global reference configuration K_R and the actual configuration K_t in Euclidean physical space E^3, we have the following local balance laws (also referred to as "field" equations):

- *Balance of mass, also called the continuity equation*

$$\dot{\rho} + \rho\,(\nabla.\mathbf{v}) = \left.\frac{\partial \rho}{\partial t}\right|_x + \nabla.(\mathbf{p}^t) = 0,\ \mathbf{p}^t := \rho\mathbf{v} \quad (1)$$

- *Balance of linear (physical) momentum (in the absence of body force)*

$$\rho\dot{\mathbf{v}} - div\,\sigma = \mathbf{0} \tag{2}$$

- *Balance of angular (physical) momentum*

$$\sigma = \sigma^T \; i.e.,\; \sigma_{ij} = \sigma_{ji} \; or \; \sigma_{[ij]} = 0 \tag{3}$$

- *First law of thermodynamics*

$$\rho\frac{d}{dt}(H^t/\rho) - \nabla.(\sigma.\mathbf{v} - \mathbf{q}) = \rho h \tag{4}$$

- *Balance of entropy*

$$\rho\frac{d}{dt}(S^t/\rho) + \nabla.(\mathbf{s}) - \rho\hat{\eta} = \rho\tilde{\eta} \tag{5}$$

- *Second law of thermodynamics*

$$\rho\tilde{\eta} \geq 0 \tag{6}$$

Here, ρ is the matter density at time t, σ is the symmetric Cauchy stress, $\mathbf{q}$ is the heat flux vector, e is the internal energy per unit mass in K_t, $h(\mathbf{x}, t)$ is a body source of energy per unit mass in K_t, η is the entropy per unit mass in K_t, $\hat{\eta}$ is a body source of entropy per unit mass in K_t, $\tilde{\eta}$ is an internal source of entropy per unit mass in B_t, S^t is the entropy per unit volume, and $\mathbf{s}$ is the entropy (in)flux vector, and we have set

$$H^t = K^t + E^t,\; K^t = \frac{1}{2}\rho(\mathbf{x}, t)\mathbf{v}^2,\; E^t = \rho e \tag{7}$$

with $\mathbf{v} = \partial\overline{\mathbf{x}}/\partial t|_X$. The standard assumptions (Coleman-Noll; see [1]) are that

$$\mathbf{s} = \mathbf{q}/\theta,\; \hat{\eta} = h/\theta \tag{8}$$

where $\theta > 0$, $\inf\theta = 0$ is the thermodynamic temperature.

Piola-Kirchhoff Format of the Local Balance Laws of Thermomechanics

On introducing the matter density ρ_0 at K_R and the first Piola-Kirchhoff stress $\mathbf{T}$ by the so-called Piola transformation,

$$\rho_0 = J_F\rho,\; \mathbf{T} = J_F\mathbf{F}^{-1}\sigma \tag{9}$$

where $J_F = \det\mathbf{F}$ and $\mathbf{F}^{-1}$ is the inverse of $\mathbf{F}$, with $\mathbf{F} := \nabla_R\overline{\mathbf{x}} = \partial\overline{\mathbf{x}}/\partial\mathbf{X}$, and using the identities,

$$\nabla_R\left(J_F\mathbf{F}^{-1}\right) = \mathbf{0},\; \nabla\left(\mathbf{J}_F^{-1}\,\mathbf{F}\right) = \mathbf{0} \tag{10}$$

we transform the set of balance equations (1) through (6) into the following set:

- *Balance of mass, also called the continuity equation*

$$\frac{\partial}{\partial t}\rho_0\Big|_X = 0 \tag{11}$$

- *Balance of linear (physical) momentum*

$$\frac{\partial}{\partial t}\mathbf{p}_R\Big|_X - div_R\mathbf{T} = \mathbf{0},\; \mathbf{p}_R := \rho_0\mathbf{v} \tag{12}$$

- *Balance of angular (physical) momentum*

$$\mathbf{FT} = \mathbf{T}^T\mathbf{F}^T \tag{13}$$

- *First law of thermodynamics*

$$\frac{\partial}{\partial t}H_R\Big|_X - \nabla_R.(\mathbf{T}.\mathbf{v} - \mathbf{Q}) = \rho_0 h \tag{14}$$

- *Balance of entropy*

$$\frac{\partial}{\partial t}S_R\Big|_X + \nabla_R.\mathbf{S} - \rho_0\hat{\eta} = \Sigma_R := \rho_0\tilde{\eta} \tag{15}$$

- *Second law of thermodynamics*

$$\Sigma_R \geq 0 \tag{16}$$

where (Piola transformations)

$$\mathbf{Q} = J_F\,\mathbf{F}^{-1}\mathbf{q},\; \mathbf{S} = J_F\,\mathbf{F}^{-1}\,\mathbf{s} \tag{17}$$

Sometimes, these equations – which are very useful in the finite strain framework – are referred to as *material equations*, as compared to the spatial equations deduced in the Cauchy format. This is a misnomer because only the

space-time parametrization and partial derivatives here refer to this framework while both (12) and (13) still have components in the physical framework (actual configuration K_t). We see below how one constructs equations that are completely in the material framework, both in terms of tensorial objects and space-time parametrization.

General Thermomechanical Theorems

- *Kinetic energy theorem*: On taking the inner product of (2) with $\mathbf{v}$, we obtain (tr = trace)

$$\rho \frac{d(K^t/\rho)}{dt} - \nabla.(\sigma.\mathbf{v}) + tr\left(\sigma.(\nabla \mathbf{v})^T\right) = 0 \quad (18)$$

- *Internal energy theorem*: On expanding (4) and combining with (18), we obtain

$$\rho \frac{d(E^t/\rho)}{dt} - tr\left(\sigma.(\nabla \mathbf{v})^T\right) + \nabla.\mathbf{q} = \rho h \quad (19)$$

- *Clausius-Duhem inequality*: Combining now (19) and (5)–(6) and introducing the free energy density $\psi = e - \eta\theta$, we obtain the following inequality:

$$\begin{aligned} &-\rho\left(\dot{\psi} + \eta\dot{\theta}\right) + tr\left(\sigma.(\nabla \mathbf{v})^T\right) \\ &-(\mathbf{q}/\theta).\nabla\theta = \rho\,\theta\tilde{\eta} \geq 0 \end{aligned} \quad (20)$$

In direct parallelism with these spatial equations, it is easy to establish the following equations in the *Piola-Kirchhoff* format:

- *Kinetic energy theorem*

$$\left.\frac{\partial K_R}{\partial t}\right|_X - \nabla_R.(\mathbf{T}.\mathbf{v}) + tr\left(\mathbf{T}.(\nabla_R \mathbf{v})^T\right) = 0 \quad (21)$$

- *Internal energy theorem*

$$\left.\frac{\partial E_R}{\partial t}\right|_X - tr\left(\mathbf{T}.(\nabla_R v)^T\right) + \nabla_R.\mathbf{Q} = \rho_0 h \quad (22)$$

- *Clausius-Duhem inequality*

$$\begin{aligned} \theta\Sigma_R = &-\left(\dot{W} + S\dot{\theta}\right) + tr\left(\mathbf{T}.(\nabla_R \mathbf{v})^T\right) \\ &-(\mathbf{Q}/\theta)\nabla_R\theta \geq 0 \end{aligned} \quad (23)$$

where we introduced the free energy $W = E_R - S\theta$, per unit volume in the reference configuration.

Thermoelastic Conductors: Standard Theory

Apart for pure elasticity, this is the simplest *thermo*mechanical behavior for deformable solids. The observable variables of state in this case are the deformation gradient $\mathbf{F}$ and thermodynamic temperature θ, so that we would a priori write the following functional dependence for the thermodynamic dependent variables (Coleman-Noll; see [1, 2]):

$$\begin{aligned} &\mathbf{T} = \overline{\mathbf{T}}(\mathbf{F},\, \theta,\, \nabla_R\theta),\, \mathbf{Q} = \overline{\mathbf{Q}}(\mathbf{F},\, \theta,\, \nabla_R\theta) \\ &W = \overline{W}(\mathbf{F},\, \theta,\, \nabla_R\theta),\, S = \overline{S}(\mathbf{F}, \theta,\, \nabla_R\theta) \end{aligned} \quad (24)$$

where the same functional dependency is assumed just as a precautionary measure (so-called *equipresence*). But in the end, however [1], [2], and [3], we have the following results:

$$\begin{aligned} &\frac{\partial \overline{W}}{\partial(\nabla_R\theta)} = \mathbf{0},\, \mathbf{T} = \tilde{\mathbf{T}}(\mathbf{F},\, \theta) = \left.\frac{\partial \tilde{\mathbf{W}}}{\partial \mathbf{F}}\right|_\theta, \\ &S = \tilde{S}(\mathbf{F},\, \theta) = -\left.\frac{\partial \tilde{\mathbf{W}}}{\partial \theta}\right|_{\mathbf{F}},\, \mathbf{Q} = \tilde{\mathbf{Q}}(\mathbf{F}, \theta; \nabla_R\theta) \end{aligned} \quad (25)$$

with

$$W = \tilde{W}(\mathbf{F},\, \theta),\, lim\, \tilde{\mathbf{Q}}(\mathbf{F},\, \theta; \nabla_R\theta \to \mathbf{0}) = \mathbf{0} \quad (26)$$

That is, entropy is formally defined just like in thermostatics, although there is thermal disequilibrium, and heat flux may still depend, as parameters, on deformation and temperature. The remaining dissipation inequality is of pure thermal origin and reads

$$\Phi_{conduction} \equiv -(\mathbf{Q}/\theta)\,.\,\nabla_R\theta \geq 0 \qquad (27)$$

A standard expression for $\mathbf{Q}$ respecting this is given by

$$\mathbf{Q} = -\mathbf{K}(\mathbf{F},\,\theta).\nabla_R\theta \qquad (28)$$

where the necessarily symmetric material tensor $\mathbf{K}$ is positive definite.

Canonical "Eshelby" Format of the Basic Equations of Thermoelasticity in Finite Strains

To be somewhat more general, we consider the possible occurrence of material inhomogeneities (dependence of properties on the material point) of both inertial and thermoelastic origins so that the material may be *nonlinear, anisotropic, and inhomogeneous* and thus giving up the three basic tenets of nineteenth-century continuum mechanics. Thus,

$$\rho_0 = \overline{\rho}_0(\mathbf{X}),\; W = \widetilde{\mathrm{W}}(\mathbf{F},\,\theta;\mathbf{X}) \qquad (29)$$

The second and third equations (25) hold good. Equation (11) is satisfied, and we assume that $h = 0$ although this is not important.

Applying $\mathbf{F}$ to the right of $(12)_1$ and accounting for the general expressions (29), after some simple manipulations, we arrive at the following fully material (co-vectorial) equation of linear momentum [4]:

$$\frac{d\,\mathbf{P}}{d\,t} - div_R\mathbf{b} = \mathbf{f}^{th} + \mathbf{f}^{inh} \qquad (30)$$

where the following quantities have been defined

$$\mathbf{P} := -\mathbf{p}_R.\mathbf{F} = -\rho_0\mathbf{v}.\mathbf{F} \qquad (31)$$

$$\mathbf{b} = -(L_W\mathbf{1}_R + \mathbf{T}.\mathbf{F}),\; L_W := K - W \qquad (32)$$

$$\begin{aligned}\mathbf{f}^{inh} &:= \partial L_W/\partial\mathbf{X}|_{expl} \equiv \partial L_W/\partial\mathbf{X}|_{fixed\,fields}\\ &= (\mathbf{v}^2/2)\nabla_R\overline{\rho}_0 - \partial\widetilde{\mathrm{W}}/\partial\mathbf{X}\Big|_{expl}\end{aligned} \qquad (33)$$

$$\mathbf{f}^{th} := S\,\nabla_R\theta,\; S = -\partial\widetilde{\mathrm{W}}/\partial\theta \qquad (34)$$

Here, $\mathbf{P}$ is the (canonical) material momentum, $\mathbf{b}$ is referred to as the (nonsymmetric) Eshelby material stress, L_W is akin to a Lagrangian density (difference between a kinetic energy and a potential energy); $\mathbf{f}^{inh}$ and $\mathbf{f}^{th}$ may be called a material force of inhomogeneity and a *thermal material force* [5], respectively. Equation (30) is entirely on the material manifold M of element $\mathbf{X}$, and so both forces are indeed on the material manifold and not in physical space. The general theory of such forces was mostly developed by the author and coworkers [6] and references therein. The thermal material force appears for the first time in small strains in a work by Bui [7].

In parallel with the transformation that led to (30), noting that $E = W + S\theta$, (22) is transformed to

$$\frac{d\,(S\theta)}{dt} + \nabla_R.Q = h^{th},\; h^{th} := S\,\dot{\theta} \qquad (35)$$

Equations (30) and (35) constitute the *canonical thermomechanics* of *materially inhomogeneous thermoelasticity*. As readily checked, they are but space and time components of a true four-dimensional (space-time) balance law, although we note that there is no « time-like » scalar equivalent to $\mathbf{f}^{inh}$ in $(35)_1$. An explicit dependence of W on time (in a *rheonomic* system) would yield a nonzero term h^{inh} and would restore a complete symmetry.

Remark 1. Associated Jump Relations. The above developed equations are supposed to be valid at any regular material point $\mathbf{X}$. They, of course, have jump relations associated with each of them at the crossing of singular surfaces. This is exposed in [1], [2] and [6].

Remark 2. Role of Canonical Equations. Balance equations such as (1)–(3), complemented by boundary and initial conditions, are exploited in the solution of practical thermoelastic problems. Only these formats can be used because data in

bulk and at boundaries are given in the present configuration K_t. In contrast, the canonical Eshelbian formulation – entirely in the material framework at K_R – is to be exploited, as in a post-processing procedure, to evaluate critical quantities of which the force acting on the tip of a crack and the energy release rate are the most popular examples, hence the main use of such equations is where field singularities and inhomogeneities are present. The main reason for this is – as remarked during the construction of such canonical equations – that quantities there are of a higher order than in the standard balance equations that do not capture efficiently such singularities (see [4] for these general concepts; cf. [9, 10]).

Remark 3. Use of the Internal Energy. The formulation (30)–(35) seems to attribute a privileged role to the Helmholtz free energy W. However, using the relation $W = E - S\theta$, one can also define an Eshelby stress tensor, $\mathbf{b}_E$ in terms of the internal energy E, so that (30) and (35) are replaced by

$$\left.\frac{\partial \mathbf{P}}{\partial t}\right|_X - div_R\, \mathbf{b}_E = \mathbf{f}_E^{th},\ \mathbf{f}_E^{th} \equiv -\theta\, \nabla_R S \tag{36}$$

$$\nabla_R \,.\, \mathbf{Q} = h_E^{th},\ h_E^{th} \equiv -\theta \dot{S} \tag{37}$$

with

$$\begin{aligned} &\mathbf{b}_E = \mathbf{b} + (\theta S)\, \mathbf{1}_R \equiv -(L_E \mathbf{1}_R + \mathbf{T}_E.\mathbf{F}),\\ &L_E \equiv K - E \end{aligned} \tag{38}$$

$$\mathbf{f}_E^{th} = \mathbf{f}^{th} - \nabla_R.\,(\theta S\, \mathbf{1}_R) \tag{39}$$

But this formulation loses the symmetry between space and time components in a four-dimensional formulation. Of course, (37) is none other than the original form of the energy equation (eventually the heat propagation equation).

Remark 4 Generalization to Complex Dissipative Media and Others. Whenever the free energy depends also on an internal variable of state denoted by α (this may be a tensor of any order) such as in thermo-elasto-plasticity, i.e., $W = \widetilde{\mathrm{W}}(\mathbf{F}, \theta, \alpha)$ in the materially homogeneous case, we obtain the following generalizations [8]:

$$\begin{aligned} &\frac{d\,\mathbf{P}}{dt} - div_R\, \mathbf{b} = \mathbf{f}^{th} + \mathbf{f}^{intr},\\ &\frac{d(S\theta)}{dt} + \nabla_R.\mathbf{Q} = h^{th} + h^{intr} \end{aligned} \tag{40}$$

where in

$$\mathbf{f}^{intr} = A.(\nabla_R \alpha)^{\mathrm{T}},\ h^{intr} = A.\dot{\alpha},\ A := -\partial \widetilde{\mathrm{W}}/\partial \alpha \tag{41}$$

where the dot product must be understood as a full saturation between the indices of tensors A and α, while the superscript notation "*intr*" refers to the processes of *intrinsic* dissipation (e.g., plasticity).

References

1. Suhubi ES (1976) Thermoelastic solids. In: Eringen AC (ed) Continuum physics, vol II. Academic, New York, pp 174–265
2. Maugin GA (1988) Continuum mechanics of electromagnetic solids. North-Holland, Amsterdam
3. Hetnarski RB (1986) Thermal stresses, vol 1, Mechanics and mathematical methods. North-Holland, Amsterdam
4. Maugin GA, Berezovski A (1999) Material formulation of finite-strain thermoelasticity and applications. J Therm Stress 22:421–449
5. Epstein M, Maugin GA (1995) Thermoelastic material forces: definition and geometric aspects. C.R. Acad. Sci. Paris, II-320:63–68
6. Maugin GA (2011) Configurational forces, Chapter 5. CRC/Chapman & Hall/Taylor and Francis, Boca Raton
7. Bui HD (1978) Mécanique de la rupture fragile. Masson Editeurs, Paris
8. Maugin GA (2002) On canonical equations of continuum thermomechanics. Mech Res Commun 33:705–710
9. Maugin GA (2013a) Article in the ETS: Thermoelastic discontinuities
10. Maugin GA (2013b) Article in the ETS: Thermoelastic fracture in terms of configurational forces

Carbon Fiber

▶ Hygrothermal Effects on Polymeric Composite Materials and Sandwich Structures

Cayley-Hamilton Theorem

▶ State-Space Approach to Thermoelasticity

Cellular Undulation

▶ Thermomechanical Growth Instability in Solidification

Cesàro Means

▶ Partition of Energy

Characteristic Method of Thermal Stresses

Naobumi Sumi
Faculty of Education, Shizuoka University, Shizuoka, Japan

Synonyms

Generalized thermoelasticity; Method of characteristics; Thermal and thermal stress waves

Overview

Thermally excited mechanical response of solid materials is of increasing interest in the engineering sciences. In the power-generating equipment, in the electromagnetic radiation pulse emitters, and in many other electronic devices, materials may be subjected to sudden large thermal fluxes, and the inertia effects characterized by the propagation of thermal stress waves become significant. The need for numerical methods for the solution of these dynamic problems is dictated by the well-known difficulty of obtaining the exact solutions.

Among the various numerical approaches, the method of characteristics, also numerical in nature, has the advantages of giving a simple description of the wavefronts, and it can give numerical solutions readily to problems with any types of input functions. Generally, the method of characteristics is a technique for solving a partial differential equation of hyperbolic type in mathematics. The method is to reduce a hyperbolic partial differential equation to a family of ordinary differential equations along which the solution can be integrated from some initial data given on a suitable hypersurface (called the characteristics). These equations (called the characteristic equations) are more suitable for numerical analysis because the use of these equations makes it possible to obtain the solution via a step-by-step integration procedure.

This entry deals with the characteristic method for the solutions of the one- and/or two-dimensional thermal stress problems. To keep the numerical treatment general, the development of the formulation is based on the generalized dynamic theory of thermoelasticity proposed by Load and Shulman [1].

One-Dimensional Problem

Generalized Theory of Thermoelasticity

According to the generalized theory of thermoelasticity proposed by Lord and Shulman, a coupling between thermal and mechanical fields is taken into account, and the classical Fourier's law is also modified by adding a thermal relaxation term to eliminate the paradox of the infinite thermal speed of the classical theory of thermoelasticity; the equations that govern the propagation of one-dimensional thermal and thermal stress waves in linear elastic, isotropic, and homogeneous materials under plane strain are given by one set of generalized equations:

1. Equation of motion

$$\rho \frac{\partial W}{\partial t} - \frac{\partial \sigma_{zz}}{\partial z} = 0 \quad : \quad W = \frac{\partial w}{\partial t} \tag{1}$$

2. Constitutive equations

$$\frac{\partial \sigma_{zz}}{\partial t} - C_{11}\frac{\partial W}{\partial z} + \beta\frac{\partial T}{\partial t} = 0 \tag{2}$$

3. Modified Fourier's law

$$\tau\frac{\partial q_z}{\partial t} + k\frac{\partial T}{\partial z} = -q_z \tag{3}$$

4. Coupled energy equation

$$\frac{\partial q_z}{\partial z} + \rho c_v\frac{\partial T}{\partial t} + T_0\beta\frac{\partial W}{\partial z} = 0 \tag{4}$$

In (1–4), t is the time; z is the Cartesian coordinate; w is the displacement and $W = \partial w/\partial t$ is the particle velocity in the direction z of wave propagation; σ_{zz} is the normal stress; q_z is the heat flux; T is the temperature change from the absolute reference temperature T_0; ρ is the density; c_v is the specific heat; k is the coefficient of thermal expansion; $C_{11} = (\lambda + 2\mu)$, $\beta = \alpha(3\lambda + 2\mu)$, where λ and μ are Lamé's constants; and α is the coefficient of thermal expansion.

In (3), τ is *the relaxation time*, which physically signifies the initiation of heat flow after the temperature gradient has been imposed. Various authors have determined the relaxation time τ for different types of materials and found it to range from 10^{-10} [sec] for gases to 10^{-14} [sec] for metals [2, 3].

The third term on the left-hand side of (4) means *the coupling term* between the deformation and heating.

Eliminating q_z from (3) and (4), we obtain the heat conduction equation:

$$k\frac{\partial^2 T}{\partial z^2} = \rho c_v\left(\tau\frac{\partial^2 T}{\partial t^2} + \frac{\partial T}{\partial t}\right) + T_0\beta\left(\tau\frac{\partial^3 w}{\partial t^2\partial z} + \frac{\partial^2 w}{\partial t\partial z}\right) \tag{5}$$

Eliminating σ_{zz} from (1) and (2), we obtain the governing equation in terms of displacement:

$$C_{11}\frac{\partial^2 w}{\partial z^2} = \rho\frac{\partial^2 w}{\partial t^2} + \beta\frac{\partial T}{\partial z} \tag{6}$$

Thus, the generalized thermoelasticity theory results in temperature and displacement fields governed by two coupled hyperbolic second-order partial differential equations, which predict finite propagation velocities for thermal and mechanical disturbances.

Characteristics and Characteristic Equations

For the method of characteristics, we use the system of four linear first-order partial differential equations (1)–(4) with W, σ_{zz}, q_z, and T as four dependent variables. In the $(z - t)$ plane, certain curves may exist, along which these variables are continuous, but their first partial derivatives may be discontinuous. These curves will be called *the characteristics*, *physical characteristics*, or *waves*, and the differential equations governing the propagation of discontinuities (waves) along characteristics will be called *the characteristic equations*. The characteristics and the characteristic equations may be derived by the conventional directional derivative method.

The total differentials of four dependent variables are written as

$$dW = \frac{\partial W}{\partial t}dt + \frac{\partial W}{\partial z}dz \tag{7}$$

$$d\sigma_{zz} = \frac{\partial \sigma_{zz}}{\partial t}dt + \frac{\partial \sigma_{zz}}{\partial z}dz \tag{8}$$

$$dq_z = \frac{\partial q_z}{\partial t}dt + \frac{\partial q_z}{\partial z}dz \tag{9}$$

$$dT = \frac{\partial T}{\partial t}dt + \frac{\partial T}{\partial z}dz \tag{10}$$

Equations (1)–(4) and (7)–(10) may be considered as linear equations with eight derivatives $\partial W/\partial t$, $\partial W/\partial z$, $\cdots \partial T/\partial t$, $\partial T/\partial z$. In matrix notation, (1)–(4) and (7)–(10) become

$$A\mathbf{X} = \mathbf{B} \quad : \quad \sum_{j=1}^{8} a_{ij}x_j = b_i, \quad (i = 1 \sim 8) \tag{11}$$

where the matrix A and vectors $\mathbf{X}$ and $\mathbf{B}$ denote

$$A = [a_{ij}] = \begin{bmatrix} \rho & 0 & 0 & -1 & 0 & 0 & 0 & 0 \\ 0 & -C_{11} & 1 & 0 & 0 & 0 & \beta & 0 \\ 0 & 0 & 0 & 0 & \tau & 0 & 0 & k \\ 0 & T_0\beta & 0 & 0 & 0 & 1 & \rho c_v & 0 \\ dt & dz & 0 & 0 & 0 & 0 & 0 & 0 \\ 0 & 0 & dt & dz & 0 & 0 & 0 & 0 \\ 0 & 0 & 0 & 0 & dt & dz & 0 & 0 \\ 0 & 0 & 0 & 0 & 0 & 0 & dt & dz \end{bmatrix}$$

$$\mathbf{X} = [x_i] = \begin{bmatrix} \partial W/\partial t \\ \partial W/\partial z \\ \partial \sigma_{zz}/\partial t \\ \partial \sigma_{zz}/\partial z \\ \partial q_z/\partial t \\ \partial q_z/\partial z \\ \partial T/\partial t \\ \partial T/\partial z \end{bmatrix}, \quad \mathbf{B} = [b_i] = \begin{bmatrix} 0 \\ 0 \\ -q_z \\ 0 \\ dW \\ d\sigma_{zz} \\ dq_z \\ dT \end{bmatrix}$$

By Cramer's formula of linear equations, the k th solution of (11) is given as

$$x_k = \frac{|A_k|}{|A|} \tag{12}$$

where the matrix A_k is obtained by exchanging the k th column of the matrix A by the column vector $\mathbf{B}$. Therefore, when both the determinants of matrices $|A_k|$ and $|A|$ become zero, the solution x_k becomes indeterminate. Calculating the determinant of matrix A be zero ($|A| = 0$), we obtain

$$\left(\frac{dz}{dt}\right)^4 - \left(\frac{C_{11}}{\rho} + \frac{k}{\rho c_v \tau} + \frac{T_0\beta^2}{\rho^2 c_v}\right)\left(\frac{dz}{dt}\right)^2 + \frac{k}{\rho^2 c_v \tau} = 0 \tag{13}$$

If we denote the four solutions of (13) as $\pm c_1, \pm c_2$, we obtain

$$\left(\frac{dz}{dt}\right)^2 = \begin{Bmatrix} c_1^2 \\ c_2^2 \end{Bmatrix} = \frac{1}{2}\left[\left(c_L^2 + \delta c_L^2 + \frac{\kappa}{\tau}\right) \pm \sqrt{\left(c_L^2 + \delta c_L^2 + \frac{\kappa}{\tau}\right)^2 - 4\frac{\kappa c_L^2}{\tau}}\right] \tag{14}$$

In (14), κ is the thermal diffusivity, c_L is the isothermal dilatation wave speed, and δ is the thermomechanical coupling parameter, respectively defined by

$$\kappa = \frac{k}{\rho c_v}, \quad c_L = \sqrt{\frac{C_{11}}{\rho}}, \quad \delta = \frac{\beta^2 T_0}{\rho c_v C_{11}} \tag{15}$$

Therefore, for the system of (1)–(4), the characteristics are found to be composed of four families of characteristic lines I_j:

$$\begin{gathered} I_j \ : \ \frac{dz}{dt} = V_j, \quad (j = 1 \sim 4) \\ (V_1, V_2, V_3, V_4) = (c_1, -c_1, c_2, -c_2) \end{gathered} \tag{16}$$

For homogeneous materials, the velocities c_1 and c_2 are constant throughout the medium, and the characteristics are straight lines of equal slope as shown in Fig. 1. The I_1 and I_2 characteristics describe two characteristic families of lines with slopes c_1 and $-c_1$, respectively. The I_3 and I_4 define another two families of lines with slopes c_2 and $-c_2$.

For the case of uncoupled theory ($\delta = 0$), the velocity of the first wavefront becomes equal to $c_1 = c_L$ and corresponds to the mechanical wave velocity of the classical theory. The velocity of the second wavefront becomes equal to $c_2 = \sqrt{\kappa/\tau}$, which is called the thermal wave velocity.

For the case of classical theory ($\tau = 0$), the velocity c_1 becomes equal to $c_1 = \sqrt{(1+\delta)}c_L$, and the velocity c_2 becomes infinite, which implies an infinite speed of thermoelastic disturbances in a solid.

The corresponding characteristic equations along characteristics are obtained by calculating the determinant of matrix A_k be zero ($|A_k| = 0$). Therefore, the characteristic equations along characteristics $I_j : dz/dt = V_j, (j = 1 \sim 4)$ are given as follows:

$$l_1^{(j)} d\sigma_{zz} + l_2^{(j)} dW + l_3^{(j)} dq_z + l_4^{(j)} dT = l_5^{(j)} q_z dt \tag{17}$$

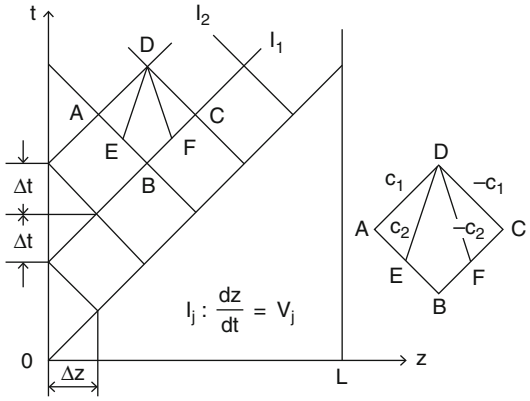

Characteristic Method of Thermal Stresses, Fig. 1 Characteristic network for numerical procedure

where

$$l_1^{(j)} = 1,\quad l_2^{(j)} = -\rho V_j,\quad l_3^{(j)} = \frac{\beta\tau V_j}{(k - \rho c_v \tau V_j^2)}$$

$$l_4^{(j)} = l_3^{(j)} \times \frac{k}{\tau V_j},\quad l_5^{(j)} = -l_3^{(j)} \times \frac{1}{\tau} \tag{18}$$

Finally, the values of W, σ_{zz}, q_z, and T may be found by solving (17) subjected to the appropriate initial and boundary conditions.

Difference Equations and Numerical Procedure

The use of characteristic (17) makes it possible to obtain the solutions by utilizing the step-by-step integration procedure. The $(z-t)$ plane is subdivided into a network constructed by two families of characteristic lines: $z \pm c_1 t = const.$ so that each element of the network is a parallelogram with the diagonals measuring $2\Delta z$ and $2\Delta t$ as shown in Fig. 1. At a typical mesh point D, we draw two characteristic lines ED, FD with slopes $\pm c_2$ through the point D. For computing the values of variables at points E and F, we use a linear interpolation between the points A, B and C, B. If we assume a linear variation in these variables between these closely spaced mesh points, the integration of the characteristic (17) along characteristic lines AD, CD, ED, FD yields their finite-difference equivalents.

$$\begin{aligned} l_1^{(j)}\sigma_{zzD} + l_2^{(j)} W_D + \left\{ l_3^{(j)} - l_5^{(j)} \frac{\Delta t_j}{2} \right\} q_{zD} \\ + l_4^{(j)} T_D = l_1^{(j)} \sigma_{zzj} + l_2^{(j)} W_j \\ + \left\{ l_3^{(j)} + l_5^{(j)} \frac{\Delta t_j}{2} \right\} q_{zj} + l_4^{(j)} T_j \end{aligned} \tag{19}$$

where the quantities with subscripts D and $(j = 1 \sim 4)$ represent the values at the points D and A, C, E, F, respectively. Therefore, the four unknowns at a point D can be calculated from these four finite-difference equations if all the quantities at neighboring points A, C, E, F are known from the previous calculations. Along the boundary points where two of the four variables are prescribed, the analysis is the same except that the two characteristic equations along two characteristics extending outside of the region should be replaced by the prescribed boundary conditions.

The characteristic equations with reference to the cylindrical and spherical coordinates are presented in [4].

For the case of nonhomogeneous or nonlinear elastic materials, material properties vary with the position z. Therefore, the wave velocities c_1, c_2 defined by (14) vary spatially, and the characteristics become curved lines. For such cases, the method needs to employ an iterative strategy to determine the mesh points in the $(z-t)$ plane [5]. Lopez and Lord [6] applied the method of characteristics to a system of second-order partial differential equation relating the second-order derivatives of temperature and strains.

Classical Uncoupled Theory of Thermoelasticity

Since the relaxation time τ is found to be very small, the heat conduction phenomenon for most engineering applications can be described by the classical Fourier's law. By deleting the term involving τ in (5), the classical theory of thermoelasticity results in temperature and displacement fields governed by two coupled partial differential equations, one equation being parabolic and the other hyperbolic. Also, in practice, the coupling term is usually neglected when its value is very small as compared with unity for the

purpose of computational convenience. By deleting the term involving τ and $T_0\beta$ from (5), we obtain the classical uncoupled heat conduction equation of parabolic type:

$$k\frac{\partial^2 T}{\partial z^2} = \rho c_v \frac{\partial T}{\partial t} \tag{20}$$

which permits the temperature state to be found independently of the mechanical state of the body.

The heat conduction (20) can be solved numerically by writing (20) in the explicit finite-difference form by using the "leap-frog" method [7] in the $(z-t)$ characteristic plane.

For the case of classical uncoupled theory ($\tau = 0,\ \delta = 0$), (1) and (2) are considered as a system of two linear first-order partial differential equations with W and σ_{zz} as two dependent variables. For this case, the velocity c_1 in (14) becomes equal to $c_1 = c_L = \sqrt{C_{11}/\rho}$, and c_2 becomes infinity that implies an infinite speed of thermoelastic disturbances predicted by the classical theory. The characteristics are found to be composed of two families of characteristic lines I_j, (j = 1,2):

$$I_j \ :\ dz/dt = (V_1, V_2) = (c_1, -c_1),\quad (j = 1,2) \tag{21}$$

The corresponding characteristic equations are

$$l_1^{(j)} d\sigma_{zz} + l_2^{(j)} dW = -\beta \frac{\partial T}{\partial t} dt,\quad (j = 1,2) \tag{22}$$

For this type of problem, it is advantageous to employ a technique called *the characteristic-difference method* [7, 8] which combines some of the advantageous of both the characteristic and finite-difference method. The numerical method employs appropriate characteristic relations (22) on the boundaries while using a more convenient explicit finite-difference approximations of (1) and (2) by using central differences in both space and time at all other intermediate points in $(z-t)$ plane.

Materials with Temperature-Dependent Properties

In many practical applications, the heat addition in materials for high-temperature applications is sufficiently intense to cause large thermal variations which, in turn, may alter the material properties considerably.

The thermal stresses in FGMs with temperature-dependent material properties are solved by the method of characteristics [9]. We assume that the material properties have nonhomogeneous character in the direction of coordinate axis and are functions of temperature. Then, the heat conduction equation becomes

$$\frac{\partial}{\partial z}\left(k\frac{\partial T}{\partial z}\right) = \rho c_v \frac{\partial T}{\partial t} \tag{23}$$

As the material parameters ρ, c_v, and k vary with the position and the temperature, (23) is of nonlinear form. Therefore, the temperature may be obtained by writing (23) in the explicit finite-difference form and by using the iteration technique to obtain the convergent solution.

The governing equations for materials with temperature-dependent properties are given by

$$\rho\frac{\partial W}{\partial t} - \frac{\partial \sigma_{zz}}{\partial z} = 0\ :\ W = \frac{\partial w}{\partial t} \tag{24}$$

$$\frac{\partial \sigma_{zz}}{\partial t} - C_{11}\frac{\partial W}{\partial z} - \frac{\partial C_{11}}{\partial t}\varepsilon + \frac{\partial}{\partial t}\left(\beta^* \int \alpha dT\right) = 0 \tag{25}$$

where $\varepsilon = \partial w/\partial z$ is the strain and

$$C_{11} = \lambda + 2\mu,\quad \beta^* = 3\lambda + 2\mu \tag{26}$$

These material properties are functions of coordinate z and temperature T.

Equations (24) and (25) constitute a system of two quasi-linear first-order partial differential equations with σ_{zz} and W as the dependent variables. The characteristics are given by (21), and the characteristic equations along $dz/dt = V_j = \pm c_1(r),\ (j = 1,2)$ are given by

$$l_1^{(j)} d\sigma_{zz} + l_2^{(j)} dW = \left\{ \frac{\partial C_{11}}{\partial t} \varepsilon - \frac{\partial}{\partial t} \beta^* \int \alpha dT \right\} dt \tag{27}$$

As ε in (27) is also unknown, we add two more equations along the plane $z = const.$, that is, along $dz/dt = 0$:

$$d\sigma_{zz} = \varepsilon dC_{11} + C_{11} d\varepsilon - d\beta^* \int \alpha dT \tag{28}$$

$$dw = W dt \tag{29}$$

By integrating (27)–(29) along four characteristics, we can obtain σ_{zz}, W, ε, and w. However, for materials with temperature-dependent properties, the velocity c_1 varies spatially and the characteristics become curved lines. Therefore, solutions must be obtained by using the iteration technique.

Two-Dimensional Problem

Generalized Theory of Thermoelasticity

The basic equations governing the propagation of two-dimensional thermal and thermal stress waves for linear elastic, isotropic, and homogeneous materials can be written in the form [10]:

1. Equation of motion

$$\begin{aligned} \frac{\partial \sigma_{xx}}{\partial x} + \frac{\partial \sigma_{zx}}{\partial z} &= \rho \frac{\partial U}{\partial t} \ : \ U = \frac{\partial u}{\partial t} \\ \frac{\partial \sigma_{zx}}{\partial x} + \frac{\partial \sigma_{zz}}{\partial z} &= \rho \frac{\partial W}{\partial t} \ : \ W = \frac{\partial w}{\partial t} \end{aligned} \tag{30}$$

2. Constitutive equations

$$\begin{aligned} \frac{\partial \sigma_{xx}}{\partial t} &= (\lambda + 2\mu) \frac{\partial U}{\partial x} + \lambda \frac{\partial W}{\partial z} - \beta \frac{\partial T}{\partial t} \\ \frac{\partial \sigma_{zz}}{\partial t} &= \lambda \frac{\partial U}{\partial x} + (\lambda + 2\mu) \frac{\partial W}{\partial z} - \beta \frac{\partial T}{\partial t} \\ \frac{\partial \sigma_{zx}}{\partial t} &= \mu \left(\frac{\partial W}{\partial x} + \frac{\partial U}{\partial z} \right) \end{aligned} \tag{31}$$

3. Modified Fourier's law

$$\begin{aligned} \tau \frac{\partial q_x}{\partial t} + q_x &= -k \frac{\partial T}{\partial x} \\ \tau \frac{\partial q_z}{\partial t} + q_z &= -k \frac{\partial T}{\partial z} \end{aligned} \tag{32}$$

4. Coupled energy equation

$$\frac{\partial q_x}{\partial x} + \frac{\partial q_z}{\partial z} + \rho c_v \frac{\partial T}{\partial t} + T_0 \beta \left(\frac{\partial U}{\partial x} + \frac{\partial W}{\partial z} \right) = 0 \tag{33}$$

where U and W are particle velocities in the x and z directions, respectively.

The equations (30) to (33) constitute a system of eight linear first-order partial differential equations with three real wave speeds.

Characteristics and Characteristic Equations

As is well known, the characteristic manifold for two-dimensional wave propagations is composed of hypersurfaces, not lines as for the one-dimensional case. The characteristic equations on characteristic surfaces are partial differential equations, not ordinary differential equations as for the one-dimensional case. The characteristic equations which relate the eight dependent variables U, W, σ_{xx}, σ_{zz}, σ_{zx}, q_x, q_z, and T along the characteristic surfaces (*bicharacteristics*) can be derived by the conventional directional derivative approach, which was used to solve the two-dimensional classical elastic problems by Clifton [11].

In matrix notation, (30)–(33) become

$$\mathbf{L}[\mathbf{X}] = A^t \mathbf{X}_{,t} + A^x \mathbf{X}_{,x} + A^z \mathbf{X}_{,z} - \mathbf{B} = 0 \tag{34}$$

where subscripts preceded by a comma denote partial differentiation with respect to the subscript variables. $\mathbf{X}$ and $\mathbf{B}$ denote the vectors

$$\mathbf{X} = \begin{bmatrix} U \\ W \\ \sigma_{xx} \\ \sigma_{zz} \\ \sigma_{zx} \\ q_x \\ q_z \\ T \end{bmatrix}, \qquad \mathbf{B} = \begin{bmatrix} 0 \\ 0 \\ 0 \\ 0 \\ 0 \\ 0 \\ -q_x \\ -q_z \\ 0 \end{bmatrix}$$

and A^t, A^x, and A^z denote the following matrices:

$$A^t = \begin{bmatrix} -\rho & 0 & 0 & 0 & 0 & 0 & 0 & 0 \\ 0 & -\rho & 0 & 0 & 0 & 0 & 0 & 0 \\ 0 & 0 & -1 & 0 & 0 & 0 & 0 & -\beta \\ 0 & 0 & 0 & -1 & 0 & 0 & 0 & -\beta \\ 0 & 0 & 0 & 0 & -1 & 0 & 0 & 0 \\ 0 & 0 & 0 & 0 & 0 & \tau & 0 & 0 \\ 0 & 0 & 0 & 0 & 0 & 0 & \tau & 0 \\ 0 & 0 & 0 & 0 & 0 & 0 & 0 & \rho c_v \end{bmatrix}$$

$$A^x = \begin{bmatrix} 0 & 0 & 1 & 0 & 0 & 0 & 0 & 0 \\ 0 & 0 & 0 & 0 & 1 & 0 & 0 & 0 \\ \lambda + 2\mu & 0 & 0 & 0 & 0 & 0 & 0 & 0 \\ \lambda & 0 & 0 & 0 & 0 & 0 & 0 & 0 \\ 0 & \mu & 0 & 0 & 0 & 0 & 0 & 0 \\ 0 & 0 & 0 & 0 & 0 & 0 & 0 & k \\ 0 & 0 & 0 & 0 & 0 & 0 & 0 & 0 \\ T_0\beta & 0 & 0 & 0 & 0 & 1 & 0 & 0 \end{bmatrix}$$

$$A^z = \begin{bmatrix} 0 & 0 & 0 & 0 & 1 & 0 & 0 & 0 \\ 0 & 0 & 0 & 1 & 0 & 0 & 0 & 0 \\ 0 & \lambda & 0 & 0 & 0 & 0 & 0 & 0 \\ 0 & \lambda + 2\mu & 0 & 0 & 0 & 0 & 0 & 0 \\ \mu & 0 & 0 & 0 & 0 & 0 & 0 & 0 \\ 0 & 0 & 0 & 0 & 0 & 0 & 0 & 0 \\ 0 & 0 & 0 & 0 & 0 & 0 & 0 & k \\ 0 & T_0\beta & 0 & 0 & 0 & 0 & 1 & 0 \end{bmatrix}$$

The condition that a surface $\Phi(t, x, z) = const.$ is a characteristic surface of (34) coincides with the condition that the determinant of the characteristic matrix A defined by

$$A = A^t \Phi_{,t} + A^x \Phi_{,x} + A^z \Phi_{,z} \tag{35}$$

is zero. If we calculate the determinant of matrix A be zero ($|A| = 0$), we obtain

$$\Phi_{,t}^2 \{\Phi_{,t}^2 - c_1^2(\Phi_{,x}^2 + \Phi_{,z}^2)\}\{\Phi_{,t}^2 - c_2^2(\Phi_{,x}^2 + \Phi_{,z}^2)\} \times \{\Phi_{,t}^2 - c_3^2(\Phi_{,x}^2 + \Phi_{,z}^2)\} = 0 \tag{36}$$

where c_1, c_2 are the dilatational wave velocities defined by (14) and c_3 is the shear wave velocity defined by

$$c_3 = \sqrt{\mu/\rho} \tag{37}$$

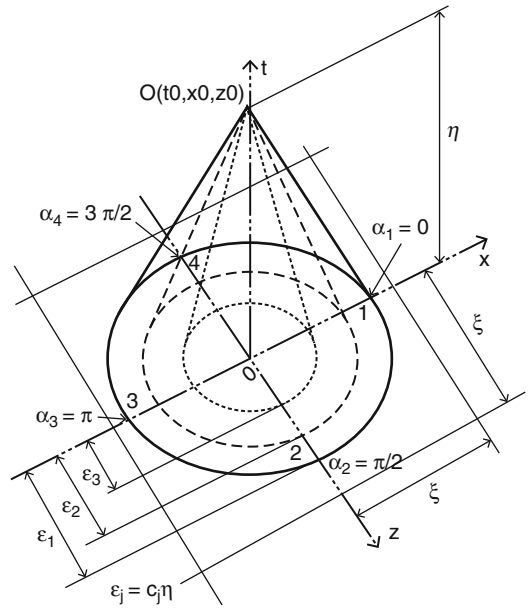

Characteristic Method of Thermal Stresses, Fig. 2 Characteristic cones for two-dimensional generalized theory of thermoelasticity

The solutions of (36) are the characteristic planes

$$\Phi(t, x, z) = c_i(t - t_0) - (x - x_0)\cos\alpha - (z - z_0)\sin\alpha, \quad c_i = (c_1, c_2, c_3) \tag{38}$$

If α is regarded as a parameter, then (38) represents one-parameter families of characteristic planes though the point (t_0, x_0, z_0). The envelopes of these one-parameter families of planes are also characteristic surfaces and constitute the characteristic cones (Monge cones [12]) through the point $(t_0, x_0, z = 0)$:

$$c_l^2(t - t_0)^2 = (x - x_0)^2 + (z - z_0)^2 \tag{39}$$

The three backward-drawn characteristic cones are shown in Fig. 2, where η is the increment of time and $\varepsilon_l = c_l\eta, (l = 1 \sim 3)$. ξ is a square mesh size for finite-difference approximation. The lines of contact of the one-parameter families of planes with their envelopes are

$$\left.\begin{aligned}\frac{dx}{dt} &= c_l\cos\alpha\\ \frac{dz}{dt} &= c_l\sin\alpha\end{aligned}\right\},\quad c_l = (c_1, c_2, c_3) \tag{40}$$

which are the bicharacteristics for (30)–(33).

If Φ is a characteristic surface of (30)–(33), then there exist null vectors $\mathbf{l}$ such that

$$\mathbf{l}A = 0 \tag{41}$$

The null vectors $\mathbf{l}$ associated with the bicharacteristic strips defined by (38) and (41) are

$$\mathbf{l} = \begin{bmatrix} -D_j\cos\alpha \\ -D_j\sin\alpha \\ D_j/c_j\cos^2\alpha \\ D_j/c_j\sin^2\alpha \\ D_j/c_j\sin 2\alpha \\ \tau c_j \\ \cos\alpha \\ \sin\alpha \end{bmatrix};\quad c_j = (c_1, c_2) \tag{42}$$

$$\mathbf{l} = \begin{bmatrix} c_3\sin\alpha \\ -c_3\cos\alpha \\ -\sin 2\alpha/2 \\ \sin 2\alpha/2 \\ \cos 2\alpha \\ 0 \\ 0 \\ 0 \end{bmatrix};\quad c = c_3 \tag{43}$$

If $\mathbf{l}$ is the null vector for a characteristic surface Φ, then the partial differential equation

$$\mathbf{l}\cdot\mathbf{L}[\mathbf{x}] = 0 \tag{44}$$

is an interior differential equation on the surface Φ. The derivatives of a function $\mathbf{x}$ in a bicharacteristic direction are given by

$$\frac{d\mathbf{X}}{dt} = \mathbf{X}_{,t} + \mathbf{X}_{,x}\frac{dx}{dt} + \mathbf{X}_{,z}\frac{dz}{dt} \tag{45}$$

Substituting (42) and (43) into (44) and partial derivatives with respect to t are eliminated by use of (45), differential relations along bicharacteristics are obtained. It is convenient to let $\alpha = 0$ for backward-drawn bicharacteristics drawn in the positive x-direction. This requires the replacement of α by $\alpha + \pi$. After making this change the (44), the characteristic equations along bicharacteristics are respectively given by

$$\begin{aligned}&\rho D_j(\cos\alpha dU + \sin\alpha dW) + \frac{D_j}{c_j}(\cos^2\alpha d\sigma_{xx}\\ &+ \sin^2\alpha d\sigma_{zz} + \sin 2\alpha d\sigma_{zx}) + \left(\frac{D_j}{c_j}\beta - \rho c_v\tau c_j\right)dT\\ &+ (\cos\alpha dq_r + \sin\alpha dq_z) = S_j(\alpha)dt, (j = 1, 2)\end{aligned} \tag{46}$$

and

$$\begin{aligned}&-\rho c_3\sin\alpha dU + \rho c_3\cos\alpha dW - \frac{1}{2}\sin 2\alpha d\sigma_{rr}\\ &+ \frac{1}{2}\sin 2\alpha d\sigma_{zz} + \cos 2\alpha d\sigma_{zx} = S_3(\alpha)dt\end{aligned} \tag{47}$$

where

$$D_j = \frac{T_0\beta\tau c_j^2}{\rho c_j^2 - (\lambda + 2\mu)},\quad (j = 1, 2) \tag{48}$$

In (46) and (47), for example, dU denotes the incremental change on U along the characteristic for an incremental change in time dt. The $S_j(\alpha), (j = 1, 2)$ and $S_3(\alpha)$ in (46) and (47) are respectively given by

$$\begin{aligned}S_j(\alpha) = &\frac{D_j}{2}\sin 2\alpha\{\sin\alpha(\sigma_{xx} - \sigma_{zz})_{,x}\\ &-\cos\alpha(\sigma_{xx} - \sigma_{zz})_{,z}\}\\ &-D_j\cos 2\alpha(\cos\alpha\sigma_{zx,z} - \sin\alpha\sigma_{zx,x})\\ &+\frac{D_j}{2c_j}\sin 2\alpha(2\mu - \rho c_j^2)(U_{,z} + W_{,x})\\ &+\left[\frac{D_j}{c_j}\{\lambda + (2\mu - \rho c_j^2)\cos^2\alpha\} + T_0\beta\tau c_j\right]\\ &(U_{,x} + W_{,z})\\ &-(D_j\beta - \rho c_v\tau c_j^2 + k)(\cos\alpha T_{,x} - \sin\alpha T_{,z})\\ &+\tau c_j\{\sin^2\alpha q_{x,x} + \cos^2\alpha q_{z,z}\\ &-\frac{1}{2}\sin 2\alpha(q_{x,z} + q_{z,x})\} - (\cos\alpha q_x + \sin\alpha q_z)\end{aligned} \tag{49}$$

$$S_3(\alpha) = -c_3 \sin^3\alpha\sigma_{xx,x} + c_3\cos^3\alpha\sigma_{zz,z} + c_3\sin2\alpha\left\{\frac{1}{2}(\sin\alpha\sigma_{xx,z} - \cos\alpha\sigma_{zz,x}) + \sin\alpha\sigma_{zx,x} - \cos\alpha\sigma_{zx,z}\right\} - \frac{1}{2}\mu\sin2\alpha(U_{,x} - W_{,z}) + \mu(\cos^2\alpha U_{,z} - \sin^2\alpha W_{,x}) \tag{50}$$

Equations (46) and (47) are the desired differential relations along the bicharacteristics.

An alternative approach to the conventional directional derivative approach, these characteristic equations may also be derived by use of Hadamard's kinematic discontinuity relations, used to derive the characteristic equations for the classical theory of elasticity by Ziv [12].

Difference Equations and Numerical Procedure

The characteristic (46) and (47) are more suitable for numerical analysis because the use of these equations makes it possible to obtain the solutions via a step-by-step integration procedure. The difference equations for computing the solution of eight variables $U, W, \sigma_{xx}, \sigma_{zz}, \sigma_{xz}, q_x, q_z$, and T at a mesh point $O(t_0, x_0, z_0)$ from known data at neighboring mesh points on the plane $t = t_0 - \eta$ can be derived by the method of Clifton [11]. These equations are obtained by linear combinations of equations resulting from integration of (46) and (47) along characteristics (40) and integration of governing equations (30)–(33) along the line $x = x_0, z = z_0$.

If a function f stands for any of eight dependent variables, the derivative of f in a characteristic direction can be written by $df = S(\alpha)dt$ as indicated in (46) and (47). Integration of this relation, along the characteristic for which $\alpha = \alpha_i$, from the point i of intersection of the characteristic with the plane $t = t_0 - \eta$ to the point O gives

$$\delta f = \frac{\eta}{2}\{S(\alpha_i)^O + S(\alpha)_i\} - (f_0 - f_i) + O(\eta^3) \tag{51}$$

where the superscript O and subscripts 0 and i denote that the associated function is evaluated at the points $O(t_0, x_0, z_0)$, $0(t_0 - \eta, x_0, z_0)$, and $i(t_0 - \eta, x_i, z_i)$, respectively. δf denotes the increment $\delta f = f^O - f_0$. Integrating (46) and (47) by use of the relation (51) along four characteristics corresponding to $\alpha_i = (i-1)\pi/2, (i = 1 \sim 4)$ on each of three characteristic cones, 12 equations involving the increments $\delta U, \delta W, \cdots, \delta T$ are obtained.

$$\rho D_j(\cos\alpha_i\delta U + \sin\alpha_i\delta W) + \frac{D_j}{c_j}(\cos^2\alpha_i\delta\sigma_{xx} + \sin^2\alpha_i\delta\sigma_{zz} + \sin2\alpha_i\delta\sigma_{zx}) + \left(\frac{D_j}{c_j}\beta - \rho c_v\tau c_j\right)\delta T + \tau(\cos\alpha_i\delta q_x + \sin\alpha_i\delta q_z) = \frac{\eta}{2}\left\{S_j(\alpha_i)^O + S_j(\alpha_i)_i\right\} - E_j(\alpha_i), \qquad (j = 1,2,\ i = 1 \sim 4) \tag{52}$$

$$-\rho c_3\sin\alpha_i\delta U + \rho c_3\cos\alpha_i\delta W - \frac{1}{2}\sin2\alpha_i\delta\sigma_{xx} + \frac{1}{2}\sin2\alpha_i\delta\sigma_{zz} + \cos2\alpha_i\delta\sigma_{zx} = \frac{\eta}{2}\{S_3(\alpha_i)^O + S_3(\alpha_i)_i\} - E_3(\alpha_i), (i = 1 \sim 4) \tag{53}$$

where

$$E_j(\alpha_i) = \rho D_j\{\cos\alpha_i(U_0 - U_i) + \sin\alpha_i(W_0 - W_i)\} + \frac{D_j}{c_j}\{\cos^2\alpha_i(\sigma_{xx0} - \sigma_{xxi}) + \sin^2\alpha_i(\sigma_{zz0} - \sigma_{zzi})\} + \sin2\alpha_i(\sigma_{zx0} - \sigma_{zxi}) + \left(\frac{D_j}{c_j}\beta - \rho c_v\tau c_j\right)(T_0 - T_i) + \tau\{\cos\alpha_i(q_{x0} - q_{xi}) + \sin\alpha_i(q_{z0} - q_{zi})\} \tag{54}$$

$$E_3(\alpha_i) = -\rho c_3\sin\alpha_i(U_0 - U_i) + \rho c_3\cos\alpha_i(W_0 - W_i) - \frac{1}{2}\sin2\alpha_i(\sigma_{xx0} - \sigma_{xxi}) + \frac{1}{2}\sin2\alpha_i(\sigma_{zz0} - \sigma_{zzi}) + \cos2\alpha_i(\sigma_{zx0} - \sigma_{zxi}) \tag{55}$$

Equations (52) and (53) contain the unknown derivatives at point O which appear in terms of having superscript O. In order to eliminate the unknown derivatives, we introduce additional eight equations, which are obtained by integration of (30)–(33) from the point 0 to the point O

along the line $x = x_0, z = z_0$. Thus, for example, from (30), we obtain

$$\rho\delta U = \frac{\eta}{2}\left[(\sigma_{xx,x} + \sigma_{zx,z})^O + (\sigma_{xx,x} + \sigma_{zx,z})_0\right]$$
$$\rho\delta W = \frac{\eta}{2}\left[(\sigma_{zx,x} + \sigma_{zx,z})^O + (\sigma_{zz,z} + \sigma_{zz,z})_0\right] \tag{56}$$

All the terms on the right-hand side of these 20 equations can be evaluated from data on the plane $t = t_0 - \eta$ except the derivatives at the point O which appear in the terms having a superscript O. Eliminating the terms having superscript O by using linear combinations of the eight equations analogous to (56) and twelve equations from (52) and (53), we obtain the final system of equations for the eight increments, which do not involve the unknown derivatives at point O. Then the final expressions for the difference equations are obtained as follows:

$$\begin{aligned}
&\rho D_j\delta U - (D_j\beta - \rho c_v\tau c_j^2)\frac{1}{k}\left(\tau + \frac{\eta}{2}\right)\delta q_x \\
&= \frac{\varepsilon_j^2}{2}\left[\rho D_j U_{,xx} + \frac{1}{c_j^2}(D_j\lambda + D_j\mu + T_0\beta\tau c_j^2)W_{,vz}\right. \\
&\quad + \frac{c_3^2}{c_j^2}\rho D_j U_{,zz} + \tau q_{z,xz} + \tau q_{x,xx}\Big]_0 \\
&\quad + \frac{\varepsilon_j}{c_j}\left[D_j(\sigma_{xx,x} + \sigma_{xz,z}) + (D_j\beta - \rho c_v\tau c_j^2)T_{,x}\right. \\
&\quad \left. + \frac{1}{k}(D_j\beta - \rho c_v\tau c_j^2)q_x\right]_0, \quad (j = 1, 2)
\end{aligned} \tag{57}$$

$$\begin{aligned}
&\rho D_j\delta W - (D_j\beta - \rho c_v\tau c_j^2)\frac{1}{k}\left(\tau + \frac{\eta}{2}\right)\delta q_z \\
&= \frac{\varepsilon_j^2}{2}\left[\rho D_j W_{,zz} + \frac{1}{c_j^2}(D_j\lambda + D_j\mu + T_0\beta\tau c_j^2)U_{,xz}\right. \\
&\quad + \frac{c_3^2}{c_j^2}\rho D_j W_{,xx} + \tau q_{z,zz} + \tau q_{x,xz}\Big]_0 \\
&\quad + \frac{\varepsilon_j}{c_j}\left[D_j(\sigma_{zz,z} + \sigma_{xz,x}) + (D_j\beta - \rho c_v\tau c_j^2)T_{,z}\right. \\
&\quad \left. + \frac{1}{k}(D_j\beta - \rho c_v\tau c_j^2)q_z\right]_0, \quad (j = 1, 2)
\end{aligned} \tag{58}$$

$$\begin{aligned}
&\frac{\lambda + 2\mu}{2(\lambda + \mu)}\frac{D_j}{c_j}\delta(\sigma_{xx} + \sigma_{zz}) \\
&+ \left\{\frac{\lambda + 2\mu}{\lambda + \mu}D_j\beta - \rho c_v\tau c_j^2\right\}\frac{1}{c_j}\delta T \\
&= \frac{\varepsilon_j^2}{2}\left[\frac{D_j}{c_j}(\sigma_{xx,xx} + \sigma_{zz,zz} + 2\sigma_{xz,xz})\right. \\
&\quad \left. - \frac{k}{c_j}(T_{,xx} + T_{,zz})\right]_0 + \varepsilon_j[D_j\rho(U_{,x} + W_{,z}) \\
&\quad + \left(\tau - \frac{\eta}{2}\right)(q_{x,x} + q_{z,z})]_0, \quad (j = 1, 2)
\end{aligned} \tag{59}$$

$$\begin{aligned}
&\left\{(\lambda + 2\mu)D_j + T_0\beta\tau c_j^2\right\}\frac{1}{2\mu c_j}\delta(\sigma_{xx} - \sigma_{zz}) \\
&\quad + \frac{\varepsilon_j\tau}{2}\left\{\left(\frac{\partial q_x}{\partial x}\right)^O - \left(\frac{\partial q_z}{\partial z}\right)^O\right\} \\
&= \frac{\varepsilon_j^2}{2}\left[\frac{D_j}{c_j}(\sigma_{xx,xx} - \sigma_{zz,zz}) - \frac{k}{c_j}(T_{,xx} - T_{,zz})\right]_0 \\
&\quad + \varepsilon_j\left[D_j\rho(U_{,x} - W_{,z}) + \left(\tau - \frac{k}{2}\right)(q_{x,x} - q_{z,z,})\right]_0, \\
&\quad (j = 1, 2)
\end{aligned} \tag{60}$$

$$\begin{aligned}
\delta\sigma_{xz} = &\frac{\varepsilon_3^2}{2}\left[(\sigma_{xx} + \sigma_{zz})_{,xz} + \sigma_{xz,xx} + \sigma_{xz,zz}\right]_0 \\
&+ \varepsilon_3\rho c_3[U_{,z} + W_{,x}]_0
\end{aligned} \tag{61}$$

In the derivation of the difference equations, the following four types of quantities to be evaluated at mesh points on the plane $t = t_0 - \eta$ are expressed by the first and second partial derivatives at point $0(t_0 - \eta, x_0, z_0)$.

$$\begin{aligned}
&f_1 - f_3 = 2c_l\eta(f_{,x})_0 + O(\eta^3) \\
&f_1 + f_3 - 2f_0 = (c_l\eta)^2(f_{,xx})_0 + O(\eta^4) \\
&\eta[(f_{,z})_1 - (f_{,z})_3] = 2c_l\eta^2(f_{,zx})_0 + O(\eta^4) \\
&\eta[(f_{,z})_1 + (f_{,z})_3 - 2(f_{,z})_0] = O(\eta^5)
\end{aligned} \tag{62}$$

$$c_1 = c_L = \sqrt{C_{11}/\rho}$$

where $c_l, (l = 1, 2, 3)$ correspond to each of three characteristic cones. Analogous quantities obtained by interchange of the role of x and z in (62) also occur. Thus $O(\eta^3)$ accuracy of

(57)–(61) is retained provided that difference approximations for the first and second partial derivatives at O are used which have accuracies $O(\eta^2)$ and $O(\eta)$, respectively. Thus, the $O(\eta^3)$ accuracy of (57)–(61) in one time step is retained provided that difference approximations for the first and second partial derivatives at point $0(t_0 - \eta, x_0, z_0)$ are used which have accuracies $O(\eta^2)$ and $O(\eta)$, respectively. Therefore, the unknowns at point $O(t_0, x_0, z_0)$ for the interior points can be computed by expanding the derivatives at point $0(t_0 - \eta, r_0, z_0)$ by the central difference for a square mesh as shown in Fig. 2 The resulting difference scheme is a nine-point scheme since the centered difference formulas for $[f_{,x}]_0$, $[f_{,z}]_0$, $[f_{,xx}]_0$, $[f_{,zz}]_0$, and $[f_{,zx}]_0$ at point 0 involve values of f at the mesh point 0 and eight neighboring points.

Consideration must specially be given to the computation of the difference solutions at boundary or corner points of the materials. The increments at these points can be obtained from the boundary conditions, and linear combinations of the above equations for which the equations along characteristics extending outside of the region are eliminated. In these cases, backward or forward differences with second-order accuracy must be used for approximating derivatives.

The characteristic method for two-dimensional classical and generalized thermoelastic problems in cylindrical coordinates is treated by Sumi [13, 14].

Future Directions for Research

The applicability of the present method is confined to cases where discontinuities may occur in the first-order derivatives of dependent variables while these variables remain continuous. The simple recurrent finite-difference equations obtained by the method of characteristics are easily adaptable to computer calculations. The method presented here is believed to be used successfully for many problems involving multiple wave reflections.

In the near future, the use of piezoelectric materials of nano-order thickness will be put into practical use as sensors and actuators in smart structural systems. Sumi and Ashida [14] have treated the thermal and mechanical wave problem in a piezoelectric plate by the method of characteristics.

References

1. Lord HW, Shulman YA (1967) A generalized dynamic theory of thermoelasticity. J Mech Phys Solids 15:299–309
2. Francis PH (1972) Thermo-mechanical effects in elastic wave propagation: a survey. J Sound Vib 21(2):181–192
3. Chandrasekharaiah DS (1986) Thermoelasticity with second sound: a review. Appl Mech Rev 39:355–376
4. Sumi N (2001) Numerical solutions of thermoelastic wave problems by the method of characteristics. J Therm Stresses 24(6):509–530
5. Sumi N (2002) Thermal and mechanical waves in nonlinear elastic solids. JSME Int J Ser A 45(2):146–152
6. Lopez AA, Lord HW (1971) A study of thermoelastic waves by the method of characteristics. Dev Theor Appl Mech 5:417–447
7. Sumi N, Noda N (1992) Dynamic thermal stresses in laminated media by the method of characteristic-difference. J Therm Stresses 15(3):379–392
8. Chou S-C, Greif R (1968) Numerical solution of stress waves in layered media. AIAA J 6(6):1067–1074
9. Sumi N, Sugano Y (1997) Thermally induced stress waves in functionally graded materials with temperature-dependent material properties. J Therm Stresses 20(3/4):281–294
10. Sumi N (2001) Two-spatial dimensional thermal and mechanical waves in finite plates by the method of characteristics. Proceedings of the 4th ICMR vol 1. Akita, Japan, p 208–213
11. Clifton RJ (1967) A difference method for plane problems in dynamic elasticity. Q Appl Math 25(1):97–116
12. Ziv M (1969) Two-spatial dimensional elastic wave propagation by the theory of characteristics. Int J Solids Struct 5:1135–1151
13. Sumi N (2001) Two-spatial dimensional thermal and mechanical wave propagations in finite medium under laser-pulse heating. Theor Appl Mech 50:103–111
14. Sumi N, Ashida F (2003) Solution for thermal and mechanical waves in a piezoelectric plate by the method of characteristics. J Therm stresses 26(11–12):1113–1123

Charge-Free Zone Model

▶ Fracture of Piezoelectric Materials

Chiral

▶ Boundary Value Problems of Elastostatics of Hemitropic Solids
▶ Mathematical Problems in Thermoelastostatics of Hemitropic Solids

Circular Plates, Statical Problems

Theodore R. Tauchert
Department of Mechanical Engineering,
University of Kentucky, Lexington, KY, USA

Overview

The "classical plate theory" (as formulated in ▶ Plates, Classical Theory), applicable to thin, isotropic, homogeneous, linearly elastic plates undergoing small deflections, is further specialized here to the case of plates of circular planform. The equations governing both in-plane stretching as well as transverse thermal bending are presented for circular plates exposed to a time-independent three-dimensional temperature distribution in combination with an applied transverse load. A general solution is presented for the mid-surface displacement of the plate for the case in which the thermal loading and boundary conditions are independent of the angular coordinate. A solution procedure is also given for non-axisymmetric bending, for the situation in which the plate experiences a thermal gradient that varies linearly through the plate thickness. References to publications treating various other axisymmetric and non-axisymmetric problems are cited.

Governing Equations

For convenience in analyzing the response of circular plates, the basic equations of classical plate theory are expressed in terms of circular cylindrical coordinates (r, θ, z). The equations which follow can be derived directly by considering the behavior of a typical element cut from the plate by axial planes and cylindrical surfaces, or they can be obtained by applying a coordinate transformation to the equations given in ▶ plates, classical theory and in [1]. Following this procedure, the in-plane strain components are found to be

$$\begin{aligned}\varepsilon_{rr} &= \frac{\partial u}{\partial r} = \varepsilon_{rr}^0 + z\kappa_r \\ \varepsilon_{\theta\theta} &= \frac{u}{r} + \frac{1}{r}\frac{\partial v}{\partial \theta} = \varepsilon_{\theta\theta}^0 + z\kappa_\theta \\ \gamma_{r\theta} &= \frac{1}{r}\frac{\partial u}{\partial \theta} + \frac{\partial v}{\partial r} - \frac{v}{r} = \gamma_{r\theta}^0 + z\kappa_{r\theta}\end{aligned} \tag{1}$$

where u and v denote the in-plane displacement components in the r and θ directions. Also, appearing in (1) are the middle-surface strains designated by the superscript $(^0)$ and curvatures, defined, respectively, by

$$\begin{aligned}\varepsilon_{rr}^0 &= \frac{\partial u^0}{\partial r}, \varepsilon_{\theta\theta}^0 = \frac{u^0}{r} + \frac{1}{r}\frac{\partial v^0}{\partial \theta} \\ \gamma_{r\theta}^0 &= \frac{1}{r}\frac{\partial u^0}{\partial \theta} + \frac{\partial v^0}{\partial r} - \frac{v^0}{r}\end{aligned} \tag{2}$$

and

$$\begin{aligned}\kappa_r &= -\frac{\partial^2 w}{\partial r^2}, \kappa_\theta = -\frac{1}{r}\frac{\partial w}{\partial r} - \frac{1}{r^2}\frac{\partial^2 w}{\partial \theta^2} \\ \kappa_{r\theta} &= -\frac{2}{r}\frac{\partial^2 w}{\partial r \partial \theta} + \frac{2}{r^2}\frac{\partial w}{\partial \theta}\end{aligned} \tag{3}$$

The resultant in-plane forces per unit length N_r, N_θ, and $N_{r\theta}$, which involve integrations of the stress components $\sigma_{rr}, \sigma_{\theta\theta}$, and $\sigma_{r\theta}$ with respect to the thickness coordinate z, become

$$\begin{aligned}N_r &= A\left(\varepsilon_{rr}^0 + \nu\varepsilon_{\theta\theta}^0\right) - N^T \\ N_\theta &= A\left(\nu\varepsilon_{rr}^0 + \varepsilon_{\theta\theta}^0\right) - N^T \\ N_{r\theta} &= \frac{1}{2}(1-\nu)A\gamma_{r\theta}^0\end{aligned} \tag{4}$$

and the resultant bending moments per unit length M_r, M_θ and the twisting moment per length $M_{r\theta}$ become

$$\begin{aligned} M_r &= D(\kappa_r + \nu\kappa_\theta) - M^T \\ M_\theta &= D(\nu\kappa_r + \kappa_\theta) - M^T \\ M_{r\theta} &= \frac{1}{2}(1-\nu)D\kappa_{r\theta} \end{aligned} \tag{5}$$

Here, $A = Eh/(1-\nu^2)$ and $D = Eh^3/12(1-\nu^2)$ represent extensional and bending stiffnesses of a plate of depth h in the z-direction, respectively; N^T and M^T are the thermal force and thermal moment, respectively, given by

$$\begin{aligned} N^T &= \frac{E\alpha}{1-\nu}\int_{-h/2}^{h/2} T(r,\theta,z)\,dz \\ M^T &= \frac{E\alpha}{1-\nu}\int_{-h/2}^{h/2} T(r,\theta,z)\,z\,dz \end{aligned} \tag{6}$$

Furthermore, the stresses in terms of their resultants become

$$\begin{aligned} \sigma_{rr} &= \frac{1}{h}(N_r + N^T) + \frac{12z}{h^3}(M_r + M^T) - \frac{E\alpha}{1-\nu}T \\ \sigma_{\theta\theta} &= \frac{1}{h}(N_\theta + N^T) + \frac{12z}{h^3}(M_\theta + M^T) - \frac{E\alpha}{1-\nu}T \\ \sigma_{r\theta} &= \frac{1}{h}N_{r\theta} + \frac{12z}{h^3}M_{r\theta} \end{aligned} \tag{7}$$

Equilibrium in the plane of the plate is then governed by the equations [1]

$$\begin{aligned} \frac{\partial N_r}{\partial r} + \frac{1}{r}\frac{\partial N_{r\theta}}{\partial \theta} + \frac{N_r - N_\theta}{r} &= 0 \\ \frac{\partial N_{r\theta}}{\partial r} + \frac{1}{r}\frac{\partial N_\theta}{\partial \theta} + \frac{2}{r}N_{r\theta} &= 0 \end{aligned} \tag{8}$$

whereas plate bending is governed by the equilibrium equations

$$\begin{aligned} \frac{\partial Q_r}{\partial r} + \frac{1}{r}\frac{\partial Q_\theta}{\partial \theta} + \frac{1}{r}Q_r + q(r,\theta) &= 0 \\ \frac{\partial M_r}{\partial r} + \frac{1}{r}\frac{\partial M_{r\theta}}{\partial \theta} + \frac{M_r - M_\theta}{r} &= Q_r \\ \frac{\partial M_{r\theta}}{\partial r} + \frac{1}{r}\frac{\partial M_\theta}{\partial \theta} + \frac{2}{r}M_{r\theta} &= Q_\theta \end{aligned} \tag{9}$$

in which Q_r, Q_θ represent shear forces per unit length (as defined in ▶ Plates, Classical Theory) and $q(r,\theta)$ is an applied transverse load.

Since the in-plane response of the plate associated with (8) represents a problem of plane stress, it can be treated using a stress-function approach; the stress function F is defined here as (see for example [2] or [3])

$$\begin{aligned} N_r &= \frac{1}{r}\frac{\partial F}{\partial r} + \frac{1}{r^2}\frac{\partial^2 F}{\partial \theta^2},\ N_\theta = \frac{\partial^2 F}{\partial r^2} \\ N_{r\theta} &= -\frac{\partial}{\partial r}\left(\frac{1}{r}\frac{\partial F}{\partial \theta}\right) \end{aligned} \tag{10}$$

in which case (8) are satisfied identically. The function F must satisfy certain compatibility requirements (see [2], p. 382), which in the present situation reduce to the single relation

$$\nabla^4 F = -(1-\nu)\nabla^2 N^T \tag{11}$$

where for cylindrical coordinates

$$\nabla^2 = \frac{\partial^2}{\partial r^2} + \frac{1}{r}\frac{\partial}{\partial r} + \frac{1}{r^2}\frac{\partial^2}{\partial \theta^2} \tag{12}$$

For the thermal bending response, the governing equations (9) can be reduced to a single differential equation for w by first eliminating the shear force resultants Q_r and Q_θ and then making use of (3) and (5). The resulting equation is

$$D\nabla^4 w = q - \nabla^2 M^T \tag{13}$$

Axisymmetric Bending

Axisymmetric bending occurs when the loading and boundary conditions are independent of the angular coordinate θ. Further, in the absence of a transverse load q, (13) reduces to

$$\nabla^4 w = -\nabla^2 M^T/D \tag{14}$$

where now

$$\nabla^2 = \frac{\mathrm{d}^2}{\mathrm{d}r^2} + \frac{1}{r}\frac{\mathrm{d}}{\mathrm{d}r} = \frac{1}{r}\frac{\mathrm{d}}{\mathrm{d}r}\left(r\frac{\mathrm{d}}{\mathrm{d}r}\right) \tag{15}$$

The general solution to (14) is [3]

$$w = C_1 + C_2 r^2 + C_3 \ln\frac{r}{a} + C_4 r^2 \ln\frac{r}{a} + \int_r^b \left(\frac{1}{r} \int_a^r \frac{M^T}{D} r \, \mathrm{d}r \right) \mathrm{d}r \tag{16}$$

in which a and b denote the inner and outer radii of the plate and C_1, C_2, C_3, and C_4 are constants of integration.

For use in satisfying boundary conditions, it is noted that the relevant moment and shear force resultants are given by

$$M_r = -D\left[2(1+\nu)C_2 - (1-\nu)\frac{C_3}{r^2} + (3+\nu)C_4 + 2(1+\nu)C_4 \ln\frac{r}{a}\right] - \frac{1-\nu}{r^2}\int_a^r M^T r \, \mathrm{d}r$$

$$M_{r\theta} = 0$$

$$Q_r = \frac{\partial M_r}{\partial r} + \frac{M_r - M_\theta}{r} = -4D\frac{C_4}{r} \tag{17}$$

From (17), it follows that in the case of a solid plate ($a = 0$) the constants $C_3 = C_4 = 0$ in order that M_r and Q_r remain finite at $r = 0$.

For a solid plate, clamped on the edge $r = b$ such that $w = \partial w/\partial r = 0$, substitution of (16) into the boundary conditions yields

$$C_1 = -b^2 C_2 = -\frac{1}{2D}\int_0^b M^T r \, \mathrm{d}r \tag{18}$$

whereas for the simply supported conditions $w = M_r = 0$ on $r = b$

$$C_1 = -b^2 C_2 = \frac{1-\nu}{2(1+\nu)D}\int_0^b M^T r \, \mathrm{d}r \tag{19}$$

Transverse deflections corresponding to other boundary conditions can be found in a similar fashion. Results for hollow circular plates having both edges clamped, or one edge clamped and one edge free, are given in [2] and [3], respectively.

Mention should also be made of an investigation by Sarkar [4] on the thermal deflection of an axisymmetric circular plate exposed to a nonstationary temperature distribution. The heat conduction equation governing the nonstationary quasi-static case was first solved, after which closed-form mathematical expressions were obtained for the resulting thermal deflections associated with different boundary conditions.

Furthermore, Biswas [5] considered the thermal deflection of a circular plate of variable thickness. Exponential variation of plate thickness was considered, and the basic governing equations derived. Two successive substitutions then lead to a confluent hypergeometric equation for which the solution is known. Both bending moments and bending stresses were calculated for simply supported and clamped plates.

Non-axisymmetric Bending

In the case of a temperature distribution which varies with the angular coordinate θ as well as r and z, we seek a solution to (14). Forray and Newman [6] consider such a problem, in which the thermal gradient is presumed to vary linearly through the plate thickness. Following their approach, it is assumed that the thermal moment M^T is expressible in the form

$$M^T = \sum_{m=0}^{\infty}\sum_{k=0}^{\infty} A_{km} r^k \cos m\theta + \sum_{m=1}^{\infty}\sum_{k=0}^{\infty} B_{km} r^k \sin m\theta \tag{20}$$

The general solution to (14) then can be expressed as

$$\begin{aligned} w = {} & a_0 + b_0 r^2 + c_0 r^2 \ln r + d_0 \ln r \\ & + (a_1 r + b_1 r^3 + c_1 r^{-1} + d_1 r \ln r)\cos\theta \\ & + (a'_1 r + b'_1 r^3 + c'_1 r^{-1} + d'_1 r \ln r)\sin\theta \\ & + \sum_{n=2}^{\infty}[(a_n r^n + b_n r^{n+2} + c_n r^{-n} + d_n r^{-n+2})\cos n\theta \\ & + (a'_n r^n + b'_n r^{n+2} + c'_n r^{-n} + d'_n r^{-n+2})\sin n\theta] \\ & + \sum_{m=0}^{\infty} g_m(r)\cos m\theta + \sum_{m=1}^{\infty} h_m(r)\sin m\theta \end{aligned} \tag{21}$$

where $a_n, a'_n, b_n, \ldots$ $(n = 0, 1, \ldots, \infty)$ are arbitrary constants and

$$(g_m, h_m) = -\frac{1}{D} r^{-m} \int \left(r^{2m-1} \int (A_{km}, B_{km}) r^{k+1-m} \mathrm{d}r \right) \mathrm{d}r \tag{22}$$

In the case of a solid plate $(a = 0)$, the constants $c_n = c'_n = d_n = d'_n = 0$ in order to avoid singularities at $r = 0$. A detailed solution and corresponding design curves are given for a clamped solid circular plate in [6].

A more complicated non-axisymmetric problem occurs when the boundary conditions vary with the angular coordinate θ. Nowacki and Olesiak [7] demonstrate application of a Green's function approach to such problem.

Cross-References

▶ Plates, Classical Theory

References

1. Tauchert TR (1986) Thermal stresses in plates – statical problems. In: Hetnarski RB (ed) Thermal stresses I. Elsevier, Amsterdam, pp 23–141
2. Boley BA, Weiner JH (1980) Theory of thermal stresses. Wiley, New York
3. Parkus H (1968) Thermoelasticity. Blaisdell, Waltham MA
4. Sarkar S (1968) Thermal deflections of a circular plate under non-stationary temperature. Applikace Mathematiki 13:208–213
5. Biswas P (1977) Thermal deflection of an elastic circular plate of variable thickness. Proc Indian Acad Sci 85A1:1–7
6. Forray M, Newman M (1961) Bending of circular plates due to asymmetric temperature distribution. J Aerosp Sci 28:773–778
7. Nowacki W, Olesiak Z (1956) Circular plate partly clamped and partly simply supported. Arch Mech Stos 8:233–255

Circular/Annular Plates, Thermal Buckling

Mohammad Reza Eslami[1] and Ahmad Reza Khorshidvand[2]
[1]Department of Mechanical Engineering, Amirkabir University of Technology, Tehran, Iran
[2]Department of Mechanical Engineering, South Tehran Branch, Islamic Azad University, Tehran, Iran

Overview

Thermal buckling of circular plates without initial geometric imperfections made of functionally graded materials with surface-bounded piezoelectric layers is studied. The material properties of the FG plates, except Poisson's ratio, are assumed to vary continuously through the plate thickness by distribution of power law, sigmoid, and exponential functions of the volume fraction of the constituent. The general thermoelastic nonlinear equilibrium and linear stability equations for the piezoelectric FG plate are derived based on the classical plate theory using the variational formulations and are used to obtain the governing equations of piezoelectric FG plate. Buckling load is derived for solid circular plates under uniform temperature rise and nonlinear and linear temperature variations through the thickness for immovable clamped edge of boundary conditions. Resulting equations are employed to obtain the closed-form solution for the critical buckling load for each loading case.

Ma and Wang [1–3] have presented the nonlinear bending and postbuckling of circular functionally graded plates subjected to mechanical and thermal loadings based on the first-order and the third-order shear deformation theories. Reddy and Khdeir [4] studied the buckling and free-vibration behavior of cross-ply rectangular composite laminated plates using the classical, first-order, and

third-order plate theories under various types of boundary conditions. Exact analytical solutions as well as the finite element numerical solutions were developed in their studies. Piezoelectric effects on the buckling and postbuckling characteristics of piezoelectric FGM hybrid plates is studied by Wang et al. [5]. Several authors have investigated the elastic stability of composite circular plates subjected to various loadings and boundary conditions. The buckling analysis of circular FGM plates under thermal loads and radial compressive load are given by Najafizadeh and Eslami [6, 7]. Khorshidvand et al. [8] presented buckling analysis of circular FGM plate integrated with piezoelectric layers subjected to three types of thermal loadings based on the classical plate theory. Javaheri and Eslami [9–12] presented the thermal and mechanical buckling of rectangular FGM plates based on the first- and higher-order plate theories. Thermo-electro-mechanical buckling and postbuckling of FGM plates with piezoelectric actuators is reported by Shen [13–15] based on the singular perturbation method. Liew et al. [16] presented postbuckling of piezoelectric FGM plates subjected to the thermo-electro-mechanical loading. They used a semi-analytical iteration to determine the postbuckling response of the plate. Axisymmetric bending of functionally graded circular and annular plates is studied by Reddy et al. [17]. They presented the solutions for deflections and force and moment resultants based on the first-order plate theory in terms of those obtained using the classical plate theory. Shariat et al. [18, 19] reported the mechanical and thermal buckling of imperfect functionally graded plates based on the classical and first-order shear deformation theories. They presented closed-form solutions for critical buckling loads for the imperfect rectangular FG plates and investigated the influence of the geometrical imperfections on stability of the plate.

Basic Assumptions

Consider a uniform thin circular plate made of FGM in the middle with two identical piezoelectric layers which are bonded to its upper and lower surfaces, as shown in Fig. 1. To extract formulations, a cylindrical coordinates system is taken in the center of plate's middle plane. The FGM profile across the thickness direction of the plate, made of ceramic and metal constituent materials, may be assumed to follow a form as

P-FGM plates

$$pr(z) = pr_m + pr_{cm}\left(\frac{2z+h}{2h}\right)^n \qquad (1)$$

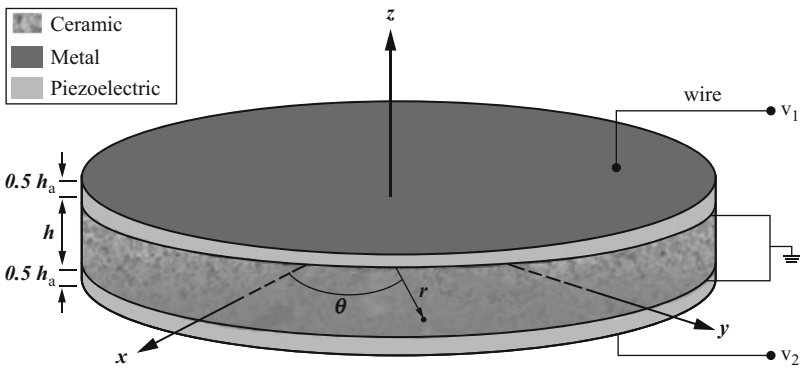

Circular/Annular Plates, Thermal Buckling, Fig. 1 Geometry of a piezoelectric coupled P-FGM circular plate

S-FGM plates (two power law functions)

$$pr(z) = pr_m + pr_{cm}\left[1 - \frac{1}{2}\left(\frac{h-2z}{h}\right)^n\right] \quad for\ 0 \le z \le h/2$$
$$pr(z) = pr_m + pr_{cm}\left[\frac{1}{2}\left(\frac{h+2z}{h}\right)^n\right] \quad for\ -h/2 \le z \le 0 \tag{2}$$

E-FGM plates (exponential function)

$$pr(z) = Ae^{B\left(\frac{2z+h}{2h}\right)},\quad A = pr_m,\quad B = \ln(pr_c/pr_m) \tag{3}$$

where pr is any material property of the FGM and is assumed to be functions of coordinate so that the effective properties are continuous through the plate thickness and are assumed to be temperature independent. This parameter represents the modulus of elasticity E and the coefficient of thermal expansion α. Term pr_m is the metal property of FGM, $pr_{cm} = pr_c - pr_m$, pr_c represents the ceramic property of FGM, and n is the power law index which takes values greater than or equal to zero, respectively. The value of n equal to zero represents a fully ceramic plate.

The material properties may be assumed to follow the power law form (PFGM), two power law functions (SFGM), and the exponential law (EFGM), indicated by (1) to (3). Note that the volume fraction of the ceramic is high near the top surface of the plate and that of metal is high near the bottom surface. In addition, the equations indicate that the top surface of the plate ($z = h/2$) is ceramic rich, whereas the bottom surface ($z = -h/2$) of the plate is metal rich. Generally, Poisson's ratio v is assumed constant across the plate thickness.

Analysis

Governing Equations

The two-dimensional stress–strain law for the plane-stress condition is given as

$$\sigma_{rr} = \frac{E(z)}{(1-v^2)}(\varepsilon_{rr} + v\varepsilon_{\theta\theta}) - \frac{E(z)\alpha(z)}{(1-v)}T(z) \tag{4}$$

$$\sigma_{\theta\theta} = \frac{E(z)}{(1-v^2)}(\varepsilon_{\theta\theta} + v\varepsilon_{rr}) - \frac{E(z)\alpha(z)}{(1-v)}T(z) \tag{5}$$

$$\sigma_{r\theta} = \frac{E(z)}{2(1+v)}\gamma_{r\theta} \tag{6}$$

The plate is assumed to be comparatively thin, and according to the Love-Kirchhoff assumptions, planes normal to the median surface are assumed to remain plane after deformation. Thus, shear deformations normal to the plate are disregarded. Using the classical plate theory (CPT), strain components at distance z from the middle plane are given in matrix form as [21]

$$\begin{Bmatrix} \varepsilon_{rr} \\ \varepsilon_{\theta\theta} \\ \gamma_{r\theta} \end{Bmatrix} = \begin{Bmatrix} u_{,r} + \frac{1}{2}(w_{,r})^2 \\ \frac{1}{r}v_{,\theta} + \frac{1}{r}u + \frac{1}{2}\left(\frac{1}{r}w_{,\theta}\right)^2 \\ \left(\frac{1}{r}u_{,\theta} + v_{,\theta} - \frac{1}{r}v_{,\theta} + \frac{1}{r}w_{,\theta}^2\right) \end{Bmatrix} + z\begin{Bmatrix} -w_{,rr} \\ -\left(\frac{1}{r}w_{,r} + \frac{1}{r^2}w_{,\theta\theta}\right) \\ \left(-\frac{1}{r}w_{,r\theta} + \frac{1}{r^2}w_{,\theta}\right) \end{Bmatrix} \tag{7}$$

where a comma in subscript indicates partial differentiation and ε_{rr}, $\varepsilon_{\theta\theta}$, and $\gamma_{r\theta}$ are the strain components along the r-, θ-, and z-directions, respectively. The stress components in plane-stress condition in FGM (with superscript h) and piezoelectric parts (with superscript p) of the plate are written as

$$\{\sigma\}^h = \begin{Bmatrix} \sigma_{rr}^h \\ \sigma_{\theta\theta}^h \\ \sigma_{r\theta}^h \end{Bmatrix} = \begin{bmatrix} Q_{11} & Q_{12} & 0 \\ Q_{12} & Q_{22} & 0 \\ 0 & 0 & Q_{44} \end{bmatrix} \begin{Bmatrix} \varepsilon_{rr} - \alpha(z)T(z) \\ \varepsilon_{\theta\theta} - \alpha(z)T(z) \\ \gamma_{r\theta} \end{Bmatrix} \tag{8}$$

$$\{\sigma\}^p = \begin{Bmatrix} \sigma_{rr}^p \\ \sigma_{\theta\theta}^p \\ \sigma_{r\theta}^p \end{Bmatrix} = \begin{bmatrix} c_{11} & c_{12} & 0 \\ c_{12} & c_{22} & 0 \\ 0 & 0 & c_{44} \end{bmatrix} \begin{Bmatrix} \varepsilon_{rr} - \alpha^p T(z) \\ \varepsilon_{\theta\theta} - \alpha^p T(z) \\ \gamma_{r\theta} \end{Bmatrix} - \begin{bmatrix} 0 & 0 & e_{31} \\ 0 & 0 & e_{32} \\ 0 & 0 & 0 \end{bmatrix} \begin{Bmatrix} E_r \\ E_\theta \\ E_z \end{Bmatrix} \tag{9}$$

where the plane-stress-reduced stiffness Q_{ij} are defined as

$$Q_{11}(z) = Q_{22}(z) = \frac{E(z)}{1-\nu^2},\ Q_{12}(z) = Q_{21}(z) = \nu Q_{11}(z),\ Q_{44}(z) = \frac{E(z)}{2(1+\nu)} \tag{10}$$

In general case, the total potential energy for FG circular plate integrated with two piezoelectric layers can be written as

$$U = U^h + U^p \tag{11}$$

in which

$$U^h = \frac{1}{2}\int_r \int_\theta \int_z [\sigma_{rr}^h(\varepsilon_{rr} - \alpha(z)T(z)) + \sigma_{\theta\theta}^h(\varepsilon_{\theta\theta} - \alpha(z)T(z)) + 2\sigma_{r\theta}^h\varepsilon_{r\theta}]rdzd\theta dr \tag{12}$$

and considering the thermal effects through the thickness of piezoelectric layers

$$U^p = \frac{1}{2}\int_r \int_\theta \int_z (\{\varepsilon - \alpha^p \Delta\{T\}\}^T[C]\{\varepsilon - \alpha^p \Delta\{T\}\} - \{E\}^T[k]\{E\} - 2\{\varepsilon - \alpha^p \Delta\{T\}\}^T[e]\{E\})rdzd\theta dr \tag{13}$$

where U^h and U^p are strain energies of the FGM and piezoelectric parts of the plate, respectively, and $\{\sigma^h\}$ indicates the stress components in middle FGM part of the plate, and $[C]$, $[k]$, and $[e]$ are matrix form of elastic, dielectric permeability, and piezoelectric material coefficients, respectively, defined as

$$[C] = \begin{bmatrix} c_{11} & c_{12} & 0 \\ c_{12} & c_{22} & 0 \\ 0 & 0 & c_{44} \end{bmatrix}, [k] = \begin{bmatrix} k_{11} & 0 & 0 \\ 0 & k_{22} & 0 \\ 0 & 0 & k_{33} \end{bmatrix}, [e] = \begin{bmatrix} 0 & 0 & e_{31} \\ 0 & 0 & e_{32} \\ 0 & 0 & 0 \end{bmatrix} \tag{14}$$

Here, c_{ij}, k_{ij}, and e_{ij} are the components of the plane-stress-reduced stiffness, dielectric permeability, and piezoelectric stiffness coefficients, respectively. Assuming that the actuator is poled along the z-direction, and viewing the piezoelectric material as a transversely isotropic material, which is true for piezoelectric ceramics, many of the parameters in the mentioned matrices will be either zero or can be expressed in terms of the other parameters. In particular, the nonzero coefficients of piezoelectric properties may be written as [20]

$$c_{11} = c_{22},\ c_{12},\ c_{44},\ e_{31} = e_{32},\ k_{11} = k_{22},\ k_{33} \tag{15}$$

Thus, the only nonzero electric field is in the z-direction and the vector of applied electric field $\{E\}$ can be shown as

$$E = \{E_r \quad E_\theta \quad E_z\}^T = \{0 \quad 0 \quad E_z\}^T \tag{16}$$

Considering relations (13) to (16) and substituting relations (4) to (9) into (12) to (13), and finally into (11) and integrating with respect to z, the total potential energy is obtained. Using variational approach, the equilibrium equations for circular plate may be obtained. Applying the Euler equations for total functional of U in (11), we obtain [21]

$$
\begin{aligned}
&N_{rr,r}+\frac{(N_{rr}-N_{\theta\theta})}{r}+\frac{1}{r}N_{r\theta,\theta}=0\\
&\frac{2}{r}N_{r\theta}+\frac{1}{r}N_{\theta\theta,\theta}+N_{r\theta,r}=0\\
&\left(rN_{rr}w_{,r}+N_{r\theta}w_{,\theta}-M_{\theta\theta}\right)_{,r}\\
&\quad+\left(\frac{1}{r}N_{\theta\theta}w_{,\theta}+N_{r\theta}w_{,r}+\frac{2}{r}M_{r\theta}\right)_{,\theta}\\
&\quad+\left(rM_{rr}\right)_{,rr}+\left(2M_{r\theta}\right)_{,r\theta}+\left(\frac{1}{r}M_{\theta\theta}\right)_{,\theta\theta}=0
\end{aligned}
\tag{17}
$$

The stability equations of the circular plate are derived using the adjacent equilibrium criterion. We assume u_0, v_0, and w_0 as the displacement components of the equilibrium state and u_1, v_1, and w_1 as the virtual displacements corresponding to a neighboring state. The displacement components and then the linear force and moment incremental resultants are

$$
u=u_0+u_1,\ v=v_0+v_1,\ w=w_0+w_1 \tag{18}
$$

$$
\begin{aligned}
&N_{rr}=N_{rr0}+N_{rr1},\ N_{\theta\theta}=N_{\theta\theta0}+N_{\theta\theta1},\\
&N_{r\theta}=N_{r\theta0}+N_{r\theta1}
\end{aligned}
\tag{19}
$$

$$
\begin{aligned}
&M_{rr}=M_{rr0}+M_{rr1},\ M_{\theta\theta}=M_{\theta\theta0}+M_{\theta\theta1},\\
&M_{r\theta}=M_{r\theta0}+M_{r\theta1}
\end{aligned}
\tag{20}
$$

Substituting relations (18) to (20) into (17), the terms with zero index satisfy the equilibrium equations, the higher-order terms are neglected and the linear terms constitute the stability equations as

$$
\begin{aligned}
&N_{rr1,r}+\frac{N_{rr1}-N_{\theta\theta1}}{r}+\frac{1}{r}N_{r\theta1,\theta}=0\\
&\frac{2}{r}N_{r\theta1}+\frac{1}{r}N_{r\theta1,\theta}+N_{r\theta1,r}=0\\
&\left(rN_{rr0}w_{1,r}+N_{r\theta0}w_{1,\theta}-M_{\theta\theta1}\right)_{,r}\\
&\quad+\left(\frac{1}{r}N_{1,\theta\theta}w_{1,\theta}+N_{r\theta0}w_{1,r}+\frac{2}{r}M_{r\theta1}\right)_{,\theta}\\
&\quad+\left(rM_{rr1}\right)_{,rr}+\left(2M_{r\theta1}\right)_{,r\theta}+\left(\frac{1}{r}M_{\theta\theta1}\right)_{,\theta\theta}=0
\end{aligned}
\tag{21}
$$

The force and moment resultants are expressed in terms of the stress components through the thickness as

$$
\begin{aligned}
\{N\}=\begin{Bmatrix}N_{rr}\\N_{\theta\theta}\\N_{r\theta}\end{Bmatrix}&=\int_{-h/2}^{+h/2}\{\sigma\}^h dz\\
&+\int_{-(h+h_a)/2}^{-h/2}\{\sigma\}^p dz+\int_{+h/2}^{+(h+h_a)/2}\{\sigma\}^p dz
\end{aligned}
\tag{22}
$$

$$
\begin{aligned}
\{M\}=\begin{Bmatrix}M_{rr}\\M_{\theta\theta}\\M_{r\theta}\end{Bmatrix}&=\int_{-h/2}^{+h/2}z\{\sigma\}^h dz\\
&+\int_{-(h+h_a)/2}^{-h/2}z\{\sigma\}^p dz+\int_{+h/2}^{+(h+h_a)/2}z\{\sigma\}^p dz
\end{aligned}
\tag{23}
$$

The stress resultants are simplified in the matrix form as

$$
\begin{aligned}
\begin{Bmatrix}\{N\}\\\{M\}\end{Bmatrix}&=\begin{bmatrix}[A+h_aC] & [B]\\ [B] & [D+LC]\end{bmatrix}\begin{Bmatrix}\{\varepsilon^{(0)}\}\\\{\varepsilon^{(1)}\}\end{Bmatrix}\\
&-\begin{Bmatrix}\{N^{(T)}\}\\\{M^{(T)}\}\end{Bmatrix}-\begin{Bmatrix}\{N^{(E)}\}\\\{M^{(E)}\}\end{Bmatrix}
\end{aligned}
\tag{24}
$$

where

$$
(A_{ij},B_{ij},D_{ij})=\int_z Q_{ij}(z)(1,z,z^2)dz,\ (i,j=1,2,3) \tag{25}
$$

Here, the quantities $\{N^{(T)}\}$, $\{M^{(T)}\}$, $\{N^{(E)}\}$, and $\{M^{(E)}\}$ are the resultants due to the applied temperature and electrical fields on the plate, respectively, and they can be computed as

$$
\begin{aligned}
\{N^{(T)}\}&=\{N^{(T)}\}_{FGM}+\{N^{(T)}\}_{piezo}\\
\{M^{(T)}\}&=\{M^{(T)}\}_{FGM}+\{M^{(T)}\}_{piezo}
\end{aligned}
\tag{26}
$$

$$\{N^{(T)}\}_{FGM} = \left\{\frac{E_4}{1-\nu}, \frac{E_4}{1-\nu}, 0\right\}^T$$
$$\{M^{(T)}\}_{FGM} = \left\{\frac{E_5}{1-\nu}, \frac{E_5}{1-\nu}, 0\right\}^T \quad (27)$$

$$\{M^{(T)}\}_{piezo} = \{(c_{11}+c_{12})(E_6+E_7), (c_{21}+c_{22})(E_6+E_7), 0\}^T \quad (28)$$

$$\{N^{(T)}\}_{piezo} = \{(c_{11}+c_{12})(E_8+E_9), (c_{21}+c_{22})(E_8+E_9), 0\}^T \quad (29)$$

$$\{N^{(E)}\} = \{e_{31}E_z h_a, e_{31}E_z h_a, 0\}^T$$
$$\{M^{(E)}\} = \{0,0,0\}^T \quad (30)$$

where

$$E_4 = \int_z \alpha(z)E(z)\Delta T dz,\ E_5 = \int_z z\alpha(z)E(z)\Delta T dz,$$
$$E_6 = \int_{h/2}^{(h+ha)/2} z\alpha^p \Delta T dz$$
$$E_7 = \int_{-(h+ha)/2}^{-h/2} z\alpha^p \Delta T dz,\ E_8 = \int_{h/2}^{(h+ha)/2} \alpha^p \Delta T dz,$$
$$E_9 = \int_{-(h+ha)/2}^{-h/2} \alpha^p \Delta T dz \quad (31)$$

Now, consider a circular plate subjected to thermal loading of the form $T = T(z)$. Taking polar symmetry condition for this case of loading, the first and third of stability equations (21), based on the displacement components, lead to

$$\left(E_1^* + c_{11}h_a\right)\left(\frac{d^2u_1}{dr^2} + \frac{1}{r}\frac{du_1}{dr} - \frac{1}{r^2}u_1\right) + E_2^*\left(-\frac{d^3w_1}{dr^3} - \frac{1}{r}\frac{d^2w_1}{dr^2} + \frac{1}{r^2}\frac{dw_1}{dr}\right) = 0$$
$$E_3^*\nabla^4 w_1 + (N_{rr0})\frac{d^2w_1}{dr^2} + \frac{1}{r}(N_{\theta\theta 0})\frac{dw_1}{dr} + Lc_{11}\nabla^4 w_1 + E_2^*\left(\frac{1}{r^2}\frac{du_1}{dr} - \frac{1}{r^3}u_1 - \frac{2}{r}\frac{d^2u_1}{dr^2} - \frac{d^3u_1}{dr^3}\right) = 0 \quad (32)$$

where $E_1^*,\ E_2^*,\ E_3^*$ are given as

$$E_1^* = E_1/(1-\nu^2) \quad E_2^* = E_2/(1-\nu^2)$$
$$E_3^* = E_3/(1-\nu^2) \quad (33)$$

$$(E_1^*, E_2^*, E_3^*) = 1/(1-\nu^2)\int_z (1, z, z^2)E(z)dz \quad (34)$$

and N_{rr0} and $N_{\theta\theta 0}$ are the prebuckling forces. For clamped and immovable edge in r direction, the boundary conditions are expressed as [22]

$$u_1(r=0) = 0\ w_1(r=0) = \text{finite}$$
$$u_1(r=a) = w_1(r=a) = \frac{d}{dr}w_1(r=a) = 0 \quad (35)$$

Prebuckling of Axisymmetric Thermal Load

Consider a circular plate subjected to transversely distributed thermal field $T = T(z)$ and constant applied voltage. Since the structure under consideration is unsymmetrical with respect to the mid-plane, the prebuckling state of the plate has to be studied carefully. For the case when thermal moments are vanished, bifurcation phenomenon may occur. However, for general cases of thermal loading, based on relations (26) to (30), thermal moments do not vanish. There is another possibility for a plate to follow the primary-secondary equilibrium path and that is when extra moments are supplied at boundaries to retain the plate flat in prebuckling regime. As known, clamped edge is capable of exhibiting such characteristic because the out-of-plane boundary conditions of a clamped edge are all essential and are not affected by thermal loading. Therefore, in this entry, only the clamped-type edge support is considered.

To study the prebuckling state of the plate, the symmetrical behavior of equilibrium state is analyzed. The lateral deflection is omitted, as the prebuckling state of the clamped plate is deflection-less. Solution of the first equilibrium equation in conjunction with the immovability condition at boundary and finiteness condition

at center reveals that radial displacement is also vanished and therefore prebuckling components are

$$u_0 = v_0 = w_0 \tag{36}$$

Here a subscript zero indicates the prebuckling state. The prebuckling force and moment resultants of the plate according to (24) are

$$\begin{aligned} &N_{rr0} = N_{\theta\theta 0} = -N_{rr0}^{(T)} - N_{rr}^{(E)} = -N_{rr0}^{(T)} - e_{31}E_z h_a \\ &N_{r\theta 0} = 0 \quad M_{rr0} = M_{\theta\theta 0} = -M^{(T)} \quad M_{r\theta 0} = 0 \end{aligned} \tag{37}$$

Solution of Stability Equations

Substituting relations (37) into the stability equations (32) yield

$$\begin{aligned} &(E_1^* + c_{11}h_a)\left(\frac{d^2u_1}{dr^2} + \frac{1}{r}\frac{du_1}{dr} - \frac{1}{r^2}u_1\right) \\ &\quad + E_2^*\left(-\frac{d^3w_1}{dr^3} - \frac{1}{r}\frac{d^2w_1}{dr^2} + \frac{1}{r^2}\frac{dw_1}{dr}\right) = 0 \\ &(E_3^* + Lc_{11})\nabla^4 w_1 + \frac{1}{r}\frac{d}{dr}\left[r\left(N_{rr0}^{(T)} + e_{31}E_z h_a\right)\frac{dw_1}{dr}\right] \\ &\quad + E_2^*\left(\frac{1}{r^2}\frac{du_1}{dr} - \frac{1}{r^3}u_1 - \frac{2}{r}\frac{d^2u_1}{dr^2} - \frac{d^3u_1}{dr^3}\right) = 0 \end{aligned} \tag{38}$$

Thus, the set of coupled stability equations must be solved. It is considered that a is the radius of solid circular plate and there is no initial imperfection. The solutions of (38) are assumed in the form

$$\begin{aligned} u_1 &= A_1 J_1(\lambda r) + A_2 Y_1(\lambda r) + A_3(1/r) + A_4 r \\ w_1 &= A_5 J_0(\lambda r) + A_6 Y_0(\lambda r) + A_7 L n r + A_8 \end{aligned} \tag{39}$$

where J_1, J_0 and Y_1, Y_0 are the Bessel functions of first, zero order, and first and second kinds, respectively. Also, A_1 to A_8 are the integration constants. Using the first and second boundary conditions yields $A_2 = A_3 = A_6 = A_7 = 0$. Satisfying the third boundary condition of relations (35) yields

$$A_4 = 0 \quad A_8 = -J_0(\lambda a)A_5 \quad J_1(\lambda a) = 0 \tag{40}$$

Thus, the smallest root is $\lambda a = 3.83$. It is seen that for the clamped edge

$$u_1 = A_1 J_1(\lambda r) \quad w_1 = A_5(J_0(\lambda r) - J_0(\lambda a)) \tag{41}$$

Substituting the expressions (41) into (38), two linear homogeneous equations are obtained as follows:

$$\begin{aligned} &-\lambda^2(E_1^* + c_{11}h_a)A_1 - \lambda^3 E_2^* A_5 = 0 \\ &\lambda^3 E_2^* A_1 + [\lambda^4(E_3^* + c_{11}L) \\ &-\lambda^2(N_{rr0}^{(T)} + e_{31}E_z h_a)]A_5 = 0 \end{aligned} \tag{42}$$

For a nontrivial solution of these equations, the determinant of coefficient must be set to zero, and when the temperature distribution of the plate is a function of thickness direction only, λ is constant and yields

$$\lambda^2 = \frac{N_{rr0}^{(T)} + e_{31}E_z h_a}{\{(E_3^* + c_{11}L) - E_2^{*2}/(E_1^* + c_{11}h_a)\}} \tag{43}$$

Table 1 presents ΔT_{cr} for thermoelastic buckling of a clamped piezoelectric circular plate made of functionally graded material under three types of thermal loads, uniform temperature rise, linear and nonlinear temperature distributions through the thickness of plate. Applied constant voltage on piezoelectric layers is considered. To validate the formulations of this entry, thermal buckling loads of the circular plate, neglecting the piezoelectric layers, are compared with those obtained by Najafizadeh and Eslami [6] for the FGM and isotropic plate. It is clear that from equation in second column, without taking piezoelectric effects, the same results are obtained for the FGM circular plate and homogeneous isotropic full ceramic circular plate in the third column.

Circular/Annular Plates, Thermal Buckling, Table 1 The results of circular plates buckling

Type of load	Thermoelastic axisymmetric buckling analysis (Piezo FGM)	Isotropic [6] FGM [6]
	$E_4 + (c_{11}+c_{12})(1-v)(E_8+E_9)$ $= \left\{\lambda^2\left[(E_3^*+c_{11}L) - \frac{E_2^{*2}}{(E_1^*+c_{11}h_a)}\right] - e_{31}E_z h_a\right\}(1-v)$	
Uniform temperature rise	$\Delta T_{cr} = \frac{(1-v)\left\{\lambda^2\left[(E_3^*+c_{11}L) - \frac{E_2^{*2}}{(E_1^*+c_{11}h_a)}\right] - e_{31}E_z h_a\right\}}{[Q_1+(c_{11}+c_{12})(1-v)\alpha^p h_a]}$ PFGM: $Q_1 = \left[\alpha_m E_m + \frac{(\alpha_m E_{cm}+\alpha_{cm}E_m)}{(n+1)} + \frac{\alpha_{cm}E_{cm}}{(2n+1)}\right]h$ SFGM: $Q_1 = \left[\frac{(4n+1)\alpha_{cm}E_{cm}}{4(4n+2)} + \frac{\alpha_{cm}E_m+\alpha_m E_{cm}}{2} + \alpha_m E_m\right]h$ EFGM: $Q_1 = \alpha_m E_m\left[\left(\lg\left[\frac{E_c}{E_m}\right] + \lg\left[\frac{\alpha_c}{\alpha_m}\right] - 1\right)\left(1.7 + \lg\left[\frac{\alpha_c}{\alpha_m}\right]\right)\right]h$	$T_{cr} = \frac{14.68}{12(1+v)}\left(\frac{h}{a}\right)^2\left(\frac{1}{\alpha_c}\right)$ $T_{cr} = \frac{14.68(1-v)}{Q_1}\left(E_3^* - \frac{E_2^{*2}}{E_1^*}\right)$
Gradient through the thickness	$\Delta T_{cr} = \frac{(1-v)}{Q_3}\left\{(-T_m - T_0)Q_1 + \lambda^2\left[(E_3^*+c_{11}L) - \frac{E_2^{*2}}{(E_1^*+c_{11}h_a)}\right] - e_{31}E_z h_a\right\}$ PFGM: $Q_3 = \frac{1}{Q_2}\left\{\alpha_m E_m/2 + \frac{1}{(n+2)}\left[(\alpha_m E_{cm}+\alpha_{cm}E_m) - \frac{E_m\alpha_m K_{cm}}{(n+1)K_m}\right]\right.$ $+ \frac{1}{(2n+2)}\left[E_{cm}\alpha_{cm} - (\alpha_m E_{cm}+\alpha_{cm}E_m)\frac{K_{cm}}{(n+1)K_m} + \frac{E_m\alpha_m K_{cm}^2}{(2n+1)K_m^2}\right]$ $+ \frac{1}{(3n+2)}\left[-\frac{E_{cm}\alpha_{cm}K_{cm}}{(n+1)K_m} + (\alpha_m E_{cm}+\alpha_{cm}E_m)\frac{K_{cm}^2}{(2n+1)K_m^2} - \frac{E_m\alpha_m K_{cm}^3}{(3n+1)K_m^3}\right]$ $+ \frac{1}{(4n+2)}\left[\frac{E_{cm}\alpha_{cm}K_{cm}^2}{(2n+1)K_m^2} - (\alpha_m E_{cm}+\alpha_{cm}E_m)\frac{K_{cm}^3}{(3n+1)K_m^3} + \frac{E_m\alpha_m K_{cm}^4}{(4n+1)K_m^4}\right]$ $+ \frac{1}{(5n+2)}\left[-\frac{E_{cm}\alpha_{cm}K_{cm}^3}{(3n+1)K_m^3} + (\alpha_m E_{cm}+\alpha_{cm}E_m)\frac{K_{cm}^4}{(4n+1)K_m^4} - \frac{E_m\alpha_m K_{cm}^5}{(5n+1)K_m^5}\right]$ $\left.+ \frac{1}{(6n+2)}\left[\frac{E_{cm}\alpha_{cm}K_{cm}^4}{(4n+1)K_m^4} - (\alpha_m E_{cm}+\alpha_{cm}E_m)\frac{K_{cm}^5}{(5n+1)K_m^5}\right] - \frac{1}{(7n+2)}\left[\frac{E_{cm}\alpha_{cm}K_{cm}^5}{(5n+1)K_m^5}\right]\right\}$ $Q_2 = 1 - \frac{K_{cm}}{(n+1)K_m} + \frac{K_{cm}^2}{(2n+1)K_m^2} - \frac{K_{cm}^3}{(3n+1)K_m^3} + \frac{K_{cm}^4}{(4n+1)K_m^4} - \frac{K_{cm}^5}{(5n+1)K_m^5}$	$T_{cr} = \frac{29.36}{12(1+v)}\left(\frac{h}{a}\right)^2\left(\frac{1}{\alpha_c}\right)$ $T_{cr} = \frac{14.68(1-v)}{Q_3}\left(E_3^* - \frac{E_2^{*2}}{E_1^*}\right)$
Linear temperature distribution	$\Delta T_{cr} = \left\{\frac{-T_1 Q_1}{(1-v)} + \lambda^2\left[(E_3^*+c_{11}L) - \frac{E_2^{*2}}{(E_1^*+c_{11}h_a)}\right] - e_{31}E_z h_a\right\}\frac{(1-v)}{\left(\frac{1}{2}Q_1+Q_4\right)}$ PFGM: $Q_4 = \left\{(\alpha_m E_{cm}+\alpha_{cm}E_m)\left[\frac{n}{(2n+2)(n+2)}\right] + \alpha_{cm}E_{cm}\left[\frac{n}{(2n+2)(2n+1)}\right]\right\}\frac{h^2}{(h+h_a)}$	

Conclusions

In this entry, the effect of piezoelectric layers on thermal buckling capacity of circular plates as closed-form solution is presented. This entry concludes with the following observations:

1. The equilibrium and stability equations are identical with the corresponding equations for FGM plates.
2. Application of piezoelectric material in thermal problems depends on an important parameter, the Curie temperature Θ_c. For PZT ceramics, the phase above the Curie temperature is a paraelectric and also non-piezoelectric (isotropic) [23].
3. The effect of piezoelectric layers on buckling of full metal plate is more relevant.
4. Applied voltage variation of the peizoelectric layers do not have much influence on the buckling of an FG plate.
5. The critical buckling temperature is reduced when volume fraction index increases, as the plate becomes more metal rich.
6. The critical buckling temperature is raised when the ratio h_a/h is increased.
7. Consideration of temperature distribution through the thickness of piezoelectric layers does not have significant effective on the increase of thermal buckling load.

References

1. Ma LS, Wang TJ (2003) Axisymmetric post-buckling of a functionally graded circular plate subjected to uniformly distributed radial compression. Materials Science Forum 423/425, pp 719–724
2. Ma LS, Wang TJ (2003) Nonlinear bending and post-buckling of a functionally graded circular plate under mechanical and thermal loadings. Int J Solids Struct 40:3311–3330
3. Ma LS, Wang TJ (2004) Relationships between the solutions of axisymmetric bending and buckling of functionally graded circular plates based on the third-order plate theory and the classical solutions for isotropic circular plates. Int J Solids Struct 41:85–101
4. Reddy JN, Khdeir AA (1989) Buckling and vibration of laminated composite plate using various plate theories. AIAA J 21:1808–1817
5. Wang CM, Liew KM, Xiang Y, Kitipornchai S (1993) Buckling of rectangular Mindlin plates with internal supports. Int J Solids Struct 30:1–17
6. Najafizadeh MM, Eslami MR (2002) Thermoelastic stability of circular plates composed of functionally graded materials based on first order theory. AIAA J 40(7):1444–1450
7. Najafizadeh MM, Eslami MR (2002) Thermoelaslic stability of orthotropic circular plates. J Ther Stress 25(10):985–1005
8. Khorshidvand AR, Jabbari M, Eslami MR (2012) Thermoelastic buckling analysis of functionally graded circular plates integrated with piezoelectric layers. J Ther Stress 35:695–717
9. Javaheri R, Eslami MR (2002) Thermal buckling of functionality graded plates. AlAA J 40(1):162–169
10. Javaheri R, Eslami MR (2002) Buckling of functionally graded plates under in-plane comppressive loading. ZAMM 82(4):277–283
11. Javaheri R, Eslami MR (2005) Buckling of functionally graded plates under in-plane compressive loading based on various theories. Trans ISME 6(1):76–93
12. Javaheri R, Eslami MR (2002) Thermal buckling of functionally graded plates based on higher order theory. J Ther Stress 25:603–625
13. Shen HS (2005) Postbuckling of FGM plates with piezoelectric actuators under thermo-electro-mechanical loadings. Int J Solids Struct 42(23):6101–6121
14. Shen HS (2005) Postbuckling of axially loaded FGM hybrid cylindrical shells in thermal environments. Comp Sci Technol 65(11–12):1675–1690
15. Shen HS, Noda N (2007) Postbuckling of pressure-loaded FGM hybrid cylindrical shells in thermal environments. Comp Struct 77(4):546–560
16. Liew KM, Yang J, Kitipornchai S (2003) Postbuckling of piezoelectric FGM plates subject to thermo-electro-mechanical loading. Int J Solids Struct 40(15):3869–3892
17. Reddy JN, Wang CM, Kitipornchai S (1999) Axisymmetric bending of functionally graded circular and annular plates. Eur J Mech A/Solids 18:195–199
18. Shriat BSA, Javaheri R, Eslami MR (2005) Buckling of imperfect functionally graded plates under in-plane compressive loading. Thin-Walled Struct 43(7):1020–1036
19. Shriat BSA, Eslami MR (2006) Thermal buckling of imperfect functionally graded plates, Int J Solids Structures 43(14–15):4082–4096
20. Moheimani SO, Fleming AJ (2006) Advances in industrial control. Springer, London
21. Brush DO, Almorth BO (1975) Buckling of bars, plates and shells. McGraw-Hill, New York
22. Reddy JN (2004) Mechanics of lminated composite plates and shells, theory and analysis. CRC Press, New York
23. Tich J, Erhart J, Kittinger E, Prvratsk J (2010) Fundamentals of piezoelectric sensorics, mechanical, dielectric, and thermodynamical properties of piezoelectric materials. Springer, New York

Classic and Generalized Thermoelastic Diffusion Theories

Moncef Aouadi
Department of Mathematics and Computer Science, Institut Supérieur des Sciences Appliquées et de Technologie de Mateur, Université de Carthage, Tunisia

Overview

The development of high technologies in the years before, during, and after the Second World War pronouncedly affected the investigations in which the fields of temperature and diffusion in solids cannot be neglected [1].

Diffusion can be defined as the movement of particles from an area of high concentration to an area of lower concentration until equilibrium is reached. It occurs as a result of second law of thermodynamics which states that the entropy or disorder of any system must always increase with time. There is now a great deal of interest in the study of diffusion, due to its many applications in geophysics and industrial applications. In integrated circuit fabrication, diffusion is used to introduce dopants in controlled amounts into the semiconductor substrate. Diffusion is used also to form the base and emitter in bipolar transistors, form integrated resistors, form the source/drain regions in MOS transistors, and dope polysilicon gates in MOS transistors. In most of these applications, the concentration is calculated using what is known as Fick's law. This is a simple law that does not take into consideration the mutual interaction between the introduced substance and the medium into which it is introduced or the effect of the temperature on this interaction. The phenomenon of diffusion is used to improve the conditions of oil extractions (seeking ways of more efficiently recovering oil from oil deposits). These days, oil companies are interested in the process of diffusion for more efficient extraction of oil from oil deposits [2].

Thermodiffusion in the solids is one of the transport processes that has great practical importance and is due to coupling of the fields of temperature, mass diffusion, and that of strain. The concept of thermodiffusion is used to describe the process of thermomechanical treatment of metals (carbonizing, nitriding steel, etc.); these processes are thermally activated, their diffusing substances being, e.g., nitrogen and carbon. They are accompanied by deformations of the solid. With the advance of a nuclear energetics, the interest in thermodiffusion has returned to metallic oxides that often heat up in inhomogeneous temperature field in connection with technological conditions.

The first theoretical works in the field of thermodiffusion of elastic deformable solid bodies belong to Pidstryhach who deduced fundamental equations of linear thermodiffusion in 1961 [3]. Nowacki, started from the linear thermoelasticity of elastic solids, continued and later developed the theory of thermodiffusion of elastic solids (see, e.g., [4]).

Classic Thermoelastic Diffusion Theory

Nowacki [4] derived the classic thermoelastic diffusion theory (by using classic Fourier's law (5) and Fick's law (8)). The governing equations for an anisotropic and homogenous solid are given by:

The equation of motion

$$\rho \ddot{u}_i = \sigma_{ji,j} + \rho F_i$$

The stress tensor relation

$$\sigma_{ij} = c_{ijkl} e_{kl} + a_{ij}\theta + b_{ij} C \tag{2}$$

The strain tensor relation

$$e_{ij} = \frac{1}{2}(u_{i,j} + u_{j,i}) \tag{3}$$

The energy equation

$$-q_{i,i} + \rho h = \rho T_0 \dot{S} \tag{4}$$

The Fourier's law

$$-\kappa_{ij}\theta_{,j} = q_i \tag{5}$$

The entropy relation

$$\rho S = -a_{ij}e_{ij} + \frac{\rho c_E}{T_0}\theta + \varpi C \tag{6}$$

The equation of conservation of mass

$$-\eta_{i,i} + r = \dot{C} \tag{7}$$

The Fick's law

$$-d_{ij}P_{,j} = \eta_i \tag{8}$$

The chemical potential relation

$$P = b_{ij}e_{ij} - \varpi\theta + \varrho C \tag{9}$$

where $\theta = T - T_0$ is the small temperature increment, T is the absolute temperature of the medium, T_0 is the reference uniform temperature of the body chosen such that $|\theta/T_0| \ll 1$, ρ is the mass density, q_i is the heat conduction vector, κ_{ij} is the thermal conductivity tensor, c_E is the specific heat at constant strain, c_{ijkm} is the tensor of elastic constants, σ_{ij} are the components of the stress tensor, $\mathbf{u} = (u_i)$ are the components of the displacement vector, e_{ij} are the components of the strain tensor, $\mathbf{F} = (F_i)$ is the external body force per unit mass, S is the entropy per unit mass, h is the heat supply per unit mass, P is the chemical potential per unit mass, C is the concentration of the diffusive material in the elastic body, d_{ij} is the diffusion tensor, r is the diffusion supply, ϖ is a measure of thermoelastic diffusion effect, ϱ is a measure of diffusive effect, and a_{ij} and b_{ij} are constitutive coefficients.

To obtain the equations of motion, we substitute from (2) and (3) into (1), we get

$$\rho\ddot{u}_i = c_{jikl}e_{kl,j} + a_{ji}\theta_{,j} + b_{ji}C_{,j} + \rho F_i \tag{10}$$

Now, substituting the divergence of both sides of (5) with (6) into (4), we obtain the equation of heat conduction

$$\rho c_E\dot{\theta} - a_{ij}T_0\,\dot{e}_{ij} + \varpi T_0\dot{C} - \rho h = \kappa_{ij}\theta_{,ij} \tag{11}$$

Substituting the divergence of both sides of (8) with (9) into (7), we obtain the equation of mass diffusion

$$d_{ij}(\varrho C + b_{ij}e_{ij} - \varpi\theta)_{,ij} + r = \dot{C} \tag{12}$$

For the case of isotropic materials, we have

$$\begin{gathered} c_{ijkl} = \lambda\delta_{ij}\delta_{kl} + \mu\delta_{ik}\delta_{jl} + \mu\delta_{il}\delta_{jk}\ a_{ij} = -\beta_1\delta_{ij} \\ b_{ij} = -\beta_2\delta_{ij}\ \kappa_{ij} = \kappa\delta_{ij}\ \ d_{ij} = \hbar\delta_{ij} \end{gathered} \tag{13}$$

where λ and μ are Lamé's constants, $\beta_1 = (3\lambda + 2\mu)\alpha_t$ and $\beta_2 = (3\lambda + 2\mu)\alpha_c$, where α_t is the coefficient of linear thermal expansion and α_c is the coefficient of linear diffusion expansion. δ_{ij} is the Kronecker symbol defined by

$$\delta_{ij} = \begin{cases} 1 & i = j \\ 0 & i \neq j \end{cases}$$

Substituting from (13) into (10)–(12), we get the governing equations for isotropic and homogenous solid

$$\begin{gathered} \rho\ddot{u}_i = (\lambda+\mu)u_{j,ji} + \mu u_{i,jj} - \beta_1\theta_{,i} - \beta_2 C_{,i} + \rho F_i \\ \rho c_E\dot{\theta} = \kappa\theta_{,ii} - \beta_1 T_0\,\dot{e}_{ii} - \varpi T_0\dot{C} + \rho h \\ \dot{C} = \hbar(\varrho C - \beta_2 e_{kk} - \varpi\theta)_{,ii} + r \end{gathered} \tag{14}$$

Generalized Thermoelastic Diffusion Theory

The classical theory of thermoelasticity is based on the conventional heat conduction equation. This equation, due to its parabolic nature, predicts that the thermal disturbances propagate at infinite speeds. This prediction may be suitable for most engineering applications, but it is a physically unacceptable assumption. To eliminate this paradox, several generalized thermoelastic theories have been developed subsequently. The development of these theories was accelerated by the advent of the second sound effects observed experimentally in materials at a very low temperature. A survey article of various representative theories in the range of generalized thermoelasticity has been brought out by Hetnarski and Ignaczak [5].

Lord and Shulman Model

The first generalization was developed by Lord and Shulman [6], which replaces the classic Fourier's law (5) with the Cattaneo-Maxwell law of heat conduction [7]

$$\tau_0 \dot{q}_i + q_i = -\kappa_{ij}\theta_{,j} \tag{15}$$

where τ_0 is the thermal relaxation time which ensures that the heat conduction equation will predict finite speeds of heat propagation. Analogous to (15) for the heat flux vector, we assume a similar equation for the mass flux vector of the form [2]:

$$\tau \dot{\eta}_i + \eta_i = -d_{ij}P_{,j} \tag{16}$$

where τ is the diffusion relaxation time, which ensures that the equation satisfied by the concentration will also predict finite speeds of propagation of matter from one medium to the other.

Sherief et al. [2] derived the generalized thermoelastic diffusion theory under Lord and Shulman model. By using (15) instead of (5) into (11) and (16) instead of (7) into (12), the authors obtained the following generalized system of governing equations:

$$\begin{aligned}
\rho\ddot{u}_i &= c_{jikl}e_{kl,j} + a_{ji}\theta_{,j} + b_{ji}C_{,j} + \rho F_i \\
\kappa_{ij}\theta_{,ij} &= \rho c_E(\dot{\theta} + \tau_0\ddot{\theta}) - a_{ij}T_0(\dot{e}_{ij} + \tau_0\ddot{e}_{ij}) \\
&\quad + \varpi T_0(\dot{C} + \tau_0\ddot{C}) - \rho(h + \tau_0\dot{h}) \\
\varrho d_{ij}C_{,ij} &= \dot{C} + \tau\ddot{C} - d_{ij}(b_{ij}e_{ij} + \varpi\theta)_{,ij} \\
&\quad - (r + \tau\dot{r})
\end{aligned} \tag{17}$$

For isotropic materials, system (17) becomes

$$\begin{aligned}
\rho\ddot{u}_i &= (\lambda + \mu)u_{j,ji} + \mu u_{i,jj} - \beta_1\theta_{,i} - \beta_2 C_{,i} \\
&\quad + \rho F_i \\
\kappa\theta_{,ii} &= \rho c_E(\dot{\theta} + \tau_0\ddot{\theta}) + \beta_1 T_0(\dot{e}_{ii} + \tau_0\ddot{e}_{ij}) \\
&\quad + \varpi T_0(\dot{C} + \tau_0\ddot{C}) - \rho(h + \tau_0\dot{h}) \\
\varrho C_{,ii} &= \beta_2 e_{kk,ii} + \varpi\theta_{,ii} + \frac{1}{\hbar}(\dot{C} + \tau\ddot{C}) \\
&\quad - \frac{1}{\hbar}(r + \tau\dot{r})
\end{aligned} \tag{18}$$

The generalized systems (17) and (18) associated with Cattaneo-Maxwell laws (15) and (16) become hyperbolic and, hence, automatically eliminate the paradox of infinite speeds.

Green and Lindsay Model

The second generalization was developed by Green and Lindsay [8] and called as temperature rate-dependent thermoelasticity. In thermoelasticity, the temperature rate dependent is included among the consecutive variables with two constants that act as two relaxation times. This does not violate the classical Fourier's law of heat conduction when body under consideration has a center of symmetry.

Rajneesh and Tarun [9] derived the generalized theory of thermoelastic diffusion under Green and Lindsay model. The thermodiffusion and thermodiffusion-mechanical relaxations are governed by four different time constants. If the material has center of symmetry, the constitutive equations take the form

$$\begin{aligned}
\sigma_{ij} &= c_{ijkl}e_{kl} + a_{ij}(\theta + \tau_1\dot{\theta}) + b_{ij}(C + \tau^1\dot{C}) \\
\rho S &= c_1 - a_{ij}e_{ij} + \frac{\rho c_E}{T_0}(\theta + \tau_0\dot{\theta}) + \varpi(C + \tau^0\dot{C}) \\
P &= b_{ij}e_{ij} - \varpi(\theta + \tau_1\dot{\theta}) + \varrho(C + \tau^1\dot{C}) + c_2
\end{aligned} \tag{19}$$

We add also the equation of motion (1), the energy equation (4), the Fourier's law (5), the equation of conservation of mass (7), and the Fick's law (8). In system (19), τ_0 and τ_1 are the thermal relaxation times, which ensure that the heat conduction equation, satisfied by the temperature θ, will predict finite speeds of heat propagation. τ^0 and τ^1 are the diffusion relaxation times which ensure that the equation, satisfied by the concentration C, will also predict finite speeds of propagation of matter from one medium to other. c_1 and c_2 are two constants.

To obtain the equations of motion, we substitute from $(19)_1$ and (3) into (1), we get

$$\rho\ddot{u}_i = c_{jikl}e_{kl,j} + a_{ji}(\theta + \tau_1\dot{\theta})_{,j} + b_{ji}(C + \tau^1\dot{C})_{,j} + \rho F_i \tag{20}$$

Now, substituting the divergence of both sides of (5) with $(19)_2$ into (4), we obtain the equation of heat conduction

$$\rho c_E(\dot{\theta}+\tau_0\ddot{\theta})-a_{ij}T_0\dot{e}_{ij}+\varpi T_0(\dot{C}+\tau^0\ddot{C})-\rho h=\kappa_{ij}\theta_{,ij} \tag{21}$$

Substituting the divergence of both sides of (8) with $(19)_3$ into (7), we arrive at the equation of mass diffusion

$$d_{ij}(\varrho(C+\tau^1\dot{C})+b_{ij}e_{ij}-\varpi(\theta+\tau_1\dot{\theta}))_{,ij}+r=\dot{C} \tag{22}$$

For isotropic materials, the governing equations (20)–(22) become

$$\begin{aligned}\rho\ddot{u}_i&=(\lambda+\mu)u_{j,ji}+\mu u_{i,jj}-\beta_1(\theta+\tau_1\dot{\theta})_{,i}\\&\quad-\beta_2(C+\tau^1\dot{C})_{,i}+\rho F_i\\ \kappa\theta_{,ii}&=\rho c_E(\dot{\theta}+\tau_0\ddot{\theta})+\beta_1T_0\,\dot{e}_{ii}\\&\quad+\varpi T_0(\dot{C}+\tau^0\ddot{C})-\rho h\\ \hbar\varrho C_{,ii}&=\hbar\beta_2e_{kk,ii}+\hbar\varpi(\theta+\tau_1\dot{\theta})_{,ii}\\&\quad+\dot{C}-\hbar\varrho\tau^1\,\dot{C}_{,ii}-r\end{aligned} \tag{23}$$

The generalized systems (20)–(22) and (23) derived under Green and Lindsay model become hyperbolic and, hence, automatically eliminate the paradox of infinite speeds.

Classic Micropolar Thermoelastic Diffusion Theory

In problems of waves and vibrations, the classical theory of elasticity fails to provide complete information, and the results obtained do not conform with experimental ones in case of media with granular structures. Most of the natural and man-made materials, including engineering, geological, and biological media, possess a microstructure. Furthermore, the micropolar elastic model is more realistic than the purely elastic theory for studying the response of materials to external stimuli. Eringen [10] developed the linear theory of micropolar elasticity. Under this theory, solids can undergo macrodeformations and microrotations. The motion in this kind of solids is completely characterized by the displacement vector $u_i(\mathbf{x},t)$ and the rotation vector $\phi_i(\mathbf{x},t)$, while in the case of classical elasticity, the motion is characterized by the displacement vector only. Micropolar solids can support couple stresses in addition to force stresses.

Tauchert et al. [11] extended the micropolar theory to include thermal effects. Aouadi [12] extended the micropolar theory to include thermal and diffusion effects. The linear system of governing equations of the classic micropolar thermoelastic diffusion theory consists of (see [12]):

The equations of motion

$$\rho\ddot{u}_i=\sigma_{ji,j}+\rho F_i\quad \epsilon_{ijk}\sigma_{jk}+\mu_{ji,j}+\rho G_i=\rho J_{ij}\,\ddot{\phi}_j \tag{24}$$

The kinematic relations

$$\varepsilon_{ji}=u_{i,j}-\epsilon_{kji}\phi_k\quad \phi_{ji}=\phi_{i,j} \tag{25}$$

The stress tensor relation

$$\sigma_{ij}=c_{ijkl}\varepsilon_{kl}+p_{ijkl}\phi_{kl}+a_{ij}\theta+b_{ij}C \tag{26}$$

The moment of couple stress tensor relation

$$\mu_{ij}=p_{ijkl}\varepsilon_{kl}+d_{ijkl}\phi_{kl}+p_{ij}\theta+q_{ij}C \tag{27}$$

The entropy relation

$$\rho S=-a_{ij}\varepsilon_{ij}-p_{ij}\phi_{ij}+\frac{\rho c_E}{T_0}\theta+\varpi C \tag{28}$$

The chemical potential relation

$$P=b_{ij}\varepsilon_{ij}+q_{ij}\phi_{ij}-\varpi\theta+\varrho C \tag{29}$$

We add also the energy equation (4), the Fourier's law (5), the equation of conservation of mass (7), and the Fick's law (8). In the above equations, μ_{ji} is the moment of couple stress tensor, ε_{ijk} is the alternating tensor, J_{ij} is the microrotation tensor, ϕ_i is the vector of internal rotations, G_i is the component of the external applied couple per unit mass, and ε_{ji} is the micro-strain tensor.

To obtain the governing equations of motion, we proceed as in previous sections, we get

$$\begin{aligned}
\rho\ddot{u}_i &= c_{jikl}\varepsilon_{kl,j} + p_{jikl}\phi_{kl,j} + a_{ji}\theta_{,j} \\
&\quad + b_{ji}C_{,j} + \rho F_i \\
\rho J_{ij}\ddot{\phi}_j &= p_{jikl}\epsilon_{kl,j} + d_{jikl}\phi_{kl,j} + p_{ji}\theta_{,j} + q_{ji}C_{,j} \\
&\quad + \varepsilon_{ijk}(c_{jkml}\varepsilon_{ml} + p_{jkml}\phi_{ml} + a_{jk}\theta \\
&\quad + b_{jk}C) + \rho G_i \\
\rho c_E\dot{\theta} &= \kappa_{ij}\theta_{,ij} + T_0 a_{ij}\,\dot{\varepsilon}_{ij} + T_0 p_{ij}\,\dot{\phi}_{ij} - T_0\varpi\dot{C} \\
&\quad + \rho h \\
\dot{C} &= d_{ij}(\varrho C + b_{ij}\varepsilon_{ij} + q_{ij}\phi_{ij} - \varpi\theta)_{,ij} + r
\end{aligned} \tag{30}$$

For the case of isotropic materials, we have

$$\begin{aligned}
c_{ijkl} &= \lambda\delta_{ij}\delta_{kl} + (\mu+\alpha)\delta_{ik}\delta_{jl} + (\mu-\alpha)\delta_{il}\delta_{jk} \\
d_{ijkl} &= \varepsilon\delta_{ij}\delta_{kl} + (\nu+\beta)\delta_{ik}\delta_{jl} + (\nu-\beta)\delta_{il}\delta_{jk} \\
a_{ij} &= -\beta_1\delta_{ij}\;\; b_{ij} = -\beta_2\delta_{ij}, \kappa_{ij} = \kappa\delta_{ij}\;\; d_{ij} = \hbar\delta_{ij} \\
J_{ij} &= J\delta_{ij}\;\; p_{ij} = q_{ij} = p_{ijkl} = q_{ijkl} = 0
\end{aligned}$$

where $\beta_1=(3\lambda+2\mu+\alpha)\alpha_t$ and $\beta_2=(3\lambda+2\mu+\alpha)\alpha_c$. Substituting the above equations into (30), we get

$$\begin{aligned}
\rho\ddot{u}_i &= (\lambda+\mu)u_{j,ji} + (\mu+\alpha)u_{i,jj} + \alpha\epsilon_{ijk}\phi_{k,j} \\
&\quad - \beta_1\theta_{,i} - \beta_2 C_{,i} + \rho F_i \\
\rho J\,\ddot{\phi}_i &= (\varepsilon+\beta)\phi_{j,ji} + \nu\phi_{i,jj} + \alpha\epsilon_{ijk}u_{k,j} \\
&\quad - 2\alpha\phi_i + \rho G_i \\
\rho c_E\dot{\theta} &= \kappa\theta_{,ii} - \beta_1 T_0\,\dot{e}_{ii} - \varpi T_0\dot{C} + \rho h \\
\dot{C} &= \hbar(\varrho C - \beta_2 e_{kk} - \varpi\theta)_{,ii} + r
\end{aligned} \tag{31}$$

Generalized Micropolar Thermoelastic Diffusion Theory

Aouadi [13] derived the generalized micropolar thermoelastic diffusion theory under Lord and Shulman model. Using the relations (15) and (16) instead of (5) and (8), respectively, the author gets the governing equations

$$\begin{aligned}
\rho\ddot{u}_i &= c_{jikl}\varepsilon_{kl,j} + p_{jikl}\phi_{kl,j} + a_{ji}\theta_{,j} + b_{ji}C_{,j} \\
&\quad + \rho F_i \\
\rho J_{ij}\ddot{\phi}_j &= p_{jikl}\varepsilon_{kl,j} + d_{jikl}\phi_{kl,j} + p_{ji}\theta_{,j} + q_{ji}C_{,j} \\
&\quad + \epsilon_{ijk}(c_{jkml}\varepsilon_{ml} + p_{jkml}\phi_{ml} + a_{jk}\theta + b_{jk}C) \\
&\quad + \rho G_i \\
\kappa_{ij}\theta_{,ij} &= \rho c_E(\dot{\theta} + \tau_0\ddot{\theta}) - a_{ij}T_0(\dot{\varepsilon}_{ij} + \tau_0\,\ddot{\varepsilon}_{ij}) \\
&\quad - p_{ij}T_0(\dot{\phi}_{ij} + \tau_0\,\ddot{\phi}_{ij}) + \varpi T_0(\dot{C} + \tau_0\ddot{C}) \\
&\quad - \rho(h + \tau_0\dot{h}) \\
d_{ij}\varrho C_{,ij} &= \dot{C} + \tau\ddot{C} - d_{ij}(b_{ij}\varepsilon_{ij} + q_{ij}\phi_{ij} - \varpi\theta)_{,ij} \\
&\quad - (r + \tau\dot{r})
\end{aligned} \tag{32}$$

For isotropic materials, system (32) becomes

$$\begin{aligned}
\rho\ddot{u}_i &= (\lambda+\mu)u_{j,ji} + (\mu+\alpha)u_{i,jj} + \alpha\varepsilon_{ijk}\phi_{k,j} \\
&\quad - \beta_1\theta_{,i} - \beta_2 C_{,i} + \rho F_i \\
\rho J\,\ddot{\phi}_i &= (\varepsilon+\beta)\phi_{j,ji} + \nu\phi_{i,jj} + \alpha\epsilon_{ijk}u_{k,j} \\
&\quad - 2\alpha\phi_i + \rho G_i \\
\kappa\theta_{,ii} &= \rho c_E(\dot{\theta} + \tau_0\ddot{\theta}) + \beta_1 T_0(\dot{e}_{ii} + \tau_0\,\ddot{e}_{ij}) \\
&\quad + \varpi T_0(\dot{C} + \tau_0\ddot{C}) - \rho(h + \tau_0\dot{h}) \\
\varrho C_{,ii} &= \beta_2 e_{kk,ii} + \varpi\theta_{,ii} + \frac{1}{\hbar}(\dot{C} + \tau\ddot{C}) \\
&\quad - \frac{1}{\hbar}(r + \tau\dot{r})
\end{aligned} \tag{33}$$

Classic Thermoelastic Theory with Voids

There are a number of theories about mechanical properties of porous materials. The concept of a distributed body introduced by Goodman and Cowin [14] in the context of granular and porous materials asserts that the mass density has the decomposition γv, where γ is the density of the matrix material and v is the volume fraction filed [15]. This representation introduces an additional degree of kinematic freedom, and by using this concept, Nunziato and Cowin [16] proposed a theory to describe the properties of homogeneous elastic materials with voids free of fluid.

Moreover, the theory of Cowin and Nunziato is more appropriated than other theories for the study of special continuum and geological materials, such as rocks, soils, and manufactured porous materials like ceramics and pressed powders. More in detail, it is used for solid material with voids but without any other phase, like liquid or gas. Generally, this theory is based on the balance of energy, where presence of the pores involves additional degree of freedom, namely, the fraction of elementary volume. Ieşan [17] has developed a linear theory of thermoelastic materials with voids. Aouadi [18] has extended the thermoelastic theory with voids to include diffusion effects. In the linear context, the equations of motion are given by

$$\rho\ddot{u}_i = \sigma_{ji,j} + \rho F_i h_{i,i} + g + \rho L = \rho J\ddot{\phi} \tag{34}$$

The constitutive equations are given by

$$\begin{aligned}
\sigma_{ij} &= c_{ijkl}e_{kl} + p_{ij}\phi + a_{ij}\theta + b_{ij}C \\
h_i &= q_{ij}\phi_{,j}, \\
g &= -p_{ij}e_{ij} - d_0\phi - \xi\theta - \zeta C \\
\rho S &= -a_{ij}e_{ij} - \xi\phi + \frac{\rho c_E}{T_0}\theta + \varpi C \\
P &= b_{ij}e_{ij} + \zeta\phi - \varpi\theta + \varrho C
\end{aligned} \tag{35}$$

To the last system, we add the energy equation (4), Fourier's law (5), Fick's law (8), and the equation of conservation of mass (7). In this system h_i are the components of the equilibrated stress vector, g is the intrinsic equilibrated body force, L is the extrinsic equilibrated body force, ϕ is the change in volume fraction from the reference volume fraction, and J is the equilibrated inertia.

To obtain the governing equations of motion, we proceed as in the above sections, we get

$$\begin{aligned}
\rho\ddot{u}_i &= c_{jikl}e_{kl,j} + p_{ji}\phi_{,j} + a_{ji}\theta_{,j} + b_{ji}C_{,j} + \rho F_i, \\
\rho J\ddot{\phi} &= -p_{ij}e_{ij} + q_{ij}\phi_{,ji} - d_0\phi - \xi\theta - \zeta C + \rho L \\
\rho c_E\dot{\theta} &= \kappa_{ij}\theta_{,ij} + T_0 a_{ij}\dot{e}_{ij} + T_0\xi\dot{\phi} - \varpi T_0\dot{C} + \rho h \\
\dot{C} &= d_{ij}(b_{ij}e_{ij} + \zeta\phi - \varpi\theta + \varrho C)_{,ij} + r
\end{aligned} \tag{36}$$

For the case of isotropic materials, the constitutive equations (35) become

$$\begin{aligned}
\sigma_{ij} &= \lambda e_{kk}\delta_{ij} + 2\mu e_{ij} + \gamma\phi\delta_{ij} - \beta_1\theta\delta_{ij} - \beta_2 C\delta_{ij} \\
h_i &= \varsigma\phi_{,i} \\
g &= -\gamma e_{kk} - d_0\phi - \xi\theta - \zeta C \\
\rho T_0 S &= \beta_1 T_0 e_{kk} - \xi T_0\phi + \rho c_E\theta + \varpi T_0 C \\
P &= -\beta_2 e_{kk} + \zeta\phi - \varpi\theta + \varrho C
\end{aligned} \tag{37}$$

and the governing equations (36) take the form

$$\begin{aligned}
\rho\ddot{u}_i &= (\lambda + \mu)u_{j,ji} + \mu u_{i,jj} + \gamma\phi_{,j} \\
&\quad - \beta_1\theta_{,i} - \beta_2 C_{,i} + \rho F_i \\
\rho J\ddot{\phi} &= \varsigma\phi_{,ii} - \gamma e_{kk} - d_0\phi - \xi\theta - \zeta C + \rho L \\
\rho c_E\dot{\theta} &= \kappa\theta_{,ii} + \xi T_0\dot{\phi} - \beta_1 T_0\,\dot{e}_{ii} - \varpi T_0\dot{C} + \rho h \\
\dot{C} &= \hbar(\varrho C - \beta_2 e_{kk} + \zeta\phi - \varpi\theta)_{,ii} + r
\end{aligned} \tag{38}$$

Generalized Thermoelastic Diffusion Theory with Voids

By using the relations (15) and (16) instead of (5) and (8), respectively, Singh [19] obtained the governing equations of the generalized thermoelastic diffusion theory with voids under Lord and Shulman model

$$\begin{aligned}
\rho\ddot{u}_i &= c_{jikl}e_{kl,j} + p_{ji}\phi_{,j} + a_{ji}\theta_{,j} + b_{ji}C_{,j} \\
&\quad + \rho F_i \\
\rho J\ddot{\phi} &= -p_{ij}e_{ij} + q_{ij}\phi_{,ji} - d_0\phi - \xi\theta - \zeta C + \rho L \\
\kappa_{ij}\theta_{,ij} &= \rho c_E(\dot{\theta} + \tau_0\ddot{\theta}) - a_{ij}T_0(\dot{e}_{ij} + \tau_0\ddot{e}_{ij}) \\
&\quad - T_0\xi(\dot{\phi} + \tau_0\ddot{\phi}) + \varpi T_0(\dot{C} + \tau_0\ddot{C}) \\
&\quad - \rho(h + \tau_0\dot{h}) \\
d_{ij}\varrho C_{,ij} &= \dot{C} + \tau\ddot{C} - d_{ij}(b_{ij}e_{ij} + \zeta\phi - \varpi\theta)_{,ij} \\
&\quad - (r + \tau\dot{r})
\end{aligned} \tag{39}$$

For isotropic materials, system (39) becomes

$$\begin{aligned}
\rho\ddot{u}_i &= (\lambda+\mu)u_{j,ji} + \mu u_{i,jj} + \gamma\phi_{,j} \\
&\quad - \beta_1\theta_{,i} - \beta_2 C_{,i} + \rho F_i \\
\rho J\ddot{\phi} &= \varsigma\phi_{,ii} - \gamma e_{kk} - d_0\phi - \xi\theta - \zeta C + \rho L \\
\kappa\theta_{,ii} &= \rho c_E(\dot{\theta} + \tau_0\ddot{\theta}) + \beta_1 T_0(\dot{e}_{ii} + \tau_0\ddot{e}_{ii}) \\
&\quad - T_0\xi(\dot{\phi} + \tau_0\ddot{\phi}) + \varpi T_0(\dot{C} + \tau_0\ddot{C}) \\
&\quad - \rho(h + \tau_0\dot{h}) \\
\varrho C_{,ii} &= \beta_2 e_{kk,ii} - \zeta\phi_{,ii} + \varpi\theta_{,ii} + \frac{1}{\hbar}(\dot{C} + \tau\ddot{C}) \\
&\quad - \frac{1}{\hbar}(r + \tau\dot{r})
\end{aligned} \tag{40}$$

Thermoelastic Diffusion Mixture Theory

The importance of the study of mixtures was recognized long ago when the basic concepts of the theory have been established and the possible applications of the mathematical models were identified. The first works on the continuum theory of mixtures were the contributions of Truesdell and Toupin [20], Kelly [21], and others.

The theory on mixtures of elastic solids is naturally described by a Lagrangian approach, and the independent constitutive variables are the displacement vector fields, their relative gradients, the temperature, and its gradient. The idea of employing interpenetrating continua as a model of composite materials was introduced by Bedford and Stern [22, 23]. In this theory, a mixture of two interacting continua s_1 and s_2 is considered. The mixture is viewed as a superposition of two continua each following its own motion and at any time each place in the mixture is occupied simultaneously by different particles, one from each constituent. The motion of a mixture is described by the equations $\mathbf{x} = \mathbf{x}(\mathbf{X}, t), \mathbf{y} = \mathbf{y}(\mathbf{Y}, t)$, where the particles under consideration occupy the same position in the reference configuration, so that $\mathbf{X} = \mathbf{Y}$. Following them, Ieşan [24] has developed a linear theory of thermoelastic mixtures. Aouadi [25] has extended the thermoelastic mixtures theory to include diffusion effects. In the linear context, the equations of motion are given by

$$\begin{aligned}
t_{ji,j} - \pi_i + \rho_1^0 F_i &= \rho_1^0\,\ddot{u}_i \\
s_{ji,j} + \pi_i + \rho_2^0 G_i &= \rho_2^0\,\ddot{w}_i
\end{aligned} \tag{41}$$

The strain measures relations

$$e_{ij} = \frac{1}{2}(u_{i,j} + u_{j,i}) \quad \mathrm{g}_{ij} = u_{j,i} + w_{i,j} \quad d_i = u_i - w_i \tag{42}$$

The constitutive equations are given by

$$\begin{aligned}
t_{ji} &= A_{jikl}e_{kl} + B_{jikl}\mathrm{g}_{kl} + a_{ji}\theta + b_{ji}C \\
s_{ji} &= B_{klij}e_{kl} + C_{ijkl}\mathrm{g}_{kl} + c_{ji}\theta + d_{ji}C \\
\pi_i &= \alpha_{ij}d_j \\
\rho_0 S &= -a_{ij}e_{ij} - c_{ij}\mathrm{g}_{ij} + \frac{\rho_0 c_E}{T_0}\theta + \varpi C \\
P &= b_{ij}e_{ij} + d_{ij}\mathrm{g}_{ij} - \varpi\theta + \varrho C
\end{aligned} \tag{43}$$

To the last system, we add the energy equation (4), Fourier's law (5), the equation of conservation of mass (7), and Fick's law (8). In the above equations ρ_α^0 are the mass density associated with the constituent s_α, t_{ij} and s_{ij} are the partial stress tensors associated with the constituent s_α, F_i and G_i are the body forces associated to s_α, π_i is the vector field characterizing the mechanical interaction between the constituents s_1 and s_2, and, finally, u_i and w_i represent the displacement vector fields associated with the constituents s_1 and s_2, respectively. To obtain the governing equations of motion, we proceed as in previous sections, we get

$$\begin{aligned}
\rho\ddot{u}_i &= A_{jikl}e_{kl,j} + B_{jikl}\mathrm{g}_{kl,j} - \alpha_{ij}d_j \\
&\quad + a_{ji}\theta_{,j} + b_{ji}C_{,j} + \rho_1^0 F_i \\
\rho\,\ddot{w}_i &= B_{klij}e_{kl,j} + C_{ijkl}\mathrm{g}_{kl,j} + \alpha_{ij}d_j \\
&\quad + c_{ji}\theta_{,j} + d_{ji}C_{,j} + \rho_2^0 G_i \\
\rho c_E\dot{\theta} &= \kappa_{ij}\theta_{,ij} + T_0 a_{ij}\,\dot{e}_{ij} + T_0 c_{ij}\,\dot{\mathrm{g}}_{ij} - \varpi T_0\dot{C} + \rho h, \\
\dot{C} &= d_{ij}(b_{ij}e_{ij} + d_{ij}\mathrm{g}_{ij} - \varpi\theta + \varrho C)_{,ij} + r
\end{aligned} \tag{44}$$

For isotropic solids, we have

$$
\begin{aligned}
A_{ijkl} &= \lambda_1\delta_{ij}\delta_{kl} + (\mu_1 + \kappa_1)\delta_{ik}\delta_{jl} + \mu_1\delta_{il}\delta_{jk}\\
C_{ijkl} &= \lambda_2\delta_{ij}\delta_{kl} + (\mu_2 + \kappa_2)\delta_{ik}\delta_{jl} + \mu_2\delta_{il}\delta_{jk}\\
B_{ijkl} &= \nu\delta_{ij}\,\delta_{kl} + \xi\delta_{ik}\,\delta_{jl} + \zeta\delta_{il}\delta_{jk},\quad \hbar_{ij} = \hbar\delta_{ij}\\
\alpha_{ij} &= \alpha\delta_{ij}\quad a_{ij} = -\beta_1\delta_{ij}\quad b_{ij} = -\beta_2\delta_{ij}\\
c_{ij} &= -\beta_3\delta_{ij}\quad d_{ij} = -\beta_4\delta_{ij}\quad \kappa_{ij} = \kappa\delta_{ij}
\end{aligned}
$$

The constitutive equations reduce to

$$
\begin{aligned}
t_{ij} &= \lambda_1 e_{kk}\delta_{ij} + (\mu_1 + \kappa_1)e_{ij} + \mu_1 e_{ji} + \nu \mathrm{g}_{rr}\delta_{ij}\\
&\quad + \xi \mathrm{g}_{ij} + \zeta \mathrm{g}_{ji} - \beta_1\theta\delta_{ij} - \beta_2 C\delta_{ij}\\
s_{ij} &= \nu e_{kk}\delta_{ij} + \xi e_{ij} + \zeta e_{ji} + \lambda_2 \mathrm{g}_{rr}\delta_{ij}\\
&\quad + (\mu_2 + \kappa_2)\mathrm{g}_{ij} + \mu_2 \mathrm{g}_{ji} - \beta_3\theta\delta_{ij} - \beta_4 C\delta_{ij}\\
\pi_i &= \alpha d_i\\
\rho_0 S &= \beta_1 e_{kk} + \beta_3 \mathrm{g}_{kk} + \frac{\rho_0 c_E}{T_0}\theta + \varpi C\\
P &= -\beta_2 e_{kk} - \beta_4 \mathrm{g}_{kk} - \varpi\theta + \varrho C
\end{aligned}
$$

By substituting the last system into (44), we obtain the governing equations of the linear theory of thermoelastic diffusion mixture for isotropic materials.

By using the relations (15) and (16) instead of (5) and (8), respectively, in the system (44), one can get the governing equations of the generalized thermoelastic diffusion mixture theory under Lord-Shulman model

$$
\begin{aligned}
\rho\,\ddot{u}_i &= A_{jikl}e_{kl,j} + B_{jikl}\mathrm{g}_{kl,j} - \alpha_{ij}d_j\\
&\quad + a_{ji}\theta_{,j} + b_{ji}C_{,j} + \rho_1^0 F_i\\
\rho\,\ddot{w}_i &= B_{klij}e_{kl,j} + C_{ijkl}\mathrm{g}_{kl,j} + \alpha_{ij}d_j\\
&\quad + c_{ji}\theta_{,j} + d_{ji}C_{,j} + \rho_2^0 G_i\\
\kappa_{ij}\theta_{,ij} &= \rho c_E(\dot{\theta} + \tau_0\ddot{\theta}) - a_{ij}T_0(\dot{e}_{ij} + \tau_0\,\ddot{e}_{ij})\\
&\quad - c_{ij}T_0(\dot{\mathrm{g}}_{ij} + \tau_0\,\ddot{\mathrm{g}}_{ij}) + \varpi T_0(\dot{C} + \tau_0\ddot{C})\\
&\quad - \rho(h + \tau_0\dot{h})\\
d_{ij}\varrho C_{,ij} &= \dot{C} + \tau\ddot{C} - d_{ij}(b_{ij}e_{ij} + d_{ij}\mathrm{g}_{ij} - \varpi\theta)_{,ij}\\
&\quad - (r + \tau\dot{r})
\end{aligned}
\tag{45}
$$

References

1. Olesiak ZS (1998) Problems of thermodiffusion of deformable solids. Mater Sci 34:297–303
2. Sherief HH, Hamza F, Saleh H (2004) The theory of generalized thermoelastic diffusion. Int J Eng Sci 42:591–608
3. Pidstryhach Ya S (1961) Differential equations of the problem of thermodiffusion in isotropic deformed solid bodies. Dop Akad Nauk Ukr SSR. 169–172
4. Nowacki W (1974) Dynamical problems of thermoelastic diffusion in solids. I. Bull Acad Pol Sci Ser Sci Tech 22:55–64, 129–135, 257–266
5. Hetnarski RB, Ignaczak J (1999) Generalized thermoelasticity. J Therm Stress 22:451–476
6. Lord H, Shulman Y (1967) A generalized dynamical theory of thermoelasticity. J Mech Phys Solid 15:299–309
7. Cattaneo C (1948) Sulla conduzione del calore. Atti Sem Mat Fis Univ Modena 3:83–101
8. Green AE, Lindsay KA (1972) Thermoelasticity. J Elast 2:1–7
9. Rajneesh K, Tarun K (2008) Propagation of Lamb waves in transversely isotropic thermoelastic diffusive plate. I. J Solids Struct 45:5890–5913
10. Eringen AC (1966) Linear theory of micropolar elasticity. J Math Mech 15:909–923
11. Tauchert TR, Jr C, Ariman T (1968) The linear theory of micropolar thermoelasticity. Int J Eng Sci 6:36–47
12. Aouadi M (2009) The coupled theory of micropolar thermoelastic diffusion. Acta Mech 208:181–203
13. Aouadi M (2009) Theory of generalized micropolar thermoelastic diffusion under Lord-Shulman model. J Therm Stress 32:923–942
14. Goodmann MA, Cowin SC (1972) A continuum theory for granular materials. Arch Ration Mech Anal 44:249–266
15. Cowin SC, Goodmann MA (1979) A nonlinear theory of elastic materials with voids. Arch Ration Mech Anal 72:175–201
16. Capriz G (1989) Continua with microstructure. In: Truesdell CA (ed) Springer tracts in natural philosophy, vol 35. Springer, Berlin
17. Ieşan D (1986) A theory of thermoelastic materials with voids. Acta Mech 60:67–89
18. Aouadi M (2010) A theory of thermoelastic diffusion materials with voids. Z Angew Math Phys 61:357–379
19. Singh B (2011) On the generalized thermoelastic solids with voids and diffusion. Eur J Mech A/Solids 30:976–982
20. Truesdell C, Toupin R (1960) The classical field theories. In: Flügge S (ed) Handbuch der Physik, vol III/3. Springer, Berlin
21. Kelly P (1964) A reacting continuum. Int J Eng Sci 2:129–153
22. Bedford A, Stern M (1972) A multi-continuum theory for composite elastic materials. Acta Mech 14:85–102

23. Bedford A, Stern M (1972) Towards a diffusing continuum theory of composite elastic materials. J Appl Mech 38:8–14
24. Ieşan D (1991) On the theory of mixtures of thermoelastic solids. J Therm Stress 14:389–408
25. Aouadi M (2010) Qualitative results in the theory of thermoelastic diffusion mixtures. J Therm Stress 33:595–615

Classical Coupled Thermoelasticity in Unbounded Domains

Remigio Russo
Department of Mathematics and Physics, Second University of Naples, Caserta, Italy

Synonyms

Coupled thermoelasticity

Overview

The purpose of this entry is to give a review of the main results concerning the system of linear coupled thermoelastodynamics in unbounded domains. In contrast with what happens in linear elastodynamics, where the hyperbolicity condition on the acoustic tensor [4] assures that the main properties of the motion of an elastic body usually stated for bounded domains, like uniqueness of the initial boundary value problem, can be extended to unbounded domain; a well-known counterexample of Tykhonov [20] about uniqueness of the solution to the Cauchy problem for the heat equation shows that this is not possible. It is necessary to require that the solution cannot grow at infinity *more rapidly* than the fundamental solution. So a condition on the temperature difference θ, like $\theta(x) = O(e^{r^2})$, should be sufficient. Actually, we show that this is thus. Indeed, we define a function class $\mathfrak{F}$ of solutions to the equations of linear thermoelastodynamics defined by a condition on θ similar to that founded by Tykhonov, and we show that for solutions in $\mathfrak{F}$, the most important properties of solutions holding in bounded domains, like the work energy theorem, uniqueness, Graffi's reciprocity relation, and the time decay to zero at infinity of the temperature difference field, can be extended to the unbounded ones. Moreover, in the last section we discuss the possibility to justify the application of a generalized Saint–Venant's principle in thermoelasticty.

Notation – We essentially follow the notation of [8, 9]. $\mathbb{N}$ and $\mathbb{R}$ denote the sets of natural and real numbers, respectively. A domain Ω is an open connected set of $\mathbb{R}^3$. $S_R = \{x \in \mathbb{R}^3 : |x - o| < R\}$, $\Omega_R = \Omega \cap S_R$, where o is the origin of the coordinate system, $r = |x - o|$, $\mathbf{x} = x - o = r\mathbf{e}_r$. $L^q(\Omega)$ $(p \geq 1)$ is the Lebesgue space endowed with its natural norm; if $\mathbf{u}$ is a regular vector field, $\hat{\nabla}\mathbf{u}$ denotes the symmetric part of $\nabla\mathbf{u}$. As is usual, if $\varphi(x)$ and $\psi(r)$ are functions defined in an unbounded domain, the symbols $\psi(x) = o(\varphi(r))$ and $\psi(x) = O(\varphi(r))$ mean, respectively, that $\lim_{|x|\to\infty} \psi(x)/\varphi(r) = 0$ and $|\psi(x)| \leq c\varphi(r)$, for large r. Finally, unless otherwise stated, c stands for a positive constant whose value is not essential for our aims; its numerical value may change, e.g., in a same line.

The System of Linear Thermoelastodynamics

Let $\mathcal{B}$ be a linearly heat-conducting elastic body, identified with an unbounded domain Ω of $\mathbb{R}^3$; it occupies in an assigned stress-free reference configuration. Let us assign the following fields expressing the material properties of $\mathcal{B}$ [5]: the *mass density* $\rho : \Omega \times (0, +\infty)$; the *elasticity tensor*, *i.e*, a map $\mathbf{C} : \Omega \times \mathrm{Lin} \to \mathrm{Sym}$, linear on Lin, such that $\mathbf{C}[\mathbf{W}] = \mathbf{0}$ for all $\mathbf{W} \in \mathrm{Skw}$ and $\mathbf{E} \cdot \mathbf{C}[\mathbf{L}] = \mathbf{L} \cdot \mathbf{C}[\mathbf{E}]$ for all $\mathbf{E}, \mathbf{L} \in \mathrm{Lin}$; a *reference temperature* Θ_0; the *specific heat* $c_e : \Omega \to (0, +\infty)$; the *conductivity tensor* $\mathbf{K} : \Omega \to \mathrm{Sym}$; and the *stress–temperature tensor* $\mathbf{M} : \Omega \to \mathrm{Sym}$.

Let $\pi[\mathbf{E}] = \mathbf{E}\cdot\mathbf{C}[\mathbf{E}]$, $\gamma[\mathbf{a}] = \mathbf{a}\cdot\mathbf{K}\mathbf{a}$. Let us assume that c_e is bounded and

- $\mathbf{C}$ is positive semi-definite, i.e., $\pi[\mathbf{E}] \geq 0$, $\forall \mathbf{E} \in \mathrm{Lin}$
- $\mathbf{K}$ is bounded and positive semi-definite, i.e., $0 \leq \gamma[\mathbf{a}] \leq c|\mathbf{a}|^2$, $\forall \mathbf{a} \in \mathbb{R}^3$.

Note that the above properties and the symmetry of $\mathbf{C}$ and $\mathbf{K}$ assure the following inequalities:

$$\begin{aligned} 2\mathbf{E}\cdot\mathbf{C}[\mathbf{F}] &\leq \xi\pi[\mathbf{E}] + \xi^{-1}\pi[\mathbf{F}], \quad \forall\, \mathbf{E},\mathbf{F} \in \mathrm{Lin}, \\ 2\mathbf{a}\cdot\mathbf{K}[\mathbf{b}] &\leq \xi\gamma[\mathbf{a}] + \xi^{-1}\gamma[\mathbf{b}], \quad \forall\, \mathbf{a},\mathbf{b} \in \mathbb{R}^3 \end{aligned} \tag{1}$$

for all $\xi > 0$.

Let $\mathbf{n}$ be the unit outward (with respect to Ω) to $\partial\Omega$ and denote by $\{\partial_1\Omega, \partial_2\Omega\}$ and $\{\partial_3\Omega, \partial_4\Omega\}$ two partitions of $\partial\Omega$. Let $\mathbf{u}_0$, $\dot{\mathbf{u}}_0$, and θ_0 be three assigned fields in Ω. The *mixed problem of the dynamical theory of thermoelasticity* is to find a pair $\mathbf{u}$ (displacement field) and θ (temperature difference field) that satisfies the equations [5]:

$$\begin{aligned} \rho\ddot{\mathbf{u}} - \mathrm{div}\,\mathbf{C}[\nabla\mathbf{u}] - \mathrm{div}\,(\theta\mathbf{M}) &= \mathbf{0} \quad \text{in } \Omega\times[0,+\infty), \\ \rho\dot{\theta} - \mathrm{div}\,(\mathbf{K}\nabla\theta) - \Theta_0\mathbf{M}\cdot\hat{\nabla}\dot{\mathbf{u}} &= 0 \quad \text{in } \Omega\times[0,+\infty), \\ \mathbf{u} &= \mathbf{0} \quad \text{on } \partial_1\Omega\times[0,+\infty), \\ (\mathbf{C}[\nabla\mathbf{u}] + \theta\mathbf{M})\mathbf{n} &= \mathbf{0} \quad \text{on } \partial_2\Omega\times[0,+\infty), \\ \theta &= 0 \quad \text{on } \partial_3\Omega\times[0,+\infty), \\ -(\mathbf{K}\nabla\theta)\mathbf{n} &= \mathbf{0} \quad \text{on } \partial_4\Omega\times[0,+\infty) \\ \mathbf{u} = \mathbf{u}_0,\ \dot{\mathbf{u}} = \dot{\mathbf{u}}_0 \quad \theta &= \theta_0 \quad \text{in } \Omega\times\{0\} \end{aligned} \tag{2}$$

Only for the sake of simplicity we assume homogeneous boundary data and zero body force. The extension of the results we derive to solutions of system (2) for nonhomogeneous data is immediate under suitable summability assumptions on them. Our aim is to find conditions on the material data assuring that a solution to (2) satisfies in a sharp function class $\mathfrak{F}$ the classical properties holding for solutions in bounded domains, like the work and energy theorem, Graffi's reciprocity relation, uniqueness [5], and the time decay to zero at infinity of the temperature difference field. Moreover, we aim at showing that a solution in $\mathfrak{F}$ decays at large spatial distance according to a generalized Saint–Venant's principle.

- Only for the sake of simplicity, through the entry we shall assume that Ω, the material data and $\mathbf{u}_0$, $\dot{\mathbf{u}}_0$, and θ_0 are of class C^∞, and we shall consider solutions $\mathbf{u}$, θ to (2) of class C^∞ in $\overline{\Omega}\times[0,+\infty)$.

The Hyperbolicity Condition and a Sharp Function Class

The *acoustic tensor* for the direction $\mathbf{m}$ ($|\mathbf{m}| = 1$) is defined by [8]

$$\mathbf{A}(x,\mathbf{m})\mathbf{a} = \rho^{-1}\mathbf{C}[\mathbf{a}\otimes\mathbf{m}]\mathbf{m}, \quad \forall\, \mathbf{a}.$$

We say that the acoustic tensor satisfies the *hyperbolicity condition* if there is a regular, positive and unbounded function $p : (a,+\infty) \to (0,+\infty)$ $(a > 0)$, with $p' > 0$ and $p'' < 0$, such that

$$|\mathbf{A}(x,\mathbf{m})| \leq [p'(r)]^{-2}, \quad \forall\, r \tag{3}$$

Note that, choosing $p(r) = \underbrace{\log\ldots\log}_{k+1 \text{ times}} r$, (3) reads $|\mathbf{A}(x,\mathbf{m})| \leq [c_1 r \underbrace{\log\ldots\log}_{k \text{ times}} r]^2$ The importance of this assumption in the isothermal case ($\theta = 0$) has been discussed in [16] (see also [4]). Roughly speaking, it assures that a signal traveling in $\mathcal{B}$ cannot reach the infinity in a finite time.

Since (2) reduces to the initial-boundary value problem for the heat equation when the elastic body is kept at rest, we cannot expect uniqueness of solution to (2) without making any assumption at infinity on the (difference) temperature field θ. Indeed, a celebrated counterexample of Tykhonov [20] (see also [6, 18]) shows that in the function class

$$\{\theta(x,t) : \theta(x,t) = O(e^{r^{2+\epsilon}}), \quad \text{for some } \epsilon > 0\},$$

the Cauchy problem for the heat equation

$$\dot{\theta} - \Delta\theta = 0 \text{ in } \mathbb{R} \times [0, +\infty)$$
$$\theta = 0 \text{ in } \mathbb{R} \times \{0\}$$

has a solution which does not identically vanish. Hence, it follows that in order to get qualitative properties of thermoelastic solutions analogous to that derived in the isothermal case, we have to define a function class where the difference temperature θ cannot grow at infinity as $e^{r^{2+\epsilon}}$, for some $\epsilon > 0$. To this end, consider the function p in (3) and set

$$R_t = \bar{p}^{-1}(p(R) + c_0 t) \tag{4}$$

for some positive c_0. We denote by $\mathfrak{F}$ the set of (regular) solutions $(\mathbf{u}, \theta)$ to system (2) such that $\nabla\theta$ satisfies for some positive κ, $\bar{R}$, the *growth condition*

$$\int_0^t ds \int_{\Omega_{R_{t-s}}} \gamma[\nabla\theta] dv = o\left(\exp\left[\int_{\bar{R}}^R (\kappa(p'(\xi))^{-1} d\xi\right]\right) \tag{5}$$

Remark 1. If we choose $p(r) = \log r$, then (5) reads

$$\int_0^t ds \int_{\Omega_{R_t}} \gamma[\nabla\theta] dv = o(e^{R^2})$$

so that, in particular, $\mathfrak{F}$ contains the set of all couple $(\mathbf{u}, \theta)$ such that $\gamma[\nabla\theta] = o(e^{r^2}/r^3)$. Other *good* functions p are $\underbrace{\log \ldots \log}_{k+1 \text{ times}} r$.

Let $(\mathbf{u}, \theta)$ be a solution to (2). We set

$$\eta[\mathbf{u}](x,t) = \frac{1}{2}\left(\rho|\dot{\mathbf{u}}|^2 + \pi[\nabla\mathbf{u}]\right)(x,t)$$
$$\varepsilon[\mathbf{u},\theta](x,t) = \eta[\mathbf{u}] + \frac{1}{2}c_e\Theta_0^{-1}\theta^2(x,t)$$

The Work and Energy Theorem

In this section, we extend to unbounded domains the classical work and energy theorem usually stated for bounded regions [5]. Beyond its intrinsic interest, it provides the main tool in establishing the results of the next sections.

Theorem 1. [15] *Let* $\mathbf{A}$ *and* $\mathbf{M}$ *satisfy* (3) *and*

$$\Theta_0(c_e\rho)^{-1}|\mathbf{M}(x)|^2 \le [p'(r)]^{-2}, \quad \forall r \tag{6}$$

If $(\mathbf{u}, \theta) \in \mathfrak{F}$ *and* $\varepsilon[\mathbf{u},\theta](x,0) \in L^1(\Omega)$, *then*

$$\int_\Omega \varepsilon[\mathbf{u},\theta](x,t)dv + \Theta_0^{-1}\int_0^t ds \int_\Omega \gamma[\nabla\theta](x,s)dv = \int_\Omega \varepsilon[\mathbf{u},\theta](x,0)dv \tag{7}$$

Proof. Let w be a regular, nondecreasing function in $\mathbb{R}$, equal to 1 in $[1, +\infty)$, vanishing in $(-\infty,0)$ and let

$$g(r,s) = w(\delta^{-1}(p(R) + c_0(t-s) - p(r))) \tag{8}$$

with $0 < \delta < p(R)$. Of course,

$$\dot{g} = -\delta^{-1}c_0 w', \quad \nabla g = -\delta^{-1}w'p'(r)\mathbf{e}_r \tag{9}$$

The support of g at instant s is the ball $S_{\bar{p}^{-1}(p(R+c(t-s)))}$, and g is equal to 1 in $S_{\bar{p}^{-1}(p(R+c(t-s))-\delta)}$.

Multiply $(2)_1$ scalarly by $g\dot{\mathbf{u}}$ and $(2)_2$ by $g\Theta_0^{-1}\theta$, respectively. Then an integration by parts yields

$$\frac{d}{ds}\int_\Omega (g\varepsilon[\mathbf{u},\theta])(x,s)dv + \Theta_0^{-1}\int_\Omega g\gamma[\nabla\theta](x,s)dv = \int_\Omega \dot{g}\varepsilon[\mathbf{u},\theta](x,s)dv - \int_\Omega \dot{\mathbf{u}}\cdot\{(\mathbf{C}[\nabla\mathbf{u}] + \theta\mathbf{M})\nabla g + \Theta_0^{-1}\theta\nabla g\cdot\mathbf{K}\nabla\theta\}(x,s)dv \tag{10}$$

By (1) and (8), we have

$$\begin{aligned}
2|\dot{\mathbf{u}}\cdot\mathbf{C}[\nabla\mathbf{u}]\nabla g| &= 2\delta^{-1}w'p'(r)\dot{\mathbf{u}}\cdot\mathbf{C}[\nabla\mathbf{u}]\mathbf{e}_r| \\
&\le \delta^{-1}w'(|p'(r)|^2\dot{\mathbf{u}}\cdot\mathbf{C}[\dot{\mathbf{u}}\otimes\mathbf{e}_r]\mathbf{e}_r + \pi[\nabla\mathbf{u}]) \\
&\le 2\delta^{-1}w'\eta[\mathbf{u}], 2|\theta\dot{\mathbf{u}}\cdot\mathbf{M}\nabla g| \\
&\le \delta^{-1}w'\left\{c_e\Theta_0^{-1}\theta^2 + c_e^{-1}\Theta_0(p'(r)|\dot{\mathbf{u}}||\mathbf{M}|)^2\right\} \\
&\le 2\delta^{-1}w'\varepsilon[\mathbf{u},\theta], |\Theta_0^{-1}\theta\nabla g\cdot\mathbf{K}\nabla\theta| \\
&\le \delta^{-1}w'\left\{\varepsilon[\mathbf{u},\theta] + \kappa\Theta_0^{-1}|p'(r)|^2\gamma[\nabla\theta]\right\}
\end{aligned} \tag{11}$$

for some positive constant κ. Therefore, choosing c_0 sufficiently large, (10) implies

$$\begin{aligned}
&\int_\Omega (g\varepsilon[\mathbf{u},\theta])(x,t)dv \\
&\quad + \Theta_0^{-1}\int_0^t ds\int_\Omega g\gamma[\nabla\theta](x,s)dv \le \int_\Omega g\varepsilon[\mathbf{u},\theta](x,0)dv \\
&\quad + (\delta\Theta_0)^{-1}\kappa\int_0^t ds\int_\Omega |p'(r)|^2\gamma[\nabla\theta](x,s)dv
\end{aligned} \tag{12}$$

By the properties of (8), we can let $\delta\to 0$ in (12) to have (see [15] for the details)

$$\begin{aligned}
&\int_{\Omega_R}\varepsilon[\mathbf{u},\theta](x,t)dv \\
&\quad + \Theta_0^{-1}\int_0^t ds\int_{\Omega_{R_{t-s}}}\gamma[\nabla\theta](x,s)dv \le \int_\Omega \varepsilon[\mathbf{u},\theta](x,0)dv \\
&\quad + \kappa\Theta_0^{-1}\int_0^t ds\int_{\Omega\cap S_{R_{t-s}}} p'(r)\gamma[\nabla\theta](x,s)da
\end{aligned} \tag{13}$$

Starting from estimate (13), let us show that the LHS of (13) is dominated uniformly on R by the initial energy. Indeed, if *per absurdum* this were not true, it should exist $\bar{R}$ such that

$$\begin{aligned}
G(R) &= \int_0^t ds\int_{\Omega_{R_{t-s}}}\gamma[\nabla\theta](x,s)dv \\
&\le \kappa\int_0^t ds\int_{\Omega\cap S_{R_{t-s}}} p'(r)\gamma[\nabla\theta](x,s)da
\end{aligned} \tag{14}$$

for $R>\bar{R}$. By the basic calculus

$$G'(R) = \int_0^t ds\int_{\Omega\cap S_{R_{t-s}}}[p'(R)/p'(R_{t-s}]\gamma[\nabla\theta](x,s)da$$

and by the properties of p,

$$p'(R_{t-s}) \le p'(R)]^2/p'(R_{t-s})$$

Therefore, (14) implies

$$G(R)\le \kappa p'(R)G'(R)$$

Hence, by a simple integration,

$$G(R)\ge G(\bar{R})\exp\left[\int_{\mathrm{R}}^{\mathrm{R}}(\kappa \mathrm{p}'(\mathrm{r})^{-1}\mathrm{d}\xi\right]$$

Since this contradicts (5), we conclude that

$$\int_{\Omega_R}\varepsilon[\mathbf{u},\theta](x,t)dv \le \int_\Omega \varepsilon[\mathbf{u},\theta](x,0)dv$$

By an analogous argument, we see that

$$\int_0^t ds\int_{\Omega_{R_{t-s}}}\gamma[\nabla\theta](x,s)dv \le \int_\Omega \varepsilon[\mathbf{u},\theta](x,0)dv$$

Thus,

$$\begin{aligned}
&\int_\Omega \varepsilon[\mathbf{u},\theta](x,t)dv \\
&\quad + \Theta_0^{-1}\int_0^t ds\int_\Omega \gamma[\nabla\theta](x,s)dv \le \int_\Omega \varepsilon[\mathbf{u},\theta](x,0)dv
\end{aligned} \tag{15}$$

Consider now (10) with $c_0=0$ and integrate over $(0,t)$. Then

$$\begin{aligned}
&\int_\Omega (g\varepsilon[\mathbf{u},\theta])(x,t)dv + \Theta_0^{-1}\int_\Omega g\gamma[\nabla\theta](x,s)dv \\
&\quad = \int_\Omega g\varepsilon[\mathbf{u},\theta](x,0)dv - \int_0^t ds\int_\Omega \dot{\mathbf{u}}\cdot\{(\mathbf{C}[\nabla\mathbf{u}] + \theta\mathbf{M})\nabla g \\
&\qquad + \Theta_0^{-1}\theta\nabla g\cdot\mathbf{K}\nabla\theta\}(x,s)dv
\end{aligned} \tag{16}$$

Since by (11)

$$\left|\int_\Omega \dot{\mathbf{u}}\cdot\{(\mathbf{C}[\nabla\mathbf{u}]+\theta\mathbf{M})\nabla g+\Theta_0^{-1}\theta\nabla g\cdot\mathbf{K}\nabla\theta\}(x,s)dv\right| \le c\int_0^t\int_{\Omega_{R_{t-s}}\setminus\Omega_{R_{t-s-\delta/c_0}}}\{\varepsilon[\mathbf{u},\theta]+\gamma[\nabla\theta]\}(x,s)dv,$$

by (15), we can let $R\to+\infty$ in (16) to get (4).

Uniqueness, Graffi's Reciprocity Relation, and Time Decay of the Temperature Difference

As a simple consequence of (7), we prove now two classical properties of linear thermoelasticity [3, 15].

Theorem 2. *Under the hypotheses of theorem 1, system* (2) *has at most one solution in the class* $\mathfrak{F}$.

Proof. If $(\mathbf{u}_1,\theta_1)$ and $(\mathbf{u}_2,\theta_2)$ are two solutions to (2), from (7) it follows that the pair $(\mathbf{u}=\mathbf{u}_1-\mathbf{u}_2,\theta=\theta_1-\theta_2)$ satisfies

$$\int_\Omega \varepsilon[\mathbf{u},\theta](x,t)dv+\Theta_0^{-1}\int_0^t ds\int_\Omega\gamma[\nabla\theta](x,s)dv=0 \tag{17}$$

By the positive semi-definiteness of $\mathbf{C}$ and $\mathbf{K}$, (17) implies

$$\int_\Omega[\rho|\dot{\mathbf{u}}|^2+c_e\Theta_0^{-1}\theta^2](x,t)dv\le 0$$

Hence, the desired result follows, taking into account that $\mathbf{u}(x,0)=0,\dot{\mathbf{u}}(x,0)=0,\theta(x,0)=0$, and that $\rho>0, c_e>0$.

Theorem 3. *Let the hypotheses of theorem 1 be satisfied. Let* $(\mathbf{u},\theta)$ *and* $\left(\tilde{\mathbf{u}},\tilde{\theta}\right)\in\mathfrak{F}$ *correspond to initial data* $(2)_7$ *and* $\tilde{\mathbf{u}}_0$, $\dot{\tilde{\mathbf{u}}}_0$, *and* $\tilde{\theta}_0$. *If* $\varepsilon[\mathbf{u},\theta](x,0)$, $\varepsilon[\tilde{\mathbf{u}},\tilde{\theta}](x,0)$, $\rho|\mathbf{u}_0|^2$, $\rho|\tilde{\mathbf{u}}_0|^2$, $c_e^{-1}\mathbf{M}\cdot\hat{\nabla}\mathbf{u}_0$, *and* $c_e^{-1}\mathbf{M}\cdot\hat{\nabla}\tilde{\mathbf{u}}_0\in L^1(\Omega)$, *then*

$$\begin{aligned}&\int_\Omega\rho[\mathbf{u}_0(x)\cdot\dot{\tilde{\mathbf{u}}}(x,t)+\dot{\mathbf{u}}_0(x)\cdot\tilde{\mathbf{u}}(x,t)]dv\\&+\int_\Omega(c_e\theta_0+\Theta_0\mathbf{M}\cdot\hat{\nabla}\mathbf{u}_0)(x)\tilde{\theta}(x,t)dv\\&=\int_\Omega\rho[\tilde{\mathbf{u}}_0(x)\cdot\dot{\mathbf{u}}(x,t)+\dot{\tilde{\mathbf{u}}}_0(x)\cdot\mathbf{u}(x,t)]dv\\&+\int_\Omega(c_e\tilde{\theta}_0+\Theta_0\mathbf{M}\cdot\hat{\nabla}\tilde{\mathbf{u}}_0)(x)\theta(x,t)dv\end{aligned}$$

The proof of theorem 3 is obtained by integrating by parts and using the methods we outlined in the proof of theorem 1 (see [2] and [15] for the details).

It is well known that the solution to a homogeneous parabolic equation in an unbounded domain decays to zero as $t\to+\infty$. The following theorem shows that, under reasonable assumptions on the initial data, the temperature difference field θ of any thermoelastic solutions $(u,\theta)\in\mathfrak{F}$ such that $\left(\dot{\mathbf{u}},\dot{\theta}\right)\in\mathfrak{F}$ tends to zero in a suitable sense at long time. In physical terms, from this property we infer that the thermoelastic solution tends, as $t\to+\infty$, to the (purely elastic) solution to the system obtained from (2) by setting $\theta=0$. Let us note that this result, proved in a very elementary way, extends to unbounded domain in a well-known result of Slemrod and Infante [17].

Theorem 4. [15] *Let the hypotheses of theorem 1 be satisfied. If* $(\mathbf{u},\theta)$, $(\dot{\mathbf{u}},\theta)\in\mathfrak{F}$ *and* $\varepsilon[\mathbf{u},\theta](x,0)$, $\varepsilon[\dot{\mathbf{u}},\dot{\theta}](x,0)\in L^1(\Omega)$, *then*

$$\lim_{t\to+\infty}\int_\Omega\gamma[\nabla\theta](x,t)dv=0 \tag{18}$$

Moreover, if $\mathbf{K}$ *is positive definite and* $\partial_3\Omega\neq\emptyset$, *then for large* R

$$\lim_{t\to+\infty}\int_{\Omega_R}\theta^2(x,t)dv=0 \tag{19}$$

Proof. By our hypotheses and (7) $\gamma[\nabla\theta]$, $\gamma[\nabla\dot{\theta}]\in L^1(\Omega\times(0,+\infty))$. Hence, it follows

that there is a sequence t_k such that $\gamma[\nabla\theta](x,t_k) \in L^1(\Omega)$ and $\lim_{k\to+\infty} \int_\Omega \gamma[\nabla\theta](x,t_k)dv = 0$. From the relation

$$\int_{\Omega_R} \gamma[\nabla\theta](x,t)dv = \int_{t_k}^{t} \left(\frac{d}{ds}\int_{\Omega_R} \gamma[\nabla\theta](x,s)dv\right)ds + \int_{\Omega_R} \gamma[\nabla\theta](x,t_k)dv = 2\int_{t_k}^{t} ds \int_{\Omega_R} (\nabla\dot{\theta})\cdot\mathbf{K}(\nabla\theta)dv + \int_{\Omega_R} \gamma[\nabla\theta](x,t_k)dv$$

by $(1)_2$, we have

$$\int_{\Omega_R} \gamma[\nabla\theta](x,t)dv \le c\left\{\int_{t_k}^{+\infty} ds \int_{\Omega} \left(\gamma[\nabla\theta] + \gamma[\nabla\dot{\theta}]\right)(x,t)dv\right\} + \int_{\Omega} \gamma[\nabla\theta](x,t_k)dv$$

Hence, letting first $R \to +\infty$, then $t \to +\infty$, it follows (18). Finally, (19) follows from (18) and the Poincaré inequality

$$\int_{\Omega_R} \theta^2(x,t)dv \le c(R)\int_{\Omega_R} |\nabla\theta|^2(x,t)dv$$

Saint–Venant's Generalized Principle

As is well known, the so-called Saint–Venant's principle of classical elastostatics is a conjecture about the stress distribution in a right, linearly elastic cylinder $\mathcal{C}$ loaded on the bases, where the ratio between the diameter of the section and the length of $\mathcal{C}$ is very small. In short, if the lateral surface is assumed to be force-free and both the tractions $\mathbf{s}$ over the bases are assumed to be – as force systems – statically equivalent to zero, the principle suggests to neglect the stress at the points of $\mathcal{C}$ that are *sufficiently far* from the bases. Accordingly, in the study of the equilibrium of $\mathcal{C}$, a solution corresponding to a surface traction distribution $\mathbf{s}$ may be replaced – at least at the interior points of $\mathcal{C}$ far from the bases – by another solution (the Saint–Venant's elementary solution, see, e.g., [7]), mathematically more manageable, corresponding to a load which vanishes on the lateral surface and is statically equivalent to $\mathbf{s}$ on each basis. It is readily understood that the criterion suggested by Saint–Venant's principle leads to a great simplification for the equilibrium problem concerning elastic bodies of a cylindrical shape. In the last 40 years, Saint–Venant's principle has been largely studied and justified by several deep researches originated by Toupin [15] (see also [7, 10]). As previous results about Saint–Venant's principle are concerned, we quote [8], p. 190. More recently, it has been realized that Saint–Venant's conjecture could be extended outside the frontiers of linear elastostatics. At a deeper glance, it should in fact be clear that such a conjecture suggests that, at least in the case of a linearly elastic cylinder, the answer is affirmative to the following question: *in a continuous system, can the effects of some particular data be neglected in region far from their supports?* In the dynamical context, this question takes a particularly interesting formulation, which will be called generalized Saint–Venant's principle: *in an evolutionary system, can the effects of a perturbation, initially confined in a bounded region, be neglected at large distance?* As far as dynamical perturbations in a purely elastic body are concerned, the answer to the above question is given by the domain of influence theorem [1, 4, 8]. Denoting by Σ the support of the data, at each instant t, the perturbation vanishes outside the envelops of the balls of radius R_t (see (4)) centered at the points of the support of $\overline{\Sigma}$. Quite different is the case of diffusion phenomena that obey equations of parabolic type – such as that of the heat conduction: it is well known that, though the thermal effects of spatially bounded heat source can be instantaneously acknowledged at any point of the space, nevertheless their *perceptibility* decays exponentially at large spatial distance. As a consequence, in the heat conduction, the thermal effects can be neglected with good approximation at points far from the heat source. In several papers, Oleinik and other authors (see, e.g., [10–15], and the

references therein) have extended the method of [19] and have applied the estimates thus obtained to the study of the asymptotic (in space and time) properties of solutions of elliptic and parabolic type. In particular, for these last ones, the generalized Saint–Venant's principle has been given an affirmative answer. In connection with this problem, this section essentially aims at providing that *thermal perturbations* in a thermoelastic body can be neglected at each point suitably far from the support of the data. Indeed, the following theorem holds true [15].

Theorem 5. *Let the hypotheses of theorem 1 be satisfied. If* $(\mathbf{u}, p) \in \mathfrak{F}$ *corresponds to initial data* $\mathbf{u}_0$, $\dot{\mathbf{u}}_0$, *and* θ_0 *with compact support in* $\overline{\Omega}$, *then there exists a positive* $\bar{R}$ *such that for all* $R > \bar{R}$

$$\int_{\mathcal{C}\Omega_{R_t}} \varepsilon[\mathbf{u}, \theta](x,t)dv + \Theta_0^{-1} \int_0^t ds \int_{\mathcal{C}\Omega_{R_s}} \gamma[\nabla\theta](x,s)dv \leq \exp\left[-\int_{\bar{R}}^{R} (\kappa p'(\xi))^{-1} d\xi\right] \int_{\Omega} \varepsilon[\mathbf{u}, \theta](x,0)dv \tag{20}$$

Proof. Consider the cutoff function

$$g(r,s) = w(\delta^{-1}(p(R) + c_0 s - p(r)))$$

and denote by f the above function with $c_0 = 0$. Then, repeating the steps in the proof of theorem (see [15] for the details), we arrive at

$$\int_{\mathcal{C}\Omega_{R_t}} \varepsilon[\mathbf{u}, \theta](x,t)dv + \Theta_0^{-1} \int_0^t ds \int_{\mathcal{C}\Omega_{R_s}} \gamma[\nabla\theta](x,s)dv \leq \kappa\Theta_0^{-1} \int_0^t ds \int_{\Omega \cap \partial S_{R_s}} \gamma[\nabla\theta](x,s)da$$

Hence, by the same argument used in the proof of theorem 1, we get (20).

References

1. Carbonaro B, Russo R (1984) Energy inequalities and the domain of influence theorem in classical elastodynamics. J Elasticity 14:163–174
2. Carbonaro B, Russo R (1985) On Graffi's reciprocal theorem in unbounded domains. J Elasticity 15:35–42
3. Carbonaro B, Russo R (1987) Uniqueness in linear coupled thermoelasticity. J Elasticity 17:85–91
4. Carbonaro B, Russo R (1991) Singularity problems in linear elastodynamics. Ann Scuola Norm Sup Pisa Classe di Scienze (4) 18: 103–133
5. Carlson DE (1972) Linear thermoelasticity. In: Truesedell C (ed) Handbuch der Physik, vol VIa/2. Springer, Berlin
6. Eidel'man SD (1969) Parabolic systems. North-Holland, Amsterdam
7. Fichera G (1979) Remarks on Saint–Venant's principle. Rend Mat Appl 12:181–200
8. Gurtin ME (1972) The linear theory of elasticity. In: Truesedell C (ed) Handbuch der Physik, vol VIa/2. Springer, Berlin
9. Hetnarski RB, Ignaczak J (2011) The mathematical theory of elasticity, 2nd edn. CRC Press, Boca Raton
10. Horgan CO (1996) Recent developments concerning Saint-Venant's principle: a second update. Appl Mech Rev 49:S101–S111
11. Iosifyan GA, Oleinik OA (1976) An analogue of the Saint-Venant principle for a second order elliptic equation, and the uniqueness of the solutions of boundary value problems in unbounded domains. Uspekhi Mat Nauk 31:261–262
12. Iosifyan GA, Oleinik OA (1977) Boundary value problems for second order elliptic equations in unbounded domains and Saint Venant's–principle. Ann Scuola Norm Sup Pisa (4) 4: 269–290
13. Oleinik OA (1979) Energetic estimates analogous to the Saint-Venant principle and their applications. Lectur Notes Math (Springer) 703:328–339
14. Russo R (1988) On generalized Saint–Venant's principle and time asymptotic behavior of solutions to a partial differential system of paparbolic type in unbounded domains. Bollettino UMI 2–B 23: 729–746
15. Russo R (1989) Classical coupled thermoelasticity in unbounded domains. J Elasticity 22:1–24
16. Russo R (2013) Linear elastodynamics in unbounded domains. In: Hetnarski R (ed) Encyclopedia of Thermal Stresses. Springer
17. Slemrod M, Infante EF (1969) An invariance principle for dynamical systems on Banach space: application to the general problem of thermoelastic stability. In: Instability of continuous systems, Iutam Symposium Herrenald
18. Täcklind S (1937) Sur les classes quasianalitiques de solutions des équations aux dériées partielles du type paraboliques. Nova Acte R Soc Sci Upsaliensis 4 (10)
19. Toupin R (1965) Saint Venant's principle. Arch Ration Mech Anal 18:83–96
20. Tykhonov AN (1935) Théorèmes d'unicité pour l'equation de la chaleur. Mat Sb 42:199–216

Classical Governing Equations for the Thermomechanical Analysis of Shells

Erasmo Carrera and Salvatore Brischetto
Department of Mechanical and Aerospace Engineering, Politecnico di Torino, Torino, Italy

Synonyms

Assumed linear temperature profile; Classical two-dimensional models; Kirchhoff hypotheses; Reissner-Mindlin hypotheses; Shell geometrical relations; Thermal stress analysis

Definition

Thermal stress analysis of multilayered shells is here proposed by using classical governing equations. Such equations are obtained from the extension of Kirchhoff model and Reissner-Mindlin model to laminated shells. The first extension gives the Classical Lamination Theory (CLT) for shell geometry; the second extension allows the First-Order Shear Deformation Theory (FSDT) to be written for the shell case. Such theories discard the thickness-stretching effect (zero transverse normal strain), and this feature suggests the uselessness of a calculated temperature profile for these models. A linear temperature profile is always considered, and it allows the main limitations of classical governing equations for the thermal stress analysis of multilayered shells to be pointed out.

Overview

The thermoelastic formulation of shells in terms of classical governing equations is a fundamental topic to investigate the effects of both high-temperature and mechanical loadings in the design process of multilayered shell structures [1]. Classical governing equations consider the temperature as an external load, and this last is defined by means of a linear assumed temperature profile through the thickness direction. The assumption of a linear temperature profile is a big limitation in the thermal stress analysis of multilayered shells, but it allows the importance of refined kinematics models to be pointed out in the case of multilayered composite structures (see the works by Brischetto and Carrera [1], Khare et al. [2], and Khdeir et al. [3]). A calculated temperature profile in thick and thin multilayered shells is fundamental for the correct definition of an opportune thermal load, and it must be used together with refined two-dimensional models to obtain a satisfactory thermal stress analysis of multilayered structures [4–7]. In the case of classical models, a linear temperature profile is employed because it is more coherent with the linear expansion of the in-plane displacement components and the constant transverse displacement assumption. This linear temperature profile remains for the quasi-3D solutions in order to better discuss the main limitations of classical theories in terms of kinematic assumptions.

Basic Methodology

The shell geometries considered have constant radii of curvature R_α and R_β as indicated in Fig. 1.

a and b are the shell dimensions, and h is the thickness value; the curvilinear reference system is indicated as (α, β, z).

Kirchhoff hypotheses [8] extended to multilayered structures give the Classical Lamination Theory (CLT); when the hypothesis of infinite transverse shear rigidity is removed (as suggested in Reissner-Mindlin hypotheses [9, 10]), a First-Order Shear Deformation Theory (FSDT) is considered for the laminated structure. Opportune geometrical relations must be written for the shell case in order to link the strains with the displacements, the constitutive equations consider both the mechanical and thermal contributions of the stress components. Constitutive equations, geometrical relations, and CLT or FSDT model must be introduced in the Principle

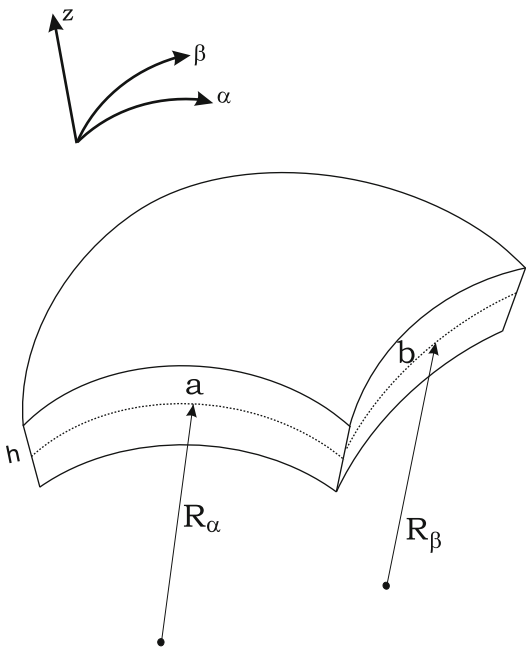

Classical Governing Equations for the Thermomechanical Analysis of Shells, Fig. 1 Geometry and reference system for a doubly curved shell

of Virtual Displacements (PVD) in order to obtain the classical governing equations for the thermal stress analysis of shells.

Classical Two-Dimensional Models and Geometrical Relations

First-Order Shear Deformation Theory (FSDT) is the extension of the Reissner-Mindlin hypotheses [9, 10] to multilayered structures, such hypotheses are:

- Straight lines that are perpendicular to the midsurface (i.e., transverse normals) before deformation remain straight after the deformation.
- The transverse normals do not experience elongation (i.e., they are inextensible).

These first two assumptions imply that the transverse displacement is independent of the transverse (or thickness) coordinate and the transverse normal strain ϵ_{zz} is zero. The displacement model and the temperature approximation in the case of shell geometry are:

$$\begin{aligned} u(\alpha,\beta,z) &= u_0(\alpha,\beta) + z\Phi_\alpha(\alpha,\beta),\\ v(\alpha,\beta,z) &= v_0(\alpha,\beta) + z\Phi_\beta(\alpha,\beta),\\ w(\alpha,\beta,z) &= w_0(\alpha,\beta),\\ \theta(\alpha,\beta,z) &= \theta_0(\alpha,\beta) + z\theta_1(\alpha,\beta) \end{aligned} \tag{1}$$

u_0, v_0, and w_0 are the midsurface displacements in the three directions α, β, and z, respectively. Φ_α and Φ_β are the two additional rotations typical of the Reissner-Mindlin model. The sovra-temperature $\theta = T - T_0$ (temperature T referred to the reference room temperature T_0) is imposed on the shell structure through the thickness, and it is given as linear by means of the mean value $\theta_0 = \frac{\theta_t+\theta_b}{2}$ and the slope $\theta_1 = \frac{\theta_t-\theta_b}{h}$. θ_t is the sovra-temperature imposed at the top of the shell, θ_b is the sovra-temperature imposed at the bottom of the shell, and h is the thickness of the structure considered.

In the case of FSDT model, the geometrical relations for shells are [11]:

$$\begin{aligned} \epsilon^k_{\alpha\alpha} &= \frac{1}{H^k_\alpha}\frac{\partial u}{\partial\alpha} + \frac{1}{H^k_\alpha R^k_\alpha} w\\ &= \frac{1}{H^k_\alpha}\frac{\partial u_0}{\partial\alpha} + \frac{z}{H^k_\alpha}\frac{\partial \Phi_\alpha}{\partial\alpha} + \frac{1}{H^k_\alpha R^k_\alpha} w_0\\ &= \left(\frac{1}{H^k_\alpha}\frac{\partial u_0}{\partial\alpha} + \frac{1}{H^k_\alpha R^k_\alpha} w_0\right)\\ &\quad + z\left(\frac{1}{H^k_\alpha}\frac{\partial \Phi_\alpha}{\partial\alpha}\right) \end{aligned} \tag{2}$$

$$\begin{aligned} \epsilon^k_{\beta\beta} &= \frac{1}{H^k_\beta}\frac{\partial v}{\partial\beta} + \frac{1}{H^k_\beta R^k_\beta} w\\ &= \frac{1}{H^k_\beta}\frac{\partial v_0}{\partial\beta} + \frac{z}{H^k_\beta}\frac{\partial \Phi_\beta}{\partial\beta} + \frac{1}{H^k_\beta R^k_\beta} w_0\\ &= \left(\frac{1}{H^k_\beta}\frac{\partial v_0}{\partial\beta} + \frac{1}{H^k_\beta R^k_\beta} w_0\right)\\ &\quad + z\left(\frac{1}{H^k_\beta}\frac{\partial \Phi_\beta}{\partial\beta}\right) \end{aligned} \tag{3}$$

$$\gamma^k_{\alpha\beta} = \frac{1}{H^k_\beta}\frac{\partial u}{\partial \beta} + \frac{1}{H^k_\alpha}\frac{\partial v}{\partial \alpha} = \frac{1}{H^k_\beta}\frac{\partial u_0}{\partial \beta} + \frac{z}{H^k_\beta}\frac{\partial \Phi_\alpha}{\partial \beta} + \frac{1}{H^k_\alpha}\frac{\partial v_0}{\partial \alpha} + \frac{z}{H^k_\alpha}\frac{\partial \Phi_\beta}{\partial \alpha} = \left(\frac{1}{H^k_\beta}\frac{\partial u_0}{\partial \beta} + \frac{1}{H^k_\alpha}\frac{\partial v_0}{\partial \alpha}\right) + z\left(\frac{1}{H^k_\beta}\frac{\partial \Phi_\alpha}{\partial \beta} + \frac{1}{H^k_\alpha}\frac{\partial \Phi_\beta}{\partial \alpha}\right) \tag{4}$$

$$\gamma^k_{\beta z} = \frac{1}{H^k_\beta}\frac{\partial w}{\partial \beta} + \frac{\partial v}{\partial z} - \frac{1}{H^k_\beta R^k_\beta} v = \left(\frac{1}{H^k_\beta}\frac{\partial w_0}{\partial \beta} + \Phi_\beta - \frac{1}{H^k_\beta R^k_\beta} v_0\right) - z\left(\frac{1}{H^k_\beta R^k_\beta}\Phi_\beta\right) \tag{5}$$

$$\gamma^k_{\alpha z} = \frac{1}{H^k_\alpha}\frac{\partial w}{\partial \alpha} + \frac{\partial u}{\partial z} - \frac{1}{H^k_\alpha R^k_\alpha} u = \left(\frac{1}{H^k_\alpha}\frac{\partial w_0}{\partial \alpha} + \Phi_\alpha - \frac{1}{H^k_\alpha R^k_\alpha} u_0\right) - z\left(\frac{1}{H^k_\alpha R^k_\alpha}\Phi_\alpha\right) \tag{6}$$

For shell geometries, even though the displacements are in Equivalent Single Layer form, the strain components depend by the k layer because of the curvature.

Classical Lamination Theory (CLT) is the extension of the Kirchhoff hypotheses [8] to multilayered structures; a third assumption is added to the two ones already considered by Reissner and Mindlin [9, 10]:

- The transverse normals rotate so that they remain perpendicular to the midsurface after the deformation.

This third assumption results in zero transverse shear strains $\gamma_{\alpha z} = \gamma_{\beta z} = 0$.

In order to obtain the kinematic model for CLT, we impose $\gamma_{\beta z} = \gamma_{\alpha z} = 0$ in (5) and (6). In this way, we obtain the relations for Φ_β and Φ_α [11]:

$$\Phi_\beta = \left(\frac{1}{H^k_\beta R^k_\beta} v_0 - \frac{1}{H^k_\beta}\frac{\partial w_0}{\partial \beta}\right)\frac{H^k_\beta R^k_\beta}{H^k_\beta R^k_\beta - z} \tag{7}$$

$$\Phi_\alpha = \left(\frac{1}{H^k_\alpha R^k_\alpha} u_0 - \frac{1}{H^k_\alpha}\frac{\partial w_0}{\partial \alpha}\right)\frac{H^k_\alpha R^k_\alpha}{H^k_\alpha R^k_\alpha - z} \tag{8}$$

In the CLT case, Φ_β and Φ_α in (7) and (8) do not depend on the k layer if we consider the mean value at the mid-reference surface for the radii of curvature R^k_α and R^k_β. The meaning of the radii of curvature R_α and R_β and the parametric coefficients $H_\alpha = (1 + z/R_\alpha)$ and $H_\beta = (1 + z/R_\beta)$ has been discussed in the section of this encyclopedia about constitutive and geometrical equations for the thermomechanical analysis of shells.

By substituting (7) and (8) in (1), we obtain the kinematic model for CLT in the case of shell geometry. The sovra-temperature remains linearly imposed through the thickness of the shell. In the same way, it is possible to write the geometrical relations for the CLT case by starting from the geometrical relations for the FSDT case ((2)–(6)), where $\gamma_{\beta z} = \gamma_{\alpha z} = 0$, and (7) and (8) give the rotations Φ_β and Φ_α.

Constitutive Equations

The constitutive equations for the FSDT model consider both mechanical $\boldsymbol{\sigma}_m$ and thermal $\boldsymbol{\sigma}_t$ contributions for the stress components in each k layer:

$$\boldsymbol{\sigma}^k = \boldsymbol{\sigma}^k_m - \boldsymbol{\sigma}^k_t = \boldsymbol{Q}^k\,\boldsymbol{\epsilon}^k - \boldsymbol{\lambda}^k\,\theta^k \tag{9}$$

The stress and strain component vectors have 5×1 dimension because the transverse normal stress σ_{zz} and strain ϵ_{zz} are zero as hypothesis in such a model:

$$\boldsymbol{\sigma}^k = \begin{bmatrix} \sigma^k_{\alpha\alpha} \\ \sigma^k_{\beta\beta} \\ \sigma^k_{\alpha\beta} \\ \sigma^k_{\beta z} \\ \sigma^k_{\alpha z} \end{bmatrix}, \quad \epsilon^k = \begin{bmatrix} \epsilon^k_{\alpha\alpha} \\ \epsilon^k_{\beta\beta} \\ \gamma^k_{\alpha\beta} \\ \gamma^k_{\beta z} \\ \gamma^k_{\alpha z} \end{bmatrix} \tag{10}$$

The sovra-temperature θ is a scalar. The matrix of elastic coefficients has 5×5 dimension, and its elastic coefficients are the reduced ones in order to overcome the Poisson locking phenomenon typical of classical two-dimensional models with zero or constant transverse normal strain ϵ_{zz} [12, 13]:

$$\boldsymbol{Q}^k = \begin{bmatrix} Q_{11}^k & Q_{12}^k & Q_{16}^k & 0 & 0 \\ Q_{12}^k & Q_{22}^k & Q_{26}^k & 0 & 0 \\ Q_{16}^k & Q_{26}^k & Q_{66}^k & 0 & 0 \\ 0 & 0 & 0 & Q_{44}^k & Q_{45}^k \\ 0 & 0 & 0 & Q_{45}^k & Q_{55}^k \end{bmatrix} \tag{11}$$

The thermomechanical coupling vector $\boldsymbol{\lambda}$ has 5×1 dimension, and it is given as a product between the elastic coefficient matrix and the thermal expansion coefficient vector $\boldsymbol{\alpha}$:

$$\boldsymbol{\lambda}^k = \boldsymbol{Q}^k \, \boldsymbol{\alpha}^k \tag{12}$$

where

$$\boldsymbol{\lambda}^k = \begin{bmatrix} \lambda_1^k \\ \lambda_2^k \\ \lambda_6^k \\ 0 \\ 0 \end{bmatrix}, \quad \boldsymbol{\alpha}^k = \begin{bmatrix} \alpha_1^k \\ \alpha_2^k \\ 0 \\ 0 \\ 0 \end{bmatrix} \tag{13}$$

In the CLT model, transverse shear stresses $\sigma_{\beta z}$ and $\sigma_{\alpha z}$ and transverse shear strains $\gamma_{\beta z}$ and $\gamma_{\alpha z}$ are zero; therefore, the vectors in (10) and (13) are reduced to 3×1 dimension by deleting the last two lines, and the matrix in (11) has 3×3 dimension obtained by deleting the last two rows and columns. The Poisson locking phenomenon appears, and it is contrasted by means of the reduced elastic coefficients as obtained in [12] and [13].

Governing Equations

The Principle of Virtual Displacements (PVD) written for multilayered shells subjected to thermal and/or mechanical loads reads [1]:

$$\sum_{k=1}^{N_l} \int_{\Omega_k} \int_{A_k} \left\{ \delta \, \epsilon^{k^T} \left(\boldsymbol{\sigma}_m^k - \boldsymbol{\sigma}_t^k \right) \right\} d\Omega_k dz = \sum_{k=1}^{N_l} \delta L_e^k \tag{14}$$

where N_l indicates the number of layers and Ω_k and A_k are the integration domains in in-plane (α, β) and z directions, respectively. k indicates the layer and T the transpose of a vector. δL_e^k is the external work for the k^{th} layer.

The steps to obtain the governing equations are:

- Substitution of geometrical relations for strain components
- Substitution of appropriate constitutive equations for stress components
- Introduction of the kinematic model for the FSDT or CLT analysis which means two-dimensional approximation for displacement vector $\boldsymbol{u}$ and sovra-temperature θ.

The general form of governing equations for a multilayered shell subjected to thermal and mechanical loadings is:

$$\delta \boldsymbol{u}^T : \quad \boldsymbol{K}_{uu} \, \boldsymbol{u} = -\boldsymbol{K}_{u\theta} \, \theta + \boldsymbol{P}_u \tag{15}$$

where $(-\boldsymbol{K}_{u\theta}\theta)$ is the thermal load and $\boldsymbol{P}_u$ is the external mechanical load. The sovra-temperature θ is always linear assumed through the thickness (mean value θ_0 and slope θ_1); the stiffness matrix $\boldsymbol{K}_{uu}$ has dimension 5×5 and 3×3 for the FSDT and CLT cases, respectively. The matrix $\boldsymbol{K}_{u\theta}$ for the thermal load has dimension 5×2 and 3×2 for the FSDT and CLT cases, respectively ($\theta^T = (\theta_0 \, \theta_1)$). The FSDT model has 5° of freedom which means vector $\boldsymbol{u}^T = (u_0 \; v_0 \; w_0 \; \Phi_\alpha \; \Phi_\beta)$; the CLT model has 3° of freedom which means vector $\boldsymbol{u}^T = (u_0 \; v_0 \; w_0)$.

In the results proposed in the next section, governing equations are solved in Navier-type closed-form solution via substitution of harmonic expressions for the displacements and temperature as well as considering materials with $Q_{16} = Q_{26} = Q_{45} = 0$ and $\lambda_6 = 0$. The following harmonic assumptions can be made for the field variables which correspond to simply supported boundary conditions for shells:

$$
\begin{aligned}
u &= \sum_{m,n} \hat{U} \cos\left(\frac{m\pi\alpha}{a}\right) \sin\left(\frac{n\pi\beta}{b}\right) \\
v &= \sum_{m,n} \hat{V} \sin\left(\frac{m\pi\alpha}{a}\right) \cos\left(\frac{n\pi\beta}{b}\right) \\
(w,\theta) &= \sum_{m,n} (\hat{W},\hat{\theta}) \sin\left(\frac{m\pi\alpha}{a}\right) \sin\left(\frac{n\pi\beta}{b}\right)
\end{aligned}
\tag{16}
$$

where $\hat{U}, \hat{V}, \hat{W}$, and $\hat{\theta}$ are the amplitudes, m and n are the wave numbers, and a and b are the shell dimensions.

Some Results

The results proposed in this section consider a linear assumed temperature profile which goes from the top value $\theta_t = +0.5K$ to the bottom value $\theta_b = -0.5K$ (bisinusoidal form in the plane with wave numbers $m = n = 1$). This temperature profile could also be calculated, but in this analysis, we always consider it linear through the thickness direction in order to better compare the classical models (CLT and FSDT) with the quasi-3D ones. The quasi-3D models, here given, have been proposed in [5] in the framework of the Carrera Unified Formulation (CUF); the case of calculated temperature profile will be discussed in dedicated sections of this encyclopedia.

Two different configurations have been analyzed for the cylindrical shell geometry which has dimensions $a = 1\,m$ and $b = \frac{\pi}{3}R_\beta = 10.47197551\,m$. The radii of curvature in the α and β directions are $R_\alpha = \infty$ and $R_\beta = 10\,m$, respectively. The considered total thickness values are $h = 2.5\,m, 1.0\,m, 0.1\,m, 0.01\,m$, which mean thickness ratios $R_\beta/h = 4, 10, 100, 1000$. The configuration 1 considers a one-layered isotropic shell in aluminum alloy $Al5086$ with Young modulus $E = 70.3GPa$, Poisson ratio $\nu = 0.33$, and thermal expansion coefficient $\alpha = 24 \times 10^{-6}K^{-1}$. The configuration 2 is a two-layered isotropic shell; the bottom layer is in $Al5086$ (the same of case 1), while the top layer is in titanium alloy $Ti22$ with Young modulus $E = 110GPa$, Poisson ratio $\nu = 0.32$, and thermal expansion coefficient $\alpha = 8.6 \times 10^{-6}K^{-1}$. The two considered layers have the same thickness $h/2$. The third configuration considers a cylindrical shell with dimensions $a = b = 1\,m$. The radii of curvature in the α and β directions are $R_\alpha = \infty$ and $R_\beta = 5\,m, 10\,m, 50\,m$. The considered total thicknesses is $h = 0.1\,m$. The ratio between Young modulus in the longitudinal and transverse direction is $E_L/E_T = 25$. The shear modulus ratio is $G_{LT}/G_{TT} = 2.5$, and the Poisson ratio is $\nu_{LT} = \nu_{TT} = 0.25$. The ratio between the thermal expansion coefficient in the transverse and longitudinal direction is $\alpha_T/\alpha_L = 3$. The two layers have the same thickness $h/2$ with lamination sequence $0°/90°$.

In Table 1, the transverse displacement $\bar{w}$ and the in-plane stress $\sigma_{\alpha\beta}$ are calculated in the middle of the shell. Different thickness ratios R_β/h are investigated. For thick shells, classical theories give an error even if the shell is isotropic and one-layered made. Such an error is smaller for thin shells, but it remains. FSDT and CLT models are very similar for thin shells because the hypothesis of zero transverse shear strains is true in this case. For thermal stress analysis, the importance of the thickness-stretching effect is important as demonstrated by the difference between CLT/FSDT models and reference solutions for each thickness ratio investigated.

The nondimensional quantities in Table 2 are normalized with the data of the aluminum alloy $Al5086$. Nondimensional transverse displacement $\bar{w}$ is considered in $z = h/4$. For classical theories, the error remains even if the shell is very thin ($R_\beta/h = 1000$); this happens because of the high transverse anisotropy due to the different elastic properties of the two layers embedded.

The displacement in Table 3 is given in the middle of the shell ($z = 0$), and it is normalized with the longitudinal thermal expansion coefficient of the composite material. The error for the classical theories remains in Table 3 because in the case of composite shells both in-plane and transverse anisotropy are evident (see both thick and thin geometries).

Classical Governing Equations for the Thermomechanical Analysis of Shells, Table 1 Configuration 1. Isotropic one-layered shell in aluminum alloy. Nondimensional transverse displacement $\bar{w} = \frac{10wh}{a^2\alpha T_1}$ and in-plane stress $\sigma_{\alpha\beta}$ in $z = 0$. $T_1 = 1.0\,K$ is the gradient of the linear temperature profile

	$\bar{w}$			$\sigma_{\alpha\beta}$		
R_β/h	10	100	1000	10	100	1000
CUF [5]	0.9468	1.2007	0.1151	$0.3209 * 10^4$	$0.1916 * 10^5$	$0.1822 * 10^5$
FSDT	1.9818	1.7943	0.1715	$0.4086 * 10^4$	$0.2846 * 10^5$	$0.2712 * 10^5$
CLT	1.9869	1.7985	0.1716	$0.4087 * 10^4$	$0.2852 * 10^5$	$0.2713 * 10^5$

Classical Governing Equations for the Thermomechanical Analysis of Shells, Table 2 Configuration 2. Two-layered isotropic shell in aluminum and titanium alloys. Nondimensional transverse displacement $\bar{w} = \frac{10wh}{a^2\alpha_{Al}T_1}$ in $z = h/4$. $T_1 = 1.0\,K$ is the gradient of the linear temperature profile

R_β/h	4	10	100	1000
CUF [5]	0.4002	0.7472	0.7468	0.0325
FSDT	1.2351	1.2694	1.1054	0.0463
CLT	1.2908	1.2914	1.1096	0.0463

Classical Governing Equations for the Thermomechanical Analysis of Shells, Table 3 Configuration 3. Two-layered carbon fiber-reinforced cylindrical shell (0°/90°). Nondimensional transverse displacement $\bar{w} = \frac{w}{b^2\alpha_L T_1}$ in $z = 0$. $T_1 = 1.0\,K$ is the gradient of the linear temperature profile

R_β/h	50	100	500
CUF [5]	1.1280	1.1434	1.1477
FSDT	1.1805	1.1959	1.1997
CLT	1.1834	1.1966	1.1997

Conclusions

The governing equations for the thermomechanical analysis of multilayered shells have been proposed for classical two-dimensional models such as the Classical Lamination Theory (CLT) and the First-Order Shear Deformation Theory (FSDT). These governing equations are very simple because they consider 3 degrees of freedom in the CLT analysis and 5 degrees of freedom for the FSDT model. However, they exhibit some limitations which are the assumption of a linear temperature profile coherent with the models and the simplified kinematic assumptions which do not consider the transverse normal strain (both CLT and FSDT model) and the transverse shear deformation (CLT analysis). Kinematic assumption limitations give several problems in the thermomechanical analysis of thick and/or in-plane and transverse anisotropic shells. The use of refined models and calculated temperature profiles appear mandatory in the thermal stress analysis of multilayered shells.

Cross References

- ▶ Calculated Temperature Profile
- ▶ Refined and Advanced Governing Equations for the Thermomechanical Analysis of Shells
- ▶ Shell Geometrical Relations
- ▶ Thermal Load
- ▶ Thermal Stress Analysis

References

1. Brischetto S, Carrera E (2009) Thermal stress analysis by refined multilayered composite shell theories. J Therm Stresses 32(1–2):165–186
2. Khare RK, Kant T, Garg AK (2003) Closed-form thermo-mechanical solutions of higher-order theories of cross-ply laminated shallow shells. Compos Struct 59(3):313–340
3. Khdeir AA, Rajab MD, Reddy JN (1992) Thermal effects on the response of cross-ply laminated shallow shells. Int J Solids Struct 29(5):653–667
4. Carrera E (2002) Temperature profile influence on layered plates response considering classical and advanced theories. AIAA J 40(9):1856–1885
5. Brischetto S (2009) Effect of the through-the-thickness temperature distribution on the response of layered and composite shells. Int J Appl Mech 1(4):581–605

6. Brischetto S, Carrera E (2011) Heat conduction and thermal analysis in multilayered plates and shells. Mech Res Commun 38(6):449–455
7. Tungikar V, Rao BKM (1994) Three dimensional exact solution of thermal stresses in rectangular composite laminates. Compos Struct 27(4):419–430
8. Kirchhoff G (1850) Über das gleichgewicht und die bewegung einer elastischen scheibe. Journal für die Reine und Angewandte Mathematik 40:51–88
9. Reissner E (1945) The effect of transverse shear deformation on the bending of elastic plates. J Appl Mech 12:69–77
10. Mindlin RD (1951) Influence of rotatory inertia and shear on flexural motions of isotropic, elastic plates. J Appl Mech 18:31–38
11. Carrera E, Brischetto S, Nali P (2011) Plates and shells for smart structures: classical and advanced theories for modeling and analysis. Wiley, New Delhi
12. Carrera E, Brischetto S (2008) Analysis of thickness locking in classical, refined and mixed multilayered plate theories. Compos Struct 82(4):549–562
13. Carrera E, Brischetto S (2008) Analysis of thickness locking in classical, refined and mixed theories for layered shells. Compos Struct 85(1):83–90

Classical Thermodynamics

Gerard A. Maugin
Institut Jean Le Rond d'Alembert, Unité mixte de recherche 7190, Universite Pierre et Marie Curie, Paris, France

Overview

Classical thermodynamics, one of the greatest scientific achievements of the nineteenth century, naturally associated with simple energetic processes, provides the basis for all further progress and complexification of a science that bears on all aspects of evolution of inert and living matter. Essentially built by pioneers such as Sadi Carnot (1795–1832), William Thomson (Lord Kelvin; 1824–1907), William Rankine (1820–1872), Rudolf Clausius (1822–1888), and James Joule (1818–1889) in a period of steam machine design, classical thermodynamics deals in a phenomenological way with the exchanges of energy in the form of heat and work between well-delineated systems. The present entry of a general scope and a discursive style introduces the relevant main concepts and definitions. In particular, are discussed the notions of energy, heat, work, and power and those of thermodynamic states and processes. The four laws of thermodynamics are enunciated together with a brief definition of various thermodynamic processes, conjugate state variables, and thermodynamics potentials. This is but a necessary prerequisite for the deeper apprehending of the thermodynamics of continua that includes thermoelasticity as a very specialized case.

Definition and Main Concepts

"Thermodynamics" is a term that goes back to James Joules and William Thomson (later Lord Kelvin) in the late 1850s. In Greek, "thermé" means "heat" and "dynamis" means "power." It was introduced to refer to the transfer of heat and of work done on or by bodies and radiation. It is acknowledged as being of universal application, to both inert and living matter, having for objects "macroscopic systems" in its "classical" framework [1–6]. In principle, any reference to the atomic description of matter is left aside. Nonetheless, a microscopic interpretation of its basic concepts was also provided by the considerations of statistical thermodynamics (not to be considered here) by James C. Maxwell (1831–1879), Ludwig Boltzmann (1844–1906), and Josiah W. Gibbs (1839–1903).

Thus, classical thermodynamics interrelates macroscopic variables such as temperature, volume, and pressure, but in a more modern context, it involves also notions such as chemical reactions, electric current, and strains. Its origins are marked by a strong interest in the possible increase of the efficiency of early steam engines. The French scientist Nicolas Léonard Sadi Carnot (1796–1832) is considered the "father of thermodynamics" with his "Reflections on the motive power of fire" (1824). He paid special attention to cyclic non-equilibrium processes although thermodynamics is essentially well understood for systems in so-called thermodynamic equilibrium. Out of equilibrium systems are much more

difficult to study while they abound in physics, chemistry, biology, and engineering science (see [6–7]).

Thus, thermodynamics deals with the study of *energy transfers* that are resolved in two distinct components, heat and work.

Here, "energy" must be understood as the capacity of a system to modify a state and to produce a work resulting in motion, in electromagnetic radiation, or in heat. It can be viewed as an "exchange currency" between physical phenomena. In the MKS (IS) system of units, energy is measured as a work in *joules* (one *joule* = force of one *newton* acting through one *meter*).

Heat itself is a transfer of thermal agitation. It can only flow from hot to cold – see Second law of thermodynamics. Heat deals with temperature scale and calorimetry. The scientific temperature scale is the so-called *absolute* one, referred to "degrees K" (or *kelvins*).

"Work" has a definite mechanical flavor: work = force × displacement.

Finally, "power" – in the physical sense – is the capacity of mobilizing energy in a more or less short (or long) interval of time. Power is measured in energy per unit of time, usually *watts*. In contrast, "action" is energy multiplied by time.

Thermodynamics uses all these notions. Carnot's fruitful fundamental views (1824) are expressed as a discourse on these notions of heat, power, energy, and engine efficiency.

Thermodynamic States and Processes

Thermodynamics describes how systems change when they interact with one another or with their surroundings. For this, one must be able to define thermodynamic systems and states and the notion of surroundings.

- A *thermodynamic system* is a precisely delineated region of the universe considered as a macroscopic physical object defined in terms of its states that can evolve in time. Macroscopic state variables have been identified in the course of empirical work. In some conditions, such variables can be related to one another through so-called *equations of state* (e.g., the celebrated equation of perfect gases: $pV = RT$, relating pressure p, volume V, and temperature T, with R a universal physical constant). Systems can be *open* (admitting mass flow, work, and heat exchanges with the surroundings), *closed* (no mass flow allowed across its boundary), or *isolated* (neither mass flow nor exchanges by heat or work with the exterior).
- *Thermodynamic processes* are the more or less rapid successions of events a thermodynamic system can undergo. Cyclic processes were of paramount importance in the initial developments of the thermodynamics of engines (e.g., in Carnot's and Rankine's works).
- The s*urroundings* of a thermodynamic system are other thermodynamic systems that can interact with it.

Thermodynamic processes are governed by a set of four universally acknowledged statements known as the *laws of thermodynamics*.

Laws of Thermodynamics

- The so-called "zeroth" *law* of thermodynamics expresses the existence of an equivalence relation on the set of considered thermodynamic systems: *If two systems are each in thermal equilibrium with a third, then they are also in thermal equilibrium with each other*. This is tacitly assumed in measurements of temperature.
- The *first law* specifies that *energy* can be exchanged between physical systems in the form of heat and thermodynamic work, more precisely: *A change in the internal energy of a closed thermodynamic system is the difference between the heat supplied to the system and the amount of work done by the system on its surroundings*. This is mathematically formulated as the *principle of conservation of energy*.
- The *second law* that deals with *entropy* expresses some limitation on the amount of work that can be delivered to an external system by a thermodynamic system. This

represents what is known as irreversibility. It is basically expressed as follows: *Heat cannot spontaneously flow from a colder region to a hotter location*. This is the expression of a universal principle of decay observable in nature that is mathematically expressed by a forbidden decrease in entropy. The latter is a measure of how much this decay process has progressed. It is measured in work (heat) per unit of temperature, i.e., in J/K.

- The *third law* (also known as Nernst heat theorem: unattainability of absolute zero temperature) is a statistical law of nature that concerns entropy and the impossibility to reach the absolute zero of temperature, more precisely: *As a system approaches absolute zero, all processes cease and the entropy of the system approaches a minimum value*. This principle provides an absolute reference point for the determination of entropy.

Special Thermodynamic Processes

These are defined as processes in which one single variable is kept constant. Most common examples are:

- Isobaric process: occurs at constant pressure p
- Isochoric process: occurs at constant volume V
- Isothermal process: occurs at constant temperature T
- Adiabatic process: occurs without loss or gain of energy by heat
- Isentropic process: a reversible adiabatic process that occurs at constant entropy
- Isolated process: occurs at constant internal energy U (and constant elementary chemical composition)

But the entropy of an isolated system which is not in equilibrium tends to increase over time, approaching a maximum value at equilibrium.

Conjugate Variables

In agreement with the notion of work, conjugate thermodynamic variables are pairs of thermodynamic variables, with one being akin to a "force" and the other to a resulting "displacement." Examples of such pairs are pressure and volume as mechanical parameters, temperature and entropy as thermal parameters, and chemical potential and particle number as material parameters. In each pair, one of the quantities is *extensive* (proportional to the quantity of matter) and the other *intensive* (independent of the quantity of matter). Examples of extensive variables are volume, number of moles, entropy, electric polarization, and magnetization. The corresponding conjugate intensive variables are pressure, concentration, temperature, electric field, and magnetic induction, respectively. Specific volume is intensive.

Thermodynamic Potentials

They are different quantitative measures of the stored energy in a system. The most familiar ones are:

- The internal energy U : function of entropy S, volume V, and particle number N
- The Helmholtz free energy $F = U - TS$, function of temperature T, volume V, and particle number N
- The enthalpy $H = U + pV$, function of entropy, pressure, and particle number
- The Gibbs free energy $G = U + pV - TS = F + pV = H - TS$, function of temperature, pressure, and particle number

The most appropriate potential to be used in measuring energy changes in systems that evolve from an initial state to a final one depends on the constraints imposed on this evolution. Thus, the Helmholtz free energy is the energy available in a system to do useful work when the temperature and volume are kept fixed. Internal energy is more appropriate to describe systems in adiabatic evolution, etc.

Various general subfields of thermodynamics are:

- The thermodynamics of engines/machines (not the object of the ETS)
- The thermodynamics of discrete systems (not the object of the ETS)

- The thermodynamics of continua

In the last case – *the thermodynamics of continua* – the "continuity" assumption made in describing the physical response of many bodies implies the application of mathematical analysis. The operational realm of this thermodynamics thus is provided by *partial differential equations* (for short, *pde*'s). One of its basic formulations provided in the nineteenth century is a paradigmatic type of such *pde*'s known as the parabolic type illustrated by the heat equation (with infinite speed of propagation) and the diffusion equation. This belongs in the general *theory of fields*, where all quantities become more or less smooth functions of space and time. *Thermoelasticity*, the main object of this encyclopedia, is the foremost application of the thermodynamics of deformable continua of the solid type. It concerns the coupling between heat and reversible deformation with basic independent state variables, temperature, and strain. *Thermoanelasticity* is its extension when the material body is also dissipative from a pure mechanical viewpoint (e.g., in viscoelasticity, plasticity). *Thermo-electro-elasticity* and *thermo-magneto-elasticity* in addition consider a possible coupling with electric properties (e.g., in piezoelectric materials) or magnetic ones (e.g., in elastic conductors of heat and electricity). For more about this see Reference [7].

Note that "energetism" – often used in opposition to atomism – is a view of physics that sees all phenomena as governed by thermodynamic principles and more particularly the fundamental concept of energy. Foremost among its propagandists was Pierre Duhem (1861–1916).

References

1. Callen HB (1960) Thermodynamics. Wiley, New York
2. Duhem P (1911) Traité d'énergétique ou de thermodynamique générale, Two volumes, Gauthiers-Villars, Paris
3. Kestin J (1966) A course in thermodynamics. Blaisdell, Waltham
4. Kondepudi D (2008) Introduction to modern thermodynamics. Wiley, Chichester
5. Bridgman PW (1943) The nature of thermodynamics. Harvard University Press, Cambridge
6. Maugin GA (1999) The thermomechanics of nonlinear irreversible behaviors. World Scientific, Singapore, see Chapters 1 and 2
7. Maugin GA (2013) Article "Continuum thermodynamics" in this Encyclopedia

Classical Thermoelasticity

▶ Fundamental Solutions in Classical Thermoelasticity

Classical Thermomechanical Models: Numerical Formulations

Kumar K. Tamma
Department of Mechanical Engineering,
University of Minnesota, Minneapolis, MN, USA

Overview

There are a significant number of general science and engineering applications wherein an accurate understanding of the multidisciplinary thermal-structural interactions are of utmost importance and concern in the design and analysis stage. The complexity and multidisciplinary nature of these structures significantly influence the response characteristics and make the combined modeling and analysis a formidable and challenging task. Furthermore, for several related applications, routine experimental and/or ground tests are highly impractical and difficult or cumbersome to simulate. As a consequence, there is a pressing need to effectively formulate accurate representative models, modeling/analysis strategies, and computational approaches to numerically simulate the combined response for a variety of situations. The focus here is upon numerical discretization for the classical thermomechanical formulations.

Introduction

Among the various numerical approaches, finite element methods have been commonly used for the modeling and analysis of thermal-structural problems. Historically, it was common to use finite difference techniques exclusively for the heat equation by the thermal analysts, whereas the finite element method was the ideal choice of structural analysts for the structural problems. For combined thermal-structural interactions, one needs to perform an accurate thermal analysis in complex structures subjected to complex boundary conditions, irregular and complicated geometries, and the like. As a consequence, the finite element method has evolved as one of the more effective general purpose approaches available for the numerical solution of these classes of problems because of the inherent advantages of the method. Furthermore, the finite element method in conjunction with direct time-integration procedures is routinely being employed for solving multidisciplinary thermal-structural problems in most commercial codes.

Traditionally, the transient governing differential equations are first discretized in space, employing the finite element method. This procedure is known as semidiscretization. The semidiscretization process reduces the partial differential equations to a system of ordinary differential equations in time. These equations are further integrated in time to obtain the transient response. The commonly adopted techniques for solving transient problems are direct time-integration methods and modal superposition methods. The direct time-integration methods are the most widely used approaches for transient analysis. Modal analysis approaches are preferred mostly for linear situations and inertial type structural dynamic problems and have not been popular for nonlinear situations and for propagation type problems where high frequencies are involved, thereby, becoming computationally intensive and unattractive. In direct time-integration methods, finite difference approximations are introduced for the time derivative terms of the semidiscretized equations for deriving the necessary algorithmic relations. The basic types of direct time-integration techniques are explicit methods, implicit methods, and mixed or variable time-integration methods.

Problems encompassing the general field of thermal-structural interactions may thus be categorized as follows: (1) thermally induced stress-wave propagation problems, (2) thermally induced inertial dynamic problems, and (3) the field of thermal stresses.

Classical Dynamic Thermoelasticity Equations

The dynamic thermoelasticity theory based on the Fourier heat conduction equation is known as the classical theory of dynamic thermoelasticity. In the classical theory, the thermal disturbances are assumed to propagate at infinite speeds through the continuum. Coupling between the deformation and the temperature fields was originally postulated by Duhamel [1]. The fundamental relations and the basic equations of thermoelasticity are given in Biot [2]. Solutions to the problems in dynamic thermoelasticity have drawn considerable interest, and the first analytic solution to an initial boundary value problem in dynamic uncoupled classical thermoelasticity is that presented by Danilovskaya [3]. This well-known Danilovskaya's problem proposed in the 1950s originally studies an elastic semi-finite medium subjected to a uniform heating on its boundary plane, the plane assumed to be always traction free. The temperature variations in the half-space were calculated from the classical heat conduction equation, neglecting thermomechanical coupling. Next, the associated thermally induced loads were used for predicting the dynamic response of the medium. These results were later extended by Danilovskaya [4] to account for boundary-layer conductance. Sternberg and Chakravorty [5] further extended the problem to include a more realistic ramp-type temperature boundary condition.

The approaches for thermoelasticity problems involve deriving two sets of finite element formulations, one for the heat conduction and the other

for the mechanical displacement. The resulting combined system of finite element matrix equations is then solved for the temperature and displacement fields.

Classical Dynamic Thermoelasticity Model Equations

Coupled

$$\rho c\,\dot{\theta} + T_o\ \beta_{ij}\dot{u}_{i,j} - (\ k_{ij}\theta_{,j})_{,i} = \rho\ Q \qquad (1)$$

$$\rho\ddot{u}_i - (D_{ijkl}\ \varepsilon_{kl} - \beta_{ij}\ \theta)_{,j} = \rho\ f_i \qquad (2)$$

And T_o is the reference temperature, and β_{ij} is the thermoelasticity tensor.

Uncoupled

The corresponding uncoupled (one-way coupled) equations are readily obtained by setting $T_o = 0$ in (1). The first equation (1) does not account for the short time response required for steady-state heat conduction to be reached when a temperature gradient is suddenly introduced. Therefore, the thermal energy transport is assumed to be transmitted instantaneously to every other point so that the speed of propagation is infinite. Such a notion of instantaneous heat diffusion does yield accurate temperature predictions for most commonly encountered practical engineering situations.

Quasi-Static Representations

The quasi-static (neglecting dynamic aspects in the structure) representations commonly employed for thermomechanical applications can be cast in the form

Coupled

$$\rho c\ \dot{\theta} + T_o\ \beta_{ij}\dot{u}_{i,j} - (k_{ij}\theta_j)_{,i} = \rho\ Q \qquad (3)$$

$$-(D_{ijkl}\ \varepsilon_{kl} - \beta_{ij}\ \theta)_{,j} = \rho\ f_i \qquad (4)$$

where there is a two-way coupling.

Uncoupled

The corresponding uncoupled equations are obtained by setting $T_o = 0$ in (3).

Static Representations

The representative steady thermal and static equations of equilibrium can be cast in the form

Coupled

$$T_o\beta_{ij}\dot{u}_{i,j} - (k_{ij}\theta_{,j})_{,i} = \rho Q \qquad (5)$$

$$-(D_{ijkl}\ \varepsilon_{kl} - \beta_{ij}\ \theta)_{,j} = \rho\ f_i \qquad (6)$$

Uncoupled

Setting $T_o = 0$ in (5) results in a one-way coupling between the thermal and mechanical models.

Boundary and Initial Conditions

Typical thermal boundary and initial conditions that may exist for a given domain $\mathbf{R}$ bounded by a closed surface $\partial\mathbf{R} = \partial\mathbf{R}_p \cup \partial\mathbf{R}_q$ are given as

Thermal

$$\theta = \theta_p \quad \text{on} \quad \partial\mathbf{R}_p \qquad (7)$$

$$q_i\ n_i = -q_S + h(\theta - \theta_h) + \sigma_T\ \varepsilon_T\,(\theta^4 - \theta_r^4) \quad \text{on} \quad \partial\mathbf{R}_q \qquad (8a)$$

or,

$$q_i\ n_i + q_S - q_h - q_r = 0 \quad \text{on} \quad \partial\mathbf{R}_q \qquad (8b)$$

and the initial condition is given as

$$\theta(\mathbf{x}, o) = \theta_0 \quad \text{in} \quad \mathbf{R} \qquad (9)$$

The first boundary condition (7) is the prescribed temperature condition on $\partial\mathbf{R}_p$. The second boundary condition (8) is the flux condition on $\partial\mathbf{R}_q$. The terms q_s, q_h, and q_r represent the surface heating rate per unit area, the rate of heat flow per unit area due to convection, and the rate of heat flow per unit area due to radiation, respectively. h is the convective heat transfer coefficient, θ_h is the convection medium temperature, σ_T is the Stefan-Boltzman constant, ε_T is the surface emissivity, and θ_r is the radiation medium temperature.

Mechanical

Typical mechanical boundary and initial conditions are given as

$$u_i = g_i \quad \text{on} \quad \partial \mathbf{R}_p \tag{10}$$

$$\sigma_{ij}\, n_j = h_i \ \text{on} \quad \partial \mathbf{R}_q \tag{11}$$

and the following initial conditions:

$$u_i\ (t = 0) = u_i^0 \quad \text{in } \mathbf{R} \tag{12a}$$

$$\dot{u}_i\ (t = 0) = \dot{u}_i^0 \tag{12b}$$

The first boundary condition is the prescribed displacement on $\partial \mathbf{R}_p$, and the second boundary condition is the traction condition on $\partial \mathbf{R}_q$.

The general representation is the classical fully coupled dynamic thermoelasticity model equations. A two-way coupled or fully coupled problem implies that the temperature field influences the displacement field and vice versa. A one-way coupled problem implies that only the temperature changes influence the displacement field. A one-way coupled problem with a transient thermal field and a static structural field leads to a quasi-static analysis. For static analysis, the transient terms in both the thermal and the structural fields are neglected.

Finite Element Discretization

Solutions of coupled/uncoupled thermomechanical problems (both dynamic and static), particularly those that admit closed-form analytical solutions are limited. Hence, numerical methods of approach seem to be a viable alternative. Nevertheless, both the multidisciplinary nature of the thermomechanical interactions and the geometric complexity of the structural components pose significant challenges for the combined modeling and analysis of these classes of problems which can be broadly categorized as (1) thermally induced wave propagation type, (2) thermally induced inertial dynamic type, and (3) the remaining class of quasi-static and static thermal stress problems.

Of the various numerical methods available for the modeling/analysis of thermal, mechanical, and multidisciplinary thermomechanical interactions, finite differences, finite volume-based techniques, finite element methods, and boundary element methods have been previously employed and have no doubt matured over the years to improved levels. The choice of the particular method has been a matter of some debate, although the selection of the finite element method seems to be quite popular. Here, for purposes of illustration, attention is confined to employing the finite element method for each of the individual disciplines and for the combined analysis of thermomechanical interactions in engineering problems.

Let the solution domain $\mathbf{R}$ be enclosed by a boundary surface $\partial \mathbf{R} = \partial \mathbf{R}_p \cup \partial \mathbf{R}_q$ where $\partial \mathbf{R}_p$ and $\partial \mathbf{R}_p$ are nonoverlapping subregions of $\partial \mathbf{R}$. For the thermal model, the boundary surface $\partial \mathbf{R}$ consists of prescribed temperature conditions on $\partial \mathbf{R}_p$ and flux boundary conditions on $\partial \mathbf{R}_q$ as given in an earlier section. For the structural model, the boundary surface $\partial \mathbf{R}$ consists of prescribed displacements on $\partial \mathbf{R}_p$ and traction conditions on $\partial \mathbf{R}_q$ also given in an earlier section. Based on the particular class of problems, the initial conditions are also given quantities for both the thermal and the mechanical models, respectively.

Within each element $\mathbf{R}_e$ contained in $\mathbf{R}$, the element variables are approximated following

$$\theta_e = \mathbf{N}^\theta\ \theta \tag{13a}$$

$$\mathbf{u}_e = \mathbf{N}^m\ \mathbf{u} \tag{13b}$$

where $\mathbf{N}^\theta$ and $\mathbf{N}^m$ are the element interpolation functions for the temperature and the displacement fields in the thermal and mechanical models, respectively, and $\boldsymbol{\theta}$ are the nodal values of the temperature field, and $\mathbf{u}$ are the nodal values of the displacement field, respectively.

Introducing the discrete approximations (13) into the general form of the governing model equations and employing the relevant constitutive relations such as the flux-temperature relations for the thermal model and the strain-displacement relations for the mechanical model, respectively,

and following the standard weak formulation associated with the initial boundary value problem, yield (boundary effects are purposely not included, and the following notations for the superscripts are used: m = mechanical, θ = thermal):

Classical Models

Semidiscretized Equations

$$\mathbf{C}^{\theta\theta}\ \dot{\boldsymbol{\theta}} + \mathbf{C}^{\theta m}\ \dot{\mathbf{u}} + \mathbf{K}^{\theta\theta}\ \boldsymbol{\theta} = \mathbf{F}^{\theta}(t) \qquad (14a)$$

$$\mathbf{M}^{mm}\ \ddot{\mathbf{u}} + \mathbf{K}^{mm}\ \mathbf{u} + \mathbf{K}^{m\theta}\ \boldsymbol{\theta} = \mathbf{F}^{m}(t) \qquad (14b)$$

where

$$\mathbf{M}^{mm} = \int_{R_e} \rho N_{\alpha}^{m} N_{\beta}^{m} dR$$

$$\mathbf{C}^{\theta\theta} = \int_{R_e} \rho c N_{\alpha}^{\theta} N_{\beta}^{\theta} dR$$

$$\mathbf{C}^{\theta m} = \int_{R_e} T_o \beta_{ij} N_{\alpha,j}^{m} N_{\alpha}^{\theta}\ dR$$

$$\mathbf{K}^{\theta\theta} = \int_{R_e} k_{ij} N_{\alpha,i}^{\theta} N_{\beta,j}^{\theta}\ dR$$

$$\mathbf{K}^{mm} = \int_{R_e} D_{ijkl} N_{\alpha,i}^{m} N_{\beta,j}^{\theta}\ dR$$

$$\mathbf{K}^{m\theta} = \int_{R_e} (-)\beta_{ij} N_{\alpha}^{m} N_{\beta,i}^{\theta}\ dR$$

$$F^{\theta} = \int_{R_e} \rho\ Q\, N_{\alpha}^{\theta} dR$$

$$\mathbf{F}^{m} = \int_{R_e} \rho f_i\ N_{\alpha}^{m}\ dR$$

For the classical models, the resulting equations are, in general, symbolically represented as

$$\mathbf{C}^{\theta}\ \mathbf{v} + \mathbf{K}^{\theta}\ \mathbf{d} = \mathbf{F}^{\theta}(t) \qquad (15a)$$

$$\mathbf{M}^{m}\ \mathbf{a} + \mathbf{C}^{m}\ \mathbf{v} + \mathbf{K}^{m}\ \mathbf{d} = \mathbf{F}^{m}(t) \qquad (15b)$$

where the thermal model is a parabolic first-order ordinary differential equation in time with the need for one initial condition on the temperature field, while the corresponding mechanical model is a hyperbolic second-order ordinary differential equation in time with the need for two initial conditions, namely, one for displacement field and one for the velocity field. In (15a), $\mathbf{C}^{\theta}$ is associated with thermal capacitance, $\mathbf{K}^{\theta}$ is associated with thermal conductance, and $\mathbf{F}^{\theta}$ is associated with heat load vectors, respectively. The vector $\mathbf{v} = \dot{\boldsymbol{\theta}}$ and vector $\mathbf{d} = \boldsymbol{\theta}$ represent the first-order time derivative of the temperature field and the temperature field, respectively. In (15b), $\mathbf{M}^{m}$ is associated with the mass matrix, $\mathbf{C}^{m}$ is associated with the damping matrix, $\mathbf{K}^{m}$ is associated with the structural stiffness, and $\mathbf{F}^{m}$ is associated with the load vector, respectively. Note that **a** is the acceleration vector, **v** is the velocity vector, and **d** is the displacement field vector, respectively.

Quasi-Static Representations

In the absence of inertial dynamic terms in the mechanical model, the resulting quasi-static semidiscretized representations are obtained as

$$\mathbf{C}^{\theta\theta}\ \dot{\boldsymbol{\theta}} + \mathbf{C}^{\theta m}\ \dot{\mathbf{u}} + \mathbf{K}^{\theta\theta}\ \boldsymbol{\theta} = \mathbf{F}^{\theta}(t) \qquad (16a)$$

$$\mathbf{K}^{mm}\ \mathbf{u} + \mathbf{K}^{m\theta}\ \boldsymbol{\theta} = \mathbf{F}^{m}(t) \qquad (16b)$$

Static Representations

In the absence of the transient/dynamic inertial terms in the thermal and mechanical models, respectively, the resulting static or steady thermomechanical semidiscretized representations are obtained as

$$\mathbf{C}^{\theta m}\ \dot{\mathbf{u}} + \mathbf{K}^{\theta\theta}\ \boldsymbol{\theta} = \mathbf{F}^{\theta}(t) \qquad (17a)$$

$$\mathbf{K}^{mm}\ \mathbf{u} + \mathbf{K}^{m\theta}\ \boldsymbol{\theta} = \mathbf{F}^{m}(t) \qquad (17b)$$

Much of the research appearing in the literature relevant to thermomechanical problems focuses emphasis on the classical approach to the thermoelasticity equations. The assumptions involved here are indeed adequately representative and quite accurate for most of the practical situations encountered in common engineering practice. *On the other hand, for certain other classes of problems, such as those applications involving very short transient durations, sudden high heat flux situations, and/or for very low temperatures near absolute zero, the notion to adopt the nonclassical models has been cited in literature as being relevant and important.*

Computational Aspects in Thermomechanical Problems

In this section, first an overview of computational algorithms and approaches for transient/dynamic

and steady/static thermomechanical problems is presented. Following this, solution strategies and computational approaches are illustrated and briefly described. Finally, a needs assessment is briefly identified based on a review of the literature and personal experiences gained by the author in working over the years in multidisciplinary flow/thermal-structural problems.

Overview: Computational Algorithms

Various computational algorithms and solution techniques for parabolic and hyperbolic-parabolic systems of equations have also no doubt matured over the years. These in conjunction with effective modeling and analysis approaches and equation solvers serve a very important role in the analysis of thermal-structural problems. There exist many numerical approximation methods which have been introduced for the time discretization and the solution of these classes of problems. These include finite difference approximations for the time derivatives which lead to the so-called direct time-integration one-step and multistep methods [6–9, 16, 17], hybrid transfinite element formulations which employ transform methods in conjunction with standard Galerkin procedures and finite elements and then numerically invert the resulting representations to obtain the solutions at desired times of interest [10–13], finite element formulations in space and time [7, 8, 14], and the like. Of the various computational algorithms available in literature for dynamic/transient problems, direct time-integration approaches have been consistently popular and most common in production codes.

Direct time-integration methods for transient thermal, structural dynamic, and combined dynamic thermal-structural problems have long been a subject matter of widespread research activity. To date, much progress has been made in the development and understanding of the direct time-integration methods. This includes the development of efficient algorithmic representations, investigations encompassing accuracy and stability properties, formulations of variable and mixed time-integration approaches, adaptive time stepping approaches, effective solution methods, implementation aspects, and the like.

Computational Algorithms: First-Order Systems

Focusing attention on the classical form of the transient parabolic thermal problems (diffusive), the first step involves the semidiscretization process on the form of the parabolic heat conduction equation. This semidiscretization process leads to a system of simultaneous ordinary differential equations, which can be represented in matrix form as

$$\mathbf{C}\ (\theta, t)\ \dot{\boldsymbol{\theta}} + \mathbf{K}\,(\theta, t)\ \boldsymbol{\theta} = \mathbf{Q}\ (\theta, t) \qquad (18)$$

$$\mathbf{C},\ \mathbf{K}, \in \mathbf{R}^{\mathrm{NEQ}}\ \mathrm{x}\ \mathbf{R}^{\mathrm{NEQ}};\ \dot{\boldsymbol{\theta}}, \boldsymbol{\theta}\ \textbf{and}\ \mathbf{Q} \in \mathbf{R}^{\mathrm{NEQ}}$$

where $\mathbf{C}$ is the capacitance matrix, $\mathbf{K}$ is the thermal conductance matrix, and $\mathbf{Q}$ is a vector of heat loads. The specific heat and density may be temperature dependent and affect the solution through the capacitance matrix. The thermal conductivity and the convection coefficient may be temperature dependent and affect the solution through the conduction and convection matrices, contained in $\mathbf{K}$, respectively. Radiation heat transfer is inherently nonlinear and affects the solution through $\mathbf{K}$ and the incident heat load vector in $\mathbf{Q}$. Also, internal heat generation, surface convection, and surface heating rates may be temperature dependent and affect the solution through the heat load vectors contained in $\mathbf{Q}$. $\boldsymbol{\theta}$ is the global nodal temperature field. The initial conditions are given as $\boldsymbol{\theta}(t = \boldsymbol{0}) = \boldsymbol{\theta}_o$.

The semidiscretized matrix representations described above usually involve integrals over the element domain and surface. Further, these matrices are customarily evaluated using numerical integration. For nonlinear situations, these element matrices are evaluated repeatedly to account for proper updating of material thermophysical parameters besides the issues involving the radiation matrix. Since the system of equations (18) does not readily permit closed-form analytical solutions, numerical time-integration schemes are mostly adopted.

Following the semidiscretization process, the next step is the time discretization. The solution is typically marched out in time at each time step Δt, starting from the initial conditions until the total duration of the transient response is reached.

Typical well-known and commonly advocated time-integration approaches for transient heat transfer analysis include the one-step generalized α-family of methods [7, 8, 16, 17]). The generalized trapezoidal α-family of methods are typically represented as

$$\mathbf{C}\dot{\boldsymbol{\theta}}^{n+1} + \mathrm{K}\boldsymbol{\theta}^{n+1} = \mathbf{Q}^{n+1} \tag{19a}$$

$$\boldsymbol{\theta}^{n+1} = \boldsymbol{\theta}^{n} + \Delta t\dot{\boldsymbol{\theta}}^{n+\alpha} \tag{19b}$$

$$\dot{\boldsymbol{\theta}}^{n+\alpha} = (1-\alpha)\dot{\boldsymbol{\theta}}^{n} + \alpha\dot{\boldsymbol{\theta}}^{n+1} \tag{19c}$$

where Δt is the time step. The parameter $\alpha(\alpha \in [0,1])$ controls the stability and accuracy of the schemes.

The initial value problem consists of finding the temperature field $\boldsymbol{\theta} = \boldsymbol{\theta}(t)$ satisfying (19) and the initial conditions $\boldsymbol{\theta}(t=0) = \boldsymbol{\theta}_o$.

The commonly advocated α−family of time-integration methods are the explicit ($\alpha = 0$) and the implicit ($\alpha = 1/2$) schemes. For $\alpha = 0$, the method is the explicit (or Euler forward), which is first-order accurate and is conditionally stable. For $\alpha = 1/2$, the method is the implicit (or Crank-Nicolson [15]), which is second-order accurate and is unconditionally stable. For $\alpha = 2/3$, the method is implicit (or Galerkin method) and is first-order accurate and unconditionally stable. For $\alpha = 1$, the method is the implicit (or Euler backward), which is first-order accurate and unconditionally stable.

Computational Algorithms: Second-Order Systems

The governing equations for the dynamic thermoelasticity models and the dynamics of structures are hyperbolic in nature.

The semidiscretized dynamical equations are typically represented in matrix form as

$$\mathbf{M}^{\theta/m}\,\mathbf{a} + \mathbf{C}^{\theta/m}\,\mathbf{v} + \mathbf{K}^{\theta/m}\,\mathbf{d} = \mathbf{F}^{\theta/m} \tag{20}$$

where $\mathbf{M}^{\theta/m}$ is associated with the mass matrix, $\mathbf{C}^{\theta/m}$ is associated with the damping, and $\mathbf{K}^{\theta/m}$ is associated with the stiffness matrix. The vectors **d**, **v**, and **a** are the displacement, velocity, and acceleration vectors, respectively. $\mathbf{F}^{\theta/m}$ is the load vector. In (20), $\mathbf{M}^{\theta/m}$ is positive-definite and symmetric, and $\mathbf{C}^{\theta/m}$ and $\mathbf{K}^{\theta/m}$ are positive semi-definite and symmetric.

The initial value problem consists of finding the vector $\mathbf{d} = \mathbf{d}(t)$ satisfying (20) and the following initial conditions:

$$\mathbf{d} = \mathbf{d}^0 \tag{21a}$$

$$\mathbf{v} = \mathbf{v}^0 \tag{21b}$$

For dynamical situations, numerous direct time-integration approaches exist for the analyses of this class of problems. Explicit, implicit, mixed explicit-implicit, and variable time-integration approaches have been employed for a variety of situations in dynamical thermal-structural problems. The direct time-integration approaches rely on deriving recursion formulas that relate the values of **d**, **v**, and **a** at one instant of time, n, to the values of these quantities at a later time, n + 1. These recursion relations make it possible for the solution to be marched out in time, starting with the initial conditions at $t = t_n$ and continuing until the desired duration of time.

The evaluation of direct time-integration methods and the current state of the art appears in Tamma et al. [7, 8, 16, 17]. As a general guideline, thermal stress-wave or mechanical stress-wave propagation problems are solved using explicit time-integration methods, while implicit methods are employed for the remainder class of inertial problems. This is because in the former, the small time steps ensure accurate tracking of the induced stress-wave fronts, while for the latter, such a restriction is not as severe.

Attention is next purposely focused on two of the approaches that have been employed for dynamic thermoelasticity problems involving the classical and the nonclassical models. The widely used Newmark-β family of direct integration methods and the generalized γ_s-family of representations for solving the dynamic equations are detailed next ([7, 8]; [16, 17]).

Newmark Family of Methods

$$\mathbf{M}\,\mathbf{a}^{n+1} + \mathbf{C}\,\mathbf{v}^{n+1} + \mathbf{K}\,\mathbf{d}^{n+1} = \mathbf{F}^{n+1} \tag{22a}$$

$$\mathbf{d}^{n+1} = \mathbf{d}^{n} + \Delta t\ \mathbf{v}^{n} + \frac{\Delta t^2}{2} \times \left[(1-2\beta)\mathbf{a}^{n} + 2\beta\mathbf{a}^{n+1}\right] \tag{22b}$$

$$\mathbf{v}^{n+1} = \mathbf{v}^{n} + \Delta t\ \left[(1-\gamma)\,\mathbf{a}^{n} + \gamma\,\mathbf{a}^{n+1}\right] \tag{22c}$$

where $\mathbf{d}^{n+1}$ in (22b) and $\mathbf{v}^{n+1}$ in (22c) are the finite difference approximations for the displacement $\mathbf{d}(t^n)$ and velocity $\mathbf{v}(t^n)$ in terms of the acceleration at the (n + 1) time level. The parameters β and γ determine the stability and accuracy of the algorithm. The values $\beta = 0$ and $\gamma = 1/2$ lead to an explicit scheme (central difference) which is conditionally stable, second-order accurate, and one of the most widely advocated explicit methods. The values of $\beta = 1/4$ and $\gamma = 1/2$ lead to the original Newmark or trapezoidal method which is implicit, unconditionally stable, and second-order time accurate.

γ_s-Family of Direct Self-Starting Methods

$$\begin{aligned}\left[\mathbf{M} + \Delta t\gamma_1\mathbf{C} + \Delta t^2\gamma_1\,\gamma_2\mathbf{K}\right]\mathbf{v}^{n+1} &= \left[\mathbf{M} - \Delta t(1-\gamma_1)\mathbf{C} - \Delta t^2\gamma_1(1-\gamma_2)\mathbf{K}\right]\mathbf{v}^{n} \\ &\quad - \Delta t\mathbf{K}\mathbf{d}^{n} + \Delta t(1-\gamma_1)\,\mathbf{F}^{n} + \Delta t\gamma_1\mathbf{F}^{n+1}\end{aligned} \tag{23a}$$

$$\mathbf{d}^{n+1} = \mathbf{d}^{n} + \Delta t\left[\gamma_3\mathbf{v}^{n+1} + (1-\gamma_3)\mathbf{v}^{n}\right] \tag{23b}$$

where $\mathbf{v}^{n+1}$, $\mathbf{d}^{n+1}$ are the current computed velocity and displacement fields and $\mathbf{v}^{n}$, $\mathbf{d}^{n}$ are the values known from the previous time step or the initial conditions.

For given initial conditions $\mathbf{v}^{n}$, $\mathbf{d}^{n}$, the γ_s-family of representations shown in (23a) directly yields the representative velocities at the current time level n + 1. Next, these velocities are substituted in (23b) to directly obtain the displacement field at time level n + 1. The evaluation of the accelerations is not involved in the computational process. The parameters for γ_s, s = 1,2,3 govern the stability and accuracy of the family of representations. For $0 \le \xi \le 1$ and $\gamma_1 = 1/2$ and $\gamma_3 = 1/2$, and $\gamma_2 = 0$, the scheme is explicit, conditionally stable, and second-order accurate. For $0 \le \xi \le 1$ and $\gamma_1 = 1/2$, $\gamma_2 = 1/2$, and $\gamma_3 = 1/2$, the scheme is implicit, unconditionally stable, and second-order accurate. $\xi \ne 0$ implies those cases where physical damping is present in the problem.

More Recent and Current State-of-the-Art Methods

Other relevant, and more recent state-of-the-art approaches which have been successfully employed to a class of transient/dynamic situations are highlighted in Tamma et al. (see, Refs. [7, 8, 16, 17]).

Concluding Remarks

The objective here was to briefly provide an overview of classical dynamic thermoelasticity models and subsequently describe computational methods for the modeling/analysis of various classes of problems encompassing thermal-structural interactions. The developments shed light on the computational aspects as related to multidisciplinary thermal-structural interactions.

References

1. Duhamel JMC (1837) Second memoire sur les phenomenes thermomecaniques. Journal de l'Ecole Polytechnique, 15 Cahier 25:1
2. Biot MA (1956) Thermoelasticity and irreversible thermodynamics. J Appl Phys 27:240
3. Danilovskaya VI (1950) Thermal stress in elastic half-space arising after a sudden heating of its boundary (in Russian). Prikl MatMekh 14:316
4. Danilovskaya VI (1952) On a dynamical problem of thermoelasticity (in Russian). Prikl Mat Mekh 16:341
5. Sternberg E, Chakravaroty JG (1959) On inertia effects in a transient thermoelastic problem. J Appl Mech 26:503
6. Tamma KK et al (2012) iINTEGRATORS: isochronous integrators and the next generation simulation toolkit for first/second order transient systems. In: 10th World Congress on Computational Mechanics (WCCM-10), July 8-13, 2012, Sao Paulo, Brazil (Semi-Plenary Lecture)
7. Tamma KK et al (2011) An overview and recent advances in vector and scalar formalisms: space/

time discretizations in computational dynamics: a unified approach. Arch Comput Meth Eng 18, (2):119–283
8. Har J, Tamma K (2012) Advances in computational dynamics of particles, materials and structures. Wiley, Chichester
9. Tamma KK (2012) Classical thermo-mechanical models: numerical formulations, Encl. thermal stresses, ETS Entry, Springer-Verlag, Germany
10. Tamma KK, Railkar SB (1987) A generalized hybrid transfinite element computational approach for nonlinear/linear unified thermal/structural analysis. Comp Struct 26(4):655
11. Tamma, KK, Railkar SB (1997) Transfinite element methodology for nonlinear/linear transient thermal modeling/analysis. Int J Numer Methods Eng 25–475.
12. Tamma KK, Railkar SB (1989) Transfinite element methodology towards a unified thermal/structural analysis. Comp Struct 25(5):649
13. Tamma KK, Railkar SB (1987) Nonlinear/linear unified thermal stress formulations: transfinite element approach. Comp Meths Appl Mech Eng 64:415
14. Argyris JM, Scharpf DW (1969) Finite elements in time and space. Aeron J Royal Aeron Soc 73:1041
15. Crank J, Nicolson P (1947) A practical method for numerical evaluation of solutions of partial differential equations of the heat-conduction type. Proc Camb Phil Soc 43:50
16. Shimada M, Tamma KK (2012) Implicit time integrators and designs for first/second order linear transient systems, Encl. thermal stresses, ETS Entry. Springer-Verlag, Germany
17. Shimada M, Tamma KK (2012) Explicit time integrators and designs for first/second order linear transient systems, Encl. thermal stresses, ETS Entry. Springer-Verlag, Germany

Classical Thermomechanical Models: Theoretical Formulations

Kumar K. Tamma
Department of Mechanical Engineering,
University of Minnesota, Minneapolis,
MN, USA

Overview

The "fusion" of both the fields of heat conduction in solids and continuum elasticity results in the so-called field of dynamic thermoelasticity. Typical in the aforementioned class of multidisciplinary problems are those associated with thermal-structural interactions (or thermoelasticity problems). Thermoelasticity represents a generalization of both the heat conduction and the elasticity theories. The theory based on the Fourier's law of heat conduction is known as the classical theory of thermoelasticity. In the classical theory, the thermal disturbances are assumed to propagate at infinite speeds. This results in a parabolic (diffusive) type of thermal response. The focus is upon classical thermomechanical formulations and the consequent theoretical formulations for linear thermoelasticity.

Introduction

Customarily, the modeling/analysis of thermally induced deformations and stresses (the general field of thermal stresses) neglects the effects of the mechanical coupling term in the heat conduction equation [1] and the inertia terms in the elasticity equations. The resulting deformations and stress fields are evaluated from known transient temperature fields as a series of quasi-static thermal stress analysis. While the mechanical coupling term may play a significant role in the case of inelastic solids at elevated temperature environments, inertia effects, however, may become important and need to be accounted for those general situations which experience sudden rapid heating or thermal shock [2]. The class of problems with the temperature field dependent upon the deformation field and vice versa are often referred to as coupled problems, while if the temperature field is independent of the deformation field, an uncoupled problem results. One may encounter (1) thermally induced stress-wave propagation problems, (2) thermally induced inertial dynamic problems, and (3) the field of thermal stresses.

The general class of coupled/uncoupled problems in interdisciplinary thermal-structural mechanics falls in the realm of "thermoelasticity" or "dynamic thermoelasticity." In the development of the governing equations relevant to the aforementioned categories, the formulations emanate starting from the principles of continuum mechanics. The conservation of mass, the conservation of momentum, and the conservation

of energy for a continuum are first described in the sections to follow for the classical models relevant to dynamic thermoelasticity.

A thermoelastic model can be defined as one in which a coupled exchange of mechanical energy and thermal energy takes place under the action of an external thermomechanical load. The field of thermoelasticity represents a generalization of both the theory of elasticity and the theory of heat conduction. The focus here is upon thermoelasticity theory influenced by classical heat conduction effects. The objectives here are to overview and briefly present the basic equations of classical dynamic thermoelasticity theories and illustrate their effects on thermal-structural problems rather than make any attempts to improve upon the various theories [3, 4]. Hence, the basic equations of the thermoelasticity theories are briefly discussed, and pertinent references are cited during the discussions that follow.

Preliminaries

A continuum occupying a volume V_o in the reference configuration occupies a volume V in the current configuration. Let X_i be the coordinates of the continuum particles in the reference configuration at time $t = 0$ which are often called as the "material coordinates," while x_i be the coordinates in the current configuration at time t which are often called as the "spatial coordinates." $\mathbf{I_i}$ and $\mathbf{e_i}$ are the unit normal vectors in the reference and the current configurations, and $\mathbf{P_o}$, $\mathbf{P}$ are the position vectors of a typical particle of the continuum in the reference and the current configuration. The two basic approaches generally followed in the derivation of governing equations for flow and motion are the Lagrangian and the Eulerian approach. The motion of the continuum may be expressed either in terms of the material coordinates (Lagrangian approach) as given by (1) or in terms of the spatial coordinates (Eulerian approach) as given by (2). Physically, the Lagrangian approach focuses attention on specific particles of the continuum, whereas the Eulerian description concerns itself with a particular region of the space occupied by the continuum.

In the Lagrangian approach, the mass of the selected particles remains constant, while the volume occupied by these particles is assumed to change with time. Hence, the spatial coordinates can be expressed as a function of the material coordinates as

$$x_i\ (X_1, X_2, X_3, t) = x_i\ (\bar{X}, t) \tag{1}$$

Alternately, in the Eulerian approach, the volume (termed as the control volume) occupied by the particles within the continuum is fixed, and the different particles are assumed to occupy the same control volume at different times. Hence, the material coordinates can be expressed in terms of the spatial coordinates on the basis of the Eulerian approach as given by (2) which essentially is the inverse relationship of (1):

$$X_i\ (x_1,\ x_2,\ x_3,\ t) = X_i\ (\overline{x}, t) \tag{2}$$

The two coordinate systems, namely, the coordinate systems representing the reference and the current configuration, can be superposed leading to the vector $\mathbf{b} = 0$. The mapping of spatial coordinates x_i and the material coordinates X_i is assumed as one-to-one with continuous partial derivatives which leads to the following relationship given by (3) where J is called as the Jacobian of the transformation:

$$dx_i = J\ \ dX_j \tag{3}$$

where

$$J = \left|\frac{dx_i}{dX_j}\right| \tag{4}$$

We focus attention here to the Lagrangian description of motion. The basic equations of dynamic thermoelasticity, namely, continuity, equations of motion, and energy, are briefly described in the sections to follow.

Conservation of Mass

In this section, the continuity equation for a single-phase continuum is derived.

The mass M occupying a region V bounded by surface ⌈ at time t can be expressed as

$$M = \int_V \rho \, dV \tag{5}$$

where $\rho = \rho(\mathbf{x}, \mathbf{y}, \mathbf{z}, t)$ is the mass density of the continuum field and dV denotes the element of V. The rate of change of mass with respect to time is given as

$$\frac{DM}{Dt} = \frac{D}{Dt} \int_V \rho \, dV \tag{6a}$$

where D/Dt is the total (material) time derivative.

From the principle of conservation of mass, the mass of a given body during motion and possible deformations remains unchanged [5]. Therefore,

$$\frac{DM}{Dt} = \frac{D}{Dt} \int_V \rho \, dV = 0 \tag{6b}$$

The material derivative of the volume integral in (6b) can be expressed [5] as

$$\int_V \left[\frac{\partial \rho}{\partial t} + (\rho v_i)_{,i} \right] dV = 0 \tag{7}$$

where v_i is the velocity component and comma (,i) denotes partial differentiation with respect to the spatial variables. Since the above equation holds for any arbitrary volume V, the integrand must vanish or

$$\frac{\partial \rho}{\partial t} + (\rho v_i)_{,i} = 0 \tag{8}$$

The above equation is called the continuity equation, which represents the conservation of the mass of the continuum. The above equation can be modified for the case of a continuum with reference density ρ_0 different from the current density ρ. The resulting expression is given [6] as

$$\frac{\rho_0}{\rho} = 1 + v_{i,i} \tag{9}$$

Conservation of Linear Momentum

The equations of motion based on the principle of conservation of linear momentum are discussed next. This principle states that the time rate of change of the total momentum of a given body equals the vector sum of all the external forces acting on the body, provided Newton's third law of action and reaction, governs the internal forces.

The total momentum over the volume is given by

$$\int_V \rho \, v_i \, dV \tag{10}$$

where v_i is the velocity, and the time rate of momentum is

$$\frac{D}{Dt} \int_V \rho \, v_i \, dV \tag{11}$$

and $\frac{D}{Dt}$ denotes the total (material) time derivative.

Using the Reynolds transport theorem [7], the material derivative of the volume integral given by (11) can be expressed as

$$\frac{D}{Dt} \int_V \rho \, v_i \, dV = \int_V \left[\frac{\partial \rho v_i}{\partial t} + (\rho v_i \, v_j)_{;j} \right] dV \tag{12}$$

$$= \int_V \left[v_i \left(\frac{\partial \rho}{\partial t} + \frac{\partial \rho v_j}{\partial x_j} \right) + \rho \left(\frac{\partial v_i}{\partial t} + v_j \frac{\partial v_i}{\partial x_j} \right) dV \right] \tag{13}$$

The first term in the parentheses (13) vanishes by the principle of conservation of mass, and the second term in the parentheses is equal to the acceleration $\dot{v}_i$. The time rate of momentum (11) stated earlier can now be expressed as

$$\frac{D}{Dt}\int_V \rho v_i \, dV = \int_V \rho \dot{v}_i \, dV \tag{14}$$

where superposed dot (.) is used to denote the material time derivative. The momentum principle now can be expressed as

$$\int_V \rho \dot{v}_i \, dV = \int_V \rho f_i \, dV + \int_S T_i dS \tag{15}$$

where ρf_i is the body force and T_i is the surface traction and is expressed in terms of the stress tensor $\sigma_{ij}(\sigma_{ij} = \sigma_{ji})$ and the unit normal n_j as $\sigma_{ij}\, n_j$. Transforming the surface integral in (15) to a volume integral by the Gauss' theorem, we have

$$\int_V \rho \dot{v}_i \, dV = \int_V \rho f_i \, dV + \int_V \sigma_{ij,j} \, dV \tag{16}$$

The above relationship holds good for all volumes V. This implies that the integrand of (16) must vanish. Thus, the equations of motion of a continuum are

$$\rho \dot{v}_i = \rho f_i + \sigma_{ij,j} \tag{17}$$

Conservation of Energy

The time rate of change of the kinetic energy added to the rate of change of internal energy is equal to the sum of the rate of work which is done on the body due to body forces ρf_i and surface tractions T_i, plus the heat produced by internal heat generation and the rate of heat input per unit time.

For a heat-conducting elastic body, the conservation principle (first law of thermodynamics) takes the form [5]

$$\frac{D}{Dt}\int_V \rho\psi \, dV + \frac{D}{Dt}\int_V \frac{1}{2}\rho v_i v_i \, dV = \int_V \rho f_i v_i \, dV + \int_S T_i v_i \, dS + \int_V \rho Q \, dV - \int_S q_i n_i \, dS \tag{18}$$

where ψ is the internal energy, ρ is the mass density, f_i is the body force per unit mass, v_i is the velocity of the particles of the body, T_i $(= \sigma_{ij} n_j$ and where $\sigma_{ij} = \sigma_{ji})$ is the external surface traction, q_i is the heat flux, Q is the heat produced by the internal heat sources per unit time and unit mass, and n_i is the exterior normal at the surface.

Following the development leading to (14), the first term in (18) can be written as

$$\frac{D}{Dt}\int_V \rho\psi \, dV = \int_V \rho\dot{\psi} \, dV \tag{19}$$

upon using local mass conservation. Proceeding similarly, we have the second term in the (18) as

$$\frac{D}{Dt}\int_V \frac{1}{2}\rho \, v_i v_i \, dV = \int_V \rho \, v_i \dot{v}_i dV \tag{20}$$

Converting the surface integrals to volume integrals, the resulting expressions (18) can be represented as

$$\int_V \Big((\rho\dot{\psi} - \sigma_{ij} v_{i,j} + q_{i,i} - \rho Q) + v_i(\rho \dot{v}_i - \sigma_{ij,j} - \rho \, f_i) \Big) dv = 0 \tag{21}$$

Further, employing the equations of motion (17) and taking advantage of the symmetry of the stress tensor, the energy equation (21) takes the form

$$\int_V (\rho\dot{\psi} - \sigma_{ij}\dot{\varepsilon}_{ij} + q_{i,i} - \rho Q) dv = 0 \tag{22}$$

or

$$\rho(\dot{\psi} - Q) = \sigma_{ij}\dot{\varepsilon}_{ij} - q_{i,i} \tag{23}$$

where

$$\varepsilon_{ij} = \frac{1}{2}(u_{i,j} + u_{j,i}) \tag{24}$$

The continuity equation, the equation of motion, and the energy equation are subsequently combined with the relevant form of the Fourier's model of heat conduction and the second law of thermodynamics for formulating the linear thermoelasticity equations.

Classical Dynamic Thermoelasticity Equations

The dynamic thermoelasticity theory based on the Fourier heat conduction equation is known as the classical theory of dynamic thermoelasticity. In the classical theory, the thermal disturbances are assumed to propagate at infinite speeds through the continuum. Coupling between the deformation and the temperature fields was originally postulated by Duhamel [8]. The fundamental relations and the basic equations of thermoelasticity are given in Biot [1]. Solutions to the problems in dynamic thermoelasticity have drawn considerable interest, and the first analytic solution to an initial boundary value problem in dynamic uncoupled classical thermoelasticity is that presented by Danilovskaya [9]. This well-known Danilovskaya's problem proposed in the 1950s originally studies an elastic semi-finite medium subjected to a uniform heating on its boundary plane, the plane assumed to be always traction-free. The temperature variations in the half-space were calculated from the classical heat conduction equation, neglecting thermomechanical coupling. Next, the associated thermally induced loads were used for predicting the dynamic response of the medium. These results were later extended by Danilovskaya [10] to account for boundary-layer conductance. Sternberg and Chakravorty [11] further extended the problem to include a more realistic ramp-type temperature boundary condition.

The linear thermoelasticity theory is based on the following fundamental equations:
Conservation of Mass (Ref. [6])

$$\frac{\rho_0}{\rho} = 1 + v_{i,i} \tag{25}$$

Conservation of Momentum (Ref. [5])

$$\sigma_{ji,j} + \rho\, f_i = \rho \dot{v}_i \tag{26}$$

where

$$\sigma_{ji} = \sigma_{ij} \tag{27}$$

Energy Equation (Ref. [5])

$$\rho(\dot{\psi} - Q) = \sigma_{ij}\, \dot{\varepsilon}_{ij} - q_{i,i} \tag{28}$$

Fourier's Law of Heat Conduction (Ref. [5])
The classical Fourier's law, on which the theory of heat conduction is based, relates the heat flux vector q_i to the temperature gradient $\theta_{,j}$ through the equation

$$q_i = -k_{ij}\, \theta_{,j} \tag{29}$$

where the thermal conductivity k_{ij} must be positive to assume a positive rate of entropy production and
ρ = mass density in current configuration
ρ_0 = mass density in reference configuration
σ_{ij} = stress tensor (Cauchy)
ε_{ij} = linear strain tensor = $\frac{1}{2}(u_{i,j} + u_{j,i})$
u_i = displacement vector
v_i = velocity vector
f_i = body force vector
q_i = heat flux vector
ψ = internal energy
Q = heat source
k_{ij} = thermal conductivity tensor ($k_{ij} = k_{ji}$)
θ = temperature ($T–T_0$)
T = absolute temperature
T_0 = initial uniform temperature (assumed to be positive)

Equations (25–29) are supplemented by the second law of thermodynamics, which demands positive production of entropy in the form of the Clausius-Duhem inequality [7]. Relevant details

are described elsewhere. Considering a function ϕ known as the free energy (or Helmholtz's function), which is a combination of the internal energy, temperature, and entropy. The Helmholtz's function is represented [12] as

$$\phi = \psi - T\eta \tag{30}$$

or

$$\dot{\phi} = \dot{\psi} - T\dot{\eta} - \eta\dot{T} \tag{31}$$

where ψ, η, and T are functions of the state, finally leading to the following to be concluded:

$$q_i \; T_{,i} \quad \leq \quad 0 \quad \text{and} \quad q_{i,i} + \rho(T\dot{\eta} - Q) = 0$$

Linear Thermoelasticity Approximations

The fundamental assumptions of the theory of linear thermoelasticity are [7] that the field variables are infinitesimally small and that the free energy is a differentiable function of only the instantaneous strain and absolute temperature.

Let θ $(= T - T_0)$ as the increment of the absolute temperature T over the reference temperature T_0. The reference temperature is assumed to be uniform throughout the body. The associated mechanical state of zero strain and zero stress is known as the natural or unstressed state. For linear thermoelasticity, it is assumed that the increment of the temperature compared with the reference temperature is small (Ref. [6]), that is,

$$\frac{|\theta|}{T_0} << 1 \tag{32}$$

For the constitutive relations, consider the free energy per unit volume φ (also known as the thermoelastic potential) which is given [6] as

$$\varphi = \rho\phi \; (\varepsilon_{ij}, T) \tag{33}$$

Expanding the function φ in a power series in terms of its arguments ε_{ij} and T $(= \theta + T_0)$, and ignoring in the series all terms of order higher than the second (a term linear in θ is disregarded since it does not appear in the equations of interest), the resulting expression [6] is

$$\varphi = \rho\phi = \varphi_0 + d_{ij}\,\varepsilon_{ij} + \frac{1}{2}\, D_{ijkl}\;\varepsilon_{ij}\;\varepsilon_{kl} - \beta_{ij}\,\varepsilon_{ij}\,\theta - \frac{1}{2}\left(\frac{\rho c}{T_0}\right)\theta^2 \tag{34}$$

where φ_0 is the energy in the initial state. The coefficient D_{ijkl} is the elasticity tensor, β_{ij} is the thermoelasticity tensor, and c is the specific heat per unit mass in the isothermal state.

In the natural state of the body, its free energy vanishes, then $\varphi_0 = 0$ and $d_{ij} = 0$ (since σ_{ij}, ε_{ij} and θ vanish simultaneously). Thus, (Ref. [6]) we have

$$\varphi = \frac{1}{2}\, D_{ijkl}\;\varepsilon_{ij}\;\varepsilon_{kl} - \beta_{ij}\,\varepsilon_{ij}\,\theta - \frac{1}{2}\left(\frac{\rho c}{\theta_0}\right)\theta^2 \tag{35}$$

From the above considerations, we obtain the following Duhamel-Neuman relations and entropy density function as (Ref. [6])

$$\sigma_{ij} = D_{ijkl}\;\varepsilon_{kl} - \beta_{ij}\,\theta \tag{36}$$

$$\rho\eta = \beta_{ij}\,\varepsilon_{ij} + \frac{\rho c}{T_0}\theta \tag{37}$$

The stress and strain tensors are symmetric.

Substituting for q_i, η, and σ_{ij} in a linearized form, we obtain the linear coupled dynamic thermoelasticity equations based on the classical theory [6] as follows:

Classical Dynamic Thermoelasticity Equations

The coupled equations are given as

$$\rho c\;\dot{\theta} + T_o\;\beta_{ij}\dot{u}_{i,j} - (k_{ij}\;\theta_{,j})_{,i} = \rho\; Q \tag{38}$$

$$\rho\ddot{u}_i - (D_{ijkl}\;\varepsilon_{kl} - \beta_{ij}\;\theta)_{,j} = \rho\; f_i \tag{39}$$

where T_o is the reference temperature and βij is the thermoelasticity tensor.

Quasi-Static Representations

The coupled quasi-static (neglecting dynamic aspects in the structure) representations commonly employed for thermomechanical applications can be cast in the form

$$\rho c\ \dot{\theta} + T_o\ \beta_{ij}\dot{u}_{i,j} - (k_{ij}\ \theta_{,j})_{,i} = \rho\ Q \qquad (40)$$

$$-\ (D_{ijkl}\ \varepsilon_{kl} - \beta_{ij}\ \theta)_{,j} = \rho\ f_i \qquad (41)$$

Static Representations

The coupled representative steady thermal and static equations of equilibrium can be cast in the form

$$T_o\ \beta_{ij}\ \dot{u}_{i,j} - (k_{ij}\ \theta_{,j})_{,i} = \rho\ Q \qquad (42)$$

$$-\ (D_{ijkl}\ \varepsilon_{kl} - \beta_{ij}\ \theta)_{,j} = \rho\ f_i \qquad (43)$$

Boundary and Initial Conditions

The general thermal boundary and initial conditions that may exist for a given domain $\mathbf{R}$ bounded by a closed surface $\partial\mathbf{R} = \partial\mathbf{R}_p \cup \partial\mathbf{R}_q$ are given as

Thermal:

$$\theta = \theta_p \quad \text{on } \partial\mathbf{R}_p \qquad (44)$$

$$q_i\, n_i = -q_S + h(\theta - \theta_h) + \sigma_T\ \varepsilon_T(\theta^4 - \theta_r^4) \text{ on } \partial\mathbf{R}_q \qquad (45)$$

or

$$q_i\, n_i + q_S - q_h - q_r = 0 \qquad \text{on} \quad \partial\mathbf{R}_q \qquad (46)$$

and

$$\theta(\mathbf{x}, o) = \theta_0 \ \text{ in } \mathbf{R} \qquad (47)$$

The above equations refer to general unsteady nonlinear thermal fields in materials with thermophysical properties dependent upon temperature. The first boundary condition (44) is the prescribed temperature condition on $\partial\mathbf{R}_p$. The second boundary condition (45) is the flux condition on $\partial\mathbf{R}_q$. The terms q_s, q_h, and q_r represent the surface-heating rate per unit area, the rate of heat flow per unit area due to convection, and the rate of heat flow per unit area due to radiation, respectively; h is the convective heat transfer coefficient, θ_h is the convection medium temperature, σ_T is the Stefan-Boltzmann constant, ε_T is the surface emissivity, and θ_r is the radiation medium temperature.

Mechanical:

Typical mechanical boundary and initial conditions are given as

$$u_i = g_i \quad \text{on } \partial\mathbf{R}_p \qquad (48)$$

$$\sigma_{ij}\, n_j = h_i \quad \text{on } \partial\mathbf{R}_q \qquad (49)$$

and the following initial conditions:

$$u_i\ (t = 0) = u_i^0 \quad \text{in } \mathbf{R} \qquad (50)$$

$$\dot{u}_i\ (t = 0) = \dot{u}_i^0 \qquad (51)$$

The first boundary condition is the prescribed displacement on $\partial\mathbf{R}_p$, and the second boundary condition is the traction condition on $\partial\mathbf{R}_q$. Equations (38–39) represent the classical fully coupled dynamic thermoelasticity equations. A two-way coupled or fully coupled problem implies that the temperature field influences the displacement field and vice versa. A one-way coupled problem implies that only the temperature changes influence the displacement field. A one-way coupled problem with a transient thermal field and a static structural field leads to a quasi-static analysis. For static analysis, the transient terms in both the thermal and the structural fields are neglected. For the numerical modeling and simulation of the class of general dynamic problems, see Refs. [13–16].

Concluding Remarks

The dynamical thermoelasticity theory is a "fusion" of the multidisciplinary areas of heat conduction in solids and continuum elasticity. The focus was

upon the classical formulations. The computational issues are indeed challenging, and the development of accurate and efficient numerical approaches is described in a separate entry. The objective was to briefly provide to the reader a quick overview of nonclassical dynamic thermoelasticity formulations and equations governing these situations.

References

1. Biot MA (1956) Thermoelasticity and irreversible thermodynamics. J Appl Phys 27:240
2. Boley BA, Weiner JH (1960) Theory of thermal stresses. Wiley, New York
3. Green AE, Lindsay KE (1972) Thermoelasticity. J Elast 2:1
4. Lord HW, Shulman Y (1967) A generalized dynamical theory of thermoelasticity. J Mech Phys Solids 15:299
5. Fung YC (1965) Foundations of solid mechanics. Prentice-Hall, Englewood Cliffs
6. Nowacki W (1975) Dynamic problems of thermoelasticity. In: Francis PH, Warsaw PWN, Polish Scientific Publishers, Poland, and Noordhoff, Industrial Publishing Company, Leyden, ISBN 90-286-0045-0, The Netherlands
7. Lawrence EM (1969) Introduction to the mechanics of a continuum medium. Prentice-Hall, Englewood Cliffs
8. Duhamel JMC (1837) Second memoire sur les phenomenes thermomecaniques. Journal de l'Ecole Polytechnique, 15 Cahier 25:1
9. Danilovskaya VI (1950) Thermal stress in elastic half-space arising after a sudden heating of its boundary, (in Russian). Prikl MatMekh 14:316
10. Danilovskaya VI (1952) On a dynamical problem of thermoelasticity, (in Russian). Prikl Mat Mekh 16:341
11. Sternberg E, Chakravaroty JG (1959) On inertia effects in a transient thermoelastic problem. J Appl Mech 26:503
12. Nowinski JL (1978) Theory of thermoelasticity with applications. Noordohf, Alphen Aan Den Rijin
13. Tamma KK et al (2012) iINTEGRATORS: Isochronous integrators and the next generation simulation toolkit for first/second order transient systems. In: 10th World congress on computational mechanics (WCCM-10), 8–13 July 2012, Sao Paulo, Brazil (Semi-Plenary Lecture)
14. Tamma KK et al (2011) An overview and recent advances in vector and scalar formalisms: space/time discretizations in computational dynamics – a unified approach. Arch Comput Methods Eng 18 (2):119–283
15. Har J, Tamma KK (2012) Advances in computational dynamics of particles, materials and structures. Wiley, Chichester
16. Tamma KK (2012) Classical thermo-mechanical models: numerical formulations, Encyclopedia. Thermal stresses, ETS Entry. Springer

Classical Two-Dimensional Models

▶ Classical Governing Equations for the Thermomechanical Analysis of Shells

Clutches

▶ Clutches, Hot Spotting Behavior
▶ Perturbation Methods in Thermoelastic Instability (TEI) with Finite Element Implementation

Clutches, Hot Spotting Behavior

Przemyslaw Zagrodzki
Raybestos Powertrain, Crawfordsville, IN, USA

Synonyms

Clutches

Overview

Hot spotting is a phenomenon observed in fiction clutches as well as many other types of sliding systems. The term hot spotting is typically used in reference to macroscopic phenomena, and all considerations here are confined to this scale. Sliding motion causes generation of frictional heat at the interface between members in relative motion. It is desired that distribution of the heat be uniform across the entire interface, meaning uniform thermal load. Geometry imperfections of mating surfaces, deformations of clutch components, and other factors cause that in practice heat distribution varies from place to place. Moderate heat variation is natural and acceptable. However, sometimes very strong local heat concentrations may occur with very low or complete lack of heat elsewhere across the nominal interface. This phenomenon is commonly known as

hot spotting. It often leads to excessive wear, malfunction, or even complete failure of the sliding system due to thermal damage. The mechanism of creation of hot spots was not understood until discovery made by J.R. Barber in the late 1960s [1] that identified the core mechanism of this phenomenon, which involves coupling between generation of frictional heat and thermoelastic deformation of sliding members. Since then, the hot spotting and the theory behind it were subject of intense exploration, and substantial progress in this area has been made.

Friction Clutches, Function, and Modes of Operation

Friction clutch is a mechanical device that transfers power from one rotating component to another. Generally, a clutch is used wherever the ability to control power flow is required: disconnecting the rotating members and connecting them. The process of connecting is initiated when the members rotate at different speeds or when one of them rotates and the other stands still. The process completes when both are brought to the same speed. This process has by nature a transient character. An important functional requirement for a friction clutch is a smooth transition during speed synchronization. An example of a clutch operating in such a mode is a so-called shifting clutch used in automotive automatic transmissions. We should note that there is a broad variety of clutches in terms of function and associated mode of operation. Friction clutches may also play a role such as maintaining some amount of speed difference between two members or transferring required amount of torque under conditions of relative motion of the members. Slip duration of a clutch operating in any of those capacities may range from short-lasting event to a long-term process.

Types and Design of Friction Clutches

Two types of clutches, wet and dry, are in common use. Wet clutches operate in a fluid such as transmission oil. Oil lubricates and cools the friction surfaces. However, friction surfaces are not intended to be separated by a fluid film during clutch engagement. Instead, boundary lubrication is developed at the interfaces during clutch slip, which helps to produce a relatively high and stable friction coefficient. Friction pair in a wet clutch is typically constituted of dissimilar materials. One of them is a ferrous material, steel, or cast iron; the other is a special friction composite. There is a variety of friction materials in use such as paper-type composites or sintered metals. Most friction materials for wet clutches have substantial porosity so that the fluid can penetrate the material.

In dry clutches, the friction pair is created by a friction material sliding against ferritic material, usually cast iron, and there is no fluid lubricant. Dry friction materials may have various compositions and are generally different from wet materials, although some sintered metals can be used in both applications. Dry friction pairs have a substantially higher friction coefficient than wet ones, which is advantageous. On the other hand, the friction coefficient of dry materials shows much greater variability. Also the wear is much greater than that of wet materials, which is accompanied by substantial production of wear debris.

From the design point of view, clutches can be classified depending on the number of friction disks. Wet clutches usually include multiple disks with layers of friction materials interleaved with disks (plates) made of steel; they are known as multidisk clutches. Rarely, they include a single friction disk with two sliding interfaces. Some wet clutches, such as those used in torque converters of automotive transmissions, may have just a single sliding interface. Most common dry clutches have a single friction disk with two sliding interfaces or two disks with four interfaces. Working surfaces in clutches are typically annular, and both mating members extend over the whole circumference.

Heat Generation in Friction Clutches

Energy is dissipated in a clutch whenever transfer of frictional torque and slip take place

concurrently. Power P dissipated in the clutch is determined by equation

$$P = M \cdot \omega \tag{1}$$

where M is the torque and ω is the relative angular speed of input member and output member. In general, both torque M and relative speed ω vary over time. For description of local phenomena on sliding surfaces, we express infinitesimal torque as

$$dM = fpr \cdot dA \tag{2}$$

where dA is the infinitesimal area of friction surface, r – the radial coordinate of dA, f – the friction coefficient, and p – the contact pressure. Then the torque can be expressed as

$$M = \int_A fpr \cdot dA \tag{3}$$

Substitution of (3) into (1) yields

$$P = \int_A fpr\omega \cdot dA = \int_A fpv \cdot dA \tag{4}$$

where local sliding speed $v = r\omega$. The integrand in (4) expresses the local frictional heat flux

$$q = fpv \tag{5}$$

Hot Spotting Engineering Perspective

It is difficult and often impossible to observe the process of formation of hot spots in clutches. That process was successfully monitored by means of infrared imaging in designs like automotive disk brakes, where a portion of the surface of the cast iron disk is exposed during operation. Most typically, however, evidence of hot spots is seen after the event, usually having the form of dark local thermal discoloration of the surface of the ferrous material. In severe cases, plastic deformation of the material caused by high thermal stress occurs. Plastic deformation is sometimes accompanied by cracks. Those evidences of hot spotting are customarily also called hot spots.

Clutches, Hot Spotting Behavior, Fig. 1 Hot spots on the surface of steel disk of a wet clutch produced after single clutch engagement

Figure 1 shows an example of hot spots created on the surface of a steel disk of a wet multidisk clutch. The hot spots are discontinuous in the sliding direction (circumferential direction), and this type of pattern is called *focal* hot spots. On the other side of the disk, which also has a working surface sliding against another friction disk, similar pattern occurs. Hot spots on two sides can be alternately located in circumferential direction, creating an *antisymmetric* mode [2]. Alternatively, they can be aligned, constituting a *symmetric* mode. Focal hot spots arise on the steel surface, and there is no similar pattern on the mating surface of friction material. However, on the surface of friction material, there might be ring-shaped traces of degraded material, a damage incurred by hot spots occurring on the mating metal surface. Of the two

Clutches, Hot Spotting Behavior, Fig. 2 Hot spots on the surface of steel disk of a wet clutch after multiple engagements

Clutches, Hot Spotting Behavior, Fig. 3 Hot spots on the surface of cast iron plate of an automotive dry clutch

materials, focal hot spots generally occur on the one with greater thermal conductivity [2]. Hot spots in Fig. 1, which exhibit a quite regular pattern, were produced during just a single cycle of clutch operation. Figure 2 shows further examples of focal hot spots on surfaces of metal disk of a wet multidisk clutch. They show a fairly irregular pattern. This irregular geometry is likely to be the result of a sequence of hot spotting events, some of them causing permanent deformation of the steel disks. The subsequent hot spotting will occur in a system that is geometrically modified and therefore produces different patterns.

Figure 3 shows a part of a dry automotive clutch with hot spots. The part is called pressure plate and is made of cast iron. It has sliding surface only on one side and slides against a single friction disk.

A quite different pattern of hot spots occurring in a wet multidisk clutch is shown in Fig. 4. The hot spots are ring-shaped and are sometimes called *band* hot spots [3]. Unlike focal hot spots, band hot spots occur on both the metal surface and the mating friction material surface.

Hot spots have been observed in sliding systems such as clutches and brakes for a long time [1, 4]. One of the most comprehensive descriptions for friction brakes was provided by Anderson and Knapp [3], where different patterns and conditions of occurrence were discussed. Many of these observations apply to friction clutches as well.

Mechanisms of Spotting

Hot spots can be caused by an imperfect geometry of the clutch disks or by clutch design features that induce nonuniform pressure distributions at sliding interfaces. These causes of hot spots are relatively easy to identify and eliminate. In most cases, however, hot spots arise in absence of such distinct contributions. Geometric profiles of surfaces measured before hot spotting often do not show correlation with hot spots' pattern observed afterward. The mechanism of hot spotting relies on interactions between thermal deformations of clutch components and the distribution of frictional heat. This mechanism was identified by James R. Barber when he studied hot spots in railway brakes [1]. It can be explained as follows. Local heat generation due to friction is proportional to the local contact pressure (5). Consequently, areas with higher contact pressure experience higher temperature rise and thereby greater thermal expansion. The increased local thermal expansion, in turn, causes further local pressure increase and further pressure concentration. This mechanism inherits a positive feedback loop, which may produce system instability. Barber called it frictionally excited thermoelastic instability (abbreviation: TEI). Numerous later studies further proved a crucial role of TEI in hot spotting in a broad variety of sliding systems, including clutches.

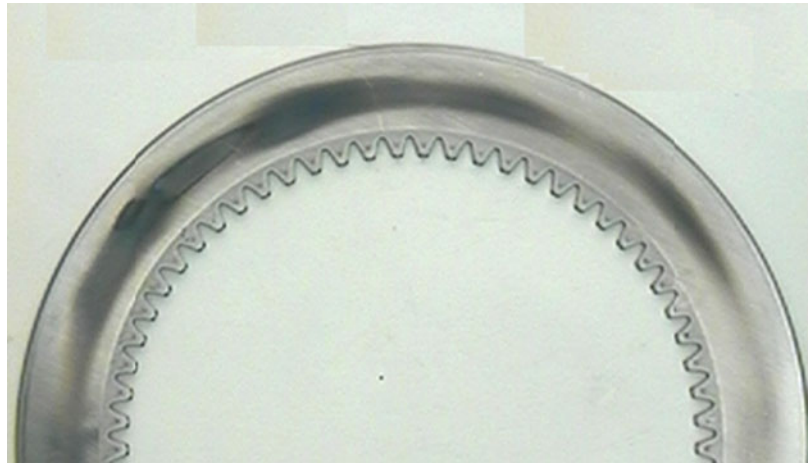

Clutches, Hot Spotting Behavior, Fig. 4 Hot spots on the surface of steel disk of a heavy-duty wet clutch

Model-Based Hot Spotting Analysis

Analytical description of thermoelastic behavior of a sliding system includes the following physical phenomena:

1. Heat conduction in the members that are in frictional contact with appropriate boundary conditions at the interface. The boundary conditions include the following: (*a*) condition of temperature continuity across the interface or definition of temperature discontinuity, such as contact resistance, and (*b*) definition of heat generation.
2. Thermal deformation of system components due to temperature field defined by problem (1), with sliding contact conditions at the interfaces.

Part of the solution of problem (2) is the contact pressure p at the interface. The pressure, in turn, defines generation of a frictional heat flux $q = fvp$ (5) in problem (1). It is clear from interrelations between the two problems that the compound thermoelastic problem is fully coupled, and equations describing thermal and thermoelastic behavior have to be solved simultaneously.

The first analytical description of this thermoelastic problem was given by Barber [1] along with his fundamental explanation of the core mechanism. The next milestone was Dow and Butron's study [5] where they considered a perturbation imposed over the solution of the unperturbed thermoelastic problem. In this way, they reduced the problem to an eigenvalue problem, which is a robust approach to stability analysis. These early works showed that stability depends on the sliding speed: when the speed exceeds some threshold, called critical speed, the system becomes unstable – the crucial finding for TEI and thereby for understanding mechanism responsible for hot spotting. Early studies provided satisfactory estimation of the critical speed in some cases, while in other, the predictions were very inaccurate [6], making practical usefulness of the analytical solution questionable. In the early models, an infinite spatial extent of the bodies in direction normal to the contact interface was adopted, and later it was found that accounting for real, finite dimensions is crucial for a realistic behavior. Furthermore, in sliding systems where both sides of metal disks have sliding interfaces, as is the case with multidisk clutches, there is strong coupling between the two sides [2, 7], which dramatically reduces stability, and this aspect has certainly to be included in the model.

We can distinguish three major approaches to modeling of the thermoelastic behavior: (1) analytical models that lead to an analytical eigenvalue stability problem [2, 5, 8], (2) numerical models to simulate thermoelastic behavior as a time-dependent process [7, 9, 10]; they usually utilize the finite element method (FEA), see Fig. 5, and (3) modal decomposition that

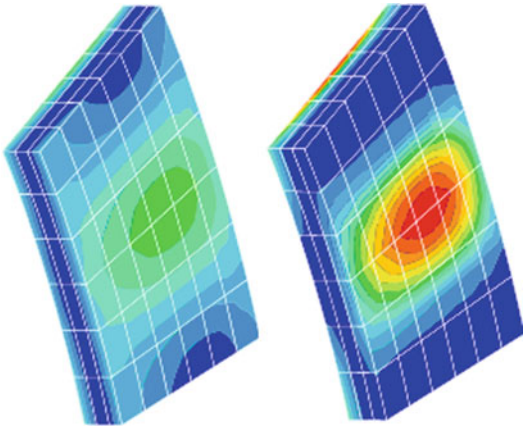

Clutches, Hot Spotting Behavior, Fig. 5 Hot spots obtained from finite element simulation of thermoelastic contact in a wet clutch

encompasses two steps: spatial discretization of the problem using FEA and then reduction to a discrete eigenvalue problem [11–14]. Each of these approaches has its own distinct features, and they are to some extent complementary.

In many practical cases, the models do not provide a highly accurate estimation of the critical speed. This is due to the complexity of phenomena involved and related involvement of many parameters, some of which exhibit inherent variability or are difficult to evaluate. For example, the friction coefficient in dry conditions exhibits significant variability that is dependent on temperature and other conditions. Nonetheless, modeling provides an exceptional insight into the mechanisms governing hot spotting, and even if quantitative accuracy is not fully satisfactory, modeling usually gives univocal directional hints. Indeed, modeling has lead to great progress in mitigation of hot spotting in clutches in recent years.

Key Findings

Existence of the critical sliding speed, that is, speed below which the system is stable and above which it is unstable, is one of the key findings. This fact was not entirely intuitive as in conventional engineering thinking, propensity to hot spotting was often associated with frictional heat flux fvp so that the pressure p was

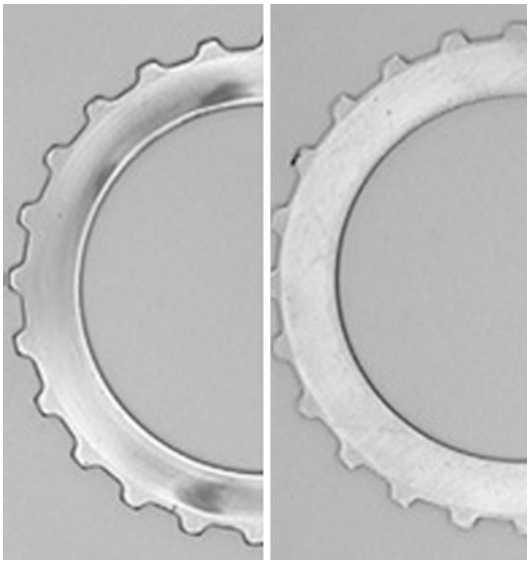

Clutches, Hot Spotting Behavior, Fig. 6 Surface of a steel disk after experimental test. Conditions: (*both cases*) single engagement, energy dissipated 28 kJ, slip duration 0.74 s; (*left*) sliding speed 32 m/s, mean contact pressure 1.14 MPa; (*right*) sliding speed 19.6 m/s, mean contact pressure 1.87 MPa

considered to be a factor as important as the speed v. TEI theory predicts independence of stability on pressure p, a fact verified experimentally (see Fig. 6). More precisely, pressure p may affect thermoelastic stability indirectly; this is the case when friction material is nonlinear with pressure-dependent properties such as modulus of elasticity.

Eigenvalue analysis of the thermoelastic sliding system provides a set of eigenmodes and associated eigenvalues. Each eigenmode represents a pattern of thermoelastic deformation or, in other words, a pattern of potential hot spots. The eigenvalue represents exponential growth rate of the mode. If the real part of an eigenvalue is negative or zero, the mode is stable, otherwise it is unstable. The eigenvalue problem is speed-dependent, and the modes and eigenvalues evolve as the sliding speed changes (Fig. 7). The speed at which the specific eigenvalue is found to be zero is the critical speed. In general, there are multiple unstable modes and multiple corresponding critical speeds. The lowest of all these speeds is considered the critical speed of the system.

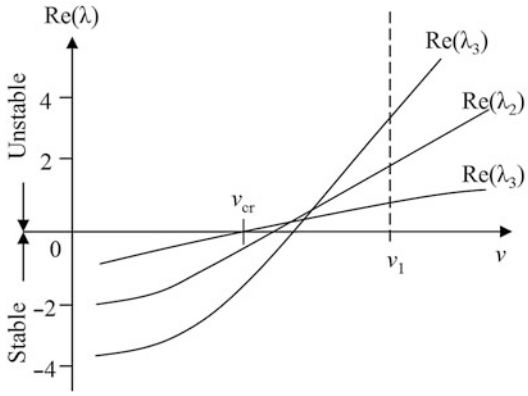

Clutches, Hot Spotting Behavior, Fig. 7 Example curves: real parts of eigenvalues as a function of sliding speed representing frictionally excited thermoelastic instability problem

If the sliding speed substantially exceeds the critical speed, more than one mode can be unstable. In this case, thermoelastic deformation represented by each of the unstable modes grows exponentially, but often one of them distinctly dominates. The dominating mode is not necessarily the one that has the lowest critical speed (i.e., the one that determines stability limit of the system). It tends to be the mode with the highest growth rate at a given sliding speed (Fig. 7). However, relative strength of excitation of individual modes also influences their magnitude and may play a meaningful role when growth rates are close [13]. Excitation is caused by different factors, one of them being pressure variation due to geometry imperfections. It is clear from this discussion that hot spots of different patterns can occur in the same clutch as the operational conditions vary. As discussed earlier, permanent deformations of disks may lead to an irregular pattern of hot spots. Similarly, sequence of hot spotting events with distinct modes may produce an irregular pattern such as that shown in Fig. 2.

In multidisk clutches, both sides of metal disks and friction disks have sliding interfaces. There is a strong thermomechanical interaction between the two sides [2, 7, 13] that promotes instability. Antisymmetric mode of deformation of the metal disk manifests this interaction, and this mode is typically by far the most unstable one [2, 11].

Mitigation of Hot Spotting

Hot spotting is not acceptable in clutches because of the detrimental consequences for clutch performance and durability. In engineering practice, a set of measures are taken to mitigate this unwanted phenomenon. It is convenient to group the factors that determine hot spotting into three categories:

- Stability of the sliding system
- Exposure of the system to operation in the unstable regime
- Excitation of unstable mode(s)

Stability of the Sliding System

Ensuring thermoelastic stability of a clutch so that the critical speed is higher than the range of operational speeds is the most desired solution. Stability depends strongly on friction coefficient, and the higher the coefficient, the lower the critical speed. Friction coefficient is typically dictated by functional requirements so that selection of this parameter is rarely a subject of practical TEI considerations. Factors by means of which TEI can be affected include (1) *structural configuration of the clutch*. Most common clutch packs have friction disks, with layers of friction material on each side, alternately arranged with metal disks. An alternative to this is a pack where each disk has a metal core with a single layer of friction material facing metal surface of the adjacent disk. These disks are called single-sided. Thermoelastic behavior of a pack with single-sided disks is much different from that of conventional pack. In particular, thermoelastic coupling between two sides of a single-sided disk is much weaker than that in the metal disk of conventional pack, thanks to differences in thermomechanical properties between the metal core and the attached friction material. As a consequence, this pack configuration has a relatively high critical speed for focal modes and in this sense is superior. However, there are also other differences that need to be considered when choosing one configuration or the other. (2) *Material properties*. Modulus of elasticity of friction material has a great influence on thermoelastic behavior. Increase of modulus decreases the stability. Modulus spans fairly wide

range, depending on the material type. Since decrease of modulus increases the critical speed [2, 10], compliant materials are generally recommended for high-speed applications, while for low speeds, relatively stiff materials can be used. Most friction materials have a very low thermal conductivity. Any increase of conductivity is advantageous particularly for stability of the focal modes. Thermal expansion coefficient of friction material plays a relatively small role in focal hot spots, but is quite substantial in band hot spots, and lower coefficient improves stability. Material properties of metal disks certainly have great influence on stability, but for steel (or cast iron), differences in properties among material grades are much less than differences among friction materials. (3) *Dimensional parameters*. Increase of the thickness of friction material generally increases the critical speed [10]. Effectiveness of this factor is greatest when the thickness is small and tends to diminish as it increases. Influence of the thickness of metal disks is fairly complex. Interestingly, for metal disks with sliding interfaces on both sides, stability of the antisymmetric mode shows counterintuitive dependence on the disk thickness. Namely, within thickness range of typical applications, the critical speed increases as the thickness decreases [2]. (4) *Cooling*. Clutches are cooled either by air or by liquid. Liquid cooling in wet clutches can be very intense. It is facilitated by forcing fluid to flow in groves made in the surface of the friction material. Heat transfer from the cooled surfaces to the fluid modifies thermal behavior and influences thermoelastic stability characteristics of the system. With intense cooling used in some modern clutches, the critical speed for TEI is noticeably increased.

Exposure of the System to Operation in the Unstable Regime

For hot spotting avoidance, clutches with long-term slip are required to operate in stable regime, which means that the span of operational speeds has to be less than the critical speed. However, for clutches operating at variable sliding speed which changes at fast rate, for example, shifting clutches in transmissions, instantaneous operation above the critical speed is not uncommon; the operational speeds may be so high that they exceed critical speeds of practical clutch solutions. This situation is acceptable under the condition that the slip time is very short so that it is insufficient for the unstable mode to substantially grow. Duration of the slip is crucial as it determines the ultimate magnitude of an unstable mode. In practical applications, the rate of change of slip speed is sometimes a controllable parameter, and by proper control, the clutch can pass the supercritical speed range sufficiently quickly to avoid hot spots.

Excitation of Unstable Mode(s)

There are different potential sources of excitation of unstable modes [13]. One, always present in a real system, is geometry imperfection of the disks that causes contact pressure nonuniformity. Evaluation of this factor requires extracting from the overall pressure distribution those components that are consistent with the modes of hot spotting [13]. For example, if an unstable mode has n waves around circumference, then the Fourier component (harmonic) of pressure with the same number of waves excites this mode. It may happen that pressure component corresponding to an unstable mode has excessive magnitude, and then by correcting the disks' geometry, the problem can be alleviated. Most typically, however, these imperfections are small (but sufficient to effectively excite unstable modes) and therefore beyond control of the manufacturing process.

In some cases, pressure variations may be caused by structural factors. A known practical example is an actuator that applies axial force to the pack of disks by means of several protrusions distributed around the circumference that produce a nonuniform pressure in the circumferential direction. Therefore, an unstable mode would be excited if the pressure pattern is consistent with the mode.

References

1. Barber JR (1969) Thermoelastic instabilities in the sliding of conforming solids. Proc R Soc London A 312:381–394
2. Lee K, Barber JR (1993) Frictionally excited thermoelastic instability in automotive disk brakes. ASME J Tribol 115:607–614

3. Anderson AE, Knapp RA (1990) Hot spotting in automotive friction systems. Wear 135:319–337
4. Parker RC, Marshall PR (1990) The measurement of the temperature of sliding surfaces with particular reference to railway blocks. Proc Inst Mech Eng 159:319
5. Dow TA, Burton RA (1972) Thermoelastic instability of sliding contact in the absence of wear. Wear 19: 315–328
6. Dow TA (1980) Thermoelastic effects in brakes. Wear 59:213–221
7. Zagrodzki P (1990) Analysis of thermomechanical phenomena in multidisk clutches and brakes. Wear 140:291–308
8. Decuzzi P, Ciavarella M, Monno G (2001) Frictionally excited thermoelastic instability in multi-disk clutches and brakes. ASME Tribol 123:865–871
9. Kao TK, Richmond JW, Douarre A (2000) Brake disc hot spotting and thermal judder: an experimental and finite element study. Int J Vehicle Design 23(3/4):276–296
10. Zagrodzki P, Truncone SA (2003) Generation of hot spots in a wet multidisk clutch during short-term engagement. Wear 254:474–491
11. Yi Y-B, Barber JR, Zagrodzki P (2000) Eigenvalue solution of thermoelastic instability problems using Fourier reduction. Proc R Soc Lond A 456: 2799–2821
12. Li J, Barber JR (2008) Solution of transient contact problems by the fast speed expansion method. Wear 265:402–410
13. Zagrodzki P (2009) Thermoelastic instability in friction clutches and brakes – transient modal analysis revealing mechanisms of excitation of unstable modes. Int J Solids Struct 46:2463–2476
14. Al-Shabibi AM, Barber JR (2009) Transient solution of the unperturbed thermoelastic contact problem. J Therm Stresses 32:226–243

Column Grid Array Assembly Under Thermal Cycling Stress

Reza Ghaffarian
Jet Propulsion Laboratory, California Institute of Technology, Pasadena, CA, USA

Overview

Understanding reliability of microelectronics under thermal cycling stresses is an integral part of implementation of advanced packaging technologies. Among these, commercial-off-the-shelf column grid array (COTS CGA) packaging technologies in high reliability versions are in use in a number of high reliability applications and space electronics systems. Establishing the process controls and identifying quality assurance (QA) indicators for reliability are critical for low-risk insertion of these advanced electronics packages.

This chapter presents extensive test data gathered during several years of investigations for CGA packages with 560–1517 columns assembled onto printed circuit boards (PCBs). The CGA assemblies are typically manufactured using a vapor-phase reflow machine or, in rare occasion, using a rework station with eutectic tin-lead paste for solder attachment. This chapter presents lessons learned from test results gathered by various manufacturing, assembly, and environmental testing along with photomicrographs taken at various test intervals showing damage progress and failures. The chapter also includes inspections results, which were performed by researchers to determine key principle parameters affecting assembly, reliability, and quality assurance controls. Thermal cycle reliability test results included up to 1819 cycles in the range of −50 °C/+75 °C, –55 °C/+100 °C, –55 °C/+125 °C, –65 °C/+150 °C, and −120 °C/+85 °C for assemblies including CGA560, CGA717, and CGA1144.

Single-Chip Packaging Trends

The trend in surface-mount packaging technology have illustrated in Fig. 1. Single-chip packages including column grid array (CGA), ball grid array (BGA), and CSPs (chip scale package) are now widely used for many electronic applications including portable and telecommunication electronics products. The CGAs are implemented for space microelectronics systems. As the I/O of CGA packages increase and become more complex with using non-hermetic flip-chip die and added passives, there is a continuous need to understand behavior under thermal cycling stresses.

Thermal stress due to column attachment for LGA and/or reworked CGA packages affects

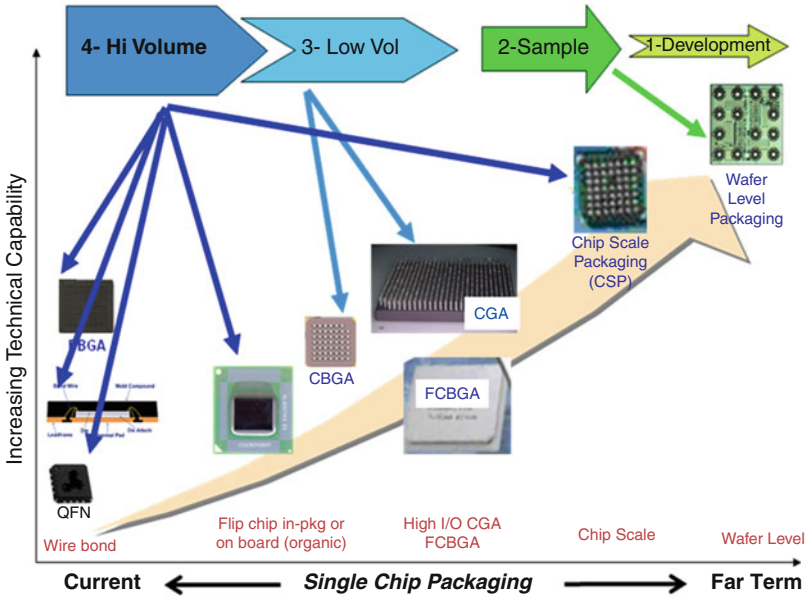

Column Grid Array Assembly Under Thermal Cycling Stress, Fig. 1 Microelectronic trends for single packaging technologies

reliability. Assembly of LGA directly onto a board using conductive adhesive may become a viable option in a near future possibly using adhesive with nanoparticulates or other approaches. With commercial industry, it is mostly implemented by Pb-free solders, and this adds currently additional challenges for high reliability applications. The options left for use of tin-lead solders are either to continue to use tin-lead solder with Pb-free columns/solder balls (backward compatibility), replace Pb-free balls/columns with tin-lead, and accommodate Pb-free in a near future with understanding associated risks and development of mitigation approaches.

Even though CGAs are commercial, off-the-shelf (COTS) packages, their high reliability package versions go through a more stringent screening with added significant cost and a long time in a delivery schedule. The issues with CGA COTS packages are essentially the same as other COTS issues and include package die source and lot-to-lot materials variations, availability of packages with radiation-hard die, outgassing for materials including underfill, etc. Assembly, inspection, and lack of individual solder re-workability issues are additional key aspects of such implementation [1–11].

CGAs/PBGAs (Up to 1000 I/Os) Under Thermal Cycling Conditions

Overview on Evaluation of CGA560/PBGA560/CGA717/PBGA728

This section presents test results for characterization of the reliability of CGA packages with 560 and 717 I/Os (CGA560/CGA717) and plastic ball grid array with 560 and 728 I/Os (PBGA560/PBGA728). The results of the 560 I/O 2nd level package assemblies with tin-lead solder cover the effect of thermal cycling temperature ranges and corner staking on the failure of CGAs and their plastic BGA counterparts. Both CGA560 and PBGA560 have an identical number of balls/columns populated at the periphery with no center population; therefore, it is a peripheral configuration. An additional discussion of first failure for low and high solder volumes CGA560 is also presented. The other set of area array packages was fully populated with 728 balls in the plastic package and 717 columns in the ceramic package. For the CGA717, the 3-corner solder columns were missing; it is purposely removed by the package manufacturer to improve reliability.

A design of experimental (DOE) technique was utilized to cover processing and other aspects

that are considered unique for the potential use of these packages in high reliability applications. Solder joint reliability is affected by many variables including solder volume. The assemblies were subjected to five types of thermal cycles. Both the process and reliability results for the CGA package assemblies are discussed below and compared to their PBGA counterparts.

CGA560/CGA717 Assemblies After Thermal Cycling

CGA560 and Effect of Solder Volume Under Thermal Cycling Stress

Figure 2 presents optical images of solder joint damage conditions for assemblies with low and high solder volume after 991 thermal cycles (−50 °C/75 °C), the low solder volume condition shows significant damage at the board site. Failures were in solder joints at the board site for the assembly with low solder volume. Note that the corner columns at the board site tilted more toward the center of the package due to the higher CTE mismatch compared to the interface at the package site.

CGA560/PBGA560 with Corner Staking Under Thermal Cycling Stress

Figure 3 compares optical and SEM photomicrographs of PBGA balls after exposure to 1819 thermal cycles Cycle A (−50 °C/75 °C) and another subjected to 588 cycles in the range of −55 °C/125 °C (Cycle C condition). Both

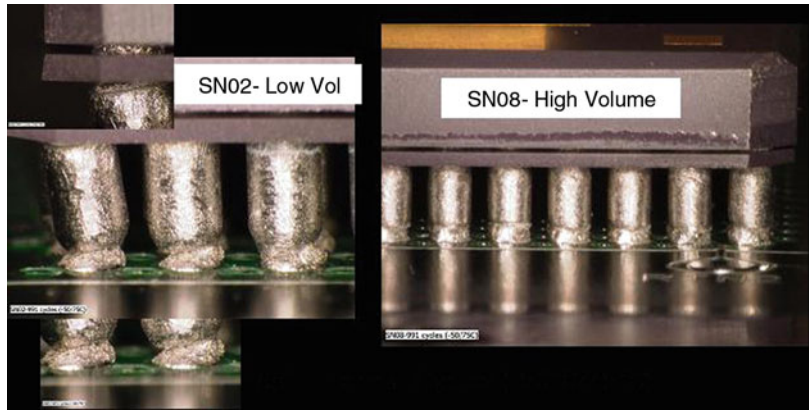

Column Grid Array Assembly Under Thermal Cycling Stress, Fig. 2 Optical photomicrographs of CGA assemblies built with an 8 mil (*left*) and 10.5 mil thick stencil after 991 cycles Cycle A (−50 °C/75 °C)

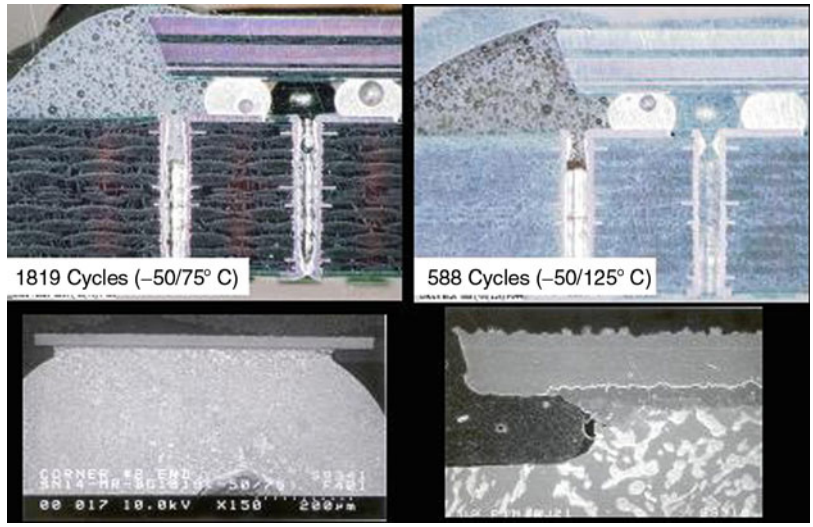

Column Grid Array Assembly Under Thermal Cycling Stress, Fig. 3 SEM Photomicrographs before and after cross-section for a PBGA package after 588 cycles (−55 °C/125 °C)

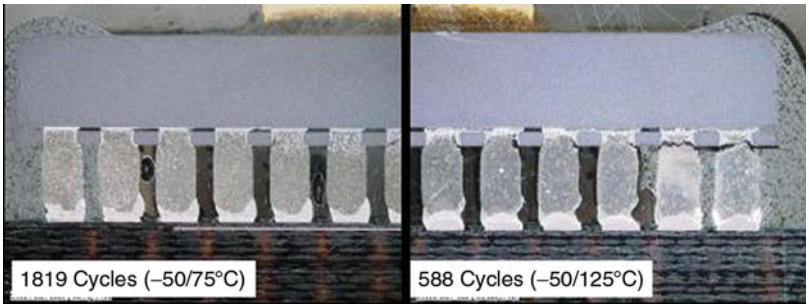

Column Grid Array Assembly Under Thermal Cycling Stress, Fig. 4 Photomicrographs of column failure at interposer with corner staking over two thermal cycle ranges

assemblies had corner staking. No significant microstructural changes for the Cycle A condition were found, whereas a small microcrack was initiated in the solder joint at the package interface for the Cycle C condition (−55 °C/125 °C). The latter photograph also clearly shows the grain growth due to exposure at elevated temperature. Similar optical photomicrographs for CGA assemblies with corner staking after the same number of cycles and conditions: 1819 (−50 °C/75 °C) and 588 (−55 °C/125 °C) are shown in Fig. 4. Although both assemblies had identical build conditions with identical corner staking materials, the failure mechanisms were different and dependent on the temperature cycle range and the maximum temperature. One failed away from staking whereas the other (−55 °C/125 °C) failed within the staking adhesive at the interposer solder interconnection interfaces.

CGA717 Damage Progress Due to Thermal Cycling Stress-Optics/SEM

Figure 5 shows optical and SEM photomicrographs of CGA717 assemblies at 950 thermal cycles Cycle B condition (−55 °C/100 °C). No failures yet detected by electrical monitoring, but signs of damage at the board and package sites are apparent.

CGA560/CGA717 and Projection of Thermal Cycles to Failure

Figure 6 compares cycles to first failures (about 5 % failure) for the CGA560 and CGA717. These plots also include extrapolations from the test results under various thermal conditions to 0 °C/100 °C, a more common thermal cycle temperature range for commercial applications. The extrapolation was carried out using the modified Coffin-Manson relationship. This relationship is one of many numerous parametric modeling analysis methods (see R. Ghaffarian in the previous chapter) that have been proposed and used by industry to project cycles to failure (CTF) from one thermal cycle condition to a field application.

Specifically, the Coffin-Manson relationship was used to correlate the test results for the CGA560 I/Os for three thermal cycling conditions with increasing temperature ranges, i.e., –50 °C/75 °C, –55 °C/100 °C, and −55 °C/125 °C to a control cycle data set in the range of 0 °C/100 °C. As the peak temperature and temperature range increases, projections become less accurate. Projection is the least accurate for the extreme range of −55 °C to 125 °C and better matches the CTF data for −50 °C/75 °C. Thus, the test results are either conservative or nonconservative depending upon how they are applied for a field application.

For example, if data generated by the package supplier, generally in the range of 0 °C/100 °C, are used as the baseline for the CTF projection to a harsher requirement of −55 °C to 125 °C, then projection could result in unrealistic nonconservative CTF data. On the other hand, if the extreme temperature data are considered, a conservative projection could cause rejection of a package that might be suitable for a field application. Microstructural and failure mechanism changes due to corner staking (demonstrated here by testing) are also unknown factors that should be considered for harsher environmental applications.

Column Grid Array Assembly Under Thermal Cycling Stress, Fig. 5 SEM photomicrographs of CGA 717 I/O assembly at 950 thermal cycles (−55 °C/100 °C) showing signs of microcracking

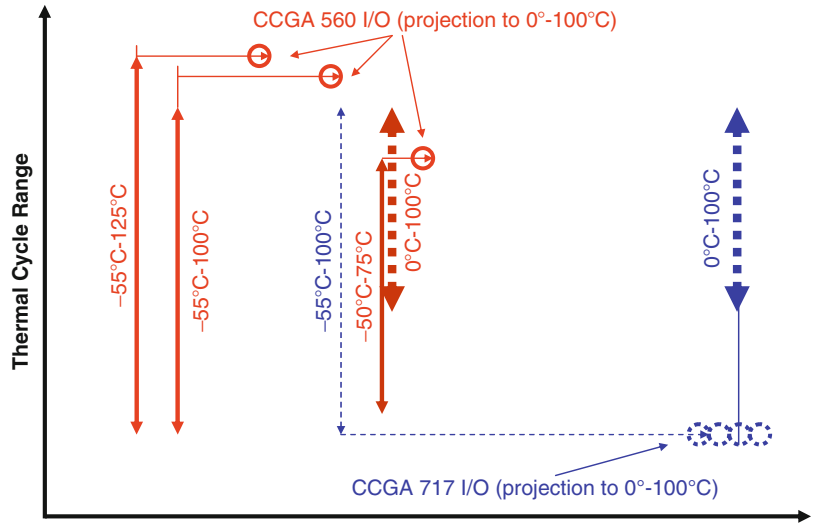

Column Grid Array Assembly Under Thermal Cycling Stress, Fig. 6 Effect of temperature range on first failure for CGA 560 I/Os and no failure yet (−55 °C/100 °C) for CGA 717 I/Os using a modified Coffin-Manson relationship

Projections made for CGA717 are also included in the plot, even though no failures were found to 950 thermal cycles for assemblies with no conformal coating and thermal cycling in the various ranges. Specifically, the plot includes projection of 950 CTF for the −55 °C/100 °C range to the control data set in the 0 °C/100 °C range. Projection made for the case of CGA717 is in contrast with those made for CGA560. Projection from a deeper cycle test data

(−55 °C/100 °C) to a milder range (0 °C/100 °C) results in higher projection values than the test results reported by the manufacturer, even though identical PCBs were used for assembling at two different facilities. Solder volume and more accurate process control and using a vapor phase machine for reflow may be one possible explanation for the improvement observed relative to the package supplier's test condition. The other possible explanation may be related to column design; the copper wrap may be such that the effects of exposure below 0 °C become less critical. None of these hypotheses have been thoroughly verified and remain as postulates until they are tested by a more comprehensive design of experiments with controlled variables, including various thermal cycle parameters.

LGA/CGAs (Up to 1517 I/Os) Under Thermal Cycling Condition

Evaluation of CGA1144 and LGA/CGA1517

The purpose of this aspect of the investigation was to characterize reliability of a new CGA package with much higher columns (1144 I/Os) than its previous version (560 & 717 I/Os). The CGA1144 package is a fully populated area array package and the chip is a field programmable gate array with a much higher number of gates than its previous version. To accommodate higher I/Os in a small package size, this package uses a finer pitch of 1 mm rather than 1.27 mm, commonly used for lower than 1000 I/O CGA versions.

The scope of our evaluation also included a ceramic array package with 1517 I/Os that came as a land grid array (LGA) with no column attachment. A number of these LGAs were converted into CGA by performing column attachment. Two facilities were used to perform column attachment, each having a unique column style. One style had copper wrapped onto a solder column with a diameter slightly lower than standard value; the other style had a micro-spring coil with no solder column, but a standard diameter. Photomicrographs of the LGA package and the two column types are shown in Fig. 7.

CGA1144 Assemblies After Thermal Cycling Stress Test

Figure 8 shows optical photomicrographs for two high I/O CGA package assemblies with corner staking adhesive and with/without conformal coating after 350 thermal cycles (−55 °C/125 °C). Appreciable surface damage is apparent for the sample with no conformal coating, but it is less evident for the one with conformal coating. Therefore, it is difficult to determine visually if conformal coating accelerates or decelerates solder damage progress due to thermal cycling.

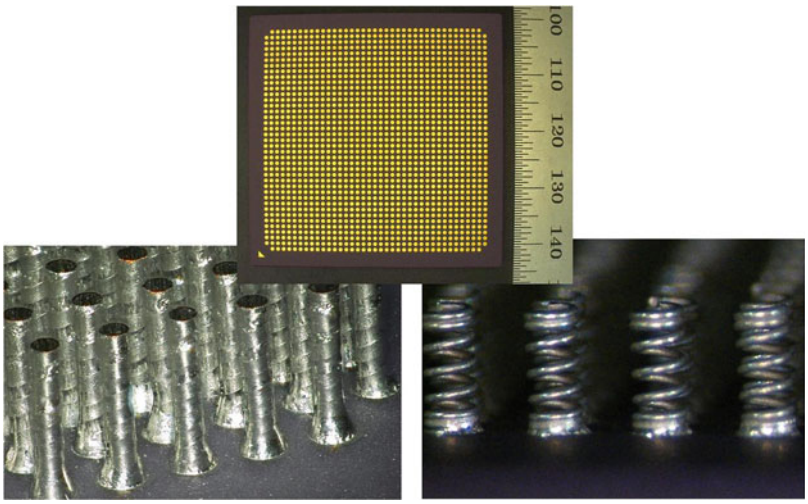

Column Grid Array Assembly Under Thermal Cycling Stress, Fig. 7 Land grid array (LGA) before column attachment (*top*) and after both copper-wrapped solder column attachment (*left*) and microspring attachment (*right*)

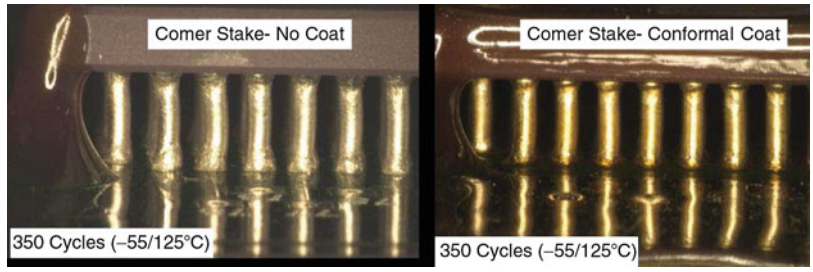

Column Grid Array Assembly Under Thermal Cycling Stress, Fig. 8 Optical photomicrographs of two high I/O CGA assemblies at 350 thermal cycles (−55 °C/125 °C). The sample on the right has conformal coating in addition to corner staking

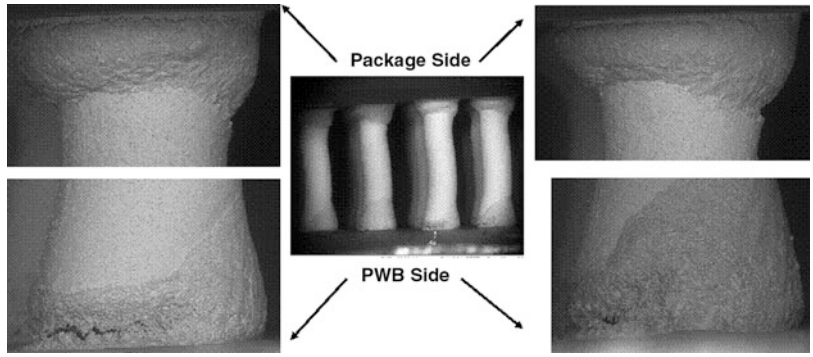

Column Grid Array Assembly Under Thermal Cycling Stress, Fig. 9 SEM photomicrographs of a high I/O CGA assembly showing crack initiation and propagation from solder starved fillet at the board side

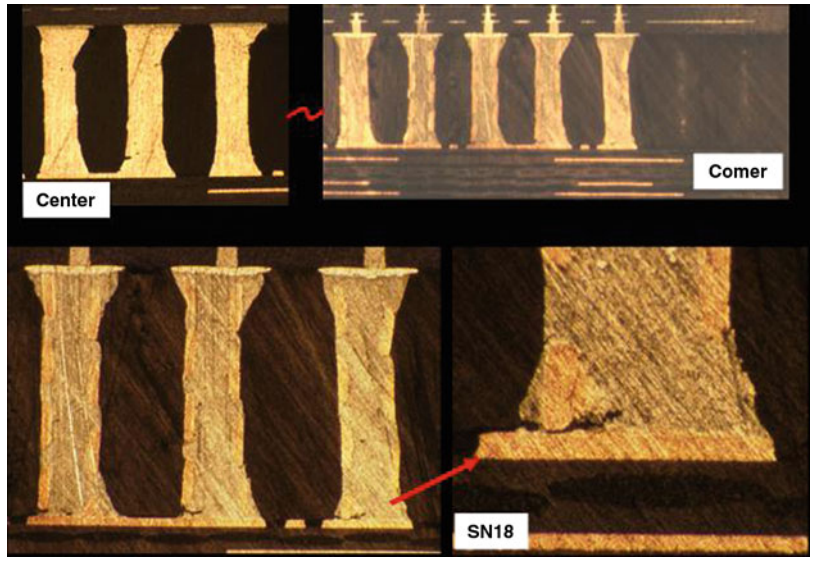

Column Grid Array Assembly Under Thermal Cycling Stress, Fig. 10 Cross-sectional optical photomicrographs of CGA 717 I/O assembly with NSMD pad design after thermal cycling

Figure 9 shows a SEM photomicrographs of an assembly after thermal cycling. It is apparent that most of the damage occurred on the board side, which shows relatively deeper cracks, whereas the cracks from the package sides, are difficult to see except at a very high magnification since they are extremely fine and are at the interfaces. It is also apparent that cracks at the board side initiated from the starved solder fillets progressing towards the good solder fillet

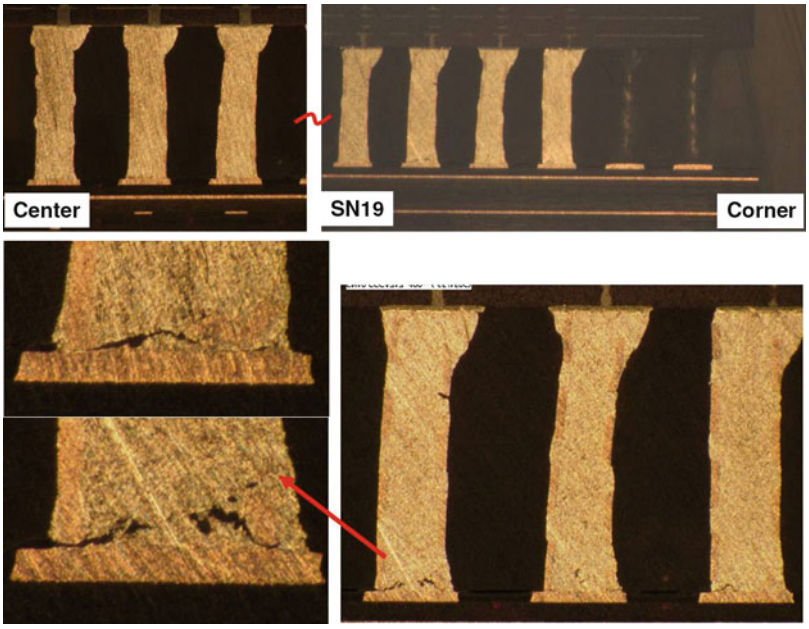

Column Grid Array Assembly Under Thermal Cycling Stress, Fig. 11 Cross-sectional optical photomicrographs of CGA 717 I/O assembly with SMD pad design after thermal cycling

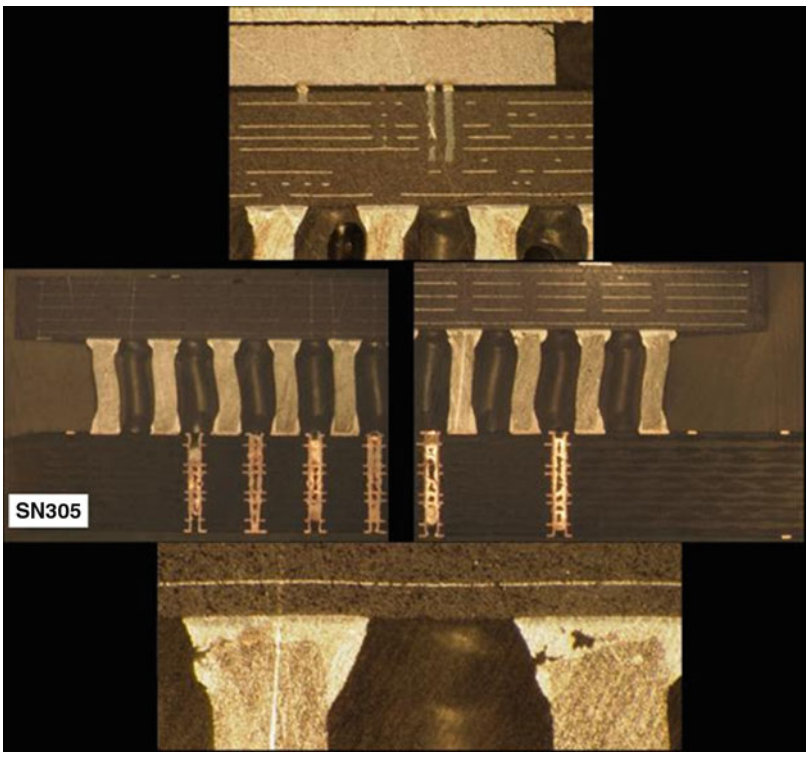

Column Grid Array Assembly Under Thermal Cycling Stress, Fig. 12 Cross-sectional photomicrograph of the CGA1144 I/O assembly after thermal cycling

areas. The extent of the cracks can only be determined by destructive techniques such as cross-sectioning.

CGA717/CGA1144 X-Sectional Verification

Figures 10 and 11 compare optical photographs of two CGA 717 I/Os with NSMD and SMD pad designs after thermal cycling, respectively. It is clear that the NSMD design solder joints show much lower damage due to cycling than the SMD design configuration. Both configurations showed signs of cracking, the NSMD cracks were penetrated to about a maximum of 50 % of the pad diameter, whereas for the SMD cracks, there are various sizes with a few at 100 % which means that the solder joints were in a failure condition.

Figure 12 shows optical photographs for the CGA1144 I/O package after thermal cycling. At the top is a photomicrograph from the package section revealing a flip chip die attach configuration with internal solder balls. The center photomicrographs clearly show tilted solder columns at the corner solder joints due to the higher CTE mismatch on these joint's furthest distances from package neutral points. There is also evidence of cracks, although the crack lengths were less than 50 % of the pad diameters.

References

1. Ghaffarian R (2012) Reliability of column/board CCGA attachment. In: IEEE intersociety thermal conference (ITherm), San Diego, May 31-June 2
2. Ghaffarian R (2011) Chapter 22. Thermal cycle and vibration/drop reliability of area array package assemblies. In: Suhir E, Connally E, Steinberg D (eds) Structural dynamics of electronics and photonic systems. Springer, New York
3. Ghaffarian R (2008) Thermal cycle reliability and failure mechanisms of CCGA and PBGA assemblies with and without corner staking. IEEE Trans Comp Packag Technol 31(2):285–296
4. Ghaffarian R (2006) Chapter 16. Area array technology for high reliability applications. In: Suhir E (ed) Micro-and opto-electronic materials and structures: physics, mechanics, design, reliability, packaging. Springer, New York
5. Ghaffarian R (2006) CCGA packages for space applications. Microelectron Reliab 46:2006–2024
6. Ghaffarian R (2004) Chapter 20. BGA assembly reliability. In: Gilleo K (ed) Area array packaging handbook. McGraw-Hill, New York
7. Fjelstad J, Ghaffarian R, Kim YG (2002) Chip scale packaging for modern electronics. Electrochemical Publications, Isle of Man, UK
8. Ghaffarian R (2001) Chip scale package assembly reliability. In: Puttlitz K, Totta PA (eds) Area array interconnection handbook. Kluwer Academic, Boston
9. Tasooji A, Ghaffarian R, Rinaldi A (2006) Design parameters influencing reliability of CCGA assembly and sensitivity analysis. In: Proceedings of Itherm, San Diego, May 30–June 2
10. Ghaffarian R (2012) Assembly and reliability of 1704 I/O FCBGA and FPBGAs. In: Proceeding IPC APEX conference, San Diego, Feb-Mar 2012
11. Column Grid Array and Rework, IBM user's guideline, 22 July 2002

Complex Variable Analysis

▶ Thermal Stresses of Thin Films on Flexible Substrates

Complex Variable Method

▶ Goursat Functions of Thermoelastic Problem of an Infinite Plate with Hypitrochoidal Hole
▶ Orthotropic Rectangular Plate with a Rigid Ribbonlike Inclusion, Thermal Stress

Composite

▶ High-Order Theory, Composite Plates
▶ Hygrothermal Effects on Polymeric Composite Materials and Sandwich Structures
▶ Thick Plates, Reissner–Mindlin Theory, Statical Problems

Composite Structures

▶ Thermomechanical Coupling in Plate and Shell Structures – Some Significant Results

Computational Methods

▶ Computational Methods in Stationary and Nonstationary Thermal-Plasticity Problems

Computational Methods in Stationary and Nonstationary Thermal-Plasticity Problems

Pavlo Steblyanko[1] and Yuriy Shevchenko[2]
[1]Dneprodzerzhinsk State Technical University, Dneprodzerzhinsk, Ukraine
[2]Timoshenko Institute of Mechanics, National Academy of Sciences of Ukraine, Kiev, Ukraine

Synonyms

Computational methods; Thermal stresses; Thermoplasticity

Overview

A geometrically linear statement of spatial stationary and nonstationary problems of the thermo-elasto-plasticity theory (TEPT) is discussed. The set of governing equations is presented by the heat conduction equation, the displacement (balance) equations, the geometrical relations, and the equations describing non-isothermal processes of loading on both rectilinear trajectories of deformation and trajectories of small curvature in view of the history of loading. The boundary and initial conditions are formulated generically. The basic numerical methods for solving the stationary and nonstationary problems of TEPT in three-dimensional cases are considered.

Introduction

In [1–9], the solutions to a number of stationary and nonstationary TEPT problems have been given. The physical relationship describing simple or almost simple processes of deformation were employed. Processes of deformation on trajectories of small curvature were also considered for non-isothermal deformation processes in an element of a solid. The fundamental relationships for describing of such processes were derived and substantiated experimentally at the Department of Thermal Plasticity of Timoshenko Institute of Mechanics, National Academy of Sciences of Ukraine [6–9].

An approach, which is based upon application of the fractional-step method or component-wise splintering method [1, 10] along with interpolation of the quested-for functions by spline functions [2–5], appears to be efficient for numerical analysis of the spatial nonstationary TEPT problems. This approach exhibits the following advantages:

- Its application is as simple as in the case of finite-difference methods.
- The solution can be found in the form of a spline for the entire domain of definition, while the finite-difference method provides a solution only on a grid [1–3, 10].
- The accuracy rate is much better, which allows for using a larger grid in comparison to the finite- difference method to achieve the same accuracy of calculations [2].

Note that two-dimensional splines were used when employing the fractional-step method [3, 5] to approximate the unknown functions and their partial derivatives on the coordinates. In the case of plane strain, the splines can be used directly, and, thus, the geometrical-parameter splintering method needs not to be involved.

Statement of TEPT Problems

The main purpose of nonstationary TEPT problems consists in determination of the displacements (displacement rates) and the stress-tensor and strain-tensor components in a solid subjected to the force loading and heating, when some of its elements perform beyond the limit of the material elasticity. Consider time-varying loading processes, those that induce displacements in some parts of a solid.

Let us consider an isotropic homogeneous body V with limiting surface S. At the initial moment of time $t = 0$, the body is in the natural non-stressed state with temperature $T_o(\theta_i)$, where $i = 1,2,3$. The body is exposed to the heating and force loading (volumetric forces influencing each element of a body, external forces acting on the entire surface or its part). On a part of the surface, the displacement rates can also be given as functions of the coordinates and time. Let us assume that the heating and loading processes progress in such a way that the rise of deformations does not change the temperature of a body element significantly, and, furthermore, the rheological properties of the material can be disregarded.

The thermophysical properties of the material can be characterized by the parameters of heat conductivity and thermal conductivity, those that are irrespective of the temperature. The heat exchange conditions can be imposed as the boundary conditions; the mechanical characteristics of the material (when studying the processes of deformation on rectilinear trajectories and small-curvature trajectories) are assumed to be in the form of instant stretching diagrams of specimens for different fixed values of the temperature.

The formulated problem is aimed to determine the temperature T, three components of the displacement-rate vector $\boldsymbol{V}$, six components of stress tensor $\boldsymbol{S}$, and six components of the strain tensor $\boldsymbol{E}$ (16 unknown functions of time and three coordinates, in toto). For this goal achievement, the displacement equations, the geometrical and physical equations, and the heat conductivity equation are to be employed.

Having neglected the generation of heat due to the deformation process, the temperature field in an isotropic body with no heat sources can be determined from the following heat conductivity equation [6]:

$$\rho C_v \dot{T} = \left(k_{ij} T_{,j}\right)_{,i} \tag{1}$$

where ρ, C_v, and k_{ij} (hereinafter $i, j, \ldots = 1, 2, 3$) are the mass density, the heat capacity per mass unit at constant volume, and the thermal conductivity, respectively.

As it was mentioned above, the initial distribution of temperature, which corresponds to the natural non-stressed state, is as follows:

$$T = T_0(\theta_i) \tag{2}$$

Let the boundary condition, which reflects the environmental influence on the temperature within the body, have a form [6]

$$\lambda \cdot \frac{\partial T}{\partial n} = -\alpha\theta - q \tag{3}$$

Here $\boldsymbol{n}$ is the external normal to the surface and $\tilde{\lambda}$ is the heat exchange coefficient. Generally, the parameters α, θ, q (α is a factor of proportionality, $\theta = T - T_0$ is the temperature difference, q denotes the heat flux) can depend on the time and position. For different values of the parameters α, θ, and q, condition (3) presents three kinds of the possible boundary conditions when (a) the temperature is given on the surface (the boundary conditions of the first kind), (b) the heat flux q through the surface is given (the boundary conditions of the second kind), and the heat exchange between the body surface and the environment of the temperature θ is assumed (the boundary conditions of the third kind).

After the temperature field for an arbitrary moment of time is found, the components of the displacement-rate vector and stress and strain tensors are to be determined from the three differential equations, six geometrical equations, and six physical equations. These 15 equations must be accompanied with certain initial and boundary conditions. The initial conditions are to be set for all 15 unknown values at $t = 0$ as follows:

$$V = V_0(\theta_i),\ S = S_0(\theta_i),\ E = E_0(\theta_i) \tag{4}$$

On a part of the surface, where external forces $\boldsymbol{b}$ are given, the stress-tensor components should satisfy three boundary conditions

$$\sigma_{in}(\theta_k, t) = \sigma_{ij} \cdot n_j \tag{5}$$

where n_j are the direction cosines of the external normal to the surface. On the other part of the

surface, where the displacement-rate-vector components are given, the boundary conditions appear as follows:

$$v_i = V_i(\theta_j, t) \tag{6}$$

The complete set of three boundary conditions can also be formed by setting any of the conditions (5) and (6).

When using a variant of the mixed solution method, the three displacement-rate-vector components and six stress-tensor components, for which the boundary conditions are imposed, as the basic unknown values. By means of the geometrical Cauchy relations, the displacements can be eliminated from physical relations (describing the non-isothermal loading processes on both the rectilinear trajectories of deformation and the trajectories of small curvature) and determined later by means of the known displacement-rate-vector components. Having solved the problem, the reliability of the used physical equations can be verified by the geometry of the deformation trajectory.

The Equations of Motion and Geometrical Relations for Three-Dimensional Bodies in Orthogonal Coordinate Systems

In geometrically linear case, the equations of motion for an infinitesimal volumetric element of a continuous medium in an orthogonal coordinate system can be written in the following form [2]:

$$\ddot{u}_i = \dot{v}_i = \frac{1}{\rho}\sigma_{ij,j} \tag{7}$$

When deriving formulae (7), the equations of motion were employed, in which the first derivatives by time of the displacement rates are used instead of the second derivatives of the displacement-rate-vector component by time:

$$v_i = \dot{u}_i, \quad i = 1, 2, 3 \tag{8}$$

The equations of equilibrium of an infinitesimal volumetric element of a continuous media in an orthogonal coordinate system in geometrically linear case can be given as [2]

$$\sigma_{ij,j} = 0 \tag{9}$$

In general case of an orthogonal coordinate system, the strain tensor and displacement-vector components are connected by the expressions [6–8]

$$\begin{aligned} 2e_{ij} &= u_{i,j} + u_{j,\,i}, \\ u_{i,j} &= \frac{\partial u_i}{\partial \theta_j} - u_k \cdot \Gamma^k_{ji} \end{aligned} \tag{10}$$

where $\Gamma^k{}_{ij}$ are the Christoffel symbols.

For the rate of deformation, the following formula

$$\dot{e}_{ij} = \frac{1}{2}\left(v_{i,j} + v_{j,\,i}\right) \tag{11}$$

can be written. The system of equations (7), (11) becomes complete by addition of the physical equations connecting stresses and deformations.

The Governing Relations of TEPT

An important aspect of the solution construction to the general nonstationary problems for nonelastic bodies lies in an appropriate choice for the governing relations connecting stresses and strains. In general case, the deformations depend on the variation of stresses and temperature and are determined through the characteristics of the entire process of deformation (not only through the current values). One can find the extended reviews on this matter in [6–9].

Let us consider some simple deformation processes, and similar to them, including ones with regard to the small-curvature trajectories. A trajectory, which swerves from the straight lines connecting the origin of the coordinates and a point on the trajectory (that corresponds to the initial yield stress) not more than the delay track of the vector properties of the material (5 to 15 of the yield stress with respect to deformation), is called a close to rectilinear

deformation trajectory. In this case, the smallest curvature radius of the deformation trajectory appears to be greater than the delay track. If the swerve from the strait line is greater than the delay track and the curvature radius of the deformation trajectory is smaller than the latter one, then the deformation occurs on the trajectory of small curvature [6–8]. Under such conditions, the stress vector is directed tangentially to the trajectories of irreversible deformations.

To derive the physical relations, suitable for analysis of both above-mentioned processes, we split the loading process onto sufficiently small stages of time. By making use of the Ilyushin's postulate [9] along with the law of elastic change in a volume for each of these stages, the relations between the stresses and strains can be written as follows:

$$\sigma_{ij} = 2G^*(e_{ij} + e_{ij}^{(n)}) + (3\lambda^* e_0 - K\alpha\theta)\delta_{ij} \quad (12)$$

where

$$\lambda^* = \frac{2G(1+v) - 2G^*(1-2v)}{3(1-2v)},$$
$$K = \frac{2G(1+v)}{1-2v},\ e_0 = \frac{1}{3}(e_{11} + e_{22} + e_{33})$$

The expressions for G^* and $e^{(n)}{}_{ij}$ may assume different forms according to the chosen plasticity relations model (simple processes off loading or processes of small curvature).

The Theory of Small Elastic–Plastic Deformations

When an element of a solid is loaded by the rectilinear deformation trajectories or by ones close to them, parameter G^* is related to the intensity of the tangential stresses and the additional shearing deformations. This function is supposed to be independent of the type of the stressed state. Therefore, it is to be determined from the experimental stretching of specimens at various temperatures [8]

$$G^* = \frac{\sigma}{2(1+v^*)e},\ v^* = \frac{1}{2} - \frac{1-2v}{2G(1+v)} \cdot \frac{\sigma}{e}$$

Here σ and e are the axial stress and strain of a specimen. In the case of active process of loading, the components of nonelastic deformation meet the condition

$$e_{ij}^{(n)} = 0;$$

or

$$e_{ij}^{(n)} = \left(\frac{1}{2G^{*(1)}} - \frac{1}{2G}\right) \cdot \left(\sigma_{ij}^{(1)} - \delta_{ij}\sigma^{(1)}\right)$$

in the case of unloading. Here the superscript $^{(1)}$ designates the corresponding values at the beginning of unloading.

Having determined the aforementioned dependency from the experiment of simple stretching of a cylindrical specimen at different fixed values of temperatures, we can construct the function

$$\sigma = F(e, \mathrm{T}) \quad (13)$$

This equation defines the so-called instant thermomechanical surface, whose appearance has been shown experimentally in [9].

Relations of the Theory of Small-Curvature Processes

When an element of a solid is loaded on the deformation trajectories of small curvature, values of G^* and $e^{(n)}{}_{ij}$, those that appear in physical relations (12), can be given as

$$G^* = G, e_{ij}^{(n)} = \sum_{k=1}^{p} \Delta_k e_{ij}^{(n)} \quad (14)$$

Here $e^{(n)}{}_{ij}$ are the nonelastic deformations accumulated during the loading process, and $\Delta_k e^{(n)}{}_{ij}$ are the increments of these deformations at each stage of loading.

It has been confirmed experimentally [9] that a function of the type (13) is irrespective of the

kind of stressed state for some classes of originally isotropic materials. As a result, it can be determined experimentally by stretching the cylindrical specimens. In this case, the nonelastic part of the relative specimen elongation can be given as

$$\varepsilon^{(n)} = \varepsilon - \frac{\sigma}{2G(1+\nu)}$$

Hence, the concretization of the governing equations can be reduced to the problem on the instant thermomechanical surface (13). To evaluate this function numerically, it must be approximated in a certain manner. When solving numerically, the equation of an instant thermomechanical surface of the kind (13) can be given in a form of experimental data table $(\sigma)_i$, $(e)_i$, $i = 0,1\ldots, N$ at fixed T.

Note that when solving nonstationary problems, the relationships (12) can be reduced to the following form:

$$\dot{\sigma}_{ij} = a_{ijkl}\,\dot{e}_{ij} - \delta_{ij}\left[K\alpha + \theta\frac{\partial(K\alpha)}{\partial T}\right]\dot{T} \qquad (15)$$

where a_{ijkl} are constants in the case of elastic material or functional of the deformation process in the case of plastic deformation [2].

Thus, apparently, formula (12) or (15) has completed the system of equations for constructing the solution of both stationary and nonstationary three-dimensional problems of thermo-elasto-plasticity. Having constructed a solution by means of one or another type of the governing equations in the Ilyushin space, the deformation trajectory is to be constructed in separate elements of the body that are being deformed beyond the framework of elasticity [6].

As it was mentioned above, the form of deformation trajectory in this space can serve as an adequacy criterion of the governing equations chosen for the considered process of deformation.

For the active loading, the condition

$$\left(\sigma_{ij} - \delta_{ij}\sigma\right)\cdot\Delta e_{ij}^{(n)} \geq 0$$

must hold. Otherwise, in compliance with the elastic law, the unloading takes place.

Methods for Solution of the Stationary Problems

There are following dominant methods for solution of the stationary TEPT problems [6–9]:

- The method of elastic solutions in the theory of simple processes of deformation;
- The method of variable elasticity parameters in the theory of simple processes of deformation;
- The method of variable elasticity parameters in the theory of small-curvature processes;
- The method of additional deformations in the theory of small-curvature processes;
- The iterative method in the theory of arbitrary deformation processes.

When the **method of elastic solutions** is used to solve the stationary TEPT problems within the framework of the theory of simple deformation processes, the system of nonlinear equations (9), (10), and (12) can be used to determine the components of stresses, strains, and displacements at each stage of deformation (loading). Nonlinearity of this system of equations is caused by the nonlinear functional dependence between the intensity of the tangential stress and the shearing strain, temperature, and time. This system can be solved in terms of either displacements or stresses. To solve the TEPT problem in terms of displacements, it is necessary to eliminate the stress and strain components from the system of 15 equations (9), (10), and (12). For this purpose, the physical relations can be represented in the form of generalized Hooke's law with additional members. Ultimately, the system of three partial differential equations in terms of displacements appears as follows:

$$G\cdot\nabla^2 u_i + (G+\lambda)\left(u_{j,j}\right)_{,i} = R_i \qquad (16)$$

where R_i are the additional members which are to be specified at each stage of loading on the basis of the previous iteration. Values of G and λ are taken at the given value of T_0. Equation (16) must be supplemented with appropriate boundary conditions. On the part of the surface, where the external forces $\boldsymbol{b}$ with components b_i are given, the stress-tensor components should satisfy three static boundary conditions

$$\sigma_{ij} \cdot n_j = b_i(\theta_k)$$

These conditions can be written in terms of displacements by means of relations (12).

On the part of the surface, where the displacement-vector components are given, the boundary conditions appear as

$$u_i = U_i(\theta_j)$$

When solving equation (16) numerically, the loading process must be split into a number of stages so that the moments of time, those that limit the separate stages, coincide with the moments of change of the deformation process from the loading to unloading and vice versa.

Besides the method of the elastic solutions, there exist other iterative methods for solution of the systems of nonlinear equations (9), (10), and (12) in the theory of simple deformation processes. One of them is the **method of variable elasticity parameters**. The central idea of this method consists in the following: the governing equations are formulated in much the same form as the Hooke's law in one of its representations with elasticity coefficients G and λ depending (except for the last one) on the temperature and stress–strain state. Hence, the solution of the TEPT problem can be reduced to the sequential solution of a number of elasticity problems with the variable coefficients, which are found for every approximation. The efficiency of this method is in a rapid convergence of the successive approximations and in the fact that it is enough to hold only one approximation for each short-term loading stage. It is necessary, however, to verify the satisfaction of the basic equations for the complete values of stresses, strains, and displacements. The basic equations are usually being solved approximately for the increments of these functions and, when they are summed up, the computational error is being accumulated necessarily. That is why it is necessary to verify this error on each stage of computation and put the results into the adjustment data for the next approximation. In addition, the tangential module of the stress–strain diagram must be accounted in the governing equations for increments of the quested-for functions. For stability of the computational process, it is necessary to approximate these diagrams by an appropriate analytical expression and then set a dense grid of transient stress–strain diagrams for specimens at different fixed values of the temperature.

The above-considered drawbacks can be obviated, in part, when applying the **method of additional strains**. In [6], this method is called the modified method of additional strains. The system of equations (9), (10), and (12) can be written for each stage of loading in terms of the total strains instead of their increments. Therefore, the successive approximation must be performed on each stage irrespectively of the stage size.

The above-mentioned methods can be used for solving TEPT problems, when the governing equations do not contain the parameters characterizing the interior geometry of the deformation trajectories of body elements. In [9], we suggested a method of successive approximations for solution of TEPT problems employing the governing equations that describe the processes of deformation (loading) on arbitrary trajectories. The physical relations, which determine the dependency between the components of stress and strain deviators based on the structural model of the environment in an implicit form, can be used as well.

The central idea of the **successive approximations in the theory of the arbitrary deformation processes** lies in the following. First, the problem is to be solved for the process of loading on the basis of the governing equations, those do not contain the parameters characterizing the geometry of deformation trajectory for each element of the body. One of the above-mentioned methods can be used for this goal achievement. Then for each element of the body, where the stress–strain state can be treated as uniform, the deformation trajectories are constructed in the five-dimensional deformation space. After that, the parameters of the structural model of the continuous environment can be specified and the process of the stresses component changes is calculated by the trajectory geometry (curvature, torsion). The obtained values should correspond to the obtained deformation trajectories and the corresponding equations of the relationship between the stresses and strains. The above-described solution

algorithm is to be repeated until achievement of the required accuracy for the stresses.

The Methods for Solution of Nonstationary Problems

The dominant methods for solution of nonstationary TEPT problems are the following [1–4, 10]:

- The finite differences method (in the theory of simple deformation processes);
- The finite elements method (in the theory of simple deformation processes and the theory of small-curvature processes);
- The method of splitting on geometrical properties (in the theory of simple deformation processes and the theory of small-curvature processes).

Within the framework of the **finite differences method** and **the method of finite elements**, the solution of nonstationary TEPT problems can be reduced to the systems of a large number of algebraic equations constructed by the classical scheme [1–3, 10]. The essence of this scheme lies in the substitution of the differential operators in the complete system of equations (9), (10), and (12) by their difference analogues. According to the form of the physical relations, different variants of these methods can be employed.

In [2], a new high-precision variant of **the method of component-wise splintering** has been suggested for solution of nonstationary thermoelasticity and thermoplasticity problems. The rates of displacements (the latter ones are determined by means of integration of the corresponding rates by time) as well as stresses, strains, and temperature are chosen to be basic unknowns. All the unknown functions appear to be functions of the time and coordinates. Then the system of equations (9), (10), and (12) yields [2]

$$\dot{W} = A_1 W_{,1} + A_2 W_{,2} + A_3 W_{,3} \qquad (17)$$

where W is a vector, whose components can be the rates of displacements v_i, the stress tensor σ_{ij}, or the strain tensor e_{ij} components.

For writing of the vector equation (17), the equations of motion (7), geometrical relations (11), and the physical relations (15) were used.

When using the component-wise splintering method, system (17) and heat conduction equation (1) are to be replaced with an equivalent system of equations. For this purpose, a time-grid with fractional step must be taken into consideration. Then the splitting scheme for equation (1) can be presented as follows [4]:

$$\begin{aligned} \rho C_v \dot{T} &= \left(k_{i1} T_{,1}\right)_{,1}, \quad t \in \left[t_p; t_{p+1/3}\right] \\ \rho C_v \dot{T} &= \left(k_{i2} T_{,2}\right)_{,2}, \quad t \in \left[t_{p+1/3}; t_{p+2/3}\right] \\ \rho C_v \dot{T} &= \left(k_{i3} T_{,3}\right)_{,3}, \quad t \in \left[t_{p+2/3}; t_{p+1}\right] \end{aligned} \qquad (18)$$

The algorithm for determination of the temperature field in a body, constructed on the basis of formulae (18), can combine the advantages of the explicit difference scheme and the implicit scheme [2, 4, 10]. At each of the consecutive steps on time, three one-dimensional equations are to be solved. The solution of the previously solved equation serves as the initial condition for the subsequent equation.

As mentioned in [2, 10], the original nonstationary spatial problem (17) can be reduced to the system of three successively solved one-dimensional problems equivalent on fraction steps on time:

$$\begin{aligned} \dot{W} &= A_1 W_{,1}, \quad t \in [t^p; t^{p+1/3}] \\ \dot{W} &= A_2 W_{,2}, \quad t \in [t^{p+1/3}; t^{p+2/3}] \\ \dot{W} &= A_3 W_{,3}, \quad t \in [t^{p+2/3}; t^{p+1}] \end{aligned} \qquad (19)$$

The solution of the previous vector equation serves as the initial condition for the subsequent equation.

Conclusions

In the given entry, questions are taken up connected with development and application of the basic numerical methods of the decision of stationary and nonstationary problems of the theory TEPT for spatial bodies at simple and complex deformation.

References

1. Steblyanko PA (1997) Spatial non-stationary problems of the theory thermo-elastic-plasticity. Institute of Mechanics NAS of Ukraine, Kyiv [in Russian]
2. Steblyanko PA (1998) Methods of decomposition in space problems of the theory of plasticity. Naukova dumka, Kyiv [in Russian]
3. Steblyanko PA (1999) Method of the decision of non-stationary problems of the theory of plasticity. Prize, Tver [in Russian]
4. Steblyanko PA (2003) The schemes of abnormally high accuracy solution of non-stationary problems of theory of the thermo-elastic-plasticity for plates and shells. Thermal Stresses and Related Topics. Proc. 5th Int. Conf., Blacksburg, Virginia, 2003, pp 231–234
5. Steblyanko PA, Shevchenko YuN (2007) Calculation of temperature non-stationary stress-strained state of composite shall on the basis of combined 2D model with 3D elements. 7th Int. Congress on Thermal Stresses and Related Topics, Taipei, Taiwan, 4–9 June 2007, pp 647–650
6. Shevchenko YN, Babeshko ME, Piskun VV, Savchenko VG (1980) Space problems thermal-plasticity. Naukova dumka, Kyiv [in Russian]
7. Shevchenko YN (1986) Space problems of the theory elasticity and the theory plasticity, vol. 6: the thermo-viscous plasticity. Naukova dumka, Kyiv [in Russian]
8. Shevchenko YN, Savchenko VG (1987) The mechanics of coupled fields in elements of constructions, vol. 2: the thermo-viscous plasticity. Naukova dumka, Kyiv [in Russian]
9. Shevchenko YN, Babeshko ME, Terehov RG (1992) Thermoviscoelastoplastic processes of the combined deformation of structural elements, Naukova dumka. Ukraine, Kyiv [in Russian]
10. Marchuk GI (1988) The method of decomposition. Nauka, Moscow [in Russian]

Computational Welding Mechanics

Lennart Karlsson[1] and John Goldak[2]
[1]Engineering Sciences and Mathematics, Luleå University of Technology, Luleå, Sweden
[2]Goldak Technologies Inc., Ottawa, Ontario, Canada

Definition

Computational welding mechanics (CWM) establishes methods and models that are usable for control and design of welding processes to obtain appropriate mechanical performance of the welded component or structure. CWM can also be used to drive solutions in product development of welded products and structures. Therefore, CWM needs to be concerned with subjects ranging from modeling of heat generation, weld pool phenomena, and heat flow to thermal stresses and deformations. Constitutive modeling (building on materials science) is an essential ingredient in the modeling of welding processes due to the severe thermal cycle(s) during welding. CWM models often need to be combined with models for microstructure evolution and other features that enable the prediction of microstructure, cracking, and other phenomena that are determined by the temperature and deformation history of the material.

Overview

The field of computational welding mechanics (CWM) is partially built upon earlier work within the fields of thermal, mechanical, and metallurgical (microstructural) properties of materials. The principles and applications of CWM have been described by Karlsson [1] Goldak [2], and Lindgren [3]. Welding simulation is a good example of how mechanics of materials and structures can be put to practical use with the support of computers. The essential features of CWM are the following: (1) it requires solving the nonlinear, coupled three-dimensional transient partial differential equations (PDEs) for heat flow (conservation of energy), microstructure evolution, and stress–strain evolution (conservation of momentum); (2) the material properties are temperature dependent and history dependent and involve phase changes; (3) the welding process usually adds material, that is, filler metal, that makes the geometric domain a time-dependent free-surface problem; (4) the boundary conditions applied by fixtures, clamps, and tack welds are complex and transient; (5) the geometry of welded structures is often complex with many parts; and (6) modeling the heat source of the arc is itself complex.

The centerpiece in welding simulations is the heat generation process. Its description belongs to the domain of thermomechanics in the case of explosive welding, friction welding, and friction stir welding. Resistance welding also includes the electrical field. However, the process becomes much more complex for fusion welding processes. Weld process modeling (WPM) focuses on modeling the physics of the heat generation. CWM models, on the other hand, start with a given heat input that replaces the details of the heat generation process and focus on the larger scales. The modeling of fluid flow and pertaining convective heat transfer may be integrated with a CWM model. However, the classical approach in CWM is to ignore the fluid flow and use a heat input model where the heat distribution is prescribed. Thus, the heat input model in CWM must be calibrated with respect to experiments or obtained from WPM models. Therefore, the classical CWM models do have some limitations in their predictive power when used to solve different engineering problems. For example, they cannot prescribe what penetration a given welding procedure will give. Appropriate procedure to determine the heat input model is therefore important in CWM.

The use of computational models does not replace experimental methods, but redefines their role. Fewer experiments are needed for evaluation of different design concepts when utilizing the power of computer models. Furthermore, the more established simulation becomes in a given field, the less validation testing is needed. However, more demands are placed on determination of material properties and boundary conditions needed for the computational model.

Constituents of Computational Welding Mechanics

As illustrated above, welding is a multiphysics problem where the physical phenomena are described by different coupled field equations that overlap or have a common boundary. Fortunately, many welding processes can be represented by simplified models. The main stream in CWM is the use of weakly coupled models where the physics in the weld is replaced by a heat input model. A general description about procedures for solving coupled systems is given in this entry, with focus on the use of the so-called staggered approach common in CWM, whereby the solution of the problem is split into a thermal and a mechanical phase. There are several options available in the thermal and mechanical analyses. One common concern is the choice of coordinate system. Most models use a fixed coordinate system. However, the moving heat source with near stationary conditions can be favorably treated by a moving coordinate system in some cases.

Decoupling of the Subdomains of Welding Simulations

In Fig. 1, a general view of the relevant fields in welding simulations is shown. The field "physics of heat generation" denotes a generic representation for all possible welding processes. Simulations of this type require weld process models in combination with the CWM model. This kind of multiphysics is not discussed further in this entry. The distribution of heat input is usually predefined in CWM models. It is determined by calibrating the model with respect to measurements. A heat input model, as illustrated in Fig. 2, replaces the "physics of heat generation" field. The domains of the fields "fluid flow" and "deformation in solid" in Fig. 1 have a common interface at the weld pool boundary.

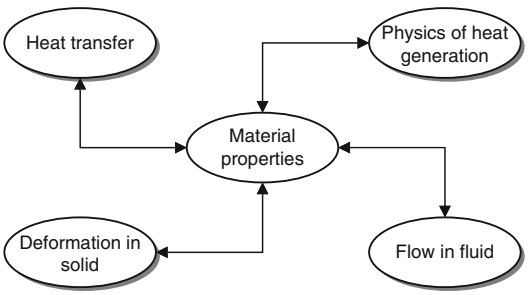

Computational Welding Mechanics, Fig. 1 Different field equations in CWM together with weld process models

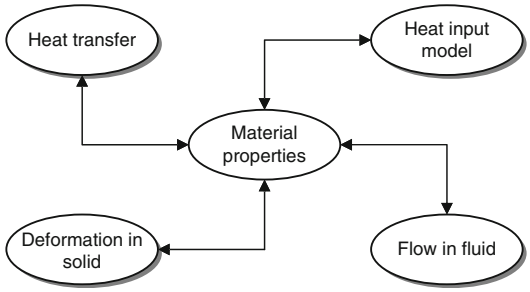

Computational Welding Mechanics, Fig. 2 Fields in CWM modeling of fusion welding, with a heat input model instead of a weld process model

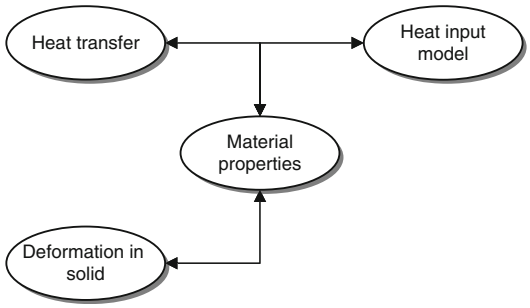

Computational Welding Mechanics, Fig. 3 Fields in classical CWM modeling of fusion welding without a welding process model and without fluid flow

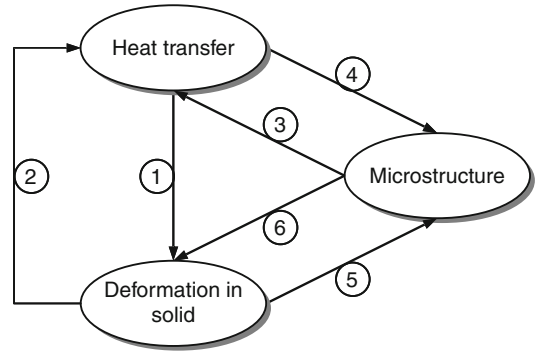

Computational Welding Mechanics, Fig. 4 Couplings in thermomechanical models

Computational Welding Mechanics, Table 1 Thermomechanical couplings in Fig. 4

Coupling	Description
1	Temperature changes drive the deformation via thermal expansion and volume changes due to phase changes denoted by coupling No 6
2	(a) Deformation generated heat
	(b) Deformation affects thermal boundary conditions
3	Thermal properties depend on microstructure, and phase changes are associated with latent heats
4	Thermal-driven phase changes
5	Deformation-driven phase changes
6	The mechanical material behavior depends on the microstructure and temperature

Most analyses in CWM ignore the fluid flow and prescribe the distribution of the heat input and the coupling scheme as shown in Fig. 3. A fully coupled solution of these fields is thoroughly discussed in Lindgren [3] Chapter 3.2 (p 16) and Chapter 3.3 (p 24).

The coupling between material behavior and temperature and deformation fields are shown in Fig. 4 and explained in Table 1. The plastic dissipated energy, coupling No 2a, is the largest contribution to the mechanically generated heat but still negligible compared to the heat input [4]. Furthermore, if the effect of the deformation on thermal boundary conditions, coupling No 2b, can be ignored, then a weakly coupled analysis can be done. The complete simulation of the heat flow is then followed by the deformation simulation. The temperature is read from the file in the latter simulation. This file was saved during the thermal simulation. However, in nearly all cases, it is most convenient to use a staggered approach for weakly coupled problems, Lindgren [3] Chapter 3.1 (p 10), as the thermal analysis does not add much to the required computer time, and one does not need the bookkeeping necessary for assuring that the correct temperature file is read during a subsequent mechanical analysis. Figure 5 shows the staggered procedure, which is convenient to use in CWM simulations.

Thermal stress problems can usually be treated as quasi-static problems. Then, the inertia forces are ignored in the mechanical analysis. This is also the case for welding processes, with the exception of explosive welding, where the deformation generates the heat.

Example

In this section, an example is presented. In this example, the CWM approach as presented above is applied, that is, the staggered approach is used. Here, the modeling and simulation software VrWeld from Goldak Technologies Inc. [5] has been used to demonstrate the proposed strategy. As will be noted below, a traditional moving heat source solution is compared to a so-called block-dumping heat source solution. The main reason for using the block-dumping technique is increased simulation efficiency, particularly for simulation-driven design applications.

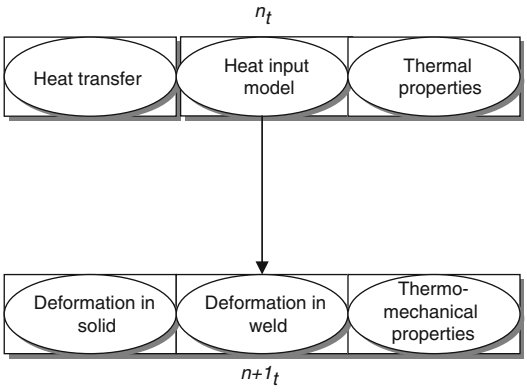

Computational Welding Mechanics, Fig. 5 Staggered approach using isothermal split starting with a heat conduction analysis with fixed geometry

Simulation Strategy

Karlsson et al. [6] proposed a welding simulation strategy for improved efficiency of welding simulation. This simulation strategy reduces the calculation time for welding simulations by replacing the traditional moving heat source with a calibrated block-dumping heat source. The block-dumping heat source is calibrated to give a good compromise between simulation accuracy and calculation time, thus allowing a larger design space to be explored during a given period of time. A rear axle bridge from a Volvo Construction Equipment wheel loader is used as a demonstrator case to show that steps 1–6 work on an industrial application. Twenty different welding sequences are compared to find the welding sequence that gives the smallest welding distortion at key positions.

Welding Case Study

The object of this case study is a rear axle bridge from a Volvo Construction Equipment wheel loader. The axle bridge is positioned in the rear frame according to Fig. 5. An axle working as a pivot for the rear axle assembly is mounted in the two holes in the axle bridge. The axle is supported by journal bearings, which are lubricated with oil from the rear axle differential. The concentricity between the two holes and the parallelism and perpendicular alignment between the plates are two important tolerance demands for the axle bridge. Due to these requirements, it is important that the welding process used to manufacture the axle bridge does not introduce excessive deformations. Therefore, the aim of this case study is to derive a suitable welding sequence that minimizes the welding distortion in the axle bridge. Identifying the proper welding sequences is done by use of the proposed simulation strategy (Fig. 6); see Table 2.

Welding and Material Properties

The three plates are joined by welds a–d in Fig. 7; the welds have a throat size of 6 mm. The axle bridge is manually tack-welded with 40-mm long tack welds at start, mid, and end of the four welds. The tack welding is performed in a separate fixture; the tack-welded axle bridge is then positioned in the welding fixture shown in Fig. 7. An automated MAG welding process then applies the four welds (see Table 3 for welding parameters).

Geometry and Preprocessing

A CAD model of the axle bridge assembly was provided by the manufacturer. This CAD model was imported to Siemens PLM NX6, where small features were removed to ease the meshing

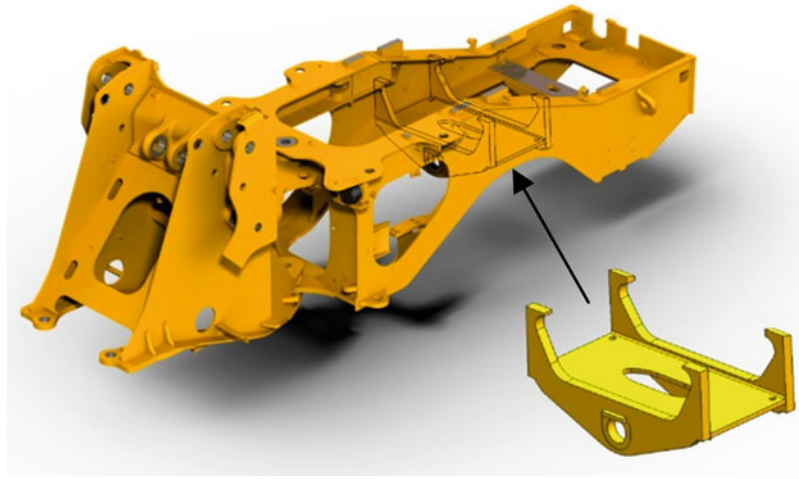

Computational Welding Mechanics, Fig. 6 Rear frame and rear axle bridge

Computational Welding Mechanics, Table 2 Welding simulation strategy for simulation-driven design

1. Welding and material parameters.	Gather information about the real welding process, such as welding method, welding speed, welding power, and welding efficiency. The material parameters include thermal and mechanical properties
2. Geometry and preprocessing.	Create CAD geometries of welded parts, and possibly each weld, and import them into the welding simulation software (STL-files in VrWeld), where the initial simulation mesh is created. Another approach is to create the initial mesh with external software and then import it into the welding simulation software (ABAQUS is one example of a mesh format supported in VrWeld). Define mechanical and thermal constraints, material models, and weld paths. Apply boundary conditions and external loads
3. Heat source and mesh calibration.	(a) Calibrate the moving heat input model, for example, by results from thermocouple measurements or weld cross section samples. (b) Calibrate the mesh for a suitable compromise between accuracy and calculation time. This is normally done by running three or more simulations with varying mesh density and then evaluating how the result converges
4. Block dump calibration.	Run a series of block dump weld simulations with varying numbers of block dumps. Compare the results from a moving heat source simulation with the block dump simulation results to evaluate how many block dumps are needed to achieve the required accuracy of the simulation. If a moving heat source simulation will be too time consuming, the needed number of block dumps can be decided by observing result convergence for an increasing number of block dumps. The level of accuracy is often case specific. Therefore, the decided number of block dumps can be applicable for similar products
5. Design space exploration (DSE)	Use the calibrated block-dumping simulation to explore the design space, for example, welding sequences, welding parameters, weld geometries, and designs. The use of design of experiments (DoE) or optimization can further increase the efficiency of the DSE
6. Verifying results with moving heat source simulation	Compare a portion of the result from the DSE to corresponding simulations with a moving heat source or with an increased number of block dumps to ensure that results obtained in the previous step are accurate enough
7. Physical testing and/or manufacturing	Proceed with physical testing and/or manufacturing based on the results achieved from the welding simulations. The amount of physical testing should at this stage have been reduced compared to a situation where no welding simulations have been performed

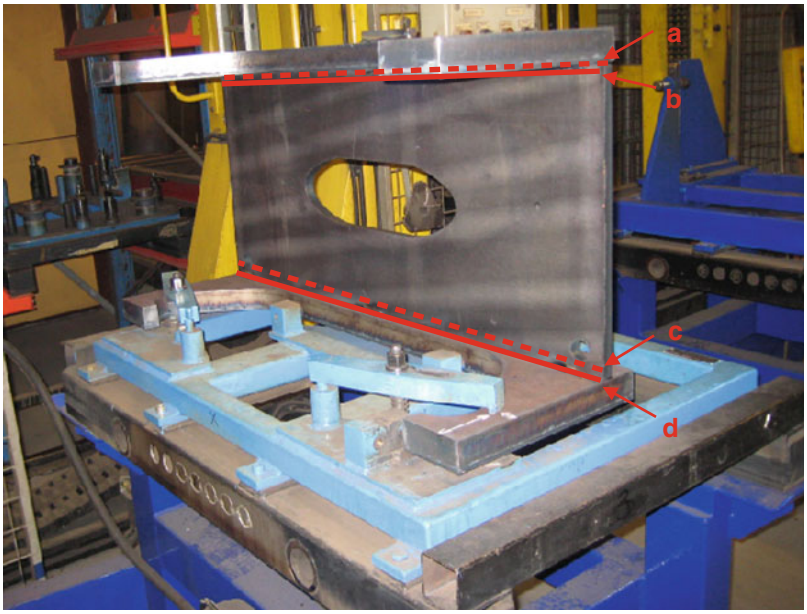

Computational Welding Mechanics, Fig. 7 Photo of real axle bridge placed in its welding fixture. The weld joints (a–d) are marked with red lines; welds a and c are placed underneath the center plate

Computational Welding Mechanics, Table 3 Welding parameters

Parameter	Value
Power	10,880 W (34 V, 320 A)
Efficiency	85 %
Welding speed	37 cm/min

process. The idealized part shown in Fig. 8 was exported to the welding simulation software (VrWeld) in STL format. The simulation model was then created in VrWeld by defining weld joints, assigning materials, creating an initial mesh and assigning initial and boundary conditions, etc. The material model described by Andersson [7] was used for both plates and filler metal. The used fixture shown in Fig. 7 prevents rigid body motions (locks six DOFs) without restraining the growth/shrinkage of the plates. This fixture modeling method was used, since the real fixture only clamps one of the plates and should therefore not have a large impact on the welding distortions. The welding distortion in the rear axle bridge was measured as the global displacement of points P1 and P2. The global ambient temperature is set to 300° K.

CWM Results

Both simulation approaches predict the same welding sequences to give the smallest and largest welding distortions in P1 and P2; see Fig. 9. Welding sequences 1–4 are welded with full-length welds only and simulated in 170 time steps. Welding sequence 20 is welded with two full-length welds and four half-length welds and simulated in 250 time steps. Welding sequences 5–19 are welded with eight half-length welds and simulated in 330 time steps. The moving heat source is simulated in 450 time steps. Hence, the number of time steps has then been reduced by 60 % (welding sequences 1–4), 45 % (welding sequence 20), and 25 % (welding sequences 5–19).

The Future of CWM

CWM was conceived in the late 1900s and has now reached a degree of maturity. The software has largely been commercialized and is rapidly being adopted by the welding industry. The next stages in the evolution of CWM in welding technology are expected to focus on the following developments:

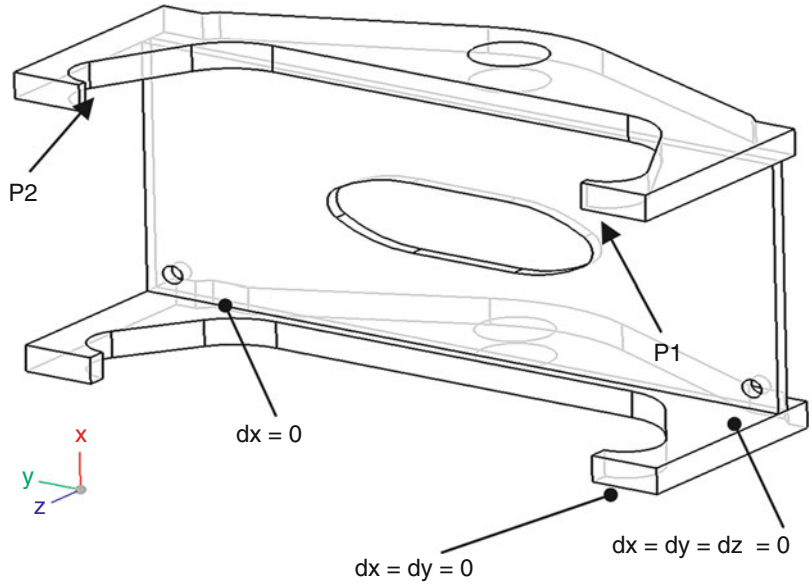

Computational Welding Mechanics,
Fig. 8 Idealized axle bridge, evaluation points and constraints

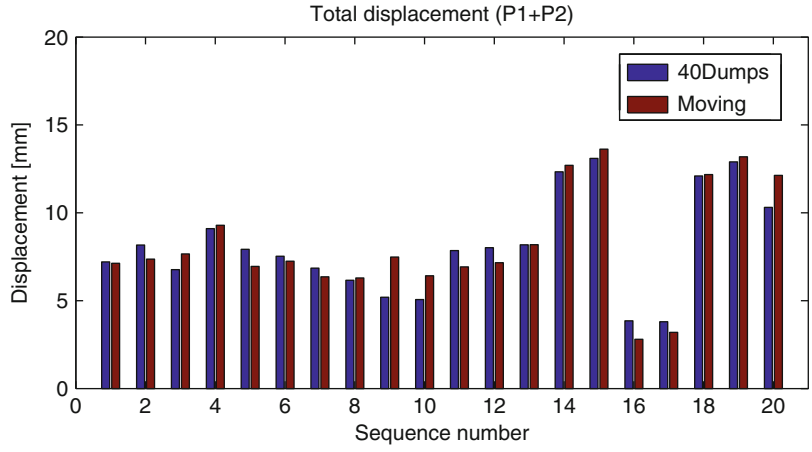

Computational Welding Mechanics,
Fig. 9 Comparison between block-dumped and moving heat source simulations

- Real-time CWM, that is, the time to solve a 3D transient nonlinear-coupled CWM problem for transient temperatures, microstructure evolution and stress, strain, and displacement while welding large welded structures with roughly 1-s temporal resolution and 1-cm spatial resolution, will be less than the welding arc time. For analysis of some large complex structures, with arc speeds that are not too fast, it is judged that commercial software for use with desktop computers will be available in 2012. If some preprocessing is permitted, then this will also most likely be available in 2012 for structures using very fast welding processes, such as laser welding. At this point, the time and cost of high-resolution CWM will become a negligible part of the total cost of product development.
- Designer-driven optimization in a design space and the design of optimal experiments will enable designers to explore larger, more complex virtual design spaces to better optimize designs and to choose optimal designs to be built and tested that reduce the time and cost of development and increase the quality of the product.

- Black boxes for welding will be developed that log data characterizing each weld. These will be similar to the black box flight recorders on aircraft. As sensors systems, cell phones and iPads are integrated into welding systems; large amounts of data will be collected for every weld in a structure. Computer vision will play a major role. This is called big data, and data analytics will be important.

CWM will become part of a holistic software analysis framework that integrates design with the manufacturing chain, in-service operation, and maintenance.

Cross-References

- ▶ Finite Element Simulation of the Fusion Welding of Metal Components including Post-Weld Heat Treatment
- ▶ Linear Friction Welding
- ▶ Minimization of Welding Distortions
- ▶ Modeling and Numerical Simulation of Resistance Spot Welding Process
- ▶ Modeling of Welding of Austenitic Stainless Steels
- ▶ Modeling Residual Stresses in Friction Stir Welding of Al Alloys
- ▶ Numerical Modelling of Underwater Welding and Cutting
- ▶ Repair Welding and Local Heat Treatment
- ▶ Shaped Metal Deposition Processes
- ▶ Thermal, Mechanical, and Microstructure Couplings
- ▶ Welding Heat Input Models
- ▶ Welding of Dissimilar Metals and Post Weld Heat Treatment
- ▶ Welding of Large Structures
- ▶ Welding Stresses

References

1. Karlsson L (1986) Thermal stresses in welding. In: Hetnarski RB (ed) Thermal stresses I. Elsevier, Amsterdam. pp 300–389
2. Goldak J, Akhlagi M (2005) Computational welding mechanics. Springer, New York
3. Lindgren L-E (2007) Computational welding mechanics. Woodhead Publishing Limited, Abington, Cambridge
4. Karlsson L, Lindgren L-E (1990) Combined heat and stress–strain calculations. In: Modeling of casting, welding and advanced solidification processes V. The Minerals, Metals & Materials Society, Davos, Switzerland
5. Goldak Technologies Inc. (2010) Available from: http://www.goldaktec.com/
6. Karlsson L, Pahkamaa A, Karlberg M, Löfstrand M, Goldak J, Pavasson J (2011) Mechanics of materials and structures: a simulation-driven design approach. J Mech Mater Struct 6(1-4):277–301, 25 s
7. Andersson BAB (1978) Thermal stresses in a submerged-arc welded joint considering phase transformations. J Eng Mater Technol, Trans ASME 100(4):356–362

Computer Simulation

- ▶ Thermal Shock and Modeling of Destruction for Refractory Linings of Metallurgical Installations

Concentrated Loading

- ▶ Magneto-Electro-Thermoelastic Problems: Fundamental Solutions and Green's Function
- ▶ Thermoelastostatics of Transversely Isotropic Materials: Fundamental Solutions and Green's Functions

Conditions of Compatibility

- ▶ Boundary-Value Problems Resulting in Thermoelastic Shock Wave Propagation
- ▶ Hyperbolic Thermoelasticity, Transient Dynamic Contact Problems
- ▶ Ray Expansion Theory
- ▶ Transient Thermoelastic Rayleigh Waves on the Surfaces of Bodies of Revolution

Conduction Shape Factors

- ▶ Two-Dimensional, Steady-State Conduction

Conformal Mapping Technique

▶ Green's Function of Thermoelastic Mixed Boundary Value Problem for Elliptic Hole

Conservation of Energy

▶ Energy and First Law of Thermodynamics

Constitutive and Geometrical Equations for the Thermomechanical Analysis of Shells

Erasmo Carrera and Salvatore Brischetto
Department of Mechanical and Aerospace Engineering, Politecnico di Torino, Torino, Italy

Synonyms

Divergence equations; Electric field-electric potential relations; Equation of heat conduction; Fourier law of heat conduction; Strain-mechanical displacement relations; Stress equations of motion

Definition

Thermal stress analysis is fundamental in the structural analysis of multilayered structures; the temperature variations are one of the most important factors for the stress fields that can cause failure of such structures. The effects of heat on the deformations and stresses of solid elastic bodies are considered by the theory of thermoelasticity. It is also possible that a deformation of the body produces changes in its temperature, which means that the effect of the temperature field on the deformation field is not a one-way phenomenon. These features demonstrate that the mechanical and thermal aspects are coupled and inseparable, and this coupling considerably complicates the computational aspect of solving actual thermoelastic problems. In order to obtain refined thermomechanical models which are able to analyze multilayered shells, the use of appropriate constitutive and geometrical relations is mandatory. These relations are here discussed in details for shell geometries; plate geometries can be seen as particular cases.

Overview

Thermal effects on a body made of traditional materials are limited to strains due to the temperature gradient, which is a datum for the stress analysis. In the case of sophisticated materials (e.g., high-performance composites), thermal effects can also include heat production due to strain rate; in this case, thermal and stress analyses are coupled [1].

Thermoelasticity is a branch of applied mechanics which investigates the effects of heat on the deformations and stresses of solid elastic bodies. It is a sort of extension of the conventional theory of isothermal elasticity to those processes in which deformations and stresses are produced by both mechanical forces and temperature variations. Thermoelastic processes are not totally reversible; in fact the elastic part may be reversed, but the thermal part may not be reversed because of the dissipation of energy which takes place during heat transfer. The effect of the temperature field on the deformation field is not a one-way phenomenon because a deformation of the body also produces changes in its temperature; these effects suggest the idea that the mechanical and thermal aspects are coupled and inseparable [2]. The thermoelastic problem, where the effects of the temperature gradient on the deformation/stress fields are considered, can be defined as a partial coupled thermomechanical problem. Otherwise full coupled thermomechanical problems are defined when also the temperature due to deformations is included.

In order to obtain a full coupled thermomechanical analysis of one-layered and multilayered isotropic and composite shells, opportune

constitutive equations must be introduced where the coupling between the elastic and thermal fields is clearly involved. Such constitutive equations can correctly be applied to shells if opportune geometrical relations are defined; these last allow the strains with the displacements and the temperature gradient with the sovra-temperature to be linked.

Basic Methodology

The coupling between the mechanical and thermal fields can be determined by using thermodynamical principles and Maxwell relations [3–6]; therefore, a Gibbs free-energy function G and a thermomechanical enthalpy density H [2, 6] must be defined. The thermomechanical enthalpy density H can be written in a quadratic form for a linear interaction, and constitutive equations are obtained as partial derivatives of this quadratic form.

The constitutive equations proposed are completely defined if the thermomechanical geometrical relations for shells are introduced; these last link the strain components with the displacement vector and the spatial gradient of temperature with the scalar sovra-temperature.

Constitutive Equations

Constitutive equations, for the thermomechanical problem, are obtained in according to that reported in Brischetto and Carrera [7] and Carrera et al. [8] where the coupling between the mechanical and thermal fields is investigated by using thermodynamical principles and Maxwell relations [3–5, 9]. Therefore, it is necessary to define a *Gibbs free-energy function* G and a *thermomechanical enthalpy density* H [2, 6]:

$$G(\varepsilon_{ij}, \theta) = \sigma_{ij}\varepsilon_{ij} - \eta\theta \tag{1}$$

$$H(\varepsilon_{ij}, \theta, \vartheta_i) = G(\varepsilon_{ij}, \theta) - F(\vartheta_i) \tag{2}$$

where σ_{ij} and ε_{ij} are the stress and strain components. η is the variation of entropy per unit of volume, and θ the sovra-temperature considered with respect to the reference temperature T_0. The function $F(\vartheta_i)$ is the dissipation function which depends on the spatial temperature gradient ϑ_i:

$$F(\vartheta_i) = \frac{1}{2}\kappa_{ij}\vartheta_i\vartheta_j - \tau_0\,\dot{h}_i \tag{3}$$

where κ_{ij} is the symmetric, positive semidefinite conductivity tensor. In the second term, τ_0 is a thermal relaxation parameter, and $\dot{h}_i$ is the temporal derivative of the heat flux h_i. The thermal relaxation parameter is usually omitted in most of the thermomechanical problems analyzed. Further details about the dissipation function $F(\vartheta_i)$ can be found in Altay and Dökmeci [3] and Yang et al. [9].

The thermomechanical enthalpy density H can be expanded in a quadratic form for a linear interaction:

$$H(\varepsilon_{ij}, \theta, \vartheta_i) = \frac{1}{2}Q_{ijkl}\varepsilon_{ij}\varepsilon_{kl} - \lambda_{ij}\varepsilon_{ij}\theta - \frac{1}{2}\chi\theta^2 - \frac{1}{2}\kappa_{ij}\vartheta_i\vartheta_j \tag{4}$$

where Q_{ijkl} is the elastic coefficients tensor considered for an orthotropic material in the problem reference system and λ_{ij} are the thermomechanical coupling coefficients. $\chi = \frac{\rho C_v}{T_0}$ where ρ is the material density, C_v is the specific heat per unit mass, and T_0 is the reference temperature [7, 8].

The constitutive equations are obtained by considering the following partial derivatives:

$$\sigma_{ij} = \frac{\partial H}{\partial \varepsilon_{ij}}, \quad \eta = -\frac{\partial H}{\partial \theta}, \quad h_i = -\frac{\partial H}{\partial \vartheta_i} \tag{5}$$

By considering (4) and (5), the constitutive equations for the thermomechanical problem are explicitly given:

$$\sigma_{ij} = Q_{ijkl}\varepsilon_{kl} - \lambda_{ij}\theta \tag{6}$$

$$\eta = \lambda_{ij}\varepsilon_{ij} + \chi\theta \tag{7}$$

$$h_i = \kappa_{ij}\vartheta_j \tag{8}$$

Single-subscript notation is introduced by using the indexes $m = q = 1, 2, 3, 4, 5, 6$ and $i = j = 1, 2, 3$:

$$\sigma_m = Q_{mq}\varepsilon_q - \lambda_m\theta \tag{9}$$

$$\eta = \lambda_q\varepsilon_q + \chi\theta \tag{10}$$

$$h_i = \kappa_{ij}\vartheta_j \tag{11}$$

From the equations written in single-subscript notations, it is easy to write their matrix form where the matrices and vectors are indicated in bold. Equations (9)–(11) are written for a generic k layer in the problem reference system (α, β, z) for a generic multilayered shell:

$$\boldsymbol{\sigma}^k = \boldsymbol{Q}^k\boldsymbol{\epsilon}^k - \boldsymbol{\lambda}^k\theta^k \tag{12}$$

$$\eta^k = \boldsymbol{\lambda}^{kT}\boldsymbol{\epsilon}^k + \chi^k\theta^k \tag{13}$$

$$\boldsymbol{h}^k = \boldsymbol{\kappa}^k\boldsymbol{\vartheta}^k \tag{14}$$

where the sovra-temperature θ^k, the term χ^k, and the entropy per unit volume η^k are scalar variables in each k layer. T indicates the transpose of a vector. The (6×1) stress and strain components are

$$\boldsymbol{\sigma}^k = \begin{Bmatrix} \sigma^k_{\alpha\alpha} \\ \sigma^k_{\beta\beta} \\ \sigma^k_{zz} \\ \sigma^k_{\beta z} \\ \sigma^k_{\alpha z} \\ \sigma^k_{\alpha\beta} \end{Bmatrix}, \quad \boldsymbol{\epsilon}^k = \begin{Bmatrix} \varepsilon^k_{\alpha\alpha} \\ \varepsilon^k_{\beta\beta} \\ \varepsilon^k_{zz} \\ \gamma^k_{\beta z} \\ \gamma^k_{\alpha z} \\ \gamma^k_{\alpha\beta} \end{Bmatrix} \tag{15}$$

The (3×1) vectors of heat flux $\boldsymbol{h}^k$ and spatial gradient of temperature $\boldsymbol{\vartheta}^k$ are

$$\boldsymbol{h}^k = \begin{Bmatrix} h^k_\alpha \\ h^k_\beta \\ h^k_z \end{Bmatrix}, \quad \boldsymbol{\vartheta}^k = \begin{Bmatrix} \vartheta^k_\alpha \\ \vartheta^k_\beta \\ \vartheta^k_z \end{Bmatrix} \tag{16}$$

The (6×1) array of thermomechanical coupling coefficients $\boldsymbol{\lambda}^k$ is

$$\boldsymbol{\lambda}^k = \boldsymbol{Q}^k\,\boldsymbol{\alpha}^k = \begin{Bmatrix} \lambda^k_1 \\ \lambda^k_2 \\ \lambda^k_3 \\ 0 \\ 0 \\ \lambda^k_6 \end{Bmatrix} \tag{17}$$

where the elastic coefficients matrix $\boldsymbol{Q}^k$ of Hooke law, in problem reference system for an orthotropic material [10], is

$$\boldsymbol{Q}^k = \begin{bmatrix} Q^k_{11} & Q^k_{12} & Q^k_{13} & 0 & 0 & Q^k_{16} \\ Q^k_{12} & Q^k_{22} & Q^k_{23} & 0 & 0 & Q^k_{26} \\ Q^k_{13} & Q^k_{23} & Q^k_{33} & 0 & 0 & Q^k_{36} \\ 0 & 0 & 0 & Q^k_{44} & Q^k_{45} & 0 \\ 0 & 0 & 0 & Q^k_{45} & Q^k_{55} & 0 \\ Q^k_{16} & Q^k_{26} & Q^k_{36} & 0 & 0 & Q^k_{66} \end{bmatrix} \tag{18}$$

the vector $\boldsymbol{\alpha}^k$ has (6×1) dimension, and it contains the thermal expansion coefficients:

$$\boldsymbol{\alpha}^k = \begin{Bmatrix} \alpha^k_1 \\ \alpha^k_2 \\ \alpha^k_3 \\ 0 \\ 0 \\ 0 \end{Bmatrix} \tag{19}$$

The matrix $\boldsymbol{\kappa}^k$ of conductivity coefficients has (3×3) dimension:

$$\boldsymbol{\kappa}^k = \begin{bmatrix} \kappa^k_{11} & \kappa^k_{12} & 0 \\ \kappa^k_{12} & \kappa^k_{22} & 0 \\ 0 & 0 & \kappa^k_{33} \end{bmatrix} \tag{20}$$

Each component proposed does not change in the case of plate geometry; the curvilinear coordinates α and β are replaced with the rectilinear ones x and y, respectively.

Geometrical Relations

A thin shell is a three-dimensional body bounded by two closely spaced curved surfaces; the distance between these two surfaces is small in comparison with the other dimensions. The middle surface of the shell is the locus of points which lie midway between these surfaces. The distance between the surfaces along the normal to the middle surface is the *thickness* of the shell at that point [11]. An example of geometry and reference system for a doubly curved shell is indicated in Fig. 1. The square of an infinitesimal linear segment in the k layer and the associated infinitesimal area and volume are

$$ds_k^2 = H_\alpha^{k2}\, d\alpha_k^2 + H_\beta^{k2}\, d\beta_k^2 + H_z^{k2}\, dz_k^2 \tag{21}$$

$$d\Omega_k = H_\alpha^k H_\beta^k d\alpha_k d\beta_k \tag{22}$$

$$dV_k = H_\alpha^k H_\beta^k H_z^k d\alpha_k d\beta_k dz_k \tag{23}$$

where the metric coefficients are

$$\begin{aligned} H_\alpha^k &= A^k(1 + z_k/R_\alpha^k), \\ H_\beta^k &= B^k(1 + z_k/R_\beta^k), \quad H_z^k = 1 \end{aligned} \tag{24}$$

k denotes the k^{th} layer of the multilayered shell; R_α^k and R_β^k are the principal radii of curvature along the coordinates α_k and β_k, respectively. A^k and B^k are the coefficients of the first fundamental form of Ω_k (Γ_k is the Ω_k boundary). If the attention is restricted to shells with constant radii of curvature (cylindrical, spherical, toroidal geometries), A^k and B^k equal 1. The geometrical relations for shells, in case of thermomechanical problems, link the mechanical strains with the displacement vector and the spatial gradient of temperature with the scalar sovra-temperature. These relations are:

$$\boldsymbol{\epsilon}^k = (\varepsilon_{\alpha\alpha}^k\ \varepsilon_{\beta\beta}^k\ \varepsilon_{zz}^k\ \gamma_{\beta z}^k\ \gamma_{\alpha z}^k\ \gamma_{\alpha\beta}^k)^T = (\boldsymbol{D}^k + \boldsymbol{A}^k)\boldsymbol{u}^k \tag{25}$$

$$\boldsymbol{\vartheta}^k = (\vartheta_\alpha^k\ \vartheta_\beta^k\ \vartheta_z^k)^T = -\boldsymbol{D}_t^k \theta^k \tag{26}$$

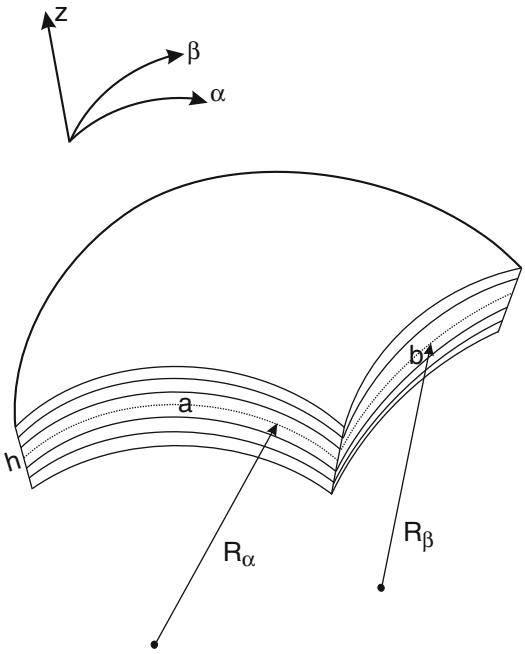

Constitutive and Geometrical Equations for the Thermomechanical Analysis of Shells, Fig. 1 Geometry and reference system for a multilayered shell

where $\boldsymbol{\epsilon}^k$ is the strain vector, $\boldsymbol{u}^k = (u^k\ v^k\ w^k)^T$ is the displacement vector, $\boldsymbol{\vartheta}^k$ is the spatial gradient of temperature, and θ^k is the scalar sovra-temperature referred to the reference external room temperature. T means the transpose of a vector. The explicit form of the introduced arrays is

$$\boldsymbol{D}^k = \begin{bmatrix} \frac{\partial_{\alpha_k}}{H_\alpha^k} & 0 & 0 \\ 0 & \frac{\partial_{\beta_k}}{H_\beta^k} & 0 \\ 0 & 0 & \partial_{z_k} \\ 0 & \partial_{z_k} & \frac{\partial_{\beta_k}}{H_\beta^k} \\ \partial_{z_k} & 0 & \frac{\partial_{\alpha_k}}{H_\alpha^k} \\ \frac{\partial_{\beta_k}}{H_\beta^k} & \frac{\partial_{\alpha_k}}{H_\alpha^k} & 0 \end{bmatrix}, \quad \boldsymbol{D}_t^k = \begin{bmatrix} \frac{\partial_{\alpha_k}}{H_\alpha^k} \\ \frac{\partial_{\beta_k}}{H_\beta^k} \\ \partial_{z_k} \end{bmatrix}$$

$$\boldsymbol{A}^k = \begin{bmatrix} 0 & 0 & \frac{1}{H_\alpha^k R_\alpha^k} \\ 0 & 0 & \frac{1}{H_\beta^k R_\beta^k} \\ 0 & 0 & 0 \\ 0 & -\frac{1}{H_\beta^k R_\beta^k} & 0 \\ -\frac{1}{H_\alpha^k R_\alpha^k} & 0 & 0 \\ 0 & 0 & 0 \end{bmatrix} \tag{27}$$

The symbols in differential operators matrices indicate the partial derivatives $\partial_{\alpha_k} = \frac{\partial}{\partial \alpha_k}$, $\partial_{\beta_k} = \frac{\partial}{\partial \beta_k}$, and $\partial_{z_k} = \frac{\partial}{\partial z_k}$. The parameters H_α^k and H_β^k equal 1 in case of plates because the radii of curvature R_α^k and R_β^k are infinite. Therefore, the pure geometrical contribute $\boldsymbol{A}^k$ equals zero in the plate case, and the coordinate system is the rectilinear one (x, y, z).

Possible Applications and Extensions

In order to define refined thermomechanical models for the accurate analysis of multilayered shells, the use of appropriate constitutive and geometrical relations is fundamental. They allow the thermomechanical effects and couplings to be evaluated and the static and dynamic response of such structures to be considered when they are subjected to mechanical and thermal loads. These equations can easily be extended to further multifield analyses (e.g., thermo-electro-mechanical problems) by considering opportune forms of the Gibbs free-energy function G and the thermo-electro-mechanical enthalpy density H and by adding the geometrical relations which link the electric field components with the electric potential.

Cross-References

- ▶ Thermal Load
- ▶ Thermal Stress Analysis

References

1. Cannarozzi AA, Ubertini F (2001) A mixed variational method for linear coupled thermoelastic analysis. Int J Solids Struct 38(4):717–739
2. Nowinski JL (1978) Theory of thermoelasticity with applications. Sijthoff & Noordhoff, The Netherlands
3. Altay GA, Dökmeci MC (1996) Some variational principles for linear coupled thermoelasticity. Int J Solids Struct 33(26):3937–3948
4. Altay GA, Dökmeci MC (1996) Fundamental variational equations of discontinuous thermopiezoelectric fields. Int J Eng Sci 34(7):769–782
5. Altay GA, Dökmeci MC (2001) Coupled thermoelastic shell equations with second sound for high-frequency vibrations of temperature-dependent materials. Int J Eng Sci 38(16):2737–2768
6. Ikeda T (1990) Fundamentals of piezoelectricity. Oxford University Press, Oxford
7. Brischetto S, Carrera E (2010) Coupled thermomechanical analysis of one-layered and multilayered isotropic and composite shells. Comput Model Eng Sci 56(3):249–301
8. Carrera E, Brischetto S, Nali P (2011) Plates and shells for smart structures: classical and advanced theories for modeling and analysis. Wiley, New Delhi
9. Yang Q, Stainer L, Ortiz M (2006) A variational formulation of the coupled thermo-mechanical boundary-value problem for general dissipative solids. J Mech Phys Solids 54(2):401–424
10. Reddy JN (2004) Mechanics of laminated composite plates and shells. Theory and analysis. CRC Press, New York
11. Leissa AW (2004) Vibration of shells. Theory and analysis. NASA SP-288, Washington, DC

Constitutive Equation for Linear Viscoelastic Materials with Temperature-Dependent Properties

Alan Wineman
Department of Mechanical Engineering,
University of Michigan, Ann Arbor, MI, USA

Overview

Polymeric materials exhibit stress relaxation, creep, and general time-dependent mechanical response that is characterized as viscoelastic. A change in the temperature of a solid polymer produces two effects: (1) thermal expansion or contraction and (2) a change in its creep and stress-relaxation properties. Spatially varying thermal expansion or contraction produces thermal stresses in polymeric structures just as in metal structures. The dependence of creep and stress relaxation on temperature is a property of polymers that has important implications for structural applications. It provides the means for calculating "frozen-in" stress distributions as well as determining the time dependence of deformed states.

This entry presents the most commonly used constitutive equation for linear viscoelastic materials with temperature-dependent properties. Only one-dimensional response is discussed in order to introduce the important concepts. The entry closes with a description of some interesting applications of the constitutive equation. Many of the modeling ideas presented here represent the current state of development. They can be expected to evolve as new experimental results lead to a better understanding of polymer response processes.

Isothermal Linear Viscoelasticity

It is useful to begin with an outline of linear isothermal viscoelasticity. A detailed development of the results presented in this section can be found in [1]. Time plays a central role in describing viscoelastic response. Let t denote the current time and let s denote a generic time, with $s \leq t$. Let $\varepsilon(s)$ and $\sigma(s)$ denote the strain and stress, respectively, at time s. For times $t \leq 0$, the material is assumed to be in its reference configuration, $\varepsilon(t) = 0$, and stress free, $\sigma(t) = 0$. When a linear viscoelastic material is subjected to a step strain history, $\varepsilon(t) = \varepsilon_0, t > 0, \varepsilon_0$ being a constant, the corresponding stress response is given by $\sigma(t) = \varepsilon_0 G(t), t > 0$. The function $G(t)$ is a material property, called the stress-relaxation modulus, that decreases monotonically with time t from $G(0)$ to an asymptotic value denoted by $G(\infty)$. When a linear viscoelastic material is subjected to a general strain history, $\varepsilon(t)$, the stress at time t depends on the preceding strain history $\varepsilon(s)$, $0 < s \leq t$, and the stress-relaxation modulus $G(t)$ through the relation:

$$\sigma(t) = \varepsilon(0)G(t) + \int_0^t G(t-s)\frac{d\varepsilon(s)}{ds}ds \qquad (1)$$

This is a constitutive equation for isothermal linear viscoelastic response whose form is motivated as follows. $d\varepsilon(s)$ denotes a step strain applied at time s, $t - s$ is the time that has elapsed since the step strain was applied, $d\sigma(s) = G(t-s)d\varepsilon(s)$ is the corresponding stress at time t, and (1) represents the superposition or sum of all stresses at time t due to all of the preceding step strains.

An equivalent approach that can be used to describe linear viscoelastic response is to subject the material to a step stress history, $\sigma(t) = \sigma_0$, $t > 0$, σ_0 being a constant. The corresponding strain response is given by $\varepsilon(t) = \sigma_0 J(t)$, $t > 0$. The function $J(t)$ is an alternate material property, called the creep compliance, that increases monotonically with time t from $J(0)$ to an asymptotic value denoted by $J(\infty)$. When a linear viscoelastic material is subjected to a general stress history, $\sigma(t)$, the strain at time t depends on the preceding stress history, $\sigma(s)$, $0 < s \leq t$, and the creep compliance $J(t)$ through the relation:

$$\varepsilon(t) = \sigma(0)J(t) + \int_0^t J(t-s)\frac{d\sigma(s)}{ds}ds \qquad (2)$$

The form of this equation can be motivated in the same way as was (1). The stress-relaxation modulus and creep compliance are not independent material properties, but satisfy the integral relation:

$$1 = G(0)J(t) + \int_0^t J(t-s)\frac{dG(s)}{ds}ds \qquad (3)$$

With the use of (3), (2) can be transformed into (1), and vice versa. In this way, (1) and (2) are considered inverses of each other.

Linear viscoelasticity can also be described by considering the response to a strain that varies sinusoidally with frequency ω, $\varepsilon(t) = \varepsilon_o \sin \omega t$, where $|\varepsilon_o| << 1$. Using (1), it can be shown that the stress has a steady state sinusoidal response described by

$$\sigma(t) = \varepsilon_o[G'(\omega)\sin \omega t + G''(\omega)\cos \omega t] \qquad (4)$$

or, equivalently,

$$\sigma(t) = \varepsilon_o G^*(\omega)\sin(\omega t + \delta(\omega)) \qquad (5)$$

where

$$G^*(\omega) = \left[G'(\omega)^2 + G''(\omega)^2\right]^{1/2}$$
$$\tan \delta(\omega) = G''(\omega)/G'(\omega) \qquad (6)$$

As seen from (5), the stress varies sinusoidally at the same frequency ω as the strain but is out of phase with the strain by $\delta(\omega)$. Both $G^*(\omega)$, the ratio of the stress and strain amplitudes, and $\delta(\omega)$, the phase difference between the stress and strain, vary with frequency ω. $G'(\omega)$ is called the storage modulus, and $G''(\omega)$ is called the loss modulus. They are an alternate set of material properties that vary with frequency. $G'(\omega)$ and $G''(\omega)$ can be calculated from the stress-relaxation modulus $G(t)$ and vice versa, but such relations are not presented here.

Similarly, the strain response to a sinusoidally oscillating stress $\sigma(t) = \sigma_o \sin \omega t$ is found from (2). The steady state strain is

$$\varepsilon(t) = \sigma_o[J'(\omega) \sin \omega t + J''(\omega) \cos \omega t] \quad (7)$$

$J'(\omega)$ is called the storage compliance, and $J''(\omega)$ is called the loss compliance. They are another set of material properties that vary with frequency. $J'(\omega)$ and $J''(\omega)$ can be calculated from the creep compliance $J(t)$ and vice versa. They can also be expressed in terms of $G'(\omega)$ and $G''(\omega)$.

Finally, it is important to point out one consequence of stress relaxation. Positive work is done when a viscoelastic solid is deformed and then returned it to its original state. Much of this work is converted to heat and leads to a rise in temperature.

Thermally Induced Dimensional Changes

Attention is restricted to materials undergoing small strains. When a viscoelastic rod is subjected to both stress and a temperature change, the total strain ε^{total} is the superposition of two separate strains, one due only to temperature change in the absence of stress, denoted by $\varepsilon^{thermal}$, and one due only to the stress, denoted by ε^{mech}. Thus,

$$\varepsilon^{total} = \varepsilon^{thermal} + \varepsilon^{mech} \quad (8)$$

Consider a viscoelastic rod that is at some constant reference temperature T_0 for $t < 0$. Let the block be subjected to a step temperature history of amount $T(t) - T_o = \Delta T_o$, $t > 0$, ΔT_o being a constant. The block appears to undergo a time-dependent thermal strain given by

$$\varepsilon^{thermal}(t) = \alpha(t)\Delta T_o \quad (9)$$

in which $\alpha(t)$ is another material property, a time-dependent coefficient of thermal expansion. Experimental results suggest that $\alpha(t)$ is a monotonically increasing function of time (see, e.g., [2]).

Suppose the viscoelastic rod is subjected to a general temperature history, $\Delta T(t) = T(t) - T_o$. It is assumed that the response to temperature changes also satisfies the conditions of superposition used in developing (1) and (2). Thus, the total thermal strain at time t depends on the preceding temperature history and $\alpha(t)$:

$$\varepsilon^{thermal}(t) = \Delta T(0)\alpha(t) + \int_0^t \alpha(t-s)\frac{d(\Delta T(s))}{ds}ds \quad (10)$$

Mechanical Response at Different Temperatures

The description of the mechanical response now involves the temperature, strain, and stress histories. Consider a series of step strain experiments carried out at the same strain but at different constant temperatures. Let $G(t, T)$ denote the stress-relaxation modulus corresponding to temperature T. If T_1 and T_2 are two temperatures with $T_2 > T_1$, then at a given time t, the stress relaxes to a smaller value at temperature T_2 than at temperature T_1, that is, $G(t, T_2) < G(t, T_1)$. In other words, the stress relaxes faster at the higher temperature.

The manner in which the stress-relaxation modulus depends on time and temperature has been the subject of a great deal of research [3]. Experimental results have led to a method of accounting for the temperature dependence known as *time-temperature superposition*. It is commonly used as a basis for calculating thermally induced stresses and deformations in viscoelastic structures.

In order to describe time-temperature superposition, the stress-relaxation modulus is expressed as a function of $\log t$:

$$G(t,T) = E(\log\ t, T) \tag{11}$$

This is done because a $\log t$ scale is more convenient for plotting stress-relaxation data over a large range of times. Time-temperature superposition is based on the following interpretation of such plots of stress-relaxation data:

1. By shifting a stress-relaxation curve for one temperature horizontally along the $\log t$ axis, it can coincide with the stress-relaxation curve for any other temperature.
2. The initial and long time values of the stress-relaxation modulus are independent of the temperature.

In order to express this mathematically, let it be assumed that the stress-relaxation modulus $E(\log t, T_0)$ is known at temperature T_0. Let $E(\log t, T_1)$ denote the stress-relaxation modulus at temperature T_1. If $T_1 > T_0$, then $E(\log t, T_1)$ is obtained by shifting $E(\log t, T_0)$ horizontally to the left, that is, to smaller times, by an amount denoted as $\log \phi(T_1, T_0)$. A given value of the stress-relaxation modulus is then reached at a smaller time at temperature T_1 than at the lower temperature T_0. The higher the temperature T_1, the larger is the amount of shift to the left. This can be expressed by writing

$$\begin{aligned} E(\log\ t, T_1) &= E(\log\ t + \log \phi(T_1, T_0), T_0) \\ &= E(\log\ \phi(T_1, T_0) t, T_0) \end{aligned} \tag{12}$$

The stress-relaxation modulus on the t -axis is obtained using (11):

$$G(t, T_1) = G(\phi(T_1, T_0) t, T_0) \tag{13}$$

For a particular viscoelastic material, the amount of shift $\log \phi(T_1, T_0)$ is constructed graphically from its stress-relaxation data. This process thus establishes the function $\phi(T_1, T_0)$ as a new material property. It is common practice to define

$$\phi(T_1, T_0) = \frac{1}{a(T_1, T_0)} \tag{14}$$

and write (13) as

$$G(t, T_1) = G\left(\frac{t}{a(T_1, T_0)}, T_0\right) \tag{15}$$

Equation (15) expresses the important result following from time-temperature superposition that the stress-relaxation modulus at any temperature can be expressed in terms of two material properties: the stress-relaxation modulus at a reference temperature $G(t, T_0)$ and a function $a(T_1, T_0)$, known as the called the *time-temperature shift function*.

If $T_1 = T_0$, the construction and (12) imply that $\phi(T_1, T_0) = a(T_1, T_0) = 1$. If $T_1 > T_0$, the construction and (12) imply that $\log \phi(T_1, T_0) > 0$, $\log a(T_1, T_0) < 0$, and $a(T_1, T_0) < 1$. On the other hand, if $T_1 < T_0$, then $a(T_1, T_0) > 1$. For a fixed value of T_0, $a(T_1, T_0)$ is a monotonically decreasing function of T_1. At a fixed temperature T_1, the argument $t/a(T_1, T_0)$ in the right side of (15) increases with increasing time t, and G monotonically decreases. At a fixed time $\hat{t}$, $a(T_1, T_0)$ decreases as T_1 increases, and the argument $\hat{t}/a(T_1, T_0)$ again increases. Thus, G decreases with increasing time or increasing temperature, and there is said to be time-temperature equivalence.

An interpretation of this result is provided by considering the sequence of changes in the configurations of a polymer's macromolecular structure during creep or stress relaxation at some specific temperature. When the temperature is changed, essentially the same sequence of macromolecular reconfigurations takes place but with a speed that depends on the temperature. A temperature rise causes a uniform speeding up of the sequence, and a temperature decrease causes a uniform slowing down of the sequence. Some researchers have described this response by saying that a polymer has an intrinsic or internal clock. Each macromolecular configuration corresponds to a time on the clock. Higher temperatures make the internal clock run faster relative to our physical clock, and lower temperatures make the internal clock run slower.

Comments on Time-Temperature Superposition

A more detailed discussion of the remarks presented here can be found in [4]. Time-temperature superposition is approximately valid for amorphous polymers. The shift function is often expressed in the form:

$$\log a(T,T_0) = \frac{C_1(T-T_g)}{C_2+T-T_g} \tag{16}$$

in which C_1, C_2 are constants associated with the reference temperature T_0. T_g is an important polymer property that is determined from a plot of the total volume per unit mass, that is, the specific volume, vs. temperature. This plot has a rapid change or "discontinuity" in slope, called the dilatometric glass transition, at a characteristic temperature T_g, called the glass transition temperature. The mechanical properties of an amorphous polymer change dramatically as the temperature passes through T_g. At temperatures above T_g, the polymer is soft and highly deformable and in a rubberlike state. At temperatures below T_g, the material is stiff and brittle and in a glass-like state. For typical polymers, the value of $a(T,T_0)$ can decrease from the order of 10^6 to the order of 10^{-2} as T increases from below to above T_g, an important observation with relevance to the mechanics of polymers.

Equation (16), referred to as the WLF Equation [3], is approximately valid for amorphous polymers above T_g. Recent work [5] has discussed forms for the shift function which can be applied for a range of temperatures above and below the glass transition.

Influence of Temperature on Material Properties

The stress-relaxation modulus at temperature T can be written in terms of a "master" relaxation function $\hat{G}(t)$ that decays monotonically from $\hat{G}(0)$ to its large time limit $\hat{G}(\infty)$:

$$G(t,T) = \hat{G}\left(\frac{t}{\tau_R(T)}\right) \tag{17}$$

$\tau_R(T)$ is a characteristic stress-relaxation time at temperature T that can be defined as the time coordinate of the centroid of the plot of $G(t,T)-G(\infty,T)$ vs. t. A specific example of a master relaxation function is given by

$$\hat{G}(t) = G_\infty + (G_0 - G_\infty)e^{-t} \tag{18}$$

in which $\hat{G}(0) = G_0$ and $\hat{G}(\infty) = G_\infty$. The stress-relaxation modulus at temperature T for the standard linear solid [1] is given by

$$G(t,T) = G_\infty + (G_0 - G_\infty)e^{-t/\tau_R(T)} \tag{19}$$

It can be seen from (15) and (17) that the characteristic stress-relaxation times at temperatures T_0 and T_1 are related by

$$\tau_R(T_1) = a(T_1,T_0)\tau_R(T_0) \tag{20}$$

From the properties of $a(T_1,T_0)$ and (20), the influence of temperature on the characteristic stress-relaxation time is seen to be summarized as

$$\begin{array}{lll} T_1>T_0, & a(T_1,T_0)<1, & \tau_R(T_1)<\tau_R(T_0) \\ T_1<T_0, & a(T_1,T_0)>1, & \tau_R(T_1)>\tau_R(T_0) \end{array} \tag{21}$$

A comment was made at the end of the preceding section that $a(T_1,T_0)$ could undergo enormous changes in value with change in temperature. Accordingly, the characteristic stress-relaxation time could change from seconds to years or vice versa, depending on the temperature change.

Let $J(t,T)$ denote the creep compliance at temperature T. It can be shown using (3) that time-temperature superposition is also valid for the creep compliance:

$$J(t,T_1) = J\left(\frac{t}{a(T_1,T_0)},T_0\right) \tag{22}$$

Letting $G'(\omega,T)$ and $G''(\omega,T)$ denote the storage and loss moduli, respectively, at temperature T, it can be shown that

$$G'(\omega, T_1) = G'(a(T_1, T_0)\omega, T_1)$$
$$G''(\omega, T_1) = G''(a(T_1, T_0)\omega, T_1) \quad (23)$$

Letting $J'(\omega, T)$ and $J''(\omega, T)$ denote the storage and loss compliances, respectively, at temperature T:

$$J'(\omega, T_1) = J'(a(T_1, T_0)\omega, T_1)$$
$$J''(\omega, T_1) = J''(a(T_1, T_0)\omega, T_1) \quad (24)$$

Suppose that $T_1 > T_0$ so that $a(T_1, T_0) < 1$. According to (23) and (24), the response at a specific frequency ω at temperature T_1 corresponds to the response at the lower frequency $a(T_1, T_0)\omega$ at the lower temperature T_0. Alternatively, the response at a specific frequency ω at temperature T_0 corresponds to the response at the higher frequency $\omega/a(T_1, T_0)$ at the higher temperature T_1. Analogous statements hold when $T_1 < T_0$.

Extension to Time-Varying Temperature Histories

There are many applications in which a viscoelastic structure experiences a time-dependent temperature history. For example, the external thermal environment may vary with time, or the temperature may rise because of energy dissipation as work is done during oscillatory deformations. In either case, it is necessary to account for the influence of time-dependent temperature histories on the material properties. The constitutive equation presented here relating stress, strain, and temperature histories was introduced by Morland and Lee [6] and makes use of time-temperature superposition.

The development uses a result that can be deduced from (15). Let G_1 and G_2 be any two values of the stress-relaxation modulus, with $G_1 > G_2$. Let t_1 and t_2 be the times when the stress-relaxation modulus reaches the values G_1 and G_2, respectively, at temperature T_1. Then, the change in value from G_1 to G_2 occurs during the time interval $t_2 - t_1$ while at temperature T_1. According to (15), at temperature T_0, the values G_1 and G_2 are reached at times $t_1/a(T_1, T_0)$ and $t_2/a(T_1, T_0)$, respectively. Thus, at temperature T_0, the change in value from G_1 to G_2 occurs during the time interval $(t_1 - t_2)/a(T_1, T_0)$.

Next, suppose a viscoelastic specimen is subjected to both a step strain history of amount ε_0 applied at time $t = 0$ and some temperature history $T(s)$, $s \in [0, t]$. Let the stress-relaxation response be denoted by

$$\sigma(t) = \varepsilon_o G\left[t, T(s)|_{s=0}^{t}\right] \quad (25)$$

This notation suggests that the stress-relaxation response depends in some way on all the values $T(s)$ from the time $t = 0$ when the step strain was applied to the current time t. The form for this temperature-dependent stress-relaxation function is determined under the following assumption:

The macromolecular reconfigurations that occur as the temperature varies with time follow the same sequence as would occur at a constant temperature. During a small time interval, the speed of the macromolecular reconfiguration process, and the resultant stress relaxation, depends only on the temperature during that interval. Time-temperature superposition can be used to relate the amount of stress relaxation during this time interval at this temperature to that during a corresponding time interval at a reference temperature.

Since the initial and residual moduli are unaffected by temperature,

$$G[0, T_1] = G[0, T_0] = G\left[0, T(s)|_{s=0}^{0}\right] \quad (26)$$

$$G[\infty, T_1] = G[\infty, T_0] = G\left[0, T(s)|_{s=0}^{\infty}\right] \quad (27)$$

Now consider a time interval $0 \le s \le t_1$ at the beginning of stress relaxation and let $\tilde{T}_1$ be an average temperature in this time interval. Using the result established above, the decrease in G at temperature $\tilde{T}_1$ during the time interval $t_1 - 0$ is the same as the decrease in G at a reference temperature T_0 during the time interval $(t_1 - 0)/a(\tilde{T}_1, T_0)$ or

$$G\left[t_1, T(s)|_{s=0}^{t_1}\right] = G\left[(t_1 - 0)/a(\tilde{T}_1, T_0), T_0\right] \tag{28}$$

During the next time interval, $t_1 \le s \le t_2$, the average value of the temperature is $\tilde{T}_2$. The decrease in G at this temperature during time interval $t_2 - t_1$ is the same as at temperature T_0 during the time interval $(t_2 - t_1)/a(\tilde{T}_2, T_0)$. G at time t_2 has reduced to a value given by

$$G\left[t_2, T(s)|_{s=0}^{t_2}\right] = G\left[(t_1 - 0)/a(\tilde{T}_1, T_0) + (t_2 - t_1)/a(\tilde{T}_2, T_0), T_0\right] \tag{29}$$

Continuing in this manner results in an expression for the stress-relaxation modulus at time t_n:

$$G\left[t_n, T(s)|_{s=0}^{t_n}\right] = G\left[\sum_{k=1}^{n} (t_k - t_{k-1})/a(\tilde{T}_k, T_0), T_0\right] \tag{30}$$

where $\tilde{T}_k$ is the average temperature during the time interval $t_{k-1} \le s \le t_k$. The approximation to the relaxation modulus at time t is improved by increasing the number of time intervals $t_{k-1} \le t_k$ and decreasing their duration $t_k - t_{k-1}$. In the limit, the expression for stress-relaxation modulus at time t is

$$G\left[t, T(s)|_{s=0}^{t}\right] = G\left[\int_0^t \frac{ds}{a(T(s), T_0)}, T_0\right] \tag{31}$$

The integral

$$\xi(t) = \int_0^t \frac{ds}{a(T(s), T_0)} \tag{32}$$

is called the "reduced time," "intrinsic time," or "pseudo time" [6]. Materials for which this model is valid are called "thermo-rheologically simple," a terminology introduced in [7].

Equation (31) has interesting implications for stress analysis when combined with the experimental results that the stress-relaxation modulus can decrease by a factor of 10^3 and the shift function $a(T_1, T_0)$ can increase to 10^6 if $T_1 < T_0$ or decrease to 10^{-4} if $T_1 > T_0$. In order to see this, consider stress relaxation in which a step strain is applied when the specimen is at temperature T_0. At time t_1, let the temperature be reduced to T_1. For $t < t_1$, it is seen from (32) that

$$\xi(t) = \int_0^t \frac{ds}{a(T_0, T_0)} = \int_0^t \frac{ds}{1} = t \tag{33}$$

The reduced time is still the physical time, and by (31), stress relaxation is given by

$$G\left[t, T(s)|_{s=0}^{t}\right] = G[t, T_0] \tag{34}$$

For $t > t_1$, the reduced time is found from (32) to be

$$\xi(t) = \int_0^{t_1} \frac{ds}{a(T_0, T_0)} + \int_{t_1}^{t} \frac{ds}{a(T_1, T_0)} = t_1 + \frac{t - t_1}{a(T_1, T_0)} \tag{35}$$

and the stress-relaxation response is given by

$$G\left[t, T(s)|_{s=0}^{t}\right] = G\left[t_1 + \frac{t - t_1}{a(T_1, T_0)}, T_0\right] \tag{36}$$

When T_1 is sufficiently low temperature, $a(T_1, T_0)$ can be large, say 10^4. The argument of G in (36) changes very little from t_1 until $t - t_1$ has increased substantially. Then, after, say 10^4 hours, the reduced time has become large enough that the relaxation modulus will begin to decrease noticeably. For a long time there is negligible stress relaxation, the stress is essentially "frozen" at the value $G(t_1, T_0)$.

Constitutive Equation for Time-Varying Temperature Histories

It is assumed that the same construction that led to (1) is valid when the temperature varies with time. Let $\varepsilon(t)$ now denote the mechanical part of the strain, defined in (8). The mechanical strain history is treated as the superposition of step strain increments. The stress at time t is the superposition at time t of responses to these step

strain increments. The additional assumption is made that the contribution to the stress at time t arising from the step strain initiated at time s depends only on the temperature history during the time interval $[s, t]$:

$$d\sigma(t) = d\varepsilon(s) G\left[\int_s^t \frac{dx}{a(T(x), T_0)}, T_0\right] \quad (37)$$

The total stress at time t is, by superposition,

$$\sigma(t) = \varepsilon(0) G\left[\int_0^t \frac{dx}{a(T(x), T_0)}, T_0\right] + \int_0^t G\left[\int_s^t \frac{dx}{a(T(x), T_0)}, T_0\right] d\varepsilon(s) \quad (38)$$

which is often written in the form:

$$\sigma(t) = \varepsilon(0) G[\xi(t), T_0] + \int_0^t G[\xi(t) - \xi(s), T_0]\, d\varepsilon(s) \quad (39)$$

It can be shown that the strain at time t can be expressed in terms of the stress history, temperature history, and creep compliance by

$$\varepsilon(t) = \sigma(0) J[\xi(t), T_0] + \int_0^t J[\xi(t) - \xi(s), T_0]\, d\sigma(s) \quad (40)$$

Applications

Equation (39), combined with the thermal history and material properties incorporated in (36), has been used in a variety of structural analyses. As an example, consider a simple structure consisting of three parallel rods connected at one end by smooth pins to a rigid support and at the other end to a rigid cross bar. A force history is applied to the cross bar, and each rod experiences a specified temperature history. Examples with different force and temperature histories are given in [1] that illustrate the use of (39) in determining (a) frozen-in deformation, (b) frozen-in bar forces, or (c) cooling-induced warping. The three-dimensional version of (39) along with a time and spatially varying temperature determined from the heat equation was used in [8] to show how a desired frozen-in stress distribution can be produced in a glass plate. There have been a number of studies that use the alternate form of constitutive equation, (4), with temperature- and frequency-dependent properties given by (23). A representative example is given by [9] which determines temperature rise during torsional oscillations of a linear viscoelastic rod.

References

1. Wineman A, Rajagopal KR (2000) Mechanical response of polymers, an introduction. Cambridge University Press, Cambridge
2. Knauss WG, Emri I (1987) Volume change and the nonlinearly thermo-viscoelastic constitution of polymers. Polym Eng Sci 27:86–100
3. Ferry JD (1980) Viscoelastic properties of polymers. Wiley, New York
4. Ward IM (1983) Mechanical properties of polymers. Wiley, NewYork
5. Losi G, Knauss W (1992) Thermal streses in nonlinearly viscoelastic solids. J Appl Mech 59:43–49
6. Morland LW, Lee EH (1960) Stress analysis for linear viscoelastic materials with temperature variation. Trans Soc Rheol 4:233–263
7. Staverman AJ, Schwarzl F (1956) Linear deformation behaviour of high polymers. In: Suart HA (ed) Die Physik der Hochpolymeren, vol 4. Springer, Berlin, pp 1–125
8. Lee EH, Rogers TG, Woo TC (1965) Residual stresses in a glass plate cooled symmetrically from both surfaces. J Am Ceram Soc 48:480–487
9. Ting EC (1972) Heat generation in a torsional spring subjected to sinusoidal oscillations. J Sound Vib 12:81–92

Constitutive Models, Physically Based Models for Plasticity

Göran Engberg
Department of Material Science, Dalarna University, Falun, Sweden

Synonyms

Mechanism-based plasticity

Definition

Physically based models for the plastic behavior of crystalline, metallic materials are discussed. However, deformation by twinning and phase transformations as well as the evolution of texture are omitted.

Overview

Slip of dislocations is the main cause for plastic deformation. Additional mechanisms are formation of twins and phase transformations (mainly austenite to martensite). Several models for deformation hardening have been proposed and most of them depict proportionality between the flow stress in shear, τ, and the square root of the total dislocation density, ρ, giving the relationship

$$\tau = \alpha G b \sqrt{\rho} \tag{1}$$

where $\alpha \sim 0.2$ for fcc and $\alpha \sim 0.4$ for bcc metals (Chapter 1 in [1]). G is the shear modulus and b is the magnitude of Burgers vector. Moving dislocations are the cause of the plastic shear rate expressed by the Orowan equation

$$\dot{\gamma}^p = \frac{d\gamma^p}{dt} = \rho_m b v \tag{2}$$

where ρ_m is the density of mobile dislocations and v is their average velocity. During deformation, the mobile dislocations move an average distance L before being immobilized, giving rise to a plastic shear strain, γ^{p}. Using (2) and assuming $d\rho_i = \rho_m dx/L$, where dx is the distance, the dislocations have moved during the time step dt, gives the relationship

$$\frac{d\rho_i}{dt} = \frac{1}{bL(\gamma^p)} \dot{\gamma}^p \tag{3}$$

where ρ_i is the immobile dislocation density. Equations 1, 2, and 3 define the fundamental relation between shear flow stress and plastic shear strain. The model can be used in crystal plasticity models, and then the relations are applied to the different slip systems. The mobile dislocation density is often assumed to be very small and constant, and then (1) and (3) are also valid for the total dislocation density. The model can be rewritten into a von Mises effective stress and effective plastic strain relation and extended to account for a variety of flow stress contributions as described shortly below.

Dislocation Density–Based Flow Stress Model

As the shear due to dislocation slip is confined to certain crystallographic planes and directions, translation to flow stress, σ, and effective plastic strain, $\bar{\varepsilon}^p$ is derived by using the Taylor factor, m. This is the inverted average of the individual Schmid factors, giving the relation between applied stress and the shear stress in the slip plane in the slip direction, in a grain. For bcc and fcc metals, the Taylor factor is approximately 2.8 (2 if assuming an infinite number of available slip systems) and 3.1 (for 12 independent slip systems), respectively. These values vary with deformation due to rotations of the individual grain(s). We thus have

$$\sigma = \sigma_0 + m\alpha G b \sqrt{\rho} \tag{4}$$

$$\frac{d\rho}{d\bar{\varepsilon}_p} = \frac{m}{bL(\bar{\varepsilon}_p)} \tag{5}$$

Here σ_0 denotes all contributions to the flow stress from other strengthening mechanisms that are independent of deformation, such as atoms in solid solution, the friction from the atomic lattice (commonly referred to as Peierls-Nabarro barriers), and precipitation of small precipitates (in comparison to the individual length of dislocation segments). It is also common to include the influence of grain size, σ_g, in σ_0 using the Petch-Hall relationship, $\sigma_g = k_g d^{-1/2}$. If L is independent of strain, we obtain the classic Ludwik relation [2]

$$\sigma = \sigma_0 + c\sqrt{\bar{\varepsilon}_p} \tag{6}$$

Equations 4 and 5 are the fundamental equations for the basic type of flow stress model discussed below. The contributions to σ_0 will be discussed in the next sections. Equation 5 describes the generation of dislocations. There are also processes that will decrease the dislocation density simultaneously due to annihilation or remobilization of immobile dislocations (see, e.g., Bergström [3]). Such processes are caused by cross-slip and diffusion-assisted climb of dislocations and by recrystallization. These additional contributions will also be discussed below. As diffusion is due to the availability and migration of vacancies in the crystal lattice, the generation of excess vacancies is also important. Recrystallization changes the grain size as well as the average dislocation density and thus also alters the flow stress.

Additional Contributions to the Flow Stress

The additional strain-independent contributions to the flow stress, first term in (4), arise from obstacles with short-range or long-range interactions with dislocations. The former are thermally activatable obstacles and the latter are not. Examples of thermally activatable obstacles are the atom lattice (Peierls-Nabarro barriers), solute atoms, and cross-slip of dislocations due to constraint of partial dislocations. Examples of long-range obstacles are precipitates where we distinguish between coarse and small precipitates with regard to the size of the dislocation network (substructure). Small precipitates act on the individual dislocation links while coarse precipitates act as regions with different elastic and plastic properties. Individual grains also belong to the second category. The flow stress is expressed as shear stress contributions, τ, in the following. The given relations can easily be translated into a normal flow stress using the Taylor factor m in order to add the contributions to (4). Some of the contributions contain a calibration parameter, and then, there is no need to include the m factor specifically as it is accommodated by the calibration parameter.

Thermally Activated Deformation Processes

Barriers to dislocations with small extension in space and of small to moderate strength can be overcome by thermal activation. Typical barriers are the individual atoms in the lattice, giving rise to the Peierls-Nabarro mechanism, substitutional and interstitial solute atoms with differing elastic properties and sizes as compared to the main specie of the metal. The mentioned barriers give rise to mainly strain-independent contributions. The effect is described by the probability, p, to overcome an activation energy multiplied with the frequency, ω, of attacks on the barrier. Thus, the average speed of the dislocation, v, can be written as

$$v = v_0 \omega p \tag{7}$$

where v_0 is the speed of the dislocation when no barriers are present. The probability can be written as

$$p = e^{-\frac{\Delta G}{kT}} \tag{8a}$$

where the activation energy is

$$\begin{aligned} \Delta G &= \int_{-r_0}^{r_0} (F - \tau^* b L^*) dr \\ &= \Delta G_1 - \tau^* b L^* 2 r_0 \\ &= \Delta G_0 - b \int_0^{\tau^*} A^* d\tau \end{aligned} \tag{8b}$$

F is the force barrier over the distance $-r_0$ to r_0 (assuming a symmetric obstacle) and $\tau^* b L^*$ is the force exerted on the barrier by the dislocation. L^* is a characteristic length of the dislocation participating in the activation event. The area swept by the dislocation during passing of the barrier, $2 r_0 L^*$, is also called the activation area, A^*, for the event. T is the temperature and k is Boltzmann's constant. ΔG_0 is the activation energy for the total barrier and ΔG_1 is the total barrier between $-r_0$ and r_0.

Inserting (7) into (2) and adapting to the polycrystal case, we obtain

$$\dot{\bar{\varepsilon}}^p = \frac{d\bar{\varepsilon}^p}{dt} = \frac{\rho_m b v_0}{m}\omega e^{-\frac{\Delta G}{kT}} \tag{9}$$

where v_0 is the speed for the dislocation moving without barriers and ω the frequency with which the dislocation attempts to overcome the barrier. Depending on the actual shape of the barrier, different relations emerge. For ferrite (bcc), it has been observed that the activation area is inversely proportional to the stress, $A^* \approx a/\tau$, and using the last relation in (8b) with a finite lower cutoff value for τ*, τ_c^*, this gives

$$\dot{\bar{\varepsilon}} = \dot{\varepsilon}_{ref}\left(\frac{\tau^*}{\tau_c}\right)^{\frac{T_0}{T}} \tag{10a}$$

$$\tau_c = \tau_c^* exp\left(\frac{\Delta G_0}{ab}\right) \tag{10b}$$

$$T_0 = \frac{ab}{k} \tag{10c}$$

$$\dot{\varepsilon}_{ref} = \frac{\rho_m b v_0 \omega}{m} \tag{10d}$$

A good description of the temperature and strain-rate dependence at low and ambient temperatures in ferrite has been achieved [4] by assuming two parallel coupled mechanisms. For interstitially dissolved carbon in ferrite, a strong asymmetric distortion of the lattice is obtained. By using the relationships for the interaction with a dislocation as proposed by [5] and assuming Friedel statistics (Chapter 2 in [1]), we obtain

$$\tau^* = \tau_0 G\sqrt{\frac{x}{x_0}\left[1 + \frac{kT}{\Delta f_0 G b^3} ln\left(\frac{\dot{\bar{\varepsilon}}^p}{\dot{\bar{\varepsilon}}_{ref}}\right)\right]} \tag{11}$$

where τ_0, Δf_0, and $\dot{\bar{\varepsilon}}_{ref}$ are constants and x is the atomic fraction of carbon in the ferrite. x_0 is a reference value, typically bulk value, of carbon.

For other barrier shapes, a more general form of the activation energy has been proposed [6]

$$\Delta G = \Delta f_0 G b^3\left[1 - \left(\frac{\tau^*}{\tau_0 G}\right)^p\right]^q \tag{12}$$

where $\Delta G0 = \Delta f0 G b^3$ is the free energy required to overcome the lattice resistance or obstacles without aid from external stress. The quantity $\hat{\tau} = \tau_0 G$ is the athermal flow strength that must be exceeded in order to move the dislocation across the barrier without aid of thermal energy. The parameters p and q allow great variations in barrier shape. Parameter q mainly determines the shape close to the barrier maximum and p determines the shape at longer distances from the maximum position. Inserting this into (9) leads to

$$\tau^* = \tau_0 G\left[1 - \left(\frac{kT}{\Delta f_0 G b^3} ln\left(\frac{\dot{\bar{\varepsilon}}_{ref}}{\dot{\bar{\varepsilon}}^p}\right)\right)^{1/q}\right]^{1/p} \tag{13}$$

It can be noted that there is a lower limit on the plastic strain rate under which the contribution should be set to zero.

Cross-slip of dislocations is another important thermally activatable process [7]. The activation energy for cross-slip of dissociated dislocations has been suggested by Escaig [8] to be

$$\Delta G_{cs} = G_0\left(1 - 1.2\frac{\tau_{cs} b}{\gamma} - 1.5\frac{\tau_{ps} b}{\gamma}\right) \tag{14a}$$

where τ_{ps} is the applied shear stress on the primary slip plane, τ_{cs} is the applied shear stress on the cross-slip plane, and γ is the stacking fault energy. The constriction energy, G_0, is given by

$$G_0 = \frac{G b^2 d_p}{37}\sqrt{\ln\left(\frac{2\sqrt{3} d_p}{b}\right)} \tag{14b}$$

where d_p is the equilibrium splitting distance between the dislocation partials given by

$$d_p = A\frac{G b^2}{\gamma} \tag{14c}$$

where A is ~0.019 and ~0.048 for screw and edge dislocations, respectively. The rate for cross-slip is then given by setting ΔG *to* ΔG_{cs} in (9).

The variants of τ^* shown above can be added into σ_0 in (4) when required.

Solution and Precipitation Hardening

The strengthening contribution of an obstacle will be determined by the distance between the obstacles along the dislocation, L_{obst}, and the strength of the obstacle, F_{obst}. Bypassing of the obstacle will occur if the force exerted by the dislocation, $\tau b L_{obst}$, equals the strength of the obstacle

$$\tau b L_{obst} = F_{obst} = 2T\cos\left(\frac{\beta}{2}\right) \qquad (15)$$

The obstacle strength can also be expressed with the angle, β, of the dislocation segments on both sides of the obstacle at the bypassing situation, Fig. 1.

$F = \tau b$ is the force on the dislocation due to the applied stress and is always perpendicular to the dislocation line, R is the radius of the dislocation segment, T is the line tension, F_{obst} is the opposing force due to the obstacle, and L_{obst} is the distance between the obstacles on the dislocation. β is the angle between two dislocation segments. The line tension is approximately

$$T \approx \frac{Gb^2}{2} \qquad (16)$$

If the obstacles are impenetrable for the dislocation, then the obstacle is bypassed by bowing around it leaving a dislocation loop behind. This is commonly referred to as the Orowan mechanism and the dislocation as completely flexible. In this case, the distance between the dislocations along the dislocation is the average distance between the obstacles in the slip plane. If the obstacles are very weak, then the dislocation moves as an almost straight line, stiff dislocation, through the lattice and the number of obstacles encountered along the dislocation line is much smaller than for the case of more flexible dislocations. For all cases in between the completely stiff and completely flexible, we denote the dislocation as partially flexible. For weak obstacles, Friedel [9] has proposed that the distance between the obstacles is given by assuming that the probability for encountering just one new obstacle when breaking away from another is exactly 1. This leads to

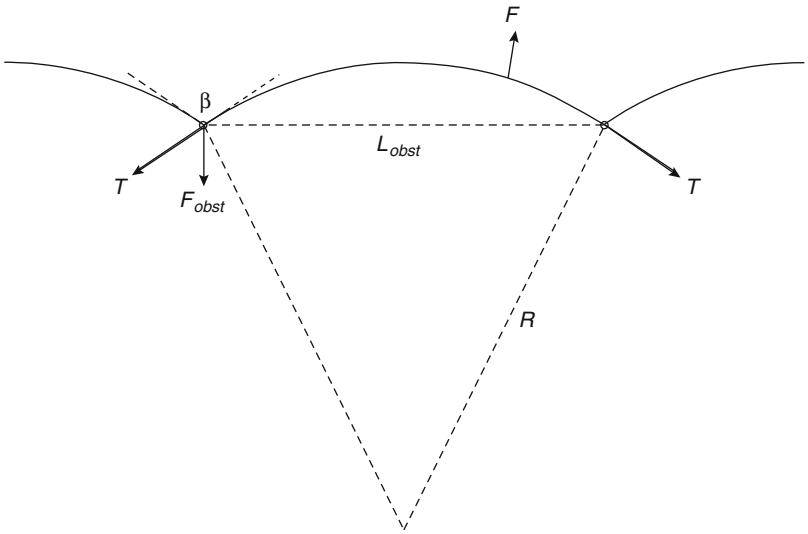

Constitutive Models, Physically Based Models for Plasticity, Fig. 1 Forces on a dislocation segment blocked by two obstacles

$$L_{obst} = \frac{L}{\sqrt{cos\left(\frac{\beta}{2}\right)}} \tag{17}$$

where L is the average distance between the obstacles in the slip plane as given by (18c) below. Brown and Ham (Chapter 2 in [1]) have summarized various computer simulations in the following equations

$$\tau_{obst} = \frac{Gb}{L}\left[cos\left(\frac{\beta}{2}\right)\right]^{3/2} \text{ for } 100^\circ \le \beta \le \pi \tag{18a}$$

$$\tau_{obst} = \frac{0.8Gb}{L} cos\left(\frac{\beta}{2}\right) \text{for } 0^o \le \beta \le \ 100^o \tag{18b}$$

$$L = \left[\sqrt{\frac{\pi}{f_{obst}}} - 2\right]\sqrt{\frac{2}{3}} r_{obst} \tag{18c}$$

where τ_{obst} is the shear stress required to overcome the obstacle, r_{obst} is the mean radius, and f_{obst} is the volume fraction of the obstacles. If we have obstacles of different strengths, then the situation is more complex. An equation of the form

$$\tau_{obst}^m = \sum\nolimits_{i=1}^{n} \tau_i^m \tag{19a}$$

is often used. τ_i denotes τ_{obst} for obstacle i according to (18a, c). A simple mixture law has also been proposed

$$\tau_{obst} f_{obst} = \sum\nolimits_{i=1}^{n} f_i \tau_i \tag{19b}$$

where f_i is the volume fraction of obstacle i and f_{obst} is the total volume fraction of obstacles ($=\Sigma f_i$). The most common values used for m are 1 or 2. Brown and Ham (Chapter 2 in [1]) also discussed these types of combinations with regard to computer simulations for two sets of point obstacles with different strengths made by Foreman and Makin [10]. In Fig. 2, the data of Forman and Makin have been reproduced and compared to (19a) with m = 1 and m = 2 and to (19b). The total number of obstacles, n_{obst}, is constant and the relative concentration c relates the individual numbers of obstacles so that $n_{obst} = (1–c)*n_{obst1} + c*n_{obst2}$. Using m = 1 is obviously wrong except for the case with a large amount of weak obstacles combined with a few strong obstacles which gives some justification to the often applied summation of hardening contributions from solute atoms and precipitates, where the former are very weak obstacles with β not far from 180 °. Using m equal to 2 gives a considerably better fit, although not perfect.

The average distance between obstacles, L, is

$$L \approx \frac{b}{\sqrt{x}} \tag{20}$$

for elements in solid solution where x is the atom fraction of the element. The interaction force between a substitutional solute atom (in the slip plane) and a screw dislocation is given by

$$F_i^S = \varepsilon_{sol} \frac{Gb^2 R_{atom}^3}{3\pi} \frac{1}{r^3} \tag{21a}$$

with the misfit parameters

$$\varepsilon_b = \frac{1}{b}\frac{db}{dx} \tag{21b}$$

$$\varepsilon_G = \frac{1}{G}\frac{dG}{dx} \tag{21c}$$

$$\varepsilon_{sol} = \left[(\alpha\varepsilon_b)^n + (\varepsilon'_G)^n\right]^{(1/n)} \tag{21d}$$

$$\varepsilon'_G = \frac{\varepsilon_G}{1 + 0.5|\varepsilon_G|} \tag{21e}$$

n equals 1 if the contributions from size and modulus misfit are summed and n equals 2 if a geometrical sum is used. R_{atom} is the atomic radius for the main specie. α is a parameter in the range of around 3–16 [5, 11]. For Si in copper a value of $\varepsilon_{sol} = 0.8$ has been given.

For an interstitial solute in ferrite, the interaction force is

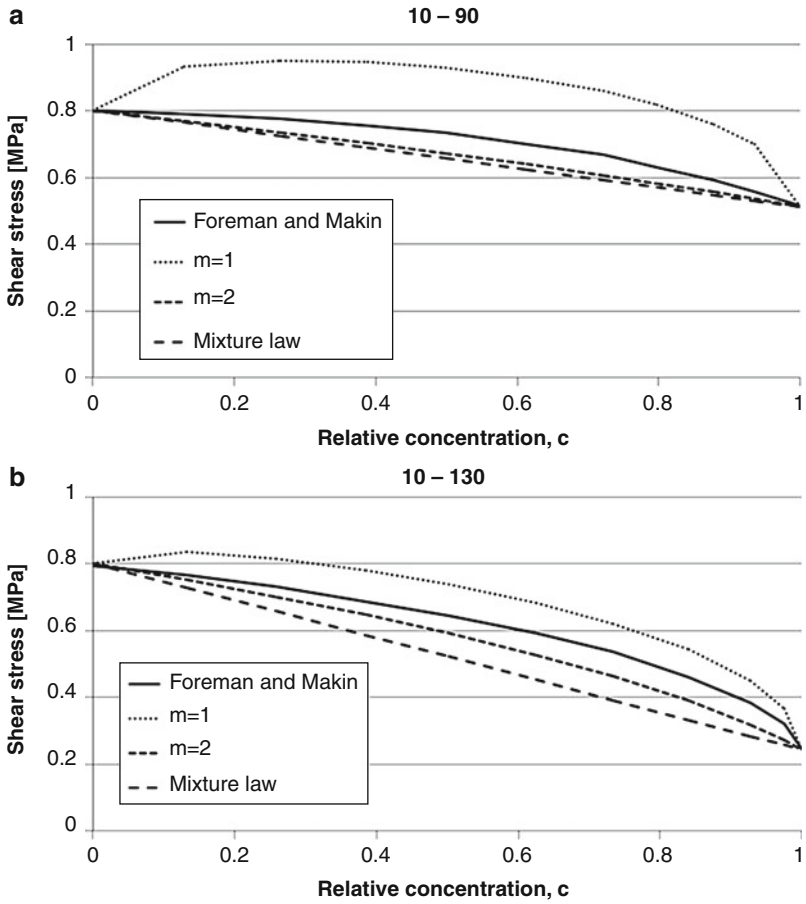

Constitutive Models, Physically Based Models for Plasticity, Fig. 2 Computer calculations by Forman and Makin [10] for obstacles with β equal to 10 ° and 90 ° (*left diagram*) and with β 10 ° and 130 ° (*right diagram*), *solid curves*. Equation (19a) with m equal to 1 and 2, *dotted curves*, and (19b), dashed curve, have been calculated using (18a, c) for the individual obstacles

$$F_i^S = \Delta\varepsilon_{sol} \frac{4\sqrt{2}GbR_{atom}^3}{9} \frac{1}{r^2} \tag{22}$$

where $\Delta\varepsilon_{sol}$ is the difference between the maximum and minimum strain of the bcc lattice due to the interstitial (equals 0.41 for carbon in ferrite).

If we use (15–16, 20) and assume that Friedel statistics, (17), (weak obstacles) are valid, then the shear stress, τ_{sol}, needed to overcome these obstacles is

$$\tau_{sol} = \frac{F_i^{S\,3/2}}{b^3} \sqrt{\frac{x}{G}} \tag{23}$$

Using the elastic interaction force up to a cutoff value of r_c combined with (8) and (9), we obtain

$$\frac{\tau_{sol}}{G\sqrt{x}} = \left[\frac{A_{sub}^{2/3}}{b^{4/3} r_c^2} + \frac{kT}{6A_{sub}^{1/3} b^{4/3} G} \ln\left(\frac{\dot{\varepsilon}^p}{\dot{\varepsilon}^p}\right) \right]^{9/4}$$
$$\text{with } A_{sub} = \varepsilon_{sol} \frac{b^2 R_{atom}^3}{3\pi} \tag{24a}$$

for substitutional species and

$$\frac{\tau_{sol}}{G\sqrt{x}} = \left[\frac{A_{int}^{1/2}}{br_c} + \frac{kT}{4A_{int}^{1/2} bG} ln\left(\frac{\dot{\varepsilon}^p}{\dot{\varepsilon}_0^p}\right) \right]^{9/3} \text{ with } A_{int}$$
$$= \Delta\varepsilon_{sol} \frac{4\sqrt{2}bR_{atom}^3}{9} \tag{24b}$$

for interstitials [(24b) was given in a simplified form in (11) above]. In Fig. 3, we have

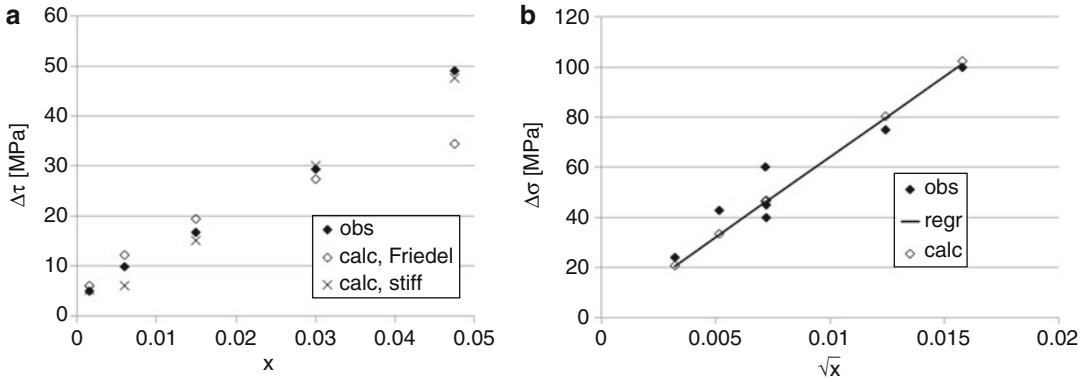

Constitutive Models, Physically Based Models for Plasticity, Fig. 3 *Left diagram*: increase in critical resolved shear stress, Δτ, due to Si in copper, data of Fleischer. *Right diagram*: yield stress, Δσ, increase due to carbon in ferrite, data of Wert. Comparison to calculated values using (24a), left diagram and (24b), right diagram (Friedel) and (26) (stiff)

applied (24b) to data for C in ferrite [12] and (24a) for Si in copper [5] using r_c = b/2 and fudge factors of 1.25 for A_{int} and 0.5 for A_{sub}. The parameter $\dot{\varepsilon}_0^p$ has been put to 1,000 s^{-1}.

The proportionality of τ_{sol} with $x^{0.5}$ in the relations above comes from the assumption of partially flexible dislocations. As the strength of substitutional species is low, the dislocation can be approximated as completely stiff (β=π), which leads to τ proportional to x. Using the theory of Labusch and Nabarro (ref. in [11]) $\tau_{o\beta\sigma\tau}$ is then predicted to be proportional to $x^{2/3}$. The maximum at room temperature of the interaction force given in (21a) is

$$F_{max} = \varepsilon_{sol}\frac{Gb^2}{120} \tag{25}$$

This corresponds to a breaking angle of 0.996*π for Si in copper. If we approximate this with a stiff dislocation, we obtain

$$\frac{\tau}{Gx} = \left[\frac{A_{sub}^{2/3}}{b^{4/3}r_c^2} + \frac{kT}{6A_{sub}^{1/3}b^{4/3}G}ln\left(\frac{\dot{\varepsilon}^p}{\dot{\varepsilon}_0^p}\right)\right]^{3/2} \text{ with } A_{sub} = \varepsilon_{sol}\frac{b^2R_{atom}^3}{3\pi} \tag{26}$$

The result using (26) for Si in copper is shown in Fig. 3 above. The used A_{sub} factor was 1.2 in this case.

According to Labusch and Nabarro (ref. in [11]), we obtain

$$\tau_{sol} = \frac{1}{2}\left[\frac{2r_0F_{\max}^4x^2}{Gb^9}\right]^{1/3} \tag{27}$$

where r_0 is the range of the maximum interaction force.

Precipitates can be bypassed by dislocations in three different ways, by bowing around the particle leaving a dislocation loop around it (often referred to as the Orowan mechanism), by cutting (shearing) through the particle, and finally by combined cross-slip and climb over the particle (see, e.g., Lagneborg [13]). When particles precipitate in solid state, they usually get a close relation between their lattice and the matrix phase. Depending on the crystal structure of the matrix and the particle, they become coherent (all lattice directions and planes coincide) or semicoherent. If the atomic spacings differ between the particle and the matrix phase, elastic coherency strains are also induced and increase as the particle grows. When these strains get too large, the particle will lose coherency with the matrix as it is more favorable to introduce phase boundary dislocations instead. This will occur at $r_{prec} \geq 2b/(3\varepsilon_{mf})$ for a spherical particle with misfit strain ε_{mf}. When cutting of the particles is possible, the contribution to the flow stress, first term in (4), will be given by one or several mechanisms.

- Increase in surface area, chemical strengthening, leading to

$$\tau_{prec}^{surf} = \frac{2}{L}\sqrt{\frac{2\gamma_{pb}^3 f_{prec}}{Gbr_{prec}}} \tag{28a}$$

where γ_{pb} is the phase boundary energy [chapter 2 in [1, 14]]. The equation predicts that the strength is reduced for larger particles, which is not observed. The mechanism is thus usually ignored [14].

- For a difference in stacking fault energy, $\Delta\gamma_{sf}$ the hardening contribution is proportional to $\Delta\gamma_{sf}$ and $\sqrt{r_{prec}f_{prec}}$ [12]
- Difference in elastic modulus, ΔG [15]

$$\tau_{prec}^{mod} = 0.16\sqrt{\frac{(\Delta G)^3 r_{prec}f_{prec}}{Gb\left(ln\left[\frac{2r_{prec}}{b\sqrt{f_{prec}}}\right]\right)^3}} \tag{28b}$$

- Coherency strains: In this case, all particles, below and above the slip plane, contribute to the strength and the problem is how to sum them. Brown and Ham (chapter 2 in [1]) used the summation according to (19a) above with m = 2. This gives

$$\tau_{prec}^{coh} = 4.1G\sqrt{\frac{|\varepsilon_{mf}|^3 f_{prec}r_{prec}}{b}} \tag{28c}$$

According to Martin [14], the constant 4.1 should be replaced by a number between 5 and 7.

For larger particles, but not large enough to cause transition to the Orowan mechanism, that is, for $b/(4|\varepsilon_{mf}|) < r_{prec} < 2b/(3|\varepsilon_{mf}|)$, the breaking angle is 0 but the dislocation leaves no loop around the particle. In this case, Brown and Ham (Chapter 2 in [1]) proposed

$$\tau_{prec}^{coh} \cong 0.7G\sqrt{f_{prec}}\left(\frac{|\varepsilon_{mf}|b^3}{r_{prec}^3}\right)^{1/4} \tag{28d}$$

neglecting the influence of particles giving larger breaking angles than 0.

- Creation of antiphase boundary, APB, with surface energy γ_{APB}:

When a dislocation cuts an ordered particle, the order is disturbed and an antiphase boundary is created. If the Friedel assumption is used, the strengthening is given by

$$\tau_{prec}^{APB} = \sqrt{\frac{8\gamma_{APB}^3 r_{prec}f_{prec}}{\pi Gb^4}} \tag{28e}$$

for a single dislocation. As a second dislocation on the same slip plane might restore the order, the dislocations are in many cases seen to move in pairs. For this case, the strengthening is given by

$$\tau_{prec}^{APB} = \frac{\gamma_{APB}}{2b}\left[\sqrt{\frac{8\gamma_{APB}r_{prec}f_{prec}}{\pi Gb^2}} - f_{prec}\right] \tag{28f}$$

according to Brown and Ham. Slightly different values of the constants have been given by other researchers [14].

The varying expressions for τ_{sol} and τ_{prec} are contributions to σ_0 in (4).

Dislocation Evolution

The evolution of dislocation density in (5) is elaborated further below. There are hardening and recovery mechanisms. Self-diffusion plays a role in the latter and is therefore also coupled to vacancy generation. Furthermore, recrystallization may enter and affect grain size as well as reduce the dislocation density.

Dislocation Generation

In (5), the variation of the mean free distance of slip, L, with strain controls the rate of generation. Bergström [3] showed that the empirical relation

$$L = L_1 + (L_0 - L_1)e^{-k\bar{\varepsilon}_p} \tag{29}$$

where the mean free distance starts at a value L_0 and asymptotically approaches a final value L_1, can give a good description for a lot of different

metals and alloys. For some materials, the final value seems to be reached at very small strains, giving rise to a parabolic stress-strain relation. This holds for low alloyed steel and copper, for example. As other dislocations impede the motion of slipping dislocations, it is reasonable to relate L to the distance between dislocations, or walls or arrays of dislocations. Thus

$$L = \frac{c_d}{\sqrt{\rho}} \tag{30}$$

For a Frank network, the proportionality constant, c_d, is close to 1. For more heterogeneous networks, the value is higher. Local rearrangement of the dislocations into cells and subgrains is facilitated by cross-slip and climb of the dislocations.

The presence of grain and phase boundaries also adds to the generation of dislocations. Ashby (Chapter 3 in ref. [1]) called this generation of geometrically necessary dislocations and also suggested values for geometrical slip distances. Thus

$$L_{gd} = c_g d \tag{31}$$

for grains with diameter d and for precipitates

$$L_{gp} = c_p \frac{r_{prec}}{f_{prec}} \tag{32}$$

For rigid, randomly distributed, spherical particles of radius r_{prec} and volume fraction f_{prec}, the proportionality constant, c_p, is 1. If the particles are not rigid, c_p should be replaced by $c_p(1–d\varepsilon_p/d\varepsilon_m)$ where $d\varepsilon_p$ is the strain increment in the particle and $d\varepsilon_m$ in the matrix. Equation 31 gives a dependence of the grain size which is almost identical to the commonly used Petch-Hall relationship where $k_y/d^{0.5}$ is added to the flow stress (k_y is an experimentally derived constant), if L_{gd} dominates L initially.

Bergström et al [16] have suggested that for dual phase steel with non-deforming martensite, the deformation is inhomogeneous in the ferrite phase and that the increase in the volume fraction that is deforming can be described by

$$f(\varepsilon_p) = f_0 + (f_1 - f_0)e^{-r\varepsilon_p} \tag{33}$$

where f_0 is the total volume fraction of ferrite and f_1 is the fraction that initially participates in the deformation. Assuming constant stress in the microstructure, the strain in the ferrite is given by $\varepsilon/f(\varepsilon)$ as it is assumed that the martensite does not deform.

Assuming that the different mechanisms give additive contributions to the increase in immobile dislocation density in (5) we can combine the different mean free distances for slip giving

$$\frac{d\rho}{d\varepsilon_p} = \frac{m}{b}\left(\frac{\sqrt{\rho}}{c_d} + \frac{1}{L_{gd}} + \frac{1}{L_{gp}}\right) \tag{34}$$

Dislocation Recovery/Annihilation

Rearrangement, remobilization, and annihilation of dislocations are mechanisms by which the dislocation density is reduced. Bergström [3] suggested that this could be described by

$$\frac{d\rho}{d\varepsilon_p} = -\Omega\rho \tag{35}$$

At higher temperatures, above ~0.5T_m (T_m is the melting temperature in Kelvin), climb of dislocations becomes an important mechanism for dislocation recovery. Assuming a Frank network, the rate is given by (ref. in [17])

$$\frac{d\rho}{dt} = -M_m\rho^2\left(1 - \frac{3f_{prec}}{4r_{prec}\sqrt{\rho}}\right) \tag{36}$$

where the rate parameter M_m is expressed as the dislocation mobility times the dislocation line tension (~0.5Gb^2) and is given by

$$M_m = \frac{M_0 x_v D_m b}{kT} Gb^2 \tag{37}$$

where M_0 is a constant. The self-diffusion coefficient is expressed as the vacancy concentration, x_v, times the migration coefficient, D_m, of vacancies. The influence of particles on the climb rate is inferred as the initial effect during and after deformation as the last term in (36).

Point Defects (Vacancies, Solute Atoms)

Plastic deformation in addition to generation of dislocations also generates point defects, vacancies. The equilibrium concentration of vacancies can be written as

$$x_v^{eq} = e^{-\frac{Q_v}{kT}} \tag{38}$$

where Q_v is the activation energy for formation of vacancies and has a value around half the activation energy for self-diffusion. According to Friedel [9], the generation is due to cutting of dislocations and should thus be proportional to the distance between dislocations. The vacancies generated will diffuse to sinks for vacancies, grain boundaries, free surfaces, and most importantly to dislocations. Assuming one-dimensional diffusion, this can be written as [17]

$$\frac{dx_v}{dt} = \frac{dx_v^{eq}}{dT}\frac{dT}{dt} + k_{v1} b \frac{d\varepsilon}{dt}\sqrt{\rho} - k_{v2} x_v D_{mv}(x_v - x_v^{eq})\sqrt{\rho} \tag{39}$$

where the first term is the change in equilibrium concentration due to temperature changes, the second is the generation due to cutting of dislocations, and the third the diffusion to sinks. kvi are model constants. Another model has been proposed by Millizer et al. [18] who assumed that nonconservative motion of jogs was responsible for vacancy generation giving

$$\frac{dx_v}{dt} = \frac{dx_v^{eq}}{dT}\frac{dT}{dt} + \kappa\frac{\sigma\Omega_0}{Q_{gv}}\frac{d\varepsilon}{dt} + \frac{c_j\Omega_0}{4b^3}\frac{d\varepsilon}{dt} - \frac{D_{mv}\rho}{\kappa^2}x_v - \frac{D_{mv}}{d^2}x_v \tag{40a}$$

where κ is a structural parameter describing the distribution of dislocations, Ω_0 is the atomic volume, and c_j is the concentration of thermal jogs

$$c_j = e^{-\frac{Gb^3}{4\pi(1-\upsilon)kT}} \tag{40b}$$

υ is Poisson's ratio. Although (39) and (40) are quite different, they give approximately the same results for the formation of vacancies. The computed vacancy formation in excess of the equilibrium value can be used to enhance the diffusion mediated by vacancies in (37). It can be noted that it is possible to account for diffusion along dislocations (pipe diffusion) as well as grain boundaries for some phenomena.

For metal alloys, we may also get drag of solute atoms impeding the movement of dislocations and grain/phase boundaries if diffusion rates are high enough. The drag force, F_{sd}, during climb of a dislocation over a distance, dy, is given by

$$F_{sd} = \frac{1}{b}\sum\nolimits_A \left[-\int_{-\infty}^{\infty} x_A \frac{dW_A}{dy} dy\right] \tag{41}$$

where W_A is the interaction energy between a solute atom and a dislocation and x_A is the corresponding atom fraction of specie A. The summation is done over all solute atoms giving drag.

A solution to Fick's second law around a moving dislocation has been given by Hirth and Lothe [19]

$$x_A = \frac{v x_A^0}{D} e^{\left(-\frac{W_A}{kT}-\frac{vy}{D}\right)} \int_{-\infty}^{y} e^{\left(\frac{W_A}{kT}+\frac{vy}{D_A}\right)} dy \tag{42}$$

where v is the climb rate in the y direction, D_A is the diffusion coefficient for the solute A, and ${x_A}^0$ is the mean concentration of A in the matrix. See Magnusson and Sandström [20] for an application showing the effect during creep in a 9 % Cr steel. The solution of (42) is not trivial and for practical reasons, a quasi-stationary solution can be used [21], giving a decrease of the mobility for climb. Then M_m in (36) is replaced by M_{msd} given by

$$M_{msd} = \frac{M_m}{1 + \sum_A \frac{D_s dx_A^0 \beta_A^2}{(kT)^2 D_A}} \tag{43}$$

The summation is done over the solute atoms, A, with diffusion coefficients D_A, mean concentration ${x_A}^0$, and interaction coefficients with the dislocation, β_A.

$$\beta_A = \frac{Gb_{edge}}{2\pi}\frac{(1+\nu)}{(1-\nu)}(\Omega_0^A - \Omega_0) \tag{44}$$

where b_{edge} is the edge component of Burgers vector and ${\Omega_0}^A$ is the atomic volume of the solute A.

Recrystallization

The kinetics of recrystallization is usually described using the JMAK-expression (Johnson-Mehl-Awrami-Kolmogorov) on the form (Sellars in [22])

$$X_{rec} = 1 - e^{-n\left(\frac{t}{t_{0.5}}\right)^k} \tag{45}$$

for the evolution of the fraction recrystallized, X_{rec}, with time t. The parameter n is usually close to 0.693. k is a parameter that varies with deformation conditions as well as the material. The time to 50 % recrystallization, $t_{0.5}$, is usually fitted by regression to relations of the form (Siwecki and Engberg in [22])

$$t_{0.5} = Ad^a\dot{\bar{\varepsilon}}_p^{-b}Z^{-c}e^{\frac{Q_{rec}}{kT}} \tag{46}$$

where A, a, b, c, and Q_{rec} are fitting parameters. Z is the Zener-Hollomon parameter. The use of equations like (45) and (46) is limited to the specific material under the specifically studied deformations/time/temperature sequences. This is a common empirical approach of curve fitting type. Humphreys [23] describes the physics of recrystallization as a process where new dislocation-free grains grow from small regions, recovered subgrains, or cells, which are already present in the deformed structure. The nucleation process as a selection process of successful embryos. The nucleation of recrystallization is considered as abnormal subgrain growth in an orientation gradient, which leads to the formation of small grains with a high angle boundary. These new grains then grow and consume the old grains, resulting in a new grain structure with low dislocation density and, as a result, the stored energy is lowered. The kinetics for recrystallization is well described using this theory for growth combined with nucleation site saturation (on old grain boundaries) and hard impingement of the growing grains. A simplified model has been shown to work quite well for CMn steel [17] and for Cr and austenitic stainless steel, Figs. 4 and 5, but the model is still fairly complex.

The model in [17] includes the dislocation density in the driving force for recrystallization. The dislocation density is reduced in the recrystallized fraction of the material, and thus, the model has two constituents, recrystallized and not recrystallized fractions. The flow stress for the recrystallized and not recrystallized regions can then be calculated and the flow stress of the material is given by a mixture law using an equation similar to (19). See [17] for details.

Phase Mixtures

The mixture laws given in (19) and (20) by themselves cannot be used for phase mixtures generally. Additional information is needed on how the strain is distributed between the phases. For lamellar structures, we can use the simple assumptions of equal strain or equal stress in the constituents if deforming parallel or perpendicular to the lamella, respectively. Equal stress is also a good approximation for many particle composites with a fraction of the softest constituent larger than 50 %. It has been proposed [24] that a mixture law given by assuming equal work in the constituents

$$\sigma_i d\varepsilon_i = \sigma_j d\varepsilon_j \tag{47a}$$

$$\sigma = \sum\nolimits_i f_i\sigma_i(\varepsilon_i) \tag{47b}$$

where i and j denote the different constituents is more general. This was shown [24] to work quite well for two iron-silver composites and for a Ti-Mn alloy with a duplex structure of α and β phase.

Final Remarks

The references [19] and [23] contain a substantial amount of useful information.

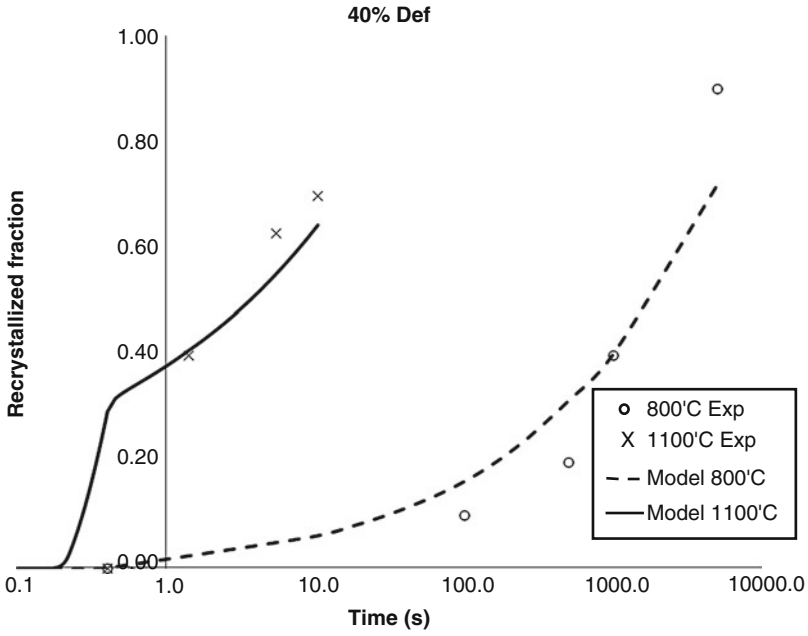

Constitutive Models, Physically Based Models for Plasticity, Fig. 4 Recrystallization after uniaxial compression of a 13 % Cr steel

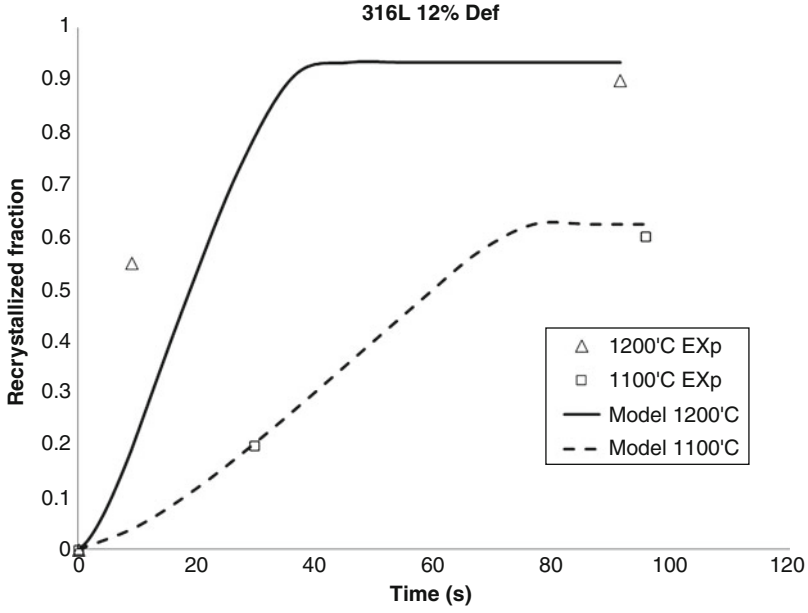

Constitutive Models, Physically Based Models for Plasticity, Fig. 5 Recrystallization after uniaxial compression of an austenitic stainless steel

The use of physically based plasticity models is expected to gain ground not only due to their relations to the physics of the deformation process but also due to their natural coupling to microstructure. It is obvious how they can be coupled with models for grain growth, precipitate growth, or dissolution, etc. There are issues like the problem of adding contributions to the flow stress from different obstacles that have still not been resolved and the development of the models and their use are expected to evolve in the future.

Cross-References

- ▶ Heat Treatment of Aluminum Alloys
- ▶ Repair Welding and Local Heat Treatment
- ▶ Shaped Metal Deposition Processes
- ▶ Welding and Heat Treatment of Alloys

References

1. Kelly A, Nicholson RB (1971) Strengthening methods in crystals. Applied Science, London
2. Ludwik P (1909) Elemente der technologischen Mekanik. Julius Springer, Berlin
3. Bergström Y (1983) The plastic deformation of metals – a dislocation model and its applicability. Reviews on powder metallurgy and physical ceramics, vol 2, no. 2 & 3, Elsevier, England
4. Engberg G, Carlsson B (2002) The strain-rate sensitivity and deformation hardening of ferritic steels. In: International conference new developments in sheet metal forming technology, Fellbach
5. Fleischer RL (1966) Substitutional solution hardening of copper. Acta Met 14:1867–1868
6. Kocks UF, Argon AS, Ashby MF (1975) Thermodynamics and kinetics of slip. Progress in materials science, vol 19. Pergamon press, Oxford
7. Gubicza J, Chinnh NQ, Lábár JL, Hegedüs Z, Langdon TG (2010) Principles of self-annealing in silver processed by equal-channel angular pressing: The significance of a very low stacking fault energy. Mater Sci Eng A 527:752–760
8. Escaig PB (1968) Cross slip of dislocations in f.c. c. structures. J Phys 29:225–239
9. Friedel J (1964) Dislocations. Pergamon press, Oxford
10. Foreman AJE, Makin MJ (1967) Can J Phys 45, Dislocation movement through random arrays of obstacles. pp. 551–557
11. Siurin H, Zander J, Sandström R (2006) Modelling solid solution hardening in stainless steels. Mat Sci Eng A 415:66–71
12. Wert CA (1950) Solid solubility of cementite in a-iron. TransAIME 188, pp. 1242–1244
13. Lagneborg R (1973) Bypassing of dislocation past particles by a climb mechanism. Scripta Met 7(6):605–613
14. Martin JW (1998) Precipitation hardening, 2nd edn. Butterworth Heinemann, Oxford
15. Melander A, Persson PA (1978) Strength of a precipitation hardened AlZnMg alloy. Acta Metall 26(2):267–278
16. Bergström Y, Granbom Y, Dirk S (2010) A dislocation based theory for the deformation hardening behavior of DP steels: Impact of martensite content and ferrite grain size. J Metallurgy, Volume 2010, Article ID 145431, 9 pages
17. Engberg G, Lissel L (2008) A physically based microstructure model for predicting the microstructural evolution of a C-Mn steel during and after hot deformation. Steel Res Int 79(7):47–58
18. Millizer M, Sun WP, Jonas JJ (1993) Effect of deformation-induced vacancies on recrystallization. Mat Sci Forum 113–115:163–168
19. Hirth JP, Lothe J (1982) Theory of dislocations, 2nd edn. Krieger, Malabar
20. Magnusson H, Sandström R (2007) Modelling of the influence of Laves phase on the creep properties in 9% Cr steels. In: Proceedings of the 8th international conference on creep and fatigue at elevated temperatures, 22–26 July 2007, San Antonio, Texas
21. Engberg G (1976) Recovery in a titanium stabilized 15% Cr – 15% Ni austenitic stainless steel. Trita-mac-00098, Materials Center, Royal Inst. of Technology, Stockholm, Sweden
22. Hutchinson B, Andersson M, Engberg G, Karlsson B, Siwecki T (1996) Thermo-mechanical processing in theory, modelling and practice [TMP]^2. In: Procedings of an International Conference 4–6 Sept 1996, Stockholm, Sweden. Published by the Swedish Society for Materials Technology.
23. Humphreys FJ, Hatherly M (2004) Recrystallization and related annealing phenomena, 2nd edn. Elsevier Science, Oxford
24. Bouaziz O, Buessler P (2004) Iso-work increment assumption for heterogeneous material behavior modeling. Adv Eng Mater 6(1–2):79–83

Contact Boundary Conditions

James R. Barber
Department of Mechanical Engineering,
University of Michigan, Ann Arbor, MI, USA

Overview

A simple idealization of a thermoelastic contact problem assumes that there is no resistance to heat flow in regions of mechanical contact and that there is no heat exchange in regions of separation. However, problems with these boundary conditions are not mathematically well posed and can exhibit nonexistence of solution. Asymptotic arguments show that for the contact of bodies with smoothly turning tangents, no solution exists when the heat flows out of the more distortive material. This difficulty is resolved if one interposes a thermal contact resistance, that is, a continuous monotonic function of contact

pressure or gap. A limiting form of this boundary condition (known as imperfect contact) can be defined which enables boundary value problems to be stated in linear form on unknown regions determined by inequalities.

Introduction

If two thermoelastic bodies at different temperatures are placed in contact, heat will flow between them through the contact area, and the resulting modification in the temperature field will generally cause thermoelastic distortion that affects the distribution of contact pressure and, in some cases, the extent of the contact area itself.

The thermal contact process itself is quite complex since surfaces are generally rough, causing actual contact to occur only at isolated points in the nominal contact area (see ▶ Thermal Contact Resistance), and also some heat can be exchanged between the bodies by radiation and convection in regions that are not in physical contact. However, for the purposes of thermoelastic analysis, it is conventional to idealize the boundary conditions.

Perfect Thermal Contact

The simplest approximation is to assume that the surfaces are smooth and that in regions of contact, the temperature is continuous across the interface, whereas in regions that are not in contact (the separation region), there is no exchange of heat between the surfaces. Mathematically, it is convenient to identify the region of the interface that is in contact as $\mathcal{A}$ in which case these conditions can be stated in the form

$$T_1(x,y) = T_2(x,y) \qquad (x,y) \in \mathcal{A} \tag{1}$$

$$q_1(x,y) = q_2(x,y) = 0 \qquad (x,y) \notin \mathcal{A} \tag{2}$$

where

$$q_i = -K_i \frac{\partial T_1}{\partial n} \tag{3}$$

is the heat flux across the interface, K is thermal conductivity, n is a local normal to the interface, and $i = 1, 2$ refers to the two contacting bodies, respectively. We shall refer to this set of boundary conditions as "perfect thermal contact." They have been used to generalize the classical Hertzian contact problem to include thermoelastic effects [1–3].

Existence and Uniqueness

Unfortunately, the boundary conditions (1, 2) are not sufficient to guarantee existence and uniqueness of a steady-state solution in thermoelastic contact (see ▶ Existence and Uniqueness for Thermoelastic Contact). The reason is that the underlying mechanical contact problem is nonlinear through the unilateral inequalities defining contact. Briefly, it is possible to push against a surface but not to pull on it, at least at conventional engineering length scales. (When we consider contact at the nanoscale, van der Waal's adhesive forces between the bodies become significant and must be taken into account, but this does not substantially alter the conclusions reached in this entry.) This is most clearly expressed by defining the normal contact pressure $p(x,y)$ and the gap $g(x,y)$ between the surfaces. We can then state the mechanical contact conditions in the dual form

$$g(x,y) = 0 \qquad (x,y) \in \mathcal{A} \tag{4}$$

$$p(x,y) > 0 \qquad (x,y) \in \mathcal{A} \tag{5}$$

$$p(x,y) = 0 \qquad (x,y) \notin \mathcal{A} \tag{6}$$

$$g(x,y) > 0 \qquad (x,y) \notin \mathcal{A} \tag{7}$$

Here, the inequalities (5, 7) serve to determine the extent of the contact area $\mathcal{A}$, and in the absence of thermoelastic effects and friction, it can be shown that the resulting solution is unique. However, the contact area also appears in the definition of the heat conduction problem and hence of the thermoelastic problem, so the two problems are coupled and must be solved together.

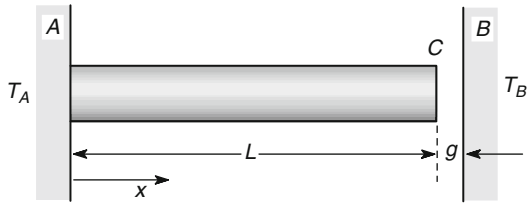

Contact Boundary Conditions, Fig. 1 A one-dimensional rod model

Dundurs and Comninou [4] showed in a simple one-dimensional example that the steady-state solution of the resulting thermoelastic contact problem may be unique, nonunique, or even nonexistent, depending on the parameters in the problem. For example, Fig. 1 shows a thermoelastic rod of length L, built in to a rigid wall at A and separated from a second rigid wall B by a small gap g. Suppose that the gap is equal to g_0, when the temperature of the rod $T = 0$. If there is no heat flow across the gap, the rod will adopt the temperature, T_A, of wall A, and elementary calculations show that the gap is reduced to $g = g_0 - \alpha L T_A$. The gap cannot be negative, so the configuration of Fig. 1 is possible only for $\alpha L T_A < g_0$.

For higher values of T_A, we anticipate contact between the rod and the wall at B and, if there is perfect thermal contact, there will be heat flow along the rod, and the steady-state temperature will vary linearly from T_A to T_B. Elementary calculations then show that the contact pressure p is given by

$$\frac{pL}{E} = \frac{\alpha L(T_A + T_B)}{2} - g_0 \tag{8}$$

This state is possible only if $p > 0$, so the system is governed by the two inequalities

$$\begin{array}{lll} \alpha L T_A & < g_0 & \text{(separation)} \\ \alpha L(T_A + T_B) & > 2g_0 & \text{(contact)} \end{array} \tag{9}$$

If $T_B > T_A$, there is a range in which *both* inequalities are satisfied, and the steady-state solution is nonunique. If $T_B < T_A$, there is a range in which *neither* inequality is satisfied and no steady-state solution exists [5].

Pressure-Dependent Contact Resistance

This mathematical difficulty can be resolved if instead we recognize the inevitable presence of a thermal contact resistance at the interface whose value depends on the contact pressure p or the gap g. Suppose that the free end of the rod in Fig. 1 is at temperature T_C in the steady state. If the thermal contact resistance is R, the steady-state heat flux q must satisfy the equations

$$q = \frac{T_C - T_B}{R}; \quad q = \frac{T_A - T_C}{KL} \tag{10}$$

and we can eliminate q to obtain

$$T_C = \frac{KRT_A + LT_B}{KR + L} \tag{11}$$

The unrestrained thermal expansion of the rod is $\alpha L(T_A + T_C)/2$ and elementary calculations then show that the gap g is defined by the equation

$$f(g) \equiv \frac{L}{KR(g) + L} = \frac{g - (g_0 - \alpha L T_A)}{\alpha L(T_A - T_B)/2} \tag{12}$$

This condition can be generalized to both contact and separation régimes by defining a generalized gap function $\tilde{g}$ through

$$\tilde{g} = g \quad ; \quad g > 0 \tag{13}$$

$$= -\frac{pL}{E} \quad ; \quad p > 0 \tag{14}$$

Physical considerations suggest that the contact resistance, $R(\tilde{g})$, should be a monotonically increasing function of $\tilde{g}$, tending to a small positive value as $\tilde{g} \to -\infty$ (very large contact pressure) and to infinity as $\tilde{g} \to \infty$ (very large gap). The corresponding function f must therefore have the general form shown in Fig. 2, constrained between the limits $0 < f < 1$.

The solution of equation (12) is defined by the intersection of the function $f(\tilde{g})$ and a straight line of slope $2/\alpha L(T_A - T_B)$ representing the right-hand side of the equation. Clearly there must be at least one intersection for all such

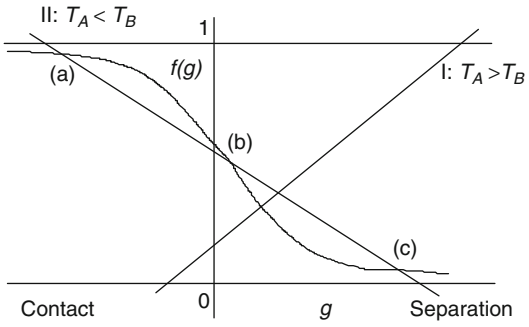

Contact Boundary Conditions, Fig. 2 Graphical solution of equation (12)

straight lines, so the problem of existence of solution is resolved. If the contact resistance and, hence, $f(\tilde{g})$ is monotonic, only one intersection can occur if the slope is positive (i.e., $T_A > T_B$). This is illustrated by line I in Fig. 2. However, multiple solutions can occur for sufficiently large negative slopes ($T_A < T_B$) as represented by line II in Fig. 2.

The contact resistance boundary condition can be generalized to two- and three-dimensional problems by defining a resistance such that

$$q(x,y) = \frac{T_1(x,y) - T_2(x,y)}{R(p,g)} \tag{15}$$

A more general discussion of existence and uniqueness with this boundary condition is given by Duvaut [6], who concludes that, as in the rod model, it is sufficient to guarantee existence, but the possibility of nonuniqueness remains, and this is believed to be a real physical effect. In effect, the steady state of the system depends on the history of loading and heating. For example, if the thermoelastic rod exists in a state involving separation and if the rod is now heated externally until it has expanded sufficiently to make contact with the wall, the temperature of the wall may now be sufficient to supply enough heat to sustain it in this new configuration.

We see therefore that the introduction of a pressure-dependent thermal contact resistance is sufficient to ensure that the steady-state thermoelastic contact problem is well posed, but at the price of making the underlying boundary value problem strongly nonlinear. By contrast, with the perfect thermal contact boundary conditions (1, 2), the nonlinearity appears only in the definition of the contact area through the inequalities (5, 7), and this can often be finessed from the problem by treating a parameter (such as the radius of $\mathcal{A}$ in an axisymmetric problem) as an independent variable.

This desirable simplification can be recovered in the limiting case where the contact pressure needed to establish almost perfect contact (negligible contact resistance) is sufficiently small. This is best understood by referring to the rod model in the case where both the separation and the contact solutions fail the inequality conditions. In this case, the introduction of a contact resistance allows the system to adopt a state where the rod expands until it is near enough to the other wall to allow enough conductance into the cold wall to prevent further expansion. This state has been characterized as "imperfect thermal contact," and in the limit, it satisfies the linear conditions

$$g(x,y) = 0 \tag{16}$$

$$p(x,y) = 0 \tag{17}$$

In effect, the thermal resistance R now becomes the dependent variable, but it must be positive from thermodynamic considerations, and hence the solution must also satisfy the inequality condition

$$\frac{T_1(x,y) - T_2(x,y)}{q(x,y)} > 0 \tag{18}$$

Boundary Value Problems

In two- and three-dimensional contact problems, it is usually found that there exists a steady-state solution satisfying the perfect thermal contact boundary conditions (1, 2) in cases where the heat flows into the body with the greater *thermal distortivity* defined as

$$\delta = \frac{\alpha(1+\nu)}{K} \tag{19}$$

where α is the coefficient of thermal expansion and ν is Poisson's ratio. For the opposite direction of heat flow, such a solution may still exist if the contact is "complete" meaning that it is determined by the shape of the contacting bodies, as in the case of the indentation of an elastic body by a rigid flat punch. In fact, the earliest indication of the mathematical difficulties described in this entry were associated with an attempt to explain the phenomenon of thermal rectification by the development of a closed region of separation completely contained within a region of perfect contact [7]. It was shown in [1] that such a state cannot occur for either direction of heat flow.

If we then consider the case of axisymmetric Hertzian contact [2], the solution involving a circular contact area satisfies the inequality conditions if and only if the heat flows into the body with the greater thermal distortivity. For the opposite case, there always exists a region near the edge of the contact circle in which the contact pressure is predicted to be negative, thus violating the inequality (5).

This situation was elucidated by Comninou and Dundurs [8] by considering the asymptotic stress and temperature fields at the transition point between perfect contact and separation, using a technique pioneered by Williams [9]. The field sufficiently near to this transition appears two-dimensional under a sufficiently large magnification and thus permits an eigenfunction expansion in terms of the eigensolution of the corresponding homogeneous problem. Comninou and Dundurs were able to demonstrate that the sign of the scalar multiplier on the dominant term in this expansion could be chosen to satisfy both the inequalities (5, 7) in the case where the local heat flow is directed into the more distortive material, but that either sign would lead to a violation of one of the two inequalities in the opposite case. Thus, this transition is impossible for this direction of heat flow.

If we also allow the possibility of regions of imperfect contact as defined by equations (16, 17) and the inequality (18), we find that an acceptable steady-state solution exists in such cases, but that there is a region of imperfect contact between regions of perfect contact and regions of separation. A formal statement of these modified boundary conditions is as follows:

Perfect Contact

$$g(x,y) = 0; \quad T_1(x,y) = T_2(x,y); \quad p(x,y) > 0$$

Imperfect Contact

$$g(x,y) = 0; \quad p(x,y) = 0; \quad \frac{T_1(x,y) - T_2(x,y)}{q(x,y)} > 0$$

Separation

$$p(x,y) = 0; \quad q(x,y) = 0; \quad g(x,y) > 0$$

Several problems have been solved using this idealization, including the axisymmetric and plane Hertzian contact problems [10, 11] and the indentation of a thermoelastic half-space by a cooled rigid punch [12]. The latter problem is of course complete, as defined above, so there exist a range of thermal conditions under which the perfect contact solution satisfies the inequality conditions. However, if the punch is cooled to a sufficiently low temperature, this solution predicts the development of a region of negative (i.e., tensile) contact pressure near the axis of symmetry. In nonthermoelastic contact problems, this would be an indication of the development of a region of separation, but we have already explained above that such a contained region cannot exist in the thermoelastic case. Thus, we must conclude that there exists a central region of imperfect contact, and the solution using this assumption does indeed satisfy all the conditions of the problem.

References

1. Barber JR (1971) The effect of thermal distortion on constriction resistance. Int J Heat Mass Trans 14:751–766
2. Barber JR (1973) Indentation of the semi-infinite elastic solid by a hot sphere. Int J Mech Sci 15:813–819

3. Jang YH, Cho H, Barber JR (2009) The thermoelastic Hertzian contact problem. Int J Solids Struct 46:4073–4078
4. Dundurs J, Comninou M (1976) On the boundary conditions in contact problems with heat conduction. In: McNitt RP (ed) Developments in theoretical and applied mechanics, vol 8. Virginia Polytechnic Institute and State University, Blacksburg, VA, pp 3–11
5. Barber JR, Dundurs J, Comninou M (1980) Stability considerations in thermoelastic contact. ASME J Appl Mech 47:871–874
6. Duvaut G (1979) Free boundary problem connected with thermoelasticity and unilateral contact. Free boundary problems, 11, Pavia.
7. Lewis DV, Perkins HC (1968) Heat transfer at the interface of stainless steel and aluminium – the influence of surface conditions on the directional effect. Int J Heat Mass Trans 11:1371–1383
8. Comninou M, Dundurs J (1979) On the Barber boundary conditions for thermoelastic contact. ASME J Appl Mech 46:849–853
9. Williams ML (1952) Stress singularities from various boundary conditions in angular corners of plates in extension. ASME J Appl Mech 19:526–528
10. Barber JR (1978) Contact problems involving a cooled punch. J Elas 8:409–423
11. Comninou M, Dundurs J, Barber JR (1981) Planar Hertz contact with heat conduction. ASME J Appl Mech 48:549–554
12. Barber JR (1982) Indentation of an elastic half space by a cooled flat punch. Q J Mech Appl Math 35:141–154

Contact Conductance Per Unit Area

▶ Thermal Contact Conductance of Rough Surfaces

Contact Fourier Problem

▶ Heat Transfer During Impact

Contact Resistance

▶ Thermomechanical Growth Instability in Solidification

Contact Stresses in an Infinite Plate with a Rigid Circular Inclusion

Ching-Kong Chao
Department of Mechanical Engineering, National Taiwan University of Science and Technology, Taipei, Taiwan, Republic of China

Overview

A class of the problem involving inclusions or bodies inserted into a hole in an elastic medium has attracted much attention in engineering community. The problem will become more complicated when separation occurs between an inclusion or insert and the surrounding medium caused by an applied loading or a nonuniform expansion of the inclusion. Unlike the corresponding problem with bonded interface between dissimilar media, there is no exact solution available for the current problem involving incomplete contact. In fact, a singular integrodifferential equation is derived to account for the incomplete contact problem that has been discussed by Muskhelishvili [1] and England [2]. A similar equation with a Prandtl type of singular integrodifferential equation has also been derived by Stippes et al. [3] and Wilson [4] in the case of separation of a circular elastic insert from the matrix. For solving the above equation, it requires some approximate methods to evaluate the contact angle and the contact stresses between an infinite plate and a smooth elastic insert. In this entry, we restrict our attention to the determination of the contact stress and the contact angle. The effect of the applied temperature gradient and a uniform temperature change on the contact stress as well as the contact angle are discussed in details and displayed in graphic form.

Problem Statement

Consider the two-dimensional problem in which an infinite plate containing a rigid circular

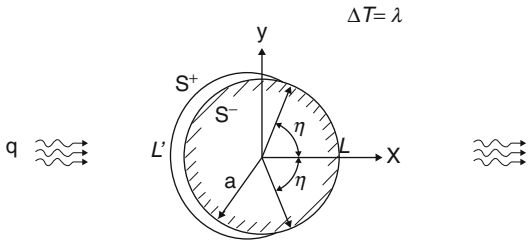

Contact Stresses in an Infinite Plate with a Rigid Circular Inclusion, Fig. 1 Contact conditions between a rigid circular inclusion and the surrounding matrix subject to a temperature gradient applied at infinity and a uniform temperature change

inclusion of radius a is subjected to a uniform temperature change as well as a remote uniform heat flux with the strength q approached from the negative x-axis (see Fig. 1). This problem is conveniently formulated in terms of the complex potentials as

$$\begin{aligned}
&\sigma_{rr}+\sigma_{\theta\theta}=2\left[\phi'(z)+\overline{\phi'(z)}\right]\\
&\sigma_{rr}+i\sigma_{r\theta}=\phi'(z)+\overline{\phi'(z)}-z\overline{\phi''(z)}-\frac{\bar{z}}{z}\overline{\psi(z)}\\
&2\mu(u_r+iu_\theta)=e^{-i\theta}\left[\kappa\phi(z)-z\overline{\phi'(z)}-\overline{\psi(z)}+2\mu\beta\int g'(z)dz\right]
\end{aligned} \tag{1}$$

where σ_{rr}, $\sigma_{r\theta}$, $\sigma_{\tau\theta}$, u_τ, u_θ are the stresses and the displacements, respectively, in polar coordinates which can be expressed in terms of two stress functions $\phi(z)$, $\psi(z)$ and a temperature function $g'(z)$. The shear modulus is denoted by μ and $\kappa=(3-\upsilon)/(1+\upsilon)$, $\beta=\alpha$ for plane stress and $\kappa=3-4\upsilon, \beta=(1+\upsilon)\alpha$ for plane strain with υ being Poisson's ratio and α the thermal expansion coefficient. Primes denotes differentiation with respect to z, and a superimposed bar denotes the complex conjugate. For this problem involving a rigid inclusion inserted into a hole in an elastic medium under thermal loads, one might expect separation to occur along the arc L', namely, $\eta\le\theta\le 2\pi-\eta$, where η is the unknown contact angle. Since the insert is assumed to be perfectly smooth, no shear stresses act on the contact arc L defined by $|\theta|\le\eta$, and then the boundary conditions for the infinite medium $|z|\ge a$ are

$$\sigma_{rr}+i\sigma_{r\theta}=0\ (\sigma\in L') \tag{2}$$

$$\sigma_{r\theta}=0\ (\sigma\in L) \tag{3}$$

$$u_r=f(\sigma)\ (\sigma\in L) \tag{4}$$

where $f(\sigma)$ is real and has the following symmetric property:

$$f(\sigma)=f(\bar{\sigma}) \tag{5}$$

This symmetry implies that there is a zero resultant force over the hole $|z|=a$ Let us suppose the region occupied by the elastic medium, the exterior of the circle $|z|=a$, is denoted by S^+ and its complement, the interior of the circle $|z|=a$, by S^-. Based on the method of analytical continuation, the traction-free boundary conditions, (2), allow us to represent the remaining boundary conditions, (3) and (4), in terms of a single stress function r and a temperature function $g'(z)$ as

$$\mathrm{Im}\left[\phi'^{+}(\sigma)-\phi'^{-}(\sigma)\right]=0\quad\sigma\in L \tag{6}$$

$$\begin{aligned}
&\mathrm{Re}\left[e^{-i\theta}\left\{\kappa\phi^{+}(\sigma)+\phi^{-}(\sigma)+2\mu\beta g^{+}(\sigma)\right\}\right]\\
&=2\mu f(\sigma)\quad\sigma\in L
\end{aligned} \tag{7}$$

where the superscript + (or −) denotes limiting values of $\phi'(z)$ for an approach to a point σ on L from outside (or inside) the hole boundary.

In the present study, we assume that the rigid circular inclusion is thermally insulated from the heat flux, and the temperature function $g'(z)$ in an infinite plate has been found as [5]

$$g'(z)=\tau\left(z+\frac{a^2}{z}\right)+\lambda \tag{8}$$

where $\tau=-q/k$ is the temperature gradient applied at infinity and λ is a uniform temperature change. Unlike the corresponding problem with perfect interface conditions, the current problem with boundary conditions is impossible to reduce

to a Hilbert problem for which an exact solution can be obtained. In order to solve this problem, we assume $\sigma_{rr} = N(\sigma)$ $(\sigma \in L)$ where the real function $N(\sigma)$ satisfies the symmetric property of (5) and then the stress function $\phi'(z)$ satisfies the Cauchy problem

$$\begin{aligned} &\phi'^{+}(\sigma) - \phi'^{-}(\sigma) = 0 \quad (\sigma \in L') \\ &\phi'^{+}(\sigma) - \phi'^{-}(\sigma) = N(\sigma) \quad (\sigma \in L) \end{aligned} \tag{9}$$

The solution to the Cauchy problem, (9), is readily obtained as

$$\phi'(z) = m'(z) - \frac{2\mu\beta\tau a^2}{1+\kappa}\frac{1}{z} \tag{10}$$

where

$$m'(z) = \frac{1}{2\pi i}\int \frac{N(\sigma)d\sigma}{\sigma - z} \tag{11}$$

Notice that the second term in the right-hand side of (10) represents the behavior of $\phi'(z)$ at infinity due to the thermal effect induced by the applied temperature gradient τ. The contour L in (11) is described in a clockwise direction. In view of the symmetric property $N(\sigma) = N(\bar{\sigma}) = \overline{N(\sigma)}$, (11) can also be represented as (see Appendix)

$$m'(z) = 2M - \overline{M'}\left(\frac{a^2}{z}\right) \tag{12}$$

where

$$M = \frac{1}{4\pi i}\int_L \frac{N(\sigma)d\sigma}{\sigma} \tag{13}$$

By approaching z to the hole boundary in (12), it is easy to show that

$$\overline{m'^{\pm}(\sigma)} = 2M - m'^{\pm}(\sigma) \tag{14}$$

Differentiating (14) will respect to σ yields

$$\overline{m''^{\pm}(\sigma)} = \frac{\sigma^2}{a^2}m''^{\pm}(\sigma) \tag{15}$$

Singular Integrodifferential Equation

For incomplete contact problems, one might expect separation to occur along the arcs L' which are unstressed, while the given normal displacement is specified over the contact region L as indicated in (7). By successively differentiating (7) with respect to the argument θ twice and combining itself, we have

$$\begin{aligned} &a\kappa[\phi'^{+}(\sigma) + \overline{\phi'^{+}(\sigma)} - \sigma\phi''^{+}(\sigma) - \frac{a^2}{\sigma}\overline{\phi''^{+}(\sigma)}] + \\ &a[\phi'^{-}(\sigma) + \overline{\phi'^{-}(\sigma)} - \sigma\phi''^{-}(\sigma) - \frac{a^2}{\sigma}\overline{\phi''^{-}(\sigma)}] + \\ &2\mu\beta a[g'^{+}(\sigma) - \sigma g''^{+}(\sigma) + \overline{g'^{+}(\sigma)} - \frac{a^2}{\sigma}\overline{g''^{+}(\sigma)}] = \\ &4\mu\left[f(\sigma) + \frac{\partial^2}{\partial\theta^2}f(\sigma)\right] \end{aligned} \tag{16}$$

With the help of (8) and (10) and using the derived formulas (14) and (15), we can rewrite the interface condition (16) in terms of $m'(\sigma)$ and $m''(\sigma)$ as

$$\begin{aligned} &a(\kappa-1)[m'^{+}(\sigma) - m'^{-}(\sigma)] - \\ &a\sigma(\kappa+1)[m''^{+}(\sigma) + m''^{-}(\sigma)] = \\ &4\mu\left[f(\sigma) + \frac{\partial^2}{\partial\theta^2}f(\sigma)\right] - 2a(\kappa+1)M - 4\mu\beta a\lambda \end{aligned} \tag{17}$$

Use of (11) and the Plemelj formulas shows that

$$m'^{+}(\sigma) - m'^{-}(\sigma) = N(\sigma) \tag{18}$$

$$m'^{+}(\sigma) + m'^{-}(\sigma) = \frac{1}{\pi i}\int_L \frac{N(\tau)d\tau}{\tau - \sigma} \tag{19}$$

Moreover, differentiating (19) with respect to σ yields

$$m''^{+}(\sigma) + m''^{-}(\sigma) = \frac{1}{\pi i}\int_L \frac{N'(\tau)d\tau}{\tau - \sigma} \tag{20}$$

Substitution of (18) and (20) into (17) gives

$$(\kappa-1)N(\sigma)-(\kappa+1)\frac{\sigma}{\pi i}\int_L \frac{N'(\tau)d\tau}{\tau-\sigma}+2(\kappa+1)M = \frac{4\mu}{a}\{f(\sigma)-\sigma f'(\sigma)-\sigma^2 f''(\sigma)\}-4\mu\beta\lambda \tag{21}$$

Equation (21) is a Prandtl type of singular integrodifferential equation for the current incomplete contact problem. Note that, by putting $\lambda = 0$ in (21), the above singular integrodifferential equation can be reduced to that for the isothermal elasticity problem [2]. Equation (21) can be rewritten in a form more convenient for the analysis by letting $a = 1$ and $f(\sigma) = 0$ as

$$(\kappa-1)N(\sigma)-(\kappa+1)\frac{\sigma}{\pi i}\int_L \frac{N'(\tau)d\tau}{\tau-\sigma}+2(\kappa+1)M = -4\mu\beta\lambda \tag{22}$$

Auxiliary Constraint Condition

In order to determine the stress distribution on the contact arc, it is necessary to solve (22) subject to the auxiliary condition that the displacements must vanish at some fixed points due to the symmetric property. For the present problem, both the normal and tangential displacements are found to vanish at the point $\sigma = 1$ since the plate and the rigid insert coincide at this point when the heat flux approaches from the negative x-axis. This condition gives

$$2\mu[u_r(\sigma)+iu_\theta(\sigma)] = \kappa\phi^+(\sigma)+\phi^-(\sigma)+2\mu\beta g^+(\sigma) \tag{23}$$

If one integrates $\phi'(z)$ in (10) with respect to z, it can be shown that

$$\phi^+(\sigma) = \phi(\sigma) = \int_\infty^\sigma m'(\xi)d\xi - \frac{2\mu\beta\tau}{1+\kappa}\log(\sigma) \tag{24}$$

and

$$\phi^-(\sigma) = \phi\left(\frac{1}{\sigma}\right) = -\int_0^{\frac{1}{\sigma}} m'(\xi)d\xi - \frac{2\mu\beta\tau}{1+\kappa}\log\left(\frac{1}{\sigma}\right) \tag{25}$$

With the help of (24) and (25) and an integration of $g'(z)$ in (8), the condition in (23) becomes

$$-\kappa\int_{1^+}^{\infty} m'(z)dz+\int_0^{1^-} m'(z)dz+2\mu\beta(0.5\tau+\lambda)=0 \tag{26}$$

Substituting (11) into (26) and performing some algebraic manipulations, we finally have (see Appendix)

$$\frac{(\kappa-1)}{2\pi}\int_0^\eta N(\theta)(\pi-\theta)\sin(\theta)d\theta+\frac{(1+\kappa)}{2\pi}\int_0^\eta N(\theta)\cos(\theta)\log[2-2\cos(\theta)]d\theta = -2\mu\beta(0.5\tau+\lambda) \tag{27}$$

where η is the contact angle to be determined.

Approximate Solutions

As we mentioned previously, there is no exact solution available for the current incomplete contact problem involving a Prandtl type of singular integrodifferential equation, (22), together with the auxiliary condition, (27). In order to solve (22) and (27) with the unknown function $N(\theta)$ and the undetermined contact angle η, we first assume that the contact normal stress is represented as

$$N(\theta) = \sqrt{\cos\theta-\cos\eta}\times\sum_{n=0}^{p} C_n\cos\left[\left(n+\frac{1}{2}\right)\theta\right] \tag{28}$$

For the problem of constructing the function $m'(z)$ corresponding to (28), we now introduce a branch function as

$$\omega(z) = [z - e^{i\eta}]^{\frac{1}{2}}[z - e^{-i\eta}]^{\frac{1}{2}} = \sqrt{z^2 - 2\cos(\eta)z + 1} \tag{29}$$

which is defined in the plane cut along L with the chosen branch such that

$$\lim_{x\to\infty}\left[\frac{\omega(z)}{z}\right] = 1 \tag{30}$$

It is easy to see that the boundary values of $\omega(z)$ on L are given by

$$\omega^{\pm}(\sigma) = \pm\sqrt{2\sigma}\cdot\sqrt{\cos(\theta) - \cos(\eta)} \tag{31}$$

By connecting the function $\omega(z)$ with the generating function for the Legendre polynomials [6], it can be shown that $\omega(z)$ has series expansions of the form

$$\omega(z) = -\sum_{k=0}^{k=\infty} D_k z^k \quad |z| < 1 \tag{32}$$

and

$$\omega(z) = z\sum_{k=0}^{k=\infty} D_k z^{-k} \quad |z| > 1 \tag{33}$$

where

$$D_0 = 1,\ D_1 = -\cos(\eta) \tag{34}$$

and

$$D_k = \frac{\cos(\eta)P_{k-1}(\cos\eta) - P_{k-1}(\cos\eta)}{k-1}\, k \geq 2 \tag{35}$$

with $P_k(x)$ being the Legendre polynomials of degree k.

In view of the fact that the contract stress function $N(\theta)$ in (28) is related to the branch function $\omega(z)$ in (31), $m'(z)$can then be approximated by a linear combination of the function $m'_n(z)$ as

$$m'(z) = \sum_{n=0}^{n=p} A_n m'_n(z) \tag{36}$$

where $m'_n(z)$ is defined by

$$m'_n(z) = (z^n + z^{-n-1})\omega(z) - D^*_{n+1} + \sum_{k=0}^{n} D_k[z^{(n+1-k)} - z^{-(n+1-k)}] \tag{37}$$

with

$$D^*_{n+1} = \delta_{0n} + D_{n+1} \tag{38}$$

and

$$\delta_{0n}\begin{cases} = 1, n = 0 \\ = 0, n \neq 0 \end{cases} \tag{39}$$

Moreover, use of (31) and the Plemelj formulas shows that

$$m'_n{}^{+}(\sigma) - m'_n{}^{-}(\sigma) \equiv N_n(\theta) = 4\sqrt{2}\cdot\cos\left[\left(n+\frac{1}{2}\right)\theta\right]\left[\cos\theta - \cos(\eta)\right]^{\frac{1}{2}} \tag{40}$$

and

$$m''_n{}^{+}(\sigma) + m''_n{}^{-}(\sigma) = \frac{\sigma}{\pi i}\int_L \frac{N'_n(\tau)d\tau}{\tau - \sigma} \equiv I_n(\theta) = 4\sum_{k=0}^{n}(n+1-k)D_k \cos[(n+1-k)\theta] \tag{41}$$

Similarly, the function M in (13) can also be approximated as

$$M = \sum_{n=0}^{n=p} A_n M_n \tag{42}$$

where $M_n(z)$ is defined by

$$M_n = \frac{1}{4\pi i}\int_L \frac{N_n(\tau)d\tau}{\tau} = -D^*_{n+1} \tag{43}$$

Substitution of (40) and (43) into (22) leads to

$$\sum_{n=0}^{n=p} A_n G_n(\theta) = -4\mu\beta\lambda + \varepsilon(\theta) \tag{44}$$

where

$$\begin{aligned} G_n(\theta) =& (\kappa-1)N_n(\theta) - (\kappa+1)I_n(\theta) \\ & - 2(\kappa+1)D^*_{n+1} \end{aligned} \tag{45}$$

and $\varepsilon(\theta)$ denotes the error in the approximate solution. If the coefficients A_n are chosen to minimize the integral

$$\int_0^\eta \varepsilon^2(\theta)d\theta \tag{46}$$

then the method of least squares requires that

$$\begin{aligned} &\sum_{n=0}^{n=p} A_n \int_0^\eta G_n(\theta)G_k(\theta)d\theta = \int_0^\eta -4\mu\beta\lambda G_k(\theta)d\theta \\ &k = 0, 1, 2.....P \end{aligned} \tag{47}$$

Substitution of (40) into (27) for the determination of the contact angle η yields the condition

$$\sum_{n=0}^{n=p} [(\kappa-1)E_n + (1+\kappa)F_n]A_n = -2\mu\beta(0.5\tau + \lambda) \tag{48}$$

where

$$\begin{aligned} E_n =& \frac{2\sqrt{2}}{\pi}\int_0^\eta (\pi-\theta)\sin(\theta)\cdot\cos\left[\left(n+\frac{1}{2}\right)\theta\right] \\ & [\cos(\theta)-\cos(\eta)]^{\frac{1}{2}}d\theta \end{aligned} \tag{49}$$

and

$$\begin{aligned} F_n =& \frac{2\sqrt{2}}{\pi}\int_0^\eta \log[2-2\cos(\theta)]\cos(\theta) \\ & \cdot\cos\left[\left(n+\frac{1}{2}\right)\theta\right]\left[\cos(\theta)-\cos(\eta)\right]^{\frac{1}{2}}d\theta \end{aligned} \tag{50}$$

The system of simultaneous equations, (47), together with the auxiliary condition, (48), is then established for solving the unknown coefficients $A_0, A_1, ...A_p$ and the contact angle η. Once the coefficients A_n and the angle η are computed, both the normal and circumferential stresses along the hole boundary can be obtained. It follows from (36) and (40) that the normal stress on the contact arc is expressed as

$$\begin{aligned} N(\theta) =& 4\sqrt{2}\cdot\sqrt{\cos(\theta)-\cos(\eta)} \\ & \times\sum_{n=0}^{n=p} A_n\cos\left[\left(n+\frac{1}{2}\right)\theta\right] \end{aligned} \tag{51}$$

Similarly, the circumferential stress can so be expressed as

$$\sigma_{\theta\theta} = N(\theta) + 4M - \frac{8\mu\beta\tau}{1+\kappa}\cos\theta \tag{52}$$

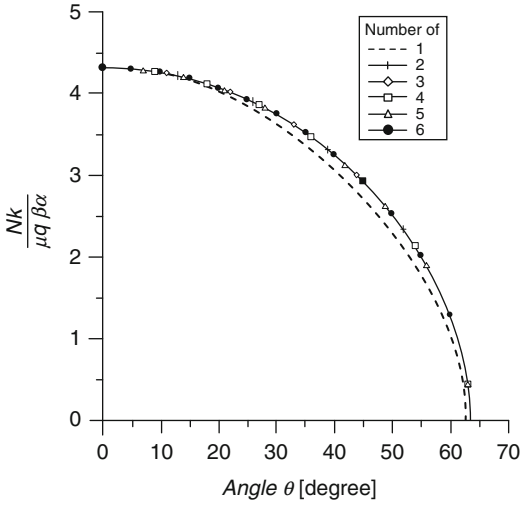

Contact Stresses in an Infinite Plate with a Rigid Circular Inclusion, Fig. 2 Normal stress on the contact arc with different number of terms for $\lambda/\tau a = 1$

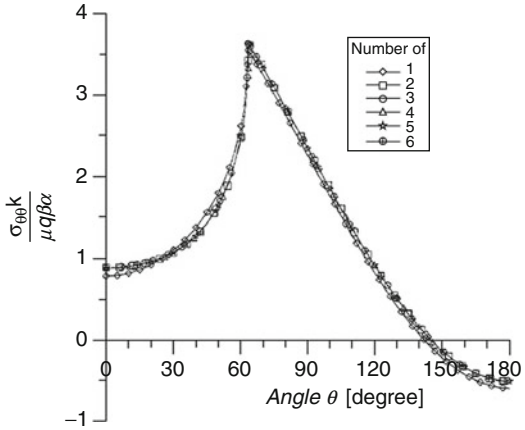

Contact Stresses in an Infinite Plate with a Rigid Circular Inclusion, Fig. 3 Circumferential stress in the plate with different number of terms for $\lambda/\tau a = 1$

Results and Discussion

The numerical calculations in (47) and (48) are performed with Simpson's quadrature formula using a maximum number of 1,000 evenly spaced subdivisions in the interval $0 \leq \theta \leq \eta$. With an initial guess of the value η for a fixed number of terms in the approximating

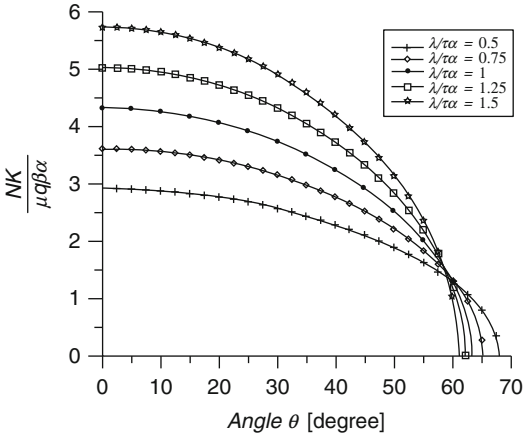

Contact Stresses in an Infinite Plate with a Rigid Circular Inclusion, Fig. 4 Normal stress on the contact arc for different values of $\lambda/\tau a$

series, (47) is solved, and the error in satisfying (48) is evaluated.

The distributions of the normal stress on the contact arc and the circumferential stress around the hole in the matrix with a different number of terms in the approximating series for the case $\lambda/\tau a = 1$ are shown in Fig. 2 and 3, respectively. It is interesting to see that the maximum circumferential stress occurs at the ends of the contact arc, while themaximum compressive normal stress occurs at the middle of the contact arc. The above conclusion can also be applied for different loading conditions as shown in Figs. 4 and 5. Although the general trend of the normal stress and the circumferential stress curves is qualitatively the same for different loading conditions, the values of the maximum stress are strongly dependent on the applied thermal loading. By increasing the value of $\lambda/\tau a$, both the maximum compressive normal stress and the maximum circumferential stress increase, whereas the contact angle decreases. Generally speaking, the magnitude of a uniform temperature change λ applied to the system plays the more important role than the applied temperature gradient τ in affecting the current problem. This can be verified from the fact that only the parameter λ

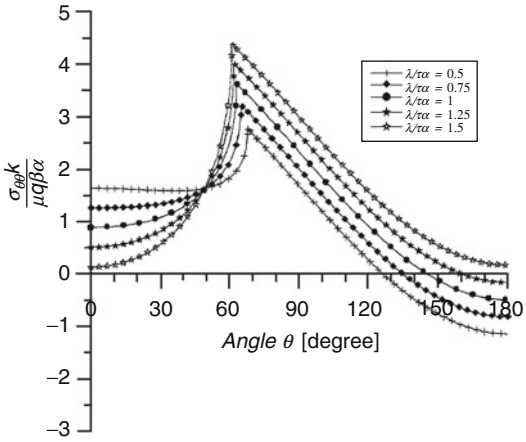

Contact Stresses in an Infinite Plate with a Rigid Circular Inclusion, Fig. 5 Circumferential stress in the plate for different values of $\lambda/\tau a$

appears in the right-hand side of a singular integrodifferential equation as indicated in (22). The presence of the temperature gradient applied at infinity can only determine the position where separation is supposed to exist. It is expected that the arc L', where separation occurs, locates near the site with higher temperature, while the contact arc L locates near the side with lower temperature.

Concluding Remarks

A Prandtl type singular integrodifferential equation governing the current incomplete contact problem is derived and solved approximately by constructing a finite series which minimizes the error in the sense of least squares. Although there is no exact solution available in the literature to check the accuracy of the approximate solution, the present derived solution seems to yield reasonable results that fit some physical considerations. The method presented here can also be applied to a related case where the plate contains an elliptic elastic insert. This problem may reduce to a singular integrodifferential equation similar to (21) but of a more complicated form.

Appendix

Derivation of (12)

By replacing z with $\frac{a^2}{z}$ in (11) and taking the conjugate, we have

$$\overline{m'}\left(\frac{a^2}{z}\right) = -\frac{1}{2\pi i}\int_L \frac{\overline{N(\tau)}d\bar{\tau}}{\bar{\tau} - \frac{a^2}{z}} \tag{53}$$

Using the property $N(\tau) = \overline{N(\tau)}$ and noting that $\tau\bar{\tau} = a^2$, (53) can be replaced by

$$\overline{m'}\left(\frac{a^2}{z}\right) = -\frac{1}{2\pi i}\int_L \frac{zN(\tau)d\tau}{\tau(z-\tau)} \tag{54}$$

Equation (54) can be rearranged as

$$\begin{aligned}\overline{m'}\left(\frac{a^2}{z}\right) &= -\frac{1}{2\pi i}\int_L \frac{N(\tau)d\tau}{\tau - z} + \frac{1}{2\pi i}\int_L \frac{N(\tau)d\tau}{\tau} \\ &= -m'(z) + 2M\end{aligned} \tag{55}$$

By approaching z to o in (55), we obtain

$$\overline{m'^{\pm}(\sigma)} = 2M - m'^{\pm}(\sigma) \tag{56}$$

Derivation of (27)

Equation (10) can be rewritten as

$$m'(z) = \frac{1}{2\pi i}\int_{L_1} \frac{N(\sigma)d\sigma}{\sigma - z} - \frac{1}{2\pi i}\int_{L_1} \frac{N(\sigma)d\bar{\sigma}}{\bar{\sigma} - z} \tag{57}$$

where the contour L_1, defined by $0 \le \arg(\sigma) \le \eta, |\sigma| = 1$, is represented as the upper part of the contact arc L.

Integrating (57) with respect to z yields

$$\int_0^1 m'(z)dz = \frac{1}{2\pi i}\left\{\int_{L_1} N(\sigma)[-\log(\sigma - z)]_0^1 d\sigma - \int_{L_1} N(\sigma)[-\log(\bar{\sigma} - z)]_0^1 d\bar{\sigma}\right\} = \frac{1}{2\pi i}\left\{\int_{L_1} N(\sigma)[-\log(\sigma - 1) + \log(\sigma)]d\sigma - \int_{L_1} N(\sigma)[-\log(\bar{\sigma} - 1) + \log(\bar{\sigma})]d\bar{\sigma}\right\} \tag{58}$$

In view of the relation $\sigma = e^{i\theta}$, $\overline{\sigma} = e^{-i\theta}$ (58) becomes

$$\begin{aligned}
&\int_0^l m'(z)dz \\
&= \frac{1}{2\pi i}\left\{\int_\theta^\eta N(\theta)[-\log(e^{i\theta} - 1) + \log(e^{i\theta})](de^{i\theta})\right. \\
&\left. - \int_\theta^\eta N(\theta)[-\log(e^{-i\theta} - 1) + \log(e^{-i\theta})]d(e^{-i\theta})\right\} \\
&= \frac{1}{2\pi i}\left\{\int_\theta^\eta N(\theta)\left[\log(e^{i\theta} - 1) - \log(e^{i\theta})\right.\right. \\
&\left. - \log(e^{-i\theta} - 1) + \log(e^{-i\theta})\right]\sin(\theta)d\theta \\
&+ \int_\theta^\eta N(\theta)\left[-\log(e^{i\theta} - 1) + \log(\sigma^{i\theta}).\right. \\
&\left.\left. - \log(e^{-i\theta} - 1) + \log(e^{-i\theta})i\cos(\theta)d\theta\right]\right\} \\
&= \frac{1}{2\pi}\int_0^\eta N(\theta)\left[-2i\theta + \log\frac{e^{i\theta} - 1}{e^{-i\theta} - 1}\right]\sin(\theta)d\theta \\
&- \frac{1}{2\pi}\int_0^\eta N(\theta)\log[(e^{i\theta} - 1)(e^{-i\theta} - 1)]i\cos(\theta)d\theta \\
&= \frac{1}{2\pi}\int_0^\eta N(\theta)(\pi - \theta)\sin(\theta)d\theta \\
&- \frac{1}{2\pi}\int_0^\eta N(\theta)\cos(\theta)\log[2 - 2\cos(\theta)]d\theta
\end{aligned} \tag{59}$$

Similarly,

$$\int_1^\infty m'(z)dz = \frac{1}{2\pi}\left\{\int_0^\eta N(\theta)(\pi - \theta)\sin(\theta)d\theta + \int_0^\eta N(\theta)\cos(\theta)\log[2 - 2\cos(\theta)]d\theta\right\} \tag{60}$$

Substitution of (59) and (60) into (27) gives

$$\begin{aligned}
&\frac{(\kappa - 1)}{2\pi}\int_0^\eta N(\theta)(\pi - \theta)\sin(\theta)d\theta \\
&+ \frac{(1 + \kappa)}{2\pi}\int_0^\eta N(\theta)\cos(\theta)\log[2 - 2\cos(\theta)]d\theta \\
&= -2\mu\beta(0.5\tau + \lambda)
\end{aligned} \tag{61}$$

References

1. Muskhelishvili NI (1953) Some basic problems of the mathematical theory of the elasticity. Noordhoff, Groningen
2. Nottingham AH (1971) Complex variable methods in elasticity. Wiley, England
3. Stippes M, Wilson HB, Krull FN (1962) A contract stress problem for a smooth disk in an infinite plate. Proceedings of the 4th U.S. National Congress of applied mechanics. ASME, vol 2, pp 799–806
4. Wilson HB (1964) Approximate determination of contact stresses in an infinite plate with a smooth circular insert. Proceedings of the 2nd southeastern conference on theoretical and applied mechanics, pp 147–163
5. Chao CK, Shen MH (1997) On bonded circular inclusions in plane thermoelasticity. ASME J Appl Mech 64:1000–1004
6. Whittaker ET, Watson GN (1952) Modern analysis, 4th edn. Cambridge University Press, Cambridge

Contact Zone

▶ Contact Zone Model for an Interface Crack in a Piezoelectric Bimaterial Under Thermoelectromechanical Loadings

Contact Zone Model for an Interface Crack in a Piezoelectric Bimaterial Under Thermoelectromechanical Loadings

Volodymyr V. Loboda[1] and Klaus P. Herrmann[2]
[1]Department of Theoretical and Applied Mechanics, Dniepropetrovsk National University, Dniepropetrovsk, Ukraine
[2]Lehrstuhl fuer Technische Mechanik, Paderborn University, Paderborn, Germany

Synonyms

Contact zone; Electrically permeable or impermeable interface cracks; Piezoelectric bimaterial; Thermal stresses; Thermomechanical loading

Overview

Piezoelectric materials are referred to the most actively developed contemporary materials which are widely used in engineering as sensors, transducers, and actuators. However, piezoelectric materials are very brittle in general and often contain various microdefects and particularly interface cracks. Such cracks are the most dangerous kind of defects, especially under essential thermal and electromechanical fields. Therefore, it is important to understand and to be able to analyze the fracture characteristics of piezoelectric materials so that reliable service life predictions of the pertinent devices can be conducted.

An interface crack in an infinite piezoelectric bimaterial under the action of a remote temperature flux has been analytically investigated in paper [1], where the representations of [2–4] extended for the piezoelectric case in paper [5] have been used. Thereby, an electrically impermeable crack has been assumed in this entry. Later a similar problem for an electrically permeable interface crack has been considered in paper [6], where also as in paper [1] the classical interface crack model has been used. The solutions obtained in the frame of this model possess the oscillating singularities at the crack tips which were found in [7]. Nevertheless, for small zone lengths of overlapping of crack faces, this solution is rather useful for an interface crack investigation because for such cases the required fracture mechanical parameters can be accurately defined by this solution. However, the existence of an essential shear loading and a temperature field lead in certain cases to the appearance of a long contact zone of the interface crack faces. In such cases the approach based upon the initial assumption concerning the existence of a contact zone [8] should be used.

A penny-shaped interface crack with a contact region between two isotropic materials under a thermomechanical loading has been investigated in papers [9, 10] by means of the method of singular integral equations. The thermal conditions in the zone of the mechanical contact of the crack faces in particular have been investigated in these papers, and important conclusions concerning the formulation of these conditions depending on the direction of the heat flux have been developed. An interface crack with a contact zone in an anisotropic bimaterial under thermomechanical loading has been analytically studied in Ref. [11], and the problems of thermoelasticity for a set of interface cracks with contact zones in isotropic and anisotropic materials were investigated in [12, 13]. A thermopiezoelectric bimaterial with an interface crack under the assumption of a contact zone model has been investigated in paper [14] by means of the Lekhnitskii-Eshelby-Stroh formalism. The method of singular integral equations has been used in this paper, and the crack faces including the contact zones were assumed to be thermally and electrically insulated.

Electrically permeable and electrically impermeable interface cracks with a frictionless contact zone at the right crack tip between two semi-infinite piezoelectric spaces under the action of a remote electromechanical loading and a temperature flux were studied in papers [15, 16].

In this entry the problem of a crack with a contact zone between two piezoelectric semi-infinite spaces under a remote electromechanical

loading and a temperature flux has been discussed. The peculiarities of an analytical consideration of this problem and the results of the analysis have been presented.

Definition

An interface crack with electrically permeable or insulated open part and mechanically frictionless contact zone in a piezoelectric bimaterial under the action of a remote mixed-mode mechanical loading as well as thermal and electrical fields is considered. By use of the matrix–vector representations of thermal, mechanical, and electrical fields via sectionally holomorphic functions, the problems of linear relationships are formulated and solved exactly for both electrically permeable and electrically impermeable interface cracks. For these cases the transcendental equations and clear analytical formulas are derived for the determination of the contact zone lengths and the associated fracture mechanical parameters. The influence of the thermal and electrical fluxes upon the mentioned values is demonstrated.

Basic Relations for a Thermopiezoelectric Solid

The constitutive relations in the absence of body forces and free charges for a linear piezothermoelectric material can be presented according to Ref. [17] in the form

$$\Pi_{iJ} = E_{iJKl} V_{K.l} - \beta_{iJ} T, \Pi_{iJ,\,i} = 0 \qquad (1)$$

$$q_i = -\lambda_{ij} T_{,j},\ q_{i,i} = 0 \qquad (2)$$

where

$$V_K = \begin{cases} u_k, & K = 1,2,3 \\ \varphi, & K = 4 \end{cases} \qquad (3)$$

$$\varphi_{iJ} = \begin{cases} \sigma_{ij}, & i,J = 1,2,3 \\ D_i, & i = 1,2,3;\ J = 4 \end{cases} \qquad (4)$$

and

$$E_{iJkl} = \begin{cases} C_{ijkl}, J, K = 1,2,3 \\ e_{lij}, J = 1,2,3; K = 4 \\ e_{ikl}, K = 1,2,3; J = 4 \\ -\varepsilon_{il}, J = K = 4 \end{cases} \qquad (5)$$

In relations (1)–(5), φ is electric potential; e_{lij}, ε_{ij}, and λ_{ij} are the piezoelectric constants, dielectric constants, and the heat conduction coefficients, respectively. The values β_{iJ} are the stress-temperature coefficients for $J = 1, 2, 3$ and β_{i4} present the pyroelectric constants. Small subscripts in (1)–(5) and afterward are always ranging from 1 to 3, capital subscripts are ranging from 1 to 4, and summation on repeated Latin suffixes has been used.

Assuming all fields are independent on the coordinate x_2, using the Lekhnitskii-Eshelby-Stroh representation and its application to piezoelectric [5] and thermopiezoelectric [1, 14] materials, the following presentations are obtained:

$$\mathbf{V} = \mathbf{A}\mathbf{f}(z) + \mathbf{c}\chi(z_t) + \bar{\mathbf{A}}\bar{\mathbf{f}}(\bar{z}) + \bar{\mathbf{c}}\bar{\chi}(\bar{z}_t) \qquad (6)$$

$$\mathbf{t} = \mathbf{B}\mathbf{f}'(z) + \mathbf{d}\chi'(z_t) + \bar{\mathbf{B}}\bar{\mathbf{f}}'(\bar{z}) + \bar{\mathbf{d}}\bar{\chi}'(\bar{z}_t) \qquad (7)$$

where $z_J = x_1 + p_J x_3$, $\mathbf{V} = [u_1, u_2, u_3, \varphi]^T$, $\mathbf{t} = [\sigma_{31}, \sigma_{32}, \sigma_{33}, D_3]^T$ (the superscript T stands for the transposed matrix), and $\mathbf{A} = [\mathbf{A}_1, \mathbf{A}_2, \mathbf{A}_3, \mathbf{A}_4]$; p_J and $\mathbf{A}_J = [a_{1J}, a_{2J}, a_{3J}, a_{4J}]^T$ are an eigenvalue and an eigenvector, respectively, of the system:

$$\left[\mathbf{Q} + p_J(\mathbf{R} + \mathbf{R}^T) + p_J^2 \mathbf{T}\right]\mathbf{A}_J = \mathbf{0} \qquad (8)$$

with the elements of the 4×4 matrices $\mathbf{Q}$, $\mathbf{R}$, and $\mathbf{T}$ defined as $Q_{JK} = E_{1JK1}$, $R_{JK} = E_{1JK3}$, and $T_{JK} = E_{3JK3}$. The vector $\mathbf{c}$ is defined by the equation

$$\left[\mathbf{Q} + \tau(\mathbf{R} + \mathbf{R}^T) + \tau^2 \mathbf{T}\right]\mathbf{c} = \mathbf{N}_1 + \tau \mathbf{N}_2 \qquad (9)$$

with $\mathbf{N}_m = [\beta_{m1}, \beta_{m2}, \beta_{m3}, \beta_{m4}]^T (m = 1,2)$, and the 4×4 matrix $\mathbf{B}$ and the vector $\mathbf{d}$ can be found by the formulas

$$\mathbf{B} = \mathbf{R}^T\mathbf{A} + \mathbf{TAP},\ \mathbf{d} = (\mathbf{R}^T + \tau\mathbf{T})\mathbf{c} - \mathbf{N}_2 \quad (10)$$

with $\mathbf{P} = diag[p_1, p_2, p_3, p_4]$

A Bimaterial Thermopiezoelectric Space with Mixed Conditions at the Interface

Further, a bimaterial composed of two different piezoelectric semi-infinite spaces $x_3 > 0$ and $x_3 < 0$ with thermomechanical properties defined by the matrices $E^{(1)}_{iJKl}$, $\lambda^{(1)}_{ij}$, $\beta^{(1)}_{iJ}$ and $E^{(2)}_{iJKl}$, $\lambda^{(2)}_{ij}$, $\beta^{(2)}_{iJ}$, respectively, is considered. We assume that the component q_3 of the temperature flux vector and the vector $\mathbf{t}$ are continuous across the whole bimaterial interface and the parts $L_t = \{(-\infty, d_1) \cup (a_1, d_2) \cup \ldots (d_n, \infty)\}$ and $L = \{(-\infty, c_1) \cup (b_1, c_2) \cup \ldots (b_n, \infty)\}$ $([d_i, a_i] \subset [c_i, b_i])$ of the interface $-\infty < x_1 < \infty$, $x_3 = 0$ are thermally and electromechanically bounded, respectively, i.e., the boundary conditions at the interface $x_3 = 0$ are the following:

$$q^{(1)}_3 = q^{(2)}_3,\ \mathbf{t}^{(1)}(x_1, 0) = \mathbf{t}^{(2)}(x_1, 0)\ for\ x_1 \in (-\infty, \infty) \quad (11)$$

$$T^{(1)} = T^{(2)}\ for\ x_1 \in L_t,\ \mathbf{V}^{(1)}(x_1, 0) = \mathbf{V}^{(2)}(x_1, 0) \quad for \quad x_1 \in L \quad (12)$$

The temperature and the thermal flux at the interface can be presented in the form

$$[T'(x_1)] = \theta''^{+}(x_1) - \theta''^{-}(x_1) \quad (13)$$

and the thermal flux can be presented as

$$q^{(1)}_2(x_1, 0) = -ik_0\left\{\theta''^{+}(x_1) + \theta''^{-}(x_1)\right\} \quad (14)$$

where $k_0 = \frac{k^{(1)}k^{(2)}}{k^{(1)}+k^{(2)}}$ ($k^{(m)}$ is defined by $\lambda^{(m)}_{ij}$) and the function $\theta(z)$ is analytic in the whole plane with a cut along $(-\infty, \infty)\backslash L_t$.

Using an approach developed for a thermoelastic case in Ref. [18] and relations (7), (11), the following expressions at the interface are obtained:

$$[\mathbf{V}'(x_1)] = \mathbf{W}^{+}(x_1) - \mathbf{W}^{-}(x_1) \quad (15)$$

$$\mathbf{t}^{(1)}(x_1, 0) = \mathbf{G}\mathbf{W}^{+}(x_1) - \bar{\mathbf{G}}\mathbf{W}^{-}(x_1) - \mathbf{g}(x_1) \quad (16)$$

where

$$[\mathbf{V}'(x_1)] = \mathbf{V}'^{(1)}(x_1, 0) - \mathbf{V}'^{(2)}(x_1, 0) \quad (17)$$

$\mathbf{G} = \mathbf{B}^{(1)}\mathbf{D}^{-1}$, $\mathbf{D} = \mathbf{A}^{(1)} - \bar{\mathbf{L}}\mathbf{B}^{(1)}$, $\mathbf{L} = \mathbf{A}^{(2)}(\mathbf{B}^{(2)})^{-1}$, $\mathbf{W}^{\pm}(x_1) = \mathbf{W}(x_1 \pm 0)$, and the vector function $\mathbf{g}(x_1) = [g_1(x_1), g_2(x_1), g_3(x_1), g_4(x_1)]^T$ can be presented in the form

$$\mathbf{g}(x_1) = \mathbf{h}\theta'^{+}(x_1) - \bar{\mathbf{h}}\theta'^{-}(x_1) \quad (18)$$

with

$$\mathbf{h} = \frac{1}{k^{(1)} + k^{(2)}} \times \left\{-\mathbf{G}(\bar{\mathbf{L}}\mathbf{d}^* - \mathbf{c}^*) - k^{(2)}\mathbf{d}^{(1)}\right\} \quad (19)$$

and

$$\mathbf{c}^* = k^{(2)}\mathbf{c}^{(1)} + k^{(1)}\bar{\mathbf{c}}^{(2)},\ \mathbf{d}^* = k^{(2)}\mathbf{d}^{(1)} + k^{(1)}\bar{\mathbf{d}}^{(2)} \quad (20)$$

It is worth to note that for the boundary conditions (12) the vector function $\mathbf{W}(z) = [W_1(z), W_2(z), W_3(z), W_3(z),]^T$ is analytic in the whole plane with a cut along $(-\infty,\infty)\backslash L$. We note as well that the matrix $\mathbf{G}$ and the vector function $\mathbf{W}(z)$ are related to the matrix $\mathbf{H}$ and the vector function $\mathbf{\Psi}'(z)$ of papers [19] and [1] as $i\mathbf{G}^{-1} = \mathbf{H}$, $\mathbf{W}(z) = -i\mathbf{H}\mathbf{\Psi}'(z)$, respectively, and relations (15), (16) can be written without any difficulties in terms of the matrix $\mathbf{H}$ and the vector function $\mathbf{\Psi}'(z)$ from these papers. But for the formulation of the problems considered in the following entries, presentations (15) and (16) appear to be more convenient than the form used in the mentioned papers. On the base of relations (15), (16), different problems of linear

relationship can be formulated for thermopiezoelectric bimaterials with cuts at the material interfaces.

The attention is focused in the following on thermopiezoelectric materials of the symmetry class 6 mm [20] poled in the direction x_3 which have an essential practical significance as so-called poled ceramics. In this case for all fields which are independent of the coordinate x_2, the displacement V_2 of the vector function $\mathbf{V}$ of equation (3) decouples in the (x_1,x_3)-plane from the components (V_1,V_3,V_4). Because of the simplicity of the V_2-determination, our attention will be focused on the plane problem for the components (V_1,V_3,V_4). In this case, similar to the contracted notations in the anisotropic elasticity [21], the following relations for the elements of the matrix $\mathbf{E}$ related to the (x_1,x_3)-plane can be introduced: $E_{1111} = C_{11}$, $E_{1133} = C_{13}$, $E_{3333} = C_{33}$, $E_{1313} = C_{44}$, $E_{1143} = e_{31}$, $E_{3343} = e_{33}$, $E_{1341} = e_{15}$, $E_{1441} = -\varepsilon_{11}$, and $E_{3443} = -\varepsilon_{33}$. Moreover, the matrix $\mathbf{G}$ without the second row and column and the vector $\mathbf{h}$ without the second element have the following structure [22]:

$$\mathbf{G} = \begin{bmatrix} G_{11} & G_{13} & G_{14} \\ G_{31} & G_{33} & G_{34} \\ G_{41} & G_{43} & G_{44} \end{bmatrix} = \begin{bmatrix} i g_{11} & g_{13} & g_{14} \\ g_{31} & i g_{33} & i g_{34} \\ g_{41} & i g_{43} & i g_{44} \end{bmatrix},$$
$$\mathbf{h} = \begin{Bmatrix} i\theta_1 \\ \theta_3 \\ \theta_4 \end{Bmatrix} \tag{21}$$

where all g_{ij} and θ_i are real.

Presentations (15), (16) play an important role for the formulations of the linear relationship problems for cracks, inclusions, etc. at the interface.

A Crack with a Contact Zone at the Material Interface

Consider a crack situated in the region $c \le x_1 \le b$, $x_3 = 0$ between two semi-infinite spaces ($x_3 > 0$, material 1 and $x_3 < 0$, material 2) which are loaded at infinity with uniform stresses $\sigma_{33}^{(m)} = \sigma$, $\sigma_{13}^{(m)} = \tau$, and $\sigma_{11}^{(m)} = \sigma_{xm}^{\infty}$, as well as with uniform electric fluxes $D_3^{(m)} = d$, $D_1^{(m)} = D_{xm}^{\infty}$ satisfying the continuity conditions at the interface. Besides, a uniform temperature flux q_0 in the x_3-direction is imposed at infinity. It is assumed that the crack surfaces are traction-free for $x_1 \in (c,a)$ while they are in frictionless contact for $x_1 \in (a,b)$, and the position of the point $a < b$ is arbitrarily chosen for the time being. It means that the interface conditions for the thermally perturbed state have the following forms:

$$x_1 \notin (c,b): \ [\boldsymbol{V}(x_1,0)] = 0, \quad [\boldsymbol{t}(x_1,0)] = 0 \tag{22}$$

$$x_1 \in (c,a): q_3^{\pm} = -q_0, \ \sigma_{13}^{(m)}(x_1,0) = 0, \sigma_{33}^{(m)}(x_1,0) = 0, \ [D_3(x_1,0)] = 0, \quad [\varphi(x_1,0)] = 0$$
– for an electrically permeable crack, (23)

$$q_3^{\pm} = -q_0, \ \boldsymbol{t}^{(m)}(x_1,0) = 0$$
– for an electrically impermeable crack, (24)

$$x_1 \in (a,b): [T] = 0, \quad [q_3] = 0, \ [u_3(x_1,0)] = 0$$
$$\sigma_{13}^{(m)}(x_1,0) = 0, [\sigma_{33}(x_1,0)] = 0, \ [D_3(x_1,0)] = 0$$
$$[\varphi(x_1,0)] = 0 \tag{25}$$

This problem is a particular case of the problem considered in the previous section for $n = 1$, $c_1 = d_1 = c$, $a_1 = a$, $b_1 = b$, and therefore, presentations (13), (14) and (15), (16) obtained there hold true in this case. Due to these presentations, the thermal problem can be reduced to a relatively simple Hilbert problem and solved exactly for both electrically permeable and electrically impermeable interface cracks.

Combining further each group of equations (15), (16) in the same way as it has been performed in Ref. [22], one arrives for the

electrically permeable crack at the following presentations:

$$\sigma_{33}^{(1)}(x_1,0)+im_j\sigma_{13}^{(1)}(x_1,0)=\vartheta_j[F_j^+(x_1)+\gamma_jF_j^-(x_1)]+\sigma_0-g_{0j}(x_1),\ (j=1,3) \tag{26}$$

$$[u_1'(x_1)]+iS_j[u_3'(x_1)]=F_j^+(x_1)-F_j^-(x_1) \tag{27}$$

where

$$F_j(z)=W_1(z)+iS_jW_3(z) \tag{28}$$

$$g_{0j}(x_1)=g_3(x_1)+im_jg_1(x_1) \tag{29}$$

$$\begin{aligned}\sigma_0 &= -g_{34}\Delta_1^{-1}(g_{43}\sigma-g_{33}d)\\ \Delta_1 &= g_{33}g_{44}-g_{43}g_{34},\end{aligned} \tag{30}$$

and the constants m_j, ϑ_j, S_j are defined by the elements of the matrix $\mathbf{G}$.

The satisfaction of the electromechanical boundary conditions (22)–(25) by use of (26), (27) leads for an electrically permeable interface crack to the following inhomogeneous-combined Dirichlet-Riemann problem for a sectionally holomorphic function $F(z)$:

$$F^+(x_1)+\gamma F^-(x_1)=\Psi_1(x_1)\quad for\quad x_1\in(c,a) \tag{31}$$

$$ImF^{\pm}(x_1)=\Psi_2(x_1)\quad for\quad x_1\in(a,b) \tag{32}$$

where the functions $\Psi_1(x_1)$ and $\Psi_2(x_1)$ are defined by the thermal solution obtained above. It is important that the solution of the problem of linear relationship (31), (32) has been presented in a closed form similar to those given in [11, 23].

For an electrically impermeable interface crack, a Hilbert problem appears in addition to problem (31), (32), but nevertheless, the analytical solutions of all obtained problems are found and all necessary thermal, mechanical, and electrical characteristics at the interface are presented in a closed form. Moreover, the clear analytical formulas for the stress intensity factors

$$k_1=\lim_{x_1\to a+0}\sqrt{2\pi(x_1-a)}\sigma_{33}^{(1)}(x_1,0)$$

$$k_2=\lim_{x_1\to b+0}\sqrt{2\pi(x_1-b)}\sigma_{13}^{(1)}(x_1,0)$$

as well as the electrical displacement intensity factor $k_4=\lim_{x_1\to a+0}\sqrt{2\pi(x_1-a)}D_3^{(1)}(x_1,0)$ have been obtained for an arbitrary value of the relative contact zone length $\lambda=\frac{b-a}{b-c}$.

Further, the real contact zone length should be obtained. For this purpose the following additional conditions

$$\begin{aligned}\sigma_{33}^{(1)}(x_1,0)\le 0\ for\ x_1\in(a,b),\\ [u_3(x,0)]\ge 0\ for\ x_1\in(c,a)\end{aligned} \tag{33}$$

should be satisfied. For an electrically permeable crack, the satisfaction of inequalities (33) gives a transcendental equation with respect to the relative contact zone length λ. The largest root λ_0 of this equation from the interval (0, 1) defines the required real contact zone length. This root can be found numerically, but for a small λ_0, an analytical formula has been obtained as well.

The numerical results were obtained for a bimaterial composed of piezoelectric cadmium selenium (the upper material) and glass (the lower one) [24]. In Fig. 1 the variation of the relative contact zone length λ_0 with respect to the dimensionless parameter p which is proportional to the intensity of the thermal flux q_0 is shown for the coefficients of normal-shear loading $k=\tau/\sigma$ equal to 0 (line1), 10 (line II), and 50 (line III). The values of λ_0 are usually rather small; therefore, the logarithmic scale is used with the definition $\vartheta_0=-ln(\lambda_0)$. It should be noted that for $k=50$ and relatively small magnitudes of p, the values of λ_0 are comparable to 1, and moreover, for any value of k, the relative contact zone length λ_0 for $p\to-\infty$ tends to the same value 7.0225×10^{-19} as for a pure thermal loading. It is important to note as well that for an electrically permeable interface crack neither the contact zone length nor the intensity factors depend on the intensity of the electrical flux d.

A more complicated situation concerning the determination of the real contact zone length

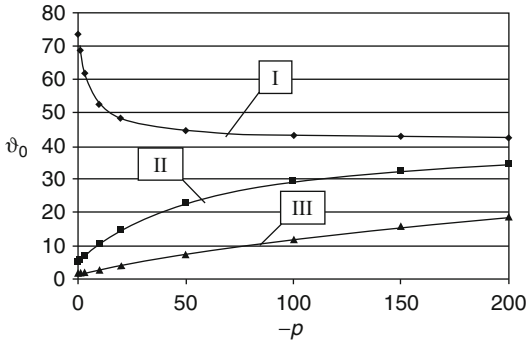

Contact Zone Model for an Interface Crack in a Piezoelectric Bimaterial Under Thermoelectromechanical Loadings, Fig. 1 The variation of the relative contact zone length λ_0 ($\vartheta_0 = -ln(\lambda_0)$) with respect to the intensity of the thermal flux for different coefficients of normal-shear loading for an electrically impermeable interface crack

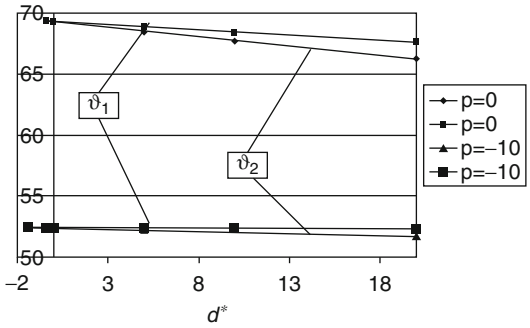

Contact Zone Model for an Interface Crack in a Piezoelectric Bimaterial Under Thermoelectromechanical Loadings, Fig. 2 The variation of the values of λ_i ($\vartheta_i = -ln(\lambda_i)$) with respect to the intensity of the electrical flux for an electrically impermeable interface crack

takes place for an electrically impermeable interface crack. In this case, inequalities (33) hold true if a is taken from the segment $[a_1, a_2]$ providing $a_1 \le a_2$ holds true, where $a = b - \lambda l$, $a_1 = b - \lambda_1 l$, $a_2 = b - \lambda_2 l$, and λ_1 is the maximum root from the interval (0,1) of the equation $k_1 = 0$ and λ_2 is the similar root of the equation $\lim_{x_1 \to a-0} \sqrt{a - x_1}[u_3'(x_1, 0)] = 0$. The required roots of the mentioned equations can be found numerically or analytically (for a small λ_1 and λ_2), and the segment $[a_1, a_2]$ can be obtained. An additional analysis based upon the theorem of the minimum potential energy shows that the real position of the point a coincides with a_1 providing $a_1 \le a_2$ holds true. If the last inequality is not valid, then the inequalities (33) cannot be satisfied and other thermal and electrical interface conditions should be introduced.

The numerical analysis showed that for the electrical flux $d = 0$, the contact zone lengths correspondent to an electrically insulated and an electrically permeable crack are practically the same. However, a nonzero electrical flux changes the real contact zone length and the associated fracture mechanical parameters for an electrically impermeable interface crack. In Fig. 2 the variations of the relative contact zone lengths λ_1 and λ_2 with respect to the intensity of the electrical flux $d^* = C_{33}^{(1)} d/(e_{33}^{(1)} \sigma)$ for $k = 0$ and two different intensities of the temperature flux are shown ($C_{33}^{(1)}$ and $e_{33}^{(1)}$ are the elastic and piezoelectric moduli, respectively). The same bimaterial as in the previous example was used, and the designation $\vartheta_i = -ln(\lambda_i)$ $(i = 1,2)$ for the logarithmic scale of Fig. 2 was adopted. It can be seen that the increasing of d leads to the increasing of the differences between λ_1 and λ_2 which for the left points of each pair of lines are equal to zero.

Contact Zone Model for an Interface Crack in a Piezoelectric Bimaterial Under Thermoelectromechanical Loadings, Table 1 Dependencies of the relative contact zone length for an electrically impermeable interface crack with respect to large values of the electrical flux

d^*	10^3	10^4	2×10^4
λ_1	6.38×10^{-13}	6.62×10^{-4}	0.0177

It is worth to be mentioned that according to the last results, the contact zone length and the associated fracture mechanical parameters depend on the electrical flux for an electrically insulated crack. However, the essential dependencies of these values on d appear for rather large relative intensities of the electrical flux only. It is particularly demonstrated by Table 1 where the values of the relative contact zone

length λ_1 are shown with respect to the intensity of the electrical flux d^* for $p = 0, k = 0$ and for the same bimaterial as earlier.

References

1. Shen S, Kuang ZB (1998) Interface crack in bi-piezothermoelastic media and the interaction with a point heat source. Int J Solids Struct 35:3899–3915
2. Lekhnitskii SG (1963) Theory of elasticity of an anisotropic elastic body. Holden-Day, San-Francisco
3. Eshelby JD, Read WT, Shockley W (1953) Anisotropic elasticity with application to dislocation theory. Acta Metall 1:251–259
4. Stroh AN (1958) Dislocations and cracks in anisotropic elasticity. Phil Mag 7:625–646
5. Barnett DM, Lothe J (1975) Dislocations and line charges in anisotropic piezoelectric insulators. Phys Stat Sol (B) 67:105–111
6. Gao CF, Wang MZ (2001) A permeable interface crack between dissimilar thermopiezoelectric media. Acta Mechanica 149:85–95
7. Williams ML (1959) The stresses around a fault or cracks in dissimilar media. Bull Seismol Soc Am 49:199–204
8. Comninou M (1977) The interface crack. J Appl Mech 44:631–636
9. Martin-Moran CJ, Barber JR, Comninou M (1983) The penny-shaped interface crack with heat flow. Part 1: perfect contact. J Appl Mech 50:29–36
10. Barber JR, Comninou M (1983) The penny-shaped interface crack with heat flow. Part 2: imperfect contact. J Appl Mech 50:770–776
11. Herrmann KP, Loboda VV (2001) Contact zone models for an interface crack in a thermomechanically loaded anisotropic bimaterial. J Therm Stresses 24:479–506
12. Kharun IV, Loboda VV (2004) A thermoelastic problem for interface cracks with contact zones. Int J Solids Struct 41:159–175
13. Kharun IV, Loboda VV (2004) A problem of thermoelasticity for a set of interface cracks with contact zones between dissimilar anisotropic materials. Mech Mater 36:585–600
14. Qin QH, Mai YW (1999) A closed crack tip model for interface cracks in thermopiezoelectric materials. Int J Solids Struct 36:2463–2479
15. Herrmann KP, Loboda VV (2003) Fracture mechanical assessment of interface cracks with contact zones in piezoelectric bimaterials under thermoelectromechanical loadings I. Electrically permeable interface cracks. Int J Solids Struct 40:4191–4217
16. Herrmann KP, Loboda VV (2003) Fracture mechanical assessment of interface cracks with contact zones in piezoelectric bimaterials under thermoelectromechanical loadings II. Electrically impermeable interface cracks. Int J Solids Struct 40:4219–4237
17. Mindlin RD (1974) Equations of high frequency vibration of thermopiezoelectric crystal plates. Int J Solids Struct 10:625–637
18. Clements DL (1983) A thermoelastic problem for a crack between dissimilar anisotropic media. Int J Solids Struct 19:121–130
19. Suo Z, Kuo CM, Barnett DM, Willis JR (1992) Fracture mechanics for piezoelectric ceramics. J Mech Phys Solids 40:739–765
20. Parton VZ, Kudryavtsev BA (1988) Electromagnetoelasticity. Gordon and Breach Science, New York
21. Sokolnikoff IS (1956) Mathematical theory of elasticity. McGraw-Hill, New York
22. Herrmann KP, Loboda VV (2000) Fracture mechanical assessment of electrically permeable interface cracks in piezoelectric bimaterials by consideration of various contact zone models. Arch Appl Mech 70:127–143
23. Nahmein EL, Nuller BM (1986) Contact of an elastic half plane and a particularly unbonded stamp [in Russian]. Prikladnaja matematica i mechanika 50:663–673
24. Ashida F, Tauchert TR (1997) Temperature determination for a contacting body based on an inverse piezothermoelastic problem. Int J Solids Struct 34:2549–2561

Continuous Data Dependence in Linear Theories of Thermoelastodynamics. Part I: Classical Theories. Basics and Logarithmic Convexity

Robin J. Knops[1] and Ramon Quintanilla[2]
[1]The Maxwell Institute of Mathematical Sciences, Heriot-Watt University, Edinburgh, Scotland, UK
[2]Matemática Aplicada 2, Universitat Politècnica de Catalunya, Terrassa, Barcelona, Spain

Overview

Parts I, II, and III, for which this section is a synoptic introduction, present accounts of

Supported by the Project "Ecuaciones en Derivadas Parciales en Termomecanica. Teoria y Aplicaciones" (MTM2009-08150) of the Spanish Ministry of Education

continuous data dependence, or structural stability, in thermoelastodynamics. A corresponding account for thermoelastostatics is presented in [1]. As in that contribution, we focus solely on linear versions of classical and nonclassical theories, with the distinction maintained between linearized and linear formulations.

Specifically, the equations studied are those for small elastic displacements and temperature deviation obtained by linearization of the full nonlinear equations either about a finitely deformed configuration (the linearized, or small deformations superposed upon large, theory) or about the natural configuration (the linear theory). Derivations are provided in [2]. Quasi-static theories are not considered.

A significant feature of linear continuum dynamics is that continuous dependence, and to some extent existence, does not require positive- or even sign-definite elastic coefficients. It follows that sign-definiteness likewise is not required for uniqueness in the initial boundary value problem. Instead, only symmetry of appropriate constitutive tensors, implied by energy conservation, is required. The problem, however, then becomes ill-posed. Fritz John [3] demonstrates how continuous dependence may be recovered provided continuity is understood in the sense of Hölder, weaker than the standard definition, and solutions belong to suitable constraint classes. Different constraint classes, however, may be required for different data. Consequently, linearity is forfeited, and treatments of separate data cannot be linearly superposed.

Several techniques are available to study continuous dependence under these relaxed conditions. Attention is confined to the techniques of logarithmic convexity and the Lagrange identity, essential features of which are briefly introduced in the respective parts to assist understanding. Both methods have been applied in [4–6] to linear elastodynamics, while somewhat earlier, Brun [7] had independently developed the Lagrange identity method to establish uniqueness in linear thermoelastodynamics and viscoelasticity. Although similar results are obtained from either method, both are included for comparative purposes as each offers slightly different advantages.

Logarithmic convexity (Part I) and Lagrange identity (Part II) arguments establish continuous dependence upon data that includes source terms, initial and boundary conditions, and mechanical and thermal constitutive tensors. Uniqueness under the same constitutive conditions may be deduced as a special case of dependence upon initial and boundary data.

Problems forward and backward in time are examined along with both bounded and unbounded regions, and in particular, exterior regions and the half-space. Proofs, details of which may be found in the cited references, are briefly described. Nor is it possible, also due to space limitations, to include the important class of problems that treat continuous dependence for the half-cylinder and similar semi-infinite bodies.

The usual positive-definite conditions recover well-posedness for the forward-in-time problem and enable the standard concept of continuity to be employed in the derivation of continuous data dependence. This permits application, for example, of semigroup theory and conservation laws. Uniqueness is again implied.

Under the same positive-definite conditions, however, the corresponding backward-in-time problem becomes ill-posed, and logarithmic convexity or Lagrange identity methods are employed to study continuous data dependence. Methods for dealing with these different circumstances in classical linear theories are illustrated in Parts I and II. Nonclassical linear theories are discussed in Part III.

Although each part is written independently of the others, all three parts are intended to form a coherent study and may be read as such. In particular, equations, expressions, and notation are often cross-referenced.

A comprehensive survey of the literature is not attempted in any part. Citations are restricted to those that help explain principal features of methods selected for presentation. Techniques not discussed, but possibly suitable for continuous data dependence in thermoelastodynamics, include weighted energy arguments, quasi-reversibility, and others listed by Payne [8].

The treatments outlined here extend easily to weak versions of the problems under consideration, and in consequence, we treat only a strong formulation. Abstract derivations include those provided by Levine [9], Dafermos [10], and Marsden and Hughes [11].

The summation and comma conventions are adopted throughout all three parts, with Roman subscripts having the range $1, 2, 3$. Greek subscripts, with the exception of η and τ which are used as additional time variables, range over $1, 2$. A vector or tensor is loosely denoted by its Cartesian components, but otherwise scalar, vector, and tensor quantities are not typographically distinguished.

Basic Initial Boundary Value Problems

Let Ω denote the (bounded) three-dimensional region occupied by a thermoelastic body in its equilibrium (undeformed) reference configuration, and let $\partial\Omega$ be the Lipschitz continuous smooth boundary of Ω. With respect to a given Cartesian system of rectangular axes, the balance law of linear momentum and the analogous law for heat, which may be either postulated or derived from the first law of thermodynamics, in linear theories are given by

$$t_{ij,j} + \rho_0 f_i = \rho_0 \ddot{u}_i \qquad (x,t) \in Q(T) \qquad (1)$$

$$q_{i,i} + \rho_0 r = \rho_0 \theta_0 \dot{S} \qquad (x,t) \in Q(T) \qquad (2)$$

where a superposed dot indicates differentiation with respect to time t. The maximal interval of existence is $[0, T]; T > 0$, $Q(t) = \Omega \times [0, t]$; $u_i(x,t)$ are the Cartesian components of the increment in displacement vector; $t_{ij}(x,t)$ are those of increments in the first Piola stress tensor; $q_i(x,t)$ are those of the increment in the heat flux vector; $\theta(x,t)$ is the increment in temperature; $S(x,t)$ is the increment in the (scalar) entropy; $\rho_0(x) > 0$ is the positive mass density in the reference configuration; $f_i(x,t)$ are components of the increment in vector body-force per unit mass of the reference configuration; $r(x,t)$ is the increment in (scalar) heat supply per unit mass of the reference configuration; and $\theta_0(x)$ is the reference temperature.

The constitutive relations in the linearized theory assume the form

$$t_{ij} = d_{ijkl} u_{k,l} - \beta_{ij}\theta \qquad (3)$$

$$S = \beta_{ij} u_{i,j} + a\theta \qquad (4)$$

$$q_i = h_{ijk} u_{j,k} + a_i \theta + k_{ij}\theta_{,j} \qquad (5)$$

where $\beta_{ij}(x), h_{ijk}(x), a_i(x), a(x)$ and $k_{ij}(x)$ are Cartesian components of various tensor, vector, and scalar constitutive coefficients assumed to be differentiable and known. The components $d_{ijkl}(x)$ of the elastic coefficient tensor, likewise supposed differentiable, are related to the differentiable elastic moduli $c_{ijkl}(x)$ by

$$d_{ijkl} = c_{ijkl} + \delta_{ik}\sigma_{jl} \qquad (6)$$

in which δ_{ij} denotes the standard Kronecker delta and σ_{ij} are Cartesian components of the symmetric Cauchy stress tensor in the large deformed equilibrium configuration. The elastic moduli possess both major symmetry and minor symmetry:

$$c_{ijkl} = c_{klij} = c_{jikl} \qquad (7)$$

so that the elastic coefficients from (6) possess only the major symmetry:

$$d_{ijkl} = d_{klij} \qquad (8)$$

Since the coefficients d_{ijkl} depend upon the large Cauchy stress σ_{ij}, which can be arbitrarily assigned, there is no *a priori* reason to suppose that they are sign-definite. Consequently, it is important to establish qualitative properties subject only to the symmetry (8). Furthermore, there is scant physical reason for supposing that the elastic moduli c_{ijkl} are sign-definite. The usual arguments are either simplistic, tautological, or occasionally spurious. Furthermore, mere mathematical expediency is inadequate as sole *a priori* justification. However, exploration

of the consequences of such mathematical postulates is perfectly legitimate.

The linear theory, which represents small deviations from the reference configuration, is obtained by setting $\sigma_{ij} = 0$ in the preceding relations. We regard the linear theory as an important, but special, case of the linearized theory and therefore do not explicitly refer to it for sign-indefinite elasticities. A significant difficulty, however, occurs when the elastic moduli are positive-definite. Then, the displacement gradient must be replaced by the symmetric linear strain tensor, and this affects integration by parts and other operations. These aspects are not discussed.

Equations of motion are derived by substitution of the constitutive relations in the balance laws (1) and (2) which, for $(x,t) \in Q(T)$, gives

$$\left(d_{ijkl}u_{k,l} - \beta_{ij}\theta\right)_{,j} + \rho_0 f_i = \rho_0 \ddot{u}_i \tag{9}$$

$$\left(h_{ijk}u_{j,k} + a_i\theta + k_{ij}\theta_{,j}\right)_{,i} + \rho_0 r = \rho_0\theta_0\left(\beta_{ij}\dot{u}_{i,j} + a\dot{\theta}\right) \tag{10}$$

When the primary configuration is at constant temperature, the heat conduction tensor becomes symmetric $(k_{ij} = k_{ji})$, while the constitutive relation for the increment in the heat flux vector simplifies to

$$q_i = k_{ij}\theta_{,j} \tag{11}$$

and consequently (10) is replaced by

$$\left(k_{ij}\theta_{,i}\right)_{,j} + \rho_0 r = \rho_0\theta_0\left(\beta_{ij}\dot{u}_{i,j} + a\dot{\theta}\right) \qquad (x,t) \in Q(T) \tag{12}$$

Material symmetries, for example, isotropy, introduce further simplifications, but these are not considered.

Specification of the initial boundary value problem is completed by adjoining standard initial and boundary conditions to the above field equations. For convenience, attention is restricted mainly to Dirichlet boundary conditions. Accordingly, the boundary conditions for $(x,t) \in \partial\Omega \times [0,T]$ are given by

$$u_i(x,t) = u_i^*(x,t) \qquad \theta(x,t) = \theta^*(x,t) \tag{13}$$

while initial conditions for $x \in \Omega$ are

$$u_i(x,0) = u_i^{(0)}(x) \qquad \dot{u}_i(x,0) = v_i^{(0)}(x) \tag{14}$$

$$\theta(x,0) = \theta^{(0)}(x) \tag{15}$$

where $u_i^*, \theta^*, u_i^{(0)}, v_i^{(0)}, \theta^{(0)}$ are prescribed functions. A further condition stated in Part III supplements (15) in the specification of the initial boundary value problem for nonclassical theories.

Suppose conditions are satisfied such that $\rho_0\theta_0$ is constant, and in consequence (11) and (12) hold. Then, the equations may be rescaled by setting

$$(\rho_0\theta_0)^{1/2}\beta_{ij} = \bar{\beta}_{ij} \tag{16}$$

$$(\rho_0\theta_0)a = \bar{a} \tag{17}$$

$$\theta = (\rho_0\theta_0)^{1/2}\bar{\theta} \tag{18}$$

$$r = (\rho_0\theta_0)^{1/2}\bar{r} \tag{19}$$

Thus, without loss, it is possible to set $\rho_0\theta_0 = 1$ in (9) and (12), provided the heat conduction tensor, k_{ij}, remains unaltered. Henceforth, under the stated conditions, it will be assumed that rescaling has occurred, with the same notation retained for rescaled quantities. As already remarked, the same conditions imply the symmetry

$$k_{ij}(x) = k_{ji}(x) \qquad x \in \Omega \tag{20}$$

Homogeneous boundary data and uniform density and reference temperature ensure that solutions to (9) and the rescaled (12) obey a conservation law.

Define the energy $E(t)$ to be

$$E(t) = \int_\Omega \left[\rho_0 u_{i,t}(t)u_{i,t}(t) + d_{ijkl}u_{i,j}(t)u_{k,l}(t) + a\theta^2(t)\right]dx \tag{21}$$

where the spatial variable in the argument is suppressed. By direct time differentiation of (21) and use of (9) and (12) rescaled, the function $J(t)$ defined by

$$J(t) = E(t) + 2\int_{Q(t)} k_{ij}\theta_{,i}(\eta)\theta_{,j}(\eta)\,dxd\eta \quad (22)$$

satisfies the relation

$$J(t) = J(0) + 2I_1(t) \quad (23)$$

in which

$$I_1(t) = \int_{Q(t)} \rho_0\big(f_i(\eta)u_{i,\eta}(\eta) + r(\eta)\theta(\eta)\big)\,dxd\eta \quad (24)$$

Consequently, $J(t)$ is conserved when source terms vanish.

More generally, consider the unscaled equations (9) and (10), for which $\theta_0(x)$ is not constant, and let

$$W(t) = E(t) + V_1(t) + V_2(t) \qquad t \in [0,T] \quad (25)$$

where $E(t)$ is defined in (21), and

$$V_1(t) = 2\int_{Q(t)} (\rho_0\theta_0)^{-1}k_{ij}\theta_{,i}(\eta)\theta_{,j}(\eta)dxd\eta \quad (26)$$

$$V_2(t) = 2\int_{Q(t)} (\rho_0\theta_0)^{-1}\big[\rho_0\theta_0 A_i(\eta)\theta_{,i}(\eta) - A_i(\eta)\theta(\eta)(\rho_0\theta_0)_{,i}\big]dxd\eta \quad (27)$$

$$A_i(t) = \big(h_{ijk}u_{j,k}(t) + a_i\theta(t)\big) \quad (28)$$

Subject to homogeneous boundary data and uniform mass density, direct differentiation of $W(t)$, and appeal to the unscaled equations (9) and (10), lead to the relation

$$W(t) = W(0) + 2I_1(t) \quad (29)$$

Zero source terms imply that $W(t)$ is conserved.

Existence of Solutions

Existence and uniqueness of weak and strong solutions with finite energy $J(t)$ to the mixed initial boundary value problem for the coupled linear classical thermoelastic system (9) and (12) on a bounded region has been established by Dafermos [10] under conditions that include positive-definiteness of the energy $J(t)$ and symmetry of the thermal coupling tensor, β_{ij}. He appeals to the Riesz representation theorem and also demonstrates that solutions are asymptotically stable with respect to time. Certain conditions, however, permit convergence of the displacement to an undamped oscillation. The same positive-definite condition enables contractive semigroup theory to be alternatively employed in the proof of existence (see [11, p. 360], and [12]).

When positive-definiteness is abandoned, it is shown in the Section entitled "Nonexistence" by a modification of the logarithmic convexity technique that a solution to linear classical problems cannot exist globally in time. Uniqueness, however, still holds.

For isotropic linear classical thermoelasticity, Lebeau and Zuazua [13] demonstrate decay with respect to time of the energy $E(t)$.

Logarithmic Convexity Arguments

Introduction

Logarithmic convexity arguments are employed in partial differential equations, for example, by Agmon [14] and applied to linear theories of elastodynamics by Knops and Payne [4, 5] who further extend the approach to classical thermoelastodynamics [15]. Elements of the method occur in the investigation of n-body dispersion by Lagrange and Jacobi and in treatments of elasticity by Lipschitz [16] and Duhem [17] (see also [18, p. 222]). Here, chief characteristics of the procedure are described before particular

features are sketched of its applications to thermoelastic systems.

A major prerequisite is a conservation law of the form

$$K(t) + V(t) \leq E(0) \qquad t \in [0, T] \tag{30}$$

where $V(t)$, a sign-indefinite function, and $K(t)$, a positive-definite function, are defined on the (weak) solution to the linear initial boundary value problem of concern, and $[0, T]$, $T > 0$ is the maximal interval of existence. Examples of $V(t)$ and $K(t)$ are the potential and kinetic energies. A second positive-definite function, $G(t)$, for example, the $L^2(\Omega)$-norm of the solution, must be identified which by virtue of the governing equations, boundary conditions, and standard inequalities ensures that the function

$$F(t) = G(t) + \gamma_1 (t + t^*)^2 \qquad t \in [0, T] \tag{31}$$

where γ_1 and t^* are positive constants to be chosen, satisfies

$$\dot{F}(t) \leq 2 \left[(G(t) + \gamma_1 (t + t^*)^2)(K(t) + \gamma_1) \right]^{1/2} \tag{32}$$

$$\ddot{F} = 2K(t) - 2V(t) + 2\gamma_1 \tag{33}$$

$$\geq 4(K(t) + \gamma_1) - 2(E(0) + \gamma_1) \tag{34}$$

The sign-indefinite function $V(t)$ has been eliminated by means of (30). Consider the differential inequality

$$\begin{aligned} F(t)\ddot{F}(t) - \dot{F}^2(t) \geq & 4\left\{ F(t)(K(t) + \gamma_1) - \dot{F}^2(t) \right\} \\ & - 2F(t)(E(0) + 2\gamma_1) \\ \geq & -2F(t)(E(0) + 2\gamma_1) \end{aligned} \tag{35}$$

where (35) follows from (32). Suppose that $E(0) < 0$ and choose $2\gamma_1 = -E(0)$ so that $F(t) > 0$, $t \in [0, T]$ and inequality (35) may be written as

$$\frac{d^2}{dt^2} (\ln F(t)) = \frac{F(t)\ddot{F}(t) - \dot{F}^2(t)}{F^2(t)} \geq 0 \tag{36}$$

which indicates that the positive-definite function $F(t)$ possesses a convex logarithm. Jensen's inequality and convexity properties lead to

$$F(t) \leq [F(0)]^{t/T} \, [F(T)]^{(1-t/T)} \tag{37}$$

$$F(t) \geq F(0) \exp \left(t\dot{F}(0)/F(0) \right) \tag{38}$$

where $t \in [0, T]$ and $\dot{F}(0)$ is positive for suitable choice of t^*. These inequalities are used to determine continuous data dependence and growth properties.

Dependence on Initial Data

Applications of logarithmic convexity to linearized classical thermoelasticity are now briefly discussed. Application to nonclassical theories is treated in Part III.

First Treatment

Let Ω be bounded and consider a strong solution to the classical system (9) and (12) rescaled so that $\rho_0 \theta_0 = 1$. The displacement and the temperature are specified everywhere on the boundary $\partial\Omega$, and Cauchy initial data is given by (14) and (15). Assume that $a \neq 0$, together with

$$\max_{\Omega} \left(\beta_{ij} \beta_{ij} + \beta_{ij,j} \beta_{ik,k} \right) \leq M_1^2 \tag{39}$$

where M_1 is a bounded positive constant, and also that there exists a positive constant k_0 such that

$$k_0 \xi_i \xi_i \leq k_{ij} \xi_i \xi_j \qquad x \in \Omega \tag{40}$$

To establish continuous dependence upon initial data, fix all other data and denote the difference in the displacements and temperatures corresponding to two distinct sets of initial data by (u_i, θ), respectively. For this problem, treated in [15], the function $F(t)$ is selected to be

$$F(t) = \int_{Q(t)} \rho_0 u_i u_i \, dx d\eta + (T-t) \times \int_\Omega \rho_0 u_i^{(0)}(x) u_i^{(0)}(x) dx + \gamma_2 \qquad (41)$$

where $t \in [0,T)$, and γ_2 is a positive constant depending upon, and vanishing with, the initial data. The differential inequality corresponding to (35) for $t \in [0,T)$, becomes

$$F\ddot{F} - \left(\dot{F}\right)^2 \geq -c_1 F\dot{F} - 2c_2 F^2 \qquad (42)$$

where c_1, c_2 are computable positive constants. A sequence of standard inequalities is deployed in the derivation of (42), details of which are given in [15]. To proceed further, it must be proved that $F(t)$ does not vanish at any point $t \in [0,T]$ for nonzero initial data. This is equivalent to uniqueness of the displacement or to proving that $F(t)$ is identically zero subject to zero initial data.

It should be remarked that Brun [7, 19], using Lagrange identities discussed in Part II, apparently was the first to prove uniqueness of solutions to coupled linearized thermoelastodynamics under the present assumptions. Nevertheless, the proof based upon logarithmic convexity is included for completeness. Assume the contrary and that there exists an open interval (t_1, t_2) on which $F(t) > 0$. Put $\tau = \exp(-c_2 t)$, and rewrite (42) as

$$\frac{d^2}{d\tau^2}\left[\ln\left(F(\tau)\tau^{-2c_1/c_2^2}\right)\right] \geq 0 \qquad (43)$$

to demonstrate the relationship with logarithmic convexity. Consequently, Jensen's inequality implies for $t_1 \leq t \leq t_2$ that there holds

$$F(\tau)\tau^{-2c_1/c_2^2} \leq \left[F(\tau_1)\tau_1^{-2c_1/c_2^2}\right]^{\frac{(\tau-\tau_2)}{(\tau_1-\tau_2)}} \times \left[F(\tau_2)\tau_2^{-2c_1/c_2^2}\right]^{\frac{(\tau_1-\tau)}{(\tau_1-\tau_2)}} \qquad (44)$$

where $\tau_\alpha = \exp(-c_2 t_\alpha), \alpha = 1,2$. Suppose that $F(t_1) = 0$, which by (44) and continuity implies that $F(t) = 0, t \in [0,t_2]$, and therefore $F(t) = 0$ on $[0,T]$. The contradiction establishes uniqueness and justifies the assumption that $F(t)$ does not vanish at any point of $[0,T]$ for nonzero initial data. Accordingly, (44) holds for $t \in [0,T]$, or equivalently,

$$F(t)\exp(2c_1 t/c_2) \leq [F(0)]^{(1-\delta(t))}\left[F(T)e^{2c_1 T/c_2}\right]^{\delta(t)} \qquad (45)$$

where

$$\delta(t) = \frac{(1-\exp(-c_2 t))}{(1-\exp(c_2 T))} \qquad (46)$$

Assume that the initial temperature, displacement, and velocity are square integrable on Ω and that the initial energy is finite. Then for smooth solutions in the constraint class

$$\int_{Q(T)} \rho_0 u_i u_i \, dx d\eta \leq N_1^2 \qquad (47)$$

for specified positive constant N_1, it follows from (45) that the $L^2(\Omega)$-norm of the displacement depends continuously upon the initial data measured by $F(0)$.

An extension of the argument enables continuous dependence of the temperature upon initial data to be similarly established but with respect to the different choice

$$P(t) = \int_{Q(t)} (t-\eta)\theta^2 \, dx d\eta + \frac{1}{2}\int_{Q(t)} (t-\eta)^2 k_{ij}\theta_{,i}\theta_{,j} \, dx d\eta \qquad (48)$$

See [15] for details.

Second Treatment

An alternative treatment, due to Wilkes [20], again assumes sign-indefinite elasticities and proves logarithmic convexity of the weaker norm

$$G(t) = \int_\Omega \rho_0 u_i u_i \, dx + a^{-1}\int_0^t \int_\Omega k_{ij}\Phi_{,i}\Phi_{,j} \, dx d\eta + \gamma_3 (t+t^*)^2 \qquad (49)$$

where

$$\Phi(x,t) = \widehat{\theta}(x,t)\, d\eta + z(x) \tag{50}$$

γ_3 and t^* are positive constants to be chosen, and for any general integrable function $\psi(x,t)$, $(x,t) \in Q(T)$, the notation

$$\widehat{\psi}(x,t) = \int_0^t \psi(x,\eta) d\eta \tag{51}$$

is introduced.

The scalar function $z(x)$, whose existence is assured by the theory of elliptic equations, is determined as the solution to the boundary value problem

$$\left(k_{ij} z(x)_{,i}\right)_{,j} = \theta^{(0)}(x) + a^{-1}\beta_{ij} u^{(0)}_{i,j}(x) \qquad x \in \Omega \tag{52}$$

$$z(x) = 0 \qquad x \in \partial\Omega \tag{53}$$

The proof avoids the boundedness condition (39) and involves the construction of the differential inequality

$$G(t)\ddot{G}(t) - \left[\dot{G}(t) - a\int_\Omega k_{ij} z_{,i} z_{,j}\, dx\right]^2 \geq -2[aJ(0) + \gamma_3]G(t) \quad (x,t) \in Q(T) \tag{54}$$

where $J(t)$ is the conserved energy defined in (22). Initial conditions that correspond to

$$a\theta^{(0}(x) + \beta_{ij} u^{(0)}_{i,j}(x) = 0 \qquad x \in \Omega \tag{55}$$

lead to $z(x) = 0$, and consequently, when $J(0) \leq 0$, the selection $\gamma_3 = -aJ(0)$, inequality (54) reduces to the convexity of $\ln\, G(t)$, already discussed. When $J(0) > 0$ and $(x,t) \in Q(T)$, (54) may be rewritten as

$$G(t)\ddot{G}(t) - \left[\dot{G}(t)\right]^2 \geq -2\left[1 + \frac{aJ(0)}{\gamma_3}\right] \times \frac{G^2(t)}{(t+t^*)^2} \tag{56}$$

where definition (49) is used. Inequality (56) may be integrated to give (see [21])

$$G(t) \leq \left(1 + \frac{t}{t^*}\right)^{2+\varepsilon} G(0) \exp\frac{t}{T} \times \ln\left[\frac{G(T)}{G(0)}\left(1 + \frac{T}{t^*}\right)^{-2-\varepsilon}\right] \qquad \varepsilon = \frac{2aJ(0)}{\gamma_3} \tag{57}$$

whose further discussion, beyond the present scope, may be found in [21].

Otherwise, two cases are distinguished dependent upon the sign of $J(0)$. For this purpose, set $\gamma_3 = t^* = 0$, and let $t \in [0,T]$. When $J(0) \leq 0$, it is proved ([20]) that

$$G(t) + a(T-t)\int_\Omega k_{ij} z_{,i} z_{,j}\, dx \leq \left[G(0) + aT\int_\Omega k_{ij} z_{,i} z_{,j}\, dx\right]^{(1-t/T)} G(T)^{t/T} \tag{58}$$

whereas when $J(0) > 0$, it follows that

$$G(t) + a(T-t)\int_\Omega k_{ij} z_{,i} z_{,j}\, dx + a^{-1}J(0) \leq e^{t(T-t)}\left[G(0) + aT\int_\Omega k_{ij} z_{,i} z_{,j}\, dx + a^{-1}J(0)\right]^{1-t/T} \times [G(T) + aJ(0)]^{t/T} \tag{59}$$

Either inequality demonstrates that solutions in the class for which $G(T)$ is bounded depend continuously in the sense of Hölder upon initial data in the half-open interval $[0,t)$. Initial data is measured by the first term on the right of each inequality which, besides $G(0)$, also requires

both the integral $A = \int_\Omega k_{ij} z_{,i} z_{,j}\, dx$ and $J(0)$ to be correspondingly small.

These conclusions impose different conditions to those required for the validity of (45) or a similar inequality that involves (48), for which boundedness of temperature at $t = T$ and smallness of A are unnecessary. Note, however, that Wilkes' derivation of continuity does not depend upon the bound (39) for the thermal coupling tensor.

Continuous Dependence upon Other Data

Source Terms and Heat Coupling Tensor

The calculations so far establish continuous dependence only upon initial data. Dependence upon other data may be derived from continuous dependence upon source terms. The problem for the rescaled system (9) and (12) is treated by Ames and Straughan [22, 23], who also appeal to logarithmic convexity and in their discussion simultaneously include dependence upon the heat coupling tensor. All other data are held fixed. Let $f_i^{(\alpha)}, r^{(\alpha)}, \beta_{ij}^{(\alpha)}, \alpha = 1, 2$ be two different sets of source terms and heat coupling tensor, and $(u_i^{(\alpha)}, \theta^{(\alpha)})$ be the corresponding displacements and temperatures. Set

$$u_i = u_i^{(2)} - u_i^{(1)} \qquad \theta = \theta^{(2)} - \theta^{(1)} \tag{60}$$

$$f_i = f_i^{(2)} - f_i^{(1)} \qquad r = r^{(2)} - r^{(1)} \tag{61}$$

$$\bar{\beta}_{ij} = \beta_{ij}^{(2)} - \beta_{ij}^{(1)} \tag{62}$$

Substitution in (9) and (12) of the difference between the solutions to the initial boundary value problems for the different coupling coefficients and source terms leads to the equations

$$\left(d_{ijkl} u_{k,l} - \beta_{ij}^{(2)} \theta\right)_{,j} + \rho_0 f_i - \left(\bar{\beta}_{ij}\, \theta^{(1)}\right)_{,j} = \rho_0\, \ddot{u}_i \tag{63}$$

$$\left(k_{ij} \theta_{,i}\right)_{,j} + \rho_0 r - \bar{\beta}_{ij}\, \dot{u}_{i,j}^{(1)} = \beta_{ij}^{(2)}\, \dot{u}_{i,j} + a\dot{\theta} \tag{64}$$

subject to homogeneous initial and boundary conditions for (u_i, θ).

Recall the notation (51) and consider the function

$$H(t) = \int_{Q(t)} \rho_0 u_i(\eta) u_i(\eta)\, dx d\eta + \int_{Q(t)} (t - \eta) k_{ij}\, \widehat{\theta}_{,i}(\eta)\, \widehat{\theta}_{,j}(\eta)\, dx d\eta + \gamma_4 \tag{65}$$

where the positive constant γ_4 is given by

$$\gamma_4 = \int_{Q(T)} \left[f_i(\eta) f_i(\eta) + 2\, \bar{\beta}_{ij}(\eta)\, \bar{\beta}_{ij}(\eta) + \bar{\beta}_{ij,j}(\eta)\, \bar{\beta}_{ik,k}(\eta) + r^2(\eta) + \widehat{r}^2(\eta)\right] dx d\eta \tag{66}$$

Differentiation, substitution from (63) and (64), followed by integration by parts, and appeal to standard inequalities show that $H(t)$ satisfies the differential inequality

$$H\ddot{H} - \left(\dot{H}\right)^2 \geq -c_3 H^2 \tag{67}$$

for computable positive constant c_3. But $H(t) > 0$ for $t \in [0, T]$ and consequently inequality (67) may be integrated to yield

$$H(t) \leq \exp(c_3 t(T - t)/2) H(0)^{(1 - t/T)} H(T)^{t/T} \tag{68}$$

where $t \in [0, T]$. Assume solutions belong to the constraint class in which displacement and temperature gradients possess bounded $L^2(Q(T))$-norms, so that $H(T) \leq N_2$, for positive constant N_2. Because $H(0) = \gamma_4$, it follows from (68) that the solution in measure $H(t)$ depends Hölder continuously upon source terms and coupling tensor.

Boundary Data

Continuous dependence upon boundary data is illustrated for Dirichlet data. Let $u_i^{*(\alpha)}(x, t), \theta^{*(\alpha)}(x, t)$, where $(x, t) \in \partial\Omega \times [0, \mathrm{T}]$, $\alpha = 1, 2$ be two specified sets of boundary data

and assume all other data are held fixed. Without confusion with the previous notation, let $u_i^{(\alpha)}, \theta^{(\alpha)}$ be the displacement and temperature in the corresponding problems, and let the respective differences be $u_i = u_i^{(2)} - u_i^{(1)}, \theta = \theta^{(2)} - \theta^{(1)}$, which accordingly satisfy (9) and (12) with zero source terms and initial data, but nonzero boundary data. Introduce the following decompositions for $(x,t) \in Q(T)$:

$$u_i(x,t) = H_i(x,t) + w_i(x,t) \tag{69}$$

$$\theta(x,t) = h(x,t) + \phi(x,t) \tag{70}$$

where

$$\rho_0 \ddot{H}_i = H_{i,jj} \qquad (x,t) \in Q(T) \tag{71}$$

$$H_i(x,0) = \dot{H}_i(x,0) = 0 \qquad x \in \Omega \tag{72}$$

and when $(x,t) \in \partial\Omega \times [0,T]$

$$H_i(x,t) = u_i^{**}(x,t) \equiv u_i^{*(2)}(x,t) - u_i^{*(1)}(x,t) \tag{73}$$

with analogous conditions for $h(x,t)$. The pair (w_i, ϕ) satisfies rescaled versions of (9) and (12) subject to homogeneous boundary conditions and with source terms given by

$$\rho_0 f_i = \left(d_{ijkl} H_{k,l} - \beta_{ij} h\right)_{,j} - \rho_0 \ddot{H}_i \tag{74}$$

$$\rho_0 r = \left(k_{ij} h_{,i}\right)_{,j} - a\dot{h} - \beta_{ij} \dot{H}_{i,j} \tag{75}$$

Substitution of the expressions (74) and (75) in (66), where terms in $\bar{\beta}_{ij}$ are no longer present, introduces terms in H_i, h, and their appropriate partial derivatives which must be bounded above by the given boundary data u_i^{**}, θ^{**}. For this purpose, let $p_i(x,\eta)$ be the solution to the dual problem, which for fixed t is specified by

$$\begin{aligned} p_{i,jj} - \rho_0 p_{i,\eta\eta} &= \rho_0 H_i(x,\eta) \quad (x,\eta) \in Q(t) \\ p_i(x,t) = \dot{p}_i(x,t) &= 0 \qquad x \in \Omega \\ p_i(x,\eta) &= 0 \qquad (x,\eta) \in \partial\Omega \times [0,t] \end{aligned}$$

with an analogous dual problem defined for the function $h(x,\eta)$.

A Rellich identity ([5]) is used in the derivation of the bound

$$\int_{Q(t)} \rho_0 H_i H_i \, dx d\eta \le c_4 \int_{Q(t)} u_i^{**} u_i^{**} \, dx d\eta$$

for computable positive constant c_4, which, together with a similar bound for h, use of estimates given in [24, 25], ultimately yields the desired bound, a typical component of which is

$$\int_{Q(T)} w_i w_i \, dx d\eta \le c_5 \left[\int_0^T \int_{\partial\Omega} \left(D_s^2 u_i^{**} D_s^2 u_i^{**} + D_s u_i^{**} D_s u_i^{**} + u_i^{**} u_i^{**} + \rho_0 u_{i,\eta\eta}^{**} u_{i,\eta\eta}^{**} \right) dS d\eta \right]^{t/T}$$

Here, c_5 is a computable positive constant, and D_s denotes the tangential derivative on the surface $\partial\Omega$. Corresponding bounds for ϕ and its time integral are obtained in similar manner. Consequently, continuous dependence upon Dirichlet boundary data is established. Precise calculations are easily adapted from [5].

Other Data

The argument of the previous section may be used to establish continuous dependence upon other constitutive coefficients, since the difference in solutions to problems for different coefficients leads to a problem of the form just discussed for nonzero source terms. Logarithmic convexity, however, is less suited to establish continuous dependence on initial geometry which is better treated by means of Lagrange identity arguments. See Part II.

Nonexistence

Wilkes [26] has applied logarithmic convexity arguments to demonstrate conditions under which the solution cannot exist globally. His procedure demonstrates that, subject to appropriate initial data, the function $G(t)$ defined in (49) possesses an exponentially increasing lower bound. The scaling operation described in [26] leads to the conclusion that the solution does not generate a semigroup and therefore cannot globally exist in time. In conjunction with results mentioned in the Section entitled

"Existence of Solutions," this conclusion implies that positive-definiteness of both elasticities and heat conduction tensor is necessary for the solution to globally exist in the form of a semi-group.

Part II examines similar properties of continuous data dependence for the initial boundary value problems of linearized classical thermoelasticity but by the alternative method of Lagrange identities. Modifications demanded by linear theories are briefly considered. Part II in addition includes a discussion of how sign-definite assumptions improve these properties.

Notation

Ω	Three-dimensional reference spatial region occupied by thermoelastic body
$\partial\Omega$	Lipschitz continuous smooth boundary of Ω
$[0,T], T>0$	Maximal closed interval of existence
t	Time variable (scalar)
x	Position vector
$Q(t)$	$\Omega \times [0,t]$
$u_i(x,t)$	Cartesian components of increment in displacement vector
$t_{ij}(x,t)$	Cartesian components of increment in first Piola stress tensor
σ_{ij}	Cartesian components of symmetric (large) Cauchy stress tensor
$q_i(x,t)$	Cartesian components of increment in heat flux vector
$\theta(x,t)$	Increment in scalar temperature
$\theta_0(x)$	Scalar reference temperature
$S(x,t)$	Increment in scalar entropy
$a(x)$	Scalar thermal capacity
$\rho_0(x)$	Mass density in reference configuration
$f_i(x,t)$	Cartesian components of increment in body-force per unit mass in reference configuration
$r(x,t)$	Increment of scalar heat supply per unit mass of reference configuration
$d_{ijkl}(x)$	Cartesian components of linearized elastic coefficient tensor
$c_{ijkl}(x)$	Cartesian components of linear elastic moduli tensor
δ_{ij}	Kronecker delta
k_{ij}	Cartesian components of heat conduction tensor
$\Omega(t_1,t_2)$	$\Omega \times Q(t_1,t_2)$
β_{ij}	Cartesian components of heat coupling tensor
$h_{ijk}, \quad a_i$	Cartesian components of material heat coefficient tensors
$E(t)$	Total energy of classical linearized thermoelastic system
$J(t)$	Augmented total energy of classical linearized system
$K(t)$	Kinetic energy of classical linearized thermoelastic system
$V(t)$	Potential energy of classical linearized thermoelastic system
$I_1(t)$	Total work done by supply terms
$F(t), G(t), H(t)$	Various solution measures
$Z(t)$	Supply term measure
α	Scalar thermal displacement
G_{ijk}, b_i, b_{ij}	Cartesian components of nonclassical thermomechanical coefficient tensors
$E_{III}(t)$	Total energy of linearized nonclassical Green-Naghdi system of type III without center of symmetry
$J_{III}(t)$	Augmented energy of linearized nonclassical Green-Naghdi system of type III without center of symmetry
$\tilde{E}_{III}(t)$	Total perturbed energy of linearized nonclassical Green-Naghdi system of type III with center of symmetry
$P_{III}(t)$	Total work done by source terms in perturbed linearized nonclassical Green-Naghdi system of type III with center of symmetry
M_i, N_i	Various specified constants

References

1. Knops RJ, Quintanilla R (2012) Spatial and structural stability in thermoelastostatics. Encyclopedia of thermal stresses (to appear)
2. Green AE (1962) Thermoelastic stresses in initially stressed bodies. Proc Roy Soc Lond A266:1–19
3. John F (1960) Continuous dependence on data for solutions of partial differential equations with a prescribed bound. Comm Pure Appl Math 13:551–585
4. Knops RJ, Payne LE (1968) Uniqueness in classical elastodynamics. Arch Ration Mech Anal 27:171–183
5. Knops RJ, Payne LE (1969) Continuous data dependence for the equations of classical elastodynamics. Math Proc Camb Phil Soc 66:481–491
6. Knops RJ, Payne LE (1988) Improved estimates for continuous data dependence in linear elastodynamics. Math Proc Camb Phil Soc 103:535–559
7. Brun L (1969) Méthodes énergétiques dans les systémes évolutifs linéaires. Premiére Partie: Séparation des énergies. Deuxiéme Partie: Théorémes d'unicité. J de Mech 8:125–166, 167–192

8. Payne LE (1975) Improperly posed problems in partial differential equations. Regional Conference Series in Applied Mathematics. SIAM, Philadelphia
9. Levine HA (1970) On a theorem of Knops and Payne in dynamical linear thermoelasticity. Arch Ration Mech Anal 38:290–319
10. Dafermos CM (1968) On the existence and the asymptotic stability of solutions to the equations of linear thermoelasticity. Arch Ration Mech Anal 29:241–271
11. Marsden JE, Hughes TJR (1983) Mathematical Foundations of Elasticity. Prentice-Hall, Englewood Cliffs
12. Navarro CB (1978) Asymptotic stability in linear thermovisco-elasticity. J Math Anal Appl 65:399–431
13. Lebeau G, Zuazua E (1999) Decay rates for the three-dimensional linear system of thermoelasticity. Arch Ration Mech Anal 148:179–231
14. Agmon S (1966) Unicité et convexité dans les problémes differentials. Sem Math Sup (1965). University Press, Montreal
15. Knops RJ, Payne LE (1970) On uniqueness and continuous dependence in dynamical problems of linear thermoelasticity. Int J Solids Struct 6:1173–1184
16. Lipschitz R (1874) Beweis eines satzes der elasticitätslehre. J Reine Angew Math 78:329–337
17. Duhem P (1906) Recherches sur l'Élasticité. Gauthier-Villars, Paris
18. Knops RJ, Wilkes EW (1973) Theory of Elastic Stability. In: Flügge S, Truesdell C (eds) Handbuch der Physik, vol VIa/3. Springer, Heidelberg/New York
19. Brun L (1965) Sur l'unicité en thermoélasticité dynamique et diverses expressions analogues la formule de Clapeyron. Comptes Rend Acad Sci Paris 261:2584–2587
20. Wilkes NS (1980) Continuous dependence and instability in linear thermoelasticity. SIAM J Appl Math 11:292–299
21. Knops RJ, Payne LE (1971) Growth estimates for solutions of evolutionary equations in Hilbert space with applications in elastodynamics. Arch Ration Mech Anal 41:363–398
22. Ames KA, Straughan B (1992) Continuous dependence results for initially prestressed thermoelastic bodies. Int J Eng Sci 30:7–13
23. Ames KA, Straughan B (1997) Non-standard and Improperly Posed Problems. Academic, San Diego/London
24. Bramble JH, Hubbard BE (1961) Some higher order identities with applications to boundary techniques. Nat Bur Stand Sect B 65:269–276
25. Sigillito V (1967) A priori inequalities and pointwise bounds for solutions of fourth order elliptic partial differential equations. SIAM J Appl Math 15:1136–1155
26. Wilkes NS (1980) On the non-existence of semigroups for some equations of continuum mechanics. Proc Roy Soc Edin A86:303–306

Continuous Data Dependence in Linear Theories of Thermoelastodynamics. Part II: Classical Theories, Lagrange Identity Methods, and Positive-Definite Arguments

Robin J. Knops[1] and Ramon Quintanilla[2]
[1]The Maxwell Institute of Mathematical Sciences, Heriot-Watt University, Edinburgh, Scotland, UK
[2]Matemática Aplicada 2, Universitat Politècnica de Catalunya, Terrassa, Barcelona, Spain

Overview

The reader is referred to the overview of Part I for a general introduction and to the section entitled "Basic Initial Boundary Value Problems," also in Part I, for the linear classical problems discussed in this Part and for the notation adopted throughout all Parts. Attention, here, however, is devoted to applications of the Lagrange identity method. Although most problems are amenable to logarithmic convexity techniques, continuous dependence upon initial geometry is selected for explicit separate treatment using Lagrange identities. Later sections consider modifications resulting from various positive-definite assumptions. The section entitled "Existence of Solutions" and the subsection entitled "Nonexistence" of the section entitled "Continuous Dependence upon Other Data" belonging to Part I.

An early appearance of Lagrange identities occurs in the context of ordinary differential equations. The extension to linear thermoelastodynamics was first achieved apparently by Brun [1, 2] as part of a comprehensive discussion primarily directed at proofs of uniqueness and stability notable for not requiring sign-definite elasticities. Subsequently, the technique has been used by several authors to establish not only uniqueness but also continuous dependence upon various data again without sign-definiteness

elasticities, provided that solutions belong to various constraint classes. The method, not devoid of subtlety, derives from a reciprocal property and introduction of corresponding adjoint systems. Several versions of the identity are possible, including those valid only on the half-open interval $[0, T/2)$. Extension to the whole interval $[0, T)$ is by iteration. Moreover, as with logarithmic convexity, continuity is in the weaker sense of Hölder. A consequence for strong solutions is an energy conservation law, which Rionero and Chirita [3] show is unnecessary for either uniqueness or continuous data dependence. For weak solutions, energy conservation must be separately postulated. Levine [4] extends the application of the Lagrange identity method to weak solutions for isothermal elasticity and emphasizes that energy conservation likewise is not required for uniqueness.

Many of the arguments applied in the context of thermoelasticity are extensions of those developed for elasticity. See, for example, [5].

Although unnecessary for the Lagrange identities themselves, the thermal conductivity tensor, nevertheless, is assumed to be positive definiteness when continuous data dependence is being discussed.

Lagrange Identities

Suppose that $(u_i(x,t), \theta(x,t))$ represent the displacement and temperature belonging to the rescaled system (9) and (12) of Part I. Let $(w_i(x,t), \phi(x,t))$ be the solution to the adjoint system defined on $Q(T)$ by

$$\left(d_{ijkl} w_{k,l}(\eta) - \beta_{ij}\phi(\eta)\right)_{,j} + \rho_0 f_i^*(\eta) = \rho_0 \ddot{w}_i(\eta) \tag{1}$$

$$-\left(k_{ij}\phi_{,i}(\eta)\right)_{,j} + \rho_0 r^*(\eta) = \beta_{ij}\dot{w}_{i,j}(\eta) + a\dot{\phi}(\eta) \tag{2}$$

where $f_i^*(x,t), r^*(x,t)$ are source terms. Dependence upon the spatial argument is implied.

Assume homogeneous Dirichlet boundary conditions of the form $u_i = w_i = \theta = \phi = 0$ for $x \in \partial\Omega$, and let

$$Q(t_1, t_2) = \Omega \times [t_1, t_2] \qquad Q(t) = Q(0, t) \tag{3}$$

Multiplication of the rescaled equations (9) and (12) of Part I, respectively, by $\dot{w}_i$ and ϕ, added to (1) and (2) multiplied, respectively, by $\dot{u}_i$ and θ, after integration by parts over $Q(t)$ leads to (cp. [6])

$$\begin{aligned}&\int_\Omega \left(\rho_0 \dot{u}_i\ \dot{w}_i + d_{ijkl} u_{i,j} w_{k,l} + a\theta\phi\right) dx\Big|_0^t \\ &= \int_{Q(t)} \rho_0 \left(f_i(\eta) w_{i,\eta}(\eta) + f_i^*(\eta) u_{i,\eta}(\eta)\right) dx d\eta \\ &\quad + \int_{Q(t)} \rho_0 (r(\eta)\phi(\eta) + r^*(\eta)\theta(\eta))\, dx d\eta\end{aligned} \tag{4}$$

Three different identities may now be deduced for particular choices of the functions (w_i, ϕ) and source terms (f_i^*, r^*). The substitution

$$w_i(x,\eta) = u_i(x,\eta) \quad \phi(x,\eta) = \theta(x,\eta) \tag{5}$$

converts the adjoint equation (2) into the original rescaled equation (12) of Part I provided the heat source is given by

$$r^* = 2\left(k_{ij}\theta_{,i}\right)_{,j} + r \tag{6}$$

Identity (4) then reduces to the conservation law (23) for $J(t)$ obtained in Part I.

Discussion of the second and third identities is facilitated by introduction of the definitions

$$K(t_1, t_2) = \int_\Omega \rho_0 u_{i,t}(t_1) u_{i,t}(t_2)\, dx \tag{7}$$

$$V(t_1, t_2) = \int_\Omega d_{ijkl} u_{i,j}(t_1) u_{k,l}(t_2)\, dx \tag{8}$$

$$W(t_1, t_2) = \int_\Omega a\theta(t_1)\theta(t_2)\, dx \tag{9}$$

where $0 \le t_1 \le t_2 \le T$. Consider, for fixed t and for $0 \le \eta \le 2t \le T$, the choice

$$w_i(\eta) = \frac{\partial u_i}{\partial \eta}(2t-\eta)$$
$$\phi(\eta) = \frac{\partial \theta}{\partial \eta}(2t-\eta) \tag{10}$$

for which the appropriate source terms are

$$f_i^*(\eta) = \frac{\partial f_i}{\partial \eta}(2t-\eta) \qquad r^*(\eta) = -\frac{\partial r}{\partial \eta}(2t-\eta) \tag{11}$$

Substitution in the fundamental identity (4) succeeded by integration over $[0,t]$ leads to the second identity, valid for $t \in [0, T/2]$:

$$\begin{aligned}
&K(t,t) - V(t,t) - W(t,t) \\
&\quad = K(0,0) - V(0,0) - W(0,0) \\
&\qquad + \int_\Omega \Big(\rho_0 u_{i,t}(0)\{u_{i,t}(2t) - u_{i,t}(0)\} \\
&\qquad - d_{ijkl} u_{i,j}(0)\{u_{k,l}(2t) - u_{k,l}(0)\} \\
&\qquad - a\theta(0)\{\theta(2t) - \theta(0)\}\Big)\, dx \\
&\qquad + 2\int_0^t \Bigg[\int_{Q(0,s)} f_i(\eta) u_{i,\eta\eta}(\tau)\, dx d\eta \\
&\qquad - \int_{Q(s,2s)} f_i(\eta) u_{i,\eta\eta}(\tau)\, dx d\eta \\
&\qquad + \int_\Omega \big(f_i(s) u_{i,s}(s) - f_i(2s) u_{i,t}(0) \big)\, dx \Bigg] ds \\
&\qquad + 2\int_0^t \Bigg[\int_{Q(0,s)} r(\eta)\theta_{,\eta}(\tau)\, dx d\eta \\
&\qquad - \int_{Q(s,2s)} r(\eta)\theta_{,\eta}(\tau)\, dx d\eta \\
&\qquad - \int_\Omega \big(r(s)\theta(s) - r(2s)\theta(0) \big)\, dx \Bigg] ds
\end{aligned} \tag{12}$$

where $\tau = 2t - \eta$ and $t \in [0, T/2]$.

The third identity is established by setting

$$\begin{aligned} w_i(\eta) &= u_i(2t-\eta) \\ \phi(\eta) &= \theta(2t-\eta) \end{aligned} \qquad 0 \le \eta \le 2t < T \tag{13}$$

and noting that $w_{i,\eta}(\eta) = -u_{i,\tau}(\tau)$, $\phi_{,\eta}(\eta) = -\theta_{,\tau}(\tau)$, $\tau = 2t - \eta$. Consequently, we have

$$\begin{aligned} f_i^*(\eta) &= f_i(2t-\eta) \\ r^*(\eta) &= -r(2t-\eta) \end{aligned} \qquad 0 \le \eta \le 2t < T \tag{14}$$

and substitution in (4) gives

$$\begin{aligned}
K(t,t) - V(t,t) - W(t,t) &= K(0,2t) - V(0,2t) \\
&\quad - W(0,2t) + \int_{Q(t,2t)} u_{i,\eta}(\eta) f_i(2t-\eta)\, dx d\eta \\
&\quad - \int_{Q(0,t)} u_{i,\eta}(\eta) f_i(2t-\eta)\, dx d\eta \\
&\quad + \int_{Q(0,2t)} \theta(\eta) r(2t-\eta)\, dx d\eta
\end{aligned} \tag{15}$$

where $0 \le 2t < T$.

Variants of the last identity are obtained as follows. Retain the previous notation, and let $u_i(x,t)$, $w_i(x,t)$, $\theta(x,t)$, and $\phi(x,t)$ denote sufficiently smooth functions. Suppose that (u_i, θ) satisfy suitably rescaled equations (9) and (12) of Part I, subject to source terms $f_i(x,t)$ and $r(x,t)$. But instead of (12) in Part I, consider its time integral:

$$\begin{aligned} &\Big(k_{ij}\, \widehat{\theta}_{,i}\,(t) \Big)_{,j} + \rho_0 \widehat{r}(t) + C = \beta_{ij} u_{i,j}(t) + a\, \dot{\widehat{\theta}}(t) \\ &\qquad (x,t) \in Q \end{aligned} \tag{16}$$

where the function $C(x) = a\theta(0) + \beta_{ij} u_{i,j}(0)$ vanishes with initial data and $\widehat{\theta}$ is defined by (51) in Part I.

Denote source terms by f_i^*, r^*, and suppose the pair (w_i, ϕ) for $(x,t) \in Q(T)$ satisfies the adjoint system

$$\big(d_{ijkl} w_{k,l}(t) - \beta_{ij}\phi(t) \big)_{,j} + \rho_0 f_i^*(t) = \rho_0 w_{i,tt}(t) \tag{17}$$

$$-\Big(k_{ij}\, \widehat{\phi}_i\,(t) \Big)_{,j} + \rho_0\, \widehat{r}^{\,*}\,(t) + C = \beta_{ij} w_{i,j}(t) + a\, \dot{\widehat{\phi}}(t) \tag{18}$$

For simplicity, assume that Ω is bounded and that the respective boundary conditions are homogeneous.

Operations similar to those leading to (4) establish the Lagrange identity (cp., Rionero and Chirita [3], and Ames and Payne [7]):

$$\begin{aligned}
&\int_\Omega \rho_0 \left[u_i(\eta) w_{i,\eta}(\eta) - u_{i,\eta}(\eta) w_i(\eta)\right] dx\Big|_0^t \\
&= \int_{Q(t)} \rho_0 \left[u_i(\eta) w_{i,\eta\eta}(\eta) - u_{i,\eta\eta}(\eta) w_i(\eta)\right] dx d\eta \\
&= \int_{Q(t)} \left[\beta_{ij} u_{i,j}(\eta)\phi(\eta) - \beta_{ij} w_{i,j}(\eta)\theta(\eta)\right] dx d\eta \\
&= \int_{Q(t)} \rho_0 \left(f_i^*(\eta) u_i(\eta) - f_i(\eta) w_i(\eta)\right) dx d\eta
\end{aligned} \tag{19}$$

by virtue of the symmetry relation (8) and (9), both of Part I, along with the adjoint equation (17). Appeal to (16) and (18) succeeded by spatial integration by parts and time integration then yields

$$\begin{aligned}
&\int_\Omega \rho_0 \left[u_i(\eta) w_{i,\eta}(\eta) - u_{i,\eta}(\eta) w_i(\eta)\right] dx\Big|_0^t \\
&= -\int_{Q(t)} \left(k_{ij} \widehat{\theta}_{,i}(\eta)\phi_{,j}(\eta) + k_{ij} \widehat{\phi}_{,i}(\eta)\theta_{,j}(\eta)\right. \\
&\quad \left. + C\left[\phi(\eta) - \theta(\eta)\right]\right) dx d\eta \\
&\quad + \int_{Q(t)} \rho_0 \left\{f_i^*(\eta) u_i(\eta) - f_i(\eta) w_i(\eta)\right. \\
&\quad \left. + \widehat{r}(\eta)\phi(\eta) - \widehat{r}^*(\eta)\theta(\eta)\right\} dx d\eta \\
&= -\int_\Omega k_{ij} \widehat{\theta}_{,i}(t) \widehat{\phi}_{,j}(t)\, dx \\
&\quad + \int_\Omega k_{ij} \widehat{\theta}_{,i}(0) \widehat{\phi}_{,j}(0)\, dx + I_2(t)
\end{aligned} \tag{20}$$

where

$$\begin{aligned}
I_2(t) = &\int_{Q(t)} C[\phi(\eta) - \theta(\eta)]\, dx d\eta \\
&+ \int_{Q(t)} \rho_0 \left[f_i^*(\eta) u_i(\eta) - f_i(\eta) w_i(\eta).\right. \\
&\left. + \widehat{r}(\eta)\phi(\eta) - \widehat{r}^*(\eta)\theta(\eta)\right] dx d\eta
\end{aligned} \tag{21}$$

Fix t and take $w_i(\eta) = u_i(\tau)$ and $\phi(\eta) = \theta(\tau)$, where $\tau = 2t - \eta$, so that

$$\widehat{\phi}(\eta) = -\widehat{\theta}(\tau) \quad f_i^*(\eta) = f_i(\tau) \quad \widehat{r}^*(\eta) = \widehat{r}(\tau) \tag{22}$$

In consequence, identity (20) becomes, for $0 \le 2t < T$,

$$\begin{aligned}
&\int_\Omega k_{ij} \widehat{\theta}_{,i}(t) \widehat{\theta}_{,j}(t)\, dx + 2\int_\Omega u_i(t) u_{i,t}(t)\, dx \\
&\quad = \int_\Omega \rho_0 \left[u_i(0) u_{i,t}(2t) + u_i(2t) u_{i,t}(0)\right] dx + I_3(t)
\end{aligned} \tag{23}$$

where

$$\begin{aligned}
I_3(t) = &\int_{Q(t)} \rho_0 \left[f_i(\eta) u_i(\tau) - f_i(\tau) u_i(\eta)\right] dx d\eta \\
&+ \int_{Q(t)} \rho_0 \left[\widehat{r}(\tau)\theta(\eta) - \widehat{r}(\eta)\theta(\tau)\right] dx d\eta \\
&+ \int_{Q(t)} C(\theta(\tau) - \theta(\eta))\, dx d\eta
\end{aligned} \tag{24}$$

Continuous data dependence may be established using any of the previous identities, and in the later section entitled "Continuous Dependence on Source Terms and Related Data," identity (20) is employed to illustrate the procedure. Meanwhile, uniqueness is discussed for the initial boundary value problem which, juxtaposed to the corresponding proof by logarithmic convexity, enables their respective advantages and disadvantages to be contrasted.

Uniqueness

Uniqueness in the linearized coupled thermoelastic initial boundary value problem on bounded regions, first due to Brun [1, 2], is proved by demonstrating that at most only the trivial solution can exist to the problem with homogeneous data. As usual, the proof is by contradiction. Assume that there exists a smooth

non-identically zero displacement $u_i(x,t)$ and temperature $\theta(x,t)$ on the maximal interval of existence $[0,T]$ to the rescaled equations (9) and (12) of Part I subject to zero source terms and zero initial and boundary data. In his proof, Brun [1, 2] combines conservation of energy expressed by (23) in Part I and explicitly given by

$$J(t) \equiv K(t,t) + V(t,t) + W(t,t) + 2\int_{Q(t)} k_{ij}\theta_{,i}\theta_{,j}\,dxd\eta = 0 \qquad (x,t) \in Q(T) \tag{25}$$

with relation (12) which becomes

$$K(t,t) - V(t,t) - W(t,t) = 0 \qquad t \in [0, T/2) \tag{26}$$

Addition of the last two expressions eliminates the term with the indefinite elasticities d_{ijkl} and gives

$$K(t,t) + \int_{Q(t)} k_{ij}\theta_{,i}\theta_{,j}\,dxd\eta = 0 \qquad (x,t) \in Q(T/2) \tag{27}$$

which by virtue of the positive-definite heat conduction tensor specified by (40) of Part I implies that $\dot{u}_i(x,t) = \theta_{,i}(x,t) = 0$, $(x,t) \in Q(T/2)$. Consequently, the conclusions $u_i(x,t) = u_i(x) = 0$, $(x,t) \in Q(T/2)$ follow from the homogeneous initial conditions, while $\theta(x,t) = \theta(t) = 0$, $t \in [0, T/2]$ follow from the homogeneous boundary conditions and continuity. In summary,

$$u_i(x,t) = \theta(x,t) = 0 \qquad (x,t) \in Q(T/2) \tag{28}$$

These results show that $u_i(x, T/2) = \dot{u}_i(x, T/2) = \theta(x, T/2) = 0$, $x \in \Omega$. Accordingly, the procedure may be repeated for the interval $[T/2, T/2 + T/4]$ so that (28) is extended to $Q(3T/4)$ and by further iterations to $Q(T)$. The contradiction proves that the solution is unique.

Brun's proof as described above relies upon energy conservation. An alternative proof due to Rionero and Chirita [3], explained in the next section, avoids this property and consequently may be extended to weak solutions. See Levine [4, 8] for an abstract version.

Continuous Dependence on Source Terms and Related Data

Consideration of continuous data dependence is commenced by a description of dependence simultaneously upon source terms and initial data. The argument differs slightly from that developed by Rionero and Chirita [3], an account of which is presented also in [9, pp. 264–267]. Furthermore, the approach provides an alternative proof of uniqueness to that originally devised by Brun [2], and does not depend upon energy conservation. As just mentioned, the distinction is important in the discussion of weak solutions. Initial and boundary data are again supposed to be zero. The Lagrange identity in the form (23) under the stated conditions and after an application of Schwarz's inequality yields

$$\begin{aligned}
&2\int_\Omega \rho_0 u_i(t) u_{i,t}(t)\,dx + \int_\Omega k_{ij}\widehat{\theta}_{,i}(t)\,\widehat{\theta}_{,j}(t)\,dx \\
&\le \left[\int_{Q(t)} \rho_0\left(f_i(\eta)f_i(\eta) + f_i(\tau)f_i(\tau) + \widehat{r}^2(\eta) + \widehat{r}^2(\tau)\right)dxd\eta\right]^{1/2} \\
&\times \left[\int_{Q(t)} \rho_0(u_i(\eta)u_i(\eta) + u_i(\tau)u_i(\tau) + \theta^2(\eta) + \theta^2(\tau))\,dxd\eta\right]^{1/2} \\
&= \left[\int_{Q(2t)} \rho_0\left(f_i(\eta)f_i(\eta) + \widehat{r}^2(\eta)\right)dxd\eta\right]^{1/2} \\
&\quad \times \left[\int_{Q(2t)} \rho_0\left(u_i(\eta)u_i(\eta) + \theta^2(\eta)\right)dxd\eta\right]^{1/2}
\end{aligned} \tag{29}$$

Consider solutions in the constraint class

$$\int_{Q(T)} \rho_0\left(u_i(\eta)u_i(\eta) + \theta^2(\eta)\right)dxd\eta \le N_3^2 \tag{30}$$

for specified positive constant N_3. Let $0 < 2s \leq T$, and integrate inequality (29) over $(0, s)$ to give

$$\int_\Omega \rho_0 u_i(s) u_i(s)\, dx + \int_{Q(s)} k_{ij}\, \widehat{\theta}_{,i}(\eta)\, \widehat{\theta}_{,j}(\eta)\, dxd\eta \leq s \left[\int_{Q(T)} \rho_0 (f_i(\eta) f_i(\eta) + \widehat{r}^2(\eta))\, dxd\eta\right]^{1/2} \times \left[\int_{Q(T)} \rho_0 \left(u_i(\eta) u_i(\eta) + \theta^2(\eta)\right) dxd\eta\right]^{1/2} \leq \frac{1}{2} T N_3 \left[\int_{Q(T)} \rho_0 (f_i(\eta) f_i(\eta) + \widehat{r}^2(\eta))\, dxd\eta\right]^{1/2} \tag{31}$$

from which follows continuous dependence upon source terms in the half-interval $[0, T/2]$.

A similar argument may be applied to the first term on the right of (23) to establish continuous dependence upon initial data in the constraint class (30). An alternative method is described in [3].

Continuous dependence upon the elasticities d_{ijkl}, coupling tensor β_{ij}, and heat conduction tensor k_{ij} are reduced to that of dependence upon source terms according to the device adopted in the subsection entitled "Source Terms and Heat Coupling Tensor" of the section entitled "Continuous Dependence upon Other Data" of Part I and employed in [3, 5, 10]. Let $d^{(\alpha)}_{ijkl}, \beta^{(\alpha)}_{ij}, k^{(\alpha)}_{ij}, \alpha = 1, 2$ denote two sets of coefficients and let $(u^{(\alpha)}_i, \theta^{(\alpha)})$ be the respective solutions of (9) and (12) in Part I that for simplicity satisfy the same source terms, initial and boundary conditions. In terms of the notation given in Part I by (58) and (59), subtraction of the governing rescaled equations yields for $(x, t) \in Q(T)$:

$$\left(d^{(2)}_{ijkl} u_{k,l} - \beta^{(2)}_{ij} \theta\right)_{,j} + \rho_0 f_i = \rho_0\, \ddot{u}_i \tag{32}$$

$$\left(k^{(2)} \theta_{,i}\right)_{,j} + \rho_0 r = \beta^{(2)}_{ij} \dot{u}_{i,jt} + a\dot{\theta} \tag{33}$$

where

$$\rho_0 f_i = \left(\bar{d}_{ijkl}\, u^{(1)}_{k,l} - \bar{\beta}_{ij}\, \theta^{(1)}\right)_{,j} \tag{34}$$

$$\rho_0 r = \left(\bar{k}_{ij}\, \theta^{(1)}_{,i}\right)_{,j} - \bar{\beta}_{ij}\, u^{(1)}_{i,jt} \tag{35}$$

$$\bar{d}_{ijkl} = d^{(2)}_{ijkl} - d^{(1)}_{ijkl} \qquad \bar{\beta}_{ij} = \beta^{(2)}_{ij} - \beta^{(1)}_{ij} \quad \bar{k}_{ij} = k^{(2)}_{ij} - k^{(1)}_{ij} \tag{36}$$

Substitution of these source terms in (31) then leads to continuous dependence upon the elasticities, coupling tensor, and heat conduction tensor, provided the component solutions $(u^{(\alpha)}_i, \theta^{(\alpha)})$ belong to the constraint class (30) and furthermore that the solution $(u^{(1)}_i, \theta^{(1)})$ satisfies the bound

$$\int_{Q(T)} \left(u^{(1)}_{i,jk} u^{(1)}_{i,jk} + u^{(1)}_{i,j\eta} u^{(1)}_{i,j\eta} + \theta^{(1)}_{,ij} \theta^{(1)}_{,ij}\right) dxd\eta \leq N_4^2 \tag{37}$$

for specified positive constant N_4.

Identity (31) is also fundamental to the treatment by Ames and Payne [7] who establish continuous dependence upon initial geometry. The analysis, outlined in the next section, extends that presented in [5] for elasticity. Song and Payne [11] in addition to continuous dependence upon initial geometry also investigate dependence upon spatial geometry, again by Lagrange identity techniques.

It must be remarked that all the above calculations are valid only on the half-interval $[0, T/2)$. Extension to the whole interval $[0, T]$ is by the recursive procedure described in [5] and leads to continuous dependence on compact subintervals in the sense of Hölder.

Dependence Upon Initial Geometry

Initial data is usually assumed to be measured instantaneously everywhere in the region Ω at say the instant $t = 0$. In practice, this is rarely, if ever, achieved. Instead, measurement usually occurs during some time interval about the instant $t = 0$, the actual time of measurement at point $x \in \Omega$ being given by $t = \varepsilon s(x), x \in \Omega$, where without loss we may assume that $|s(x)| \leq 1$. It becomes of interest to estimate the error in the solution due to the error between initial data measured at the actual and presumed times.

Such investigations, initiated and developed by Payne [12, 13] employing Lagrange identity arguments, are extended by Ames and Payne [7] to linear coupled thermoelasticity subject to homogeneous Dirichlet boundary data and zero source terms. Their proof is summarized as follows:

Let $Q_s(T) = \{(x,t) : \varepsilon s(x) \le t \le T, x \in \Omega\}$, and assume that the function $s(x)$ is sufficiently smooth and that ε is sufficiently small. More general conditions on $s(x)$ are possible; see [7]. Let $(u_i^{(2)}, \theta^{(2)})$ be the solution defined on $Q_s(T)$ generated by initial data $(u_i^{(0)}(x), \theta^{(0)}(x))$ prescribed on $t = \varepsilon s(x)$, and let $(u_i^{(1)}, \theta^{(1)})$ be the solution defined on $Q(T)$ generated by the same initial data but prescribed at $t = 0$. Set

$$u_i(x,t) = u_i^{(2)}(x,t) - u_i^{(1)}(x,t) \qquad (x,t) \in Q(\varepsilon, T) \tag{38}$$

$$\theta(x,t) = \theta^{(2)}(x,t) - \theta^{(1)}(x,t) \qquad (x,t) \in Q(\varepsilon, T) \tag{39}$$

Homogeneous Dirichlet data is assumed on the respective lateral boundaries, and solutions are supposed to belong to the constraint set

$$\sup_{\varepsilon s \le t \le T} \int_\Omega \rho_0 u_i^{(\alpha)} u_i^{(\alpha)}\, dx \le N_5^2 \tag{40}$$

$$\int_\varepsilon^T \left\{ \left[\int_\Omega \rho_0 \theta^{(1)2} \right]^{1/2} + \left[\int_\Omega \rho_0 \theta^{(2)2} \right]^{1/2} \right\} d\eta \le N_6 \tag{41}$$

$$\int_\varepsilon^T \left\{ \left[\int_\Omega \rho_0 \theta_{,i}^{(1)} \theta_{,i}^{(1)} \right]^{1/2} + \left[\int_\Omega \rho_0 \theta_{,i}^{(2)} \theta_{,i}^{(2)} \right]^{1/2} \right\} d\eta \le N_7 \tag{42}$$

where N_5, N_6, N_7 are prescribed positive constants.

Lagrange identity (23) is applied to the difference solutions (u_i, θ) followed by integration with respect to time over $[\varepsilon, t)$ and the determination of a suitable bound for $I_3(t)$. Deployment of Schwarz's inequality similar to that in the previous section leads to the bound

$$\begin{aligned} \int_\Omega \rho_0 u_i u_i\, dx + \int_{Q(\varepsilon,t)} k_{ij} \theta_{,i} \theta_{,j}\, dx d\eta \\ \le \frac{1}{2} \int_\Omega \rho_0 u_i(\varepsilon) u_i(\varepsilon)\, dx \\ + M_2 \left(\int_\Omega \rho_0 u_i(\varepsilon) u_i(\varepsilon)\, dx \right)^{1/2} \\ + M_3 \int_\Omega \rho_0 u_{i,\eta}(\varepsilon) u_{i,\eta}(\varepsilon)\, dx \\ + M_4 \left(\int_\Omega \phi^2(\varepsilon)\, dx \right)^{1/2} \\ \varepsilon \le t \le (T+\varepsilon)/2 \end{aligned} \tag{43}$$

where M_2, M_3, M_4 are certain positive constants dependent upon N_5, N_6, N_7 and time T. The integrals on the right are estimated by continuing the solutions backward in time to $t = -\varepsilon$ subject to the previously stated conditions for $s(x)$. Backward continuation is achieved by defining new solutions to be

$$\widetilde{u}_i^{(1)}(x,t) = \begin{cases} u_i^{(1)}(x,t), & 0 < t < T \quad x \in \Omega \\ u_i^{(0)}(x) & t \le 0 \quad x \in \Omega \end{cases} \tag{44}$$

$$\widetilde{u}_i^{(2)}(x,t) = \begin{cases} u_i^{(2)}(x,t) & \varepsilon s(x) < t < T \quad x \in \Omega \\ u_i^{(0)}(x) & t \le \varepsilon s(x) \quad x \in \Omega \end{cases} \tag{45}$$

with similar continuations for velocities and temperatures. It follows, for example, that because $u_i(x, -\varepsilon) = 0$, we may use Poincaré's inequality to obtain

$$\begin{aligned} \int_{-\varepsilon}^{\varepsilon} \int_\Omega \rho_0 u_i u_i\, dx d\eta \le \left(\frac{4\varepsilon}{\pi} \right)^2 \\ \times \int_{-\varepsilon}^{\varepsilon} \int_\Omega \rho_0 u_{i,\eta} u_{i,\eta}\, dx d\eta \end{aligned} \tag{46}$$

Further computations, details of which are presented in [7], employ the governing equations to construct the bound

$$\int_\Omega \rho_0 u_i(\varepsilon) u_i(\varepsilon)\, dx \le \varepsilon M_5^2 \tag{47}$$

and companion bounds for velocity and temperature, where M_5 is a computable positive constant. Substitution of these respective expressions in (6) yields

$$\int_\Omega \rho_0 u_i u_i\, dx + \int_{Q(\varepsilon,t)} k_{ij}\theta_{,i}\theta_{,j}\, dx d\eta \le \varepsilon^{1/2} M_6 \qquad \varepsilon \le t \le (T+\varepsilon)/2 \tag{48}$$

for computable positive constant M_6 and establishes the desired continuous dependence upon initial geometry as $\varepsilon \to 0$. Extension to the whole interval $[\varepsilon, T]$ is achieved by a recurrence operation similar to before.

Exterior Unbounded Regions: The Half-Space

Arguments presented in the section entitled "Continuous Dependence Upon Source Terms and Related Data" may be extended to exterior unbounded regions and the half-space by employing certain weighted integrals to derive a weighted Lagrange identity. The procedure, in thermoelasticity due to Rionero and Chirita [3], in part depends upon those developed in [14–17] for corresponding problems in linear elastodynamics. Further discussion is provided by Flavin and Rionero [18]. Asymptotic behavior must be suitably restricted to ensure solutions both exist and are unique. Counterexamples, presented, for example, in [18] and by John [19] for the heat conduction equation, illustrate the difficulty.

Suppose Ω is an unbounded three-dimensional region exterior to a bounded three-dimensional region Ω_1. The half-space is treated later. Let $g(x)$ be the weight function given by

$$g(x) = \exp(-c_6|x|) \qquad |x| = (x_i x_i)^{1/2} \tag{49}$$

where c_6 is a prescribed positive constant, and consider solutions that, in addition to the constraint class (30), belong to the class which for $t \in [0, T]$ requires the spatial asymptotic behavior to be

$$|u_i(x,t)| + |u_{i,j}(x,t)| + |\theta(x,t)| + |k_{ij}\,\widehat{\theta}_{,i}\,\widehat{\theta}_{,j}| = O(\exp(c_6|x|)) \qquad \text{as } |x| \to \infty \tag{50}$$

and

$$\lim_{c_6 \to 0} c_6^2 \int_{Q(T)} \rho_0^{-1} \exp(c_6|x|) \times \left(u_{i,j}u_{i,j} + \theta^2 + k_{ij}\,\widehat{\theta}_{,j}\,k_{ip}\,\widehat{\theta}_{,p}\right) dx d\eta = 0 \tag{51}$$

Similar arguments to before are now applied to the governing equations after each has been multiplied by the weight function $g(x)$ in order to establish continuous dependence upon source terms and initial data, first on the half-interval $[0, T/2]$ and then by iteration on the whole interval $[0, T]$.

When Ω is assumed to be the half-space $x_3 \ge 0$, the weight function is chosen to be

$$g(x) = \exp -\{c_7(x_\alpha x_\alpha)^{c_8} + c_9 x_3\} \tag{52}$$

where c_7, c_8, c_9 are positive constants.

Subject to certain transverse spatial asymptotic behavior as $(x_\alpha x_\alpha)^{1/2} \to \infty$, and asymptotic conditions similar to (51), suitable Lagrange identities are derived in [3] that enable continuous data dependence to be established for solutions in the constraint class (30).

Backward in Time

Problems in this category are concerned with an investigation of the previous history of the process when "present" data is prescribed at $t = 0$. The problem is ill-posed, even under positive-definiteness assumptions, and is studied on some reverse maximal interval of existence $[-T, 0]$. A pertinent comment by J. Clerk Maxwell is quoted by Flavin and Rionero [18, p.156].

The problem is converted into one forward in time on replacing t by $-t$, so that rescaled equations (9) and (12) of Part I for $(x,t) \in Q(T)$ become

$$\left(d_{ijkl}u_{k,l} - \beta_{ij}\theta\right)_{,j} + \rho_0 f_i = \rho_0 \ddot{u}_i \tag{53}$$

$$\left(k_{ij}\theta_{,i}\right)_{,j} + \beta_{ij}\dot{u}_{i,j} + a\dot{\theta} + \rho_0 r = 0 \tag{54}$$

Of course, boundary conditions on $\partial\Omega \times [0,T]$ and initial conditions on $\Omega \times \{0\}$ also must be prescribed.

Lagrange identities are used by Ames and Payne [6] in conjunction with an energy inequality to establish continuous dependence upon initial data for elasticities d_{ijkl} that are either positive-definite, negative-definite, or indefinite and for positive or negative a. Conditions imposed on the coupling tensor and heat conduction tensor are similar to those already adopted in Part I and also in this Part, while the constraint set requires only that the $L^2(\Omega)$-norm of the temperature is uniformly bounded on $[0,T]$. The arguments, which broadly repeat earlier ones, are presented in [6] and summarized in [9]. Ciarletta [20] provides a closely related discussion.

As previously remarked, uniqueness is recovered as a special case.

Nonlocalization of Energy

By means of uniqueness in the forward and backward in time problems, we may prove that the solution cannot be locally compact in time, or otherwise expressed, cannot be localized in time. Assume the contrary, and let the support of the solution be contained in the time interval (t_1, t_2). At $t_0 < t_1$, the Cauchy data vanishes, and uniqueness for the forward in time problem creates a contradiction. Similarly, at $t_{00} > t_2$, the solution vanishes by hypothesis, and backward uniqueness again establishes a contradiction. Obviously, the last part of the argument also demonstrates that for nonzero initial data, the solution cannot vanish in finite time, which is of significance for asymptotic behavior with respect to time.

Sign-Definite Assumptions

This section is devoted to a discussion of how conditions for uniqueness and continuous data dependence are modified by the assumptions of positive-definite elasticities and heat conduction tensor.

Suppose that there exists a positive constant d_0 such that

$$d_0\psi_{ij}\psi_{ij} \le d_{ijkl}\psi_{ij}\psi_{kl} \qquad \forall \psi_{ij} \tag{55}$$

Buckling and similar phenomena may cause this condition to be violated.

Also suppose that the coefficient a is positive and, as in Part I, that there exists a positive constant k_0 such that

$$k_0\xi_i\xi_i \le k_{ij}\xi_i\xi_j \qquad \forall \xi_i \tag{56}$$

Diverse methods, in general reliant upon energy conservation laws, are equally applicable to the problems under consideration. As illustration, one possible method is selected for each problem with the common objective of deriving estimates for continuous data dependence and uniqueness. For simplicity, throughout this section, homogeneous Dirichlet boundary conditions continue to be assumed. Source terms may or may not be zero.

Consider the rescaled system (9) and (12) of Part I and the nonnegative energy function defined by expression (21) also of Part I.

The conservation law (23) of Part I in the absence of source terms ($I_1(t) = 0$) implies that

$$\begin{aligned} E(t) &= E(0) - 2\int_{Q(t)} k_{ij}\theta_{,i}\theta_{,j}\,dxd\eta \\ &\le E(0) \end{aligned} \tag{57}$$

from which it is easy to deduce uniqueness and continuous dependence upon initial data in energy measure. When source terms are present, differentiation of (23) in Part I gives

$$\begin{aligned} \dot{E}(t) &= -2\int_\Omega k_{ij}\theta_{,i}\theta_{,j}\,dx + 2\int_\Omega \rho_0\left(f_i u_{i,t} + r\theta\right)dx \\ &\le 2Z^{1/2}(t)\left[\int_\Omega \rho_0\left(u_{i,t}u_{i,t} + \theta^2\right)dx\right]^{1/2} \end{aligned} \tag{58}$$

$$\leq 2c_{10}Z^{1/2}(t)E^{1/2}(t) \tag{59}$$

where

$$Z(t) = \int_\Omega \rho_0 \left(f_i f_i + r^2\right) dx \tag{60}$$

and

$$c_{10}^2 = \max_\Omega \left(1, \rho_0 a^{-1}\right) \tag{61}$$

Integration of (59) yields

$$E^{1/2}(t) \leq E^{1/2}(0) + c_{10} \int_0^t Z^{1/2}(\eta)\, d\eta \tag{62}$$

Provided $Z(t) \leq M_7^2$ and $t \in [0, T]$, for positive constant M_7, it may be concluded that the displacement gradient, temperature, and, by Poincaré's inequality, also the displacement are bounded in $L^2(\Omega)$-norm. The same procedure applied to (9) and (12) of Part I, after differentiation with respect to time, delivers a bound for the gradient of the velocity subject to bounded time derivatives of the source terms. These results are used in the discussion of continuous dependence upon the thermal coupling tensor undertaken at the end of this section.

Meanwhile, the analysis is extended to the systems (9) and (10) of Part I valid when the reference temperature $\theta_0(x)$ is not uniform and the previous rescaling cannot be undertaken. In addition to the positive-definite assumptions (18) and (19), we suppose that the following bounds are satisfied:

$$\max_\Omega \left(a_i a_i + a_{i,j} a_{i,j}\right) \leq M_8^2 \tag{63}$$

$$\max_\Omega \; h_{ijk} h_{ijk} \leq M_9^2 \tag{64}$$

$$M_{10}^2 \leq \inf_\Omega \; \theta_0^2 \qquad \sup_\Omega \; \theta_{0,i}\theta_{0,i} \leq M_{11}^2 \tag{65}$$

where $M_i, i = 8, 9, , \ldots 11$ are specified positive constants.

A time differentiation of the energy function given by (21) in Part I and substitution from (9) and (10) in the same Part together with homogeneous boundary conditions lead immediately to the expression

$$\begin{aligned} \dot{E}(t) = &- \int_\Omega \frac{1}{\theta_0} \left(h_{ijk} u_{j,k} + a_i \theta + k_{ij} \theta_{,j}\right) \theta_{,i}\, dx \\ &+ \int_\Omega \frac{\theta_{0,i}\theta}{\theta_0^2} \left(h_{ijk} u_{j,k} + a_i \theta + k_{ij} \theta_{,j}\right) dx \\ &+ \int_\Omega \rho_0 \left(r\theta\theta_0^{-1} + f_i u_{i,t}\right) dx \end{aligned} \tag{66}$$

Standard inequalities and appeal to the bounds (63)–(65) then yield the inequality

$$\dot{E}(t) \leq c_{11} E(t) + c_{12} E^{1/2}(t) Z^{1/2}(t) \tag{67}$$

where the function $Z(t)$ is defined by (60) and c_{11}, c_{12} are positive computable constants.

In order to integrate (30), set $y(t) = E^{1/2}(t)$, and rewrite (67) in the form

$$\begin{aligned} \frac{d}{dt}\left(y e^{-(c_{11}t/2)}\right) &\leq \frac{c_{12}}{2} e^{-(c_{11}t/2)} Z^{1/2}(t) \\ &\leq \frac{c_{12}}{2} Z^{1/2}(t) \end{aligned} \tag{68}$$

to obtain

$$E^{1/2}(t) \leq \frac{1}{2}\left(2E^{1/2}(0) + c_{12} \int_0^t Z^{1/2}(\eta)\, d\eta\right) e^{(c_{11}t/2)} \tag{69}$$

Subject to the stipulated conditions, uniqueness to the initial boundary value problem is easily derived from (69). More generally, we may obtain continuous dependence upon initial data and source terms. By means of operations similar to before, continuous dependence upon constitutive coefficients may be deduced. Dependence obviously is established with respect to the energy norm, although use of Poincaré's and similar embedding inequalities enables dependence to be derived in the $L^2(\Omega)$-norm.

But instead of appealing to these methods, it is possible to directly establish continuous

dependence upon most coefficients. The technique is illustrated by reference to dependence upon the heat coupling tensor β_{ij} in the linearized classical problem with all other data assumed fixed. For simplicity, consider the rescaled systems (9) and (12) of Part I, and let $(u_i^{(\alpha)}, \theta^{(\alpha)}), \alpha = 1, 2$ be the displacement and temperature corresponding to the heat coupling tensor $\beta_{ij}^{(\alpha)}$. This problem has been treated in Part I in the section entitled "Source Terms and Heat Coupling Tensor" and in the section entitled "Continuous Dependence on Source Terms and Related Data" of this part, but for indefinite elasticities. Consequently, retain the notation (58)–(60) of Part I, and consider (61) and (62), again from Part I, with data specified by

$$\begin{aligned} u_i(x,0) = \dot{u}_i(x,0) = \theta(x,0) = 0 \qquad & x \in \Omega \\ u_i(x,t) = \theta(x,\mathrm{t}) = 0 \qquad & (x,\mathrm{t}) \in \partial\Omega \times [0,T] \\ \rho_0 f_i(x,t) = -\left(\bar{\beta}_{ij}\,\theta^{(1)}\right)_{,j} \qquad & x \in Q(T) \\ \rho_0 r(x,t) = -\bar{\beta}_{ij}\,\dot{u}_{i,j}^{(1)} \qquad & x \in Q(T) \end{aligned}$$

The conservation relation (23) from Part I after an integration by parts and appeal to Schwarz's inequality successively yields

$$\begin{aligned} J(t) &= 2\int_{Q(t)} \beta_{ij}\left(\theta^{(1)} u_{i,j\eta} - u_{i,j\eta}^{(1)}\theta\right) dxd\eta \\ &\le \bar{\bar{\beta}}\left[\int_{Q(t)} \left(\left(\theta^{(1)}\right)^2 + \theta^2\right) dxd\eta\right. \\ &\quad \left.\int_{Q(t)} \left(u_{i,j\eta}^{(1)} u_{i,j\eta}^{(1)} + u_{i,j\eta} u_{i,j\eta}\right) dxd\eta\right]^{1/2} \\ &\le 6\bar{\bar{\beta}}\left[\int_{Q(T)} \left(\theta^{(\alpha)}\theta^{(\alpha)}\right) dxd\eta\right. \\ &\quad \left.\int_{Q(T)} \left(u_{i,j\eta}^{(\alpha)} u_{i,j\eta}^{(\alpha)}\right) dxd\eta\right]^{1/2} \end{aligned} \tag{70}$$

where

$$\bar{\bar{\beta}}^2 = \max_{\Omega}\ \bar{\beta}_{ij}\,\bar{\beta}_{ij}$$

It is inferred from the bound (62) that the integrals on the right of (70) remain bounded for $T < \infty$ subject to the respective component source terms and their time derivatives remaining bounded. The positive-definite assumptions (55) and (56) imply that the displacement and temperature vanish in the $L^2(\Omega)$ -norms as $\bar{\bar{\beta}} \to 0$. Accordingly, continuous dependence upon the heat coupling tensor is established. Unlike conditions imposed in the previous discussions, the gradient of $\bar{\beta}_{ij}$ is not required to be bounded.

Linear Thermoelasticity

Many of the conclusions of the previous sections are valid for the linear theory for which the positive-definite condition (55) is replaced by

$$c_0 \xi_{ij}\xi_{ij} \le c_{ijkl}\xi_{ij}\xi_{kl} \qquad \forall \xi_{ij} = \xi_{ji} \tag{71}$$

where c_0 is a specified positive constant. The restriction, however, of (71) to symmetric tensors present certain difficulties outwith the scope of the present discussion.

Backward in Time

Continuous data dependence results for the backward in time problem for the rescaled systems (9) and (12) specified in Part I subject to homogeneous Dirichlet boundary data are due to Ames and Payne [6] and are also described in [9]. The heat conduction tensor satisfies the positive-definite condition (56), but the elasticities d_{ijkl} are assumed to be positive semi-definite. By combining Lagrange identities with energy conservation, it is demonstrated for $t \in [0, T/2]$ that

$$\begin{aligned} E(t) \le &\left[\left(4M_{12}^2 + E(0)\right)^{1/2} E(0)^{1/2} + 3E_1(0)\right] \\ &\times \exp(c_{13}t) \end{aligned}$$

where

$$E_1(t) = \frac{1}{2}\int_{\Omega} \left(\rho_0\,\dot{u}_i\,\dot{u}_i + d_{ijkl}u_{i,j}u_{k,l}\right) dx$$

and c_{13} is a computable positive constant. The positive constant M_{12} constrains the temperature according to the bound

$$\int_{\Omega} \theta^2(t)\, dx \leq M_{12}^2 \qquad t \in [0, T]$$

Specialization of this conclusion to uniqueness in conjunction with the corresponding problem forward in time demonstrates that the solution cannot have compact support in the time interval. Expressed otherwise, for nonzero initial data, localization of the solution with respect to time is not possible.

Part III describes the application of both logarithmic convexity and Lagrange identity methods to nonclassical linear theories of thermoelasticity and also examines consequences of sign-definite assumptions.

Notation

Ω	Three-dimensional reference spatial region occupied by thermoelastic body
$\partial\Omega$	Lipschitz continuous smooth boundary of Ω
$[0, T], T > 0$	Maximal closed interval of existence
t	Time variable (scalar)
x	Position vector
$Q(t)$	$\Omega \times [0, t]$
$u_i(x, t)$	Cartesian component of increment in displacement vector
$t_{ij}(x, t)$	Cartesian component of increment in first Piola stress tensor
σ_{ij}	Cartesian component of symmetric (large) Cauchy stress tensor
$q_i(x, t)$	Cartesian component of increment in heat flux vector
$\theta(x, t)$	Increment in scalar temperature
$\theta_0(x)$	Scalar reference temperature
$S(x, t)$	Increment in scalar entropy
$a(x)$	Scalar thermal capacity
$\rho_0(x)$	Mass density in reference configuration
$f_i(x, t)$	Cartesian component of increment in body force per unit mass in reference configuration
$r(x, t)$	Increment of scalar heat supply per unit mass of reference configuration
$d_{ijkl}(x)$	Cartesian component of linearized elastic coefficient tensor
$c_{ijkl}(x)$	Cartesian component of linear elastic moduli tensor
δ_{ij}	Kronecker delta
k_{ij}	Cartesian component of heat conduction tensor
$Q(t_1, t_2)$	$\Omega \times (t_1, t_2)$
β_{ij}	Cartesian component of heat coupling tensor
$h_{ijk}, \quad a_i$	Cartesian component of material heat coefficient tensors
$E(t)$	Total energy of classical linearized thermoelastic system
$J(t)$	Augmented total energy of classical linearized system
$K(t)$	Kinetic energy of classical linearized thermoelastic system
$V(t)$	Potential energy of classical linearized thermoelastic system
$I_1(t)$	Total work done by supply terms
$F(t)$, $G(t)$, $H(t)$	Various solution measures
$Z(t)$	Supply term measure
α	Scalar thermal displacement
G_{ijk}, b_i, b_{ij}	Cartesian components of nonclassical thermomechanical coefficient tensors
$E_{III}(t)$	Total energy of linearized nonclassical system of Green-Naghdi type III without center of symmetry
$J_{III}(t)$	Augmented energy of linearized nonclassical Green-Naghdi of type III without center of symmetry
$\tilde{E}_{III}(t)$	Total perturbed energy of linearized nonclassical Green-Naghdi system of type III with center of symmetry
$P_{III}(t)$	Total work done by source terms in perturbed linearized nonclassical Green-Naghdi system of type III with center of symmetry
M_i, N_i	Various specified constants

Acknowledgments Supported by the project "Ecuaciones en Derivadas Parciales en Termomecanica. Teoria y Aplicaciones" (MTM2009-08150) of the Spanish Ministry of Education.

References

1. Brun L (1965) Sur l'unicité en thermoélasticité dynamique et diverses expressions analogues la formule de Clapeyron. Comptes Rend Acad Sci Paris 261:2584–2587
2. Brun L (1969) Méthodes énergétiques dans les systémes évolutifs linéaires. Premiére Partie:

Séparation des énergies. Deuxiéme Partie: Théorémes d'unicité. J de Mech 8:125–166, 167–192
3. Rionero S, Chirita S (1987) The Lagrange identity method in linear thermoelasticity. Int J Eng Sci 25:935–947
4. Levine HA (1977) An equipartition of energy theorem for weak solutions of evolutionary equations in Hilbert space. The Lagrange identity method. J Diff Equ 24:197–2120
5. Knops RJ, Payne LE (1988) Improved estimates for continuous data dependence in linear elastodynamics. Math Proc Camb Phil Soc 103:535–559
6. Ames KA, Payne LE (1991) Stabilizing solutions of the equations of dynamical linear thermoelasticity backward in time. Stab Appl Anal Cont Media 1:243–260
7. Ames KA, Payne LE (1995) Continuous dependence on initial-time geometry for a thermoelastic system with sign-indefinite elasticities. J Math Anal Appl 189:693–714
8. Levine HA (1970) On a theorem of Knops and Payne in dynamical linear thermoelasticity. Arch Ration Mech Anal 38:290–319
9. Ames KA, Straughan B (1997) Non-standard and improperly posed problems. Academic Press, San Diego/London
10. Knops RJ, Payne LE (1969) Continuous data dependence for the equations of classical elastodynamics. Math Proc Camb Phil Soc 66:481–491
11. Song JC, Payne LE (1989) Continuous dependence on the time and spatial geometry for the equations of thermoelasticity. Math Method Appl Sci 11:317–329
12. Payne LE (1985) On stability and growth of solutions to second-order operator equations. In: Mathematical methods and models in mechanics, vol 15. Banach Center Publications, Warsaw, pp 465–475
13. Payne LE (1987) On geometric and modelling perturbations in partial differential equations. In: Knops RJ, Lacey AA (eds) Proceedings of LMS Durham symposium on non-classical continuum mechanics. Cambridge University Press, Cambridge, pp 108–128
14. Galdi GP, Rionero S (1979) Continuous dependence theorems in linear elasticity on exterior domains. Int J Eng Sci 17:521–526
15. Galdi GP, Rionero S (1983) Continuous data dependence in linear elastodynamics on unbounded domains without definiteness conditions on the elasticities. Proc R Soc Edin A93:299–306
16. Galdi GP, Rionero S (1985) Weighted energy methods in fluid dynamics and elasticity. In: Lecture notes in mathematics, vol 1134. Springer, Berlin/Heidelberg/New York/Tokyo
17. Galdi GP, Knops RJ, Rionero S (1986) Uniqueness and continuous dependence in the linear elastodynamic exterior and half-space problems. Math Proc Camb Phil Soc 99:357–366
18. Flavin JN, Rionero S (1996) Qualitative estimates for partial differential equations. An introduction. CRC Press, Boca Raton
19. John F (1982) Partial differential equations, 4th edn. Springer, Berlin/New York
20. Ciarletta M (2003) On the uniqueness and continuous dependence of solutions in dynamical thermoelasticity backward in time. J Therm Stress 25:969–984

Continuous Data Dependence in Linear Theories of Thermoelastodynamics. Part III: Nonclassical Theories

Robin J. Knops[1] and Ramon Quintanilla[2]
[1]The Maxwell Institute of Mathematical Sciences, Heriot-Watt University, Edinburgh, Scotland, UK
[2]Matemática Aplicada 2, Universitat Politècnica de Catalunya, Terrassa, Barcelona, Spain

Overview

Parts I and II discuss continuous data dependence for classical linearized thermoelasticity. In this part, these properties are examined for selected nonclassical linearized theories using the methods of logarithmic convexity and Lagrange identities presented in Parts I and II, respectively. Implications of sign-definite assumptions are also treated. A general introduction to these investigations is included in the first section of Part 1, which also defines the notation employed in all three parts of this coordinated study. Additional notation is introduced as appropriate.

The Fourier theory of heat conduction predicts that heat propagates with infinite speed, which in certain practical circumstances is unrealistic. Alternative theories free from this defect include those formulated by Maxwell [1] and Cattaneo [2]. Books by Ames and Straughan [3], Iesan [4], Ignaczak and Ostoja-Starzewski [5], and Straughan [6] contain further references. Several relaxed heat conduction models have successfully been incorporated into thermoelasticity, and of these we select for study those proposed by Green and Naghdi. Other notable models are due to Lord and Shulman [7] and Green and Lindsay [8]. A general theory,

developed within the context of extended thermodynamics, is constructed by Müller and Ruggeri and presented in their book [9]. The Green-Naghdi theories [10–12] depend upon an entropy balance law rather than upon the usual entropy production inequality. Three related theories, called Types I, II, and III, are developed. The linearized version of the field equations belonging to Type I is identical to those of classical thermoelasticity, while those corresponding to Type II, also known as *thermoelasticity without energy dissipation*, is the limiting case of Type III in which the heat conduction tensor, k_{ij}, vanishes and exhibits energy conservation. By contrast, equations for Type III exhibit energy dissipation and do not necessarily admit a finite speed of heat propagation. The corresponding linearized equations in the absence of a center of symmetry and for $(x,t) \in Q(T)$ are represented by

$$\left(d_{ijkl}u_{k,l} - \beta_{ij}\theta + G_{ijk}\alpha_{,k}\right)_{,j} + \rho_0 f_i = \rho_0 \ddot{u}_i \tag{1}$$

$$\left(G_{jki}u_{j,k} + b_i\theta + k_{ij}\theta_{,j} + b_{ij}\alpha_{,j}\right)_{,i} + b_i\theta_{,i} + \rho_0 r = \rho_0\theta_0\left(\beta_{ij}\,\dot{u}_{i,j} + a\dot{\theta}\right) \tag{2}$$

$$\dot{\alpha} = \theta \tag{3}$$

where $\alpha(x,t)$ is the thermal displacement and G_{ijk}, b_i, b_{ij} are components of constitutive tensor coefficients, which satisfy the symmetries

$$G_{ijk} = G_{jik} \qquad b_{ij} = b_{ji} \tag{4}$$

A center of symmetry induces odd order constitutive tensors to vanish, so that

$$G_{ijk} = b_i = 0 \tag{5}$$

Moreover, in what follows it is assumed that under appropriate conditions, (1)–(3) have been rescaled such that $\rho_0\theta_0 = 1$, and that the heat conduction tensor is symmetric so that

$$k_{ij}(x) = k_{ji}(x) \tag{6}$$

Boundary conditions are specified for the displacement and temperature, and when of Dirichlet type are given by Part I, (13). Initial conditions (14) and (15) of Part I, however, are for $x \in \Omega$ augmented by

$$\alpha(x,0) = \alpha^{(0)}(x) \qquad \dot{\alpha}(x,0) = \theta(x,0) = \theta^{(0)}(x) \tag{7}$$

Without loss, it may be assumed that $\alpha^0(x) = 0$, since otherwise terms involving nonzero $\alpha^{(0)}(x)$ may be absorbed into the respective source terms.

Subject to homogeneous boundary conditions, uniform coefficients, b_i, and on defining the energy $E_{III}(t)$ to be

$$E_{III}(t) = \int_\Omega \left[\rho_0\dot{u}_i\dot{u}_i + d_{ijkl}u_{i,j}u_{k,l} + 2G_{ijk}u_{i,j}\alpha_{,k} + b_{ij}\alpha_{,i}\alpha_{,j} + a\theta^2\right] dx \tag{8}$$

the following conservation law may easily be proved:

$$J_{III}(t) \equiv E_{III}(t) + 2\int_{Q(t)} k_{ij}\theta_{,i}(\eta)\theta_{,j}(\eta)\,dx d\eta \tag{9}$$

$$= J_{III}(0) + 2I_1(t) \tag{10}$$

where $I_1(t)$ is defined in Part I, (24).

Equations governing Type II theory are obtained on setting $k_{ij} = 0$ in the preceding Type III equations. In consequence, (2) reduces to

$$\left(G_{ijk}u_{j,k} + b_i\theta + b_{ij}\alpha_{,j}\right)_{,i} + b_i\theta_{,i} + \rho_0 r = \rho_0\theta_0\left(\beta_{ij}\,\dot{u}_{i,j} + a\dot{\theta}\right) \qquad (x,t) \in Q(T) \tag{11}$$

which in the presence of a center of symmetry becomes invariant forward and backward in time.

For homogeneous boundary conditions, the Type III conservation law (10) indicates that the energy $E_{III}(t)$ for the linearized Type II theory satisfies

$$E_{III}(t) = E_{III}(0) + 2I_1(t) \tag{12}$$

and is conserved when both source terms vanish.

Scope of Part III

Many of the techniques explained in Parts I and II are applicable to nonclassical linear theories of thermoelastodynamics. Rather than an exhaustive treatment, we confine attention to the Green-Naghdi theories of Types II and III whose reference configurations possess a center of symmetry. Principal investigations include those by Quintanilla and Straughan [13] and Quintanilla [14, 15] who employ logarithmic convexity and Lagrange identities to establish uniqueness, continuous data dependence, and growth estimates for bounded and unbounded spatial regions and sign-indefinite elasticities. Logarithmic convexity is employed by Bofill, Leseduarte, and Quintanilla [16] to obtain uniqueness and growth estimates in the linear theories of Lord and Shulman and of Green and Lindsay subject to sign-indefinite elasticities and positive-definite heat conduction tensor. Other conditions are implied by an entropy production inequality proposed by Green and Lindsay [8], who prove uniqueness for positive semi-definite elasticities.

Type II and III theories without a center of symmetry require certain positive-definite assumptions and are considered by Quintanilla [17].

The methods of either logarithmic convexity, Lagrange identities, or energy conservation for positive-definite elasticities are applicable in principle to both Type II and Type III theories. But for illustrative purposes, different problems are selected for each method. Conditions are supposed satisfied that enable the equations to be rescaled to give $\rho_0\theta_0 = 1$.

Logarithmic Convexity

Type II

Consider the system specified by (1), (3), and (11) modified by assumption (5), and seek to establish continuous dependence upon initial data with zero source terms and boundary conditions.

Initial data is specified in Part I by conditions (14) and (15), and by (7), while the tensor b_{ij} is supposed symmetric and positive definite:

$$b_{ij} = b_{ji} \qquad b_0\xi_i\xi_i \le b_{ij}\xi_i\xi_j \qquad \forall \xi_i \tag{13}$$

for positive constant b_0.

The logarithmic convexity analysis developed in [13] employs a new variable which in the notation of Part I, (51) is given by

$$\omega(x,t) = \widehat{\alpha}(x,t) + \zeta(x) \tag{14}$$

where $\alpha(x,t)$ is defined by (3) and $\zeta(x)$ is the solution to the elliptic equation

$$\left(b_{ij}\zeta_{,j}\right)_{,i} = \beta_{ij}u^{(0)}_{i,j}(x) + a\theta^{(0)}(x) \tag{15}$$

This enables (11) to be written in the alternative forms

$$\left(b_{ij}\alpha_{,j}\right)_{,i} = \beta_{ij}\,\dot{u}_{i,j} + a\ddot{\alpha} \tag{16}$$

$$\left(b_{ij}\omega_{,j}\right)_{,i} = \beta_{ij}u_{i,j} + a\ddot{\omega} \tag{17}$$

It may be shown [13] that the function $F(t)$, defined by

$$F(t) = \int_\Omega \left(\rho_0 u_i u_i + b_{ij}\omega_{,i}\omega_{,j}\right) dx + \gamma_5(t + t^{**})^2 \tag{18}$$

where γ_5, t^{**} are positive constants to be chosen, satisfies the differential inequality

$$F(t)\ddot{F}(t) - \left(\dot{F}(t)\right)^2 \ge -2F(t)(2E_{III}(0) + \gamma_5) \tag{19}$$

in which $E_{III}(t)$ is the conserved quantity defined by (12). The discussion of (19) now proceeds as before. In particular, zero initial data implies $E_{III}(0) = 0$, and on selecting $\gamma_5 = 0$, we have $F(0) = 0$. Uniqueness is recovered both forward and backward in time, demonstrating that the solution cannot have compact support in $[0,T]$. Green and Naghdi [11] prove uniqueness for the isotropic Type II theory using Lagrange identities considered in the section entitled "Lagrange Identities."

When initial data is such that $E_{III}(0) \le 0$ or > 0, it may be deduced from inequality (19)

with $\gamma_5 = -2E_{III}(0)$ or $\gamma_5 = 0$ that the solution grows according to

$$F(t) \geq F(0)\exp\left(\frac{F'(0)}{F(0)}t\right) \tag{20}$$

Detailed arguments are presented in [13].

Because the rescaled (11) with a center of symmetry is invariant with respect to a time reversal, the results of this section apply both forward and backward in time. In particular, localization of the solution subject to nonzero initial data is not possible.

Type III

Logarithmic convexity arguments may also be applied to the Green-Naghdi Type III theory with a center of symmetry. The problem is studied by Quintanilla [14] who derives continuous dependence on source terms and coupling coefficients for homogeneous materials. The initial boundary value problem treated consists of (1)–(3) subject to (5) and the boundary and initial conditions specified in Part I by (13)–(15) supplemented by (7) of this part. Suppose that k_{ij} and b_{ij} are symmetric and satisfy the positive conditions

$$k_{ij}\xi_i\xi_j \geq k_0\xi_i\xi_i \qquad b_{ij}\xi_i\xi_j \geq 0 \quad \forall\xi_i \tag{21}$$

where k_0 is a positive constant. Let (u_i, θ, α) denote the difference in displacement, temperature, and thermal displacement for two different sets of source terms $f_i^{(\alpha)}, r^{(\alpha)}, \alpha = 1, 2$ and coupling coefficients $\beta_{ij}^{(\alpha)}$. Other data are held fixed.

Subtraction of the respective equations and use of the definitions

$$u_i = u_i^{(2)} - u_i^{(1)} \qquad \theta = \theta^{(2)} - \theta^{(1)} \tag{22}$$

$$f_i = f_i^{(2)} - f_i^{(1)} \qquad r = r^{(2)} - r^{(1)} \tag{23}$$

for $(x, t) \in Q(T)$ leads to

$$\left(d_{ijkl}u_{k,l} - \beta_{ij}^{(2)}\theta - \bar{\beta}_{ij}\,\theta^{(1)}\right)_{,j} + \rho_0 f_i = \rho_0\,\ddot{u}_i$$
$$\left(k_{ij}\theta_{,i} + b_{ij}\alpha_{,i}\right)_{,j} + \rho_0 r - \bar{\beta}_{ij}\,\dot{u}_{i,j}^{(1)} = \beta_{ij}^{(2)}\,\dot{u}_{i,j} + a\dot{\theta}$$

adjoined to which are homogeneous initial and boundary conditions.

Assume solutions are constrained to have the temperature and temperature spatial gradient bounded and the displacement and velocity gradients bounded according to

$$\max_{\Omega}\Big((\dot{u}_{i,j} - v_{i,j}^{(0)})(\dot{u}_{i,j}^{(2)} - v_{i,j}^{(0)}) + (u_{i,j}^{(2)} - u_{i,j}^{(0)} - tv_{i,j}^{(0)})$$
$$(u_{i,j}^{(2)} - u_{i,j}^{(0)} - tv_{i,j}^{(0)})\Big) \leq N_7^2$$

where N_7 is a specified positive constant.

In terms of the notation given by (51) of Part I, the function $F(t)$ defined by

$$F(t) = \int_{Q(t)}\left(\rho_0 u_i u_i + k_{ij}\widehat{\alpha}_{,i}\,\widehat{\alpha}_{,j} + (t-\eta)k_{ij}\alpha_{,i}\alpha_{,j}\right)dxd\eta$$
$$+ \int_{Q(T)}\left(\rho_0^2 f_i f_i + 2\bar{\beta}_{ij}\bar{\beta}_{ij} + \rho_0^2(R_1^2 + R_2^2)\right)dxd\eta$$
$$R_1(t) = \widehat{r}(\eta) \qquad R_2 = \widehat{\widehat{r}}(\eta) \tag{24}$$

may be shown [14] to satisfy the differential inequality

$$F(t)\ddot{F}(t) - \left(\dot{F}(t)\right)^2 \geq -c_{14}F^2(t) \qquad t \in [0, T]$$

where c_{14} is a computable positive constant. Consequently, $F(t)$ possesses a convex logarithm on $[0, T]$ which, for computable positive constant M_{13}, leads after integration to the inequality

$$F(t) \leq M_{13}\left[\int_{Q(T)}\left(\rho_0^2 f_i f_i + 2\beta_{ij}\beta_{ij}\right.\right.$$
$$\left.\left.+\rho_0^2(R_1^2 + R_2^2)\right)dxd\eta\right]^{(1-t/T)}$$

In consequence, continuous dependence is established upon source terms and the coupling tensor.

Lagrange Identities

Application of the technique of Lagrange identities to nonclassical thermoelastic theories is illustrated

by the proof of uniqueness for the Green-Naghdi Type III theory with a center of symmetry. Continuous dependence upon various other data may be derived by obvious extension of the discussion in Parts I and II for classical theories. The relevant initial boundary value problem is specified by (1)–(3) subject to (5), together with conditions (13)–(15) of Part I augmented by (7). It is preferable to express (2) alternatively as

$$\left(k_{ij}\,\dot{\alpha}_{,j}\right)_{,i} + \left(b_{ij}\alpha_{,j}\right)_{,i} + \rho_0 r = \beta_{ij}\dot{u}_{i,j} + a\ddot{\alpha} \quad (25)$$

Recall that the solution satisfies the conservation law (10) subject to homogeneous boundary conditions. In what follows, it is necessary to require only the positive semi-definite conditions

$$k_{ij}\xi_i\xi_j \geq 0 \qquad \forall \xi_i \quad (26)$$

$$b_{ij}\xi_i\xi_j \geq 0 \qquad \forall \xi_i \quad (27)$$

As usual, to prove uniqueness, it is sufficient to assume homogeneous initial and boundary conditions, and zero source terms. Computations similar to those outlined in Part II lead for $t \in [0, T/2]$ to the identity

$$\int_\Omega \left\{\rho_0 \dot{u}_i(t)\,\dot{u}_i(t) - d_{ijkl}u_{i,j}(t)u_{k,l}(t) - a\theta^2(t) + b_{ij}\alpha_{,i}(t)\alpha_{,j}(t)\right\} dx = 0 \quad (28)$$

The sign-indefinite terms may be eliminated by combining with the conservation law (10) to give

$$\int_\Omega \left(\rho_0 \dot{u}_i\dot{u}_i + b_{ij}\alpha_{,i}\alpha_{,j}\right) dx + \int_{Q(t)} k_{ij}\theta_{,i}\theta_{,j}\,dx d\eta = 0 \quad (29)$$

which from (26), (27), and homogeneous initial conditions implies that $u_i(x,t) \equiv 0$, $(x,t) \in Q(T/2)$. Insertion into (10) leads to the conclusion that $\theta(x,t) \equiv 0, (x,t) \in Q(T/2)$ and uniqueness is established in $Q(T/2)$ and by recursion in $Q(T)$.

Inclusion of nonzero source terms modifies the above argument in a manner similar to that presented in Part II. Continuous dependence on constitutive coefficients again reduces to the consideration of nonzero source terms.

Type II theory is, of course, included as a special case in these results. Note, however, that the backward in time problem for sign-indefinite elasticities appears to await investigation for both Type II and III theories by means of Lagrange identities, even though continuous data dependence, uniqueness, and related properties for Type II backward in time may be derived using logarithmic convexity methods as discussed in the section entitled "Logarithmic Convexity, Type II."

Sign-Definite Assumptions

As already mentioned, provided it is accepted that the maximal interval of existence may be finite and continuity may be in a weak sense, sign-definite elasticities are not essential for proofs of continuous data dependence. Nevertheless, it is instructive to examine the improvement gained by introduction of these assumptions. The analysis has been undertaken by Quintanilla [15] for dependence upon various coefficients and for the isotropic version of the Type III theory with center of symmetry. The treatment is sketched for the corresponding anisotropic version and for dependence upon the elasticities, coupling tensor, and the heat conduction tensor subject to $a > 0$. Furthermore, the positive conditions

$$d_0\zeta_{ij}\zeta_{ij} \leq d^{(\alpha)}_{ijkl}\zeta_{ij}\zeta_{kl} \qquad \forall \zeta_{ij} \quad (30)$$

$$0 \leq k^{(\alpha)}_{ij}\xi_i\xi_j \qquad \forall \xi_i \quad (31)$$

$$0 \leq b^{(\alpha)}_{ij}\xi_i\xi_j \qquad \forall \xi_i \quad (32)$$

where the superscript $\alpha = 1, 2$ refers to the different sets of coefficients and d_0 is a specified positive constant are assumed also to hold.

Quintanilla and Racke [18] under the same conditions have established exponential stability (i.e., continuous dependence upon initial conditions) with respect to the energy norm for the linearized version of Type III both in one dimension and for radially symmetric solutions.

These authors appeal to energy methods and spectral analysis. Similar behavior is examined by Zhang and Zuazua [19].

Recall that the solutions $(u_i^{(\alpha)}(x,t), \theta^{(\alpha)}(x,t)), \alpha = 1,2$ satisfy the respective conservation laws (10), and supplement the notation (22) and (23), by

$$\bar{d}_{ijkl} = d_{ijkl}^{(2)} - d_{ijkl}^{(1)} \quad \bar{\beta}_{ij} = \beta_{ij}^{(2)} - \beta_{ij}^{(1)} \quad \bar{k}_{ij} = k_{ij}^{(2)} - k_{ij}^{(1)} \tag{33}$$

$$\alpha(x,t) = \alpha^{(2)}(x,t) - \alpha^{(1)}(x,t) \tag{34}$$

$$\bar{b}_{ij}(x) = b_{ij}^{(2)}(x) - b_{ij}^{(1)}(x) \tag{35}$$

Dirichlet boundary conditions are assumed fixed, while initial data may alter, so that

$$u_i(x,t) = \theta(x,t) = 0 \qquad (x,t) \in \partial\Omega \times [0,T] \tag{36}$$

$$u_i(x,0) = u_i^{(00)}(x) \quad \dot{u}_i(x,0) = v_i^{(00)}(x) \quad x \in \Omega \tag{37}$$

$$\theta(x,0) = \theta^{(00)}(x) \quad \alpha(x,0) = \alpha^{(00)}(x) \quad x \in \Omega \tag{38}$$

where $u_i^{(00)}(x), v_i^{(00)}(x), \theta^{(00)}(x), \alpha^{(00)}(x)$ are prescribed functions.

A center of symmetry enables $G_{ijk} = b_i = 0$ to be taken in (1) and (2). Subtraction of the respective equations leads to the system

$$\left(d_{ijkl}^{(2)} u_{k,l} - \beta_{ij}^{(2)}\theta\right)_{,j} + X_i = \rho_0 \ddot{u}_i \tag{39}$$

$$\left(k_{ij}^{(2)}\theta_{,i} + b_{ij}^{(2)}\alpha_{,i}\right)_{,j} + R = \beta_{ij}^{(2)}\dot{u}_{i,j} + a\dot{\theta} \tag{40}$$

where

$$X_i(x,t) = \rho_0 f_i + \left(\bar{d}_{ijkl}\, u_{k,l}^{(1)} - \bar{\beta}_{ij}\,\theta^{(1)}\right)_{,j} \tag{41}$$

$$R(x,t) = \rho_0 r + \left(\bar{k}_{ij}\,\theta_{,i}^{(1)} + \bar{b}_{ij}\,\alpha_{,i}^{(1)}\right)_{,j} - \bar{\beta}_{ij}\,\dot{u}_{i,j}^{(1)} \tag{42}$$

Multiplication of (39) by $\dot{u}_i$ and addition of the resulting expression to (40) multiplied by $\theta = \dot{\alpha}$, succeeded by integration over $Q(t)$, yields the conservation identity

$$\tilde{E}_{III}(t) = \tilde{E}_{III}(0) + P_{III}(t) \tag{43}$$

where

$$\begin{aligned}\tilde{E}_{III}(t) = &\frac{1}{2}\int_\Omega \Big(\rho_0\,\dot{u}_i(t)\,\dot{u}_i(t) + d_{ijkl}^{(2)} u_{i,j}(t) u_{k,l}(t) \\ &+ b_{ij}^{(2)}\alpha_{,i}(t)\alpha_{,j}(t) + a\theta^2(t)\Big)\,dx \\ &+ \int_{Q(t)} k_{ij}^{(2)}\theta_{,i}(\eta)\theta_{,j}(\eta)\,dx d\eta\end{aligned} \tag{44}$$

$$P_{III}(t) = \int_{Q(t)} \left(X_i u_{i,\eta} + R\theta\right) dx d\eta \tag{45}$$

Set

$$\bar{d}^2 = \max_\Omega \left(\bar{d}_{ijkl}\bar{d}_{ijkl} + \bar{d}_{ijkl,j}\bar{d}_{ipkl,p}\right) \tag{46}$$

$$\bar{\beta}^2 = \max_\Omega \left(\bar{\beta}_{ij}\bar{\beta}_{ij} + \bar{\beta}_{ij,j}\bar{\beta}_{ip,p}\right) \tag{47}$$

$$\bar{k}^2 = \max_\Omega \left(\bar{k}_{ij}\bar{k}_{ij} + \bar{k}_{ij,j}\bar{k}_{ip,p}\right) \tag{48}$$

$$\bar{b}^2 = \max_\Omega \left(\bar{b}_{ij}\bar{b}_{ij} + \bar{b}_{ij,j}\bar{b}_{ip,p}\right) \tag{49}$$

and assume that $(u_i^{(1)}, \theta^{(1)})$ satisfies the bound

$$\begin{aligned}\int_{Q(T)} \Big(&u_{i,j}^{(1)}u_{i,j}^{(1)} + u_{i,jk}^{(1)}u_{i,jk}^{(1)} + u_{i,j\eta}^{(1)}u_{i,j\eta}^{(1)} + \theta_{,i}^{(1)}\theta_{,i}^{(1)} \\ &+ \theta_{,ij}^{(1)}\theta_{,ij}^{(1)} + \alpha_{,i}^{(1)}\alpha_{,i}^{(1)} + \alpha_{,ij}^{(1)}\alpha_{,ij}^{(1)}\Big)\,dx d\eta \le N_8^2\end{aligned} \tag{50}$$

where N_8 is a specified positive constant. It is subsequently proved later in this section that imposition of a stricter bound than (50) leads to improved result for continuous data dependence provided the heat conduction tensor k_{ij} is positive definite.

Standard inequalities applied to the second term on the right of (43) yield

$$P_{III}(t) \leq \left[\int_{Q(t)} \left(X_i X_i + R^2\right) dxd\eta\right]^{1/2} \left[\int_{Q(t)} \left(u_{i,\eta} u_{i,\eta} + \theta^2\right) dxd\eta\right]^{1/2} \leq D_1 \left[\int_0^t \tilde{E}_{III}(\eta)\, d\eta\right]^{1/2} \tag{51}$$

where

$$D_1^2 = 6c_{15}\left[\int_{Q(T)} \rho_0\left(f_i f_i + r^2\right) dxd\eta + (\bar{d}^2 + \bar{\beta}^2 + \bar{k}^2 + \bar{b}^2)N_8^2\right]^{1/2}$$

$$c_{15} = \max_{\Omega}\left(1, \rho_0^{-1}, a^{-1}\rho_0 a^{-1}\right)$$

It immediately follows that $D_1 \to 0$ as the differences between the respective source terms and constitutive coefficients vanish provided $T<\infty$.

Let

$$y(t) = \int_0^t \tilde{E}_{III}(\eta)\, d\eta$$

Substitution of (51) in (43) gives the differential inequality

$$\dot{y}(t) \leq \tilde{E}_{III}(0) + D_1 y^{1/2}(t) \tag{52}$$

$$\leq \tilde{E}_{III}(0) + \frac{1}{2}D_1^2 + \frac{1}{2}y(t) \tag{53}$$

Comment on two special cases is appropriate prior to discussion of the general integration of inequality (53). Variation of initial data alone implies $D_1 = 0$, and continuous dependence in E_{III}-measure follows immediately from (52). By contrast, subject to fixed initial data and variable other data, (52) may be integrated to obtain

$$y(t) \leq D_1^2 t^2/4 \tag{54}$$

$$\dot{y}(t) = \tilde{E}_{III}(t) \leq D_1^2 t/2 \tag{55}$$

and continuous dependence again follows.

More generally, integration of (52) gives

$$y(t) \leq 2\left(\tilde{E}_{III}(0) + \frac{D_1^2}{2}\right)\left(e^{t/2} - 1\right) \tag{56}$$

and consequently substitution in (52) gives

$$\tilde{E}_{III}(t) \leq \tilde{E}_{III}(0) + D_1\left[2\left(\tilde{E}_{III}(0) + \frac{D_1^2}{2}\right)\left(e^{t/2} - 1\right)\right]^{1/2} \tag{57}$$

When $t \to 0$, the second term in (57) vanishes, and the bound reduces to an identity. Moreover, the bound for $t > 0$ establishes continuous dependence in turn upon the initial data, source terms, and constitutive coefficients. Differences in all data must simultaneously approach zero, or each datum must be considered independently with the remainder held fixed during the limiting process. Convergence is respect to the E_{III}-measure, although Poincaré's inequality may be used to obtain $L^2(\Omega)$-norm convergence for the displacement. In particular, these conclusions imply that Type III theory converges to Type II as $k_{ij} \to 0$, all other data being fixed.

Positive definiteness of the heat conduction tensor, given by

$$k_0 \xi_i \xi_i \leq k_{ij}^{(\alpha)} \xi_i \xi_j \qquad \forall \xi_i \tag{58}$$

where k_0 is a prescribed positive constant, enables improved estimates for continuous data dependence to be determined, subject to a constraint class stricter than (50).

An integration by parts with respect to both space and time gives

$$P_{III}(t) = \int_{Q(t)} \left(\rho_0 f_i u_{i,\eta} + \Phi_{ij,\eta} u_{i,j} + \rho_0 r\theta + \Psi_i \theta_{,i}. + \beta_{ij,j} u_{i,\eta}^{(1)} \theta\right) dxd\eta \tag{59}$$

where

$$\Phi_{ij}(x,t) = \left(\bar{d}_{ijkl}\dot{u}_{k,l}^{(1)} - \bar{\beta}_{ij}\dot{\theta}^{(1)}\right) \tag{60}$$

$$\Psi_i(x,t) = \left(\bar{k}_{ij}\,\theta^{(1)}_{,j} + \bar{b}_{ij}\,\alpha^{(1)}_{,j} + \bar{\beta}_{ji}\,u^{(1)}_{j,\eta}\right) \tag{61}$$

An application of Schwarz's inequality leads to

$$\begin{aligned} P_{III}(t) \le D_3 &\left[\int_{Q(t)} \left(\rho_0 u_{i,\eta}u_{i,\eta} + u_{i,j}u_{i,j}\right.\right. \\ &\left.\left. + (\rho_0+1)\theta^2\right) dx d\eta\right]^{1/2} \\ &+ D_4\left[\int_{Q(t)} \theta_{,i}\theta_{,i}\,dx d\eta\right]^{1/2} \\ &+ D_5\left[\int_\Omega u_{i,j}(t)u_{i,j}(t)\,dx\right]^{1/2} + D_6 \\ &\le D_7\left[\int_0^t \tilde{E}_{III}(\eta)\,d\eta\right]^{1/2} + D_8\,\tilde{E}^{1/2}_{III}(t) + D_6 \end{aligned} \tag{62}$$

where $D_i, i = 3, \ldots 8$ are positive constants computable in terms of the data.

Substitution of (62) in (43) gives

$$\begin{aligned} \tilde{E}_{III}(t) &\le \tilde{E}_{III}(0) + D_6 + D_7\left[\int_0^t \tilde{E}_{III}(\eta)\,d\eta\right]^{1/2} \\ &\quad + D_8\,\tilde{E}^{1/2}_{III}(t) \\ &\le 2(\tilde{E}_{III}(0) + D_6) + D_8^2 \\ &\quad + 2D_7\left[\int_0^t \tilde{E}_{III}(\eta)\,d\eta\right]^{1/2} \end{aligned} \tag{63}$$

after an appeal to the arithmetic–geometric mean inequality. Inequality (63) is of the same form as inequality (52) and may be discussed as previously subject, however, to the bound (50) being replaced by

$$\int_{Q(T)} \left(u^{(1)}_{i,j\eta}(\eta)u^{(1)}_{i,j\eta}(\eta) + \left(\theta^{(1)}_{,\eta}\right)^2 + \theta^{(1)}_{,i}(\eta)\theta^{(1)}_{,i}(\eta) + \alpha^{(1)}_{,i}(\eta)\alpha^{(1)}_{,i}(\eta)\right) dx d\eta \le N_9^2 \tag{64}$$

$$\sup_{t\in[0,T]}\left\{\int_\Omega u^{(1)}_{i,j}(t)u^{(1)}_{i,j}(t) + \left(\theta^{(1)}(t)\right)^2\right\} \le N_{10}^2 \tag{65}$$

where N_9, N_{10} are prescribed positive constants. Of course, sufficient smoothness of $u^{(1)}_i, \theta^{(1)}$, and $\alpha^{(1)}$ is implicit in these assumptions. In this regard, the bound (64) is superfluous for terms involving time derivatives since we can derive from (1), (2), and (3), differentiated with respect to time, a modified conservation law which leads to the required bound provided initial data are sufficiently smooth.

Backward in Time

The backward in time problem for the Green-Naghdi Type III linear theory is discussed by Quintanilla [20]. Uniqueness is proved for positive-definite elasticities and heat conduction tensor. Consequently, in view of uniqueness for the forward in time problem, localization of the solution in the time interval becomes impossible.

Notation

Ω	Three-dimensional reference spatial region occupied by thermoelastic body
$\partial\Omega$	Lipschitz continuous smooth boundary of Ω
$[0,T], T > 0$	Maximal closed interval of existence
t	Time variable (scalar)
x	Position vector
$Q(t)$	$\Omega \times [0,t]$
$u_i(x,t)$	Cartesian component of increment in displacement vector
$t_{ij}(x,t)$	Cartesian component of increment in first Piola stress tensor
σ_{ij}	Cartesian component of symmetric (large) Cauchy stress tensor
$q_i(x,t)$	Cartesian component of increment in heat flux vector
$\theta(x,t)$	Increment in scalar temperature
$\theta_0(x)$	Scalar reference temperature
$S(x,t)$	Increment in scalar entropy
$a(x)$	Scalar thermal capacity
$\rho_0(x)$	Mass density in reference configuration
$f_i(x,t)$	Cartesian component of increment in body force per unit mass in reference configuration

(*continued*)

$r(x,t)$	Increment of scalar heat supply per unit mass of reference configuration
$d_{ijkl}(x)$	Cartesian component of linearized elastic coefficient tensor
$c_{ijkl}(x)$	Cartesian component of linear elastic moduli tensor
δ_{ij}	Kronecker delta
k_{ij}	Cartesian component of heat conduction tensor
$Q(t_1,t_2)$	$\Omega \times (t_1,t_2)$
β_{ij}	Cartesian component of heat coupling tensor
h_{ijk}, a_i	Cartesian component of material heat coefficient tensors
$E(t)$	Total energy of classical linearized thermoelastic system
$J(t)$	Augmented total energy of classical linearized system
$K(t)$	Kinetic energy of classical linearized thermoelastic system
$V(t)$	Potential energy of classical linearized thermoelastic system
$I_1(t)$	Total work done by supply terms
$F(t)$, $G(t)$, $H(t)$	Various solution measures
$Z(t)$	Supply term measure
α	Scalar thermal displacement
G_{ijk}, b_i, b_{ij}	Cartesian components of nonclassical thermomechanical coefficient tensors
$E_{III}(t)$	Total energy of linearized nonclassical system of Green-Naghdi Type III without center of symmetry
$J_{III}(t)$	Augmented energy of linearized nonclassical Green-Naghdi of Type III without center of symmetry
$\tilde{E}_{III}(t)$	Total perturbed energy of linearized nonclassical Green-Naghdi system of Type III with center of symmetry
$P_{III}(t)$	Total work done by source terms in perturbed linearized nonclassical Green-Naghdi system of Type III with center of symmetry
M_i, N_i	Various specified constants

Acknowledgement Supported by the project "Ecuaciones en Derivadas Parciales en Termomecanica. Teoria y Aplicaciones" (MTM2009-08150) of the Spanish Ministry of Education

References

1. Maxwell JC (1867) On the dynamical theory of gases. Phil. Trans R Soc Lon A 157:49–88
2. Cattaneo C (1948) Sulla conduzione del calore. Atti Sem Mat Fis Univ Modena 3:83–101
3. Ames KA, Straughan B (1997) Non-standard and Improperly Posed Problems. Academic, San Diego/London
4. Ieşan D (2004) Thermoelastic Models of Continua. Springer, Berlin/Heidelberg/New York
5. Ignaczak J, Ostoja-Starzewski M (2010) Thermoelasticity with Finite Wave Speeds. Oxford University Press, Oxford
6. Straughan B (2011) Heat Waves. Springer, New York
7. Lord HW, Shulman Y (1967) A generalized dynamical theory of thermoelasticity. J Mech Phys Solids 15:299–309
8. Green AE, Lindsay KA (1972) Thermoelasticity. J Elast 2:1–7
9. Müller I, Ruggeri T (1998) Rational Extended Thermodynamics. Springer Tracts in Natural Philosophy, 2nd edn. Springer, Berlin
10. Green AE, Naghdi PM (1992) On undamped heat waves in an elastic solid. J Therm Stress 15:253–264
11. Green AE, Naghdi PM (1993) Thermoelasticity without energy dissipation. J Elast 31:189–208
12. Green AE, Naghdi PM (1995) A unified procedure for construction of theories of deformable media. I. Classical continuum physics. II. Generalized continua. III. Mixtures of interacting continua. Proc R Soc Lond A 448:335–356, 357–377, 379–388
13. Quintanilla R, Straughan B (2000) Growth and uniqueness in thermoelasticity. Proc R Soc Lond A 56:1419–1429
14. Quintanilla R (2001) Structural stability and continuous dependence of solutions of thermoelasticity of type III. Discrete Cont Syst Ser B 1:463–470
15. Quintanilla R (2003) Convergence and structural stability in thermoelasticity. Appl Math Comput 135:287–300
16. Bofill F, Leseduarte MC, Quintanilla R (2005) Uniqueness and growth in hyperbolic thermoelastic theories. Proceedings of sixth international congress on thermal stresses, Vienna, pp 149–152
17. Quintanilla R (2002) Existence in thermoelasticity without energy dissipation. J Therm Stress 25:195–202
18. Quintanilla R, Racke R (2003) Stability and thermoelasticity of type III. Discrete Cont. Dyn Syst Ser B 3:383–400
19. Zhang X, Zuazua E (2003) Decay of solutions of the system of thermoelasticity of type III. Comm Contemp Math 5:25–83
20. Quintanilla R (2007) On the impossibility of localization in linear thermoelasticity. Proc R Soc Lond A 463:3311–3322

Continuous Dependence

▶ Continuous Dependence Results
▶ Well-Posed Problems

Continuous Dependence on Constitutive Quantities

▶ Structural Stability in Linear Thermoelasticity

Continuous Dependence Results

Cătălin Galeş
Department of Mathematics, Faculty of Mathematics, "Al. I. Cuza" University of Iaşi, Iaşi, Romania

Synonyms

Continuous dependence; Nonlinear theory; Stability; Thermoelasticity

Overview

A close connection between thermodynamics and stability has been reported in various papers [4, 7, 10]. For the nonlinear thermoelasticity without heat conduction, the problem of stability has been investigated by Dafermos [6], who established the continuous dependence of smooth thermodynamic processes upon initial state and supply terms. The proof is based on the local convexity of internal energy (or the strong ellipticity condition).

The results obtained by Dafermos have been completed by Chiriţă [3], who studied the general case of heat-conducting thermoelastic materials. Using the consequences of the Clausius–Duhem inequality, Chiriţă [3] proved uniqueness and continuous dependence results for smooth admissible thermodynamic processes, under the further condition stating that the elastic material behaves as a definite conductor of heat.

This method has been utilized and extended recently to viscoelastic materials [9, 11, 12] and to some generalized models of continua [2, 8].

Based on the papers [3, 6], this work describes the method in question. Thus, in the next section, we recall the basic equations of the nonlinear thermoelasticity. Then, an evolutionary identity controlling the time evolution of the so-called distance between two processes is presented. A discussion concerning the technical ingredients in the proof of the stability theorem, for both types of elastic materials: nonconductors and conductors of heat, is also given. Finally, a uniqueness theorem and the continuous dependence of smooth thermodynamic processes upon initial state and body loads are presented.

Basic Formulation

We consider a body that at time $t = 0$ occupies the regular region B of the three-dimensional Euclidean space and is bounded by a piecewise smooth surface ∂B. We denote by $\overline{B}$ the closure of B. The configuration of the body at time $t = 0$ is taken as the reference configuration. We refer the motion of the body to the reference configuration and to a fixed system of rectangular axes. We identify a typical particle X of the body with its position $\mathbf{X}$ in the reference configuration. The coordinates of a typical particle X in B are X_K $(K = 1, 2, 3)$. The coordinates of this particle in the position $\mathbf{x}$ at time t are denoted by x_i. The deformation of the body is described by

$$\mathbf{x} = \mathbf{x}(\mathbf{X}, t), \qquad \mathbf{X} \in \overline{B},\ t \in [0, t_0) \tag{1}$$

We assume the continuous differentiability of $\mathbf{x}$ with respect to the variables X_K and t as many times as required and

$$J = \det\left(\frac{\partial x_i}{\partial X_K}\right) > 0 \tag{2}$$

In the following, we shall employ the following notations and conventions: Latin subscripts are understood to range over the integers $(1, 2, 3)$; summation over repeated subscripts is implied; subscripts preceded by a comma denote partial differentiation with respect to the corresponding Cartesian coordinate; a superposed dot denotes time differentiation; N_K are the components of the unit outward normal vector to the surface ∂B;

the symbol $|\cdot|$ denotes a norm, either in the Euclidean vector space or in a tensor space, while $\|\cdot\|_{L^2(B)}$ denotes the L^2 –norm. We say that a function f defined on $B \times [0, t_0)$ is of class $C^{M,N}$, where M and N are given nonnegative numbers, if the functions $\partial^m f^{(n)} \equiv \frac{\partial^m}{\partial x_i \partial x_j \ldots \partial x_s}\left(\frac{\partial^n f}{\partial t^n}\right)$, $m \in \{0, 1, \ldots M\}$, $n \in \{0, 1, \ldots, N\}$, and $m + n \leq \max\{M, N\}$ exist and are continuous on $B \times [0, t_0)$.

We assume that an elastic material fills B. Then, the fundamental equations of the nonlinear theory of thermoelasticity are [1, 3]

– The equations of motion

$$S_{Ki,K} + \rho_0 b_i = \rho_0 \ddot{x}_i \tag{3}$$

– The energy equation

$$\rho_0 T \dot{S} = -Q_{K,K} + \rho_0 r \tag{4}$$

– The constitutive equations

$$\begin{aligned} \psi &= \hat{\psi}(x_{i,K}, T; X_L) \\ S_{Ki} &= \rho_0 \frac{\partial \hat{\psi}}{\partial x_{i,K}} \\ S &= -\frac{\partial \hat{\psi}}{\partial T} \\ Q_K &= \hat{Q}_K(x_{i,K}, T, T_{,K}; X_L) \end{aligned} \tag{5}$$

where $\rho_0(X_L) > 0$ is the reference mass density, $b_i(X_K, t)$ is the body force, $r(X_K, t)$ is the heat supply, S_{Ki} is the first Piola–Kirchhoff stress tensor, $T(X_K, t) > 0$ is the absolute temperature, S is the entropy, Q_K is the heat flux vector and ψ is the free energy. The response functions $\hat{\psi}$ and $\hat{Q}_K$ are assumed to be of class C^1 on their domains of definition. The domain of $\hat{\psi}$ is the set of all $(x_{i,K}, T; X_L)$, where $\det(x_{i,K}) > 0$, $T > 0$, and $\mathbf{X} \in B$, while the domain of $\hat{Q}_K$ is the set of all $(x_{i,K}, T, T_{,K}; X_L)$, where $\det(x_{i,K}) > 0$, $T > 0$, and $\mathbf{X} \in B$. Moreover, the functional $\hat{Q}_K$ must satisfy the following restrictions [1, 3]:

$$\begin{aligned} &\hat{Q}_K T_{,K} \leq 0 \\ &\hat{Q}_K(x_{i,K}, T, 0; X_L) = 0 \end{aligned} \tag{6}$$

An *admissible thermodynamic process*, corresponding to an elastic material characterized by the density ρ_0 and the response functions $\hat{\psi}$, $\hat{Q}_K$, is the ordered array $[x_i, T, \psi, S_{Ki}, S, Q_K, b_i, r]\ (X_M, t)$ having the regularity properties:

$\alpha)$ $x_i \in C^{1,2}$ on $\overline{B} \times [0, t_0)$

$\beta)$ $T, \psi, S \in C^1$ on $\overline{B} \times [0, t_0)$

$\gamma)$ $Q_K, S_{Ki} \in C^{1,0}$ on $\overline{B} \times [0, t_0)$

$\delta)$ $b_i, r \in C^0$ on $\overline{B} \times [0, t_0)$

and satisfying (3)–(6).

We shall say that $U = \{x_i, T\}$ is a *smooth admissible state* corresponding to the load (b_i, r) if $[x_i, T, \psi, S_{Ki}, S, Q_K, b_i, r]$ is an admissible thermodynamic process.

For admissible thermodynamic processes, we have the relation

$$\begin{aligned} &\frac{\partial}{\partial t}\left[\rho_0\left(\psi + TS + \frac{1}{2}\dot{x}_i \dot{x}_i\right)\right] \\ &\quad = \left(S_{Ki}\dot{x}_i - Q_K\right)_{,K} + \rho_0(b_i \dot{x}_i + r) \end{aligned} \tag{7}$$

which follows by adding (4) and the relations (3) multiplied by $\dot{x}_i$, and then by using

$$\begin{aligned} \rho_0 \dot{\psi} &= \rho_0 \frac{\partial \hat{\psi}}{\partial x_{i,K}} \dot{x}_{i,K} + \rho_0 \frac{\partial \hat{\psi}}{\partial T} \dot{T} \\ &= S_{Ki} \dot{x}_{i,K} - \rho_0 S \dot{T} \end{aligned} \tag{8}$$

In the following, we denote by $\mathbf{F}$ the deformation gradient, $\mathbf{g}$ the temperature gradient, and $\mathbf{v}$ the velocity. Their components will be denoted by F_{iK}, g_K, and v_i, respectively, namely,

$$F_{iK} = x_{i,K}, \quad g_K = T_{,K}, \quad v_i = \dot{x}_i \tag{9}$$

Preliminary Results

Let $U = \{x_i, T\}$ and $\overline{U} = \{\overline{x}_i, \overline{T}\}$ be two smooth admissible states on $B \times [0, t_0)$ corresponding to

the loads (b_i, r) and $(\overline{b}_i, \overline{r})$, respectively. We define the function D on $[0, t_0)$ by

$$D = \int_B \left[\frac{1}{2}\rho_0(v_i - \overline{v}_i)(v_i - \overline{v}_i) + \rho_0\psi - \rho_0\overline{\psi} - \overline{S}_{Ki}(F_{iK} - \overline{F}_{iK}) + \rho_0 S(T - \overline{T})\right] dV \tag{10}$$

where

$$\begin{aligned} \overline{F}_{iK} &= \overline{x}_{i,K},\ \overline{g}_K = \overline{T}_{,K},\ \overline{v}_i = \dot{\overline{x}}_i \\ \overline{\psi} &= \hat{\psi}(\overline{F}_{iK}, \overline{T}; X_K) \\ \overline{S} &= -\frac{\partial \overline{\psi}}{\partial \overline{T}} \\ \overline{S}_{Lj} &= \rho_0 \frac{\partial \overline{\psi}}{\partial \overline{F}_{jL}} \\ \overline{Q}_L &= \hat{Q}_L(\overline{F}_{iK}, \overline{T}, \overline{g}_K; X_K) \end{aligned} \tag{11}$$

On account of (5), (9), and (11), it is easy to see that D is of quadratic order in

$$\left\|\mathbf{v} - \overline{\mathbf{v}}, \mathbf{F} - \overline{\mathbf{F}}, T - \overline{T}\right\|_{L^2(B)}$$

The evolution in time of this function is described by the following theorem:

Theorem 1. *If $U = \{x_i, T\}$ and $\overline{U} = \{\overline{x}_i, \overline{T}\}$ are two smooth admissible states on $B \times [0, t_0)$ corresponding to the loads (b_i, r) and $(\overline{b}_i, \overline{r})$ in $L^\infty(B \times [0, t_0))$, then*

$$\dot{D} = \int_{\partial B} \Gamma dA + \int_B \left[\Lambda + Z + \rho_0(b_i - \overline{b}_i)(v_i - \overline{v}_i) + \frac{\rho_0}{T}(r - \overline{r})(T - \overline{T}) - \frac{1}{T\overline{T}}\left(-\overline{Q}_{K,K} + \rho_0\overline{r}\right)(T - \overline{T})^2\right] dV \tag{12}$$

where

$$\Gamma = \left[(S_{Ki} - \overline{S}_{Ki})(v_i - \overline{v}_i) - \frac{1}{T}(Q_K - \overline{Q}_K)(T - \overline{T})\right] N_K \tag{13}$$

$$\Lambda = \dot{\overline{F}}_{iK}\left[S_{Ki} - \overline{S}_{Ki} - \frac{\partial \overline{S}_{Ki}}{\partial \overline{F}_{jL}}(F_{jL} - \overline{F}_{jL}) - \frac{\partial \overline{S}_{Ki}}{\partial \overline{T}}(T - \overline{T})\right] - \rho_0\overline{T}\left[S - \overline{S} - \frac{\partial \overline{S}}{\partial \overline{F}_{iK}}(F_{iK} - \overline{F}_{iK}) - \frac{\partial \overline{S}}{\partial \overline{T}}(T - \overline{T})\right] \tag{14}$$

$$Z = (Q_K - \overline{Q}_K)\left(\frac{T - \overline{T}}{T}\right)_{,K} \tag{15}$$

Proof. From (10) we obtain

$$\begin{aligned} \dot{D} = \int_B \Bigg\{ & \frac{\partial}{\partial t}\left[\rho_0\left(\psi + TS + \frac{1}{2}v_i v_i\right)\right] \\ & - \frac{\partial}{\partial t}\left[\rho_0\left(\overline{\psi} + \overline{T}\,\overline{S} + \frac{1}{2}\overline{v}_i\overline{v}_i\right)\right] \\ & - \rho_0\left(v_i\dot{\overline{v}}_i + \dot{v}_i\overline{v}_i - 2\overline{v}_i\dot{\overline{v}}_i\right) - \dot{\overline{S}}_{Ki}\left(F_{iK} - \overline{F}_{iK}\right) \\ & - \overline{S}_{Ki}\left(\dot{F}_{iK} - \dot{\overline{F}}_{iK}\right) - \rho_0\dot{\overline{T}}\left(S - \overline{S}\right) \\ & - \rho_0\overline{T}\left(\dot{S} - \dot{\overline{S}}\right)\Bigg\} dV \end{aligned} \tag{16}$$

Using the balance laws (3), (7), we may write (16) in the form

$$\begin{aligned} \dot{D} = \int_B \Big\{ & \left[(S_{Ki} - \overline{S}_{Ki})(v_i - \overline{v}_i)\right]_{,K} + \rho_0(b_i - \overline{b}_i)(v_i - \overline{v}_i) \\ & + \rho_0 r - Q_{K,K} - \rho_0\overline{r} + \overline{Q}_{K,K} - \dot{\overline{S}}_{Ki}(F_{iK} - \overline{F}_{iK}) \\ & + \dot{\overline{F}}_{iK}(S_{Ki} - \overline{S}_{Ki}) - \rho_0\dot{\overline{T}}(S - \overline{S}) - \rho_0\overline{T}\left(\dot{S} - \dot{\overline{S}}\right)\Big\} dV \end{aligned} \tag{17}$$

Introducing the notations

$$\begin{aligned} R = & -\dot{\overline{S}}_{Ki}(F_{iK} - \overline{F}_{iK}) + \dot{\overline{F}}_{iK}(S_{Ki} - \overline{S}_{Ki}) \\ & - \rho_0\dot{\overline{T}}(S - \overline{S}) + \rho_0\dot{\overline{S}}(T - \overline{T}) \end{aligned} \tag{18}$$

$$P = \rho_0 r - Q_{K,K} - \rho_0\overline{r} + \overline{Q}_{K,K} - \rho_0\left(\dot{\overline{S}}T + \dot{S}\overline{T} - 2\dot{\overline{S}}\overline{T}\right) \tag{19}$$

we have

$$\begin{aligned} \dot{D} = \int_B \Big\{ & \left[(S_{Ki} - \overline{S}_{Ki})(v_i - \overline{v}_i)\right]_{,K} \\ & + \rho_0(b_i - \overline{b}_i)(v_i - \overline{v}_i) + R + P\Big\} dV \end{aligned} \tag{20}$$

It follows from (11) that

$$\dot{\overline{S}}_{Ki} = \frac{\partial \overline{S}_{Ki}}{\partial \overline{F}_{jL}} \dot{\overline{F}}_{jL} + \frac{\partial \overline{S}_{Ki}}{\partial \overline{T}} \dot{\overline{T}}$$
$$\dot{\overline{S}} = \frac{\partial \overline{S}}{\partial \overline{F}_{iK}} \dot{\overline{F}}_{iK} + \frac{\partial \overline{S}}{\partial \overline{T}} \dot{\overline{T}} \tag{21}$$

With the help of (21), we find that

$$R = \Lambda \tag{22}$$

On the other hand, using (4) we have

$$\begin{aligned} P &= \rho_0 r - Q_{K,K} - \rho_0 \dot{\bar{r}} + \overline{Q}_{K,K} - \rho_0 \dot{\overline{S}}(T - \overline{T}) \\ &\quad - \rho_0 \overline{T}\left(\dot{S} - \dot{\overline{S}}\right) = \rho_0 r - Q_{K,K} - \rho_0 \dot{\bar{r}} + \overline{Q}_{K,K} \\ &\quad + \frac{\overline{T}}{T}\left(-\overline{Q}_{K,K} + \rho_0 \bar{r}\right) - \frac{\overline{T}}{T}\left(-Q_{K,K} + \rho_0 r\right) \\ &\quad - \left(-\overline{Q}_{K,K} + \rho_0 \bar{r}\right)\left(\frac{\overline{T}}{T} - 2 + \frac{T}{\overline{T}}\right) \\ &= \frac{\rho_0}{T}(r - \bar{r})(T - \overline{T}) - \left[\left(Q_K - \overline{Q}_K\right)\frac{T - \overline{T}}{T}\right]_{,K} \\ &\quad + \left(Q_K - \overline{Q}_K\right)\left(\frac{T - \overline{T}}{T}\right)_{,K} \\ &\quad - \frac{1}{T\overline{T}}\left(-\overline{Q}_{K,K} + \rho_0 \bar{r}\right)(T - \overline{T})^2 \end{aligned} \tag{23}$$

Collecting (20), (22), (23) and using (13), (14), (15) and the divergence theorem, we conclude that (12) holds. The proof is complete.

Remark 1. For a nonconductor of heat elastic material ($Q_K = \overline{Q}_K = 0$), the right-hand side of (12) is of quadratic order in

$$\left\|\mathbf{v} - \bar{\mathbf{v}}, \mathbf{F} - \overline{\mathbf{F}}, T - \overline{T}, \mathbf{b} - \bar{\mathbf{b}}, r - \bar{r}\right\|_{L^2(B)}$$

provided the smooth admissible states satisfy the same boundary conditions.

On the other hand, since $D(t)$ is of quadratic order in

$$\left\|\mathbf{v} - \bar{\mathbf{v}}, \mathbf{F} - \overline{\mathbf{F}}, T - \overline{T}\right\|_{L^2(B)},$$

then from (12) some stability results may be obtained by applying Gronwall-type inequalities. This was the case studied by Dafermos [6].

Remark 2. For the general case of elastic materials which are conductors of heat, it is clear that the right-hand side of (12) is of quadratic order in

$$\left\|\mathbf{v} - \bar{\mathbf{v}}, \mathbf{F} - \overline{\mathbf{F}}, T - \overline{T}, \mathbf{g} - \bar{\mathbf{g}}, \mathbf{b} - \bar{\mathbf{b}}, r - \bar{r}\right\|_{L^2(B)}$$

provided the smooth admissible states satisfy the same boundary conditions. So, in order to apply a Gronwall-type inequality, some further results giving an estimate involving the function Z, defined by the relation (15), are needed. In [3], Chiriţă showed how to overcome this problem for *definite heat-conducting* elastic materials.

In the following, we consider the general case of elastic materials which are conductors of heat. First, we recall the notion of definite conductor, introduced by Coleman and Gurtin [5] and utilized by Chiriţă [3], to study the stability of smooth admissible states.

From (11), it follows that

$$\begin{aligned} Q_K = \overline{Q}_K &- \overline{K}_{KL}(g_L - \overline{g}_L) - \overline{\varepsilon}_{KiL}\left(F_{iL} - \overline{F}_{iL}\right) \\ &- \overline{\alpha}_K(T - \overline{T}) + Q_K^0 \end{aligned} \tag{24}$$

where

$$\begin{aligned} \overline{K}_{KL} &= -\frac{\partial \widehat{Q}_K}{\partial g_L}\left(\overline{F}_{kM}, \overline{T}, \overline{g}_M; X_M\right) \\ \overline{\varepsilon}_{KiL} &= -\frac{\partial \widehat{Q}_K}{\partial F_{iL}}\left(\overline{F}_{kM}, \overline{T}, \overline{g}_M; X_M\right) \\ \overline{\alpha}_K &= -\frac{\partial \widehat{Q}_K}{\partial T}\left(\overline{F}_{kM}, \overline{T}, \overline{g}_M; X_M\right) \end{aligned} \tag{25}$$

and Q_K^0 is a function of order $o(\rho)$, ρ being defined by

$$\rho = \left|\mathbf{F} - \overline{\mathbf{F}}\right| + \left|T - \overline{T}\right| + \left|\mathbf{g} - \bar{\mathbf{g}}\right| \tag{26}$$

Definition 1. *We say that the admissible state $\overline{U}$ resides in the region where the material is a definite heat conductor if*

$$\overline{k}_{KL} = \frac{1}{2}\left(\overline{K}_{KL} + \overline{K}_{LK}\right) \tag{27}$$

is positive definite.

We introduce the following notation:

$$y(t) = \left\| (\mathbf{F} - \overline{\mathbf{F}}, T - \overline{T})(\cdot, t) \right\|_{L^2(B)}, \quad t \in [0, t_0) \tag{28}$$

Theorem 2. *Let $\overline{U} = \{\overline{x}_i, \overline{T}\}$ be a smooth admissible state residing in the region where the material is a definite conductor of heat. Then there exist the positive constants δ, m_1 and with the following property: if $U = \{x_i, T\}$ is any smooth admissible process defined on $B \times [0, t_0)$, such that*

$$\rho = |\mathbf{F} - \overline{\mathbf{F}}| + |T - \overline{T}| + |\mathbf{g} - \overline{\mathbf{g}}| < \delta \tag{29}$$

on $B \times [0, t_0)$, then

$$\int_B Z dV \le m_1 y^2(t), \qquad t \in [0, t_0) \tag{30}$$

Proof. Since $\overline{U} = \{\overline{x}_i, \overline{T}\}$ resides in the region of state where the elastic material behaves as a definite conductor of heat, it follows that there is a positive constant λ such that

$$\begin{aligned} &\int_B \frac{1}{T} \overline{K}_{KL} (g_K - \overline{g}_K)(g_L - \overline{g}_L) dV \\ &\quad = \int_B \frac{1}{T} \overline{k}_{KL} (g_K - \overline{g}_K)(g_L - \overline{g}_L) dV \\ &\quad \ge \lambda \int_B (g_K - \overline{g}_K)(g_K - \overline{g}_K) dV \end{aligned} \tag{31}$$

Then in view of (15), (24), and the above inequality, we conclude that there exist a positive constant δ such that when (29) is satisfied, then

$$\begin{aligned} &\int_B Z dV \le -\lambda \int_B (g_K - \overline{g}_K)(g_K - \overline{g}_K) dV \\ &+ \int_B \Big[I_{KiL} (g_K - \overline{g}_K)(F_{iL} - \overline{F}_{iL}) \\ &+ G_K (g_K - \overline{g}_K)(T - \overline{T}) \\ &+ H_{iK} (F_{iK} - \overline{F}_{iK})(T - \overline{T}) + E(T - \overline{T})^2 \Big] dV \end{aligned} \tag{32}$$

where

$$\begin{aligned} I_{KiL} &= -\frac{1}{T} \overline{\varepsilon}_{KiL}, \quad G_L = \frac{1}{T^2} \left(g_K \overline{K}_{LK} - \overline{\alpha}_L T \right) \\ H_{iL} &= \frac{1}{T^2} g_K \overline{\varepsilon}_{KiL}, \quad E = \frac{1}{T^2} g_L \overline{\alpha}_L \end{aligned} \tag{33}$$

Applying the Schwarz inequality and the mean arithmetic–geometric inequality

$$a_1 a_2 \le \frac{1}{2} \left(\varepsilon a_1^2 + \frac{a_2^2}{\varepsilon} \right), \quad \varepsilon > 0 \tag{34}$$

to the last terms in (32), we obtain

$$\begin{aligned} 2 \int_B Z dV \le\ & (\varepsilon_1 + \varepsilon_2 - 2\lambda) \| (\mathbf{g} - \overline{\mathbf{g}})(\cdot, t) \|^2_{L^2(B)} \\ &+ \left(\frac{M_1^2}{\varepsilon_1} + M_4^2 + 1 \right) \left\| T - \overline{T})(\cdot, t) \right\|^2_{L^2(B)} \\ &+ \left(\frac{M_2^2}{\varepsilon_2} + M_3^2 \right) \left\| (\mathbf{F} - \overline{\mathbf{F}})(\cdot, t) \right\|^2_{L^2(B)} \end{aligned} \tag{35}$$

where ε_1, ε_2 are arbitrary positive constants and

$$\begin{aligned} M_1 &= \max |\mathbf{G}|, \quad M_2 = \max |\mathbf{I}| \\ M_3 &= \max |\mathbf{H}|, \quad M_4^2 = 2 \max |E|, \quad \text{on } \overline{B} \times [0, t_0) \end{aligned} \tag{36}$$

Now, choosing the arbitrary constants ε_1 and ε_2 so that

$$\varepsilon_1 + \varepsilon_2 - 2\lambda \le 0 \tag{37}$$

from (35), it follows the inequality (30) with

$$m_1 = \frac{1}{2} \max \left(\frac{M_1^2}{\varepsilon_1} + M_4^2 + 1, \frac{M_2^2}{\varepsilon_2} + M_3^2 \right) \tag{38}$$

The proof is complete.

Stability of Smooth Admissible States

Definition 2. *A smooth admissible state $\overline{U} = \{\overline{x}_i, \overline{T}\}$ resides in the convexity region of*

internal energy if [6] *the following two conditions are satisfied*:

(i) *For each* $(\mathbf{X}, t) \in \overline{B} \times [0, t_0)$, *there exists a positive constant* μ *such that*

$$\frac{\partial \overline{\psi}}{\partial \overline{F}_{iK} \overline{F}_{jL}} \xi_{iK} \xi_{jL} \geq \mu \, \xi_{iK} \xi_{iK}, \qquad \text{for all } \xi_{iK} \tag{39}$$

$$\text{(ii)} \qquad \frac{\partial \overline{S}}{\partial \overline{T}} > 0 \tag{40}$$

The study on stability and uniqueness is based on the following Gronwall-type inequality [6]:

Lemma 1. *Assume that the nonnegative functions* $z(t) \in L^{\infty}[0, s]$ *and* $g(t) \in L^{1}[0, s]$ *satisfy the inequality*

$$z^2(\tau) \leq M^2 z^2(0) + 2 \int_0^{\tau} [(\alpha + 2\beta\tau) z^2(t) + N g(t) z(t)] dt \quad \tau \in [0, s] \tag{41}$$

with α, β, M, *and* N *nonnegative constants. Then*

$$z(s) \leq \left[M z(0) + N \int_0^s g(t) dt \right] \exp\left(\sigma s + \beta s^2\right) \tag{42}$$

where $\sigma = \alpha + \beta/\alpha$.

Now, we are ready to state the following stability result:

Theorem 3. *Let* $\overline{U} = \{\overline{x}_i, \overline{T}\}$ *be a smooth admissible state on* $B \times [0, t_0)$ *corresponding to the loading* $(\overline{b}_i, \overline{r}) \in L^{\infty}(B \times [0, t_0))$ *and residing in the region where the internal energy is a convex function and the elastic material is a definite conductor of heat. Then there exist the positive constants* δ_1, α_0, M_0, *and* N_0 *with the following property*: *if* $U = \{x_i, T\}$ *is any smooth admissible state on* $B \times [0, t_0)$ *corresponding to the loading* $(b_i, r) \in L^{\infty}(B \times [0, t_0))$, *such that*

$$\rho = \left|\mathbf{F} - \overline{\mathbf{F}}\right| + \left|T - \overline{T}\right| + |\mathbf{g} - \bar{\mathbf{g}}| < \delta_1 \tag{43}$$

on $B \times [0, t_0)$ *and*

$$\begin{aligned} &(v_i - \overline{v}_i)(S_{Ki} - \overline{S}_{Ki}) N_K = 0 \\ &(T - \overline{T})(Q_K - \overline{Q}_K) N_K = 0, \qquad \text{on } \partial B \times [0, t_0) \end{aligned} \tag{44}$$

then for any $s \in [0, t_0)$, *we have*

$$z_0(s) \leq \left[M_0 z_0(0) + N_0 \int_0^s g_0(t) dt \right] \exp(\alpha_0 s) \tag{45}$$

where

$$z_0(s) = \left\| (\mathbf{v} - \bar{\mathbf{v}}, \mathbf{F} - \overline{\mathbf{F}}, T - \overline{T})(\cdot, s) \right\|_{L^2(B)} \tag{46}$$

$$g_0(s) = \|(\mathbf{b} - \bar{\mathbf{b}}, r - \bar{r})(\cdot, s)\|_{L^2(B)} \tag{47}$$

Proof. From (13) and (44) we have $\Gamma = 0$. In view of (12), (14), (30), and Schwarz inequality, it follows that there exist the positive constants δ, v_1, and v_2 such that whenever (29) holds, we have

$$\dot{D}(t) \leq v_1 y^2(t) + v_2 g_0(t) w(t), \qquad t \in [0, t_0) \tag{48}$$

where $y(t)$ is defined by (28) and

$$w(t) = \left\| (\mathbf{v} - \bar{\mathbf{v}}, T - \overline{T})(\cdot, t) \right\|_{L^2(B)} \tag{49}$$

Let us fix $s \in [0, t_0)$ and integrate (48) over $[0, \tau]$, with $\tau \in [0, s]$. Then, we have

$$D(\tau) \leq D(0) + v_1 \int_0^{\tau} z_0^2(t) dt + v_2 \int_0^{\tau} g_0(t) z_0(t) dt \tag{50}$$

Here we used the inequalities $y(t) \leq z_0(t)$ and $w(t) \leq z_0(t)$, $t \in [0, t_0)$.

On the other hand, in view of (5), (9), and (11), we obtain

$$\rho_0\psi - \rho_0\overline{\psi} - \overline{S}_{Ki}\left(F_{iK} - \overline{F}_{iK}\right) + \rho_0 S\left(T - \overline{T}\right) = \frac{\rho_0}{2}\frac{\partial\overline{\psi}}{\partial\overline{F}_{iK}\partial\overline{F}_{jL}}\left(F_{iK} - \overline{F}_{iK}\right)\left(F_{jL} - \overline{F}_{jL}\right) + \frac{1}{2}\frac{\partial\overline{S}}{\partial\overline{T}}\left(T - \overline{T}\right)^2 + o\left(\left|\mathbf{F} - \overline{\mathbf{F}}\right|^2 + \left|T - \overline{T}\right|^2\right) \tag{51}$$

It follows from (10), (39), (40), and (51) that there exist the positive constants δ_0 and v_3 such that, whenever

$$\left|\mathbf{F} - \overline{\mathbf{F}}\right| + \left|T - \overline{T}\right| < \delta_0 \tag{52}$$

we have

$$v_3 z_0(t) \leq 2D(t), \qquad t \in [0, t_0) \tag{53}$$

Setting $\delta_1 = \min(\delta, \delta_0)$ in (43), from (50) and (53), we obtain

$$v_3 z_0^2(\tau) \leq 2D(0) + 2v_1\int_0^\tau z_0^2(t)dt + 2v_2\int_0^\tau g_0(t)z_0(t)dt \tag{54}$$

Using the estimate

$$D(0) \leq v_4 z_0(0), \qquad v_4 > 0 \tag{55}$$

and the notations

$$M_0^2 = \frac{2v_4}{v_3}, \qquad \alpha_0 = \frac{v_1}{v_3}, \qquad N_0 = \frac{v_2}{v_3} \tag{56}$$

then (54) implies that

$$z_0^2(\tau) \leq M_0^2 z_0(0) + 2\int_0^\tau \left[\alpha_0 z_0^2(t)dt + N_0 g_0(t)z_0(t)\right]dt \tag{57}$$

An application of the Lemma 1 completes the proof.

A direct consequence of the above theorem is the following uniqueness result:

Theorem 4. *Let U and $\overline{U}$ be as in Theorem 3. Assume that the corresponding body loads coincide on $B \times [0, t_0)$ and U and $\overline{U}$ originate from the same state, namely,*

$$x_i(\mathbf{X}, 0) = \overline{x}_i(\mathbf{X}, 0), \quad v_i(\mathbf{X}, 0) = \overline{v}_i(\mathbf{X}, 0) \quad T(\mathbf{X}, 0) = \overline{T}(\mathbf{X}, 0), \quad \mathbf{X} \in B \tag{58}$$

Then U and $\overline{U}$ coincide on $B \times [0, t_0)$.

Remark 3. Theorem 3 describes the continuous dependence of smooth thermodynamic processes upon initial state and the body loads, while Theorem 4 deals with the uniqueness of processes. Both results are local, and they are established under the assumption that the internal energy is a convex function and the elastic material behaves as a definite conductor of heat.

Similar results are obtained when the convexity of internal energy is replaced by a weaker condition expressing that $\overline{U}$ resides in the strong ellipticity region (for more details see [3, 6]).

References

1. Carlson DE (1972) Linear thermoelasticity. In: Truesdell C (ed) Handbuch der Physik VI a/2. Springer, Berlin/Heidelberg/New York, pp 297–345
2. Ciarletta M, Scalia A (1993) On the nonlinear theory of nonsimple thermoelastic materials with voids. ZAMM 73:67–75
3. Chiriţă S (1982) Uniqueness and continuous data dependence in dynamical problems of nonlinear thermoelasticity. J Therm Stress 5:331–346
4. Coleman BD, Dill EH (1973) On thermodynamics and the stability of motions of materials with memory. Arch Ration Mech Anal 51:1–53
5. Coleman BD, Gurtin ME (1965) Waves in materials with memory III. Thermodynamic influences in the growth and decay of acceleration waves. Arch Ration Mech Anal 19:266–298
6. Dafermos CM (1979) The second law of thermodynamics and stability. Arch Ration Mech Anal 70:167–179
7. Ericksen JL (1966) A thermo–kinetic view of elastic stability. Int J Solid Struct 2:573–580
8. Galeş C (2010) On the nonlinear theory of micromorphic thermoelastic solids. Math Probl Eng 2010: 16 p, Article ID 415304
9. Galeş C (2011) On uniqueness and continuous dependence in nonlinear thermoviscoelasticity. J Therm Stress 34:366–377

10. Gurtin ME (1975) Thermodynamics and stability. Arch Ration Mech Anal 59:63–96
11. Ieşan D (2006) Continuous dependence in a nonlinear theory of viscoelastic mixtures. Int J Eng Sci 44:1127–1145
12. Ieşan D, Nappa L (2008) On the theory of viscoelastic mixtures and stability. Math Mech Solid 13:55–80

Control of Crack Propagation

Akihide Saimoto
Graduate School of Engineering,
Nagasaki University, Nagasaki, Japan

Overview

A thermal stress induced by a localized temperature change in the vicinity of crack tip often causes crack to propagate. Taking advantage of this phenomenon, brittle plates can be cleaved without any mechanical tool but with adequate temperature control [1, 2]. This technique is useful in the division of thin glass plates into parts and is called thermal stress cleaving. That is, in the thermal stress cleaving, a crack propagation is controlled by the control of temperature change in the body. Since the generated surface by thermal stress cleaving is strong, smooth, and not stained by coolant nor cutting fluid, this method is expected as one of the desired technique for dividing brittle plates. In this entry, the fundamental background and some numerical results of thermal stress cleaving are presented.

Mechanics of Crack Growth Under Thermal Stress Induced by Point Heating

When an infinite plate of thickness B is heated by a continual point heat source applied at an origin of the coordinate system, the temperature rise $T(r,t)$ at a point of radial distance r from the origin, after heating duration t, is given by [3]

$$T(r,t) = \frac{Q}{4\pi\lambda} E_1\left(\frac{r^2}{4\kappa t}\right) \tag{1}$$

where Q is a magnitude of heat source per thickness, λ is a thermal conductivity, κ is a thermal diffusivity, and $E_1(x)$ is an exponential integral function defined as

$$E_1(x) = \int_x^\infty \frac{e^{-u}}{u} du \tag{2}$$

Note that (1) expresses the mean value of temperature rise in thickness and no heat dissipation from surfaces of plate is assumed. The asymmetric thermal stress field corresponding to (1) is calculated by

$$\begin{aligned} \sigma_r(r,t) &= -\frac{\alpha EQ}{8\pi\lambda}\left\{\frac{1-e^{-p}}{p} + E_1(p)\right\} \\ \sigma_\theta(r,t) &= \frac{\alpha EQ}{8\pi\lambda}\left\{\frac{1-e^{-p}}{p} - E_1(p)\right\} \end{aligned} \tag{3}$$

in which p is a nondimensional parameter defined by $p = r^2/4\kappa t$. E is Young's modulus and α is a coefficient of linear expansion.

The thermoelastic field of (1) and (3) is plotted in Fig. 1. Contrast to the distributions T and σ_r, which do not change their sign, σ_θ varies from negative to positive value depending on the parameter $r^2/4\kappa t$. A positive σ_θ around the heating point can be used for the crack extension force. That is, if the crack exists along the radial direction to the point of heat, the mode I singular stress field would be produced in the vicinity of the crack tip. In this entry, it is assumed that the heat transfer coefficient γ which characterizes the heat dissipation from surfaces of plate to atmosphere is independent of the temperature rise. Therefore, γ is constant regardless of temperature. When line crack of length $2a$ exists along the radial direction from the heating point as illustrated in Fig. 2, the crack tip stress intensity factor (SIF) is estimated by

$$K_{\mathrm{I}}^N = \frac{\alpha EQ}{8\pi\lambda}\frac{d}{\sqrt{\pi a}}\int_1^{1+2a/d} S_\theta(X)\sqrt{\frac{2a/d+1-X}{X-1}}\,dX \tag{4}$$

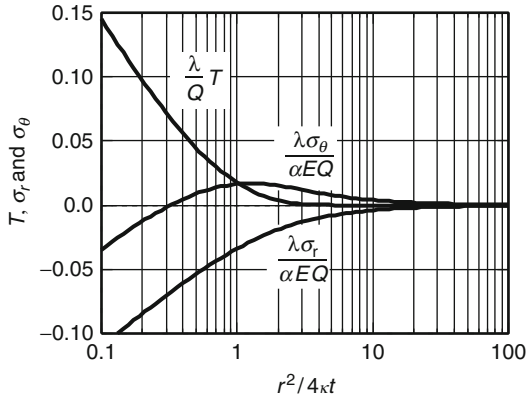

Control of Crack Propagation, Fig. 1 Thermoelastic field due to a point heat source acting in an infinite plate

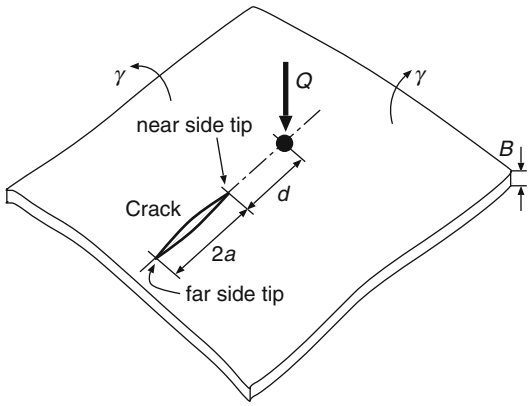

Control of Crack Propagation, Fig. 2 Radial crack in an infinite plate heated by a point heat source of magnitude Q

for near side tip and

$$K_{\mathrm{I}}^{F}=\frac{\alpha EQ}{8\pi\lambda}\frac{d}{\sqrt{\pi a}}\int_{1}^{1+2a/d}S_{\theta}(X)\sqrt{\frac{X-1}{2a/d+1-X}}\,dX \tag{5}$$

for far side tip, respectively. In (4) and (5), it is assumed that the crack opening does not alter the temperature distribution. $S_\theta(X)$ is a function defined as

$$S_{\theta}(X)=\int_{X^2/P}^{\infty}e^{-\Gamma X^2/u}\left(\frac{1-e^{-u}}{u^2}-2\frac{e^{-u}}{u}\right)du \tag{6}$$

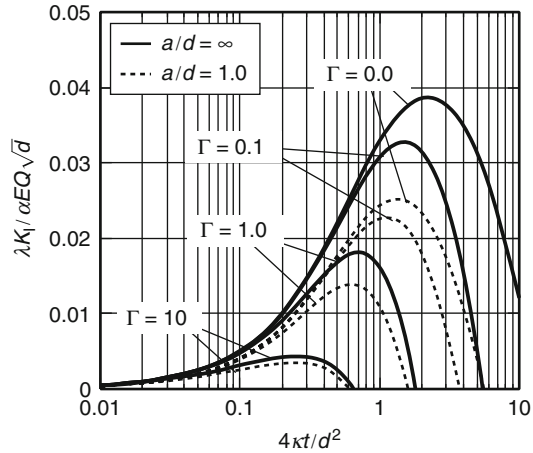

Control of Crack Propagation, Fig. 3 SIF at near side tip in Fig. 2 $\left(\Gamma=\frac{\gamma d^2}{4B\lambda}\right)$

where d is the distance between point of heat and the near side crack tip, Γ and P are the nondimensional parameters defined by $\Gamma=\gamma d^2/4B\lambda$ and $P=d^2/4\kappa t$, respectively. K_{I}^{N} is plotted against $4\kappa t/d^2$ in Fig. 3. As seen in this figure, the degree of heat dissipation from the surface of plate influences significantly on the value of resulted SIF. That is, the peak value of K_{I}^{N} decreases with increase of Γ.

If the magnitude of point heat source Q is suitable, the crack may propagate toward to a heating point. This crack propagation then causes the decrease of distance d. Once the distance d decreases to some level, the crack tip SIF becomes small and the crack would be finally arrested. In order to hold the SIF at some material dependent level so that the crack could grow continuously, the heating point should be moved so as to hold an appropriate distance d [1]. The quasi-steady stress σ_y distribution along the x axis when the point heat moves in a constant velocity v on x axis is given by

$$\sigma_y(\xi)=\frac{\alpha EQ}{8\pi\lambda}\int_0^{\infty}e^{-\Gamma u}\left[\frac{1-e^{-(\xi+Vu)^2/u}}{(\xi+Vu)^2}-\frac{2}{u}e^{-(\xi+Vu)^2u}\right]du \tag{7}$$

and the SIF of a semi-infinite crack following the point of heat with the identical velocity is obtained from

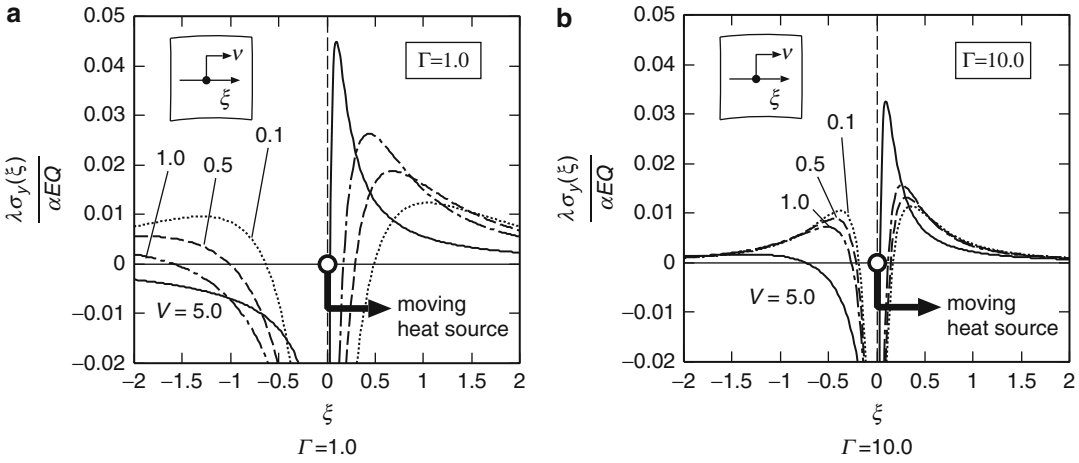

Control of Crack Propagation, Fig. 4 σ_y around a moving heat source that moves along x axis with constant velocity

$$K_{\mathrm{I}} = \sqrt{\frac{2d}{\pi}} \int_1^{\infty} \frac{\sigma_y(-\xi)}{\sqrt{\xi - 1}} d\xi \tag{8}$$

In (7), V is a nondimensional parameter defined by $V = vd/4\kappa$.

σ_y induced by a moving heat along the x axis exhibits the different tendency in the forward ($\xi > 0$) and in the backward ($\xi < 0$) regions. In the backward region, the $\sigma_y = 0$ boundary goes far off with increase of moving velocity as seen in Fig. 4. In Fig. 5, the nondimensional SIF of a semi-infinite crack which follows the moving heat source keeping a constant distance d_0 is plotted against nondimensional cutting velocity $vd_0/4\kappa$. It is found that if the values of v and Q are appropriate, the thermal stress cleaving could be continued stationary. It is also seen that there exist the limit velocity under which the steady crack growth is realized. This limit velocity becomes large with increase of the degree of heat dissipation from the surfaces of plate Γ. The variation of SIF can also be calculated when the cutting velocity is assumed at a constant v_0. Then the SIF is the function of distance d, as seen in Fig. 6.

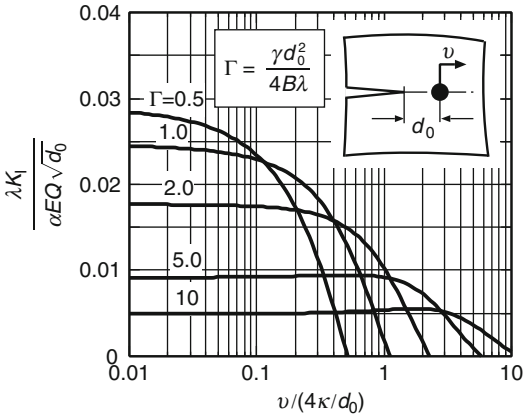

Control of Crack Propagation, Fig. 5 SIF vs nondimensional cutting velocity (d_0: constant, v: variable)

Point Heat Source in a Rectangular Plate

When the plate is large enough to be regarded as *an infinite*, some results shown so far would be useful for the explanation of mechanics of thermal stress cleaving. However, there are many situations in which the size effect cannot be ignored.

Thermoelastic Fields in a Rectangular Plate

The transient temperature field $T(x, y, t)$ in a rectangle with insulated boundaries heated by an instantaneous point heat can be expressed by series expansion as

$$T(x,y,t) = \frac{\kappa q}{ab\lambda}\left[e^{-\gamma\kappa(t-\tau)/\lambda B} + 2\sum_{n=1}^{\infty} f_n + 2\sum_{m=1}^{\infty} g_m + 4\sum_{m,n=1}^{\infty} h_{mn}\right] \tag{9}$$

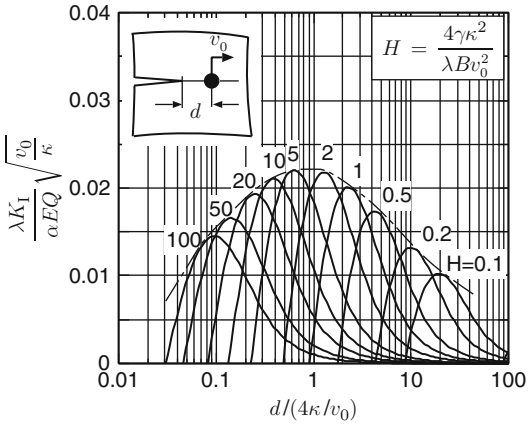

Control of Crack Propagation, Fig. 6 SIF vs nondimensional distance (v_0: constant, d: variable)

$$f_n = e^{-\left\{\left(\frac{n\pi}{b}\right)^2+\frac{\gamma}{Bz}\right\}\kappa(t-\tau)}\cos\frac{n\pi\eta}{b}\cos\frac{n\pi y}{b} \tag{10}$$

$$g_m = e^{-\left\{\left(\frac{m\pi}{a}\right)^2+\frac{\gamma}{Bz}\right\}\kappa(t-\tau)}\cos\frac{m\pi\xi}{a}\cos\frac{m\pi x}{a} \tag{11}$$

$$h_{mn} = e^{-\left\{\left(\frac{m\pi}{a}\right)^2+\left(\frac{n\pi}{b}\right)^2+\frac{\gamma}{Bz}\right\}\kappa(t-\tau)}\cos\frac{m\pi\xi}{a}\cos\frac{m\pi x}{a} \times \cos\frac{n\pi\eta}{b}\cos\frac{n\pi y}{b} \tag{12}$$

In (9–12), (x, y) are the coordinates of reference point, (ξ, η) are the coordinates of heating point, $(t-\tau)$ is the progress time after heating, a and b are the length and width of the rectangle, and q is the magnitude of an instantaneous point heat source per thickness. The temperature field in (9) can be used as the Green function. In fact, by integrating it with respect to heating time τ and heating position (ξ, η), the temperature fields due to the continual point heat source, area heating, and line heating can be obtained.

The thermoelastic field corresponding to the temperature field of (9) can be obtained through the thermoelastic displacement potential Φ for plane stress. That is, the stress components are given by [3, 4]

$$\sigma_x = \alpha E\left(\frac{\partial^2\Phi}{\partial x^2} - \Delta\Phi\right), \quad \sigma_y = \alpha E\left(\frac{\partial^2\Phi}{\partial y^2} - \Delta\Phi\right), \tau_{xy} = \alpha E\frac{\partial^2\Phi}{\partial x\partial y} \tag{13}$$

wherein Φ is the solution of

$$\Delta\Phi(x, y, t) = T(x, y, t) \tag{14}$$

In (13) and (14), Δ is the Laplacian. In general, the stress field corresponding to the particular solution of Φ in (14) does not satisfy the mechanical boundary conditions. In that case, the suitable isothermal stress field must be superposed onto (13) in order to fulfill the boundary condition.

Some Numerical Results

SIF by Circular Heating

Equation (9) is integrated over the circular area assuming that the heating density is uniform as illustrated in Fig. 7. The SIF normalized by using a total heating energy Q is plotted against a normalized heating duration in Fig. 8. The SIF increases monotonically with increase of the heating duration and decreases with the increase of heating radius r. Since the decrease of heating radius leads a localized overheating that may bring a thermal damage, the heating radius should not be set too small. The ratio of SIF and the temperature rise at the center of heating circle T_c is plotted in Fig. 9. It is found that the ratio K_I/T_c increases with increase of the heating area. This inclination is especially remarkable in the beginning of heating.

In Fig. 10, the nondimensional SIF normalized using Q is plotted against the crack length c/b when the heating radius is $r/b = 0.25$. The SIF becomes maximum when the position of crack tip coincides with the edge of heating circle. When the crack length is small, say $c/b < 0.15$, the SIF becomes negative for any heating duration. In order to make such small crack to grow, the heating position ξ should be placed nearer to the crack tip. The SIF is still positive when the crack tip exists within the heating area $0.75 < c/b < 1.15$.

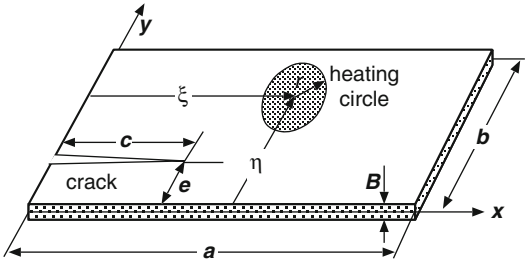

Control of Crack Propagation, Fig. 7 A rectangle heated in a circular area

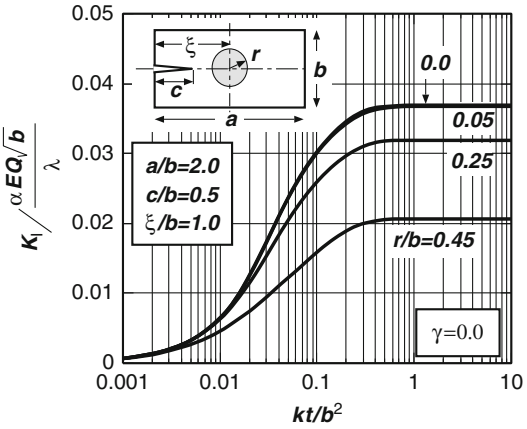

Control of Crack Propagation, Fig. 8 Effect of heating radius on K_I/Q ($e = \eta = b/2$ in Fig. 7)

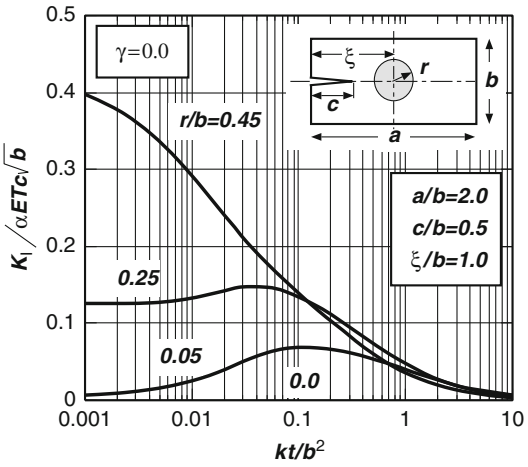

Control of Crack Propagation, Fig. 9 Effect of heating radius on K_I/T_c ($e = \eta = b/2$ in Fig. 7)

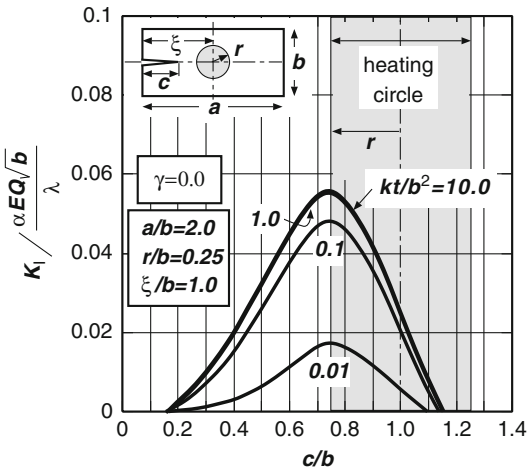

Control of Crack Propagation, Fig. 10 Variation of SIF as the function of c/b ($e = \eta = b/2$ in Fig. 7)

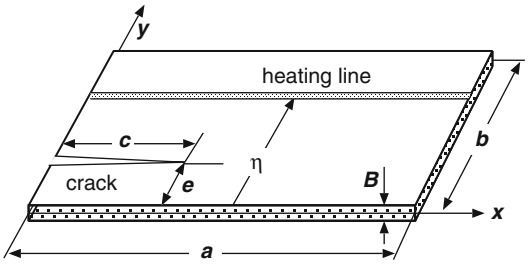

Control of Crack Propagation, Fig. 11 A rectangle heated by a line heat source

SIF Under Line Heating

The temperature rise shown in (9) and corresponding stress tensors in (13) can also be extended to the problem of line heating as seen in Fig. 11. In Figs. 12 and 13, the SIFs normalized using Q (the total heating energy) and T_c (temperature rise at heating line) are plotted against the heating duration. It is found from both figures that the line heating is effective when the length of crack is small. It is also found from Fig. 13 that the maximum value of K_I/T_c appears when $\kappa t/b^2 \sim 0.5$ almost independently of the crack length [5]. Figure 14 shows the variation of K_I/Q as the function of c/b. The SIF increases rapidly, while the crack length is small and then takes almost constant

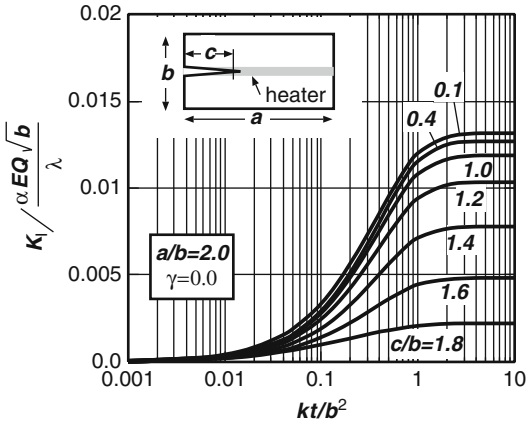

Control of Crack Propagation, Fig. 12 Effect of crack length on K_I/Q ($e = \eta = b/2$ in Fig. 11)

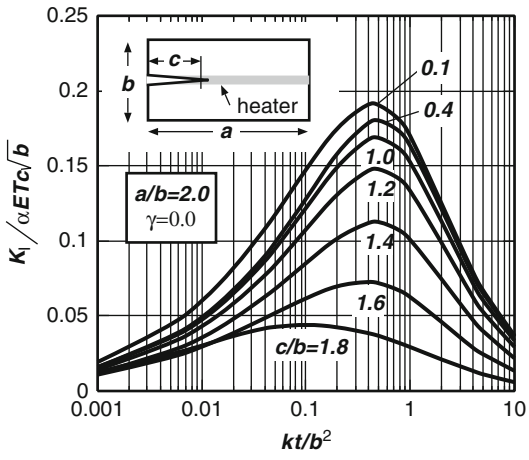

Control of Crack Propagation, Fig. 13 Effect of crack length on K_I/T_c ($e = \eta = b/2$ in Fig. 11)

within the range $c/b \in [0.2, 0.5]$. In this K - constant range, the steady crack growth could be observed.

The temperature field under line heating is independent of the length a, but the function of width b and heating position η. On the other hand, the SIF strongly depends upon the aspect ratio a/b. The effect of aspect ratio on the SIF is shown in Fig. 15. It can be said that the more the rectangle becomes slender ($a/b \rightarrow$ large), the larger the SIF becomes at the same heating duration.

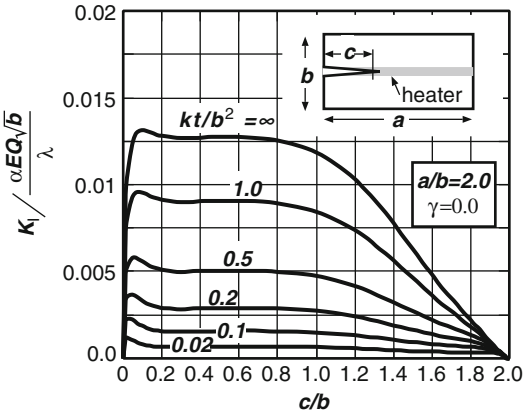

Control of Crack Propagation, Fig. 14 Variation of SIF as the function of c/b ($e = \eta = b/2$ in Fig. 11)

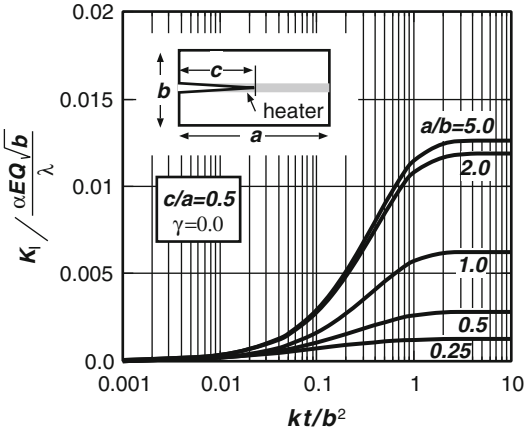

Control of Crack Propagation, Fig. 15 Effect of aspect ratio a/b on SIF ($e = \eta = b/2$ in Fig. 11)

References

1. Imai Y et al (1989) Possibility of employing thermal stress as a cutting device for brittle materials. Trans. Jpn Soc Mech Engrs 55–509:147 (in Japanese)
2. Saimoto A, Imai Y, Sawada H (1997) Thermal stress cleaving of a thin strip using a point heat source. Advances in Fracture Research (ICF9) 4:2095
3. Takeuchi Y, Noda N (1989) Analysis of thermal stress, 4th edn. Nissin Syuppan, Tokyo (in Japanese)
4. Timoshenko SP, Goodier JN (1987) Theory of elasticity, 3rd edn. McGraw–Hill, London, 22nd printing
5. Saimoto A, Sawada H, Imai Y (1998) Thermal Stress Cleaving of a Brittle Thin Strip Using Line Heat Source and the Size Effect. J Soc Mat Sci Jpn 47–8:813, (in Japanese)

Control of Thermal Residual Stresses

Nina Orlovskaya[1], Mykola Lugovy[2], V. Slyunyayev[2] and Jakob Kuebler[3]
[1]Department of Mechanical, Materials and Aerospace Engineering, University of Central Florida, Orlando, FL, USA
[2]Institute for Problems of Materials Science, Kiev, Ukraine
[3]Lab for High Performance Ceramics, EMPA, Duebendorf, Switzerland

Overview

Thermal residual stresses play the key role in the mechanical behavior of various composite materials. The control of residual stresses in materials allows the highest possible mechanical properties to be achieved. This is of special importance to ceramics-matrix composites, which are being used in numerous crosscutting industrial applications due to their excellent hardness, wear, corrosion resistance, and ability to withstand high temperatures. The best approach to increasing the fracture toughness and reliability, which enables the structural application of ceramics, is through the development of ceramic layered structures. Several publications on ceramics show that the use of layered materials is the most promising method for controlling cracks by deflection, bifurcation, microcracking, or internal stresses [1–5]. Layered structures clearly offer a key to greater reliability at a moderate cost, and new applications may result as more complex structures are tailored to specific applications [6].

One can increase the strength and apparent fracture toughness of ceramics by creating a layer with compressive stresses on the surface. This way, surface cracks will be arrested, and, therefore, higher failure stresses are achieved [7]. The variable layer composition, as well as the system's geometry, allows the designer to control the magnitude of the residual stresses in such a way that compressive stresses in the outer layers near the surface increase strength, flaw tolerance, fatigue strength, resistance to oxidation, and stress corrosion cracking. The changes in compressive and tensile stresses depend on the mismatch of coefficients of thermal expansion (CTEs), Young's moduli, as well as on the thickness ratio of layers [8, 9]. Compressive thermal stress arises after cooling from fabrication temperature if the CTE of the corresponding layer is less than CTEs of the surrounding layers. There have also been a number of experimental studies on laminated ceramics attempting to maximize the mechanical properties through control of thermal stresses [10–13].

Calculation of Thermal Stresses in a Layered Structure

The main assumptions of the calculation are:

1. The layered composite is considered as a rectangular cross section beam loaded in pure bending in the plane perpendicular to the layers.
2. The material of each layer is assumed elastic, strictly obeying Hooke's law.
3. The plane sections remain plane.
4. Temperature gradients, edge effects, and shear stresses are neglected.
5. The interface between two layers is suggested to be indestructible, and two layers are bonded rigidly (without sliding).

The cross section of the multicomponent layered beam is shown in Fig. 1. The total thickness of the specimen of its rectangular cross section is w, its width is b, and the total number of layers is n. It is most appropriate to put the coordinate origin on the free surface of the first layer. Note that the geometry of the multilayered material is such that the problem can be reduced to one dimension. The thickness of the i-th layer is w_i, $w = \sum_{i=1}^{n} w_i$, and the coordinate of interface between i-th and $(i+1)$-th layers is $y_i = \sum_{j=1}^{i} w_j$. Note that $y_0 = 0$ and $y_n = w$. In a case when deformation is a function of coordinate y only, it

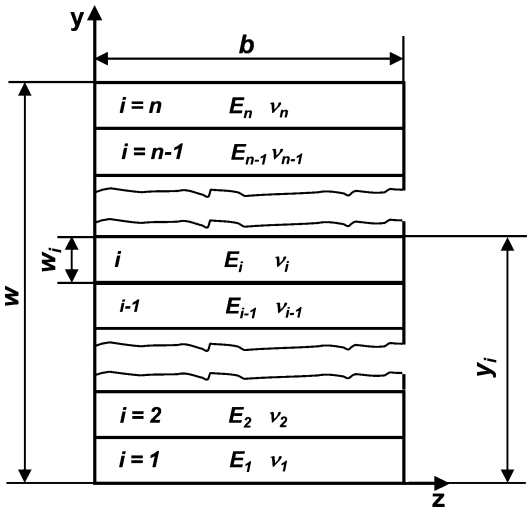

Control of Thermal Residual Stresses, Fig. 1 The cross section of the multicomponent layered beam

follows from strain compatibility that overall deformation must be linear for elastic material:

$$\varepsilon(y) = k_0 y + \varepsilon_0 \tag{1}$$

where k_0 is the curvature of surface when ε=0 and ε_0 is the overall strain at y=0. Note that in general, the overall strain is the sum of strains related to the applied bending moment and thermal expansions. The parameters k_0 and ε_0 can be found from a system of linear equations:

$$\begin{cases} b\int_0^w \sigma(y)dy = 0 \\ M + b\int_0^w y\sigma(y)dy = 0 \end{cases}, \tag{2}$$

where $\sigma(y)$ is the stress at the point with coordinate y and M is the applied bending moment. In fact, the system of linear equations (2) is the static balance conditions for the considered cross section.

The stress in the i-th layer can be expressed by

$$\begin{aligned} \sigma_i(y) &= E'_i(\varepsilon(y) - \alpha_i \Delta T) \\ &= E'_i(k_0 y + \varepsilon_0 - \alpha_i \Delta T),\ y_{i-1} < y < y_i \end{aligned} \tag{3}$$

where $E'_i = \frac{E_i}{1-\nu_i}$; E_i and ν_i are the Young modulus and Poisson ratio of the i-th layer, respectively; $\alpha_i \Delta T$ is the i-th layer thermal expansion strain; α_i is the coefficient of thermal expansion of i-th layer, $\Delta T = T - T_{join}$; T is the current temperature; and T_{join} is the joining temperature which is determined to be the temperature at which the layers constituting the material are rigidly joined.

For a layered structure, the system (2) can be transformed to

$$\begin{cases} b\sum_{i=1}^{n}\int_{y_{i-1}}^{y_i} \sigma_i(y)dy = 0 \\ M + b\sum_{i=1}^{n}\int_{y_{i-1}}^{y_i} y\sigma_i(y)dy = 0 \end{cases} \tag{4}$$

Accounting for (3), the system (4) can be written as

$$\begin{cases} L_0\varepsilon_0 + L_1 k_0 = J_0 \\ L_1\varepsilon_0 + L_2 k_0 = J_1 - M/b \end{cases} \tag{5}$$

where

$$\begin{aligned} L_j &= \frac{1}{j+1}\sum_{i=1}^{n} E'_i\left[(y_i)^{j+1} - (y_{i-1})^{j+1}\right],\ j = 0,1,2 \\ J_j &= \frac{1}{j+1}\sum_{i=1}^{n} \alpha_i \Delta T E'_i\left[(y_i)^{j+1} - (y_{i-1})^{j+1}\right],\ j = 0,1 \end{aligned} \tag{6}$$

Note that L_j is only related to the elastic properties of layers and layered structure geometry. Then it follows from (5) that

$$\begin{aligned} \varepsilon_0 &= \frac{L_2 J_0 - L_1 J_1 + L_1 M/b}{L_0 L_2 - L_1^2} \\ k_0 &= \frac{L_0 J_1 - L_1 J_0 - L_0 M/b}{L_0 L_2 - L_1^2} \end{aligned} \tag{7}$$

It is evident that $\varepsilon_0 = \varepsilon_0^{(r)} + \varepsilon_0^{(a)}$ where

$$\varepsilon_0^{(r)} = \frac{L_2 J_0 - L_1 J_1}{L_0 L_2 - L_1^2} \tag{8}$$

is associated with thermal expansion and thermal stresses, and

$$\varepsilon_0^{(a)} = \frac{L_1 M/b}{L_0 L_2 - L_1^2} \tag{9}$$

is associated with applied bending moment. Correspondingly, $k_0 = k_r + k_a$, where

$$k_r = \frac{L_0 J_1 - L_1 J_0}{L_0 L_2 - L_1^2} \text{ and } k_a = -\frac{L_0 M/b}{L_0 L_2 - L_1^2} \tag{10}$$

It is convenient to present $\sigma_i(y)$ as $\sigma_i(y) = \sigma_i^{(r)}(y) + \sigma_i^{(a)}(y)$ where

$$\sigma_i^{(r)}(y) = E'_i(k_r y + \varepsilon_0^{(r)} - \alpha_i \Delta T) \tag{11}$$

is the stress related to thermal expansion of layers and

$$\sigma_i^{(a)}(y) = E'_i(k_a y + \varepsilon_0^{(a)}) \tag{12}$$

is the stress related to applied bending moment. Note that the stresses are linear functions of y inside each layer. The stresses have jumps at interfaces due to the difference of elastic constants and CTEs between layers. Also note that the thermal expansion can generally result in nonzero curvature of the layered beam even in the case of zero-applied bending moment.

Often, only two-component layered composites with symmetric macrostructure are considered [14]. In this case, the layers consisting of different components alternate one after another, and the external layers consist of the same component. The total number of layers n in such a composite sample is odd. Often, the layer of each component has some constant thickness, and the layers of same component have identical thickness. In this case, all layers of the first component including the two external (top) layers can be designated by index 1, and all layers of the second component (internal) can be designated by index 2. The number of layers designated by index 1 is $(n+1)/2$, and the number of layers designated by index 2 is $(n-1)/2$.

The residual thermal stresses in the case of a two-component material with a symmetrical layered structure can be derived from (11):

$$\sigma_1^{(r)} = \frac{E'_1 E'_2 f_2(\alpha_2 - \alpha_1)\Delta T}{E'_1 f_1 + E'_2 f_2} \tag{13}$$

and

$$\sigma_2^{(r)} = \frac{E'_2 E'_1 f_1(\alpha_1 - \alpha_2)\Delta T}{E'_1 f_1 + E'_2 f_2} \tag{14}$$

where $f_1 = \frac{(n+1)w_1}{2w}$ and $f_2 = \frac{(n-1)w_2}{2w}$. Note that k_0=0 in this case, and thermal stresses are not a function of y.

The mismatch of thermal expansion coefficients between different layers inevitably generates thermal residual stresses during subsequent cooling of layered ceramics with strong interfaces [15]. The relative thickness of different layers determines the relative magnitudes of compressive and tensile stress, while the strain mismatch between the layers dictates the absolute values of the residual stresses. The important trends are a decreasing of tensile residual stress and an increasing of compressive residual stress with an increase in the thickness of layers under tension and a decrease in the thickness of layers under compression. In this way, a change of a layer thickness ratio allows for control of the residual stress level in laminates.

Designing Laminates to Enhance Apparent Fracture Toughness

The compressive thermal stresses in the outer layers of a layered composite shield natural and artificial cracks. Therefore, the resistance to fracture of such a structure increases. The more compressive residual stress is induced, the greater shielding occurs. In the case of layered material, the so-called apparent fracture toughness is usually considered [14]. Such an approach does not take into account the stress distribution near the crack tip in layered media, but it is still a useful characteristic allowing for the effective contribution of thermal stresses to be accounted for.

In fracture mechanics, both thermal and applied stresses are usually included in the crack driving force. However, thermal stresses can be considered as a part of the crack resistance. Therefore, in layered composites, the higher resistance to failure results from a reduction of crack driving force rather than from an increase in intrinsic material resistance to crack extension [16].

The calculation of thermal stresses is a powerful tool of laminate design because it enables predicting its mechanical behavior. The design of a layered structure is one way to control thermal stresses. Compositions of the layers should be selected depending on the intended application of the composite. Then, the relevant material constants entering the design are determined. The constants for design are the coefficient of thermal expansion, Young's modulus, Poisson's ratio, the density of the corresponding constituents, and the joining temperature. Effective coefficients of thermal expansion, effective Young's modulus, average density, and the thickness ratio of layers are determined using the rule of mixtures. An important step in the design is the selection of the number of layers. Really, this can be any appropriate number depending on the total thickness of the specimen. Usually, the thickness of the thinnest possible layer is limited by the manufacturing technology. Note that a compressive layer should be thin enough to reach a high level of thermal stress. Another important requirement is the determination of thickness of layers with higher CTE where tensile stress arises. Any appropriate thickness can be used as a first approximation. After this, the calculation of thermal stresses is done using (11) or (13) and (14). The total thickness of the specimen is determined for selected layer thicknesses. The layer thickness is changed after analysis of the thermal stress and the total thickness of the specimen. Other conditions being equal, increasing the tensile layer thickness decreases tensile thermal stress. However, it can result in increasing total thickness of specimen. After changing the thicknesses, calculation is repeated. Such iterations are continued to find optimal layer thicknesses that produce the maximum possible compressive thermal stress, low tensile thermal stress, and required total thickness of the specimen. A design algorithm is presented in Fig. 2.

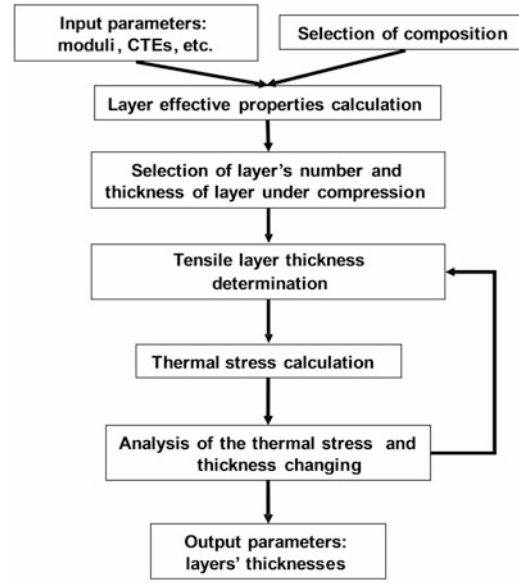

Control of Thermal Residual Stresses, Fig. 2 A design algorithm

The maximum possible apparent fracture toughness of the corresponding layered structure is also determined in all iterations as an indicative parameter of the design [14]. The determination of the apparent fracture toughness uses the compressive thermal stress and the thickness of an outer layer as a crack length at any given iteration. These two parameters (the compressive thermal stress and the thickness of the outer layer) have trends acting in opposite directions. A decrease in the outer layer thickness can increase the thermal stress in the layer, but it also decreases the maximum length of the crack. To obtain the highest resistance to failure, the tensile layer should be made as stiff as possible (i.e., high elastic modulus), whereas the compressive layers should be as compliant as feasible (i.e., low elastic modulus) [13].

Examples of Control of Thermal Residual Stresses in Laminates

Silicon-Nitride-Based Laminates

The structures investigated were a combination of alternative Si_3N_4 layers and (1) Si_3N_4-20wt%

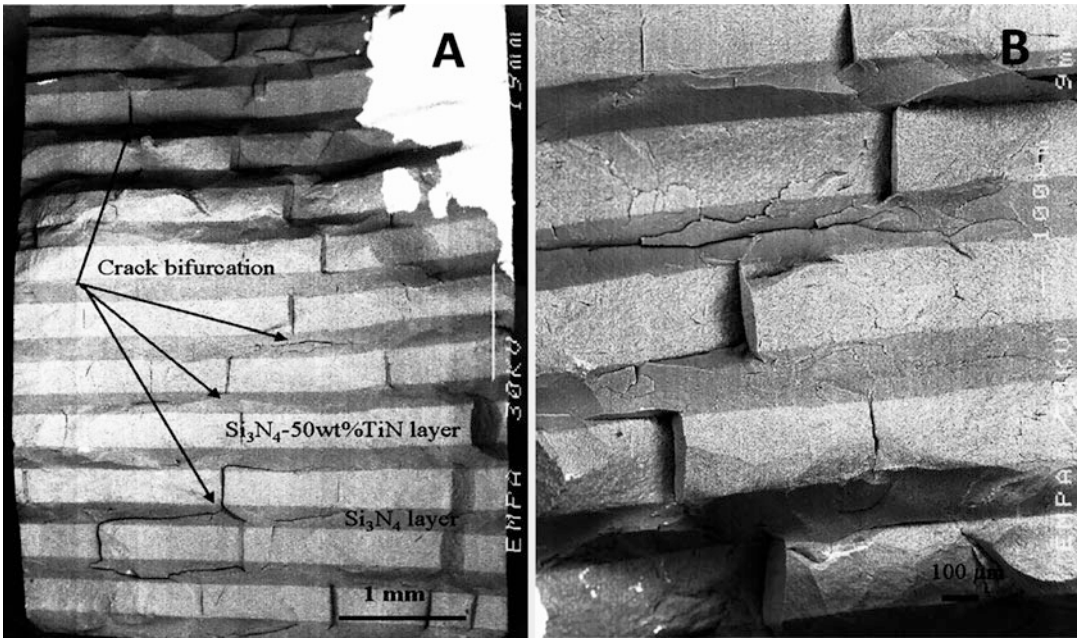

Control of Thermal Residual Stresses, Fig. 3 Fracture surface of Si_3N_4/Si_3N_4-50%wt%TiN composite

TiN layers, (2) Si_3N_4-30wt%TiN layers, and (3) Si_3N_4-50wt%TiN layers [12, 17–19]. While the strength of Si_3N_4/Si_3N_4-20 wt% TiN laminates are approximately on the same level as the Si_3N_4 specimens, further increase of the TiN content to 50 wt% results in a significant decrease in both strength and Young's modulus.

The Si_3N_4/Si_3N_4-20 wt% TiN laminates showed an increase in apparent fracture toughness. This increase can be explained by the introduction of residual bulk compressive stresses in Si_3N_4 layers. There was an increase in apparent fracture toughness (8.5 ± 0.01 MPa $m^{1/2}$) for the laminates with 20 wt% TiN. The reason for this is a significant residual compressive stress in the Si_3N_4 layers and, at the same time, a decrease of the residual tensile stress in the Si_3N_4-20 wt% TiN layers.

For the Si_3N_4/Si_3N_4-30 wt% TiN laminate with an Si_3N_4 top compressed layer, the apparent fracture toughness increases up to 17 MPa $m^{1/2}$. The failure of all samples occurred at 351 ± 13 MPa. The toughness decreases from 17 to 5 MPa $m^{1/2}$, if the crack tip is located in the second Si_3N_4-30 wt% TiN layer with a residual tensile stress. The next increase from 5 to 14 MPa $m^{1/2}$ occurs if the crack tip is located in the third Si_3N_4 layer with a residual compressive stress.

All surface cracks of sufficient length will cause failure at the same stress because these will grow in non-catastrophic regime up to some threshold stress due to an increase of apparent fracture toughness in the layer with compressive stress. At the same time, if the residual compressive stress in the top layer is not high enough, the small cracks can cause catastrophic failure once they start to grow. Therefore, obtaining a high residual compressive stress in the first layer is an effective way of providing high toughness at small crack lengths, thereby ensuring improved flaw tolerance and surface damage resistance.

An increase of TiN content to 50 wt% resulted in a significant increase in the residual tensile stress of the laminates. The tensile stress became higher than the tensile strength of the material, resulting in much cracking and a decrease in all mechanical properties. Fracture surface of Si_3N_4/Si_3N_4-50%wt%TiN composite is shown in Fig. 3.

Boron-Carbide-Based Laminates

A symmetric three-layered B_4C/B_4C-30wt%SiC laminate was investigated [20]. The layers with residual tensile and compressive stresses are the B_4C and B_4C-30wt%SiC layers, respectively. The outer layers have residual compressive stress. The laminates were designed in such a way that the tensile stresses were maintained at low values. The apparent fracture toughness was 7.42 ± 0.82 MPa $m^{1/2}$ [21], which is still a very high value for brittle boron-carbide-based composites.

The research [22] represents the first step in boron-carbide-based laminate development and should provide higher performance. The control of thermal residual stresses was used to develop optimal design parameters. As a result, laminates with high compressive residual stresses (up to 650 MPa) and low tensile residual stresses (below 150 MPa) were developed. The feasibility of manufacturing laminate composite systems with enhanced toughness through the incorporation of thin layers with high compressive stresses in the ceramics was demonstrated.

Possible Effect of Uncontrolled Thermal Stresses

A laminate with outer B_4C-30wt%SiC layers having a thickness of 1,650 μm and the thick B_4C layer having a thickness of 9,000 μm was fabricated [22]. For such a design, the level of residual tensile stress was raised to 210 MPa after cooling from 2,200 °C. Such high residual tensile stress led to a complete fracture of the tile during decompression of the graphite die to separate the tile after hot pressing (Fig. 4). The failure apparently started from the tile edges with cracks propagating further into the tile body.

This example shows the importance of control of thermal residual stress in layers. However, the tensile strength of layers usually exhibits an essential scattering. One of the problems is that the mechanical properties of an individual layer of laminate can significantly deviate from the ones of a corresponding bulk material. The critical tensile stress can be easily calculated if the intrinsic fracture toughness and the size of the critical flaw inside the layer are determined. However, the critical defect in the layer cannot usually be identified. There is a possibility of determining the stress for crack tunneling in the tensile layer [23]. Such stress depends only on the intrinsic fracture toughness and the layer thickness and is in fact the threshold stress for tensile layer cracking. Another way is to use an empirical value of tensile strength. Such an approach, in fact, is also rather successful in eliminating cracking in laminates.

Control of Thermal Residual Stresses, Fig. 4 Possible effect of uncontrolled thermal stresses

References

1. Clegg WJ, Kendall K, McN AN, Button TW, Birchall JD (1990) A simple way to make tough ceramics. Nature 347:455–457
2. Clegg WJ (1999) Controlling cracks in ceramics. Science 286:1097–1099
3. Rao MP, Sanchez-Herencia AJ, Beltz GE, McMeeking RM, Lange FF (1999) Laminar ceramics that exhibit a threshold strength. Science 286:102–105
4. Moon H, Pontin MG, Lange FF (2004) Crack interactions in laminar ceramics that exhibit a threshold strength. J Am Ceram Soc 87:1694–1700
5. Lugovy M, Slyunyayev V, Subbotin V, Liang F, Gou J, Orlovskaya N, Graule T, Kuebler J (2011) Mechanical behavior and failure mechanisms of boron carbide based three-layered laminates with weak interfaces. Ceram Int 37:2255–2261

6. Chan H (1997) Layered ceramics: processing and mechanical behaviour. Annu Rev Mater Sci 27:249–282
7. Honeyman-Colvin P, Lange FF (1996) Infiltration of porous alumina bodies with solution precursors: strengthening via compositional grading, grain size control, and transformation toughening. J Am Ceram Soc 79:1810–1814
8. Oechsner M, Hillman C, Lange F (1996) Crack bifurcation in laminar ceramic composites. J Am Ceram Soc 79:1834–1838
9. Sanchez-Herencia A, Pascual C, He J, Lange F (1999) ZrO_2/ZrO_2 layered composites for crack bifurcation. J Am Ceram Soc 82:1512–1518
10. Lakshminarayanan R, Shetty DK, Cutler RA (1996) Toughening of layered ceramic composites with residual surface compression. J Am Ceram Soc 79:79–87
11. Blattner A, Lakshminarayanan R, Shetty DK (2001) Toughening of layered ceramic composites with residual surface compression: effect of layer thickness. Eng Fract Mech 68:1–7
12. Lugovy M, Slyunyayev V, Orlovskaya N, Blugan G, Kuebler J, Lewis M (2005) Apparent fracture toughness in Si_3N_4-based laminates with residual compressive or tensile stresses in surface layers. Acta Mater 53:289–296
13. Hbaieb K, McMeeking RM (2002) Threshold strength predictions for laminar ceramics with cracks that grow straight. Mech Mater 34:755–772
14. Orlovskaya N, Lugovy M, Kuebler J, Yarmolenko S, Sankar J (2006) Design of tough ceramic laminates by residual stresses control. In: Low IM (ed) Ceramic matrix composites: microstructure/property relationship. Woodhead Publishing, Cambridge, pp 178–215
15. Chartier T, Merle D, Besson JL (1995) Laminar ceramic composites. J Eur Ceram Soc 16:101–107
16. Sglavo VM, Larentis L, Green DJ (2001) Flaw-insensitive ion-exchanged glass: I, Theoretical aspects. J Am Ceram Soc 84:1827–1831
17. Lugovy M, Orlovskaya N, Berroth K, Kuebler J (1999) Macrostructural engineering of ceramic matrix layered composites. Compos Sci Technol 59:1429–1437
18. Lugovy M, Slyunyayev V, Subbotin V, Orlovskaya N, Gogotsi G (2004) Crack arrest in Si_3N_4-based layered composites with residual stress. Compos Sci Technol 64:1947–1957
19. Yaroshenko V, Orlovskaya N, Einarsrud M-A, Kovylayev V (1998) Processing of multilayered Si_3N_4-TiN hot-pressed ceramic composites. In: Haddad YM (ed) Advanced multilayered and fibre-reinforced composites. Kluwer, Dordrech, pp 285–295
20. Orlovskaya N, Lugovy M, Subbotin V, Radchenko O, Adams J, Chheda M, Shih J, Sankar J, Yarmolenko S (2003) Design and manufacturing B_4C-SiC layered ceramics for armor applications. Ceram Trans 151:59–70
21. Orlovskaya N, Adams J, Chheda M, Shih J, Yarmolenko S, Sankar J, Lugovy M, Subbotin V (2003) Boron carbide – silicon carbide laminate ceramics for ballistic protection. In: Sankar J (ed) Proceedings of 2003 ASME international mechanical engineering congress, vol 3. Washington, DC, pp 319–326
22. Orlovskaya N, Lugovy M, Subbotin V, Radchenko A, Adams J, Chheda M, Shih J, Sankar J, Yarmolenko S (2005) Robust design and manufacturing of ceramic laminates with controlled thermal residual stresses for enhanced toughness. J Mater Sci 40:5483–5490
23. Ho S, Suo Z (1993) Tunnelling cracks in constrained layers. J Appl Mech-Trans ASME 60:890–894

Cosserat Surfaces

▶ Saint-Venant's Problem for Cosserat Elastic Shells

Coupled and Generalized Thermoviscoelasticity

Ahmed S. El-Karamany
Department of Mathematical and Physical Sciences, Nizwa University, Nizwa, Oman

Synonyms

Amorphous polymers; Biopolymers; Bitumen materials; Metals at very high temperatures; Plexiglas; Semicrystalline polymers

Definition

In the theory of linear elasticity, the response behavior can be described by Hooke's law, that is, if the deformations are small, the stress is proportional to the strain and is independent of the strain rate. When the load is removed, the material returns to its undeformed state. On the other hand, the viscous fluid is described by Newton's law, that is, the stress is proportional to the strain rate, provided it is small [1].

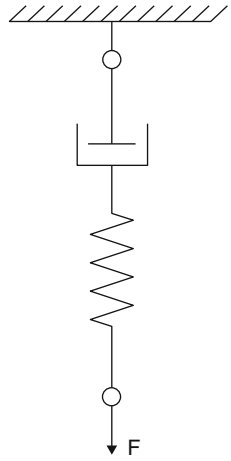

Coupled and Generalized Thermoviscoelasticity, Fig. 1 Maxwell element

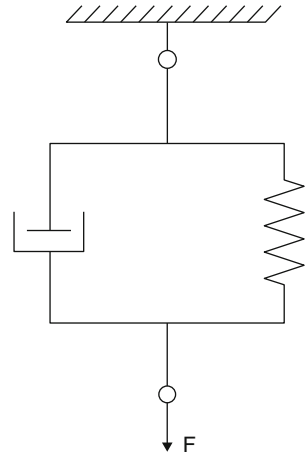

Coupled and Generalized Thermoviscoelasticity, Fig. 2 Kelvin–Voigt element

Viscoelastic material exhibits both viscous and elastic characteristics and do not conserve energy. The theory of linear viscoelasticity is a generalization to the classical theories of linear elasticity and hydromechanics of viscous fluid.

The simple viscoelastic solid has the following properties:

1. *Stress relaxation* when constant strain causes decreasing stress (Maxwell element represented by a spring and a dashpot in series Fig. 1). Then, $\dot{\varepsilon} = (\dot{\sigma}/2\mu) + (\sigma/2\eta)$, where η – the coefficient of viscosity, μ – the shear modulus. Assuming $\varepsilon(t) = \varepsilon(0) = const.$, $\sigma(0) = \sigma_0.$, and integrating the preceding equation, we get $(\sigma(t)/\sigma_0) = \exp(-t/\tau)$, where $\tau = \eta/\mu$ is the stress relaxation time.
2. *Creep* [2] which results when the body undergoes continuous deformation under constant load or stress and the strain tends to limiting value as $t \to \infty$, (Kelvin–Voigt element represented by a spring and a dashpot in parallel Fig. 2). Then, $\sigma = 2\mu\varepsilon + 2\eta\dot{\varepsilon}$. Assuming $\varepsilon(0) = 0$, $\sigma(t) = \sigma_0 = const.$, and integrating the preceding equation, we get $(2\mu\varepsilon(t)/\sigma_0) = [1 - \exp(-t/\lambda_r)]$, where $\lambda_r = \eta/\mu$ in case of creep is called the retardation time.

Overview

Boltzmann [3] in 1874 apparently supplied the first formulation of a three-dimensional theory of isotropic viscoelasticity, while Volterra [4] obtained comparable forms for anisotropic solids in 1909. The mechanical model representation of linear viscoelastic behavior was investigated by many authors [5]. Notable works in these fields include those of Gurtin and Sternberg [6] and Sternberg [7].

The linear viscoelasticity remains an important area of research not only due to the advent and use of polymers but also because most solids when subjected to dynamic loading exhibit viscous effects. The stress–strain law for many materials such as polycrystalline metals and high polymers can be approximated by the linear viscoelasticity theory. Recently, thermoviscoelasticity has an increasing role in modeling soft tissues and bones.

Governing Equations of the Linear Coupled Thermoviscoelasticity

We assume a linear thermoviscoelastic material occupies a regular region V with a piecewise smooth boundary surface ∂V in the three-dimensional Euclidean space. All the functions are considered to be functions of position $\boldsymbol{x} = (\boldsymbol{x}_1, \boldsymbol{x}_2, \boldsymbol{x}_3)$ and time t. A superposed dot denotes differentiation with respect to time, and the comma followed by a subscript denotes partial differentiation with respect to the space variables x_i. The summation notation is used.

The equation of motion is

$$\sigma_{ji,j} + \rho b_i = \rho \ddot{u}_i \tag{1}$$

The kinematical relations are

$$\varepsilon_{ij} = \frac{1}{2}(u_{i,j} + u_{j,i}) \tag{2}$$

The energy equation is

$$T_0 \dot{S} = Q - q_{i,i} \tag{3}$$

and *the heat conduction law* for the coupled thermoviscoelasticity is the classical Fourier law [5]

$$q_i = -k_{ij}\theta_{,j} \tag{4}$$

where $u_i, \varepsilon_{ij}, \sigma_{ij}, \theta, S, q_i, b_i, \rho, k_{ij}$, and Q are respectively the displacement vector, strain tensor, stress tensor, temperature deviation from a reference temperature T_0, entropy per unit volume, heat flux vector, mass force, density, thermal conductivity tensor, and the intensity of applied heat source per unit volume.

The initial conditions on $\bar{V} = V \cup \partial V$ are

$$\begin{aligned} u_i(\boldsymbol{x}, 0) &= u_i^0(\boldsymbol{x}) \quad \dot{u}_i(\boldsymbol{x}, 0) = v_i^0(\boldsymbol{x}) \\ \theta(\boldsymbol{x}, 0) &= \theta^0(\boldsymbol{x}) \quad \dot{\theta}(\boldsymbol{x}, 0) = \vartheta^0(\boldsymbol{x}) \end{aligned} \tag{5}$$

where the functions u_i^0, v_i^0, θ^0, and ϑ^0 are prescribed functions of $\boldsymbol{x}$ on $\bar{V}$.

The boundary conditions on $\partial V \times [0, \infty)$ are

$$\begin{aligned} u_i(\boldsymbol{x},\ t) &= \hat{u}_i \quad \text{on} \quad \partial V_u \quad \text{and} \\ \sigma_{ji} n_j &= \hat{f}_i(\boldsymbol{x},\ t) \quad \text{on} \quad \partial V_\sigma \end{aligned} \tag{6}$$

$$\begin{aligned} \theta(\boldsymbol{x},\ t) &= \hat{\theta} \quad \text{on} \quad \partial V_\theta \quad \text{and} \\ q_i n_i &= \hat{q}(\boldsymbol{x},\ t) \quad \text{on} \quad \partial V_q \end{aligned} \tag{7}$$

where $\partial V = \partial V_\sigma \cup \partial V_u = \partial V_q \cup \partial V_\theta$ and $\emptyset = \partial V_u \cap \partial V_\sigma = \partial V_\theta \cap \partial V_q$ and $n_i = n_i(\boldsymbol{x}_{\partial V})$. The functions $\hat{u}_i$ and $\hat{\theta}$ are prescribed functions of $(\boldsymbol{x}_{\partial V},\ t)$ on $\partial V_\chi \times [0, \infty)$, where $(\chi = u$ and $\theta)$. The functions $\hat{f}_i$ and $\hat{q}$ are prescribed functions of $(\boldsymbol{x}_{\partial V},\ t)$ on $\partial V_{\chi^c} \times [0, \infty)$, where $\chi^c = \sigma$ and q.

The constitutive laws are

$$\sigma_{ij}(\boldsymbol{x}, t) = (G_{ijkl} * \dot{\varepsilon}) - (\gamma_{ij} * \dot{\theta}) \tag{8}$$

$$S(\boldsymbol{x}, t) = (\beta * \dot{\theta}) + (\gamma_{ij} * \dot{\varepsilon}_{ij}) \tag{9}$$

where

$$(f * g) = \int_0^t f(\boldsymbol{x}, t - \tau) g(\boldsymbol{x}, \tau)\, d\tau$$

Comparing with the corresponding elasticity tensors $C_{ijkl}(\boldsymbol{x})$, $\gamma_{ij}(\boldsymbol{x})$, and $\beta(\boldsymbol{x})$ which are independent of time, the relaxation tensors $G_{ijkl}(\boldsymbol{x}, t)$, $\gamma_{ij}(\boldsymbol{x}, t)$, and $\beta(\boldsymbol{x}, t)$ are time-dependent and highly temperature sensitive fourth order, second order, and zero order tensors [8].

Basic Assumptions (*Thermoviscoelastic State*)

The ordered array of field histories $\{u_i, \theta, \varepsilon_{ij}, \sigma_{ij}\}$ belongs to the class of thermoviscoelastic state on $V \times (-\infty, \infty)$ corresponding [7] to the data $G_{ijkl}, \gamma_{ij}, \beta$ if (a) G_{ijkl}, γ_{ij}, and β *vanish* on $\bar{V} \times (-\infty, 0)$, are twice continuously differentiable functions of $\boldsymbol{x}$ and t on $\bar{V} \times [0, \infty)$; (b) the symmetry relations $G_{ijkl} = G_{klij} = G_{jikl} = G_{ijlk}$, $\gamma_{ij} = \gamma_{ji}$, hold on $V \times [0, \infty)$ and $k_{ij}(\bar{x}) = k_{ji}(\bar{x})$ on V; (c) $u_i, \theta, \varepsilon_{ij}, \sigma_{ij}$ *vanish* on $\bar{V} \times (-\infty, 0)$, θ, ε_{ij} being once – and u_i twice continuously differentiable functions of $\boldsymbol{x}$ and t on $V \times [0, \infty)$; (d) (1)–(9) hold on $V \times [0, \infty)$; and (e) the equilibrium elastic moduli $G_{ijkl}(\infty)$, $\gamma_{ij}(\infty)$, and $\beta(\infty)$ exist [9].

From (3), (4), and (9), the heat transport equation results in the form

$$\begin{aligned} T_0^{-1}(k_{ij}\theta_{,j}(t))_{,i} = \frac{\partial}{\partial t}[(\beta * \dot{\theta}) + (\gamma_{ij} * \dot{\varepsilon}_{ij})] \\ - T_0^{-1} Q(t) \end{aligned} \tag{10}$$

For convenience, we suppressed the argument $\boldsymbol{x}$

The isotropic forms of the constitutive laws (8), (9), and (10) can be obtained by setting $k_{ij} = k\delta_{ij}$, $\gamma_{ij}(t) = \gamma(t)\delta_{ij}$, and

$$G_{ijkl}(t) = \frac{1}{3}(G_2(t) - G_1(t))\delta_{ij}\delta_{kl} + \frac{1}{2}G_1(t)(\delta_{ik}\delta_{jl} + \delta_{il}\delta_{jk}) \tag{11}$$

where $G_1(t)$ and $G_2(t)$ are two independent relaxation functions and δ_{ij} is the Kronecker's delta. We introduce the deviatoric components of strain and stress tensors

$$e_{ij} = \varepsilon_{ij} - \frac{\varepsilon_{kk}}{3}\delta_{ij}, \quad s_{ij} = \sigma_{ij} - \frac{\sigma_{kk}}{3}\delta_{ij} \tag{12}$$

Then, (8), (9), (11), and (12) lead to

$$\begin{aligned} s_{ij}(t) &= (G_1 * \dot{e}_{ij}), \\ \sigma_{kk}(t) &= (G_2 * \dot{\varepsilon}_{kk}) - 3(\gamma * \dot{\theta}) \end{aligned} \tag{13}$$

where $G_1(0) = 2\mu$, $G_2(0) = 3\lambda + 2\mu = 3K$, $\gamma(0) = \gamma_0 = 3K\alpha_T$, λ, μ, K, and α_T are Lame constants, bulk modulus, and coefficient of linear thermal expansion. $G_v(0)$ and $(v = 1, 2)$ are the instantaneous elastic moduli.

The heat transport (10) for isotropic solids takes the form

$$T_0^{-1}(k\theta_{,i}(t))_{,i} = \frac{\partial}{\partial t}[(\beta * \dot{\theta}) + (\gamma * \dot{\varepsilon}_{kk})] - T_0^{-1}Q(t) \tag{14}$$

For an isotropic solid, the *creep laws* are

$$\begin{aligned} e_{ij}(t) &= (J_1 * \dot{s}_{ij}), \\ \varepsilon_{kk} &= (J_2 * \dot{\sigma}_{kk}) + 3(\alpha_T * \dot{\theta}) \end{aligned} \tag{15}$$

where J_v are two independent compliance functions, α_T the coefficient of linear thermal expansion, and $J_v = G_v^{-1}$, $\dfrac{\partial J_v}{\partial t} > 0$, $\dfrac{\partial G_v}{\partial t} < 0$.

The Generalized Thermoviscoelasticity Theories

(A) Lord–Shulman Thermoviscoelasticity Theory

Equations (1)–(3) and (5)–(9) remain the same. Equation (4) is replaced by the Maxwell–Cattaneo law [10]

$$q_i + \tau_0\dot{q}_i = -k_{ij}\theta_{,j} \tag{16}$$

where $\tau_0 > 0$ is the relaxation time. Using (9), (11), (13), and (16), we obtain the heat transport equation for the Lord–Shulman generalized thermoviscoelasticity (with one relaxation time [11])

$$T_0^{-1}(k_{ij}\theta_{,j}(t))_{,i} = \left(\frac{\partial}{\partial t} + \tau_0\frac{\partial^2}{\partial t^2}\right)[\beta * \dot{\theta}) + (\gamma_{ij} * \dot{\varepsilon}_{ij})] - T_0^{-1}\left(Q + \tau_0\frac{\partial Q}{\partial t}\right) \tag{17}$$

For an isotropic solid, we get

$$T_0^{-1}(k\theta_{,i}(t))_{,i} = \left(\frac{\partial}{\partial t} + \tau_0\frac{\partial^2}{\partial t^2}\right)[\beta * \dot{\theta}) + (\gamma * \dot{\varepsilon}_{kk})] - T_0^{-1}\left(Q + \tau_0\frac{\partial Q}{\partial t}\right) \tag{18}$$

(B) Green–Lindsay Thermoviscoelasticity Theory

The second generalization to the coupled theory of elasticity is the theory of thermoelasticity with two relaxation times or the theory of temperature-rate-dependent thermoelasticity [12]. This theory contains two constants that act as relaxation times and modify all the equations of the coupled theory, not only the heat equation [13]. Therefore, (8), (9), and (4) in this theory take the form

$$\sigma_{ij}(t) = (G_{ijkl} * \dot{\varepsilon}_{kl}) - (\gamma_{ij} * (\dot{\theta} * v\ddot{\theta})) \tag{19}$$

$$\begin{aligned} S(t) &= (\beta * (\dot{\theta} + \tau_1\ddot{\theta})) + (\gamma_{ij} * \dot{\varepsilon}_{ij}) - a_i\theta_{,i} \\ q_i(t) &= -(k_{ij}\theta_{,j} + T_0 a_i\dot{\theta}) \end{aligned}$$

where a_i are components of a constant vector such that $a_i = 0$ if the medium under consideration has a center of symmetry; τ_1 and ν are two relaxation times $0 < \tau_1 \leq \nu$.

The heat transport equation takes the form

$$T_0^{-1}(k_{ij}\theta_{,j})_{,i} + 2a_i\dot{\theta}_{,i} = \frac{\partial}{\partial t}[(\beta * (\dot{\theta} + \tau_1\ddot{\theta})) + (\gamma_{ij} * \dot{\varepsilon}_{ij})] - T_0^{-1}Q \quad (20)$$

For an isotropic solid, we get

$$s_{ij} = (G_1 * \dot{e}_{ij}), \quad \sigma_{kk} = (G_2 * \dot{\varepsilon}_{kk}) - 3(\gamma * (\dot{\theta} + \nu\ddot{\theta})) \quad (21)$$

$$T_0^{-1}(k\theta_{,i})_{,i} = \frac{\partial}{\partial t}[(\beta * (\dot{\theta} + \tau_1\ddot{\theta})) + (\gamma * \dot{\varepsilon}_{kk})] - T_0^{-1}Q \quad (22)$$

(C) **The Dual-Phase-Lag Thermoviscoelasticity** In this model, the Fourier law is replaced by the equation [14]

$$\left(1 + \tau_q\frac{\partial}{\partial t} + \frac{1}{2}\tau_q^2\frac{\partial^2}{\partial t^2}\right)q_i = -k_{ij}\left(1 + \tau_\theta\frac{\partial}{\partial t}\right)\theta_{,j} \quad (23)$$

where τ_θ and τ_q are the phase lags of the temperature gradient and of the heat flux. Equations (8), (9), and (13) remain the same. Introducing the notation $\Omega f = (\tau_q\frac{\partial}{\partial t} + \frac{1}{2}\tau_q^2\frac{\partial^2}{\partial t^2})f$, the heat transport equation takes the form

$$T_0^{-1}\left[k_{ij}\left(1 + \tau_\theta\frac{\partial}{\partial t}\right)\theta_{,j}\right]_{,i} = (1 + \Omega)\left[\frac{\partial}{\partial t}(\beta * \dot{\theta}) + \frac{\partial}{\partial t}(\gamma_{ij} * \dot{\varepsilon}_{ij}) - T_0^{-1}Q\right] \quad (24)$$

For an isotropic solid, we obtain

$$T_0^{-1}\left[k\left(1 + \tau_\theta\frac{\partial}{\partial t}\right)\theta_{,i}\right]_{,i} = (1 + \Omega)\left[\frac{\partial}{\partial t}(\beta * \dot{\theta}) + \frac{\partial}{\partial t}(\gamma * \dot{\varepsilon}_{kk}) - T_0^{-1}Q\right] \quad (25)$$

Example: Generalized Thermoviscoelasticity in a Semi-space. We consider a semi-space homogeneous viscoelastic medium occupying the region $x \geq 0$ with quiescent initial state. A thermal shock is applied to the boundary plane $x = 0$, which is assumed traction-free. Then, the boundary condition is

$$\theta(0, t) = \theta_0 H(t), \quad \sigma_{xx}(0, t) = 0 \quad (26)$$

where θ_0 is constant and $H(t)$ is the Heaviside unit step function.

Since the solution is unbounded at infinity, the initial conditions should be so adjusted that the infinite terms are eliminated. The relaxation functions for the homogeneous solid depend only upon time and may be taken in the form

$$G_1(t) = 2\mu(1 - A_1\int_0^t f(\tau)d\tau) = 2\mu R_\mu(t),$$

$$G_2(t) = 3K(1 - A_2\int_0^t f(\tau)d\tau) = 3KR_K(t)$$

$$\gamma(t) = G_2(t)\alpha_T, \quad \beta(t) = \beta(0)(1 - A_3\int_0^t f(\tau)d\tau) = \beta_0 R_\beta(t), \quad \beta_0 = \beta(0) = \rho C_E/T_0 \quad (27)$$

where $f(t) = t^{\zeta-1}e^{-\beta^* t}$, A, A_0, β^*, ζ are empirical constants [15], C_E is the specific heat at constant strain, and $0 < A_3 \leq A_2 \leq A_1 < \frac{(\beta^*)^\zeta}{\Gamma(\zeta)}$ $\beta^* > 0$, $0 < \zeta < 1$.

For the one-dimensional problems, all the considered functions will depend only on the space variable x and the time t. The displacement vector has components $(u(x, t), 0, 0)$. Then, considering $A_1 = A_2 = A_3 = A$, we get $R_\xi(t) = R(t)$, $\xi = \mu, K, \beta$. Equations (13) and (17), in absence of heat source, take the form

$$\sigma_{xx} = (\lambda + 2\mu)(R * \dot{e}) - 3K\alpha_T(R * \dot{\theta}), T_0^{-1}k\frac{\partial^2\theta}{\partial x^2} = \left(\frac{\partial}{\partial t} + \tau_0\frac{\partial^2}{\partial t^2}\right)[\beta_0(R * \dot{\theta}) + \gamma_0(R * \dot{e})],$$

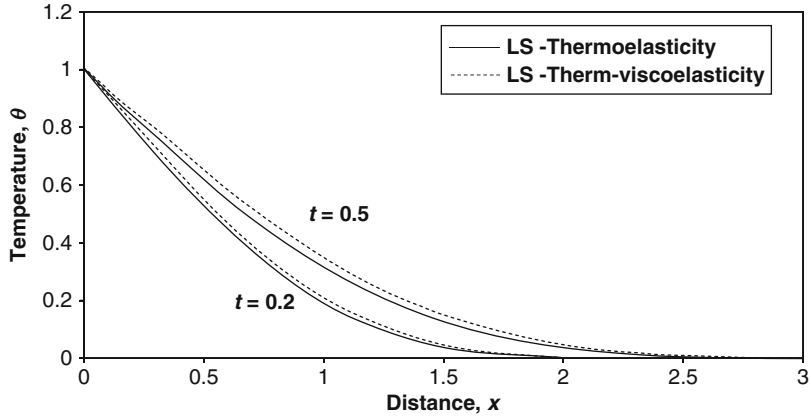

Coupled and Generalized Thermoviscoelasticity, Fig. 3 Temperature distribution for a semi space problem under Lord-Shulman thermoelasticity and thermoviscoelasticity theories

where $e = \frac{\partial u}{\partial x}$. Introducing the following non-dimensional variables

$$x' = C_0\,\eta\,x, \quad t' = C_0^2\,\eta\,t, \sigma'_{ij} = \sigma_{ij}/(\lambda + 2\mu),$$
$$\theta' = \theta\gamma_0/\rho C_0^2,$$

where $C_0^2 = (\lambda + 2\mu)/\rho$, $\eta = \rho C_E/k$, we get suppressing primes

$$\sigma_{xx} = (R * (\dot{e} - \dot{\theta})), \quad \frac{\partial^2\theta}{\partial x^2} = \left(\frac{\partial}{\partial t} + \tau_0\frac{\partial^2}{\partial t^2}\right)$$
$$(R * (\dot{\theta} + \varepsilon\dot{e})), \quad \frac{\partial\sigma_{xx}}{\partial x} = \frac{\partial^2 u}{\partial t^2}, \quad \varepsilon = \frac{T_0\gamma_0^2}{k\eta\rho C_0^2}$$

Performing Laplace transform defined by $L\{f(t)\} = \bar{f}(s) = \int_0^\infty e^{-st} f(t)dt$, we get

$$\sigma_{xx} = sR\left(\frac{\partial u}{\partial x} - \theta\right), \quad \frac{\partial^2\theta}{\partial x^2} = s^2(1 + \tau_0 s)$$
$$R\left(\theta + \varepsilon\frac{\partial u}{\partial x}\right), \quad s^2 u = \frac{\partial\sigma_{xx}}{\partial x},$$
$$sR = 1 - \frac{A\Gamma(\zeta)}{(s + \beta^*)^\zeta}$$

Choosing as state variables the temperature deviation θ, the displacement component u and their gradients, applying the state space approach [16], we obtain the solution in Laplace transform domain:

$$\theta(x,s) = \frac{1}{s\,(k_1^2 - k_2^2)}\left[\left(k_1^2 - \frac{s}{R}\right)e^{-k_1 x} - \left(k_2^2 - \frac{s}{R}\right)e^{-k_2 x}\right] \tag{28}$$

$$u(x,s) = -\frac{1}{s\,(k_1^2 - k_2^2)}\left[k_1\,e^{-k_1 x} - k_2\,e^{-k_2 x}\right] \tag{29}$$

$$\sigma_{xx}(x,s) = \frac{s}{(k_1^2 - k_2^2)}\left[e^{-k_1 x} - e^{-k_2 x}\right] \tag{30}$$

where k_1 and k_2 are the roots of the characteristic equation

$$k^4 - \left[\frac{s}{R} + (1+\varepsilon)\,s^2 R\omega\right]k^2 + s^3\,\omega = 0, \omega = 1 + \tau_0 s$$

In order to invert the Laplace transform in the above equations, we adopt a numerical inversion method based on a Fourier series expansion [17]. The calculations are carried out for a copper-like material, and the constants are $\varepsilon = 0.0168$. $\zeta = 0.5$, $\beta^* = 0.05$, $A = 0.106$. For Lord–Shulman theory, $\tau_0 = 0.02$, and for the coupled theory, $\tau_0 = 0$. Results are illustrated graphically in Figs. 3, 4, and 5.

Figures 4 and 5 show that the viscoelastic effect is to decrease the magnitude of stress component with increase of the temperature deviations.

Figure 5 demonstrates clearly the difference between the coupled and the generalized theory

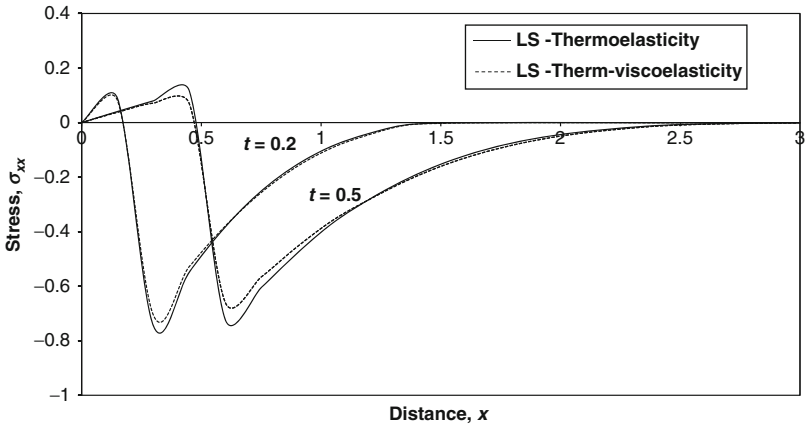

Coupled and Generalized Thermoviscoelasticity, Fig. 4 Thermal stress distribution for a semi space problem under Lord-Shulman thermoelasticity and thermoviscoelasticty theories

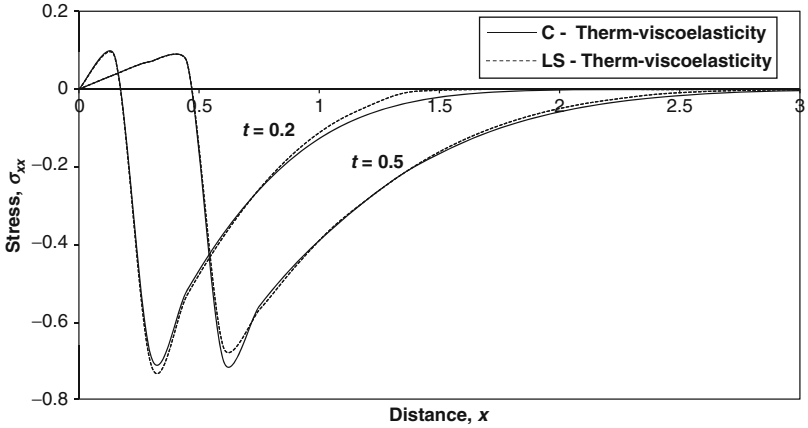

Coupled and Generalized Thermoviscoelasticity, Fig. 5 Thermal stress distribution for a semi space problem under coupled and Lord-Shulman thermoviscoelasticity theories

of thermoviscoelasticity with one relaxation time. In the first and older theory, the waves propagate with infinite speeds, so the value the stress component is not identically zero (though it may be very small) for any large value of x. In the generalized theory, the response to the thermal and mechanical effects does not reach infinity instantaneously but remains in a bounded region of space.

Cross-References

- ▶ Creep Analysis
- ▶ Dual Phase-Lag Thermoelasticity
- ▶ Generalized Theory of Thermoelasticity with One Relaxation Time
- ▶ Laplace Transform
- ▶ State-Space Approach to Generalized Thermoelasticity
- ▶ Wave Propagation in Coupled and Generalized Thermoelastic Media

Appendix

Kelvin–Voigt Model

$$\begin{aligned} s_{ij}(t) &= 2\mu e_{ij}(t) + 2\eta \dot{e}_{ij}(t), \quad \sigma = \frac{\sigma_{kk}}{3} \\ &= K\left(1 + \lambda_r \frac{\partial}{\partial t}\right)\left(e - 3\alpha_T \theta\right) \end{aligned} \tag{31}$$

Equations (31) lead to the equation

$$\sigma_{ij} = \left(1 + \lambda_r \frac{\partial}{\partial t}\right)\left(\lambda e \delta_{ij} + 2\mu \varepsilon_{ij} - 3K\alpha_T \theta\right) \tag{32}$$

The heat transport equation is

$$T_0^{-1}(k\theta_{,i})_{,i} = \beta(0)\dot{\theta} + \gamma(0)\dot{\varepsilon}_{kk} - T_0^{-1}Q \quad (33)$$

Maxwell Model

$$\dot{e}_{ij}(t) = \frac{1}{2\mu}\dot{s}_{ij}(t) + \frac{1}{2\eta}s_{ij}(t),$$
$$\dot{e} = \dot{\varepsilon}_{kk} = \frac{1}{K}\left(\dot{\sigma} + \frac{\sigma}{\tau}\right) + 3\alpha_T\left(\dot{\theta} + \frac{\theta}{\tau}\right) \quad (34)$$
$$\tau = \eta/\mu$$

Equation (34) lead to

$$\dot{\varepsilon}_{ij} = \frac{1+\nu}{E}(\dot{\sigma}_{ij} + \frac{\sigma_{ij}}{\tau}) - \frac{\nu}{E}(\dot{\sigma}_{kk} + \frac{\sigma_{kk}}{\tau})\delta_{ij} + \alpha_T(\dot{\theta} + \frac{\theta}{\tau})\delta_{ij} \quad (35)$$

where E and ν are modulus of elasticity and Poisson's ratio.

The heat transport equation in this case is the same (33).

Replacing θ by $\hat{\theta} = \theta + \tau_0\dot{\theta}$ in (31–35), we get the corresponding equations for the generalized Kelvin–Voigt and Maxwell models with one relaxation time.

References

1. Haddad YM (1995) Viscoelasticity of engineering materials. Chapman & Hall, London
2. Hetnarski RB, Reza Eslami M (2008) Thermal stresses: advanced theory and applications. Springer, New York
3. Boltzmann L (1874) Zur Theorie der elastichen Nachwirkung, Sitzber, Kaiserl. Acad. Wiss. Wien, Math. Naturw. KI. 70:275–30
4. Volterra V (1909) Sulle equazioni integro-differenziali della teoria della'elasticita. Atti Reale Accad Lincei 18:295–301
5. Christensen RM (1982) Theory of viscoelasticity –an introduction. Academic Press, New York
6. Gurtin ME, Sternberg E (1962) On the linear theory of viscoelasticity. Arch Ration Mech Anal 11:291–356
7. Sternberg E (1964) On the analysis of thermal stresses in viscoelastic solids, high temperature structures and materials. In: Proceedingds of the 3rd symposium on naval structural mechanics. Pergamon Press, New York
8. Hilton HH (2011) Equivalences and contrasts of thermo-elasticity and thermo-viscoelasticity: a comprehensive critique. J Therm Stresses 34(5):488–535
9. Fabrizio M, Morro A (1992) Mathematical problems in linear viscoelasticity, vol 12. SIAM Studies in Applied Mathematics, Philadelphia
10. Hetnarski RB, Ignaczak J (1999) Generalized thermoelasticity. J Therm Stresses 22:451–476
11. Sherief HH (1986) Fundamental solutions of the generalized thermoelastic problem for short times. J Therm Stresses 9:151–164
12. Ignaczak J (1989) Generalized thermoelasticity and its applications. In: Hetnarski RB (ed) Thermal stresses III. Elsevier, New York, pp 279–354
13. Ignaczak J, Ostoja-Starzeweski M (2009) Thermoelasticity with finite wave speeds. Oxford University Press, Oxford
14. Chandrasekharaiah DS (1998) Hyperbolic thermoelasticity. A review of recent literature. Appl Mech Rev 51:705–729
15. Koltunov MA (1976) Creeping and relaxation, Izd. Vyschaya Shkola, Moscow
16. Bahar L, Hetnarski R (1978) State space approach to thermoelasticity. J Therm Stresses 1:135–145
17. Honig G, Hirdes U (1984) A method for the numerical inversion of the Laplace transforms. J Comp Appl Math 10:113–132

Coupled Displacement Fields

▶ Thermal Post-Buckling Paths of Beams

Coupled Dynamic Micropolar Problems of Thermoelasticity: Stress–Temperature Equations of Motion of Ignaczak Type

Mountajab Al-Hasan[1] and Janusz Dyszlewicz[2]
[1]Department of Mathematics, Al-Baath University, Homs, Syrian Arab Republic
[2]Faculty of Fundamental Problems of Technology, Institute of Mathematics and Computer Science, Wrocław Technical University, Wrocław, Poland

Overview

In linear classical elastodynamics, the mixed initial-boundary value problem may be reduced to solving one tensorial stress equation with certain initial-boundary conditions expressed in stresses

by Hetnarski and Ignaczak [1, pp. 212–218], Gurtin [2, p. 212], and Eringen [3]. Ignaczak [4] proved that solving the stress initial-boundary value problem (SIBVP) in linear micropolar isothermal elastodynamics is equivalent to solving the system of two coupled tensor stress equations with appropriately formulated initial-boundary conditions in terms of stresses. Closely related to the subject are the pure stress field equations presented by Ieşan [5] and Olesiak [6]. In this entry stress-temperature initial-boundary value problems (STIBVP) of Ignaczak type for the coupled dynamical thermoelasticity for the Eringen–Nowacki (E–N) model of a micropolar body with six degrees of freedom (three-dimensional (3D) and two-dimensional (2D) problems) will be presented. The foundations of the linear theory of the general Cosserat continuum can be found in the following monographs: Eringen [7], Nowacki [8], Kupradze, Gegelia, Basheleishvili and Burchuladze [9], Kunin [10], Rubin [11], Ieşan [12], and Ostoja-Starzewski [13]. In the newest survey article of Altenbach et al. [14], a few hundreds of papers are listed, and in the introduction, the authors gave an extensive and detailed historical description of the development of scientific theories of Cosserat type. In this entry, we collect some basic relations and equations for the linear coupled dynamical thermoelasticity (the E–N model) on the basis of the monograph [8] (see also ▶ Dynamic Micropolar Thermoelasticity).

Notations

The right-hand orthogonal Cartesian coordinate system $Ox_1x_2x_3$, the Cartesian tensor index notation is used, and the extended summation convention is applied – small Latin indices i, j, and k assume the values 1, 2, and 3, Greek indices α, β, and γ assume the values 1 and 2. The partial derivatives with respect to the position variables are denoted by an apostrophe, and the derivative with respect to the time t is denoted by a superscribed dot: $\dot{f} \equiv \partial f/\partial t$. Symbol ϵ_{ijk} denotes the Levi-Civitá tensor, δ_{ij} is the Kronecker symbol, $\mathbb{R}$ denotes the set of real numbers, $\mathbb{R}^3$ is the three-dimensional Euclidean space, $x_i \equiv (x_1, x_2, x_3)$ are points in $\mathbb{R}^3$, Ω is a region in $\mathbb{R}^3$ with piecewise smooth boundary $\partial\Omega$, and n_j are the components of the unit outward normal vector to $\partial\Omega$. Further, the closed region $\overline{\Omega}$ is the union of the sets Ω and $\partial\Omega$ ($\overline{\Omega} = \Omega \cup \partial\Omega$); the time intervals are denoted as follows: $\mathbf{T} = [0, \infty) = \{t \in \mathbb{R} : t \geq 0\}$, $\mathbf{T}_+ = (0, \infty) = \{t \in \mathbb{R} : t > 0\}$, and symbol $\Omega \times \mathbf{T}$ denotes the Cartesian product of the sets Ω and $\mathbf{T}$. A function f belongs to the class C^n in the set Ω ($f \in C^n(\Omega)$) if f and all its partial derivatives up through the n-th order are continuous in the set Ω ($n = 0, 1, 2, \ldots$). The fact that the function f is defined in the set $\Omega \times \mathbf{T}$ will be denoted as follows: $f : \Omega \times \mathbf{T} \to \mathbb{R}$. The parameters $(\mu, \lambda, \alpha, \beta, \gamma, \varepsilon, \rho, J, \kappa, \eta_0, \nu_T) \in \mathbb{R}$ are thermo-elastodynamical constants in the E–N model. For the plain strain state (causes and effects do not depend on the variable x_3), the above notation should be adapted to the Cartesian coordinate system Ox_1x_2. Throughout the entry, the numbers of equations and formulae are sometimes furnished with natural indices, which indicate which equation or formula from a given group is selected. Thus, for instance, $(7)_{3,4}$ denotes the third and the fourth formulae from the group (7).

Basic Equations of the E–N Model: The 3D Problem

The linear E–N model of the micropolar body is subject to certain restrictions. The micropolar body is elastic, homogeneous, isotropic, and centrosymmetric. Considerations are referred to the medium $\Omega(\mu, \lambda, \alpha, \beta, \gamma, \varepsilon, \rho, J, \kappa, \eta_0, \nu_T)$ described by the set of thermo-elastodynamic real-valued parameters given in the parentheses. The initial configuration of the medium is the region Ω. All the physical fields defining the thermo-elastodynamical states of the medium are real-valued functions of the position variables x_i and the time variable t. The basic equations of the E–N model can be divided into the following groups:

- *The equations of motion in* $\Omega \times \mathbf{T}_+$ [8, p. 11]

$$\sigma_{ji,j} + X_i = \rho\, \ddot{u}_i, \qquad \epsilon_{ijk}\, \sigma_{jk} + \mu_{ji,j} + Y_i = J\, \ddot{\varphi}_i \quad (1)$$

where σ_{ji} and $\mu_{ji} \in C^1(\Omega \times \mathbf{T}_+)$ are 3×3 matrices with physical components of the asymmetric force-stress tensor and the asymmetric couple-stress tensor; X_i and $Y_i \in C^0(\Omega \times \mathbf{T})$ are the fields of body loadings and body moments, respectively; u_i and $\varphi_i \in C^2(\Omega \times \mathbf{T}_+)$ are components of the displacement and the rotation vectors, respectively; ρ is the density; and J is the rotational inertia of the medium.

- *The equations of compatibility in* $\Omega \times \mathbf{T}$ [8, p. 21]

$$\gamma_{li,h} - \gamma_{hi,l} - \epsilon_{khi}\,\kappa_{lk} + \epsilon_{kli}\,\kappa_{hk} = 0,\ \kappa_{li,h} - \kappa_{hi,l} = 0 \tag{2}$$

where γ_{ji} and $\kappa_{ji} \in C^1(\Omega \times \mathbf{T})$ are the 3×3 matrices with physical components of the asymmetric strain tensor and the asymmetric micro-strain (torsion-flexure) tensor.

The tensors γ_{ji} and κ_{ji} are defined by [8, pp. 12, 14]:

- *The geometric relations in* $\Omega \times \mathbf{T}_+$

$$\gamma_{ji} = u_{i,j} - \epsilon_{kji}\,\varphi_k, \qquad \kappa_{ji} = \varphi_{i,j} \tag{3}$$

- *The constitutive relations in* $\Omega \times \mathbf{T}$

$$\begin{aligned} \sigma_{ji} &= (\mu + \alpha)\gamma_{ji} + (\mu - \alpha)\gamma_{ij} + (\lambda\gamma_{kk} - \nu_T\theta)\delta_{ij} \\ \mu_{ji} &= (\gamma + \varepsilon)\kappa_{ji} + (\gamma - \varepsilon)\kappa_{ij} + \beta\kappa_{kk}\delta_{ij} \end{aligned} \tag{4}$$

where μ, λ, α, β, γ, and ε are the elasticity constants of the medium; $\nu_T = (2\mu + 3\lambda)\alpha_t$; and α_t is the linear coefficient of thermal expansion of the medium.

The function $\theta = T - T_0$ describes the temperature field, and it satisfies [8, p. 203]:

- *The coupled heat equation in* $\Omega \times \mathbf{T}_+$

$$\theta_{,ii} - \frac{1}{\kappa}\dot{\theta} - \eta_0\,\dot{u}_{j,j} = -\frac{Q}{\kappa} \tag{5}$$

where

$$Q = \frac{\kappa W}{\lambda_0}, \qquad \kappa = \frac{\lambda_0}{c_\varepsilon}, \qquad \eta_0 = \frac{\nu_T T_0}{\lambda_0}$$
$$\theta \in C^2(\Omega \times \mathbf{T}_+)$$

Q stands for the heat sources in the body, W is the amount of heat generated in a unit volume and unit time, λ_0 represents the heat conduction coefficient, T_0 means the natural state temperature, and c_ε denotes the specific heat for constant deformation.

- *The initial-boundary conditions:*
  - The boundary conditions on $\partial\Omega \times \mathbf{T}$

$$\sigma_{ji}n_j = p_i, \qquad \mu_{ji}n_j = m_i, \qquad \theta = \vartheta \tag{6}$$

where the functions p_i, m_i, and $\vartheta : \partial\Omega \times \mathbf{T} \to \mathbb{R}$ are given.

  - The initial conditions in $\Omega \times \{0\}$

$$\begin{aligned} u_i &= h_i, \qquad \varphi_i = k_i, \qquad \theta = l \\ \dot{u}_i &= \psi_i, \qquad \dot{\varphi}_i = \chi_i \end{aligned} \tag{7}$$

where the functions h_i, k_i, l, ψ_i, and $\chi_i : \Omega \to \mathbb{R}$ are given.

Definition 1. *By stress and temperature fields corresponding to the solution of the problem given by (1)–(7), we understand the triple* $(\boldsymbol{\sigma}, \boldsymbol{\mu}, \theta)$ *with such properties that there exists a quadruple* $(\mathbf{u}, \boldsymbol{\varphi}, \boldsymbol{\gamma}, \boldsymbol{\kappa})$*, such that the system of functions* $(\mathbf{u}, \boldsymbol{\varphi}, \boldsymbol{\gamma}, \boldsymbol{\kappa}, \boldsymbol{\sigma}, \boldsymbol{\mu}, \theta)$ *is a solution of (1)–(7), where* $\mathbf{u}, \boldsymbol{\varphi}, \boldsymbol{\gamma}, \boldsymbol{\kappa}, \boldsymbol{\sigma}, \boldsymbol{\mu}$ *are the vectors of displacements, rotations and the tensors of strain, micro-strain, force-stress, couple-stress, respectively.*

Let us assume that we know the triple $(\boldsymbol{\sigma}, \boldsymbol{\mu}, \theta)$ and the pair $(\boldsymbol{\gamma}, \boldsymbol{\kappa})$. Then the pair $(\mathbf{u}, \boldsymbol{\varphi})$ can be obtained from the pair $(\boldsymbol{\gamma}, \boldsymbol{\kappa})$ by integrating the geometric relations (3) with respect to the position coordinates x_i, and arbitrary integration functions $A_{ij}(x_k, t)$, $B_{ij}(x_k, t)$ $(j \neq k)$ can be determined by using the compatibility equations (2). In section "Stress-Temperature Equations of Motion for the 3D Problem," we offer an alternative method of recovering $(\mathbf{u}, \boldsymbol{\varphi})$ from $(\boldsymbol{\gamma}, \boldsymbol{\kappa})$.

Stress–Temperature Equations of Motion for the 3D Problem

Let us turn to the derivation of the stress-temperature equations of motion of Ignaczak type

(STEMP). Using the geometric relations (3), we obtain from the equations of motion (1) the following equations in $\Omega \times \mathbf{T}_+$:

$$\rho^{-1} R_{i,j} - J^{-1}\,\epsilon_{kji}\, M_k = \ddot{\gamma}_{ji}, \qquad J^{-1} M_{i,j} = \ddot{\kappa}_{ji} \quad (8)$$

where $R_i = \sigma_{ji,j} + X_i, M_i = \epsilon_{ijk}\,\sigma_{jk} + \mu_{ji,j}$. In view of equations (3), the coupled heat equation (5) takes the form in $\Omega \times \mathbf{T}_+$

$$\theta_{,ii} - \frac{1}{\kappa}\dot{\theta} - \eta_0\,\dot{\gamma}_{kk} = -\frac{Q}{\kappa} \quad (9)$$

The constitutive relations (4), when solved for strains, take the following equivalent form in $\Omega \times \mathbf{T}$:

$$\begin{aligned} \gamma_{ji} &= \frac{1}{2\mu}\sigma_{(ji)} + \frac{1}{2\alpha}\sigma_{[ji]} - \frac{1}{2\mu}(\lambda e - \nu_T\theta)\delta_{ij} \\ \kappa_{ji} &= \frac{1}{2\gamma}\mu_{(ji)} + \frac{1}{2\varepsilon}\mu_{[ji]} - \frac{\beta}{2\gamma(2\gamma+3\beta)}\mu_{kk}\delta_{ij} \end{aligned} \quad (10)$$

where $e = \frac{1}{2\mu+3\lambda}(\sigma_{kk} + 3\nu_T\theta)$ and the parentheses $(\,.\,)$ and brackets $[\,.\,]$ denote the symmetric part and the antisymmetric part of a tensor, respectively. By using relations (10), we reduce equations (8) and (9) to the form in $\Omega \times \mathbf{T}_+$:

$$\begin{aligned} &\rho^{-1} R_{i,j} + J^{-1}\,\epsilon_{ijk}\, M_k - \frac{1}{2\mu}\,\ddot{\sigma}_{(ji)} - \frac{1}{2\alpha}\,\ddot{\sigma}_{[ji]} \\ &\qquad + \frac{1}{2\mu}(\lambda\ddot{e} - \nu_T\ddot{\theta})\delta_{ij} = 0 \\ &J^{-1} M_{i,j} - \frac{1}{2\gamma}\,\ddot{\mu}_{(ji)} - \frac{1}{2\varepsilon}\,\ddot{\mu}_{[ji]} + \frac{\beta}{2\gamma(2\gamma+3\beta)}\,\ddot{\mu}_{kk}\,\delta_{ij} = 0 \\ &\theta_{,ii} - \frac{1}{\kappa}\dot{\theta} - \eta_0\dot{e} = -\frac{Q}{\kappa} \end{aligned} \quad (11)$$

where

$$\dot{e} = \frac{1}{2\mu+3\lambda}(\dot{\sigma}_{kk} + 3\nu_T\dot{\theta}),\ \ddot{e} = \frac{1}{2\mu+3\lambda}(\ddot{\sigma}_{kk} + 3\nu_T\ddot{\theta})$$

The initial conditions for the triple $(\boldsymbol{\sigma}, \boldsymbol{\mu}, \theta)$ which satisfies the field equations (11) follow from the initial conditions (7), the constitutive relations (4), the geometric relations (3), and the coupled heat equation (5). We obtain the following matrices of initial values of stresses $\boldsymbol{\sigma}^0, \boldsymbol{\mu}^0$ and stress velocities $\dot{\boldsymbol{\sigma}}^0, \dot{\boldsymbol{\mu}}^0$:

$$\boldsymbol{\sigma}^0 \equiv [\sigma^0_{ji}], \qquad \boldsymbol{\mu}^0 \equiv [\mu^0_{ji}] \quad (12)$$

$$\dot{\boldsymbol{\sigma}}^0 \equiv [\dot{\sigma}^0_{ji}], \qquad \dot{\boldsymbol{\mu}}^0 \equiv [\dot{\mu}^0_{ji}] \quad (13)$$

where

$$\begin{aligned} \sigma^0_{ji} &= (\mu+\alpha)\gamma^0_{ji} + (\mu-\alpha)\gamma^0_{ij} + (\lambda e^0 - \nu_T l)\delta_{ij} \\ \mu^0_{ji} &= (\gamma+\varepsilon)k_{i,j} + (\gamma-\varepsilon)k_{j,i} + \beta k_{k,k}\delta_{ij} \\ \gamma^0_{ji} &= h_{i,j} - \epsilon_{kji}\,k_k, \qquad e^0 = h_{k,k} \end{aligned} \quad (14)$$

and

$$\begin{aligned} \dot{\sigma}^0_{ji} &= (\mu+\alpha)\,\dot{\gamma}^0_{ji} + (\mu-\alpha)\,\dot{\gamma}^0_{ij} \\ &\quad + \left[(\lambda + \nu_T\kappa\eta_0)\,\dot{e}^0 - \nu_T(\kappa\, l_{,kk} + Q^0)\right]\delta_{ij} \\ \dot{\mu}^0_{ji} &= (\gamma+\varepsilon)\chi_{i,j} + (\gamma-\varepsilon)\chi_{j,i} + \beta\chi_{k,k}\delta_{ij} \\ \dot{\gamma}^0_{ji} &= \psi_{i,j} - \epsilon_{kji}\,\chi_k, \qquad \dot{e}^0 = \psi_{k,k} \end{aligned} \quad (15)$$

where Q^0 is the initial value of the heat sources. Let us formulate the following useful lemma [15].

Lemma 1. *Assume that the fields* $\mathbf{u}, \boldsymbol{\varphi}, \boldsymbol{\sigma}$, *and* $\boldsymbol{\mu}$ *are sufficiently smooth on* $\overline{\Omega} \times \mathbf{T}$. *Then the fields* $\mathbf{u}, \boldsymbol{\varphi}, \boldsymbol{\sigma}$, *and* $\boldsymbol{\mu}$ *satisfy the equations of motion* (1) *and the initial conditions* (7) *if and only if the following relations hold in* $\Omega \times \mathbf{T}$:

$$\begin{aligned} u_i &= \psi_i t + h_i + \rho^{-1}(t * R_i) \\ \varphi_i &= \chi_i t + k_i + J^{-1}(t * M_i) \end{aligned} \quad (16)$$

where $*$ *denotes the convolution* [16]:

$$t * f(x_1, x_2, x_3, t) = \int_0^t (t-\tau) f(x_1, x_2, x_3, \tau)\, d\tau$$

Definition 2. *(STEMP). By the stress-temperature equations of motion problem*

of linear, homogeneous, isotropic, coupled, dynamical, micropolar thermoelasticity for a three-dimensional body, we understand the initial-boundary value problem, in which the field equations (11) are satisfied, together with the initial conditions in $\Omega \times \{0\}$

$$\begin{aligned} \boldsymbol{\sigma} &= \boldsymbol{\sigma}^0, \qquad \boldsymbol{\mu} = \boldsymbol{\mu}^0, \qquad \theta = l \\ \dot{\boldsymbol{\sigma}} &= \dot{\boldsymbol{\sigma}}^0, \qquad \dot{\boldsymbol{\mu}} = \dot{\boldsymbol{\mu}}^0 \end{aligned} \tag{17}$$

and the boundary conditions (6) on $\partial\Omega \times \mathbf{T}$.

Theorem 1. *(Formulation of the problem in terms of stresses and temperature). Let the systems of functions* $(\mathbf{u}, \boldsymbol{\varphi})$,$(\boldsymbol{\sigma}, \boldsymbol{\mu}, \theta)$, *and* $(\boldsymbol{\gamma}, \boldsymbol{\kappa})$ *be sufficiently smooth on* $\overline{\Omega} \times \mathbf{T}$. *Then* $\boldsymbol{\sigma}$, $\boldsymbol{\mu}$, *and* θ *are the stress fields and the temperature field, respectively, corresponding to the solution of the initial-boundary value problem (1)–(7) if and only if equations (11) hold and the initial conditions (17) and the boundary conditions (6) are satisfied.*

Proof. *Necessity*. It has been shown that the relations (1) and (3)–(7) give the field equations (11), the boundary conditions (6), and the initial conditions (17).

Sufficiency. Let us assume that the stress and temperature fields $\boldsymbol{\sigma}$, $\boldsymbol{\mu}$, and θ correspond to the solution of STEMP. Therefore, by using (10), we determine the strain fields $\boldsymbol{\gamma}$ and $\boldsymbol{\kappa}$. Next, we determine the displacement field $\mathbf{u}$ and the rotation field $\boldsymbol{\varphi}$ by means of the relations (16). Let us notice that the conditions (16), (10), and (11) imply the relations (3). The system of functions $(\mathbf{u}, \boldsymbol{\varphi}, \boldsymbol{\sigma}, \boldsymbol{\mu})$ satisfies the equations of motion (1) and the initial conditions $(7)_{1,2,4,5}$ if and only if the relations (16) hold. Since it is easy to notice that $(11)_3$ and $(17)_3$ imply the heat conduction equation (5) and the initial condition $(7)_3$, we conclude that the system of functions $(\mathbf{u}, \boldsymbol{\varphi}, \boldsymbol{\gamma}, \boldsymbol{\kappa}, \boldsymbol{\sigma}, \boldsymbol{\mu}, \theta)$ is a solution of the problems (1)–(7). This completes the proof.

Remark 1. *When solving a STEMP, one does not have to refer to the compatibility equations (2) since equations (2) are implied by equations (11), (17), and (12)–(15).*

Remark 2. *A STEMP makes sense when the initial stress, stress rate, and temperature are presented in an arbitrary way. However, in such a general case, the compatibility equations (2) will not be satisfied at* $t = 0$, *and the problem does not belong to classical micropolar dynamical thermoelasticity.*

A Singular Solution of STEMP for an Infinite 3D Space

Let us consider harmonic vibrations of an infinite micropolar thermoelastic space which correspond to the following concentrated loads:

- *The case of body loadings*

$$(X_i, Y_i) = (P_0, M_0) e^{-i\omega t} \delta(x_1)\delta(x_2)\delta(x_3)\delta_{is} \tag{18}$$

- *The case of heat source*

$$Q = Q_0 e^{-i\omega t} \delta(x_1)\delta(x_2)\delta(x_3) \tag{19}$$

  where $\delta(.)$ is the Dirac delta distribution, ω is the vibration frequency, and P_0 and M_0 refer to the unit force and the unit moment, respectively, $Q_0 = 1$.

A singular solution of STEMP for an infinite space corresponding to the loads X_i, Y_i, and Q given by (18) and (19), respectively, will be obtained with the help of differential equations for the stress components and for the temperature, which are obtained from the field equations (11) in the form:

- The equation for force-stresses

$$\begin{aligned} D_2\Box_3(\Box_2\Box_4 + 4\alpha^2\Delta)\sigma_{ij} &= -2\alpha\epsilon_{ijk}D_2L_1Y_{s,sk} \\ &+ 2\alpha D_2\Box_3\left[(\mu+\alpha)\epsilon_{jsk}Y_{k,si}\right. \\ &\left.+(\mu-\alpha)\epsilon_{isk}Y_{k,sj} + \epsilon_{ijk}\Box_2 Y_k\right] \\ &+ 2\mu\Box_3(DL_2 - v_T\eta_0\partial_t\Box_4)X_{k,kij} \\ &- D_2\Box_3\left\{\Box_4\left[(\mu+\alpha)X_{j,i} + (\mu-\alpha)X_{i,j}\right]\right. \\ &\left.+ 4\alpha^2(X_{j,i} - X_{i,j})\right\} - \Box_3(\Box_2\Box_4 + 4\alpha^2\Delta) \\ &\times (\lambda D - v_T\eta_0\partial_t)X_{k,k}\delta_{ij} \\ &- \frac{v_T}{\kappa}\Box_3(\Box_2\Box_4 + 4\alpha^2\Delta)\left[2\mu Q_{,ij} + (\lambda\Delta - \Box_1)Q\delta_{ij}\right] \end{aligned} \tag{20}$$

where

$$L_1 = (\beta+\gamma-\varepsilon)\Box_2 - 4\alpha^2$$
$$L_2 = (\lambda+\mu-\alpha)\Box_4 - 4\alpha^2$$
$$\Box_1 = (\lambda+2\mu)\Delta - \rho\partial_t^2,\ \ \Box_2 = (\mu+\alpha)\Delta - \partial_t^2$$
$$\Box_3 = (\beta+2\gamma)\Delta - 4\alpha - J\partial_t^2,\ \Box_4 = (\gamma+\varepsilon)\Delta - 4\alpha - J\partial_t^2$$
$$D = \Delta - \frac{1}{\kappa}\partial_t,\ \ D_2 = D\Box_1 - \eta_0 v_T \partial_t \Delta$$

$\Delta(\,.\,) = (\,.\,)_{,ii}$, the symbol ∂_t denotes the partial derivative with respect to time.

- The equation for couple-stresses

$$\begin{aligned}\Box_3(\Box_2\Box_4 + 4\alpha^2\Delta)\mu_{ij} &= 2\alpha\Box_3\left[(\gamma+\varepsilon)\epsilon_{jsk}X_{k,si} + (\gamma-\varepsilon)\epsilon_{isk}X_{k,sj}\right] \\ &\quad - \Box_2\Box_3\left[(\gamma+\varepsilon)Y_{j,i} + (\gamma-\varepsilon)Y_{i,j}\right] \\ &\quad + 2\gamma L_1 Y_{k,kij} - \beta(\Box_2\Box_4 + 4\alpha^2\Delta)Y_{k,k}\delta_{ij}\end{aligned} \tag{21}$$

- The equation for temperature

$$D_2\theta = -\left(\eta_0\partial_t X_{k,k} + \frac{1}{\kappa}\Box_1 Q\right) \tag{22}$$

First, a singular solution to STEMP will be obtained for the case $P_0 \neq 0$, $M_0 = 0$, and $Q_0 = 0$. Applying the method of integral transformations based on the Fourier transformation (direct and inverse) of a function $f(\mathbf{x})$ [17, p. 27]

$$\begin{aligned}\tilde{f}(\boldsymbol{\xi}) &= (2\pi)^{-\frac{n}{2}}\int_{\mathbb{R}^n} f(\mathbf{x})e^{i\boldsymbol{\xi}\circ\mathbf{x}}d\mathbf{x} \\ f(\mathbf{x}) &= (2\pi)^{-\frac{n}{2}}\int_{\mathbb{R}^n} \tilde{f}(\boldsymbol{\xi})e^{-i\boldsymbol{\xi}\circ\mathbf{x}}d\boldsymbol{\xi}\end{aligned} \tag{23}$$

where

$$\mathbf{x} = (x_1, \ldots, x_n) \in \mathbb{R}^n$$
$$\boldsymbol{\xi} = (\xi_1, \ldots, \xi_n) \in \mathbb{R}^n$$
$$\boldsymbol{\xi}\circ\mathbf{x} = \xi_1 x_1 + \cdots + \xi_n x_n$$

(for $n = 4$), and using $(18)_1$, we obtain from equations (20)–(22) the following formulae:

– For the force-stresses

$$\begin{aligned}\sigma_{ij}^{(s)} = \frac{P_0 e^{-i\omega t}}{4\pi\rho\omega^2}\Bigg[&\frac{\rho\omega^2\alpha}{\mu l^2(\lambda_1^2-\lambda_2^2)}\left(\delta_{is}F_{1,j} - \delta_{js}F_{1,i}\right) \\ &+ 2\mu(K_1 - K_2)_{,ijs} + \left(\lambda G_2 - \frac{\rho\omega^2 q\varepsilon}{\mu_1^2-\mu_2^2}\Gamma_1\right)_{,s}\delta_{ij} \\ &+ (\mu+\alpha)\delta_{js}G_{1,i} + (\mu-\alpha)\delta_{is}G_{1,j}\Bigg]\end{aligned} \tag{24}$$

where

$$K_1 = \frac{1}{R}\left(A_1 e^{i\lambda_1 R} + A_2 e^{i\lambda_2 R}\right)$$
$$K_2 = \frac{1}{R}\left(E_1 e^{i\mu_1 R} - E_2 e^{i\mu_2 R}\right)$$
$$G_1 = \frac{1}{R}\left(A_1\lambda_1^2 e^{i\lambda_1 R} + A_2\lambda_2^2 e^{i\lambda_2 R}\right)$$
$$G_2 = \frac{1}{R}\left(E_1\mu_1^2 e^{i\mu_1 R} - E_2\mu_2^2 e^{i\mu_2 R}\right)$$
$$F_1 = \frac{1}{R}\left(e^{i\lambda_1 R} - e^{i\lambda_2 R}\right)$$
$$\Gamma_1 = \frac{1}{R}\left(e^{i\mu_1 R} - e^{i\mu_2 R}\right)$$
$$A_1 = \frac{\sigma_2^2-\lambda_2^2}{\lambda_1^2-\lambda_2^2}, A_2 = \frac{\sigma_2^2-\lambda_1^2}{\lambda_2^2-\lambda_1^2}, R = \sqrt{x_j x_j}$$
$$E_1 = \frac{(\mu_1^2-q)\sigma_1^2}{\mu_1^2(\mu_1^2-\mu_2^2)}, \qquad E_2 = \frac{(\mu_2^2-q)\sigma_1^2}{\mu_2^2(\mu_1^2-\mu_2^2)}$$
$$\sigma_i = \frac{\omega}{c_i}\ (i = 1,\ 2,\ 3,\ 4)$$
$$c_1 = \sqrt{\frac{\lambda+2\mu}{\rho}}, c_2 = \sqrt{\frac{\mu+\alpha}{\rho}}, c_3 = \sqrt{\frac{\beta+2\gamma}{J}}$$
$$c_4 = \sqrt{\frac{\gamma+\varepsilon}{J}}$$
$$v_0^2 = 2p = \frac{4\alpha}{\gamma+\varepsilon}, \qquad s = \frac{2\alpha}{\mu+\alpha}, \qquad \eta_0^2 = ps$$

The values λ_1^2 and λ_2^2 are the roots of the equation

$$\begin{aligned}W_4(\lambda) = \lambda^4 - \lambda^2\left[\sigma_2^2 + \sigma_4^2 + p(s-2)\right] \\ + \sigma_2^2(\sigma_4^2 - 2p) = 0\end{aligned}$$

with the determinant $\Delta_W = (\sigma_2^2 - \sigma_4^2 - \eta_0^2 + v_0^2)^2 + 4\sigma_2^2\eta_0^2 > 0$. The polynomial $W_4(\lambda)$ is obtained

from the operator $\Box_2\Box_4 + 4\alpha^2\Delta$. The roots λ_1^2 and $\lambda_2^2 \in \mathbb{R}$ are different, and

$$\lambda_{1,2}{}^2 = \tfrac{1}{2}\big[\sigma_2^2 + \sigma_4^2 + \eta_0^2 - \nu_0^2 \pm \sqrt{(\sigma_2^2 - \sigma_4^2 - \eta_0^2 + \nu_0^2)^2 + 4\sigma_2^2\eta_0^2}\big].$$

Since we assume only real-phase velocities in (24), we let $J\omega^2 - 4\alpha > 0$ in order to satisfy the inequalities $\lambda_1^2 > 0$ and $\lambda_2^2 > 0$ (see [8, p. 50] and [9, p. 71]). The values μ_1^2 and μ_2^2 are the roots of the equation $W_4(\mu) = 0$. The polynomial $W_4(\mu)$ with complex coefficients, obtained from the operator D_2, has the following form:

$$W_4(\mu) = \mu^4 - \big[\sigma_1^2 + q(1+\varepsilon)\big]\mu^2 + q\sigma_1^2 = (\mu^2 - \mu_1^2)(\mu^2 - \mu_2^2)$$

where $q = i\omega/\kappa$, $\varepsilon = \kappa\eta_0 m$, and $m = \nu_T/(2\mu+\lambda)$. Thus, we obtain $\mu_{1,2}{}^2 = \frac{1}{2}[\sigma_1^2 + q(1+\varepsilon) \pm \sqrt{[\sigma_1^2 + q(1+\varepsilon)]^2 - 4q\sigma_1^2}]$. The roots μ_1 and μ_2 are complex-valued. For a detailed discussion of this problem, see [18] and [19, pp. 96–102]:

– For the couple-stresses

$$\mu_{ij}^{(s)} = \frac{P_0 e^{-i\omega t}}{8\pi\mu l^2}\frac{1}{(\lambda_1^2 - \lambda_2^2)} \times \big[(\gamma+\varepsilon)\,\epsilon_{jks}F_{1,ik} + (\gamma-\varepsilon)\,\epsilon_{iks}F_{1,jk}\big] \tag{25}$$

where $l^2 = \frac{(\gamma+\varepsilon)(\mu+\alpha)}{4\alpha\mu}$.

– For the temperature

$$\theta^{(s)} = \frac{P_0 e^{-i\omega t}}{4\pi\rho\omega^2}\frac{q\varepsilon\sigma_1^2}{m(\mu_1^2 - \mu_2^2)}\Gamma_{1,s} \tag{26}$$

Formulas (24)–(26) represent a singular solution $(\boldsymbol{\sigma}^{(s)}, \boldsymbol{\mu}^{(s)}, \theta^{(s)})$, which corresponds to the load $(18)_1$. In order to obtain displacement and rotation fields associated with the solution, we use relations (16). For this purpose, we need to specify the initial values of displacements, rotations, and their velocities. It follows from equations (14), (15), (24), and (25) that

$$\psi_i^{(s)} = -i\omega h_i^{(s)}, \qquad \chi_i^{(s)} = -i\omega k_i^{(s)} \tag{27}$$

and

$$h_i^{(s)} = A_0\Big[(K_1 - K_2)_{,is} + \delta_{is}G_1\Big]$$
$$k_i^{(s)} = \frac{\rho\omega^2}{2\mu l^2}\frac{1}{\lambda_1^2 - \lambda_2^2}A_0\,\epsilon_{iks}F_{1,k} \tag{28}$$

where $A_0 = \frac{P_0}{4\pi\rho\omega^2}$. Hence, from equations (16), (24), (25), (27), and (28) and the relations

$$\int_0^t (t-\tau)e^{-i\omega\tau}d\tau = \omega^{-2}\big(1 - i\omega t - e^{-i\omega t}\big)$$
$$A_1 + A_2 = 1, \qquad E_1 - E_2 = 1$$
$$\Delta\left(\frac{e^{i\lambda_1 R}}{R}\right) = \Delta\left(\frac{1}{R}\right) - \lambda_1^2\frac{e^{i\lambda_1 R}}{R} \tag{29}$$

we obtain

$$u_i^{(s)} = A(t)\Big[(K_1 - K_2)_{,is} + \delta_{is}G_1\Big]$$
$$\varphi_i^{(s)} = \frac{\rho\omega^2}{2\mu l^2}\frac{1}{\lambda_1^2 - \lambda_2^2}A(t)\,\epsilon_{iks}F_{1,k} \tag{30}$$

where $A(t) = A_0 e^{-i\omega t}$. One can check that when $R \to \infty$, the stress fields (24) and (25), the temperature field (26), as well as the displacement and rotation fields (30), all tend to zero. Also, by taking into account relations $(18)_1$, (24)–(26), and (30) and the formula

$$\frac{1}{4\pi}\Delta\left(\frac{1}{R}\right) = -\delta(x_1)\delta(x_2)\delta(x_3) \tag{31}$$

we note that the equations of motion (1) and the coupled heat equation (5) are satisfied identically.

Next, a singular solution to STEMP is obtained for the case $P_0 = 0$, $M_0 \neq 0$, and

$Q_0 = 0$. Proceeding in a way similar to that of nonzero mass forces, we receive:

– The force-stresses

$$\sigma_{ij}^{(s)} = \frac{M_0 e^{-i\omega t}}{4\pi}\left\{-p(\epsilon_{ijk}K_{3,ks} + \epsilon_{ijs}F_2) + \frac{1}{2\mu l^2(\lambda_1^2-\lambda_2^2)}\left[(\mu+\alpha)\epsilon_{jks}F_{1,ik} + (\mu-\alpha)\epsilon_{iks}F_{1,jk}\right]\right\} \tag{32}$$

where

$$K_3 = \frac{1}{R}\left(C_1 e^{i\lambda_1 R} + C_2 e^{i\lambda_2 R} + C_3 e^{i\lambda_3 R}\right)$$
$$F_2 = \frac{1}{R}\left(A_1 e^{i\lambda_2 R} + A_2 e^{i\lambda_1 R}\right)$$
$$C_1 = A_2\frac{1}{\lambda_1^2}, \qquad C_2 = A_1\frac{1}{\lambda_2^2}, \qquad C_3 = -\frac{\sigma_2^2}{\lambda_1^2\lambda_2^2}$$
$$\lambda_3 = \sqrt{\sigma_3^2 - \tau_0^2} > 0, \qquad \tau_0^2 = \frac{4\alpha}{\beta+2\gamma}$$

– The couple-stresses

$$\mu_{ij}^{(s)} = \frac{M_0 e^{-i\omega t}}{4\pi J c_4^2}\left[2\gamma K_{3,ijs} + \frac{\beta(\gamma+\varepsilon)}{\beta+2\gamma}\left(\frac{e^{i\lambda_3 R}}{R}\right)_{,s}\delta_{ij} + (\gamma+\varepsilon)\delta_{js}F_{2,i} + (\gamma-\varepsilon)\delta_{is}F_{2,j}\right] \tag{33}$$

In this case, the formula for the temperature $\theta^{(s)}$ reads

$$\theta^{(s)} \equiv 0 \tag{34}$$

Formulas (32)–(34) represent a singular solution $(\boldsymbol{\sigma}^{(s)}, \boldsymbol{\mu}^{(s)}, \theta^{(s)})$ of STEMP for an infinite space corresponding to the load $(18)_2$. Furthermore, initial values of displacements, rotations, and their velocities are given by the formulas (see (27))

$$\psi_i^{(s)} = -i\omega h_i^{(s)}, \qquad \chi_i^{(s)} = -i\omega k_i^{(s)} \tag{35}$$

and

$$h_i^{(s)} = \frac{Jc_4^2}{2\mu l^2}\frac{1}{\lambda_1^2-\lambda_2^2}C_0\,\epsilon_{iks}F_{1,k}$$
$$k_i^{(s)} = C_0(K_{3,is} + \delta_{is}F_2), \qquad C_0 = \frac{M_0}{4\pi J c_4^2} \tag{36}$$

Finally, the formulas for the displacements and the rotations read

$$u_i^{(s)} = \frac{Jc_4^2}{2\mu l^2}\frac{1}{\lambda_1^2-\lambda_2^2}C(t)\,\epsilon_{iks}F_{1,k}$$
$$\varphi_i^{(s)} = C(t)(K_{3,is} + \delta_{is}F_2) \tag{37}$$

where $C(t) = C_0 e^{-i\omega t}$. One can check that when $R \to \infty$, the stress fields (32), (33), the temperature field (34), as well as the displacement and rotation fields (37), all tend to zero. Also, by taking into account relations $(18)_2$, (32)–(34), (37), and (31), we note that the equations of motion (1) and the coupled heat equation (5) are satisfied identically. Let us note that in this case a temperature field vanishes.

Finally, in case $P_0 = 0$, $M_0 = 0$, and $Q_0 \neq 0$, from equations (24) and (26), we obtain

$$D_2\sigma_{ij} = -\frac{\nu_T}{\kappa}\left[2\mu Q_{,ij} + (\lambda\Delta - \Box_1)Q\delta_{ij}\right] \tag{38}$$

$$D_2\theta = -\frac{1}{\kappa}\Box_1 Q \tag{39}$$

Applying to equations (38), (39), and (19), the same integration method based on the four-dimensional Fourier transform (23) as in the previous cases, we obtain the following results in a closed form:

– The force-stresses

$$\sigma_{ij} = -\frac{Q_0 e^{-i\omega t}}{4\pi}\frac{m}{\kappa}\left[\frac{2\mu}{\mu_1^2-\mu_2^2}\Gamma_{1,ij} + \left(2\mu\Gamma_2 - \frac{\lambda\sigma_1^2}{\mu_1^2-\mu_2^2}\Gamma_1\right)\delta_{ij}\right] \tag{40}$$

– The temperature

$$\theta = \frac{Q_0 e^{-i\omega t}}{4\pi}\frac{1}{\kappa}\Gamma_2 \tag{41}$$

where $\Gamma_2 = \frac{1}{\mu_1^2-\mu_2^2}(\Delta+\sigma_1^2)\Gamma_1 = \frac{1}{R}(E_1 e^{i\mu_2 R} - E_2 e^{i\mu_1 R})$. By using equation (21), in this case, for the couple-stresses, we obtain the formula

$$\mu_{ij} \equiv 0 \tag{42}$$

The pair $(\mathbf{u}, \boldsymbol{\varphi})$ given by formula (16) is determined by a method described in the previous cases. The initial values of displacements, rotations, and their velocities take the form:

$$\psi_i = -i\omega h_i, \qquad \chi_i = -i\omega k_i \tag{43}$$

and

$$h_i = -B_0 \frac{1}{\mu_1^2 - \mu_2^2}\Gamma_{1,i}, \qquad k_i = 0 \tag{44}$$

where $B_0 = \frac{mQ_0}{4\pi\kappa}$. Using these formulas as well as relations (16) and (29), we obtain results for u_i and φ_i in the following form:

$$u_i = -B(t)\frac{1}{\mu_1^2 - \mu_2^2}\Gamma_{1,i}, \qquad \varphi_i = 0 \tag{45}$$

where $B(t) = B_0 e^{-i\omega t}$. When $R \to \infty$, all physical fields obtained above tend to zero. Besides, taking into account relations (40)–(42), (45), (19), and (31), we note that the equations of motion (1) and the heat conduction equation (5) are satisfied identically. Formulas (40), $(45)_1$, and (41) determine the fields of stresses $\boldsymbol{\sigma}$, displacements $\mathbf{u}$, and temperature θ corresponding to the heat source (19). This is the classical result $(\varphi_i \equiv 0, \mu_{ij} \equiv 0)$.

Remark 3. *The results for the physical fields produced by the loads* (18) and (19) *which were obtained by the STEMP method* [20, p. 37] *correspond to the results given in* [8, pp. 238–244], [21], *and* [20, pp. 24, 29].

STEMP for a Plane State of Strain: The 2D Problem

Let us discuss briefly, for didactic purposes, STIBVP for the case of the plane state of deformation for a coupled dynamic thermoelasticity. In the plane state of strain, all causes and results depend on two (x_1, x_2) variables only. In the case of the action of a temperature field $\theta(x_1, x_2, t)$, the deformation of the body is described by the vectors

$$\begin{aligned} \mathbf{u} &= [u_1(x_1, x_2, t), u_2(x_1, x_2, t), 0] \\ \boldsymbol{\varphi} &= [0, 0, \varphi_3(x_1, x_2, t)] \end{aligned} \tag{46}$$

The force- and couple-stress tensor fields $\boldsymbol{\sigma}$ and $\boldsymbol{\mu}$ and the strain and micro-strain tensor fields $\boldsymbol{\gamma}$ and $\boldsymbol{\kappa}$ can be written as the matrices

$$\boldsymbol{\sigma} \equiv \begin{bmatrix} \sigma_{11} & \sigma_{12} & 0 \\ \sigma_{21} & \sigma_{22} & 0 \\ 0 & 0 & \sigma_{33} \end{bmatrix}, \quad \boldsymbol{\mu} \equiv \begin{bmatrix} 0 & 0 & \mu_{13} \\ 0 & 0 & \mu_{23} \\ \mu_{31} & \mu_{32} & 0 \end{bmatrix} \tag{47}$$

$$\boldsymbol{\gamma} \equiv \begin{bmatrix} \gamma_{11} & \gamma_{12} & 0 \\ \gamma_{21} & \gamma_{22} & 0 \\ 0 & 0 & 0 \end{bmatrix}, \qquad \boldsymbol{\kappa} \equiv \begin{bmatrix} 0 & 0 & \kappa_{13} \\ 0 & 0 & \kappa_{23} \\ 0 & 0 & 0 \end{bmatrix} \tag{48}$$

The basic equations of the E–N model can be divided into the following groups [8, p. 250]:

- *The equations of motion in* $\Omega \times \mathbf{T}_+$

$$\begin{aligned} &\sigma_{\beta\alpha,\beta} + X_\alpha = \rho\, \ddot{u}_\alpha \\ &\epsilon_{\alpha\beta}\, \sigma_{\alpha\beta} + \mu_{\alpha 3,\alpha} + Y_3 = J\, \ddot{\varphi}_3 \end{aligned} \tag{49}$$

  Here $\mathbf{X} \equiv (X_1, X_2, 0)$ and $\mathbf{Y} \equiv (0, 0, Y_3)$ are the vectors of body force and body moment, respectively.

- *The compatibility equations in* $\Omega \times \mathbf{T}$

$$\begin{aligned} &\kappa_{23,1} - \kappa_{13,2} = 0, \qquad \kappa_{13} - \gamma_{21,1} + \gamma_{11,2} = 0 \\ &\kappa_{23} + \gamma_{12,2} - \gamma_{22,1} = 0 \end{aligned} \tag{50}$$

- *The geometric relations in* $\Omega \times \mathbf{T}_+$

$$\gamma_{\alpha\beta} = u_{\beta,\alpha} + \epsilon_{\beta\alpha}\,\varphi_3, \qquad \kappa_{\alpha 3} = \varphi_{3,\alpha} \tag{51}$$

- *The constitutive relations in* $\Omega \times \mathbf{T}$

$$\begin{aligned} &\sigma_{\alpha\beta} = (\mu+\alpha)\gamma_{\alpha\beta} + (\mu-\alpha)\gamma_{\beta\alpha} + (\lambda e_1 - \nu_T\theta)\delta_{\alpha\beta} \\ &\sigma_{33} = \nu\sigma_{\alpha\alpha} - \frac{\mu}{\mu+\lambda}\nu_T\theta \\ &\mu_{\alpha 3} = (\gamma+\varepsilon)\kappa_{\alpha 3}, \qquad \mu_{3\alpha} = \frac{\gamma-\varepsilon}{\gamma+\varepsilon}\mu_{\alpha 3} \end{aligned} \tag{52}$$

where $e_1 = \gamma_{\varepsilon\varepsilon}$ and $\nu = \frac{\lambda}{2(\mu+\lambda)}$ is Poisson's ratio.

- *The coupled heat equation in* $\Omega \times \mathbf{T}_+$

$$\theta_{,\alpha\alpha} - \frac{1}{\kappa}\dot{\theta} - \eta_0\,\dot{u}_{\varepsilon,\varepsilon} = -\frac{Q}{\kappa} \tag{53}$$

- *The initial-boundary conditions:*
  - The boundary conditions on $\partial\Omega \times \mathbf{T}$

$$\sigma_{\beta\alpha}n_\beta = p_\alpha, \qquad \mu_{\alpha 3}n_\alpha = m_3, \qquad \theta = \vartheta \tag{54}$$

where the functions p_α, m_3, and $\vartheta : \partial\Omega \times \mathbf{T} \to \mathbb{R}$ are given.

  - The initial conditions in $\Omega \times \{0\}$

$$u_\alpha = f_\alpha, \quad \varphi_3 = f_3, \quad \theta = l, \quad \dot{u}_\alpha = g_\alpha, \quad \dot{\varphi}_3 = g_3 \tag{55}$$

where the functions f_α, f_3, l, g_α, and $g_3 : \Omega \to \mathbb{R}$ are given.

Definition 1 remains valid and takes the form.

Definition 3. *By stress and temperature fields corresponding to the solution of the problem* (49)–(55)*, we mean a triplet* $(\boldsymbol{\sigma}, \boldsymbol{\mu}, \theta)$ *with the property that there exists a system of functions* $(\mathbf{u}, \boldsymbol{\varphi}, \boldsymbol{\gamma}, \boldsymbol{\kappa})$ *such that* $(\mathbf{u}, \boldsymbol{\varphi}, \boldsymbol{\gamma}, \boldsymbol{\kappa}, \boldsymbol{\sigma}, \boldsymbol{\mu}, \theta)$ *is a solution of the problem given by* (46)–(55).

Let us suppose that we know $(\boldsymbol{\sigma}, \boldsymbol{\mu}, \theta)$ and the deformations $(\boldsymbol{\gamma}, \boldsymbol{\kappa})$. Note that we obtain a triplet (u_1, u_2, φ_3) from a pair $(\boldsymbol{\gamma}, \boldsymbol{\kappa})$ by integrating (51), and $C_1(x_1,t)$, $C_2(x_2,t)$, $C_3(x_1,t)$, $C_4(x_2,t)$, $C_5(x_1,t)$, and $C_6(x_2,t)$ – arbitrary functions of integration – are determined from the compatibility equations (50). Next, we offer an alternative method of recovering (u_1, u_2, φ_3) from $(\boldsymbol{\gamma}, \boldsymbol{\kappa})$.

Let us turn to the derivation of STEMP. From equations (49), by use of (51), we obtain the following equations in $\Omega \times \mathbf{T}_+$:

$$\rho^{-1}R_{\alpha,\beta} + J^{-1}\,\epsilon_{\alpha\beta}\,R_3 = \ddot{\gamma}_{\beta\alpha}, \qquad J^{-1}R_{3,\alpha} = \ddot{\kappa}_{\alpha 3} \tag{56}$$

where $R_\alpha = \hat{R}_\alpha + X_\alpha$, $R_3 = \hat{R}_3 + Y_3$, $\hat{R}_\alpha = \sigma_{\beta\alpha,\beta}$, and $\hat{R}_3 = \epsilon_{\alpha\beta}\,\sigma_{\alpha\beta} + \mu_{\alpha 3,\alpha}$. From equation (53), by use of (51), we get in $\Omega \times \mathbf{T}_+$:

$$\theta_{,\alpha\alpha} - \frac{1}{\kappa}\dot{\theta} - \eta_0\,\dot{\gamma}_{\varepsilon\varepsilon} = -\frac{Q}{\kappa} \tag{57}$$

Let us write down (52) in an equivalent form in $\Omega \times \mathbf{T}$:

$$\begin{aligned} &\gamma_{\alpha\beta} = \tfrac{1}{2\mu}\sigma_{(\alpha\beta)} + \tfrac{1}{2\alpha}\sigma_{[\alpha\beta]} - \tfrac{1}{2\mu}(\lambda e_1 - \nu_T\theta)\delta_{\alpha\beta} \\ &\kappa_{\alpha 3} = \tfrac{1}{\gamma+\varepsilon}\mu_{\alpha 3}, \qquad e_1 = \tfrac{1}{2(\mu+\lambda)}(\sigma_{\varepsilon\varepsilon} + 2\nu_T\theta) \end{aligned} \tag{58}$$

Next, equations (56) and (57) are used to transform (58) into

$$\begin{aligned} &\rho^{-1}R_{\alpha,\beta} + J^{-1}\,\epsilon_{\alpha\beta}\,R_3 - \tfrac{1}{2\mu}\,\ddot{\sigma}_{(\alpha\beta)} + \tfrac{1}{2\alpha}\,\ddot{\sigma}_{[\alpha\beta]} \\ &\qquad + \frac{1}{2\mu}\left(\lambda\,\ddot{e}_1 - \nu_T\ddot{\theta}\right)\delta_{\alpha\beta} = 0 \\ &c_4^2 R_{3,\alpha} - \ddot{\mu}_{\alpha 3} = 0 \\ &\theta_{,\alpha\alpha} - \frac{1}{\kappa}\dot{\theta} - \eta_0\,\dot{e}_1 = -\frac{Q}{\kappa} \qquad \text{in } \Omega \times \mathbf{T}_+ \end{aligned} \tag{59}$$

where

$$\begin{aligned} \dot{e}_1 &= \frac{1}{2(\mu+\lambda)}(\dot{\sigma}_{\varepsilon\varepsilon} + 2\nu_T\dot{\theta}) \\ \ddot{e}_1 &= \frac{1}{2(\mu+\lambda)}(\ddot{\sigma}_{\varepsilon\varepsilon} + 2\nu_T\ddot{\theta}) \end{aligned}$$

The initial conditions for a triplet $(\boldsymbol{\sigma}, \boldsymbol{\mu}, \theta)$ that satisfies equations (59) are implied by (55) and (51)–(53). We obtain the following matrices of initial values $\boldsymbol{\sigma}^0, \boldsymbol{\mu}^0$, $\dot{\boldsymbol{\sigma}}^0$, and $\dot{\boldsymbol{\mu}}^0$ for stresses and their velocities:

$$\boldsymbol{\sigma}^0 \equiv \begin{bmatrix} \sigma_{11}^0 & \sigma_{12}^0 & 0 \\ \sigma_{21}^0 & \sigma_{22}^0 & 0 \\ 0 & 0 & \sigma_{33}^0 \end{bmatrix}, \boldsymbol{\mu}^0 \equiv \begin{bmatrix} 0 & 0 & \mu_{13}^0 \\ 0 & 0 & \mu_{23}^0 \\ \mu_{31}^0 & \mu_{32}^0 & 0 \end{bmatrix} \tag{60}$$

$$\dot{\boldsymbol{\sigma}}^0 \equiv \begin{bmatrix} \dot{\sigma}_{11}^0 & \dot{\sigma}_{12}^0 & 0 \\ \dot{\sigma}_{21}^0 & \dot{\sigma}_{22}^0 & 0 \\ 0 & 0 & \dot{\sigma}_{33}^0 \end{bmatrix}, \dot{\boldsymbol{\mu}}^0 \equiv \begin{bmatrix} 0 & 0 & \dot{\mu}_{13}^0 \\ 0 & 0 & \dot{\mu}_{23}^0 \\ \dot{\mu}_{31}^0 & \dot{\mu}_{32}^0 & 0 \end{bmatrix} \tag{61}$$

where

$$\begin{aligned} \sigma_{\alpha\beta}^0 &= (\mu+\alpha)\gamma_{\alpha\beta}^0 + (\mu-\alpha)\gamma_{\beta\alpha}^0 + (\lambda e_1^0 - \nu_T l)\delta_{\alpha\beta} \\ \mu_{\alpha 3}^0 &= (\gamma+\varepsilon) f_{3,\alpha}, \quad \gamma_{\alpha\beta}^0 = f_{\beta,\alpha} - \epsilon_{\alpha\beta} f_3, \quad e_1^0 = f_{\varepsilon,\varepsilon} \\ \dot{\sigma}_{\alpha\beta}^0 &= (\mu+\alpha)\,\dot{\gamma}_{\alpha\beta}^0 + (\mu-\alpha)\,\dot{\gamma}_{\beta\alpha}^0 \\ &\quad + \left[(\lambda + \nu_T \kappa \eta_0)\, \dot{e}_1^0 - \nu_T (\kappa l_{,\delta\delta} + Q^0)\right]\delta_{\alpha\beta} \\ \dot{\mu}_{\alpha 3}^0 &= (\gamma+\varepsilon) g_{3,\alpha}, \quad \dot{\gamma}_{\alpha\beta}^0 = g_{\beta,\alpha} - \epsilon_{\alpha\beta}\, g_3, \quad \dot{e}_1^0 = g_{\varepsilon,\varepsilon} \end{aligned} \tag{62}$$

For the initial moment $t = 0$, we have $Q = Q^0$. Now we present the following lemma.

Lemma 2. Let $\mathbf{u}$ and $\boldsymbol{\varphi}$ *given by* (46) *and* $\boldsymbol{\sigma}$ and $\boldsymbol{\mu}$ *given by* (47) *be smooth functions on* $\overline{\Omega} \times \mathbf{T}$. *Then* $\mathbf{u}$, $\boldsymbol{\varphi}$, $\boldsymbol{\sigma}$, *and* $\boldsymbol{\mu}$ *satisfy the equations of motion* (49) *as well as the initial conditions* $(55)_{1,\,2,\,4,\,5}$ *if and only if in* $\Omega \times \mathbf{T}$

$$\begin{aligned} u_\alpha &= g_\alpha t + f_\alpha + \rho^{-1}(t * R_\alpha) \\ \varphi_3 &= g_3 t + f_3 + J^{-1}(t * R_3) \end{aligned} \tag{63}$$

where $*$ *stands for the convolution product on the* t *-axis.*

Proof. We integrate the equations of motion (49) twice with respect to time and take into account the initial conditions $(55)_{1,\,2,\,4,\,5}$ to obtain (63) in $\Omega \times \mathbf{T}$. To show that (63) implies (49) and $(55)_{1,\,2,\,4,\,5}$, we proceed in a way similar to that in [15] and [4, p. 93]. □

Definition 4. *By STEMP associated with the linear homogeneous isotropic micropolar coupled dynamic thermoelasticity problem in the plane state of deformation, we mean the initial-boundary value problem in which the fields equations* (59) *are satisfied together with the initial conditions* (17) *and the boundary conditions* (54). *Of course, the expressions* $\boldsymbol{\sigma}$, $\boldsymbol{\mu}$, $\boldsymbol{\sigma}^0$, $\boldsymbol{\mu}^0$, $\dot{\boldsymbol{\sigma}}^0$, *and* $\dot{\boldsymbol{\mu}}^0$ *are now described by the expressions* (47), (60), *and* (61), *respectively.*

Remarks 1 and 2 remain valid here. We can formulate the following theorem.

Theorem 2. *(Characterization of the problem under consideration in terms of stress and temperature). Let the systems of functions* $(\mathbf{u}, \boldsymbol{\varphi})$,$(\boldsymbol{\sigma}, \boldsymbol{\mu}, \theta)$, *and* $(\boldsymbol{\gamma}, \boldsymbol{\kappa})$ *be sufficiently smooth on* $\overline{\Omega} \times \mathbf{T}$. *Then the fields* $\boldsymbol{\sigma}$, $\boldsymbol{\mu}$, *and* θ *correspond to the solution of the initial-boundary value problem given by* (46)–(55) *if and only if the equations* (59), *the initial conditions* (17), *as well as the boundary conditions* (54) *are satisfied.*

In the paper [22], we describe a pure stress–temperature initial-boundary value problem (STIBVP) of a micropolar coupled dynamic thermoelasticity, taking into account the stress–temperature equations of motion of Ignaczak type (STEMP) for the cases of the plane and axisymmetric state of deformation of the E–N model and to illustrate this method by the time-harmonic Green functions for an unbounded space. Now we will present here some results from [22]. It should be noted that the singular solutions to this problem (the plane state of strain) have been obtained before by Crăciun [23] by means of the method of direct determination of displacements, rotations, and temperature.

Let us consider harmonic vibrations of an infinite micropolar space produced by the following concentrated loadings:

- *The body force*

$$X_\alpha = P_1 e^{-i\omega t}\delta(x_1)\delta(x_2)\delta_{\alpha 1}, \quad Y_3 = 0, \quad Q = 0 \tag{64}$$

- *The heat source*

$$Q = Q_0 e^{-i\omega t}\delta(x_1)\delta(x_2), \quad X_\alpha = 0, \quad Y_3 = 0 \tag{65}$$

Remark 4. *The coefficients P_0, P_1, P_2, M_0, and Q_0 in (18), (19), (64), and (65) are introduced to comply with SI units (see [20, p. 36]) and to have the singular solutions in a dimensional form.*

A singular solution generated by X_α and Q by solving a STEMP associated with the loadings (64) and (65) will be obtained by means of differential equations for individual stress components and temperature implied from (59) in the form:

- The force-stress equations

$$\begin{aligned}
&D_2(\Box_2\Box_4 + 4\alpha^2\Delta_1)\sigma_{\alpha\beta} \\
&= -\frac{v_T}{\kappa}(\Box_2\Box_4 + 4\alpha^2\Delta_1)\left[2\mu Q_{,\alpha\beta} + (\lambda\Delta_1 - \Box_1)Q\delta_{\alpha\beta}\right] \\
&\quad + 2\alpha D_2\left[(\mu+\alpha)\epsilon_{\beta\gamma}Y_{3,\gamma\alpha} + (\mu-\alpha)\epsilon_{\alpha\gamma}Y_{3,\gamma\beta} + \epsilon_{\alpha\beta}\Box_2 Y_3\right] \\
&\quad + 2\mu(DL_2 - v_T\eta_0\partial_t\Box_4)X_{\gamma,\gamma\alpha\beta} \\
&\quad - (\Box_2\Box_4 + 4\alpha^2\Delta_1)(\lambda D - v_T\eta_0\partial_t)X_{\gamma,\gamma}\delta_{\alpha\beta} \\
&\quad + 4\alpha^2\epsilon_{\alpha\beta}\epsilon_{\delta\gamma}D_2X_{\delta,\gamma} \\
&\quad - D_2\Box_4\left[(\mu+\alpha)X_{\beta,\alpha} + (\mu-\alpha)X_{\alpha,\beta}\right]
\end{aligned} \tag{66}$$

- The couple-stress equations

$$(\Box_2\Box_4 + 4\alpha^2\Delta_1)\mu_{\alpha 3} = -(\gamma+\varepsilon)(2\alpha\epsilon_{\delta\gamma}X_{\delta,\gamma\alpha} + \Box_2 Y_{3,\alpha}) \tag{67}$$

- The temperature equation

$$D_2\theta = -\left(\eta_0\dot{X}_{\delta,\delta} + \frac{1}{\kappa}\Box_1 Q\right) \tag{68}$$

Here the operators $\Box_1, \Box_2, \Box_4, L_2, D$ and D_2 are the same as in section "A Singular Solution of STEMP for an Infinite 3D Space," but the Laplace operator Δ must be replaced by the operator Δ_1 ($\Delta_1 f = f_{,\alpha\alpha}$).

Remark 5. *From the equation (68), it can be seen that action of the body moments Y_3 in the infinite space will not cause the temperature field θ.*

Let us turn to the case of the body force (64). Applying an integration method based on the triple Fourier integral transform (23) (for $n = 3$ with respect to the position variable x_α and time t) to equations (64) and (66)–(68), and using [24, pp. 182–183] and [25], we obtain the closed-form results.

The force-stress components $\sigma_{\alpha\beta}$ are given by

$$\begin{aligned}
\sigma_{\alpha\beta} = \frac{iP_1 e^{-i\omega t}}{4\rho\omega^2}\Bigg[&\frac{\rho\omega^2 ps}{\lambda_1^2 - \lambda_2^2}\epsilon_{\alpha\beta}F_{1,2} + 2\mu(\psi_1 - \psi_2)_{,1\alpha\beta} \\
&+ \left(\lambda G_2 - \frac{\rho\omega^2 q\varepsilon}{\mu_1^2 - \mu_2^2}F_2\right)_{,1}\delta_{\alpha\beta} \\
&+ (\mu+\alpha)\delta_{\beta 1}G_{1,\alpha} + (\mu-\alpha)\delta_{\alpha 1}G_{1,\beta}\Bigg]
\end{aligned} \tag{69}$$

where

$$\begin{aligned}
F_1 &= H_0^{(1)}(\lambda_1 r) - H_0^{(1)}(\lambda_2 r), \ r = (x_\alpha x_\alpha)^{1/2} \\
i &= \sqrt{-1}, \quad F_2 = H_0^{(1)}(\mu_1 r) - H_0^{(1)}(\mu_2 r) \\
\psi_1 &= A_1 H_0^{(1)}(\lambda_1 r) + A_2 H_0^{(1)}(\lambda_2 r) \\
\psi_2 &= E_1 H_0^{(1)}(\mu_1 r) - E_2 H_0^{(1)}(\mu_2 r) \\
G_1 &= A_1\lambda_1^2 H_0^{(1)}(\lambda_1 r) + A_2\lambda_2^2 H_0^{(1)}(\lambda_2 r) \\
G_2 &= E_1\mu_1^2 H_0^{(1)}(\mu_1 r) - E_2\mu_2^2 H_0^{(1)}(\mu_2 r)
\end{aligned}$$

$H_0^{(1)}(z)$ is the Hankel function of the first kind, and

$$\int_{-\infty}^{+\infty}\int_{-\infty}^{+\infty}\frac{e^{-i\xi_\alpha x_\alpha}}{\xi^2 - a^2}\,d\xi_1\,d\xi_2 = i\pi^2 H_0^{(1)}(ar)$$

a^2 is either a real number or a complex one, and $\xi^2 = \xi_\alpha\xi_\alpha$. Other symbols are the same as in section "A Singular Solution of STEMP for an Infinite 3D Space."

The couple-stress components $\mu_{\alpha 3}$ are given by

$$\mu_{\alpha 3} = -\frac{iP_1 s e^{-i\omega t}}{4(\lambda_1^2 - \lambda_2^2)}F_{1,2\alpha} \tag{70}$$

The temperature θ is given by

$$\theta = \frac{iP_1 e^{-i\omega t}}{4\rho\omega^2} \frac{q\varepsilon\sigma_1^2}{m(\mu_1^2 - \mu_2^2)} F_{2,1} \tag{71}$$

Formulae (69), (70), $(52)_{2,4}$, and (71) determine the stress fields $\boldsymbol{\sigma}$ and $\boldsymbol{\mu}$ and the temperature field θ, respectively, corresponding to the singular solution. To obtain the displacement and rotation fields associated with the singular solution under consideration we use the formulae (63). Clearly, we need to know the initial values for the displacements and rotations, as well as their velocities. Combining (62) with (69)–(71) yields

$$g_\alpha = -i\omega f_\alpha, \quad g_3 = -i\omega f_3 \tag{72}$$

and

$$\begin{aligned} f_\alpha &= \frac{iP_1}{4\rho\omega^2}\left[(\psi_1 - \psi_2)_{,1\alpha} + \delta_{\alpha 1} G_1\right] \\ f_3 &= -\frac{iP_1 s}{4Jc_4^2(\lambda_1^2 - \lambda_2^2)} F_{1,2} \end{aligned} \tag{73}$$

Now, using (63), (69), (70), (72), (73), and $(29)_{1,2}$ and the relation

$$\Delta_1 H_0^{(1)}(\lambda_1 r) = \frac{2i}{\pi}\Delta_1(\ln r) - \lambda_1^2 H_0^{(1)}(\lambda_1 r) \tag{74}$$

we obtain the formulas for the triplet (u_1, u_2, φ_3):

$$\begin{aligned} u_\alpha &= \frac{iP_1 e^{-i\omega t}}{4\rho\omega^2}\left[(\psi_1 - \psi_2)_{,1\alpha} + \delta_{\alpha 1} G_1\right] \\ \varphi_3 &= -\frac{iP_1 s e^{-i\omega t}}{4Jc_4^2(\lambda_1^2 - \lambda_2^2)} F_{1,2} \end{aligned} \tag{75}$$

Now, let us turn to the case of the heat source (65). Proceeding in a way similar to that of the above case, we obtain the closed-form results.

The force-stress components $\sigma_{\alpha\beta}$ are given by

$$\begin{aligned} \sigma_{\alpha\beta} = &-\frac{iQ_0 e^{-i\omega t}}{4}\frac{m}{k}\left[\frac{2\mu}{\mu_1^2 - \mu_2^2} F_{2,\alpha\beta}\right. \\ &\left. + \left(2\mu G_4 - \frac{\lambda\sigma_1^2}{\mu_1^2 - \mu_2^2} F_2\right)\delta_{\alpha\beta}\right] \end{aligned} \tag{76}$$

where $G_4 = E_1 H_0^{(1)}(\mu_2 r) - E_2 H_0^{(1)}(\mu_1 r)$.

The couple-stress components $\mu_{\alpha 3}$ are given by

$$\mu_{\alpha 3} \equiv 0 \tag{77}$$

The temperature θ is given by

$$\theta = -\frac{iQ_0 e^{-i\omega t}}{4}\frac{1}{\kappa} G_4 \tag{78}$$

Formulae (76), (77), $(52)_{2,4}$, and (78) determine the stress fields $\boldsymbol{\sigma}$ and $\boldsymbol{\mu}$ and the temperature field θ, respectively, corresponding to the singular solution. The initial values for the displacement and rotation fields and their velocities are given by (72) and

$$f_\alpha = -\frac{iQ_0}{4}\frac{m}{\kappa}\frac{1}{\mu_1^2 - \mu_2^2} F_{2,\alpha}, \qquad f_3 \equiv 0 \tag{79}$$

Then the displacements u_α and the rotation φ_3 are given by

$$u_\alpha = -\frac{iQ_0 e^{-i\omega t}}{4}\frac{m}{\kappa}\frac{1}{\mu_1^2 - \mu_2^2} F_{2,\alpha}, \qquad \varphi_3 \equiv 0 \tag{80}$$

Remark 6. *Let us notice that the heat source provokes the classical fields only.*

It can easily be verified that the stress fields (69), (70), (76), and (77) and the temperature fields (71) and (78) as well as the displacement rotation fields (75) and (80) tend to zero as $r \to \infty$. Furthermore, upon taking into account (64) and (65); formulae (69), (70), (76), and (77); formulae (71) and (78); formulae (75) and (80), respectively; and the relation

$$\Delta_1(\ln r) = 2\pi\delta(x_1)\delta(x_2) \tag{81}$$

we verify that the equations of motion (49) and the coupled heat equation (53) are identically satisfied.

Remark 7. *From the singular solutions in the E–N model, we can obtain the singular solutions for the limiting theories by performing the corresponding limits* [20, p. 27].

Cross-References

▶ Dynamic Micropolar Thermoelasticity

References

1. Hetnarski RB, Ignaczak J (2011) The mathematical theory of elasticity, 2nd edn. CRC Press, Boca Raton
2. Gurtin ME (1972) The linear theory of elasticity. In: Flügge S (ed) Encyclopaedia of physics, vol VIa/2, Springer, Berlin/Heidelberg/New York
3. Eringen AC (1999) Microcontinuum field theories I: foundation and solids. Springer, New York/Berlin/Heidelberg
4. Ignaczak J (1971) Tensorial equations of motion for elastic materials with microstructure. In: Trends in elasticity and thermoelasticity. Groningen (Witold Nowacki Anniversary Volume), Wolters–Noordh Publ, pp. 89–111
5. Ieşan D (1968) On the plane coupled micropolar thermoelasticity. Bull Acad Polon Sci, Sér Sci Techn 16:379–384
6. Olesiak ZS (1970) Stress differential equations of the micropolar elasticity. Bull Acad Polon Sci, Sér Sci Techn 18:177–184
7. Eringen AC (1968) Theory of micropolar elasticity. In: Liebowitz H (ed) Theory of micropolar elasticity, vol II. Academic, New York, pp. 621–729
8. Nowacki W (1986) Theory of asymmetric elasticity. Polish Scientific/Warsaw and Pergamon Press, Oxford/New York/Paris/Frankfurt
9. Kupradze VD, Gegelia TG, Basheleishvili MO, Burchuladze TV (1976) Three-dimensional problems of the mathematical theory of elasticity and thermoelasticity. Izd Nauka, Moscow (in Russian)
10. Kunin IA (1975) Theory of elastic bodies with microstructure. Izd Nauka, Moscow (in Russian)
11. Rubin MB (2000) Cosserat theories: shells, rods and points. Kluwer Academic, Dordrecht
12. Ieşan D (2004) Thermoelastic models of continua. Kluwer Academic, Dordrecht
13. Ostoja-Starzewski M (2008) Microstructural randomness and scaling in mechanics of materials. Chapman & Hall/CRC Press/Taylor & Francis, Boca Raton/London/New York
14. Altenbach J, Altenbach H, Eremeyev VA (2010) On generalized Cosserat-type theories of plates and shells: a short review and bibliography. Arch Appl Mech 80:73–92
15. Ieşan D (1969) On the linear theory of micropolar elasticity. Int J Eng Sci 7(12):1213–1220
16. Mikusiński J (1959) Operational calculus. Pergamon, New York
17. Sneddon IN (1972) The use of integral transforms. McGraw–Hill, New York
18. Chadwick P, Sneddon IN (1958) Plane waves in an elastic solid conducting heat. J Mech Phys of Solids 6:223–230
19. Nowacki W (1966) Dynamical problems of thermoelasticity. Polish Scientific Publishers, Warsaw (in Polish)
20. Dyszlewicz J (2004) Micropolar theory of elasticity. In: Pfeiffer F, Wriggers P (eds) Lecture notes in applied and computational mechanics, vol 15. Springer, Berlin/Heidelberg/New York
21. Stefaniak J (1969) Concentrated loadings in asymmetric thermoelasticity. Rozprawy No 40 (in Polish), Technical University of Poznań, Poland
22. Al-Hasan M, Dyszlewicz J (1998) Plane state of deformation in the coupled dynamic micropolar problem of thermoelasticity. Stress equations of Ignaczak type. Reports No. 93 and 94, Institute of Mathematics, Wrocław University of Technology, Poland
23. Crăciun IA (1987) On fundamental solutions in the plane micropolar thermoelasticity. Bull Pol Ac Tech 35:490–503
24. Vladimirov VS (1984) Equations of mathematical physics. Mir Publishers, Moscow (in Russian)
25. Hadamard J (1923) Lectures on Cauchy's problem in partial differential equations. Yale University Press, New Haven

Coupled Generalized Thermoelasticity of Functionally Graded Materials

Mridula Kanoria
Department of Applied Mathematics, University of Calcutta, Kolkata, West Bengal, India

Synonyms

Coupled thermoelasticity

Overview

There are materials in which the elastic coefficients are position dependent. Such materials are called nonhomogeneous materials. In solid mechanics, many of engineering materials, such as composites and a large variety of bonded materials and structural components, are generally modeled as nonhomogeneous continua. A composite is a solid material that results when two or more different substances, each with its

own characteristics, are combined to create a new substance whose properties are superior to those of the original components in a specific application. Most primitive composite materials comprised straw and mud in the form of bricks for building construction. Plywood is a common composite material encountered in everyday life.

A functionally graded material is a nonhomogeneous composite which consists of a graded change in the volume fraction of constituents from one location to other in a component. The concept of FGMs was initially proposed in 1984 by a group of scientists in Sendai, Japan [18, 27]. Since then, FGMs have been of intensive research interests. Due to the continuously varying material properties in space on the microscopic scale, FGMs are usually superior to conventional traditional materials in mechanical behavior, especially under thermal loads. Nitride, steel, for instance, could be regarded as FGM. Modern FGMs are constructed for complex requirements, such as the heat shield of a rocket or implants for humans. FGMs have potential applications in automotive brakes and clutches. It can be more resistant to crack initiation and propagation. FGMs made from ceramic and metal are suitable for use in high-temperature-generating systems, e.g., the use of ceramic composite microstructure in gas turbines can protect metals and improve the life and reliability of thermal barrier coating.

The classical uncoupled theory of thermoelasticity [8] predicts two phenomena not compatible with physical observations. First, the equation of heat conduction of this theory does not contain any elastic terms contrary to the fact that elastic changes produce heat effects. Second, the heat equation is of parabolic type predicting infinite speeds of propagation for heat waves. Although Biot's [4] theory of coupled thermoelasticity eliminates the first paradox of classical theory, both theories share the second shortcoming since the heat equation for the coupled theory is also parabolic.

During last five decades, nonclassical thermoelasticity theories involving hyperbolic type heat transport equations admitting finite speeds for thermal signals have been formulated. According to these theories, heat propagation is to be viewed as a wave phenomenon rather than a diffusion phenomenon. These nonclassical theories are referred to as *generalized thermoelasticity theories* and are motivated by experiments [1–3, 12, 16, 17, 20, 21, 24, 26] exhibiting the actual occurrence of thermal wave at low temperatures and for small intervals of time. A wide variety of problems revealing interesting phenomenon characterizing these theories have been investigated, and the relevant literature can be found in [5, 6, 13–15].

According to Lord-Shulman theory, Fourier's law of heat conduction is modified by introducing a single relaxation time [19]. In Green-Lindsay theory, two relaxation times are introduced by modifying the stress–strain relations and the entropy density [9]. Green and Naghdi proposed two models known as Green-Naghdi model II and III which permit propagation of thermoelastic waves with a finite speed. The Green-Naghdi model II does not sustain dissipation of thermal energy [11]. The Green-Naghdi model III [10] admits the dissipation of energy.

Dual-phase lag thermoelasticity was proposed by Chandrasekharaiah [7] and Tzou [25] (CT model) in which the Fourier law is replaced by an approximation to a modification of the Fourier law with two different time translations for the heat flux and the temperature gradient. Tzou [25] introduced two-phase-lags to both the heat flux vector and the temperature gradient.

The latest in this row is three-phase-lag thermoelasticity theory proposed by Roychoudhuri [22]. In this theory, he established a generalized mathematical model of a coupled thermoelasticity theory that includes three-phase lags in the heat flux vector, the temperature gradient, and in the thermal displacement gradient. The more general model established reduces to the previous models as special cases.

Basic Equations for Functionally Graded Material

Strain–Displacement Relations

$$e_{ij} = \frac{1}{2}(u_{i,j} + u_{j,i}), i,j = 1,2,3 \qquad (1)$$

where e_{ij} is the strain tensor and u_i is the displacement component.

Stress–Strain Temperature Relations

$$\tau_{ij} = C_{ijkl}e_{kl} - \beta_{ij}[(T - T_0) + t_1\alpha_0\dot{T}]$$

or

$$e_{ij} = S_{ijkl}\tau_{kl} + \alpha_{ij}[(T - T_0) + t_1\alpha_0\dot{T}] \quad i,j,k,l = 1,2,3, \tag{2}$$

where

$$\begin{aligned} C_{ijkl} &= C_{jikl} = C_{ijlk} = C_{klij}, \\ S_{ijkl} &= S_{jikl} = S_{ijlk} = S_{klij}, \\ S_{ijkl} &= (C_{ijkl})^{-1}; \end{aligned} \tag{3}$$

and τ_{ij}, C_{ijkl}, and S_{ijkl} are stress tensor, elasticity tensor, and elastic compliance tensor, respectively; $\beta_{ij} = C_{ijkl}\alpha_{kl}, \alpha_{ij} = S_{ijkl}\beta_{kl}$; and β_{ij} and α_{ij} are thermal moduli and thermal expansion tensor, respectively, and T is the absolute temperature.

Law of Heat Conduction

$$q_i + t_2\tau_q\dot{q}_i + t_3\frac{\tau_q^2}{2}\ddot{q}_i = -\left((\tau_v^\star)_{ij}T_{,j} + \tau_T K_{ij}\dot{T}_{,j} + K_{ij}^\star v_{,j}\right), \quad i,j = 1,2,3 \tag{4}$$

where q_i is the component of the heat flux vector and K_{ij} is the thermal conductivity tensor, $\dot{v} = T$, $(\tau_v^\star)_{ij} = K_{ij} + \tau_v K_{ij}^\star$.

Energy Equation

$$-q_{i,i} + \rho Q = \rho C_v(\dot{T} + t_4\alpha_1\ddot{T}) + T_0\beta_{ij}\dot{e}_{ij}, i,j = 1,2,3 \tag{5}$$

where Q is the heat source acting per unit mass per second and C_v is the specific heat at constant strain and the term $T_0\beta_{ij}\dot{e}_{ij}$ brings about coupling between temperature and strain field.

Heat Equation

Elimination of q_i from (4) and (5) leads to the following hyperbolic type heat transport equation in unified form:

$$\begin{aligned} &((\tau_v^\star)_{ij}\dot{T}_{,j})_{,i} + \tau_T(K_{ij}\ddot{T}_{,j})_{,i} + (K_{ij}^\star T_{,j})_{,i} = \\ &\left(1 + t_2\tau_q\frac{\partial}{\partial t} + t_2\frac{1}{2}\tau_q^2\frac{\partial^2}{\partial t^2}\right)\left[\rho C_v T_0\frac{\partial}{\partial t}(\dot{T} + t_4\alpha_1\ddot{T})\right] \\ &+ \left(1 + t_2\tau_q\frac{\partial}{\partial t} + t_2\frac{1}{2}\tau_q^2\frac{\partial^2}{\partial t^2}\right)(\beta_{ij}\ddot{e}_{ij} - \rho\dot{Q}) \end{aligned} \tag{6}$$

where t_1, t_2, t_3, t_4 are unified parameters.

In the case when $t_1 = 0, t_2 = 1, t_3 = 0, t_4 = 0$, $\tau_T = 0$, $\tau_q = \tau_0$, $K_{ij}^\star = 0$, $\tau_v = 0$, and hence $(\tau_v^\star)_{ij} = K_{ij}$, this theory clearly reduces to L-S theory. τ_0 is called relaxation time, which is the time required to maintain steady-state heat conduction in an element of volume of an elastic body when a sudden temperature gradient is imposed on that volume element. When $t_1 = 1, t_2 = 0, t_3 = 0$, $t_4 = 1$, $\tau_T = 0$, $\tau_q = 0$, $\tau_q^2 = 0$, $K_{ij}^\star = 0$, $\tau_v = 0$, and hence $(\tau_v^\star)_{ij} = K_{ij}$, $t_1 = 1$, and $t_2 = 1$, this theory clearly reduces to G-L theory, where α_1 and α_2 $(\alpha_1 \geq \alpha_2 \geq 0)$ are two constitutive constants having the dimension of time. For $t_1 = 0$, $t_2 = 0$, $t_3 = 0$, $t_4 = 0$, $\tau_T = 0$, and $\tau_v = 0$, this theory reduces to (for much low thermal conductivity) Green-Naghdi's second model of generalized thermoelasticity without energy dissipation. For $t_1 = 0, t_2 = 0, t_3 = 0, t_4 = 0, \tau_T = 0, \tau_v = 0$, and hence $(\tau_v^\star)_{ij} = K_{ij}$, this theory becomes third model of Green-Naghdi. Here, v is the thermal displacement and $K_{ij}^\star$ is the tensor of additional material constant for Green-Naghdi theory. Further in the case, when $t_1 = 0$, $t_2 = 1$, $t_3 = 1$, $t_4 = 0$, $K_{ij}^\star = 0$, $\tau_v = 0$, and hence $(\tau_v^\star)_{ij} = K_{ij}$, this theory clearly reduces to dual-phase-lag model. Finally, for $t_1 = 0$, $t_2 = 1$, $t_3 = 1$, and $t_4 = 0$, this theory reduces to three-phase-lag model. The delay time τ_T is called the phase lag of the temperature gradient and the other delay time τ_q, the phase lag of the heat flux. The delay time τ_T is caused by the microstructural interactions (small scale effects of heat transport in space such as phonon–electron interaction or phonon

scattering). The second delay time τ_q is caused due to the fast transient effects of thermal inertia (or small scale effects of heat transport in time). The phase lags τ_q and τ_T are small, positive, and assumed to be intrinsic properties of the medium. The third delay time τ_v may be interpreted, following Tzou [25], as the phase lag of the thermal displacement gradient.

Equations of Motion

$$\tau_{ij,j} + \rho F_i = \rho \ddot{u}_i,\ i,j = 1,2,3 \tag{7}$$

where F_i is the component of body force per unit mass and ρ (>0) the mass density.

Equations (2), (6), and (7) constitute complete mathematical model of different hyperbolic thermoelasticity theories.

The relations given above, valid for an anisotropic body, readily reduce to the corresponding relations for an isotropic body by means of the relations

$$C_{ijkl} = \mu(\delta_{ik}\delta_{jl} + \delta_{il}\delta_{jk}) + \lambda\delta_{ij}\delta_{kl}$$

$$S_{ijkl} = \mu'(\delta_{ik}\delta_{jl} + \delta_{il}\delta_{jk}) + \lambda'\delta_{ij}\delta_{kl}$$

$$\beta_{ij} = \beta\delta_{ij}, \alpha_{ij} = \alpha_t\delta_{ij}, K_{ij} = K\delta_{ij}, K^{\star}_{ij} = K^{\star}\delta_{ij}$$

where

$$\mu' = \frac{1}{4\mu},\ \lambda' = -\frac{\lambda}{2\mu(3\lambda + 2\mu)}$$
$$\beta = 3k\alpha_t,\ k = \lambda + \frac{2}{3}\mu$$

Here, λ and μ are Lamé constants, k is the compressibility modulus, and α_t the coefficient of linear thermal expansion for an isotropic body.

Application to a Problem

We consider a functionally graded infinite isotropic thermoelastic body at a uniform reference temperature θ_0 in the presence of periodically varying heat sources distributed over a plane area. We shall consider one-dimensional disturbance of the medium, so that the displacement vector $\vec{u}$ and temperature field θ can be expressed in the following form:

$$\vec{u} = (u(x,t), 0, 0)$$
$$\theta = \theta(x,t) \tag{8}$$

In the context of linear theory of generalized thermoelasticity based on Green-Naghdi model II (Green and Naghdi, 1993), the equation of motion, heat equation, and constitutive equation can be written as

$$f(x)\left[(\lambda_0 + 2\mu_0)\frac{\partial^2 u}{\partial x^2} - \gamma_0\frac{\partial\theta}{\partial x}\right] + \left[(\lambda_0 + 2\mu_0)\frac{\partial u}{\partial x} - \gamma_0(\theta - \theta_0)\right]\frac{\partial f(x)}{\partial x} = \rho_0 f(x)\frac{\partial^2 u}{\partial t^2} \tag{9}$$

$$\frac{\partial}{\partial x}\left[K_0^{\star} f(x)\frac{\partial\theta}{\partial x}\right] + \rho_0 f(x)\dot{Q} = \rho_0 f(x) c_v \ddot{\theta} + \gamma_0 f(x)\theta_0\ddot{\Delta} \tag{10}$$

$$\tau_{xx} = f(x)[(\lambda_0 + 2\mu_0)e_{xx} - \gamma_0(\theta - \theta_0)] \tag{11}$$

where

$$e_{xx} = \frac{\partial u}{\partial x} \tag{12}$$

and it is assumed that variation of material properties are dependent on f(x). Introducing the following nondimensional variables:

$$x' = \frac{x}{l}, u' = \frac{\lambda_0 + 2\mu_0}{\gamma_0\theta_0 l}u, t' = \frac{ct}{l}, \theta' = \frac{\theta - \theta_0}{\theta_0}$$

$$f'(x') = f(x), \tau'_{x'x'} = \frac{\tau_{xx}}{\gamma_0\theta_0}, e'_{x'x'} = e_{xx} \tag{13}$$

where l is a standard length and c is a standard speed, and omitting the primes (9)–(12) can be rewritten in nondimensional form as

$$f(x)\left(\frac{\partial^2 u}{\partial x^2}-\frac{\partial \theta}{\partial x}\right)+\left(\frac{\partial u}{\partial x}-\theta\right)\frac{\partial f(x)}{\partial x}=f(x)\frac{1}{C_P^2}\frac{\partial^2 u}{\partial t^2} \tag{14}$$

$$C_T^2\frac{\partial}{\partial x}\left[f(x)\frac{\partial \theta}{\partial x}\right]+f(x)Q_0=f(x)\frac{\partial^2 \theta}{\partial t^2} + \varepsilon_T f(x)\frac{\partial^3 u}{\partial t^2 \partial x} \tag{15}$$

$$\tau_{xx}(x,t)=f(x)\left[\frac{\partial u}{\partial x}-\theta\right] \tag{16}$$

$$e_{xx}(x,t)=\frac{\gamma_0\theta_0}{\lambda_0+2\mu_0}\frac{\partial u}{\partial x} \tag{17}$$

where

$$C_T^2=\frac{K_0^\star}{\rho_0 c_v c^2}, \varepsilon_T=\frac{\gamma_0^2\theta_0}{(\lambda_0+2\mu_0)\rho_0 c_v}$$

$$C_P^2=\frac{\lambda_0+2\mu_0}{\rho_0 c^2}, Q_0=\frac{l}{\theta_0 c_v c}\frac{\partial Q}{\partial t}$$

We assume that the medium is initially at rest. The undisturbed state is maintained at reference temperature. Then, we have

$$u(x,0)=\dot{u}(x,0)=\theta(x,0)=\dot{\theta}(x,0)=0 \tag{18}$$

We take exponential variation of nonhomogeneity (i.e., $f(x)=e^{-kx}$, where k is a dimensionless constant).

Applying Laplace-Fourier double integral transform defined by

$$\bar{g}(x,p)=\int_0^\infty g(x,t)e^{-pt}dt, Re(p)>0$$
$$\hat{\bar{g}}(\alpha,p)=\frac{1}{\sqrt{2\pi}}\int_{-\infty}^{\infty}\bar{g}(x,p)e^{i\alpha x}dx \tag{19}$$

to the (14)–(17) and solving the resulting equation, we get solutions for $\hat{\bar{u}}(\alpha,p)$, $\hat{\bar{\theta}}(\alpha,p)$, $\hat{\bar{\tau}}_{xx}(\alpha,p)$, and $\hat{\bar{e}}_{xx}(\alpha,p)$ as follows:

$$\hat{\bar{u}}(\alpha,p)=\frac{\hat{\bar{Q}}_0(i\alpha+k)}{M(\alpha)} \tag{20}$$

$$\hat{\bar{\theta}}(\alpha,p)=\frac{\hat{\bar{Q}}_0\left(\alpha^2+\frac{p^2}{C_P^2}-i\alpha k\right)}{M(\alpha)} \tag{21}$$

$$\hat{\bar{\tau}}_{xx}(\alpha,p)=-\frac{p^2\hat{\bar{Q}}_0}{M(\alpha+ik)} \tag{22}$$

$$\hat{\bar{e}}_{xx}(\alpha,p)=\frac{\beta_1\hat{\bar{Q}}_0\,\alpha(\alpha-ik)}{M(\alpha)} \tag{23}$$

where

$$\begin{aligned}M(\alpha)&=C_T^2\alpha^4-2ikC_T^2\alpha^3+p^2\left(1+\varepsilon_T+\frac{C_T^2}{C_P^2}\right)\alpha^2\\&\quad-C_T^2k^2\alpha^2-\left[p^2ik\left(1+\varepsilon_T+\frac{C_T^2}{C_P^2}\right)\right]\alpha+\frac{p^4}{C_P^2},\\&=C_T^2(\alpha-\alpha_1)(\alpha-\alpha_2)(\alpha-\alpha_3)(\alpha-\alpha_4)\end{aligned} \tag{24}$$

Periodically Varying Heat Source

Now, let us take the heat source in the following form:

$$\begin{aligned}Q_0&=Q_0^\star\delta(x)\sin\left(\frac{\pi t}{\tau}\right)\text{ for }0\le t\le\tau\\&=0\text{ for }t>\tau;\end{aligned} \tag{25}$$

then,

$$\hat{\bar{Q}}_0=\frac{Q_0^\star\pi\tau(1+e^{-p\tau})}{\sqrt{2\pi}(\pi^2+p^2\tau^2)} \tag{26}$$

Thus, the expressions for displacement, temperature, stress, and strain in Laplace transform domain take the following form:

$$\bar{u}(x,p)=\int_{-\infty}^{\infty}\frac{Q_0^\star\tau(1+e^{-p\tau})(i\alpha+k)e^{-i\alpha x}d\alpha}{2(\pi^2+p^2\tau^2)M(\alpha)} \tag{27}$$

Coupled Generalized Thermoelasticity of Functionally Graded Materials,

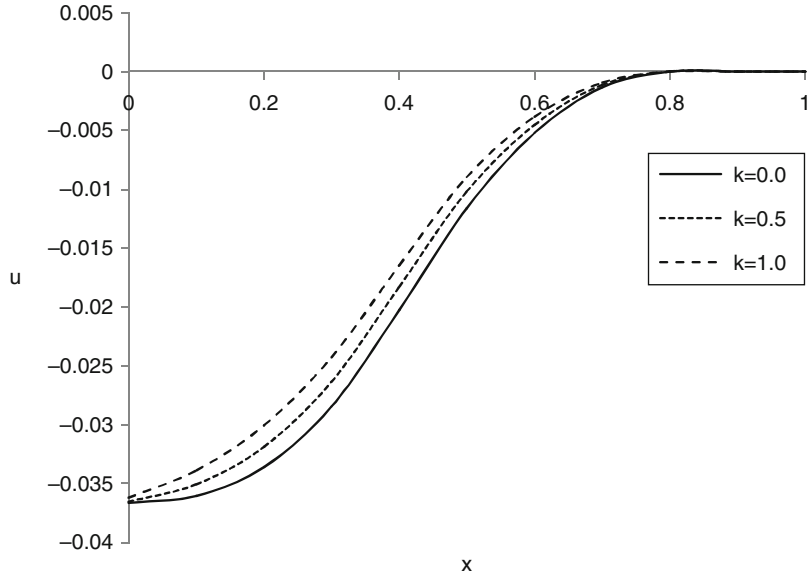

Fig. 1 Variation of displacement u with distance x for t = 0.4

$$\bar{\theta}(x,p)=\int_{-\infty}^{\infty}\frac{Q_0^{\star}\tau(1+e^{-p\tau})(\alpha^2+\frac{p^2}{C_p^2}-i\alpha k)e^{-i\alpha x}d\alpha}{2(\pi^2+p^2\tau^2)M(\alpha)} \tag{28}$$

$$\bar{\tau}_{xx}(x,p)=\int_{-\infty}^{\infty}\frac{-Q_0^{\star}\tau(1+e^{-p\tau})p^2e^{-i\alpha x}d\alpha}{2(\pi^2+p^2\tau^2)M(-\alpha)} \tag{29}$$

$$\bar{e}_{xx}(x,p)=\int_{-\infty}^{\infty}\frac{\beta_1 Q_0^{\star}\tau(1+e^{-p\tau})\alpha(\alpha-ik)e^{-i\alpha x}d\alpha}{2(\pi^2+p^2\tau^2)M(\alpha)} \tag{30}$$

Applying contour integration to the (27)–(30), we obtain the solution for displacement ($\bar{u}(x,p)$), temperature ($\bar{\theta}(x,p)$), stress ($\bar{\tau}_{xx}(x,p)$), and strain ($\bar{e}_{xx}(x,p)$) in Laplace transform domain as follows:

$$\begin{aligned}\bar{u}(x,p) &= -F(p)\sum_{\substack{j=1\\ Im(\alpha_j)<0}}^{4} A_j\bar{u}_j e^{-i\alpha_j x},\ x>0\\ &= F(p)\sum_{\substack{j=1\\ Im(\alpha_j)>0}}^{4} A_j\bar{u}_j e^{-i\alpha_j x},\ x<0\end{aligned} \tag{31}$$

$$\begin{aligned}\bar{\theta}(x,p) &= -F(p)\sum_{\substack{j=1\\ \mathrm{Im}(\alpha_j)<0}}^{4} A_j\bar{\theta}_j e^{-i\alpha_j x},\ x>0\\ &= F(p)\sum_{\substack{j=1\\ \mathrm{Im}(\alpha_j)>0}}^{4} A_j\bar{\theta}_j e^{-i\alpha_j x},\ x<0\end{aligned} \tag{32}$$

$$\begin{aligned}\bar{\tau}_{xx}(x,p) &= F(p)\sum_{\substack{j=1\\ \mathrm{Im}(l_j)<0}}^{4} B_j e^{-il_j x},\ x>0\\ &= -F(p)\sum_{\substack{j=1\\ \mathrm{Im}(l_j)>0}}^{4} B_j e^{-il_j x},\ x<0\end{aligned} \tag{33}$$

$$\begin{aligned}\bar{e}_{xx}(x,p) &= -F(p)\sum_{\substack{j=1\\ \mathrm{Im}(\alpha_j)<0}}^{4} A_j\bar{e}_j e^{-i\alpha_j x},\ x>0\\ &= F(p)\sum_{\substack{j=1\\ \mathrm{Im}(\alpha_j)>0}}^{4} A_j\bar{e}_j e^{-i\alpha_j x},\ x<0\end{aligned} \tag{34}$$

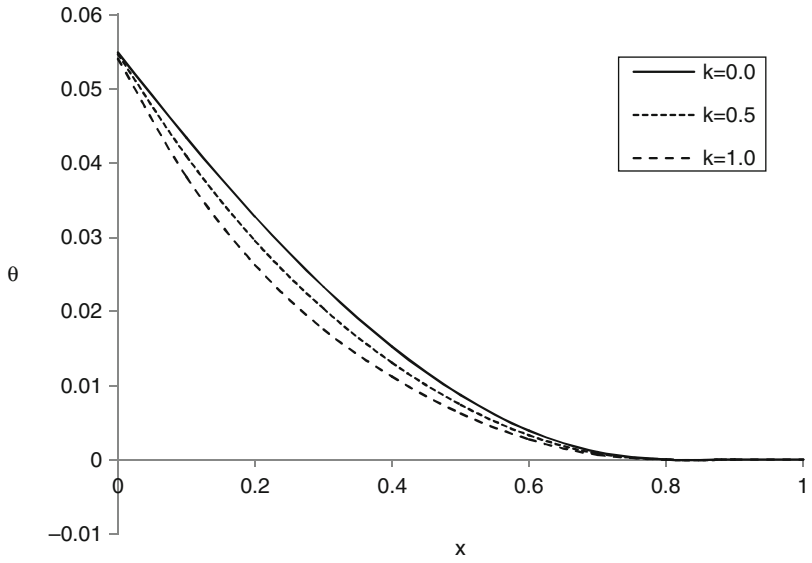

Coupled Generalized Thermoelasticity of Functionally Graded Materials, Fig. 2 Variation of temperature θ with distance x for t = 0.4

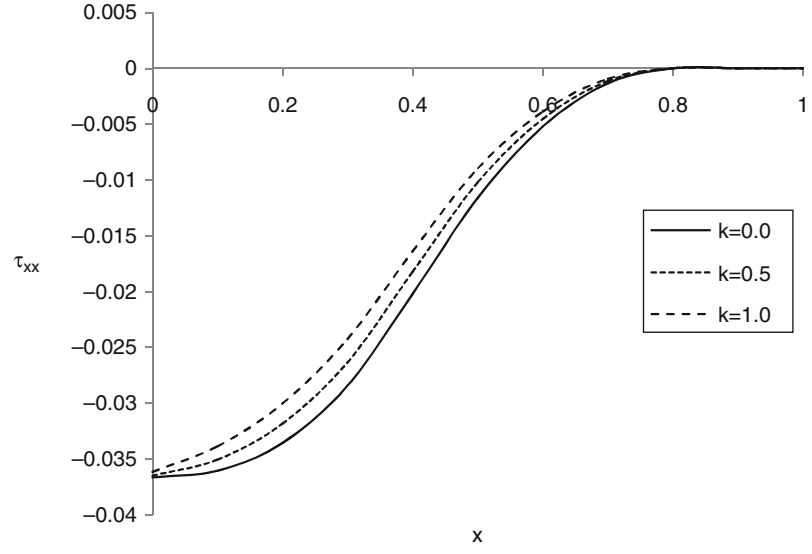

Coupled Generalized Thermoelasticity of Functionally Graded Materials, Fig. 3 Variation of stress τ_{xx} with distance x for t = 0.4

where A_j's, B_j's, F(p), $\bar{u}_j$, $\bar{\theta}_j$, and $\bar{e}_j$ are given by

$$A_j = \prod_{\substack{n=1 \\ n \neq j}}^{4} \frac{1}{(\alpha_j - \alpha_n)}$$
$$B_j = \prod_{\substack{n=1 \\ n \neq j}}^{4} \frac{1}{(l_j - l_n)}, j = 1,2,3,4 \quad (35)$$

$$F(p) = \frac{iQ_0^{\star}\pi\tau(1+e^{-p\tau})}{C_T^2(\pi^2+p^2\tau^2)} \quad (36)$$

$$\begin{aligned} \bar{u}_j &= (i\alpha_j + k) \\ \bar{\theta}_j &= (\alpha_j^2 + \tfrac{p^2}{C_p^2} - i\alpha_j k) \\ \bar{e}_j &= \alpha_j(\alpha_j - ik) \end{aligned} \quad (37)$$

and α_j, l_j, and (j = 1(1)4) are roots of the equations $M(\alpha) = 0$ and $M(-\alpha) = 0$, respectively.

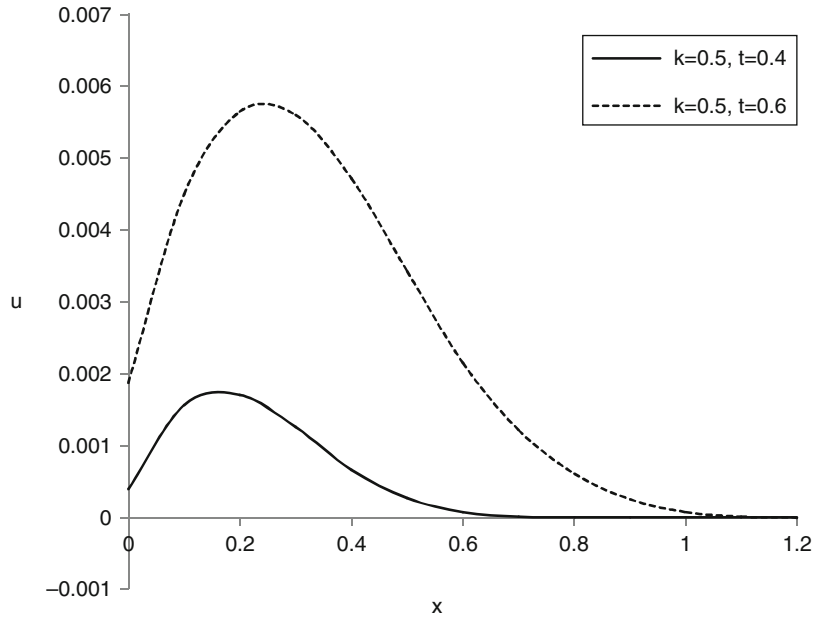

Coupled Generalized Thermoelasticity of Functionally Graded Materials, Fig. 4 Variation of displacement u with distance x for t = 0.4 and t = 0.6

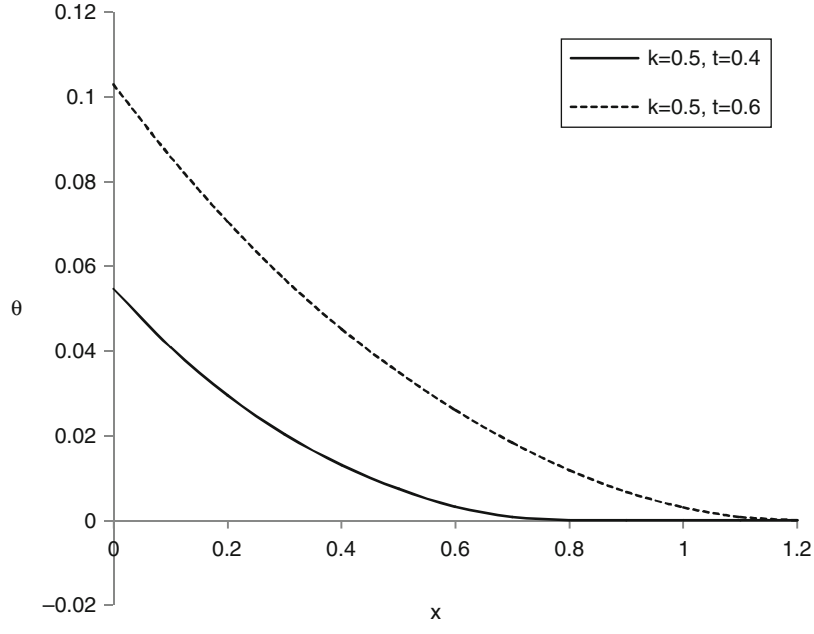

Coupled Generalized Thermoelasticity of Functionally Graded Materials, Fig. 5 Variation of temperature θ with distance x for t = 0.4 and t = 0.6

Numerical Results and Discussion

To get the solution for thermal displacement, temperature, stress, and strain in space-time domain, we have to apply Laplace inversion formula to the (31)–(34), respectively. This has been done numerically using a method based on Fourier series expansion technique. For the purpose of illustration, we consider copper-like material with material constants as follows [23]:

$$\lambda = 1.387 \times 10^{12} dynes/cm^2$$
$$\mu = 0.448 \times 10^{12} dynes/cm^2$$

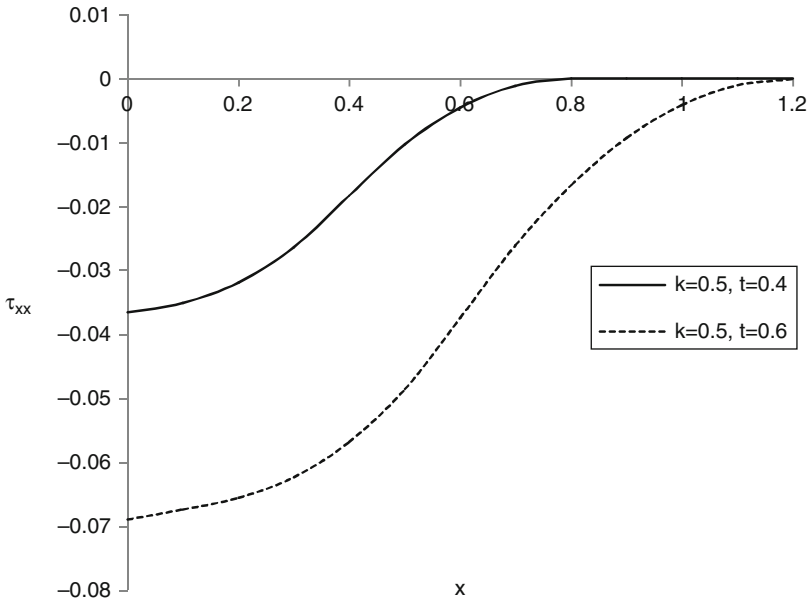

Coupled Generalized Thermoelasticity of Functionally Graded Materials,
Fig. 6 Variation of stress τ_{xx} with distance x for t = 0.4 and t = 0.6

$$\varepsilon_T = 0.0168, \alpha_t = 1.67 \times 10^{-8}/^0C, \ \theta_0 = 1^0C$$

Also, we have taken $Q_0^\star = 1$, $\tau = 1, C_P = 1$, and $C_T = 2$, so the faster wave is the thermal wave.

Figure 1 depicts variation of thermal displacement versus distance for time $t = 0.4$ when the nonhomogeneity parameter $k = 0, 0.5, 1.0$. It is observed that as the value of the nonhomogeneity parameter k decreases, the peak of thermal displacement also decreases. The effect of nonhomogeneity is seen in the interval $0 < x < 3$. Figure 2 is plotted to show the variation of temperature θ with distance x. It is seen from figure that as the value of k increases, the magnitude of the temperature decreases for fixed x and ultimately θ approaches to zero value. This is because heat source varies periodically with the time for a short duration. This can also be verified from the expression of $\bar{\theta}$ given in (32) involving $e^{-i\alpha_j x}$, $\mathrm{Im}(\alpha_j) < 0$ for $x \geq 0$. Figure 3 shows variation of thermal stress versus distance x. Here, the stress takes negative values for $k = 0, 0.5, 1.0$ and the magnitude of stress increases as k decreases for the particular value of x. Figures 4–6 are plotted to show the variation of thermal displacement, temperature, and thermal stress, respectively, against x for $k = 0.5$ and $t = 0.4, 0.6$. It is observed from these figures that as time t increases, the magnitude of displacement, temperature, and thermal stress increases.

References

1. Ackerman CC, Bertman B, Fairbank HA, Guyer RA (1967) Second sound in solid helium. Phys Rev Lett 16:309–789
2. Ackerman CC, Guyer RA (1968) Temperature pulses in dielectric solids. Ann Phys 50:128–185
3. Ackerman CC, Overton WC Jr (1969) Second sound in solid helium-3. Phys Rev Lett 22:764–766
4. Biot M (1956) Thermoelasticity and irreversible thermodynamics. J Appl Phys 27:240–253
5. Chandrasekharaiah DS (1986) Thermoelasticity with second sound: a review. Appl Mech Rev 39(3):355–376
6. Chandrasekharaiah DS (1996) A note on the uniqueness of solution in the linear theory of thermoelasticity without energy dissipation. J Elasticity 43:279–283
7. Chandrasekharaiah DS (1998) Hyperbolic thermoelasticity: a review of recent literature. Appl Mech Rev 51:705–729
8. Duhamel JMC (1837) Second memoire sur les phenomes thermomechaniques. J de l'Ecole Polytech 15(25):1–57
9. Green AE, Lindsay KA (1972) Thermoelasticity. J Elasticity 2:1–7

10. Green AE, Naghdi PM (1992) On undamped heat waves in an elastic solid. J Therm Stresses 15:252–264
11. Green AE, Naghdi PM (1993) Thermoelasticity without energy dissipation. J Elasticity 31: 189–208
12. Guyer RA, Krumhansl JA (1966) Solution of the linearized phonon Boltzmann equation. Phys Rev 148(2):766–778
13. Hetnarski RB, Eslami MR (2008) Thermal stresses-advanced theory and applications. Springer, Dordrecht
14. Ignaczak J (1989) Generalized thermoelasticity and its applications. In: Hetnarski RB (ed) Thermal stresses, vol III. Elsevier, Oxford Chap. 4
15. Ignaczak J, Ostoja-Starzewski M (2009) Thermoelasticity with finite wave speeds. Oxford University Press, Oxford
16. Jackson HF, Walker CT (1971) Thermal conductivity, second sound and phonon-phonon interactions in NaF. Phys Rev B 3:1428–1439
17. Jackson HE, Walker CT, McNelly TF (1970) Second sound in NaF. Phys Rev Lett 25:26–28
18. Koizumi M (1993) Concept of FGM. Ceramic Trans 34:3–10
19. Lord H, Shulman Y (1967) A generalized dynamical theory of thermoelasticity. J Mech Phys Solids 15:299–309
20. Narayanmurti V, Dynes RC (1972) Observation of second sound in bismuth. Phys Rev Lett 28:1461–1465
21. Rogers SJ (1971) Transport of heat and approach to second sound in some isotropically pure alkali-halide crystals. Phys Rev B 3: 1440–1457
22. Roychoudhuri SK (2007) On a thermoelastic three-phase-lag model. J Therm Stresses 30: 231–238
23. Roychoudhuri SK, Dutta PS (2005) Thermoelastic interaction without energy dissipation in an infinite solid with distributed periodically varying heat sources. Int J Solids Struct 42: 4192–4203
24. Taylor B, Maris HJ, Elbaum C (1969) Phonon focusing in solids. Phys Rev Lett 23:416–419
25. Tzou DY (1995) A unified field approach for heat conduction from macro to micro scales. ASME J Heat Transfer 117:8–16
26. Von Gutfeld RJ, Nethercot AH Jr (1966) Temperature dependence of heat pulse propagation in sapphire. Phys Rev Lett 17:868–871
27. Yamanouchi M, Koizumi M, Hirai T, Shiota I (1990) (eds) Proceeding of the first international symposium on functionally gradient materials, functionally gradient materials forum and the society of non-traditional technology, Tokyo, pp 197–202, 1990

Coupled Problem of Thermoelasticity: Solution in a Series of Functions Form

Richard B. Hetnarski
Department of Mechanical Engineering,
Rochester Institute of Technology, Rochester, NY, USA
Naples, FL, USA

Overview

In the classic uncoupled thermoelasticity, the field of the temperature is governed by the partial differential equation, the Fourier equation of heat conduction. This equation does not contain stress or displacement terms. And since this equation is of parabolic type, its solutions are smooth; thus, the temperature effects described by the solutions are felt instantly up to infinity. This theory of uncoupled thermal stresses is considered in a number of textbooks, including [1, 2], and [3]. In these books, the field equations of dynamic theory of thermal stresses, in which there is no coupling between the mechanical and thermal fields, are thoroughly analyzed. In this classic theory, the transient thermal stresses are produced by a time-dependent temperature field that satisfies the parabolic heat conduction equation, separate from the dynamic displacement–temperature field equations. This theory does not explain simple experimental results, for example, why a steel specimen gets hot during a standard tension test.

As early as 1837, J. M. C. Duhamel [4] proposed a set of equations that would remedy this situation. However, the more extensive research in this area started only a few decades ago. It was in 1956 that the theory of coupled thermoelasticity was introduced in 1956 by M. Biot [5]. This theory provides the coupling between the temperature field and the stress field and thus removes the paradox that elastic changes have no effect on the temperature. As for the displacement–temperature equations, they are of

hyperbolic–parabolic type. And this is the theory of which one problem we will solve in this encyclopedia entry.

Coupled Thermoelasticity

The governing equations of coupled thermoelasticity for a linear homogeneous isotropic material are:

The equation of motion

$$\operatorname{div}\mathbf{S}+\mathbf{b}=\rho\ddot{\mathbf{u}},\quad \mathbf{S}=\mathbf{S}^{T} \tag{1}$$

The strain–displacement relation

$$\mathbf{E}=\frac{1}{2}(\nabla\mathbf{u}+\nabla\mathbf{u}^{T}) \tag{2}$$

Hooke's law

$$\mathbf{S}=2\mu\mathbf{E}+\lambda(\operatorname{tr}\mathbf{E})\mathbf{1}-\gamma T\mathbf{1},\quad T=\theta-\theta_0 \tag{3}$$

The energy equation

$$\nabla^2 T-\frac{1}{\kappa}\dot{T}-\frac{\gamma\theta_0}{k}\operatorname{tr}\dot{\mathbf{E}}=-\frac{Q}{\kappa} \tag{4}$$

Here $\mathbf{1}$ is the unit second-order tensor, θ is the temperature, θ_0 is the reference temperature, and T is temperature change. From the combination of the first three equations, the displacement–temperature equation of motion is obtained:

$$\mu\nabla^2\mathbf{u}+(\lambda+\mu)\nabla(\operatorname{div}\mathbf{u})-\gamma\nabla\mathbf{T}+\mathbf{b}=\rho\ddot{\mathbf{u}} \tag{5}$$

Equations (4) and (5) represent the displacement–temperature equations of coupled thermoelasticity for a solid elastic body. The full description of the problem requires the energy equation and the equation of motion complemented by appropriate initial and boundary conditions for thermal and mechanical loads.

Coupled Thermoelasticity Problem for an Infinite Body

As an example, it will be shown now the approach to a solution of a coupled problem of spherical stress and temperature waves in an infinite elastic space, initially at rest [6]. The contents of the same paper [6] are the topic of Section 3.3 of the book by JP Nowacki [7]. It is assumed that there acts an instantaneous point source of heat $Q=Q_0\delta(t)\,\delta(R)$, where Q_0 is a constant and R is the radial distance from the source to a representative point in the space. Assuming the body force $\mathbf{b}$ to be zero in (5) and writing the energy equation (4) in slightly changed rendition, the fundamental equations are

$$\mu\nabla^2\mathbf{u}+(\lambda+\mu)\nabla(\operatorname{div}\mathbf{u})-\gamma\nabla T=\rho\ddot{\mathbf{u}} \tag{6}$$

and

$$\nabla^2 T-\frac{1}{\kappa}\dot{T}-\frac{\gamma\,\theta_0}{k}\operatorname{div}\dot{\mathbf{u}}=-\frac{Q(P,t)}{\kappa} \tag{7}$$

where P means the position of a representative point. Write the displacement vector $\mathbf{u}$ as a sum of two parts, namely, an irrotational part and a potential part [8],

$$\mathbf{u}=\nabla\phi+\nabla\times\Psi \tag{8}$$

where ϕ denotes a scalar potential and Ψ denotes a vector potential.

Equation (8) is substituted into (6) and (7) to obtain

$$\begin{aligned}
&\nabla^2\phi-\frac{1}{c_1^2}\ddot{\phi}=\frac{\gamma}{\lambda+2\mu}T\\
&\nabla^2\Psi_i-\frac{1}{c_2^2}\ddot{\Psi}_i=0\qquad i=1,2,3\\
&\nabla^2 T-\frac{1}{\kappa}\dot{T}-\frac{\gamma\,\theta_0}{k}\nabla^2\dot{\phi}=-\frac{Q(P,t)}{\kappa}
\end{aligned} \tag{9}$$

where c_1 and c_2 stand, respectively, for the speed of propagation of the elastic longitudinal wave and the speed of the shear wave.

Elimination of T from the first and the third of (9) leads to a single differential equation for ϕ

$$\left(\nabla^2 - \frac{1}{\kappa}\frac{\partial}{\partial t}\right)\left(\nabla^2 - \frac{1}{c_1^2}\frac{\partial^2}{\partial t^2}\right)\phi - \frac{\gamma^2\,\theta_0}{(\lambda+2\mu)k}\nabla^2\dot{\phi} = -\frac{\gamma}{\lambda+2\mu}\frac{Q(P,t)}{\kappa} \tag{10}$$

The immediate goal is to find the scalar potential ϕ from (10). Once ϕ is determined, both the stresses and the temperature can be calculated. Now, introduce a nondimensional *coupling parameter* ε defined as

$$\varepsilon = \frac{\gamma^2\,\theta_0}{c\,\rho\,(\lambda+2\mu)} \tag{11}$$

and the expression for $Q(P,t)$ and apply the Laplace transform to (10) subject to homogeneous initial conditions. The result is

$$\left[\left(\nabla^2 - \frac{p}{\kappa}\right)\left(\nabla^2 - \frac{p^2}{c_1^2}\right) - \frac{\varepsilon}{\kappa}\,p\,\nabla^2\right]\overline{\phi} = -\frac{\gamma}{\lambda+2\mu}\frac{Q_0\,\delta(R)}{\kappa} \tag{12}$$

Let Laplacians be treated as numbers, and use the notation $h_1 = p/c_1$, where $c_1 = \sqrt{(\lambda+2\mu)/\rho}$ and $h_2 = \sqrt{p/\kappa}$, with p being the Laplace transform parameter. This leads to

$$\begin{aligned}\overline{\phi} &= -\frac{\gamma}{\lambda+2\mu}\frac{Q_0}{\kappa}\frac{1}{(\nabla^2-h_1^2)(\nabla^2-h_2^2) - \varepsilon h_2^2\nabla^2}\,\delta(R)\\ &= \frac{\gamma}{\lambda+2\mu}\frac{Q_0}{\kappa}\frac{1}{(\nabla^2-h_1^2)(\nabla^2-h_2^2)}\\ &\quad\times\left[\frac{1}{1 - h_2^2\varepsilon\frac{\nabla^2}{(\nabla^2-h_1^2)(\nabla^2-h_2^2)}}\right]\delta(R)\end{aligned} \tag{13}$$

Expand now the expression in square brackets into the power series in terms of ε:

$$\begin{aligned}\overline{\phi} &= -\frac{\gamma}{\lambda+2\mu}\frac{Q_0}{\kappa}\frac{1}{(\nabla^2-h_1^2)(\nabla^2-h_2^2)}\\ &\quad\times\left\{1 + h_2^2\varepsilon\frac{\nabla^2}{(\nabla^2-h_1^2)(\nabla^2-h_2^2)} + \left[h_2^2\varepsilon\frac{\nabla^2}{(\nabla^2-h_1^2)(\nabla^2-h_2^2)}\right]^2 + \ldots\right\}\delta(R)\end{aligned} \tag{14}$$

or

$$\overline{\phi} = A\left[\sum_{n=0}^{\infty}\frac{\left(h_2^2\,\varepsilon\,\nabla^2\right)^n}{\left(\nabla^2-h_1^2\right)^{n+1}\left(\nabla^2-h_2^2\right)^{n+1}}\right][-4\pi\delta(R)] \tag{15}$$

where

$$A = \frac{\gamma}{4\pi(\lambda+2\mu)}\frac{Q_0}{\kappa} \tag{16}$$

It is known that for an infinite space [9],

$$\begin{aligned}\left(\nabla^2 - h_1^2\right)\frac{\exp(-h_1R)}{R} &= -4\pi\delta(R)\\ \left(\nabla^2 - h_2^2\right)\frac{\exp(-h_2R)}{R} &= -4\pi\delta(R)\end{aligned} \tag{17}$$

Combining these two equations results in

$$\frac{1}{(\nabla^2-h_1^2)(\nabla^2-h_2^2)}[-4\pi\delta(R)] = \frac{\exp(-h_1R) - \exp(-h_2R)}{(h_1^2-h_2^2)R} \tag{18}$$

Now, introduce two nondimensional parameters ω_1 and ω_2 and replace h_1^2 by $\omega_1 h_1^2$ and h_2^2 by $\omega_2 h_2^2$, and get

$$\frac{1}{\left(\nabla^2-\omega_1h_1^2\right)\left(\nabla^2-\omega_2h_2^2\right)}[-4\pi\delta(R)] = \frac{\exp\left(-\sqrt{\omega_1}h_1R\right) - \exp\left(-\sqrt{\omega_2}h_2R\right)}{\left(\omega_1h_1^2 - \omega_2h_2^2\right)R} \tag{19}$$

Consecutive differentiation of $\left(\nabla^2 - \omega_1h_1^2\right)^{-1}$ with respect to ω_1 leads to

$$\frac{\partial}{\partial\omega_1}\left(\nabla^2-\omega_1h_1^2\right)^{-1}=1\cdot h_1^2\left(\nabla^2-\omega_1h_1^2\right)^{-2}$$
$$\frac{\partial^2}{\partial\omega_1^2}\left(\nabla^2-\omega_1h_1^2\right)^{-1}=1\cdot2\cdot\left(h_1^2\right)^2\left(\nabla^2-\omega_1h_1^2\right)^{-3}$$
$$\vdots$$
$$\frac{\partial^n}{\partial\omega_1^n}\left(\nabla^2-\omega_1h_1^2\right)^{-1}=n!\left(h_1^2\right)^n\left(\nabla^2-\omega_1h_1^2\right)^{-n-1}\tag{20}$$

$$\frac{\partial^n}{\partial\omega_2^n}\left(\nabla^2-\omega_2h_2^2\right)^{-1}=n!\left(h_2^2\right)^n\left(\nabla^2-\omega_2h_2^2\right)^{-n-1}\tag{21}$$

Substitute expressions appearing in (20) and (21) with $\omega_1=\omega_2=1$ in (15)

Similarly,

$$\overline{\phi}=A\left\{\sum_{n=0}^{\infty}\frac{\varepsilon^n\left(\nabla^2\right)^n}{(n!)^2}\frac{1}{\left(h_1^2\right)^n}\frac{\partial^{2n}}{\partial\omega_1^n\,\partial\omega_2^n}\frac{1}{(\nabla^2-\omega_1h_1^2)(\nabla^2-\omega_2h_2^2)}\left[-4\pi\delta(R)\right]\right\}\Bigg|_{\omega_1=\omega_2=1}\tag{22}$$

Introduce (19) into (22) and denote the inverse Laplace transform by $L^{-1}\{\overline{f}(p)\}$. Then,

$$\phi(R,t)=L^{-1}\left\{\overline{\phi}(R,p)\right\}=A\left\{\sum_{n=0}^{\infty}\frac{\varepsilon^n\left(\nabla^2\right)^n}{(n!)^2}\frac{\partial^{2n}}{\partial\omega_1^n\,\partial\omega_2^n}L^{-1}\left[\frac{\exp(-\sqrt{\omega_1}h_1R)-\exp(-\sqrt{\omega_2}h_2R)}{\left(h_1^2\right)^n(\omega_1h_1^2-\omega_2h_2^2)R}\right]\right\}\Bigg|_{\omega_1=\omega_2=1}\tag{23}$$

To make (23) simpler for performing inverse Laplace transformation, the following relations are used:

$$\left(\nabla^2\right)^n\frac{\exp(-\sqrt{\omega_1}h_1R)}{R}=\omega_1^nh_1^{2n}\frac{\exp(-\sqrt{\omega_1}h_1R)}{R}\tag{24}$$

and

$$\left(\nabla^2\right)^n\frac{\exp(-\sqrt{\omega_2}h_2R)}{R}=\omega_2^nh_2^{2n}\frac{\exp(-\sqrt{\omega_2}h_2R)}{R}\tag{25}$$

Substitute (24) and (25) into (23) and get

$$\phi(R,t)=L^{-1}\left\{\overline{\phi}(R,p)\right\}=A\left\{\sum_{n=0}^{\infty}\frac{\varepsilon^n}{(n!)^2}\times\frac{\partial^{2n}}{\partial\omega_1^n\,\partial\omega_2^n}L^{-1}\left[\frac{\omega_1^nh_1^{2n}\exp(-\sqrt{\omega_1}h_1R)-\omega_2^nh_2^{2n}\exp(-\sqrt{\omega_2}h_2R)}{\left(h_1^2\right)^n(\omega_1h_1^2-\omega_2h_2^2)R}\right]\right\}\tag{26}$$

and take the expression in braces for $\omega_1=\omega_2=1$. The result obtained is the power series in terms of the coupling parameter ε. The first term, for $n=0$, gives the solution to the classic (uncoupled) problem, while the following terms show the effect of the coupling.

This problem in the classic (uncoupled) case is extensively discussed in Subsection 11.2.1 of [3]. It should be noted that the Laplace transform parameter p appears in h_1 and h_2.

After performing the required operations, both ω_1 and ω_2 should be made equal one.

The next step is the inversion of the Laplace transform of the expression in brackets in (26). The method of inversion of this Laplace transform is not the topic of this encyclopedia entry. A detailed method of obtaining the inverse transform is a quite lengthy process and requires special formulas of which some are given in "Cross-References." The entire inversion of the first two terms of the series, as well as the analysis and discussion of the results, with tables and figures, is to be found in [6]. After the potential $\phi(R,t)$ is determined, the stresses and the temperature are arrived at by using the formulas

$$S_{RR} = -\frac{4\mu}{R}\frac{\partial\phi}{\partial R} + \rho\frac{\partial^2\phi}{\partial t^2} \tag{27}$$

$$S_{\varphi\varphi} = S_{\vartheta\vartheta} = -2\mu\left(\frac{1}{R}\frac{\partial\phi}{\partial R} + \frac{\partial^2\phi}{\partial R^2}\right) + \rho\frac{\partial^2\phi}{\partial t^2} \tag{28}$$

$$S_{R\varphi} = S_{\varphi\vartheta} = S_{R\vartheta} = 0 \tag{29}$$

$$T = \frac{\lambda + 2\mu}{\gamma}\left(\frac{\partial^2\phi}{\partial R^2} + \frac{2}{R}\frac{\partial\phi}{\partial R} - \frac{1}{c_1^2}\frac{\partial^2\phi}{\partial t^2}\right) \tag{30}$$

The method of attacking one of the basic problems of coupled thermoelasticity illustrates the fact that solution of problems of coupled thermoelasticity is not a simple matter, and only few such problems have been solved without recurrence to numerical methods.

Cross-References

- ▶ Application of the Generalized Functions Method for Analysis of Thermal Stresses in Piecewise-Homogeneous Solids
- ▶ Laplace Transforms of Specific Exponential Form Encountered in Thermoelasticity

References

1. Noda N, Hetnarski RB, Tanigawa Y (2003) Thermal stresses, 2nd edn. Taylor & Francis, New York
2. Hetnarski RB, Eslami MR (2009) Thermal stresses – advanced theory and applications. Springer, Dordrecht
3. Hetnarski RB, Ignaczak J (2011) The mathematical theory of elasticity. CRC Press, Boca Raton
4. Duhamel J-M-C (1837) Second mémoire, sur les phenomenes thermo-mechaniques. J de L'École Polytechnique, tome 15, cahier 25: 1–57
5. Biot M (1956) Thermoelasticity and irreversible thermodynamics. J Appl Phys 27:240–253
6. Hetnarski RB (1964) Solution of the coupled problem of thermoelasticity in the form of series of functions. Arch Mech Stosow 4:919–941
7. Nowacki W (1975) In: Francis PH, Hetnarski RB (eds) Dynamic problems of thermoelasticity. Nordhoff International Publishing\PWN – Polish Scientific Publishers, Leyden\Warszawa, pp 256–269
8. Nowacki JP (1986) Thermoelasticity, 2nd edn. Pergamon Press\PWN – Polish Scientific Publishers, Oxford\Warszawa, p 52
9. Morse PM, Feshbach H (1953) Methods of theoretical physics, vol 1. McGraw-Hill, New York

Coupled Thermoelasticity

- ▶ Application of Meshless Local Petrov-Galerkin (MLPG) and Generalized Finite Difference (GFD) Methods in Coupled Thermoelasticity Analysis of Thick Hollow Cylinder
- ▶ Asymptotic Expansions in Coupled and Generalized Thermoelasticity
- ▶ Classical Coupled Thermoelasticity in Unbounded Domains
- ▶ Coupled Generalized Thermoelasticity of Functionally Graded Materials
- ▶ Coupled Thermoelectroelasticity in Extended Thermodynamics
- ▶ Deterministic and Stochastic Coupled Thermoelasticity Analysis in Thick Hollow Cylinder Subjected to Thermal Shock Loading Using Green-Naghdi Theory
- ▶ Thermoelastic Wave Propagation Analysis in Thick Hollow Cylinder Based on Green-Naghdi Theory of Coupled Thermoelasticity Using Analytical Method

Coupled Thermoelasticity of Shells

▶ Thermoelasticity of Thin Shells

Coupled Thermoelectroelasticity in Extended Thermodynamics

A. F. Ghaleb
Department of Mathematics, Faculty of Science, Cairo University, Cairo, Giza, Egypt

Synonyms

Coupled thermoelasticity

Overview

The experimental evidence of heat propagating as thermal wave at low temperature, a phenomenon commonly called "second sound," has fueled scientific research in the past few decades. The aim was to remove the paradox of infinite speed of propagation of waves in classical thermodynamics, in which Fourier law for heat conduction plays a central role, leading to a partial differential equation of parabolic type for temperature. It was recognized at an early stage that the cause of this paradox was an insufficient description of the nonequilibrium thermodynamical state in the existing model.

An early attempt to modify Fourier law for heat conduction was undertaken by Cattaneo [1] who introduced in the classical law a new term involving a time derivative of the heat flux vector. Chester [2] notes that "this generalized law itself is a truncated form of a more extensive relation obtained earlier by Maxwell who, in view of the problems he was treating then, casually neglected the time derivative term as well as many others." An example of such an extensive law is given by Grad [3]. Although the kinetic formula proposed by Cattaneo does not satisfy the fundamental principle of frame indifference, it can nevertheless be considered as an important step in the way of formulating more sophisticated laws which are in conformity with the general principles of thermodynamics and continuum mechanics. Within this framework, several contributions have been devoted to the study of thermodynamical models, relativistic or nonrelativistic, including rate-type constitutive relations. This trend has been given the general appellation of extended thermodynamics. Among the pioneering contributions in this field of research, we cite those by Müller [4, 5]; Lord and Y. Shulman [6]; Gurtin and Pipkin [7]; Fox [8]; Green and Lindsay [9]; Maugin [10]; Atkin, Fox, and Vasey [11]; Israel [12]; Massa and Morro [13]; Lebon, Jou, and Casas-Vasquez [14]; Bampi and Morro [15]; Coleman, Fabrizio, and Owen [16]; Ghaleb [17]; Green and Naghdi [18]; and Öncü and Moodie [19].

Many of the established models were later on generalized to include interaction with electric and magnetic fields. Apart from the importance of studying generalized thermoelastic effects in polarizable and magnetizable continuous media at low temperatures, recent experimental evidence by Rybalko [20] has shown that heat pulses at low temperatures are accompanied by some electrical activity. An explanation of this phenomenon is undertaken by Rybalko et al. [21] and Pashitskii et al. [22, 23]. The investigation of such phenomena, together with the problem of experimental determination of new physical parameters, clearly points out at the importance of developing and investigating complex models on the basis of rational thermodynamics, involving electromagneto-thermomechanical interactions.

There is ample literature on the subject of electromagneto-thermoelastic interactions in generalized thermodynamics. Ersoy [24, 25] proposes a new nonlinear theory of constitutive equations for electrically and thermally conducting magnetothermoelastic solids in which the electric current and heat flux vectors are considered to be independent variables in the argument of each constitutive function. Chandrasekharaiah [26] developed a model of

thermoelasticity for piezoelectric materials in which the heat flux figures among the independent thermodynamical variables. He showed that the linearized model still admits finite velocity of propagation of thermal signals. Singh [27] formulated the governing equations for generalized thermopiezoelectric solids using Green-Lindsay and Lord-Shulman theories. Montanaro [28] derived thermodynamic restrictions on the constitutive equations for an electrically polarizable, heat-conducting elastic continuous medium subjected to an electric field.

Several papers were devoted to the investigation of different phenomena in polarizable and magnetizable media in extended thermodynamics, most are concerned with piezoelectric ceramics. Bassiouny and Ghaleb [29] studied the propagation of thermoelastic waves in a semi-infinite rod of a piezoelectric material. Roy Choudhuri [30] studied the propagation of plane electro-magneto-thermo-elastic harmonic waves in an unbounded isotropic conducting medium permeated by a primary uniform magnetic field when the entire medium rotates with a uniform angular velocity. Sherief [31] solved the electromagneto-thermoelastic wave propagation problem in an infinitely long circular solid cylinder. Majhi [32] investigated the propagation of discontinuities in generalized thermoelastic wave propagation in a semi-infinite piezoelectric rod. Sherief and Ezzat [33] addressed the same problem, but for an annular circular cylinder. Tianhu, Xiaogeneg, and Yapeng [34, 35] studied shock-wave propagation in piezoelectric rods and plates. Restuccia and Maruszewski [36] described the behavior of anisotropic piezoelectric crystals defective by dislocations, using a nonconventional model based on the extended irreversible thermodynamics in which a dislocation tensor and its flux are introduced as internal variables. Xia Lu and Hanagud [37] investigated the self-heating or dissipation in piezoelectric ceramics within Onsager's theory, with application to actuators. Singh [27] solved a two-dimensional problem for a thermopiezoelectric solid. He, Tian, and Shen [38] studied a generalized electromagneto-thermoelastic problem for an infinitely long solid cylinder. Aouadi [39–41], and [42] studied one- and two-dimensional problems of thermoelastic diffusion. Youssef and Bassiouny [43] studied two-temperature generalized thermopiezoelasticity for one-dimensional problems using state-space approach.

In what follows, we present a fully nonlinear model for electrically polarizable, heat-conducting elastic continuous media including several couplings between the mechanical, thermal, and electric fields. A consistent approach to build such models can be conducted within the frame of the theory of relativity, which is a common natural frame for mechanics, thermodynamics, and electromagnetism. This was achieved in [10, 12, 13], and [15]. Our attention, however, will be restricted to the quasi-electrostatic case, and this can be carried out in the nonrelativistic approximation. The ensuing field equations and constitutive relations are formulated in the reference configuration. This makes the model particularly suitable for handling many situations, for example, problems with moving boundaries. The rationalized MKS system of units is used throughout. The basic unknown functions in the proposed system of nonlinear equations are the mechanical displacement, the electric field, and the temperature. The number of unknown functions may be reduced by noting that the electric field is derived from a scalar electric potential. Details concerning the definitions and the derivations may be found in the textbook by Maugin [44], and also in Maugin [45].

Notation and Kinematics

We use the standard Cartesian tensor notation in orthogonal Cartesian coordinate systems, and the summation convention over repeated indices is adopted. The "comma" denotes covariant derivative and the "dot," the material time derivative, as defined in [44]. The motion between the reference configuration K_R, thought of as a natural configuration free of loads, strains, and fields and where the mass density and the temperature have uniform values ρ_R and θ_0,

respectively, and the current configuration K_t at time t is represented by the law of the motion

$$x_i = \tilde{x}_i(X_K, t), \quad i, K = 1, 2, 3 \tag{1}$$

$$J \equiv \det(x_{i,K}) > 0 \tag{2}$$

where x_i and X_K are the Eulerian and the material coordinates, respectively. By inversion, one has

$$X_K = \tilde{X}_K(x_i, t) \tag{3}$$

and the following relations hold:

$$x_{i,K} X_{K,j} = \delta_{ij}, \qquad X_{K,i} x_{i,L} = \delta_{KL}$$

the δ_{ij} and δ_{KL} being the usual Kronecker symbols. The deformation gradient tensor F is defined through its components as

$$F_{iK} = x_{i,K} \qquad F^{-1}_{Ki} = X_{K,i}$$

One also needs to introduce the finite-strain symmetric Lagrangian tensors $\mathbb{C}$ and $\mathbb{E}$ with respective components

$$C_{KL} = x_{i,K} x_{i,L}, \qquad E_{KL} = \frac{1}{2}(C_{KL} - \delta_{KL})$$

The components u_i and U_K of the displacement vector in K_t and K_R, respectively, are given by

$$u_i = x_i - \delta_{iK} X_K, \qquad U_K = \delta_{Ki} x_i - X_K$$

where δ_{iK} and δ_{Ki} are the so-called shifters. By differentiation, one obtains

$$x_{i,K} = \delta_{iK} + u_{i,K}, \qquad X_{K,i} = \delta_{Ki} - U_{K,i}$$

and therefore,

$$E_{KL} = \frac{1}{2}(U_{K,L} + U_{L,K} + U_{M,K} U_{M,L}) \tag{4}$$

The following developments may be useful in finding successive approximations from the basic equations:

$$x_{i,K} = \delta_{iL}(\delta_{LK} + U_{L,K}) \tag{5}$$

$$\begin{aligned} X_{K,i} = {} & \delta_{Ki} - U_{K,L}\,\delta_{Li} + U_{K,L}\,U_{L,M}\,\delta_{Mi} \\ & - U_{K,L}\,U_{L,M}\,U_{M,N}\,\delta_{Ni} + \cdots \end{aligned} \tag{6}$$

$$\begin{aligned} J = {} & 1 + U_{K,K} + \frac{1}{2}(U_{K,K})^2 \\ & - \frac{1}{2} U_{K,L}\,U_{L,K} + \frac{1}{3!}(U_{K,K})^3 \\ & - \frac{1}{2} U_{K,K}\,U_{M,N}\,U_{N,M} \\ & + \frac{1}{3} U_{M,L}\,U_{L,N}\,U_{N,M} + \cdots \end{aligned} \tag{7}$$

The velocity field $\mathbf{v}$ is defined through its components v_i as

$$v_i = \left(\frac{\partial x_i}{\partial t}\right)_{X_K} \tag{8}$$

All fields appearing in the subsequent equations are material fields, depending on the variables (X_K, t), unless otherwise stated.

Equations for the Electric Field

All effects connected with the magnetic field will be disregarded. Definitions and details concerning the material form of the electric quantities may be found in the books by Nelson [46] and by Maugin [44]. In quasistatic approximation and in the absence of external electric charges, the equations in material form satisfied by the electric fields are

$$\nabla_{\mathbf{R}} \cdot \bar{\mathbf{D}} = 0 \tag{9}$$

$$\nabla_{\mathbf{R}} \times \bar{\mathbf{E}} = 0 \tag{10}$$

where subscript R refers to the referential configuration and the material fields are endowed with a "bar." The material electric field $\bar{\mathbf{E}}$ and electric induction $\bar{\mathbf{D}}$ are related to the corresponding quantities $\mathbf{E}$ and $\mathbf{D}$ in the Eulerian configuration by

$$\bar{\mathbf{E}} = \mathbf{E}F, \qquad \bar{\mathbf{D}} = JF^{-1}\mathbf{D} \tag{11}$$

or in components

$$\bar{E}_K = E_i\, x_{i,K}, \qquad \bar{D}_K = JX_{K,i}\, D_i \tag{12}$$

Recalling the relation between the Eulerian electric induction and electric field

$$\mathbf{D} = \varepsilon_0 \mathbf{E} + \mathbf{P} \tag{13}$$

where $\mathbf{P}$ denotes the polarization per unit volume of the medium and $\varepsilon_0 = \frac{1}{36\pi} \times 10^{-9}\, Fm^{-1}$ is the permittivity of a vacuum. Introducing the material polarization per unit volume

$$\bar{\mathbf{P}} = JF^{-1}\mathbf{P} \tag{14}$$

the material counterpart of (13) takes the form

$$\bar{\mathbf{D}} = \varepsilon_0 J \mathbb{C}^{-1}\bar{\mathbf{E}} + \bar{\mathbf{P}} \tag{15}$$

or in components

$$\bar{D}_K = \varepsilon_0 JX_{K,i}\, X_{L,i}\, \bar{E}_L + \bar{P}_L \tag{16}$$

According to (10), the electric field is derived from a vector potential, Φ say, so that one may write

$$\mathbf{E} = -\nabla_{\mathbf{R}}\Phi \tag{17}$$

The boundary conditions related to the above equations may be derived in the usual way. On a surface of discontinuity with unit normal $\mathbf{N}$, these conditions read

$$[\bar{\mathbf{D}}.\mathbf{N}] = 0, \qquad [\Phi] = 0, \tag{18}$$

where [.] denotes the jump in crossing the surface along $\mathbf{N}$.

Equations of Motion

In the absence of body forces of nonelectric origin, the equations of motion in material form are (cf. [44], p. 194)

$$\rho_R \frac{\partial^2 u_i}{\partial t^2} = T_{Ki,K} \tag{19}$$

where T_{Ki} are the components of the "total" Piola-Kirchhoff stress tensor, given as the sum of mechanical (labelled E) and electrical (labelled F) contributions:

$$T_{Ki} = T^E_{Ki} + T^F_{Ki} \tag{20}$$

This tensor is related to the Eulerian stress tensor

$$t = t^E + t^F \tag{21}$$

by the relation

$$T = JF^{-1}t \tag{22}$$

Tensor t^E is assumed symmetric. At this stage, it is convenient to introduce the "total" second Piola-Kirchhoff stress tensor (cf. [44], p. 196)

$$\bar{T} = \bar{T}^E + \bar{T}^F \tag{23}$$

through the relation

$$T = \bar{T}F^T \tag{24}$$

This may be rewritten in components as

$$T_{Ki} = x_{i,L}\,(\bar{T}^E_{KL} + \bar{T}^F_{KL}) \tag{25}$$

Tensor $\bar{T}^E$ is clearly symmetric. Its components will be determined later on within the constitutive theory, while the electric part is given by the expression

$$\bar{T}^F_{KL} = X_{L,j}\, X_{M,j}\,(\bar{D}_K\ \bar{E}_M - \frac{1}{2}\,\bar{E}_N\ \bar{D}_N\ \delta_{KM}) \tag{26}$$

this being taken directly from the well-known Eulerian counterpart

$$t^F_{ji} = E_i D_j - \frac{1}{2} E_k D_k\, \delta_{ij} \tag{27}$$

The skew-symmetric part of tensor $\bar{T}^F$ has components

$$\bar{T}^F_{[KL]} = \bar{D}_{[K} X_{L],j} X_{M,j} \bar{E}_M \tag{28}$$

and is related to the density of volume and surface couples of electric origin acting on the medium through the formula

$$\bar{T}^F - (\bar{T}^F)^T = -JF^{-1}(C + M)(F^T)^{-1} \tag{29}$$

The components of the Eulerian, skew-symmetric second-order tensors C and M are related to those of the body torque per unit volume $\mathbf{c} = (c_i)$ and contact torque per unit area $\mathbf{m}_{(\mathbf{n})} = (m_{ji}n_j)$, where $\mathbf{n}$ denotes the unit normal to the surface, by the formulae

$$C_{ij} = \varepsilon_{ijk}\, c_k, \qquad M_{ij} = \varepsilon_{ijk}\, m_{kr,r} \tag{30}$$

where ε_{ijk} denote the components of the Levi-Civita completely skew-symmetric tensor.

The boundary condition corresponding to the equation of motion (19) is

$$[N_K T_{K,i}] = 0 \tag{31}$$

Equation of Heat Conduction

Let $\mathbf{q}$ denote the heat flow vector, $\mathbf{Q}$ its material counterpart defined as

$$\mathbf{Q} = JF^{-1}\mathbf{q} \tag{32}$$

and r the heat supply. Then, the equation of heat conduction in material form reads (cf. [44], p. 196)

$$\dot{\Sigma} = T^E_{KL}\dot{E}_{KL} + \bar{\mathbf{E}}.\dot{\bar{\mathbf{P}}} - Q_{K,K} + \rho_R\, r \tag{33}$$

where the left-hand side is related to the time rate of change of the specific internal energy e by

$$\dot{\Sigma} = \rho_R \dot{e} \tag{34}$$

and the "dot" means differentiation w.r. to time under constant X_K.

Clausius-Duhem Inequality

The second law of thermodynamics yields the following material equation for the time rate of variation of the specific entropy η:

$$\rho_R \dot{\eta} = -\left(\frac{Q_K}{\theta}\right)_{,K} + \sigma, \quad \sigma \geq 0 \tag{35}$$

where θ is the absolute temperature and σ the dissipation function.

Introducing the specific free energy ψ by the relation

$$\psi = e - \theta\eta \tag{36}$$

and using (35) and (44), the equation of energy (33) yields the well-known Clausius-Duhem inequality:

$$\begin{aligned} -\rho_R(\dot{\psi} + \eta\dot{\theta}) + T^E_{KL}\dot{E}_{KL} + \bar{\mathbf{E}}.\dot{\bar{\mathbf{P}}} \\ -\theta^{-1}\mathbf{Q}.\nabla_{\mathbf{R}}\theta = \sigma \geq 0 \end{aligned} \tag{37}$$

Constitutive Relations

The following constitutive assumption is made concerning the dependence of the free energy on the different thermodynamical variables:

$$\psi = \psi(E_{KL}, \bar{P}_K, \theta, Q_K) \tag{38}$$

The problem of inclusion of flow rates as thermodynamical arguments in the free energy was discussed by several authors, among whom we cite [16, 24], and [17]. In addition, one also assumes the validity of the following set of constitutive relations:

$$T^E_{KL} = \rho_R \frac{\partial\psi}{\partial E_{KL}} \tag{39}$$

$$\bar{E}_K = \rho_R \frac{\partial \psi}{\partial \bar{P}_K} \tag{40}$$

$$\eta = -\frac{\partial \psi}{\partial \theta} \tag{41}$$

A systematic deduction of these equations may be found in [28]. In view of the above, the Clausius-Duhem inequality (37) reduces to

$$\sigma = -\rho_R \frac{\partial \psi}{\partial Q_K} \dot{Q}_K - \theta^{-1} Q_K \theta_{,K} \geq 0 \tag{42}$$

Cattaneo-Type Evolution Equation for the Heat Flux

The present model can accommodate an evolution equation of Cattaneo's type for the heat flow vector. A detailed investigation of this matter was carried out by Montanaro [28]. Following this last reference, we postulate the existence of the evolution equation

$$\tau_{KL} \dot{Q}_L = Q_K + \kappa_{KL} \theta_{,L} \tag{43}$$

where tensors τ and κ are positive definite, and that the free energy ψ can be represented in the form

$$\psi = \psi_0(E_{KL}, \bar{P}_K, \theta) + \frac{1}{2} N_{KL}\, Q_K Q_L \tag{44}$$

with (N_{KL}) a symmetric tensor. Substituting for $\dot{Q}_K$ from (43) and for ψ from (44) into the reduced Clausius-Duhem inequality (42) and choosing

$$N_{KL} = -\rho_R^{-1} \theta^{-1}\, \kappa^{-1}_{(K|S} \tau_{S|L)} \tag{45}$$

one finally arrives at the following expression for the dissipation function:

$$\sigma = \theta^{-1} \kappa^{-1}_{KL} Q_K Q_L \tag{46}$$

and this is nonnegative in view of the above property of tensor κ.

Conclusions

1. A model has been presented for elastic, electrically polarizable, and heat-conducting continuous media within the frame of extended thermodynamics.
2. The present model complies with the basic assumptions of Continuum Mechanics and Thermodynamics.
3. The used approach is nonrelativistic, and the equations of electromagnetism are taken in the quasistatic approximation, when all phenomena including the magnetic field can be disregarded.
4. All equations are formulated in material form in the reference configuration, which carries some advantages in many situations, especially in treating problems with moving boundaries.
5. The model is fully nonlinear and involves couplings between the mechanical, thermal, and electric fields.
6. A Cattaneo-type evolution equation for the heat flow vector could be obtained by assuming an extra dependence of the free energy, as compared to the classical model, on the heat flow vector. At the same time, the frequently used Onsager-type theory to deduce the kinetic equations has to be abandoned.
7. Proofs and details of calculations were omitted for the sake of conciseness. These may be found in the relevant literature.

References

1. Cattaneo C (1948) Sulla conduzione del calore. Atti Sem Mat Fis Univ Modena 3:83–101
2. Chester M (1963) Second sound in solids. Phys Rev 131:2013–2015
3. Grad H (1958) Principles of the kinetic theory of gases. In: Flügge S (ed) Handbuch der physik, vol 12. Springer, Berlin, p 271
4. Müller I (1967) Zum Parodoxon der Warmleitungstheorie. Z Phys 198:329–344
5. Müller I (1967) On the entropy inequality. Arch Ration Mech Anal 26:118–141
6. Lord H, Shulman Y (1967) A generalized dynamical theory of thermoelasticity. J Mech Phys Solids 15(5):299–309
7. Gurtin ME, Pipkin AC (1968) A general theory of heat conduction with finite wave speeds. Arch Ration Mech Anal 31:113–126

8. Fox N (1969) Generalized thermoelasticity. Int J Eng Sci 7:437–445
9. Green AE, Lindsay KA (1972) Thermoelasticity. J Elast 2(1):1–7
10. Maugin GA (1974) Constitutive equations for heat conduction in general relativity. J Phys A7:465–484
11. Atkin RJ, Fox N, Vasey MW (1975) A continuum approach to the second sound effect. J Elast 5:237–248
12. Israel W (1976) Nonstationary irreversible thermodynamics: a causal relativistic theory. Ann Phys 100:310–331
13. Massa A, Morro A (1978) A dynamical approach to relativistic continuum thermodynamics. Ann Inst Henri Poincaré 29:423–454
14. Lebon G, Jou D, Casas-Vasquez J (1980) An extension of the local equilibrium hypothesis. J Phys A13:275–290
15. Bampi F, Morro A (1980) Two approaches to nonstationary relativistic thermodynamics. J Math Phys 21:1201–1204
16. Coleman BD, Fabrizio M, Owen DR (1982) On the thermodynamics of second sound in dielectric crystals. Arch Ration Mech Anal 80:135–158
17. Ghaleb AF (1986) A model of continuous, thermoelastic media within the frame of extended thermodynamics. Int J Eng Sci 24:765–771
18. Green AE, Naghdi PM (1991) A reexamination of the basic postulates of thermomechanics. Proc R Soc Lond 432:171–194
19. Öncü TS, Moodie TB (1992) On the constitutive relations for second sound in elastic solids. Arch Ration Mech Anal 121:87–99
20. Rybalko AS (2004) Observation of the electric induction due to a second-sound wave in HeII. J Low Temp Phys 30:994–997
21. Rybalko AS, Rudavskii E, Rubets S, Tikhiy V, Derkach V, Tarapov S (2007) Electric induction in He II. J Low Temp Phys 148:527–534
22. Pashitskii EA, Ryabchenko SM (2007) On the cause of electric activity of superfluid helium upon excitation of a second sound wave and normal-component velocity oscillations in it. J Low Temp Phys 33:12–21
23. Pashitskii EA, Tkachenko OM, Grygoryshyn KV, Lev BI (2009) On the nature of electrical activity in superfluid helium at second sound excitation. Ukr J Phys 54:89–93
24. Ersoy Y (1984) A new nonlinear constitutive theory for conducting magnetothermoelastic solid. Int J Eng Sci 22:683–705
25. Ersoy Y (1986) A new nonlinear constitutive theory of electric and heat conductions for magnetoelastothermo-electrical anisotropic solids. Int J Eng Sci 24:867–882
26. Chandrasekharaiah DS (1988) A generalized linear thermoelasticity theory for piezoelectric media. Acta Mech 71:39–49
27. Singh B (2005) On the theory of generalized thermoelasticity for piezoelectric materials. Appl Math Comput 171(1):398–405
28. Montanaro A (2011) On the constitutive relations for second sound in thermo-electroelasticity. Arch Mech 63(3):225–254
29. Bassiouny E, Ghaleb AF (1984) A one-dimensional problem in the generalized theory of thermopiezoelasticity. In: Maugin GA (ed) The mechanical behavior of electromagnetic solid continua. Elsevier Science Publisher B.V./IUTAM-IUPAP, North Holland, pp 79–84
30. Roy Choudhuri SK (1984) Electromagneto-thermoelastic plane waves in rotating media with thermal relaxation. Int J Eng Sci 22(5):519–530
31. Sherief HH (1994) Problem in electromagneto thermoelasticity for infinitely long solid conducting circular cylinder with thermal relaxation. Int J Eng Sci 32(7):1137–1149
32. Majhi MC (1995) Discontinuities in generalized thermoelastic wave propagation in a semi-infinite piezoelectric rod. J Tech Phys 36:269–278
33. Sherief HH, Ezzat MA (1998) A problem in generalized magneto-thermoelasticity for an infinitely long annular cylinder. J Eng Math 34:387–402
34. Tianhu H, Xiaogeneg T, Yapeng S (2002) State space approach to one-dimensional shock problem for a semi-infinite piezoelectric rod. Int J Eng Sci 40:1081–1097
35. Tianhu H, Xiaogeneg T, Yapeng S (2002) Two-dimensional generalized thermal shock a thick piezoelectric plate of infinite extent. Int J Eng Sci 40:2249–2264
36. Restuccia L, Maruszewski BT (2004) Thermomechanics of piezoelectrics defective by dislocations. Proceedings of the 7th conference on applied and industrial mathematics in Italy, Venice, Italy, 20–24 September 2004. In: Primicerio M, Spigler R, Valente V (eds) Series on advances in mathematics for applied sciences, vol 69. World Scientific, New Jersey/London/Singapore, pp 475–486
37. Xia L, Hanagud SV (2004) Extended irreversible thermodynamics modeling for self-heating and dissipation in piezoelectric ceramics. IEEE Trans Ultrason Ferroelectr Freq Control 51(12):1582–1592
38. He T, Tian X, Shen Y (2005) A generalized electromagneto-thermoelastic problem for an infinitely long solid cylinder. Eur J Mech A/Solids 24(2):349–359
39. Aouadi M (2006) A generalized thermoelastic diffusion problem for an in finitely long solid cylinder. Int J Math Math Sci 2006:1–15
40. Aouadi M (2006) Variable electrical and thermal conductivity in the theory of generalized thermoelastic diffusion. Z Angew Math Phys 57(2):350–366
41. Aouadi M (2007) Generalized thermoelastic-piezoelectric problem by hybrid Laplace transform-finite element method. Eng Sci Mech 8(3):137–147

42. Aouadi M (2010) A contact problem of a thermoelastic diffusion rod. Z Angew Math Phys 90(4):278–286
43. Youssef HM, Bassiouny E (2008) Two-temperature generalized thermopiezoelasticity for one-dimensional problems. State space approach. Comput Methods Sci Technol 14(1):55–64
44. Maugin GA (1989) Electrodynamics of continua. Springer, New York
45. Maugin GA (2011) Electromagnetics in deformable solids. In: Ogden RW, Steigman DJ (eds) Mechanics and electrodynamics of magneto and electro elastic materials, vol 527, CISM courses and lectures. Springer, Wien/New York, pp 1–55
46. Nelson DF (1979) Electric, optic and acoustic interactions in dielectrics. Wiley, New York

Coupling Constitutive Coefficients

► Cylindrical Orthotropic Thermoelastic Shells Modeled by Direct Approach

Coupling of Electromechanical and Temperature Fields Under Monoharmonic Electrical and Mechanical Loading

► Piezothermo-Inelastic Behavior of Structural Elements: Vibrations and Dissipative Heating

Coupling of Mechanical and Temperature Fields Under Harmonic Loading

► Forced Harmonic Vibrations and Dissipative Heating of Nonelastic Bodies

CPLPS

► Photoluminescence Piezo-Spectroscopy Method for Measurement of Residual Stresses

Cr^{3+} Fluorescence Spectroscopy

► Photoluminescence Piezo-Spectroscopy Method for Measurement of Residual Stresses

Cr^{3+} Photoluminescence Piezo-spectroscopy

► Photoluminescence Piezo-Spectroscopy Method for Measurement of Residual Stresses

Crack

► Crack Closure
► Crack Detection/Arrest with Joule Heating
► Cracks in Transversely Isotropic and Inhomogeneous Elastic Solids
► Creep Crack Growth
► Curvilinear Cracks
► Interaction Problem Between a Hole and a Crack
► Thermal Shock and Modeling of Destruction for Refractory Linings of Metallurgical Installations

Crack Closure

Stelios K. Georgantzinos and Nikolaos K. Anifantis
Department of Mechanical Engineering and Aeronautics, University of Patras, Patras, Greece

Synonyms

Crack; Crack surface interference; Crack surfaces contact

Definitions

A crack in a body subjected to tension loading is completely open only at high load levels, or in

other words, at low load levels a part of the crack near the tip remains closed during the loading as well as the unloading phase of the cycle. Moreover, in the mechanism that is called crack breathing phenomenon, the crack moves from an upper position with respect to the direction of an alternating thermal and/or mechanical loading where the load forces the crack to be "closed" to the opposite position in which the crack is forced to be "open." Furthermore, the contact of the surfaces of a crack subjected to sudden heating implies that the crack is no longer fully open. The interference of deformations of crack faces in previous situations is commonly referred to the literature as crack closure, and this phenomenon effects and considerably controls various aspects of the crack propagation.

Overview

The concept of crack closure was first proposed by Elber [1] in 1970 to explain the characteristics of fatigue crack growth in aluminum alloys. Beyond the mechanical loading, insert wear characterized by small cracks and fissures caused by temperature fluctuations and the crack closure phenomenon exists resulting from cyclic stresses due to temperature changes. The study of crack interference under given thermal loadings is becoming increasingly important and has attracted considerable attention in the design of various machine components. The presence of imperfect contact and thermal resistance, which depends on the pressure between the contacting faces, leads to coupling of the thermal and stress field in such problems. Indicative modeling efforts [2] dealing with heat transfer and thermoelastic problems take into account the imperfect contact and thermal resistant. The conditions presented in the crack area depend on the mechanical pressure applied in the crack surfaces. According to the nature of the load, the crack can remain open, and then there is no sliding contact phenomenon. In addition, the symmetry of an imposed thermal load does not permit any heat exchange between the crack faces. Therefore, neither thermal contact resistance nor gap conductance could exist in such a problem. On the other hand, the loading conditions may lead to crack closure, resulting in heat flux between the crack faces that is mediated by the thermal contact resistance [3, 4].

Special interest has been given in the determination of fracture characteristics of thermally stressed cracks contained in elastic solids, mainly because of their importance in the theory of brittle fracture and in many industrial applications. The complicated geometry configurations of structures combined with the developed step temperature gradients enforce failures reducing safety and reliability standards. According to the finite element method (FEM) formulation that is usually followed, the overlapping of the crack faces is prevented by assuming proper constraints between adjacent nodes. Three states of contact are possible: the open, stick, and slip state. It is assumed that slip occurs under dry Coulomb friction conditions. Due to the presence of friction, the problems considered are solved in an incremental–iterative fashion.

Contact Between Two Crack Faces

The crack surface interference problem is usually treated like a classical contact problem between deformable but interconnected bodies at the crack front. In order to approach frictional contact between these sub-bodies, it is assumed that possible sliding obeys Coulomb's law of friction and that penetration between contacting areas is not allowed. The breathing crack behavior is usually treated as a contact problem between the crack surfaces ${}^{I}S$ and ${}^{II}S$, which intersect in the crack area. As shown in Fig. 1, these surfaces may come into contact on an interface ${}^{c}S$, given by ${}^{c}S = {}^{I}S \cap {}^{II}S$. The size of ${}^{c}S$ can vary during the interaction between the load and the structure, but it usually consists of two parts, an adhesive (${}^{a}S$) and a slipping (${}^{s}S$) part, depending on the friction conditions maintained between the contacting surfaces. In the open crack state, the ${}^{o}S$ part of the crack surface is subject to the traction-free condition.

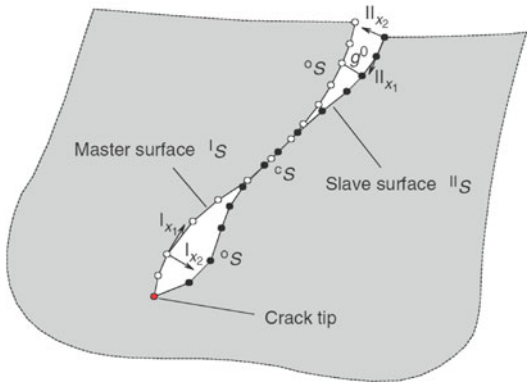

Crack Closure, Fig. 1 Contact of crack surfaces

Contact State

The open crack model requires crack faces to be thermally insulated and traction-free. Under thermal loading, these assumptions are no longer valid because partial crack closure may occur. Assume that the body is subject to small strains and small deformations due to the action of thermal load and that this thermal load eventually causes the closure of the crack.

The contact area along ^{c}S can be divided then into three possible states of contact: the open, slip, and adhesion state. The relationships between the normal and tangential traction in the local coordinate system for each one of these contact states are

$$p_{x_1} = p_{x_2} = 0 \text{ (open)} \tag{1}$$

$$p_{x_1} = \pm \mu p_{x_2} = 0 \text{ (slip)} \tag{2}$$

$$\left|p_{x_1}\right| < \mu \left|p_{x_2}\right| = 0 \text{ (adhesion)} \tag{3}$$

where μ is the coefficient of friction of ^{c}S. As it can be seen from the above equation, it is assumed that slip occurs under Coulomb friction conditions. The crack surfaces are defined by local coordinate systems $\left(\left({}^{j}x_1, {}^{j}x_2\right),\ \text{with J} = \text{I, II}\right)$. Subscripts 1 and 2 represent the tangential and normal directions, respectively, to the crack surfaces. Both axes $^{j}x_2$ define the direction of the unit outward normal vector of the corresponding surfaces, while the corresponding axes $^{j}x_1$ define the slipping direction.

The so-called slave–master concept that is widely used for the implementation of contact analysis can be adopted for prediction of the crack surface interference. Assuming that the crack surface ^{I}S is the slave, the nodes on this surface are called slave nodes. Then the surface ^{II}S is the master one, and the nodes that belong to this are called master nodes. Contact segments that span master nodes cover the contact surface of the structure. Therefore, the above problem can be regarded as contact between a slave node and a point on a master segment. This point may be located at a node, an edge, or a point of a master segment. A slave point makes contact with only one point on the master segments, but one master segment can make contact with one or more slave nodes at each time. For every contact pair, the mechanical contact conditions are expressed in a local coordinate system in the direction of the average normal to the boundaries of the bodies.

Contact problems are in general nonlinear since the extent of contact is not known in advance and because the friction phenomena at the contact area lead to the load history dependency of the boundary conditions. Therefore, these problems have to be formulated in an incremental and iterative fashion. In the steady-state problems, the extent of contact may be load independent. Despite this fact, an incremental procedure is generally needed to deal with such problems because the areas of stick and slip can be still load dependent. However, if the partition of stick–slip regions in the contact area is load independent as well, then these problems can be solved iteratively, with one step using the total load. When the external loading varies, then the regions on which the adhesion, slip, and traction-free conditions occur also vary. The existence of pressure-dependent thermal contact leads to coupling of temperature and stress fields. Therefore, the inherent nonlinearity of the problem demands simultaneous treating of both thermal and mechanical boundary integral equations, while iterative procedures are introduced to ensure equilibrium of mechanical and thermal contact conditions at each step of the process. Under crack contact conditions, the near crack tip

displacements and stresses keep their essential singular behavior, despite the imposed contact constraints. However, because of the nonlinearity of the contact phenomenon, an accurate analytical solution is not possible.

Incremental Solution

Since the frictional contact problems are inherently nonlinear and irreversible, an incremental approach could be implemented. The discretized nonlinear system of equations can be written as a set of algebraic equations in the form

$$[\mathbf{K}_{\mathrm{T}}(\mathbf{U})]\{\mathbf{U}\} = \{\mathbf{F}\} \tag{4}$$

In (1), $\{\mathbf{F}\}$ is the external force vector, and $\{\mathbf{U}\}$ is the structural displacement vector, respectively.

To trace the nonlinear structural response, a load stepping procedure must be used. Assuming that the load is applied in M equal small increments of the form $\{\Delta\mathbf{F}^m\} = \{\mathbf{F}^m\} - \{\mathbf{F}^{m-1}\}$, $m = 1, 2, \ldots, M$, an incremental procedure is then set up. The incremental procedure makes use of the fact that the solution for $\{\mathbf{U}^{m-1}\}$ is known when the load term $\{\mathbf{F}^{m-1}\}$ is applied to the structure. Such a method can yield reasonable results and guaranteed to converge if a suitably small increment of $\{\mathbf{F}\}$ is chosen.

The application of a trial load $\{\Delta\mathbf{F}^m\}$ at the step m of the procedure yields the incremental form of (1) in the form

$$[\mathbf{K}_{\mathrm{T}}]\{\Delta\mathbf{U}^m\} = \{\Delta\mathbf{F}^m\} \tag{5}$$

where $[\mathbf{K}_{\mathrm{T}}]$ is the tangent stiffness matrix and $\{\Delta\mathbf{U}^m\} = \{\mathbf{U}^m\} - \{\mathbf{U}^{m-1}\}$ is the increment in the structural displacement. At any increment m, it must be satisfied also the equilibrium condition

$$\{\mathbf{R}^m\} = \{\mathbf{P}^m\} - \{\mathbf{F}^m\} \approx \{\mathbf{0}\} \tag{6}$$

where $\{\mathbf{R}^m\}$ is the residual and $\{\mathbf{P}^m\}$ is the vector of internal forces. The solution of the problem posed by (5) and (6) cannot approach directly, and some form of iteration will be always required to zero the residual and restore the equilibrium for every load step. The iterative procedure approximately achieves the solution, and some tolerance limits are set to terminate the iteration and ensure the convergence of the iterative procedure.

Under the FEM approach and load reversing, in adjacent node pairs, the tractions vary according to the type of contact (1–3). This means that some displacement components are constrained and force components are altering. The time variation of the external loading imposes changes in the nodal pairs on which these constrains are valid. Recalling the equilibrium condition between the components of the incremental force is always maintained by the following equations:

$$^{\mathrm{I}}\Delta f_i^{\,m} + {}^{\mathrm{II}}\Delta f_i^{\,m} = 0, \quad i = 1, 2, 3 \tag{7}$$

In the open crack state (surface $^{\mathrm{o}}S$), the incremental traction components are simplified as follows:

$$^{\mathrm{I}}\Delta f_i^{\,m} = -{}^{\mathrm{II}}f_i^{\,m-1}, \quad i = 1, 2, 3 \tag{8}$$

By the definition of adhesion, on the corresponding crack surfaces ($^{\mathrm{a}}S$), the incremental displacement components are interconnected by the equation

$$^{\mathrm{I}}u_i^{\,m-1} + {}^{\mathrm{I}}\Delta u_i^{\,m} = {}^{\mathrm{II}}u_i^{\,m-1} + {}^{\mathrm{II}}\Delta u_i^{\,m}, \quad i = 1, 2 \tag{9}$$

When exists a gap g^0 in the normal direction, then the incremental displacement component along the normal direction is

$$^{\mathrm{I}}u_3^{\,m-1} + {}^{\mathrm{I}}\Delta u_3^{\,m} = {}^{\mathrm{II}}u_3^{\,m-1} + {}^{\mathrm{II}}\Delta u_3^{\,m} - g^0 \tag{10}$$

where g^0 is the initial normal gap between the master and slave node of the corresponding node pair. The slip state does not prohibit the existence of a gap between the crack surfaces, so (7) is still

Crack Closure, Table 1 Definition of contact status

	Decision	
Assumption	Open	Contact
Open	${}^{\mathrm{II}}\Delta u_3{}^m - {}^{\mathrm{I}}\Delta u_3{}^m > {}^{\mathrm{I}}u_3{}^{m-1} - {}^{\mathrm{II}}u_3{}^{m-1} + g^0$	${}^{\mathrm{II}}\Delta u_3{}^m - {}^{\mathrm{I}}\Delta u_3{}^m \le {}^{\mathrm{I}}u_3{}^{m-1} - {}^{\mathrm{II}}u_3{}^{m-1} + g^0$
Contact	${}^{\mathrm{I}}f_3{}^{m-1} + {}^{\mathrm{I}}\Delta f_3{}^m \ge 0$	${}^{\mathrm{I}}f_3{}^{m-1} + {}^{\mathrm{I}}\Delta f_3{}^m < 0$
	Adhesion	Slip
Adhesion	$\left\lvert {}^{\mathrm{I}}f_i{}^{m-1} + {}^{\mathrm{I}}\Delta f_i{}^m \right\rvert < \left\lvert \mu \left({}^{\mathrm{I}}f_3{}^{m-1} + {}^{\mathrm{I}}\Delta f_3{}^m \right) \right\rvert$, $i = 1,\ 2$	$\left\lvert {}^{\mathrm{I}}f_i{}^{m-1} + {}^{\mathrm{I}}\Delta f_i{}^m \right\rvert \ge \left\lvert \mu \left({}^{\mathrm{I}}f_3{}^{m-1} + {}^{\mathrm{I}}\Delta f_3{}^m \right) \right\rvert$, $i = 1,\ 2$
Slip	$\left({}^{\mathrm{I}}f_i{}^{m-1} + {}^{\mathrm{I}}\Delta f_i{}^m \right) \left({}^{\mathrm{I}}\Delta f_i{}^m - {}^{\mathrm{II}}\Delta f_i{}^m \right) > 0, i = 1,\ 2$	$\left({}^{\mathrm{I}}f_i{}^{m-1} + {}^{\mathrm{I}}\Delta f_i{}^m \right) \left({}^{\mathrm{I}}\Delta f_i{}^m - {}^{\mathrm{II}}\Delta f_i{}^m \right) \le 0, i = 1,\ 2$

valid in this case. However, the coplanar force components are defined in terms of friction

$$ {}^{\mathrm{I}}f_i{}^{m-1} + {}^{\mathrm{I}}\Delta f_i{}^m = \pm\mu \left({}^{\mathrm{I}}f_3{}^{m-1} + {}^{\mathrm{I}}\Delta f_3{}^m \right), \quad i = 1,\ 2 \tag{11} $$

where μ is the coefficient of Coulomb friction. Lowercase symbols ${}^{\mathrm{j}}u_i{}^m$ and ${}^{\mathrm{j}}f_i{}^m$, $i = 1,\ 2$ denote nodal displacement and force components, respectively, defined on the local coordinate systems $({}^{j}x_1, {}^{j}x_2)$, j = I, II. For reasons of simplicity, the subscripts that indicate nodal numbers were dropped out.

The constraints appearing in (7)–(11) can be embedded in the previously reported incremental FEM procedure if they are transformed to the global coordinate system and properly assembled to the master system of (5). Assume that the problem has been solved for the step $m - 1$ and consequently that the total nodal values $\{\mathbf{U}^{m-1}\}$, $\{\mathbf{F}^{m-1}\}$ are known for the whole structure. To determine the corresponding total nodal values of the step m, the contact conditions must be satisfied first. Therefore, the iterative procedure must be applied by initially utilizing the convergent contact status c = a ∪ s ∪ o of the previous step $m - 1$. The procedure initially assumes that ${}^{\mathrm{I}}\Delta f_i{}^m = 0, i = 1,\ 2,\ 3$. Then, the accurate values of incremental forces can be estimated via the iterative procedure. The contact state for every node pair is examined according to Table 1.

This Table describes criteria to check if violations involving geometrical compatibility and force continuity have occurred. Where necessary, appropriate changes from open to contact and from adhesion to slip state, and vice versa are made to seek the equilibrium state of contact conditions. For the node pair closest to a change, the new contact condition is applied. If the change is from open state to contact state, then the adhesion condition is adjusted. When the iterative procedure is converged, the incremental nodal values $\{\Delta\mathbf{U}^m\}$, $\{\Delta\mathbf{F}^m\}$ become known for the whole structure. After calculating the total nodal values, the procedure goes to the next step of the load increment and continues until the final increment M is reached. Then, the solution of the problem is evidently attained.

In order to solve the thermomechanical problem, the computational simplicity of the incremental–iterative procedure depends strongly on the way that thermal contact is formulated. Many researchers – in order to resolve the thermal crack closure phenomenon – assumed that the crack faces were insulated [4], while others assumed perfect thermal contact between the crack faces when in frictionless mechanical contact. In other works [6], imperfect thermal contact conditions were assumed in order to solve general frictionless thermoelastic contact problems.

In adiabatic crack contact approach, it is assumed that the crack faces are fully adiabatic being in mechanical contact or not. This assumption uncouples the thermal solution of the problem from the mechanical one, in the sense that during the incremental procedure the thermal part of the problem does not need to be resolved according to the new contact

state because thermal conditions in the contact region are not affected.

In general, thermal contact conditions are defined according to the assumption that the heat flow between the contacting areas is dependent on thermal resistance R which is regarded as a function of contact pressure. The thermomechanical contact conditions for a node pair being in adhesion, slip, and open state, respectively, are:

1. Adhesion state

$$ {}^{\mathrm{I}}q = -{}^{\mathrm{II}}q;\ {}^{\mathrm{I}}\theta = {}^{\mathrm{II}}\theta - R({}^{\mathrm{I}}t_{x_2})\,{}^{\mathrm{I}}q \tag{12} $$

$$ {}^{\mathrm{I}}t_{x_1} = -{}^{\mathrm{II}}t_{x_1};\ {}^{\mathrm{I}}t_{x_2} = -{}^{\mathrm{II}}t_{x_2};\ {}^{\mathrm{I}}u_{x_1} = {}^{\mathrm{II}}u_{x_1};\ {}^{\mathrm{I}}u_{x_2} = {}^{\mathrm{II}}u_{x_2} - g^0_{x_2} \tag{13} $$

where θ and q denote temperature and heat flux.

2. Slip state

$$ {}^{\mathrm{I}}q = -{}^{\mathrm{II}}q;\ {}^{\mathrm{I}}\theta = {}^{\mathrm{II}}\theta - R({}^{\mathrm{I}}t_{x_2})\,{}^{\mathrm{I}}q \tag{14} $$

$$ {}^{\mathrm{I}}t_{x_1} = -{}^{\mathrm{II}}t_{x_1},\ {}^{\mathrm{I}}t_{x_2} = -{}^{\mathrm{II}}t_{x_2},\ {}^{\mathrm{I}}t_{x_1} = \pm\mu\,{}^{\mathrm{I}}t_{x_2},\ {}^{\mathrm{I}}u_{x_2} = {}^{\mathrm{II}}u_{x_2} - g^0_{x_2} \tag{15} $$

3. Open state

$$ {}^{\mathrm{I}}q = -{}^{\mathrm{II}}q;\ {}^{\mathrm{I}}q^m = 0 \tag{16} $$

$$ {}^{\mathrm{I}}t_{x_1} = -{}^{\mathrm{II}}t_{x_1};\ {}^{\mathrm{I}}t_{x_2} = -{}^{\mathrm{II}}t_{x_2};\ {}^{\mathrm{I}}t_{x_1} = 0;\ {}^{\mathrm{I}}t_{x_2} = 0 \tag{17} $$

In addition, the boundary conditions along the interface of the bodies are

$$ {}^{\mathrm{I}}q = -{}^{\mathrm{II}}q;\ {}^{\mathrm{I}}\theta = {}^{\mathrm{II}}\theta \tag{18} $$

$$ {}^{\mathrm{I}}t_{x_1} = -{}^{\mathrm{II}}t_{x_1};\ {}^{\mathrm{I}}t_{x_2} = -{}^{\mathrm{II}}t_{x_2};\ {}^{\mathrm{I}}u_{x_1} = {}^{\mathrm{II}}u_{x_1};\ {}^{\mathrm{I}}u_{x_2} = {}^{\mathrm{II}}u_{x_2} \tag{19} $$

As it can be seen, the interface is regarded as perfect. For convenience, the boundary condition (18, 19) are as well expressed in aforementioned local coordinate system. Finally, it is noted that for the previously given thermal boundary conditions (12, 14, 16) there is

$$ {}^{\mathrm{I}}q = {}^{\mathrm{I}}k\left(\frac{\partial T}{\partial x_2}\right);\ {}^{\mathrm{II}}q = {}^{\mathrm{II}}k\left(\frac{\partial T}{\partial x_2}\right) \tag{20} $$

where ${}^{\mathrm{I}}k$ and ${}^{\mathrm{II}}k$ are thermal conductivities of the bodies I and II, respectively. Someone may use the aforementioned thermal and mechanical contact conditions in order to solve the thermomechanical crack closure phenomenon implementing the boundary element approach [5].

References

1. Elber W (1970) Fatigue crack closure under cyclic tension. Eng Fract Mech 2:37–45
2. Comninou M, Barber JR (1984) The thermoelastic Hertz problem with pressure dependent contact resistance. Int J Mech Sci 26:549–554
3. Keppas LK, Giannopoulos GI, Anifantis NK (2008) Transient coupled thermoelastic contact problems incorporating thermal resistance: a BEM approach. Comput Model Eng Sci 25:181–196
4. Kokini K, Reynolds RR (1991) Transient heating vs cooling of interfacial cracks in ceramic-to-metal bonds. Eng Fract Mech 38:371–383
5. Giannopoulos GI, Anifantis NK (2007) A BEM analysis for thermo-mechanical closure of interfacial cracks incorporating friction and thermal resistance. Comput Method Appl Mech Eng 196:1018–1029
6. Martynyak RM, Honchar KhI, Nahalka SP (2003) Simulation of thermomechanical closure of an initially open interface crack with heat resistance. Mater Sci 39:672–681

Crack Detection/Arrest with Joule Heating

Thomas Jin-Chee Liu
Department of Mechanical Engineering,
Ming Chi University of Technology, Taishan,
New Taipei City, Taiwan, Republic of China

Synonyms

Crack

Definitions

The Joule heating effect is a thermoelectric coupling phenomenon, which can be used to achieve crack detection and arrest.

In electrically conductive materials subjected to an electric current, locally higher values of electric current density occur near fillets, holes, and crack/notch tips. This phenomenon is analogous to stress concentration in solid mechanics. By the Joule heating effect, a higher temperature will be induced in those regions experiencing higher electric current densities. Additional thermal stresses and deformations are thus also induced.

By varying the size of the external current, crack arrest or crack detection can be achieved. When a sufficiently large amount of electrical energy is applied to a material containing cracks, crack tips can melt, causing the formation of a crack tip hole during the cooling process. This crack tip hole can arrest further crack growth.

On the other hand, when a lower amount of electrical energy is applied to the material, crack tips will not melt, but a local hot region will form around the crack tip. These hot spots can be detected using thermal sensors or an infrared sensing system. In this way, the Joule heating effect enables the detection of cracks on surfaces of a structure. This method is one kind of nondestructive testing (NDT).

Overview

When a conductive material carries electric current, the electric current density field is concentrated at fillets, holes, and crack/notch tips. Figure 1 illustrates this electric current density concentration effect. This effect is similar to stress concentration in solid mechanics. Like the stress field in solid mechanics, the electric current density field also has a singularity at the crack tip. The current density theoretically approaches an infinite value at the singular point.

Due to the electric current density concentration and the Joule heating effect, a local hot region will form around the crack tip (as shown in Fig. 2a). This hot spot can be used to detect and arrest cracks. The hot spot can also be detected by thermal sensors or an infrared sensing system, so the crack tip location can be determined. If sufficiently high values of electric current and energy are applied, the crack tip temperature may surpass the material melting point. At this point, the crack tip melts, and a circular hole may form at the tip during the cooling process (as shown in Fig. 2b, c).

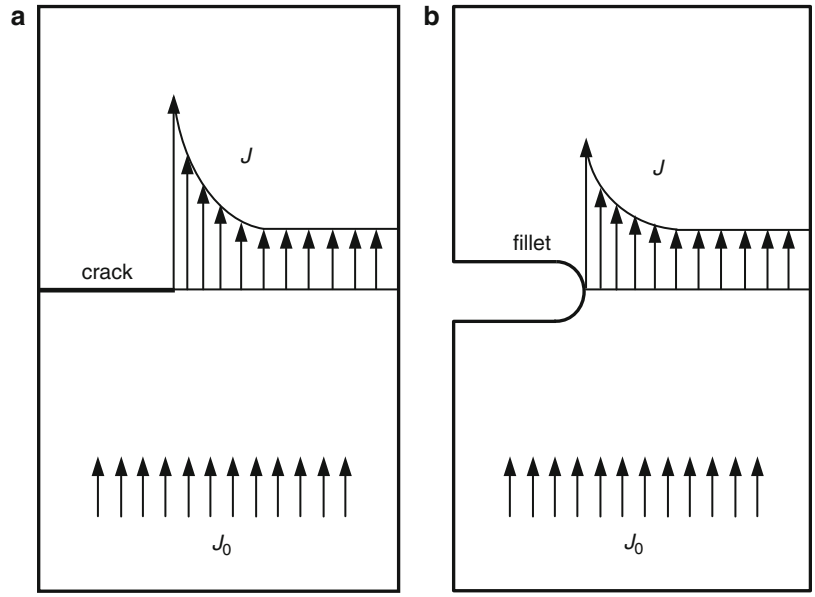

Crack Detection/Arrest with Joule Heating, Fig. 1 Electric current density concentration. (**a**) Concentration at crack tip and (**b**) concentration at fillet (J, J_0 : electric current density)

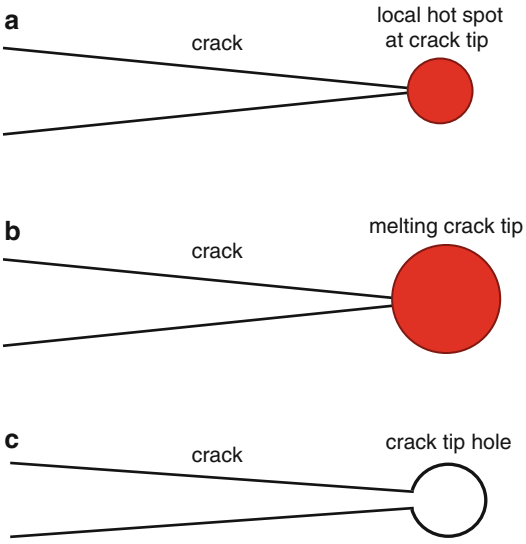

Crack Detection/Arrest with Joule Heating, Fig. 2 (**a**) Local hot spot at crack tip, (**b**) melting crack tip and (**c**) crack tip hole

This crack tip hole, like a drilled hole, halts crack propagation, and crack arrest is achieved.

In 1982, Parton et al. [1, 2] reported that the Joule heating effect can induce local compressive thermoelastic stresses and melting at the crack tip to arrest crack propagation. Recently, Librescu et al. [3–5] used mathematical and analytical methods to investigate cracked conducting plates and shells under electric current. They reported that significant Joule heating concentration occurs around the crack tip.

Experimental studies have shown the creation of a crack tip hole using the Joule heating effect to be an effective crack arrest technique. The crack tip can melt under high electric current loading and a crack tip hole occurs during the subsequent cooling process [6–9]. A typical fine phase transformation microstructure is obtained around the crack tip as a result of rapid heating and cooling [6]. It was found that ductility and wear capacity around the crack tip were increased and promoted [6]. In addition to experiments, finite element analyses of the Joule heating crack arrest mechanism have been performed by Cai and Yuan [10, 11] and Liu [12, 13]. The finite element results can provide more practical and complete information that analytical and experimental methods cannot obtain. The melting crack tip and crack arrest theories are proved from the numerical solutions. In ref. [13], it is proposed that electric currents on the order of 20,000–30,000 A cause melting in the vicinity of the crack tip. The resistance spot welding technique, associated with high currents up to 30,000 A, can be applied to the Joule heating crack arrest method [13].

For crack detection, very high electric currents are not necessary, since melting of the crack tip is not desired. However, a local hot spot at the crack tip is still necessary for the crack detection process. The magnitude of the applied current will thus affect the crack detection performance.

Basic Methodology

Fundamental Equations

The fundamental equations for the crack detection/arrest analysis are listed as follows [12–16]:

1. Electric current analysis

$$\mathbf{E} = -\nabla\phi,\ \mathbf{J} = \frac{1}{\rho}\mathbf{E},\ \nabla\cdot\mathbf{J} = 0 \tag{1}$$

where $\mathbf{E}$, $\mathbf{J}$, ϕ, and ρ are the electric field (V/m), electric current density (A/m^2), electric potential (V), and resistivity (Ω-m), respectively.

2. Thermal analysis

$$\mathbf{q}'' = -k\nabla T,\ k\nabla^2 T + \dot{q} = \beta C_p \frac{\partial T}{\partial t},\ \dot{q} = \rho|\mathbf{J}|^2 \tag{2}$$

where $\mathbf{q}''$, k, T, $\dot{q}$, β, C_p, and t are the heat flux (W/m^2), thermal conductivity (W/m-K), temperature (K), heat generation (W/m^3) of Joule heating, mass density (kg/m^3), specific heat (J/kg-K), and time (s), respectively.

3. Thermoelastic analysis

$$\sigma_{ji,j} + X_i = \beta\ddot{u}_i,\ i,j = x,y,z \tag{3}$$

$$\varepsilon_{ij} = \frac{1}{2}(u_{i,j} + u_{j,i}),\ i,j = x,y,z \tag{4}$$

$$\varepsilon_{ij} = \frac{1}{E}\left[(1+\nu)\sigma_{ij} - (\nu I_1 - E\alpha\Delta T)\delta_{ij}\right],\quad i,j = x,y,z \tag{5}$$

where σ_{ij}, ε_{ij}, X_i, u_i, $\ddot{u}_i$, E, ν, I_1, α, ΔT, and δ_{ij} are the stress (Pa = N/m^2), strain (dimensionless), body force (N/m^3), displacement (m), acceleration (m/s^2), Young's modulus (Pa), Poisson's ratio (dimensionless), stress invariant ($I_1 = \sigma_{xx} + \sigma_{yy} + \sigma_{zz}$), coefficient of thermal expansion (1/K), temperature difference ($\Delta T = T - T_0$ where T_0 is the reference temperature), and Kronecker delta, respectively.

Coupled-Field Analysis

Crack detection/arrest analysis is represented by the thermo-electro-structural coupled-field problem. Equations (1)–(5) need to be coupled, but the equations are difficult to solve by analytical methods. Using numerical methods, such as the finite element method, is the preferred way to solve this complicated problem.

In this study, the finite element equations of the thermo-electro-structural coupled-field analysis are as follows [17]:

$$\begin{bmatrix} \mathbf{M} & 0 & 0 \\ 0 & 0 & 0 \\ 0 & 0 & 0 \end{bmatrix} \begin{bmatrix} \ddot{\mathbf{U}} \\ \ddot{\mathbf{T}} \\ \ddot{\mathbf{V}} \end{bmatrix} + \begin{bmatrix} \mathbf{C} & 0 & 0 \\ \mathbf{C^{tu}} & \mathbf{C^{t}} & 0 \\ 0 & 0 & 0 \end{bmatrix} \begin{bmatrix} \dot{\mathbf{U}} \\ \dot{\mathbf{T}} \\ \dot{\mathbf{V}} \end{bmatrix} + \begin{bmatrix} \mathbf{K} & \mathbf{K^{ut}} & 0 \\ 0 & \mathbf{K^{t}} & 0 \\ 0 & 0 & \mathbf{K^{v}} \end{bmatrix} \begin{bmatrix} \mathbf{U} \\ \mathbf{T} \\ \mathbf{V} \end{bmatrix} = \begin{bmatrix} \mathbf{F} \\ \mathbf{Q} \\ \mathbf{I} \end{bmatrix} \tag{6}$$

where $\mathbf{U}$, $\mathbf{T}$, $\mathbf{V}$, $\mathbf{F}$, $\mathbf{Q}$, and $\mathbf{I}$ are the vector forms of the displacement (m), temperature (K), electric potential (V), force (N), heat flow rate (W), and electric current (A), respectively. The material constant matrices $\mathbf{M}$, $\mathbf{C}$, $\mathbf{C^t}$, $\mathbf{C^{tu}}$, $\mathbf{K}$, $\mathbf{K^t}$, $\mathbf{K^{ut}}$, and $\mathbf{K^v}$ are the structural mass, structural damping, thermal specific heat, thermoelastic damping, structural stiffness, thermal conductivity, thermoelastic stiffness, and electric conductivity, respectively. The coupled heat flow matrix $\mathbf{Q}$ contains the effects of thermal loading and electrical Joule heating. $\mathbf{C^{tu}}$ and $\mathbf{K^{ut}}$ are thermoelastic coupled terms. Equation (6) is a directly coupled nonlinear equation which is solved using the Newton–Raphson iterative method. Equations (1)–(6) can be solved using the finite element software ANSYS [17].

Temperature-Dependent Material Constants

In analytical or numerical studies of crack detection/arrest, it is more practical and accurate to use temperature-dependent material constants. The material constants of mild steel are listed in Table 1 [13, 18]; however, it is difficult to find complete temperature-dependent material constant data for other materials from past references. Many material constants and data at high temperatures are yet to be measured.

Simulating the creation of a crack tip hole is more difficult than the simple heated case, since it includes a solid–fluid phase change and material shrinkage during the cooling process. To simplify the analysis and ignore the phase change, only the temperature contour is adopted to estimate the size of the melted crack tip [12, 13].

Crack Contact

During the Joule heating process, the two surfaces of a crack may contact each other. The contact area becomes a thermo-electro-structural coupled-field problem. As shown in Fig. 3, this complicated problem includes structural contact, electrical contact, and thermal contact. Structural contact means the contact pressure exists on the crack surfaces. Electrical and thermal contact means that electric current and heat flow can pass through the crack contact surfaces.

The contact problem is not easily solved analytically; a simpler way is to use the finite element method. The structural contact problem is a standard analysis in many finite element software packages. However, the nature of the electrical and thermal contact is more complex. Indeed, the contact resistance depends on the temperature and contact pressure [19]. It is difficult to find the physical constants of the contact interface for the numerical calculation. Typical and simplified values of the contact

Crack Detection/Arrest with Joule Heating, Table 1 Temperature-dependent material constants of mild steel (SI units) [13, 18]

Temperature T (°C)	Young's modulus E (GPa)	Coefficient of thermal expansion α (1/°C)	Thermal conductivity k (W/m-°C)	Specific heat C_p (J/kg-°C)	Resistivity ρ (Ω-m)
21	206.8	10.98×10^{-6}	64.60	444	0.14224×10^{-6}
93	196.5	11.52×10^{-6}	63.15	452.38	0.18644×10^{-6}
204	194.4	12.24×10^{-6}	55.24	511.02	0.26670×10^{-6}
315.5	186	12.96×10^{-6}	49.87	561.29	0.37592×10^{-6}
426.7	169	13.50×10^{-6}	44.79	611.55	0.49530×10^{-6}
537.8	117	14.04×10^{-6}	39.71	661.81	0.64770×10^{-6}
648.9	55	14.58×10^{-6}	34.86	762.34	0.81788×10^{-6}
760	6.9	14.05×10^{-6}	30.46	1,005.3	1.0109×10^{-6}
871	–	13.05×10^{-6}	28.37	1,005.3	1.1151×10^{-6}
982	–	–	27.62	1,005.3	1.1582×10^{-6}
1,093	–	–	28.52	1,189.6	1.1786×10^{-6}
1,204	–	–	–	1,189.6	1.2090×10^{-6}

Poisson's ratio $v = 0.3$, density $\beta = 7{,}861.2$ kg/m^3, melting point = 1,521 °C

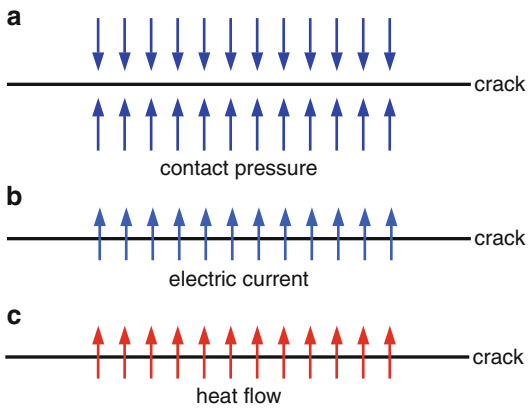

Crack Detection/Arrest with Joule Heating, Fig. 3 (**a**) Structural contact, (**b**) electrical contact, and (**c**) thermal contact

resistance or conductance of mild steel can be found in ref. [13, 18].

Electric Current Density Factor

In linear elastic fracture mechanics (LEFM), the stress near the crack tip has an $r^{-1/2}$ singularity. Likewise, in the electric current problem, the electric current density field near the crack tip also has an $r^{-1/2}$ singularity [10, 20, 21]. Analogous to the stress intensity factor (SIF), the electric current density factor (ECDF) K_J was introduced in [10, 20, 21] as a parameter for describing the current density singularity.

In a cracked conductive material carrying electric current, the near-field solutions of the current density field near the crack tip are expressed as follows [21]:

$$J_x = \frac{-K_J}{\sqrt{2\pi r}} \sin\frac{\theta}{2} \tag{7}$$

$$J_y = \frac{K_J}{\sqrt{2\pi r}} \cos\frac{\theta}{2} \tag{8}$$

where J_x and J_y are electric current density components along the $x-$ and $y-$ directions. For (7) and (8), the local coordinate system at the crack tip is defined in Fig. 4. Furthermore, the ECDF can be defined as [21]

$$K_J = \lim_{r\to 0} \sqrt{2\pi r} J_y(r, 0) \tag{9}$$

For an infinite plane subjected to a remote current density J_0 (shown in Fig. 5), the analytical solution of a central crack of length $2a$ is [21]

$$K_J = J_0\sqrt{\pi a} \tag{10}$$

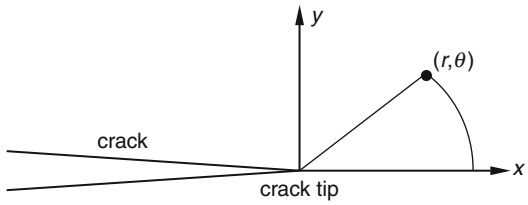

Crack Detection/Arrest with Joule Heating, Fig. 4 Local coordinate system at crack tip

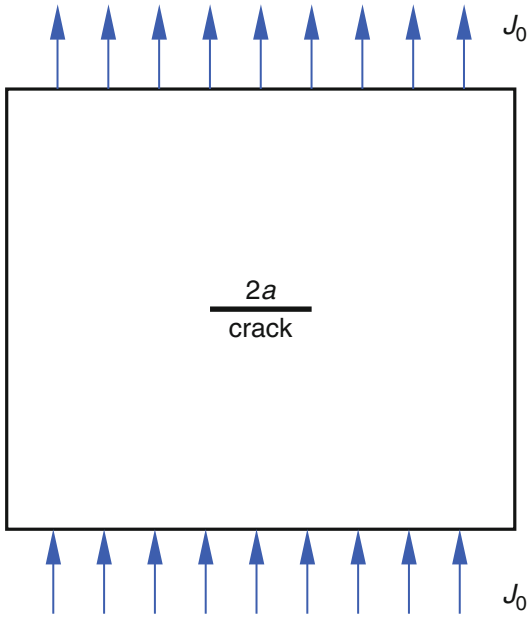

Crack Detection/Arrest with Joule Heating, Fig. 5 Infinite plane with central crack carrying electric current (J_0, remote electric current density; $2a$, crack length)

Equation (10) is similar to the SIF of the Griffith crack problem in LEFM.

The definition of K_J is similar to the concept of LEFM. In ref. [22], the analogy between the electric current density and antiplane shear (Mode-III) problem has been reported. Both fields are governed by the Laplace equation as follows [22]:

$$\nabla^2 \phi = 0 \tag{11}$$

$$\nabla^2 w = 0 \tag{12}$$

where w is the antiplane (z-direction) displacement. However, the ECDF and SIF for the Griffith crack problem of both fields are similar as

$$K_J = J_0\sqrt{\pi a}, K_{III} = \tau_0\sqrt{\pi a} \tag{13}$$

where τ_0 and K_{III} are the remote antiplane shear stress and Mode-III SIF. Analogous to the previous equations, both factors from the near-field solutions are also similar [12, 13]:

$$K_J = \frac{\eta\phi}{2\sin\frac{\theta}{2}}\sqrt{\frac{2\pi}{r}} \tag{14}$$

$$K_{III} = \frac{Gw}{2\sin\frac{\theta}{2}}\sqrt{\frac{2\pi}{r}} \tag{15}$$

where η is the electrical conductivity ($\eta = 1/\rho$) and G is the shear modulus.

Finite Element Model

The crack detection/arrest problem is nonlinear, and the finite element method is suitable for solving this complicated problem. In doing so, a thermo-electro-structural coupled-field analysis has to be adopted.

The finite element model for crack detection/arrest analysis must include the following items:

1. Finite element mesh
2. Element type with the capability of thermo-electro-structural coupled-field analysis
3. Quarter-point elements (QPE) [23] to simulate the crack tip singularity (as shown in Fig. 6)
4. Temperature-dependent material constants
5. Contact analysis and parameters between crack surfaces
6. Structural, thermal, and electrical boundary conditions

Validation of Finite Element Model by ECDF

To calculate the ECDF from the finite element results, the limited electric potential extrapolation technique (LEPET) [12, 13] for calculating K_J is adopted as follows. As shown in Fig. 7, each K_J at nodes C, D, and E along the crack surface can be computed using (14) [12, 13].

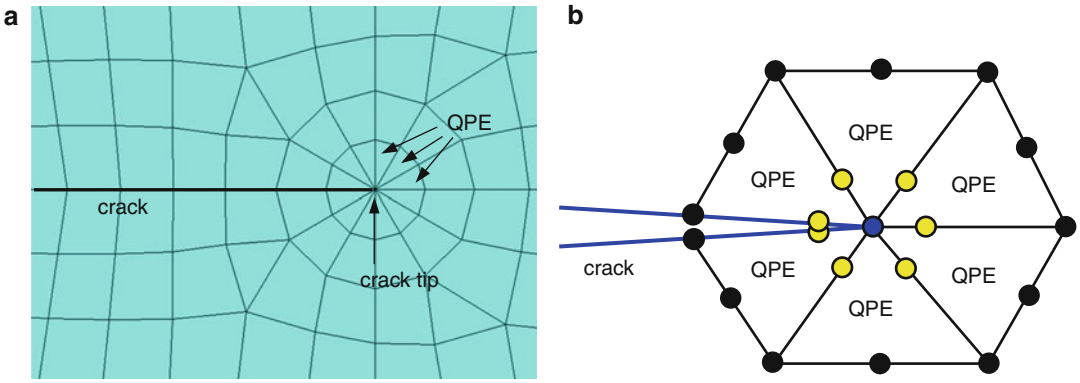

Crack Detection/Arrest with Joule Heating, Fig. 6 (**a**) Arrangement of QPEs and (**b**) QPEs with node shifting [23]

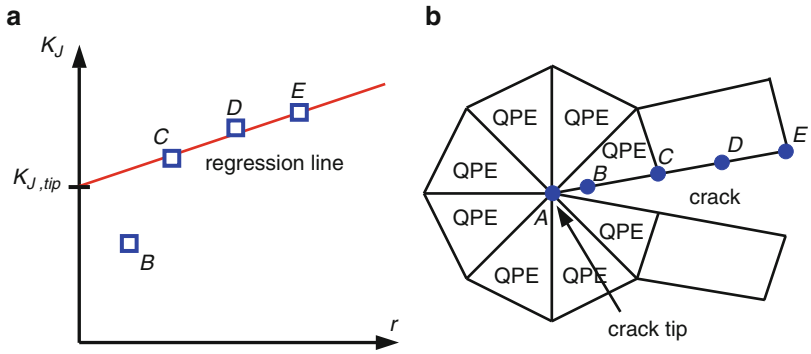

Crack Detection/Arrest with Joule Heating, Fig. 7 LEPET method. (**a**) linear regression and (**b**) node position [12, 13]

The electric potential ϕ at each node can be obtained from the finite element results. Referring to Fig. 4, the angles $\theta = 180^\circ$ and $\theta = -180^\circ$ denote the two crack surfaces. In Fig. 7, three nodal values of K_J are used to fit a straight line using linear regression. This line is extrapolated to $r = 0$ to obtain K_J at the crack tip. The concept of the LEPET [12] is adopted from the LDET method [24].

The accuracy of the finite element mesh can be confirmed using the ECDF. For example, a finite element mesh with a central crack and relatively large boundary can be established to simulate an infinite plane. Then the finite element solution of K_J can be compared with (10).

Case Study I: Crack Detection

A case study for crack detection extracted from Ref. [25] is described herein. As shown in Fig. 8, the thin plate is made of the mild steel (ASTM A36), with dimensions $L = 200$ mm, $W = 25$ mm, and $e = 0.1$ mm, where e is the thickness. The plate contains an edge crack of length $a = 4.3301$ mm.

The main conditions adopted in this analysis are listed as follows:

1. Thermoelectric coupled-field analysis.
2. Three-dimensional analysis.
3. Temperature-dependent material properties in Table 1 are considered.
4. Contact conditions on crack surfaces are ignored.

In addition, the electric input i_0 is direct current (DC). The convection conditions $h = 15$ W/m^{2}K and $T_\infty = 25$ °C are applied on all surfaces of the plate. The initial temperature T_0 is 25 °C.

The finite element software ANSYS was adopted, and the plate was modeled using SOLID226 elements, i.e., 20-node isoparametric solid elements, with the thermoelectric coupled-field analysis [17]. The nodal degrees of freedom

of SOLID226 are T and ϕ. Figure 9 shows the ANSYS finite element mesh.

Under $i_0 = 150$ A, Fig. 10 shows the electric current density vectors at $t = 1$ s. It is clear that there is a field concentration at the crack tip. Similar to the elastic stress field, the electric current density also exhibits an $r^{-1/2}$ singularity at the crack tip. Figure 11 shows the temperature contour of the plate, and it can be seen that the Joule heating effect causes a high temperature area around the crack tip. The crack tip location can be detected by a thermal sensor.

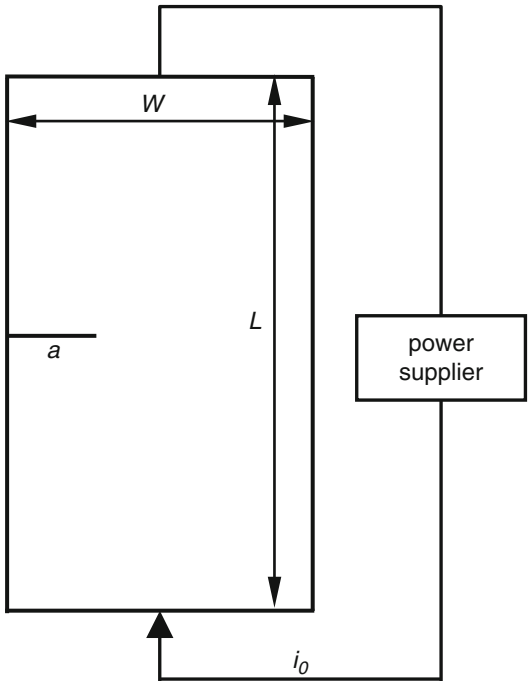

Crack Detection/Arrest with Joule Heating, Fig. 8 Configuration of case study I: a plate with an edge crack for crack detection research [25]

Figure 12 shows the temperature distribution in front of the crack tip at $t = 1$ s under $i_0 = 10$ A and $i_0 = 150$ A. The temperature decreases from the crack tip to the surrounding area. When the external current i_0 is larger, the value of the temperature gradient near the crack tip is larger. If the temperature gradient near the crack tip is too small, it is hard to detect the crack tip. For example, in Fig. 12a, the temperature variation from point A to B under $i_0 = 10$ A is 0.035 °C. Thermal sensing equipment without a high resolution may not detect such a small temperature variation. In Fig. 12b, the temperature variation from point A to B under $i_0 = 150$ A is 18.46 °C, which is much easier to detect [25].

Case Study II: Crack Arrest

This case study for crack arrest research is adopted from ref. [13]. As shown in Fig. 13, the thin plate contains a central crack of length $2a$. The dimensions of the plate are $L = W = 50$ mm,

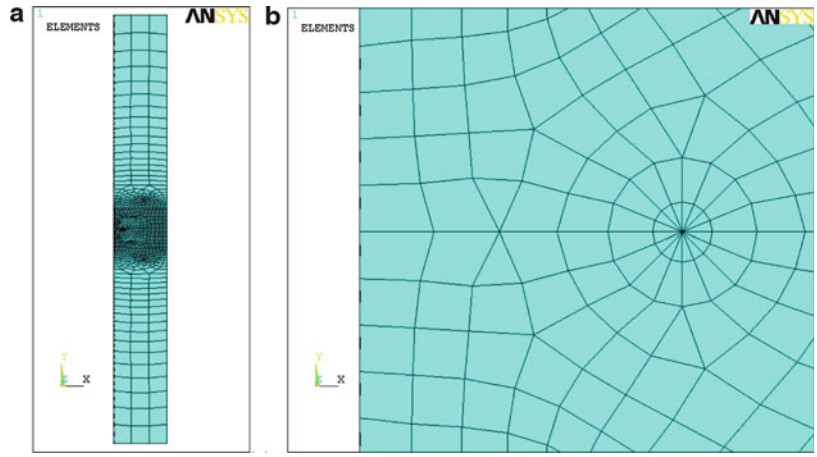

Crack Detection/Arrest with Joule Heating, Fig. 9 Finite element mesh. (**a**) Global view and (**b**) local view near crack tip

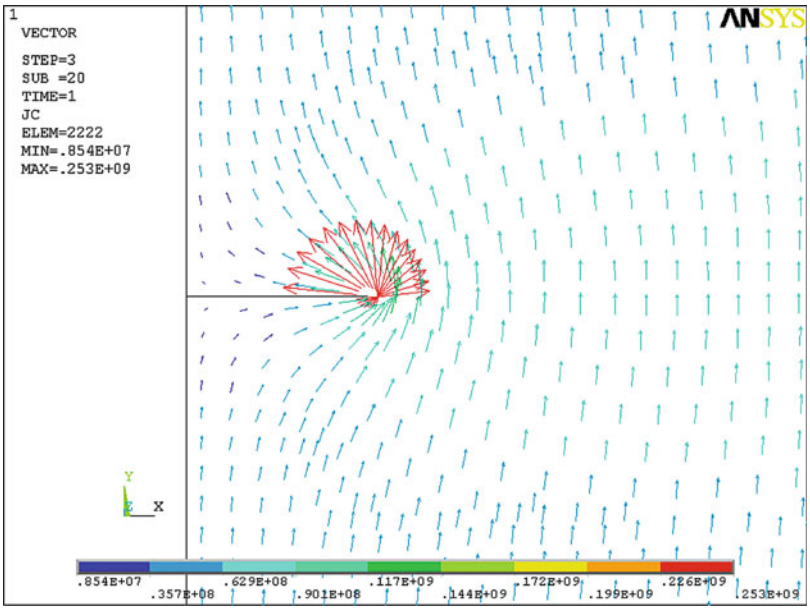

Crack Detection/Arrest with Joule Heating, Fig. 10 Electric current density vectors (units: A/m^2)

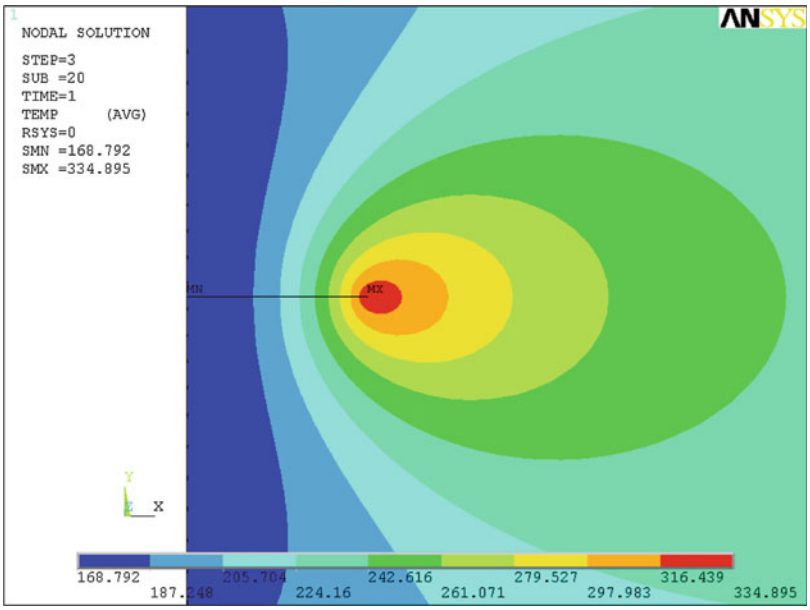

Crack Detection/Arrest with Joule Heating, Fig. 11 Distribution of temperature field (units: °C)

$a = 10$ mm, and $e = 1$ mm, where e is the thickness, and the plate material is mild steel (ASTM A36).

The main conditions adopted in this analysis are listed as follows:

1. Thermo-electro-structural coupled-field analysis.
2. Two-dimensional analysis.
3. Plane stress condition.
4. Linear elastic property.
5. Temperature-dependent material properties in Table 1 are considered.
6. Contact conditions on crack surfaces are considered.

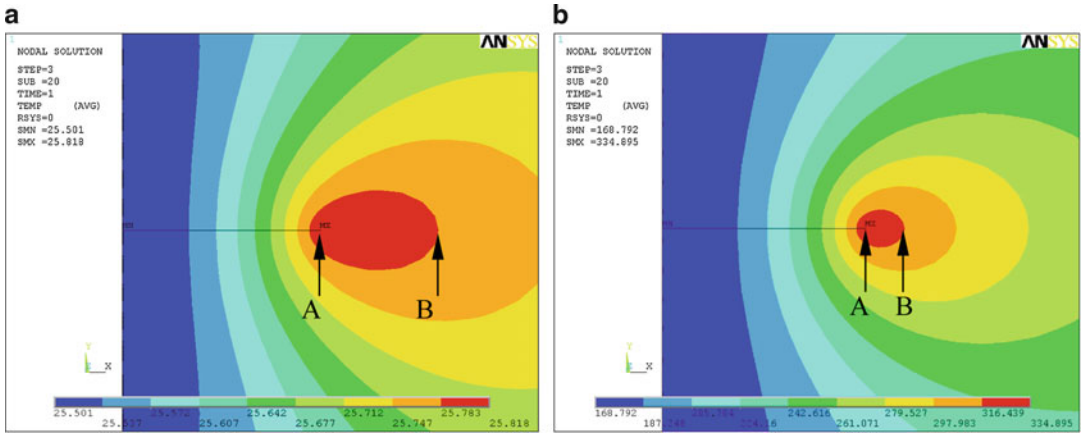

Crack Detection/Arrest with Joule Heating, Fig. 12 Temperature contour. (**a**) Under $i_0 = 10$ A; (**b**) $i_0 = 150$ A (units: °C)

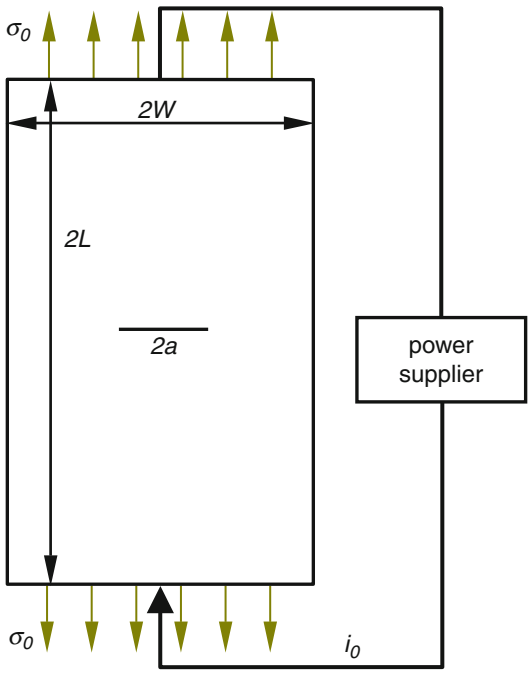

Crack Detection/Arrest with Joule Heating, Fig. 13 Configuration of case study II: a plate with a central crack for crack arrest research [13]

The plate is subjected to a remote stress σ_0. Also, the electric input is alternating current (AC) $i_0(t) = i_A \sin(2\pi ft)$ where t, i_A, and f are the time, amplitude, and frequency, respectively. As the time span is relatively short in the transient thermal analysis, all surfaces of the plate are assumed to undergo adiabatic processes [11]. The initial temperature T_0 is 21 °C.

The finite element software ANSYS was utilized here. The plate is modeled using ANSYS type PLANE223 elements, i.e., 8-node isoparametric plane elements with thermo-electro-structural coupled-field analysis [17]. The nodal degrees of freedom of PLANE223 are u_x, u_y, T, and ϕ. The plane stress option is used. Due to symmetry, only half of the region is analyzed. Figure 14 shows the ANSYS finite element mesh.

In this case study, a current $i_0(t) = 28000\sin(120\pi t)$ A is applied to the plate. The AC frequency is 60 Hz, and there are five cycles (1 cycle = 1/60 s) in the process.

Figure 15 shows the crack tip temperature variation with time under varying mechanical load σ_0. When a compressive stress $\sigma_0 = -20$ MPa is applied, the two crack surfaces contact each other, and the crack tip cannot melt at the end of the last cycle ($t = 0.0833$ s). Due to the contact, the electric current density vectors can pass through the crack so that the crack tip concentration and temperature are simultaneously reduced.

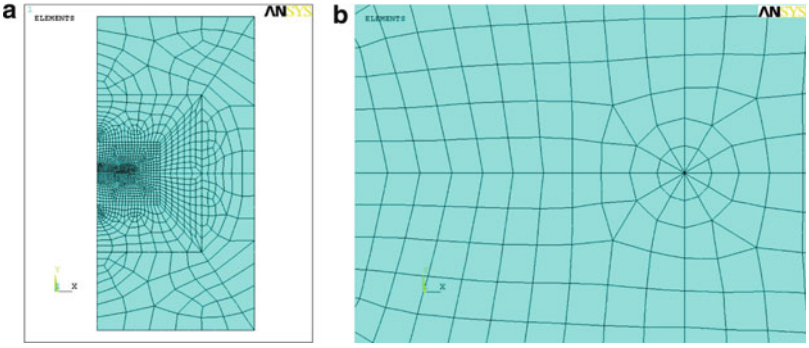

Crack Detection/Arrest with Joule Heating, Fig. 14 Finite element mesh (1/2 symmetrical model). (**a**) Global view and (**b**) local view near crack tip

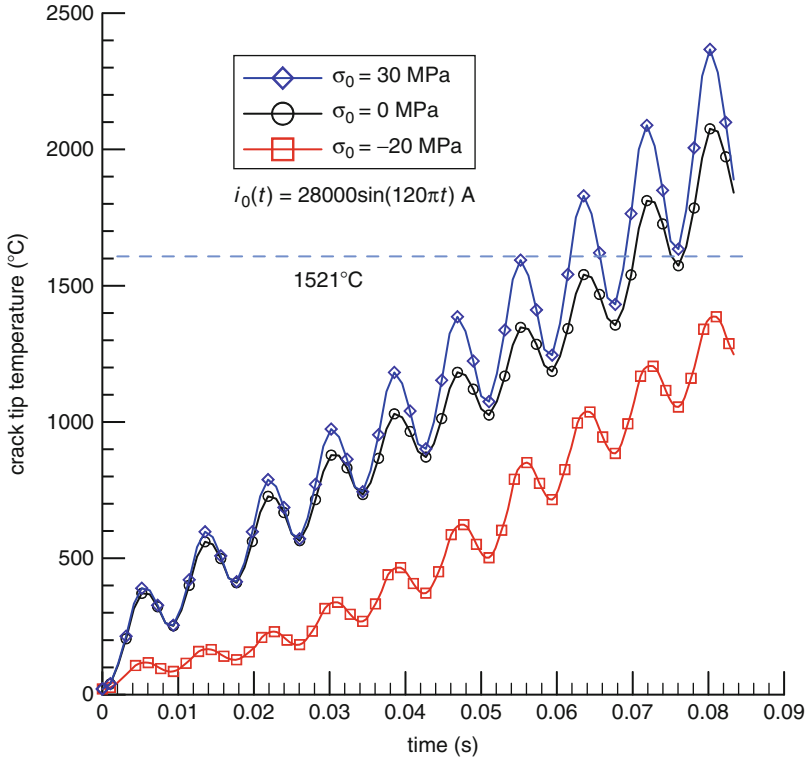

Crack Detection/Arrest with Joule Heating, Fig. 15 Crack tip temperature variation with time [13]

In Fig. 15, the results from $\sigma_0 = 30$ MPa yield the highest temperature. The tensile load makes the crack open enough to cause a high current density concentration at the crack tip so that the crack tip can melt. When there is no mechanical load ($\sigma_0 = 0$ MPa), crack contact occurs near the crack tip. This contact is due to thermal deformation and results in a lower crack tip temperature. However, for some internal cracks in the structure, it is difficult to make the crack open using tensile loading only. In this case, a larger electric power and longer process time are required to induce melting of the crack tip.

Figure 16 shows a time history of the temperature change near the crack tip. The crack tip

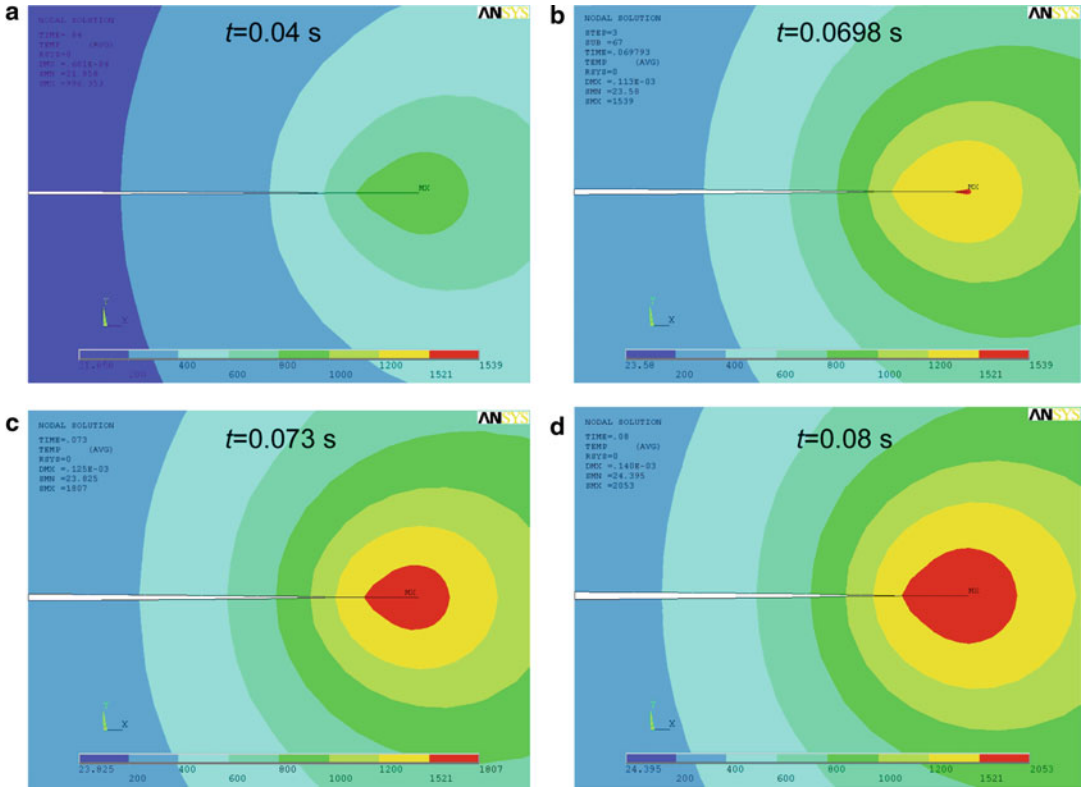

Crack Detection/Arrest with Joule Heating, Fig. 16 Temperature contour at different times (units: °C)

temperature increases with time under electric current. The red color denotes the melted region ($T > 1{,}521$ °C). According to experimental results [6–9], this melted region at the crack tip can shrink to a hole during the cooling process. This hole prevents crack growth, and crack arrest is achieved.

References

1. Parton VZ, Kudryavtsev BA (1988) Electromagnetoelasticity. Gordon and Breach, New York
2. Kudryavtsev BA, Parton VZ, Rubinskii BD (1982) Electromagnetic and thermoelastic fields in a conducting plate with a cut of finite length. Solid Mech 17:110–118
3. Librescu L, Hasanyan D, Qin Z (2007) Joule heating, its implications on crack detection/arrest and other magneto-thermo-elastic issues in multifunctional thin-walled structures. In: Proceedings of the seventh international congress on thermal stresses, Taipei
4. Qin Z, Librescu L, Hasanyan D (2007) Joule heating and its implications on crack detection/arrest in electrically conductive circular cylindrical shells. J Therm Stress 30:623–637
5. Hasanyan D, Librescu L, Qin Z, Young RD (2005) Thermoelastic cracked plates carrying nonstationary electrical current. J Therm Stress 28:729–745
6. Fu YM, Bai XZ, Qiao GY, Hu YD, Luan JY (2001) Technique for producing crack arrest by electromagnetic heating. Mater Sci Technol 17:1653–1656
7. Bai XZ, Tian ZG, Zheng J (2009) Thermo-electric effects in fracture mechanics. National Defense Industry Press, Beijing (in Chinese)
8. Wu J, Li XH, Bai XZ (2005) Application of high voltage pulse discharging in metal crack arrest. J Exp Mech 20:411–416 (in Chinese)
9. Fu YM, Bai XZ, Zheng LJ (2001) Numerical simulation and experimental research on crack arresting using electromagnetic heat effects. Int J Nonlinear Sci Numer 2:375–378
10. Cai GX, Yuan FG (1998) Stresses around crack tip due to electric current and its self-induced magnetic field. Adv Eng Softw 29:297–306

11. Cai GX, Yuan FG (1999) Electric current-induced stresses at the crack tip in conductors. Int J Fract 96:279–301
12. Liu TJC (2008) Thermo-electro-structural coupled analyses of crack arrest by Joule heating. Theor Appl Fract Mech 49:171–184
13. Liu TJC (2011) Finite element modeling of melting crack tip under thermo-electric Joule heating. Eng Fract Mech 78:666–684
14. Cheng DK (1983) Field and wave electromagnetics. Addison-Wesley, Reading
15. Incropera FP, DeWitt DP (2002) Fundamentals of heat and mass transfer, 5th edn. Wiley, New York
16. Boresi AP, Chong KP (2000) Elasticity in engineering mechanics, 2nd edn. Wiley, New York
17. ANSYS, Inc. (2005) ANSYS HTML online documentation. SAS IP, Inc., USA
18. Tsai CL, Dai WL, Dickinson DW, Papritan JC (1991) Analysis and development of a real-time control methodology in resistance spot welding. Weld J 70:s339–s351
19. Braunovic M, Konchits VV, Myshkin NK (2007) Electrical contacts: fundamentals, applications and technology. CRC Press, Boca Raton
20. Liu S, Liu J, Ao T, Bai XZ (2004) Electric current density factor and its distribution. J Basic Sci Eng 12:121–126 (in Chinese)
21. Fan HL, Chen P (2005) Crack arrest effect in thin plates. Acta Armamentarii 26:791–794 (in Chinese)
22. Jin XQ, Li H (2006) On the analogy between the current density distribution in a thin conductive plate and the anti-plane shear problem. Mech Eng 28:23–27 (in Chinese)
23. Barsoum RS (1976) On the use of isoparametric finite elements in linear fracture mechanics. Int J Numer Meth Eng 10:25–37
24. Lim IL, Johnston IW, Choi SK (1992) Comparison between various displacement-based stress intensity factor computation techniques. Int J Fract 58:193–210
25. Liu TJC (2012) Local hot region at crack tip or notch tip under electric load and Joule heating effect. In: Proceedings of the 12th international conference on creep and fracture of engineering materials and structures (Creep 2012), Kyoto

Crack Surface Interference

► Crack Closure

Crack Surfaces Contact

► Crack Closure

Cracks in Transversely Isotropic and Inhomogeneous Elastic Solids

Ernian Pan[1,2], Chunying Dong[3], Ali Sangghaleh[2] and Yanfei Zhao[2]
[1]Henan Key Engineering Laboratory for Anti-fatigue Manufacturing Technology and the School of Mechanical Engineering, Zhengzhou University, Zhengzhou, People's Republic of China
[2]Department of Civil Engineering, Computer Modeling and Simulation Group, University of Akron, Akron, OH, USA
[3]Department of Mechanics, School of Aerospace Engineering, Beijing Institute of Technology, Beijing, People's Republic of China

Synonyms

Crack

Overview

Fracture mechanics is essential to the mechanical safety of structures, in which cracks and the corresponding stress intensity factors (SIFs) near their tips (fronts) are important [1]. In 1957, Irwin [2] introduced the SIFs to describe the stress and displacement fields near a crack tip. As it is well known, there are three basic crack modes: opening (mode I), sliding (mode II), and tearing (mode III). Determining the SIFs near the crack tip (or front) in linear elasticity is interesting yet challenging. While most previous studies in SIFs were focused on one or two fracture modes, mixed three-dimensional (3D) modes need to be considered as materials could be mostly failed under combined tensile/compressive, shearing, and tearing loads or the material under consideration is anisotropic (as for most composite materials). For 3D isotropic elastic materials, Singh et al. [3] obtained the SIFs using the concept of a universal crack closure integral. For transversely isotropic (TI), orthotropic, and anisotropic solids, Pan and Yuan [4] presented

the general relationship between the SIF and the relative crack opening displacement (COD). Lazarus et al. [5] compared the calculated SIFs with experimental results for brittle solids under mixed mode I-III or I-II-III loadings. The 3D SIFs were also calculated by Zhou et al. [6] using the variable-order singular boundary element. More recently, Yue et al. [7] employed the boundary element method (BEM) [8, 9] in their calculation of the 3D SIFs of an inclined square crack within a finite but bimaterial domain. Other representative works in this direction are those by Liu et al. [10], Blackburn [11], dell'Erba and Aliabadi [12], Partheymüller [13], Hatzigeorgiou and Beskos [14], Popov [15], Ariza and Dominguez [16], Lo et al. [17], and Zhao et al. [18]. The weakly singular and weak-form integral equation method recently proposed by Rungamornrat [19] and Rungamornrat and Mear [20] is also efficient in crack analysis in anisotropic media. Besides the analytical (integral equation) and BEM methods [21], other common methods, such as the finite difference (FD) [22–24] and finite element (FE) [25, 26], were also applied to the 3D SIF analysis. Since both the FD and FE methods require discretization of the whole problem domain, they could be time consuming and more expensive than the BEM in fracture analyses.

While BEM is an excellent choice for fracture mechanics analysis in a linear and homogeneous solid, material heterogeneity or inhomogeneity introduces complexity to this approach. Nevertheless, various progresses have been made in modifying BEM for the inhomogeneity systems, including composites, rock structures, porous and cracked media. Bush [27] investigated the interaction between a crack and a particle cluster in composites using the BEM. Also applying the BEM, Knight et al. [28] analyzed the effect of the constituent material properties, fiber spatial distribution, and microcrack damage on the local behavior of fiber-reinforced composites. Dong et al. [29] presented a general-purpose integral formulation in order to study the interaction between the inhomogeneity and cracks embedded in 3D isotropic matrices. Based on a symmetric Galerkin BEM, Kitey et al. [30] investigated the crack growth behavior in materials embedded with a cluster of inhomogeneities. Lee and Tran [31] applied the Eshelby equivalent inclusion method to carry out the stress analysis when a penny-shaped crack interacts with inhomogeneities and voids. Dong et al. [32] investigated the interaction between cracked TI inhomogeneous solids using a special BEM formulation. Interface cracks in two or more isotropic materials were also studied by Sladek and Sladek [33] and Liu and Xu [34]. Recent representative developments in this direction include the three-step multi-domain BEM solver [35], the subregion-by-subregion approach based on the Krylov solver [36, 37], and the well-known fast multipole BEM [38, 39].

In this entry, we will give a brief account on 3D linear fracture mechanics in TI inhomogeneous materials, based on the BEM approach. The field responses, the relative crack opening displacement (COD), as well as the SIFs will be discussed.

Governing Equations

– Equations of equilibrium

$$\sigma_{ij,j} + b_i = 0, \quad i,j = 1,2,3 \tag{1}$$

where σ_{ij} is the stress tensor; b_i the body force; and the subscript "j" denotes the partial differentiation with respect to the coordinates x, y, and z.

– Strain and displacement relation

$$\varepsilon_{ij} = 0.5\left(u_{i,j} + u_{j,i}\right), \quad i,j = 1,2,3 \tag{2}$$

where u_i is the elastic displacement.

– Constitutive relation

Again, we assume that the material is TI and we let the global z-axis be along the symmetry axis of the material. Then, the constitutive relation for this case can be written as

$$\begin{aligned}
\sigma_{xx} &= c_{11}\varepsilon_{xx} + c_{12}\varepsilon_{yy} + c_{13}\varepsilon_{zz} \\
\sigma_{yy} &= c_{12}\varepsilon_{xx} + c_{11}\varepsilon_{yy} + c_{13}\varepsilon_{zz} \\
\sigma_{zz} &= c_{13}\varepsilon_{xx} + c_{13}\varepsilon_{yy} + c_{33}\varepsilon_{zz} \\
\sigma_{yz} &= 2c_{44}\varepsilon_{yz};\ \sigma_{xz} = 2c_{44}\varepsilon_{xz};\ \sigma_{xy} = 2c_{66}\varepsilon_{xy}
\end{aligned} \tag{3}$$

where c_{ij} are the stiffness coefficients with $c_{66} = (c_{11}\text{-}c_{12})/2$. Thus, in a TI, there are only five independent material coefficients. In terms of the compliance coefficients (the inverse of the stiffness), the physical meanings of the five independent coefficients are: the Young's modulus and Poisson's ratio in the isotropic plane (i.e., the xoy plane), the Young's modulus and Poisson's ratio in the plane normal to the isotropic plane, and the shear modulus in the plane normal to the isotropic plane.

It is noted that since a crack may be oriented in any direction with respect to the TI material system, one usually needs to introduce two orientation angles, for instance, ψ and β [4, 40], to describe the relation between the material system and the crack orientation. Furthermore, one may need extra coordinate transforms between the material systems and the global space-fixed coordinate system if multiple material domains (inhomogeneous materials) are involved and/or the boundary conditions are described in terms of the global system.

The BEM for a Cracked Matrix with a Single Inhomogeneity

We start with a cracked matrix containing only one inhomogeneity. The single crack is located in the matrix. We now present the solution process based on the BEM. First, we discretize the cracked matrix in terms of the single-domain BEM [4]. In other words, we apply the following displacement and traction boundary integral equations [4]

$$\begin{aligned} b_{ij}u_j(y_S) = &\int_S U_{ij}(y_S, x_S)\, t_j(x_S) dS(x_S) \\ &- \int_S T_{ij}(y_S, x_S)\, u_j(x_S) dS(x_S) \\ &- \int_{\Gamma+} T_{ij}(y_S, x_{\Gamma+})\, [u_j(x_{\Gamma+}) \\ &- u_j(x_{\Gamma-})] d\Gamma(x_{\Gamma+}) + u_i^0(y_S) \end{aligned} \tag{4}$$

$$\begin{aligned} &[t_l(y_{\Gamma+}) - t_l(y_{\Gamma-})]/2 + n_m(y_{\Gamma+}) \\ &\int_S c_{lmik} T_{ij,k}(y_{\Gamma+}, x_S) u_j(x_S) dS(x_S) \\ &+ n_m(y_{\Gamma+}) \int_{\Gamma+} c_{lmik} T_{ij,k}(y_{\Gamma+}, x_{\Gamma+}) \\ &[u_j(x_{\Gamma+}) - u_j(x_{\Gamma-})] d\Gamma(x_{\Gamma+}) \\ &= n_m(y_{\Gamma+}) \int_S c_{lmik} U^*_{ij,k}(y_{\Gamma+}, x_S) t_j(x_S) dS(x_S) \\ &+ [t_l^0(y_{\Gamma+}) - t_l^0(y_{\Gamma-})]/2 \end{aligned} \tag{5}$$

to the cracked matrix. In (4) and (5), b_{ij} are the coefficients that depend only on the local geometries of the inhomogeneity–matrix interface S at $\boldsymbol{y}_s$. A point on the positive (negative) side of the cracks is denoted by $\boldsymbol{x}_{\Gamma+}$ ($\boldsymbol{x}_{\Gamma-}$), and on the inhomogeneity–matrix interface S by both $\boldsymbol{x}_s$ and $\boldsymbol{y}_s$; n_m is the unit outward normal of the positive side of the crack surface at $\boldsymbol{y}_{\Gamma+}$; c_{lmik} is the fourth-order stiffness tensor of the TI material; $u_i^0(y_s)$ is the i-th displacement component at point $\boldsymbol{y}_s$ corresponding to the given remote loading, and $t_l^0(y_{\Gamma+})$ and $t_l^0(y_{\Gamma-})$ the corresponding traction components along the l-direction at points $\boldsymbol{y}_{\Gamma+}$ and $\boldsymbol{y}_{\Gamma-}$; u_i and t_i are the displacements and tractions on the inhomogeneity–matrix interface S (or the crack surface Γ); U_{ij} and T_{ij} are the Green's functions of the displacements and tractions; $U_{ij,k}$ and $T_{ij,k}$ are, respectively, the derivatives of the Green's displacements and tractions with respect to the source point. The displacement and traction Green's functions are taken from Pan and Chou [41] while their derivatives are taken from Pan and Yuan [4]. It is noted that the single-domain boundary integral equations similar to (4) and (5) were applied to a cracked homogeneous solid before and it has been demonstrated that this single-domain BEM approach is very efficient. However, if there is also an inhomogeneity in the cracked domain, one needs another BEM equation. In other words, the displacement integral equation

needs to be applied to the surface of the inhomogeneity as follows [32]:

$$b_{ij}u_j(y_S) = \int_S U_{ij}(y_S, x_S)\, t_j(x_S) dS(x_S) - \int_S T_{ij}(y_S, x_S)\, u_j(x_S) dS(x_S) \tag{6}$$

Equations (4), (5), and (6) then can be utilized to investigate the effect of the inhomogeneity on the SIFs of the crack in a TI matrix as well as the internal field behaviors both within the inhomogeneity and the matrix. In discretization of these equations, the nine-node quadrilateral curved elements can be applied to the inhomogeneity–matrix interface and the crack surface with the crack front being treated by special elements [4].

Taking each node in turn as the collocation point and performing the involved integrals, we finally obtain the compact forms of the discretized equations from (4), (5), and (6) as

$$\begin{bmatrix} \mathbf{H}_{11} & \mathbf{H}_{12} \\ \mathbf{H}_{21} & \mathbf{H}_{22} \end{bmatrix} \begin{bmatrix} \mathbf{U}_m \\ \Delta\mathbf{U}_c \end{bmatrix} + \begin{bmatrix} \mathbf{B}_1 \\ \mathbf{B}_2 \end{bmatrix} = \begin{bmatrix} \mathbf{G}_{11} & \mathbf{G}_{12} \\ \mathbf{G}_{21} & \mathbf{G}_{22} \end{bmatrix} \begin{bmatrix} \mathbf{T}_m \\ \mathbf{T}_c \end{bmatrix} \tag{7}$$

and

$$\mathbf{H}_i\mathbf{U}_i = \mathbf{G}_i\mathbf{T}_i \tag{8}$$

where the subscripts i and m represent, respectively, the inhomogeneity and matrix; $\mathbf{H}$ and $\mathbf{G}$ are, respectively, the influence coefficient matrices containing integrals of the fundamental Green's function solutions; $\mathbf{B}_1$ and $\mathbf{B}_2$ are, respectively, the displacement and traction vectors induced by the remote loading; $\mathbf{U}_\mathrm{m}$ ($\mathbf{U}_\mathrm{i}$) and $\mathbf{T}_\mathrm{m}$ ($\mathbf{T}_\mathrm{i}$) are, respectively, the nodal displacement and traction vectors on the matrix side (inhomogeneity side) of the inhomogeneity–matrix interface; $\Delta\mathbf{U}_\mathrm{c}$ and $\mathbf{T}_\mathrm{c}$ are, respectively, the discontinuous displacement and traction vectors over the crack surface. In this entry, we assume that the tractions on both sides of the crack are equal and opposite, and thus, $\mathbf{T}_\mathrm{c}$ is equal to zero.

Using the continuity condition of the displacement and traction vectors along the interface, i.e., $\mathbf{U}_\mathrm{m} = \mathbf{U}_\mathrm{i}$ and $\mathbf{T}_\mathrm{m} = -\mathbf{T}_\mathrm{i}$, between the inhomogeneity and matrix, we can combine (7) and (8) into

$$\begin{bmatrix} \mathbf{H}_{11} + \mathbf{G}_{11}\mathbf{G}_i^{-1}\mathbf{H}_i & \mathbf{H}_{12} \\ \mathbf{H}_{21} + \mathbf{G}_{21}\mathbf{G}_i^{-1}\mathbf{H}_i & \mathbf{H}_{22} \end{bmatrix} \begin{Bmatrix} \mathbf{U}_m \\ \Delta\mathbf{U}_c \end{Bmatrix} = -\begin{Bmatrix} \mathbf{B}_1 \\ \mathbf{B}_2 \end{Bmatrix} \tag{9}$$

which can be solved for the unknowns $\mathbf{U}_\mathrm{m}$ and $\Delta\mathbf{U}_\mathrm{c}$. After that, a boundary integral equation similar to (4) or (6) can be applied to find the internal displacements and their gradients (by taking the derivatives) inside the matrix or the inhomogeneity. It is pointed out that in discretizing the boundary and the crack face, besides the regular shape functions, special ones need to be applied. For instance, the discontinuous elements need to be introduced to handle the common edge of the displacement and traction boundary conditions, and the common edge of the displacement/traction boundary and the crack surface. Furthermore, special shape functions have to be utilized to the elements adjacent to the crack front to make sure that the relative COD is proportional to $\sqrt{r}$ where r is the distance behind the crack front. These discontinuous/special elements along with their corresponding shape functions can be found in Pan and Yuan [4].

Once the relative COD $\Delta\mathbf{U}_\mathrm{c}$ is solved in the global coordinates, it can be transformed to the local coordinates (or the crack-tip coordinates) to find the SIFs. Assuming that the crack front is smooth and that the crack tip is away from the possible corner of the problem geometry, then the singular term (in the sense of stresses) in the asymptotic expansion of the displacement field near the crack tip (front) satisfies the generalized plane-strain condition in the local coordinates. Actually, if we let r be the distance behind the crack front, then in terms of the relative CODs in

the crack-tip coordinate, the three SIFs can be expressed as follows:

$$\begin{Bmatrix} K_{II} \\ K_I \\ K_{III} \end{Bmatrix} = 2\sqrt{\frac{2r}{\pi}}\mathbf{L}^{-1}\begin{Bmatrix} \Delta u_1 \\ \Delta u_2 \\ \Delta u_3 \end{Bmatrix} \tag{10}$$

where $\mathbf{L}$ is the Barnett-Lothe tensors [42] which depends only on the anisotropic properties of the solid in the crack-front coordinates, and Δu_1, Δu_2, and Δu_3 are the relative CODs in the local crack-front coordinates. We also point out that r in (10) was selected to be a very small value as compared to the crack size [4, 32, 40]. For a penny-shaped crack lying in the isotropic plane of the TI material, the SIF can be calculated analytically [43], which can be used as the benchmark for BEM modeling. The result was extended to the bimaterial case where the crack was located on the interface plane [44].

General Inhomogeneity Problems with Multiple Cracks

It is obvious that the approach presented above can be extended to the multi-inhomogeneity case with multiple cracks. However, there are more efficient approaches proposed recently to the problems in inhomogeneous or heterogeneous media, as discussed briefly below.

Three-step Multi-domain BEM

The three-step multi-domain BEM solution technique [35] can be used to effectively solve the problems consisting of any number of arbitrarily distributed sub-domains. In the multi-domain BEM technique, nodes are arranged in the following order: The "self nodes" which are used only by the considered sub-domain itself are collocated first; the "common nodes" which are shared by two adjacent sub-domains are collocated next; and the "internal nodes" which are located inside a sub-domain are arranged in the last step. The three-step multi-domain BEM solution technique will produce condensations by eliminating the internal unknowns (internal nodal displacements) and boundary unknowns (self-nodal quantities) so that the final multi-domain BEM formula only contains the common nodal displacements. Since the number of degrees of freedom in the system is reduced by this technique and the coefficient matrix is blocked sparse, the computational efficiency of large-scale problems can be improved.

Subregion-by-subregion with Krylov Solver

In general, this approach contains two main parts: (1). A robust subregion-by-subregion (SBS) technique, which is necessary for coping with heterogeneous materials. (2). The efficient integration procedures, which are needed for evaluating the singular and nearly singular integrals involved in the BEM. The SBS technique is based on the use of the Krylov solver, which allows the treatment of a large number of inhomogeneities. The diagonal-preconditioned bi-conjugate gradient solver is employed to solve the resulting linear system of equations. A detailed description on this method can be found in the work by Araujo and coworkers [36, 37].

Fast Multipole BEM

With the development of the fast multipole methods (FMMs) [39, 45] for solving boundary integral equations, large models with several million degrees of freedom can be solved readily on a desktop computer. Rokhlin and Greengard [46], who pioneered the FMM, and coworkers [47] have done extensive research on the FMM in the context of potential fields. Fu et al. [48] formulated the boundary integral equations for the 3D elastic inclusion problem using the FMM. Solutions for up to 343 spherical voids in an elastic domain were computed using the parallel FMM BEM code with total degrees of freedom around 400 K. Some other developments of the fast multipole BEM can be found in Pierce and Napier [49] and Popov and Power [50] for general elasticity problems, and in Nishimura et al. [51], Yoshida et al. [52], and Lai and Rodin [53] for crack problems. To develop an FMM for BEM, one needs simple and appropriate expressions of the two-point Green's functions of the associated problem domain, and their suitable expansion, i.e., the multipole expansion.

For most linear systems, the two-point Green's functions can be successfully expanded and therefore, the three key translations in FMM can be achieved (M2M, L2L, and M2L) [38, 39].

Future Directions for Research

Solution to the penny-shaped crack problem in pure elasticity is a benchmark, and it has been extended to the multiphase material couplings [54–57]. For instance, Zhao et al. [54] derived the solution for an ellipsoidal cavity in an infinite TI magneto-electro-elastic medium, and obtained the exact closed-form solution for a penny-shaped crack by letting the minor axis of the ellipsoidal cavity approach zero. Zhao et al. [55] analyzed the planar crack of arbitrary shape in the isotropic plane of a 3D TI magneto-electro-elastic medium by using the hyper-singular integral equation method. Niraula and Wang [56] derived an exact closed-form solution for a penny-shaped crack in an infinite magneto-electro-thermo-elastic medium under a temperature field, where the problem was transformed into the dual integral equations which were solved directly. Wang and Niraula [57] further considered the transient thermal fracture problem of TI magneto-electro-elastic materials, where the problem is reduced to an integral equation which was treated exactly using the Abel's integral equation. The fracture properties of a penny-shaped crack embedded in a magneto-electro-elastic layer of finite height under both thermal flow and radial shear loads were investigated by Feng et al. [58]. Thermally insulated crack surface assumption is adopted. By means of the Hankel transform technique, the problem was reduced to a Fredholm integral equation, which is different to that addressed previously [54–57].

Acknowledgment This work was partially supported by the Dept. of Civil Engineering, University of Akron, Henan Province, National Natural Science Foundation of China (11072034, 11172273), and the Major Program of National Natural Science Foundation of China (11132011).

References

1. Anderson TL (1995) Fracture mechanics – fundamentals and applications. CRC Press, London
2. Irwin GR (1957) Analysis of stresses and strains near the end of a crack traversing a plate. J Appl Mech 24:361–364
3. Singh R, Carter BJ, Wawrzynek PA, Ingraffea AR (1998) Universal crack closure integral for SIF estimation. Eng Fract Mech 60(2):133–146
4. Pan E, Yuan FG (2000) Boundary element analysis of three-dimensional cracks in anisotropic solids. Int J Numer Meth Eng 48:211–237
5. Lazarus V, Leblond JB, Mouchrif SE (2001) Crack front rotation and segmentation in mixed mode I + III or I + II + III. part I: calculation of stress intensity factors. J Mech Phys Solids 49:1399–1420
6. Zhou W, Lim KM, Lee KH, Tay AAO (2005) A new variable-order singular boundary element for calculating stress intensity factors in three-dimensional elasticity problems. Int J Solids Struct 42:159–185
7. Yue ZQ, Xiao HT, Pan E (2007) Stress intensity factors of square crack inclined to interface of transversely isotropic bi-material. Eng Anal Bound Elem 31:50–65
8. Hong HK, Chen JT (1988) Derivations of integral equations of elasticity. J Eng Mech ASCE 114(6):1028–1044
9. Chen JT, Hong HK (1999) Review of dual boundary element methods with emphasis on hypersingular integrals and divergent series. Appl Mech Rev ASME 52(1):17–33
10. Liu Y, Liang LH, Hong QC, Antes H (1999) Nonlinear surface crack analysis by three-dimensional boundary elements with mixed boundary conditions. Eng Fract Mech 63:413–424
11. Blackburn WS (1999) Three dimensional calculation of growth of cracks starting in parallel planes by boundary elements. Int J Fatigue 21:933–939
12. dell'Erba DN, Aliabadi MH (2000) On the solution of three-dimensional thermoelastic mixed-mode edge crack problems by the dual boundary element method. Eng Fract Mech 66:269–285
13. Partheymüller P, Haas M, Kuhn G (2000) Comparison of the basic and the discontinuity formulation of the 3D-dual boundary element method. Eng Anal Bound Elem 24:777–788
14. Hatzigeorgiou GD, Beskos DE (2000) Static analysis of 3D damaged solids and structures by BEM. Eng Anal Bound Elem 26:521–526
15. Popov V, Power H, Walker SP (2003) Numerical comparison between two possible multipole alternatives for the BEM solution of 3D elasticity problems based upon Taylor series expansions. Eng Anal Bound Elem 27:521–531
16. Ariza MP, Dominguez J (2004) Dynamic BE analysis of 3-D cracks in transversely isotropic solids. Comput Meth Appl Mech Eng 193:765–779

17. Lo SH, Dong CY, Cheung YK (2005) Integral equation approach for 3D multiple-crack problems. Eng Fract Mech 72:1830–1840
18. Zhao MH, Fan CY, Yang F, Liu T (2007) Analysis method of planar cracks of arbitrary shape in the isotropic plane of a three-dimensional transversely isotropic magnetoelectroelastic medium. Int J Solids Struct 44:4505–4523
19. Rungamornrat J (2006) Analysis of 3D cracks in anisotropic multi-material domain with weakly singular SGBEM. Eng Anal Bound Elem 30:834–846
20. Rungamornrat J, Mear ME (2008) Weakly-singular, weak-form integral equations for cracks in three-dimensional anisotropic media. Int J Solids Struct 45:1283–1301
21. Noda NA, Xu C (2008) Controlling parameter of the stress intensity factors for a planar interfacial crack in three-dimensional biomaterials. Int J Solids Struct 45(3–4):1017–1031
22. Chen YM (1975) Numerical computation of dynamic stress intensity factors by a Lagrangian finite-difference method (the HEMP code). Eng Fract Mech 7(4):653–660
23. Altus E (1984) The finite difference technique for solving crack problems. Eng Fract Mech 19(5): 947–957
24. Dorogoy A, Banks-Sills L (2005) Effect of crack face contact and friction on Brazilian disk specimens—a finite difference solution. Eng Fract Mech 72(18): 2758–2773
25. Leung AYT, Su RKL (1995) A numerical study of singular stress field of 3D cracks. Finite Elem Anal Des 18:389–401
26. He WJ, Lin Y, Ding HJ (1997) A three-dimensional formula for determining stress intensity factors in finite element analysis of cracked bodies. Eng Fract Mech 57(4):409–415
27. Bush MB (1997) The interaction between a crack and a particle cluster. Int J Fract 88:215–232
28. Knight MG, Wrobel LC, Henshall JL (2003) Fracture response of fibre-reinforced materials with macro/microcrack damage using the boundary element technique. Int J Fract 121:163–182
29. Dong CY, Lo SH, Cheung YK (2003) Numerical analysis of the inclusion-crack interactions using an integral equation. Comput Mech 30:119–130
30. Kitey R, Phan AV, Tippur HV, Kaplan T (2006) Modeling of crack growth through particulate clusters in brittle matrix by symmetric-Galerkin boundary element method. Int J Fract 141:11–25
31. Lee HK, Tran XH (2010) On stress analysis for a penny-shaped crack interacting with inclusions and voids. Int J Solids Struct 47:549–558
32. Dong CY, Yang X, Pan E (2011) Analysis of cracked transversely isotropic and inhomogeneous solids by a special BIE formulation. Eng Anal Bound Elem 35:200–206
33. Sladek J, Sladek V (1995) Boundary element analysis for an interface crack between dissimilar elastoplastic materials. Comput Mech 16:396–405
34. Liu YJ, Xu N (2000) Modeling of interface cracks in fiber-reinforced composites with the presence of interphases using the boundary element method. Mech Mater 32(12):769–783
35. Gao XW, Guo L, Zhang CH (2007) Three-step multi-domain BEM solver for nonhomogeneous material problems. Eng Anal Bound Elem 31:965–973
36. Araujo FC, Gray LJ (2008) Analysis of thin-walled structural elements via 3D standard BEM with generic substructuring. Comp Mech 41:633–645
37. Araujo FC, d'Azevedo EF, Gray LJ (2010) Boundary-element parallel-computing algorithm for the micro-structural analysis of general composites. Comp Struct 88:773–784
38. Nishimura N (2002) Fast multipole accelerated boundary integral equation methods. Appl Mech Rev 55:299–324
39. Liu YJ (2009) Fast multipole boundary element method, Theory and applications in engineering. Cambridge University Press, Cambridge
40. Chen CS, Chen CH, Pan E (2009) Three-dimensional stress intensity factors of a central square crack in a transversely isotropic cuboid with arbitrary material orientations. Eng Anal Bound Elem 33:128–136
41. Pan YC, Chou TW (1976) Point force solution for an infinite transversely isotropic solid. J Appl Mech 43:608–612
42. Ting TCT (1996) Anisotropic elasticity: theory and applications. Oxford University Press, Oxford
43. Hoenig A (1982) Near-tip behavior of a crack in a plane anisotropic elastic body. Eng Fract Mech 16:393–403
44. Qu J, Xue Y (1999) Three-dimensional interface cracks in anisotropic bimaterials – The non-oscillatory case. J Appl Mech 65:1048–1055
45. Liu YJ, Nishimura N, Otani Y, Takahashi T, Chen XL, Munakata H (2005) A fast boundary element method for the analysis of fiber-reinforced composites based on a rigid-inclusion model. J Appl Mech 72:115–128
46. Rokhlin V, Greengard LF (1987) A fast algorithm for particle simulations. J Comput Phys 73:325–348
47. Cheng H, Rokhlin V, Greengard LF (1999) A fast adaptive multipole algorithm in three dimensions. J Comput Phys 155:468–498
48. Fu Y, Klimkowski KJ, Rodin GJ, Berger E, Browne JC, Singer JK, Geijn RAVD, Vemaganti KS (1998) A fast solution method for three-dimensional many-particle problems of linear elasticity. Int J Numer Meth Eng 42:1215–1229
49. Peirce AP, Napier JAL (1995) A spectral multipole method for efficient solution of large-scale boundary element models in elastostatics. Int J Numer Meth Eng 38:4009–4034

50. Popov V, Power H (2001) An O(N) Taylor series multipole boundary element method for three-dimensional elasticity problems. Eng Anal Bound Elem 25:7–18
51. Nishimura N, Yoshida K, Kobayashi S (1999) A fast multipole boundary integral equation method for crack problems in 3D. Eng Anal Bound Elem 23:97–105
52. Yoshida K, Nishimura N, Kobayashi S (2001) Application of fast multipole Galerkin boundary integral equation method to crack problems in 3D. Int J Numer Meth Eng 50:525–547
53. Lai YS, Rodin GJ (2003) Fast boundary element method for three-dimensional solids containing many cracks. Eng Anal Bound Elem 27:845–852
54. Zhao MH, Yang F, Liu T (2006) Analysis of a penny-shaped crack in a magneto-electro-elastic medium. Philos Mag 86:4397–4416
55. Zhao MH, Fan CY, Liu T, Yang F (2007) Extended displacement discontinuity Green's functions for three-dimensional transversely isotropic magneto-electro-elastic media and applications. Eng Anal Bound Elem 31:547–558
56. Niraula OP, Wang BL (2006) Thermal stress analysis in magneto- electro-thermo-elasticity with a penny-shaped crack under uniform heat flow. J Therm Stresses 29:423–437
57. Wang BL, Niraula OP (2007) Transient thermal fracture analysis of transversely isotropic magneto-electro-elastic materials. J Therm Stresses 30: 297–317
58. Feng WJ, Pan E, Wang X (2008) Stress analysis of a penny-shaped crack in magneto-electro-thermo-elastic layer under uniform heat flow and shear loads. J Therm Stresses 31:497–514

Crack-Tip Singular Fields in Functionally Graded Materials

Zhihe Jin
Department of Mechanical Engineering, University of Maine, Orono, ME, USA

Overview

This entry introduces the asymptotic temperature, thermal flux, stress, and displacement fields near the tip of a crack in a functionally graded material (FGM) with continuous and piecewise differentiable material properties. This entry begins with the introduction of basic equations of heat conduction, thermoelasticity, and thermoplasticity for FGMs. The eigenfunction expansion method is then employed to prove that the governing equations of the crack-tip dominant solutions of temperature and stress functions remain the same as the corresponding equations for homogeneous materials in every differentiable piece near the crack tip. Hence, the inverse square-root singular thermal flux and stress fields still prevail at the crack tip in a thermoelastic FGM, and the near-tip HRR field exists for a power-law hardening FGM. The effects of material property gradients on the dominance of the crack-tip singular fields are also discussed.

Introduction

Functionally graded materials (FGMs) represent a new concept of tailoring materials with microstructural and property gradients to achieve optimized performance. FGMs were originally conceived as high-temperature-resistant materials for aircraft and aerospace applications. The FGM concept has since spread to other areas, for example, tribological coatings, diesel engines, energy conversion systems, biomedical engineering, and so on. An FGM is a multiphase material with volume fractions of the constituents varying gradually in a predetermined (designed) profile, thus yielding a nonuniform microstructure in the material with continuously graded properties. In applications involving severe thermal gradients, FGMs exploit the heat, oxidation, and corrosion resistance typical of ceramics and the strength, ductility, and toughness typical of metals. Damage tolerance and defect assessments for structural integrity of FGM components require knowledge of the fracture behavior of FGMs.

From the fracture mechanics point of view, materials fail by the initiation and unstable growth of macroscopic cracks. Fracture parameters often arise from analyses of the asymptotic stress and deformation fields near the crack tip. The validity of continuum fracture mechanics to predict material failure lies in the fact that the fracture process zone around the crack tip is contained in a singular field of continuum

mechanics and the failure is governed by the controlling parameter(s) of the crack-tip singular fields. The study of fracture mechanics of FGMs thus begins with analyses of crack-tip asymptotic stress and deformation fields.

This entry introduces the asymptotic temperature, thermal flux, stress, and displacement fields near the tip of a crack in an FGM. Both thermoelastic and thermoelastic-plastic FGMs are considered. The material properties of the FGM are assumed to be continuous and piecewise continuously differentiable. The remainder of this entry is organized as follows. The basic thermoelasticity and thermoplasticity equations of FGMs are described in Section 2. Section 3 presents the asymptotic temperature and heat flux fields near a crack tip. Section 4 introduces the crack-tip stress and displacement fields in a thermoelastic FGM. Section 5 considers a crack in a thermoelastic-plastic FGM. The effects of material gradation on the dominance of the crack-tip singular fields are also discussed.

Thermoelasticity and Thermoplasticity Equations of FGMs

Fracture behavior of FGMs is generally investigated in the standard micromechanics/continuum framework, that is, FGMs are treated as macroscopically nonhomogeneous materials with space-dependent thermomechanical properties approximately evaluated from the conventional micromechanics models of composite materials. Moreover, an uncoupled approach is adopted in quasi-static thermal fracture problems in which the influence of deformation on temperature is ignored, and hence the temperature field is obtained independently of deformations.

Heat Conduction

The Fourier law of heat conduction in isotropic FGMs is given by

$$q_i = -k(\boldsymbol{x})\frac{\partial T}{\partial x_i} \tag{1}$$

where T is the temperature, q_i the heat fluxes, and $k(\boldsymbol{x})$ the space-dependent thermal conductivity. The Latin indices have the range 1, 2, and 3, and repeated indices imply summation over the range of the index. Equation (1) has been written in rectangular Cartesian coordinates $\boldsymbol{x} = (x_1, x_2, x_3)$ which will also be denoted by (x, y, z).

The governing equation of the temperature for isotropic FGMs without consideration of a heat source/sink is

$$k(\boldsymbol{x})\nabla^2 T + \frac{\partial k}{\partial x_i}\frac{\partial T}{\partial x_i} = \rho(\boldsymbol{x})c(\boldsymbol{x})\frac{\partial T}{\partial t} \tag{2}$$

where t is time, $\rho(\boldsymbol{x})$ the mass density, $c(\boldsymbol{x})$ the specific heat, and ∇^2 the Laplacian operator.

Thermoelasticity

The basic equations of thermoelasticity of isotropic FGMs include the equations of equilibrium (in the absence of body forces)

$$\sigma_{ij,j} = 0 \tag{3}$$

the strain–displacement relations for infinitesimal deformations

$$\varepsilon_{ij} = \frac{1}{2}\left(u_{i,j} + u_{j,i}\right) \tag{4}$$

and the constitutive relation

$$\varepsilon_{ij} = \frac{1+\nu(\boldsymbol{x})}{E(\boldsymbol{x})}\sigma_{ij} - \frac{\nu(\boldsymbol{x})}{E(\boldsymbol{x})}\sigma_{kk}\delta_{ij} + \alpha(\boldsymbol{x}) \times (T - T_0)\delta_{ij}. \tag{5}$$

In (3–5), σ_{ij} denote stresses, ε_{ij} strains, u_i displacements, δ_{ij} the Kronecker delta, $E(\boldsymbol{x})$ Young's modulus, $\nu(\boldsymbol{x})$ Poisson's ratio, $\alpha(\boldsymbol{x})$ the coefficient of thermal expansion, T_0 the reference temperature, and a comma followed by the index j implies partial derivative with respect to x_j.

Under plane stress conditions, the equilibrium equations can be satisfied by expressing stresses in terms of the Airy stress function F as follows:

$$\sigma_{xx} = \frac{\partial^2 F}{\partial y^2}, \sigma_{yy} = \frac{\partial^2 F}{\partial x^2}, \sigma_{xy} = -\frac{\partial^2 F}{\partial x \partial y} \tag{6}$$

The governing equation of the Airy function can be obtained using the constitutive relation (5) and the strain compatibility conditions as follows:

$$\nabla^2\left(\frac{1}{E}\nabla^2 F\right) - \frac{\partial^2}{\partial y^2}\left(\frac{1+v}{E}\right)\frac{\partial^2 F}{\partial x^2} - \frac{\partial^2}{\partial x^2} \times \left(\frac{1+v}{E}\right)\frac{\partial^2 F}{\partial y^2} + 2\frac{\partial^2}{\partial x \partial y}\left(\frac{1+v}{E}\right)\frac{\partial^2 F}{\partial x \partial y} = -\nabla^2[\alpha(T-T_0)] \tag{7}$$

where ∇^2 is the Laplacian operator in the x-y plane. For plane strain deformations, E, v, and α are replaced by $E/(1-v^2)$, $v/(1-v)$, and $(1+v)\alpha$, respectively.

The material parameters of an FGM (E, v, α, and so on) can be calculated from micromechanics models or can be assumed as elementary functions which are consistent with the micromechanics analyses. The properties are usually continuous and piecewise continuously differentiable functions of spatial coordinates.

Thermoplasticity

When investigating stationary crack-tip fields in elastic–plastic FGMs, it may be appropriate to use the constitutive law of deformation plasticity with space-dependent material properties. For a power-law hardening material described by the Ramberg-Osgood model, the stress–strain relationship of the deformation plasticity can be expressed as

$$\varepsilon_{ij} = \frac{1+v}{E}s_{ij} + \frac{1-2v}{3E}\sigma_{kk}\delta_{ij} + \frac{3}{2}\alpha_p {\sigma_e}^{n-1} s_{ij} + \alpha(T-T_0)\delta_{ij} \tag{8}$$

where $\alpha_{\mathrm{p}} = \alpha_{\mathrm{p}}(\boldsymbol{x})$ is a (dimensional) material parameter in the Ramberg-Osgood model, $n = n(\boldsymbol{x})$ is the hardening exponent, s_{ij} are the deviatoric stress components given by

$$s_{ij} = \sigma_{ij} - \frac{1}{3}\sigma_{kk}\delta_{ij} \tag{9}$$

and σ_{e} is the effective stress defined by

$$\sigma_{\mathrm{e}} = \sqrt{\frac{3}{2}s_{ij}s_{ij}} \tag{10}$$

Under plane stress conditions, the basic equation of the Airy stress function for the power-law hardening FGM is given by

$$\nabla^2\left(\frac{1}{E}\nabla^2 F\right) - \frac{\partial^2}{\partial y^2}\left(\frac{1+v}{E}\right)\frac{\partial^2 F}{\partial x^2} - \frac{\partial^2}{\partial x^2}\left(\frac{1+v}{E}\right) \times \frac{\partial^2 F}{\partial y^2} + 2\frac{\partial^2}{\partial x \partial y}\left(\frac{1+v}{E}\right)\frac{\partial^2 F}{\partial x \partial y} + \frac{\partial^2}{\partial x^2} \left[\alpha_p \sigma_e^{n-1}\left(\frac{\partial^2 F}{\partial x^2} - \frac{1}{2}\frac{\partial^2 F}{\partial y^2}\right)\right] + \frac{\partial^2}{\partial y^2} \left[\alpha_p \sigma_e^{n-1}\left(\frac{\partial^2 F}{\partial y^2} - \frac{1}{2}\frac{\partial^2 F}{\partial x^2}\right)\right] + 3\frac{\partial^2}{\partial x \partial y} \left[\alpha_p \sigma_e^{n-1}\frac{\partial^2 F}{\partial x \partial y}\right] + \nabla^2[\alpha(T-T_0)] = 0 \tag{11}$$

Temperature and Heat Flux Fields near a Crack Tip

Consider a crack in an FGM with continuous and piecewise differentiable thermal properties, as shown in Fig. 1, where (r, θ) are the polar coordinates centered at the crack tip which terminates at the boundary L between two differentiable pieces. The thermal properties of the FGM are continuously differentiable in each piece, continuous across the boundary L, and their derivatives with respect to the spatial coordinates may undergo jumps across L. Assume that the temperature has the following asymptotic expansion in each differentiable piece at the crack tip:

$$\begin{aligned} &T = R_1(t) r^{\delta_1}\tilde{T}_1(\theta), r \to 0, -\pi < \theta < -(\pi - \theta_L) \\ &T = R_2(t) r^{\delta_2}\tilde{T}_2(\theta), r \to 0, -(\pi - \theta_L) < \theta < \theta_L \\ &T = R_3(t) r^{\delta_3}\tilde{T}_3(\theta), r \to 0, \theta_L < \theta < \pi \end{aligned} \tag{12}$$

where δ_{i} ($i = 1, 2, 3$) are the eigenvalues to be determined and $\tilde{T}_i(\theta)$ ($i = 1, 2, 3$) are the angular distributions of the temperature. The thermal properties can be expanded into Taylor series at

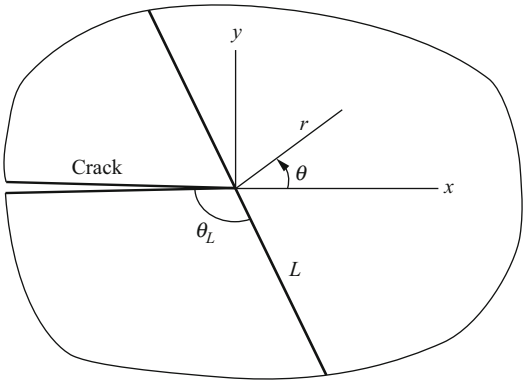

Crack-Tip Singular Fields in Functionally Graded Materials, Fig. 1 A crack terminating at the boundary between two differentiable pieces in a functionally graded material

the crack tip in each differentiable piece. For example, the thermal conductivity has the expansion as follows:

$$\begin{aligned} k &= k_{tip} + a_{11}x + b_{11}y + \ldots, \ -\pi < \theta < -(\pi - \theta_L) \\ k &= k_{tip} + a_{12}x + b_{12}y + \ldots, \ -(\pi - \theta_L) < \theta < \theta_L \\ k &= k_{tip} + a_{13}x + b_{13}y + \ldots, \ \theta_L < \theta < \pi \end{aligned} \tag{13}$$

where $(x, y) = (r\cos\theta, r\cos\theta)$ are the rectangular coordinates, k_{tip} is the thermal conductivity at the crack tip, and a_{ij} and b_{ij} are constants related to the derivatives of the thermal conductivity at the crack tip in the differentiable pieces. Similarly, the mass density and specific heat can also be expanded into Taylor series in each differentiable piece. By substituting (12) and (13) and the expansions of specific heat and mass density into the governing equation (2), we can find that the first term on the left-hand side dominates the other terms near the crack tip, and hence the dominant term for the temperature still satisfies the Laplacian equation in every differentiable piece, that is,

$$\nabla^2 T = 0 \tag{14}$$

which is the same as that for homogeneous materials. Thus, the dominant solution for the homogeneous material [1] is also the solution for the FGM in every differentiable piece and satisfies the temperature and heat flux continuity conditions across the boundary between the differentiable pieces as long as the thermal conductivity is continuous. Hence, the crack-tip temperature and heat flux fields have the following forms:

$$T = R(t)\sqrt{2r}\sin\frac{\theta}{2} \tag{15}$$

$$\begin{aligned} q_r &= -k_{tip}\frac{\partial T}{\partial r} = -k_{tip}\frac{R(t)}{\sqrt{2r}}\sin\frac{\theta}{2}, \\ q_\theta &= -k_{tip}\frac{\partial T}{r\partial\theta} = -k_{tip}\frac{R(t)}{\sqrt{2r}}\cos\frac{\theta}{2} \end{aligned} \tag{16}$$

where $R(t)$ describes the intensity of the crack-tip singular thermal flux field and cannot be determined by the local asymptotic analysis. The above conclusion on the crack-tip temperature and heat flux fields in FGMs was reached by Jin and Noda [2] and Noda and Jin [3].

Crack-Tip Fields in Thermoelastic FGMs

Consider a cracked thermoelastic FGM, as shown in Fig. 1, where the crack tip terminates at the boundary between the two differentiable pieces. We assume that Young's modulus $E(\boldsymbol{x})$, Poisson's ratio $\nu(\boldsymbol{x})$, and the coefficient of thermal expansion $\alpha(\boldsymbol{x})$ are continuous and piecewise differentiable functions of spatial position. Jin and Noda [2] and Noda and Jin [3] proved that the crack-tip stress and deformation fields in FGMs with continuous and piecewise differential properties have the same forms as those for homogeneous elastic materials, which is an extension of Eischen's result [4] for nonhomogeneous materials with continuously differentiable properties. Assume the following asymptotic expansion of the Airy stress function near the crack tip:

$$\begin{aligned} F &= r^{s_1}\tilde{F}_1(\theta), \ r \to 0, -\pi < \theta < -(\pi - \theta_L) \\ F &= r^{s_2}\tilde{F}_2(\theta), \ r \to 0, -(\pi - \theta_L) < \theta < \theta_L \\ F &= r^{s_3}\tilde{F}_3(\theta), \ r \to 0, \theta_L < \theta < \pi \end{aligned} \tag{17}$$

where s_{i} $(i = 1, 2, 3)$ are the eigenvalues to be determined and $\tilde{F}_i(\theta)$ $(i = 1, 2, 3)$ are the angular distributions of the Airy function. At the same

time, the elastic modulus can be expanded into a Taylor series at the crack tip in each differentiable piece as follows:

$$\begin{aligned} E &= E_{tip} + a_{11}x + b_{11}y + \ldots, \ -\pi < \theta < -(\pi - \theta_L) \\ E &= E_{tip} + a_{12}x + b_{12}y + \ldots, \ -(\pi - \theta_L) < \theta < \theta_L \\ E &= E_{tip} + a_{13}x + b_{13}y + \ldots, \ \theta_L < \theta < \pi \end{aligned} \tag{18}$$

where E_{tip} is the modulus at the crack tip and a_{ij} and b_{ij} are constants related to the derivatives of Young's modulus at the crack tip in the differentiable pieces. Similarly, Poisson's ratio and the coefficient of thermal expansion can also be expanded into Taylor series in each differentiable piece. Substituting (17) and (18) and the temperature field (15) into the governing equation (7) and keeping only the dominant terms, we obtain

$$\nabla^2\nabla^2 F = 0 \tag{19}$$

which holds true in every differentiable piece. The singular solution to homogeneous materials [5] satisfies the same equation. Thus, it is also the dominant solution to the FGM in every differentiable piece. The continuities in displacements and tractions across the boundary between the differentiable pieces are maintained by this solution as long as Young's modulus and Poisson's ratio are continuous. Hence, the crack-tip stress and displacement fields in FGMs have the same forms as those in homogeneous materials [6] provided the material properties are continuous and piecewise differentiable. Thus, the crack-tip stress and displacement fields are given as follows:

$$\begin{aligned} \sigma_{xx} &= \frac{K_I}{\sqrt{2\pi r}} \cos\frac{\theta}{2}\left(1 - \sin\frac{\theta}{2}\sin\frac{3\theta}{2}\right) \\ &\quad - \frac{K_{II}}{\sqrt{2\pi r}} \sin\frac{\theta}{2}\left(2 + \cos\frac{\theta}{2}\cos\frac{3\theta}{2}\right) \\ \sigma_{yy} &= \frac{K_I}{\sqrt{2\pi r}} \cos\frac{\theta}{2}\left(1 + \sin\frac{\theta}{2}\sin\frac{3\theta}{2}\right) \\ &\quad + \frac{K_{II}}{\sqrt{2\pi r}} \sin\frac{\theta}{2}\cos\frac{\theta}{2}\cos\frac{3\theta}{2} \\ \sigma_{xy} &= \frac{K_I}{\sqrt{2\pi r}} \sin\frac{\theta}{2}\cos\frac{\theta}{2}\cos\frac{3\theta}{2} \\ &\quad + \frac{K_{II}}{\sqrt{2\pi r}} \cos\frac{\theta}{2}\left(1 - \sin\frac{\theta}{2}\sin\frac{3\theta}{2}\right) \end{aligned} \tag{20}$$

$$\begin{aligned} u_x &= \frac{K_I}{4\mu_{tip}}\sqrt{\frac{r}{2\pi}}\left[(2\kappa_{tip} - 1)\cos\frac{\theta}{2} - \cos\frac{3\theta}{2}\right] \\ &\quad + \frac{K_I}{4\mu_{tip}}\sqrt{\frac{r}{2\pi}}\left[(2\kappa_{tip} + 3)\sin\frac{\theta}{2} + \sin\frac{3\theta}{2}\right] \\ u_y &= \frac{K_I}{4\mu_{tip}}\sqrt{\frac{r}{2\pi}}\left[(2\kappa_{tip} + 1)\sin\frac{\theta}{2} - \sin\frac{3\theta}{2}\right] \\ &\quad - \frac{K_I}{4\mu_{tip}}\sqrt{\frac{r}{2\pi}}\left[(2\kappa_{tip} - 3)\cos\frac{\theta}{2} + \cos\frac{3\theta}{2}\right] \end{aligned} \tag{21}$$

where K_{I} and K_{II} are mode I and mode II stress intensity factors (SIFs), respectively, μ_{tip} is the shear modulus at the crack tip, $\kappa_{\text{tip}} = 3 - 4\nu_{\text{tip}}$ for plane strain, and $\kappa_{\text{tip}} = (3 - \nu_{\text{tip}})/(1 + \nu_{\text{tip}})$ for plane stress with ν_{tip} being the Poisson's ratio at the crack tip. Equations (20) and (21) indicate that material nonhomogeneities influence the crack-tip stress and displacement solutions only through SIFs. The sameness of the crack-tip fields between homogeneous and nonhomogeneous materials implies that the SIF concept can still be used to study the linear elastic fracture behavior of FGMs and the SIF is the fracture driving force.

Equations (20) and (21) are the dominant stress and displacement solutions near the crack tip. They can be used to represent the complete stress and displacement fields at points very close to the crack tip as compared with the crack length or any other characteristic lengths of the cracked body. The region in which the solutions (20) and (21) hold is called the *K*-dominance zone. While gradients of the elastic modulus do not influence the inverse square-root singularity, they may affect the size of the *K*-dominance zone. Jin and Batra [7] estimated the effect of material gradation on the size of the *K*-dominance zone based on the governing equation (7) and the asymptotic solution (20). Equation (7) can be rewritten as

$$\begin{aligned} &\frac{1}{E}\nabla^2\nabla^2 F + 2\left[\frac{\partial}{\partial x}\left(\frac{1}{E}\right)\frac{\partial\nabla^2 F}{\partial x} + \frac{\partial}{\partial y}\left(\frac{1}{E}\right)\frac{\partial\nabla^2 F}{\partial y}\right] \\ &+ \nabla^2\left(\frac{1}{E}\right)\nabla^2 F - \frac{\partial^2}{\partial y^2}\left(\frac{1+\nu}{E}\right)\frac{\partial^2 F}{\partial x^2} \\ &- \frac{\partial^2}{\partial x^2}\left(\frac{1+\nu}{E}\right)\frac{\partial^2 F}{\partial y^2} + 2\frac{\partial^2}{\partial x\partial y}\left(\frac{1+\nu}{E}\right)\frac{\partial^2 F}{\partial x\partial y} \\ &+ \nabla^2[\alpha(T - T_0)] = 0 \end{aligned} \tag{22}$$

We know from (20) that for a model I crack, at a radial distance r from the crack tip,

$$\frac{\partial^2 F}{\partial x_\alpha \partial x_\beta} \sim \frac{K_I}{\sqrt{2\pi r}} \tag{23}$$

to within an angular multiplier of order unity. This singularity is due to the first term in (22). Neglecting gradients of Poisson's ratio, the dominance of this first term over other terms involving modulus gradients in (22) leads to the K-dominance conditions related to material nonhomogeneities

$$\frac{1}{E}\left|\frac{\partial E}{\partial x_\alpha}\right| << \frac{1}{r}, \frac{1}{E}\left|\frac{\partial^2 E}{\partial x_\alpha \partial x_\beta}\right| << \frac{1}{r^2} \tag{24}$$

The above condition indicates that the size of the K-dominance zone decreases with increasing magnitude of modulus gradients. The K-dominance zone becomes vanishingly small for a crack located in a nearly sharp interface region where the modulus gradients are extremely steep. For the stress intensity factor to be a meaningful fracture parameter, the crack-tip fracture process zone should be engulfed in the K-dominance zone.

Crack-Tip Fields in Thermoelastic-Plastic FGMs

Consider a crack in a thermoelastic-plastic FGM with continuous and piecewise differentiable elastic–plastic properties. We still assume that the crack tip terminates at the boundary between the two differentiable pieces as shown in Fig. 1. Jin and Noda [2] and Noda and Jin [3] proved that the crack-tip stress and displacement fields in the thermoelastic-plastic FGM with continuous and piecewise differential properties have the same forms as those for the corresponding homogeneous material. This entry focuses on the thermoelastic power-law hardening material described in Section 2.3.

As in the case of thermoelastic FGMs, we still assume the following asymptotic expansion of the Airy stress function near the crack tip:

$$\begin{aligned} F &= r^{s_1}\tilde{F}_1(\theta),\ r \to 0,\ -\pi < \theta < -(\pi - \theta_L) \\ F &= r^{s_2}\tilde{F}_2(\theta),\ r \to 0,\ -(\pi - \theta_L) < \theta < \theta_L \\ F &= r^{s_3}\tilde{F}_3(\theta),\ r \to 0,\ \theta_L < \theta < \pi \end{aligned} \tag{25}$$

where s_i ($i = 1, 2, 3$) are the eigenvalues to be determined and $\tilde{F}_i(\theta)$ ($i = 1, 2, 3$) are the angular distributions of the Airy function. At the same time, the hardening exponent $n(\boldsymbol{x})$ and the parameter $\alpha_p(\boldsymbol{x})$ can be expanded into Taylor series at the crack tip in each differentiable piece as follows:

$$\begin{aligned} n &= n_{tip} + a_{11}x + b_{11}y + \ldots,\ -\pi < \theta < -(\pi - \theta_L) \\ n &= n_{tip} + a_{12}x + b_{12}y + \ldots,\ -(\pi - \theta_L) < \theta < \theta_L \\ n &= n_{tip} + a_{13}x + b_{13}y + \ldots,\ \theta_L < \theta < \pi \end{aligned} \tag{26}$$

$$\begin{aligned} \alpha_p &= \alpha_p^{tip} + c_{11}x + d_{11}y + \ldots, -\pi < \theta < -(\pi - \theta_L) \\ \alpha_p &= \alpha_p^{tip} + c_{12}x + d_{12}y + \ldots, -(\pi - \theta_L) < \theta < \theta_L \\ \alpha_p &= \alpha_p^{tip} + c_{13}x + d_{13}y + \ldots, \theta_L < \theta < \pi \end{aligned} \tag{27}$$

where n_{tip} and α_p^{tip} are the values of the hardening exponent and parameter α_p at the crack tip, a_{ij} and b_{ij} are constants related to the derivatives of the hardening exponent at the crack tip in the differentiable pieces, and c_{ij} and d_{ij} are constants related to the derivatives of the parameter α_p at the crack tip in the differentiable pieces. Substituting (25) through (27), the Taylor series expansions of the thermoelastic properties and the temperature field (15) into (11), we find that the plastic deformation dominates the elastic and thermal ones. Hence, the governing equation of the Airy function reduces to the following in the crack-tip region in each differentiable piece:

$$\frac{\partial^2}{\partial x^2}\left[\sigma_e^{n_{tip}-1}\left(\frac{\partial^2 F}{\partial x^2}-\frac{1}{2}\frac{\partial^2 F}{\partial y^2}\right)\right] + \frac{\partial^2}{\partial y^2}\left[\sigma_e^{n_{tip}-1}\left(\frac{\partial^2 F}{\partial y^2}-\frac{1}{2}\frac{\partial^2 F}{\partial x^2}\right)\right] + 3\frac{\partial^2}{\partial x\partial y}\left[\sigma_e^{n_{tip}-1}\frac{\partial^2 F}{\partial x\partial y}\right]=0 \tag{28}$$

Equation (28) is the same as the governing equation for the homogenous power-law hardening material with constant properties of n_{tip} and α_p^{tip}. Thus, the HRR field for the homogeneous power-law hardening material [8, 9] is also the dominant solution to the FGM in every differentiable piece. The continuities in displacements and tractions across the boundary between the differentiable pieces are maintained by this solution as long as the hardening exponent n and parameter α_{p} are continuous. Hence, the crack-tip stress and displacement fields in the FGM are still the HRR field provided the material properties are continuous and piecewise differentiable. We note that if the Ramberg-Osgood model is expressed in a dimensionless form, the yield stress and yield strain should also be continuous and piecewise differentiable. The crack-tip stress and displacement fields are thus given as follows:

$$\sigma_{\alpha\beta}(r,\theta)=K_M r^{-1/(n_{tip}+1)}\tilde{\sigma}_{\alpha\beta}(\theta) \tag{29}$$

$$\varepsilon_{\alpha\beta}(r,\theta)=\alpha_p^{tip}(K_M)^{n_{tip}}r^{-n_{tip}/(n_{tip}+1)}\tilde{\varepsilon}_{\alpha\beta}(\theta) \tag{30}$$

$$u_\alpha(r,\theta)=\alpha_p^{tip}(K_M)^{n_{tip}}r^{1/(n_{tip}+1)}\tilde{u}_\alpha(\theta) \tag{31}$$

where K_{M} represents the intensity of the singular stress field and $\tilde{\sigma}_{\alpha\beta}(\theta)$, $\tilde{\varepsilon}_{\alpha\beta}(\theta)$, and $\tilde{u}_\alpha(\theta)$ are the angular variations of the crack-tip stress, strain, and displacement fields, respectively. These angular distributions can be found in Hutchinson [8] and Rice and Rosengren [9].

We note that the properties of a homogeneous material in a thermal gradient become space-dependent when the temperature dependence of material properties is taken into consideration. Yuan and Kalkhof [10] studied crack-tip fields in a power-law hardening material with temperature-dependent properties using a finite element method. Their numerical results showed that the HRR field exists in the crack-tip region if the temperature gradient is not very severe.

We have seen that the crack-tip fields in a power-law hardening FGM have the same forms as those for a homogeneous material (HRR field) as long as the material properties are continuous and piecewise continuously differentiable. The size of the region in which the crack-tip fields (29) through (31) dominate (HRR dominance zone), however, will be affected by the material property gradients. Jin [11] estimated the effect based on the crack-tip solutions (29) through (31) and the basic equation (11). To simplify the analysis, only mode I deformation is considered. For a power-law hardening material, it follows from the HRR solution (29) that at a radial distance r from the crack tip,

$$\frac{\partial^2 F}{\partial x_\alpha \partial x_\beta}\sim K_M r^{-1/(n_{tip}+1)}$$
$$F\sim K_M r^{(2n_{tip}+1)/(n_{tip}+1)},\quad r\to 0 \tag{32}$$

By comparing the magnitude of the dominant terms in (11) related to the asymptotic solution (29) and the magnitude of the terms related to the material gradation, we can show that the crack-tip solutions (29) through (31) will dominate at points for which

$$\frac{1}{\alpha_p}\left|\frac{\partial\alpha_p}{\partial x_\alpha}\right| << \frac{1}{r},\quad \frac{1}{\alpha_p}\left|\frac{\partial^2\alpha_p}{\partial x_\alpha\partial x_\beta}\right| << \frac{1}{r^2} \tag{33}$$

$$\frac{1}{n}\left|\frac{\partial n}{\partial x_\alpha}\right| << \frac{1}{r|\ln(r/A)|},\quad \frac{1}{n}\left|\frac{\partial^2 n}{\partial x_\alpha\partial x_\beta}\right| << \frac{1}{r^2|\ln(r/A)|} \tag{34}$$

where A is a length parameter. We note that (33) and (34) are the estimates on the order of magnitude of the HRR dominance zone size and the selection of A does not affect the asymptotic nature of (34) when $r\to 0$. Equations (33) and (34) indicate that the size of the HRR dominance zone decreases with increasing magnitude of material property gradients in the crack-tip

region. The HRR dominance conditions (33) and (34) involve only the plastic properties of the material (α_p and n).

References

1. Sih GC (1965) Heat conduction in the infinite medium with lines of discontinuities. ASME J Heat Transfer 87:293–298
2. Jin ZH, Noda N (1994) Crack tip singular fields in nonhomogeneous materials. ASME J Appl Mech 61:738–740
3. Noda N, Jin ZH (1995) Crack-tip singularity fields in nonhomogeneous body under thermal stress fields. JSME Int J Ser A 38:364–369
4. Eischen JW (1987) Fracture of nonhomogeneous materials. Int J Fract 34:3–33
5. Williams ML (1957) On the stress distribution at the base of a stationary crack. J Appl Mech 24:109–114
6. Sun CT, Jin ZH (2012) Fracture mechanics. Academic Press, Boston
7. Jin ZH, Batra RC (1996) Some basic fracture mechanics concepts in functionally graded materials. J Mech Phy Solids 44:1221–1235
8. Hutchinson JW (1968) Singular behaviour at the end of a tensile crack in a hardening material. J Mech Phy Solids 16:13–31
9. Rice JR, Rosengren GF (1968) Plane strain deformation near a crack tip in a power-law hardening material. J Mech Phy Solids 16:1–12
10. Yuan H, Kalkhof D (1999) Effects of temperature gradients on crack characterization under thermal-mechanical loading conditions. Int J Fract 100:355–377
11. Jin ZH (2004) Effect of material nonhomogeneities on the HRR dominance. Mech Res Commun 31:203–211

Creep Analysis

Marko Čanađija
Department of Engineering Mechanics, Faculty of Engineering, University of Rijeka, Rijeka, Croatia

Overview

Engineers designing structures operating at higher temperatures noticed that at a constant level of stress, structural deformation continues to increase. Such behavior is known as creep and strains that occur are known as creep strains. An opposite effect is also seen: if a structure is subjected to a constant strain at elevated temperatures, the stress level will decrease. This phenomenon is known as stress relaxation. Strain rate becomes an important factor in the design and it is assumed to be influenced by the stress level and temperature. This strain accompanies usual, elastic strain. Most applications involving creep are concerned with the behavior below yielding point, but creep can be accompanied by the instantaneous plastic strain as well. The creep process is not limited to constant levels of stress; it occurs as well in the case of variable stress levels. Although higher temperatures are usually understood as a trigger for creep and relaxation behavior, the phenomenon is present at room temperature in the case of some polymers and even metals – lead for an example. Besides already mentioned temperature and stress as basic variables influencing creep, grain size, alloying, prestrain, and recovery are additional factors influencing creep.

This entry is intended to give a brief introduction to the problems of creep and relaxation analysis. The outline is as follows – initially typical curves representing this behavior are described. Discussion of creep mechanisms follows. Relations between stress and strain are presented for the uniaxial case and extended to the multiaxial case. To familiarize the reader with the problem, three different applications are selected: stress relaxation of a uniaxially loaded bar, creep of a thin-walled tube, and stress relaxation in a beam. At the end, some conclusions are given.

Creep and Relaxation Curves

Typical creep curve for the constant load level and constant temperature is shown in Fig. 1 [1–3]. The uniaxial creep test could be performed under constant load or constant stress assumption. Although both assumptions give the same result at the beginning of the test, at the later stage they diverge. Since the testing apparatus for constant load is much simpler, this is the preferred

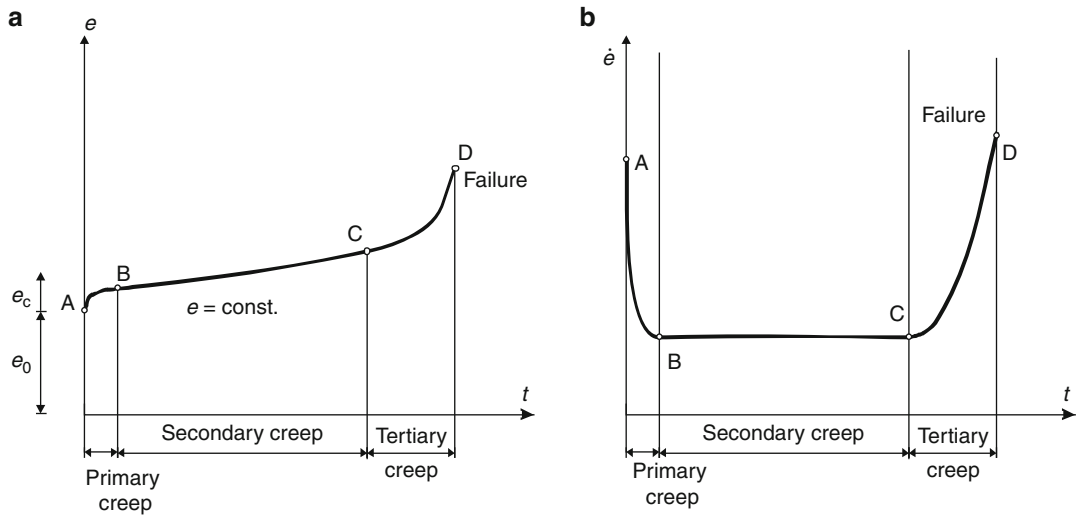

Creep Analysis, Fig. 1 Creep curves: (**a**) Strain versus time; (**b**) strain rate versus time

approach although from the metallurgical point of view, creep is a stress function. The curve obtained in that way can be divided into three distinctive parts. Upon instantaneous-elastic (and possibly plastic) strain e_0, the first part of the curve describes primary or transient creep. It is characterized by decrease of the creep strain rate and is relatively short compared to the second part. The second phase is known as secondary or steady-state creep. The name itself implies that during this phase creep strain rate is constant, leading to linear rise of the creep strain with respect to time. It is the longest step in the creep process. Under favorable conditions, the final, tertiary, or accelerating creep stage is reached. Creep strain rate now starts to rapidly increase, eventually leading to the failure of the specimen. This phase is accompanied by the necking of the test specimen. The creep curve in Fig. 1 is only a typical one. Often creep curves do not have the tertiary phase or the secondary is either completely absent or very short. For example, for lower temperatures and loads, after primary creep phase, creep might cease to propagate entirely. Some general guidance [4–8] is that at temperatures up to 0.3 T/T_M, where T_M is melting temperature in degrees kelvin, primary creep is most significant, while secondary creep is negligible. At moderate temperatures ($T/T_M < 0.7$) both primary and secondary creep are important, while at the temperatures near melting point primary creep can be neglected and secondary creep takes the dominant role.

If strain is kept constant then under suitable environment conditions, stresses are going to decrease through relaxation process. The phenomenon is closely related to creep and it is believed that it could be analyzed by the same underlying mechanism as the creep itself. Therefore, a typical relaxation test is carried out by constraining the contraction of a previously uniaxially loaded specimen. During the test, stresses are registered and obtained curve should look like the one given in Fig. 2. In the first part of the relaxation curve, the stress decrease rate is the highest but it soon starts to slow down. The source of stress decrease is that elastic strain, Fig. 2b, is gradually substituted by the creep strain. It should be noted that total strain remains constant throughout the whole process. Probably the most frequently met problem of this kind is found in bolts joining two flanges of a pipeline operating at high temperature.

Creep Mechanisms

To keep it very simple, it could be said that creep occurs either through the movement of

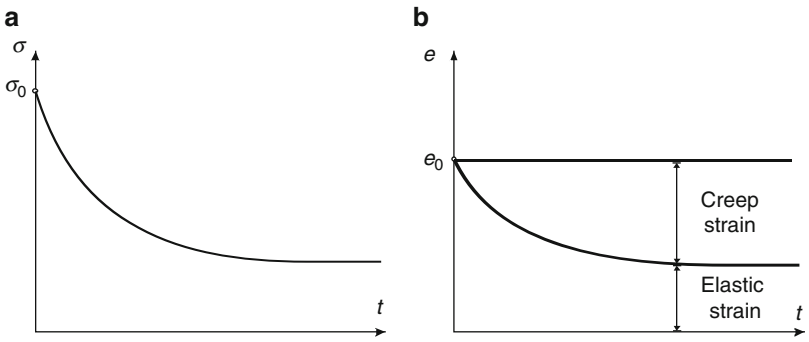

Creep Analysis, Fig. 2 Relaxation curves: (**a**) Stress versus time; (**b**) strain versus time

dislocations or through diffusion. Both can take place simultaneously. Dislocation creep is dominated by the movement of dislocations, i.e., crystallographic defects [9–13]. Since the movement of dislocations involves higher stresses needed to overcome obstacles, such creep arises only if the stresses are high enough. Similar behavior is found in plastic deformation. However, differently from plastic deformation where stresses are used to unlock the dislocation, at elevated temperatures diffusional movement of vacancies is exploited to unlock the dislocations. This is known as the climb. So, although movement of dislocations is the cause of creep, diffusion of vacancies should be present as well for the process to occur. Temperatures in the creep of metals should be at least 0.3–0.4 T_M in most cases. Due to the climb, sliding of dislocations does not necessary have to be in the same plane like in plasticity. When sufficient number of vacancies is diffused away a dislocation can change a slip plane in order to avoid an obstacle, evidently increasing the deformation of the material. In dislocation creep, a certain threshold stress is frequently introduced below which no creep is present (or can be neglected). To describe such creep a power law is often used.

Diffusional creep is dominant as temperature is approaching the melting point in materials with fine grain crystal structure. The stress level could be low. Two kinds of diffusion are important in the creep of metals: interstitial and vacancy diffusion. Interstitial diffusion exploits the small gaps between atoms, i.e., smaller atoms in the crystal lattice can diffuse through the gaps if their energy level is sufficiently high. For example, steel – the most widely used structural material nowadays – could creep in that manner since carbon atoms are small enough to travel through these gaps. It has to be emphasized that interstitial diffusion is less frequently found than vacancy diffusion. Vacancy diffusion occurs in crystals with the approximately equal size of atoms in the lattice. Since the atoms are of equal size, neither atom can squeeze through the gaps; instead a vacancy in the lattice must be present if the atom is going to move. Obviously, grain boundaries or other defects in the lattice are places where such missing atoms could be found in larger numbers. In that way, diffusion is greatly enhanced by the presence of grain boundaries or other defects [11]. Therefore, vacancies move from the one grain boundary to the next, grouping at the boundaries. The flow of vacancies is not random; they have tendency to move and group in the direction perpendicular to the axis at which tensile stresses are positioned – in the region with compressive stresses. On the other side, atoms move in the opposite direction, from the compressive stresses zone to the tensile stresses zone. If the temperature is high enough, diffusion will occur also through the crystal. The movement of dislocations does not have to take place. As a consequence of such diffusion, grains elongate what effectively enhances creep. Diffusional creep can be rather accurately described by linear stress dependence on the strain rate.

Constitutive Models of Creep

Uniaxial Model of Creep Strain Evolution

The uniaxial model of creep must provide an approximation to the creep curve, Fig. 1, i.e., of strain change versus time. A starting hypothesis is partition of strain e into the instantaneous elastic and the creep parts:

$$e = e_e + e_c \tag{1}$$

where is e_e linear elastic strain and is e_c creep strain. Linear elastic strain is calculated as usual:

$$e_e = \sigma/E \tag{2}$$

while creep strain remains to be approximated from the test results. It should be emphasized that instantaneous plastic strain can also be added besides elastic strain, but such cases are not the topic of this entry. For more details, the interested reader should refer to some of the standard textbooks on elastoplasticity.

To describe the evolution of creep strain a number of models were developed. Since the secondary creep phase is usually most significant, the greatest number of models deal with this phase. Some models can be used to describe both primary and secondary phase, while some deals with the tertiary creep. In the text that follows only models dealing with primary and secondary creep are considered. The general approach is to assume that creep strain is a function of stress, temperature, and time:

$$e_c = F(\sigma, T, t) \tag{3}$$

The usual assumption is that influence of each particular variable can be uncoupled, i.e. [14]:

$$e_c = \sum_{i=1}^{N} f_i(\sigma) g_i(T) h_i(t) \tag{4}$$

where f, g, and h are functions of stress, temperature, and time, respectively. Such an approach is strongly supported by the testing procedures – usually both stress and temperature are kept fixed and creep strain variation in time is monitored. Alternatively, temperature and strain are held fixed and stress is allowed to vary. The results can be then compared at given time t. It is not rare to see that temperature is not explicitly introduced into the equation, but rather material parameters are considered to be functions of temperature.

Majority of the models used for creep are based on the Arrhenius equation:

$$\dot{e}_c = f(\sigma) e^{-\frac{Q}{RT}} \tag{5}$$

where Q is the activation energy (J mol^{-1}) and R is the universal gas constant (8.31 J mol^{-1} K^{-1}). In Arrhenius equation, strain rate is an exponential function of temperature and therefore it is usually to find the same functional dependence in empirical equations.

List of possible creep models is very long [15, 16]. Some are more suitable for metals, others for ceramics or plastics. The most common options are summarized below. Most simple cases are based on the time dependence only, for example, logarithmic law:

$$e_c = A \ln t + B \tag{6}$$

where A and B are material parameters. The law is suitable for temperature ratios $0.05 < T/T_M < 0.3$ and primary creep. Strain rate for the model described by (6) is:

$$\dot{e}_c = A/t \tag{7}$$

therefore giving infinitely large strain rate at the $t = 0$. An alternative form that circumvents the problem is given by

$$e_c = A \ln(1 + Ct) \tag{8}$$

Various more or less sophisticated time dependence models can be envisaged; just to give an idea of these forms, combined exponential-power and logarithmic-power laws are provided:

$$\begin{aligned} e_c &= A\left(1 + Bt^{1/3}\right)e^{Ct} - A \\ e_c &= A \ln(t) + Bt^C + Dt \end{aligned} \tag{9}$$

Probably the most popular model is the Bailey-Norton law, in which stress function in (5) is considered to be a power law on the stress:

$$e_c = A\sigma^B t^C \tag{10}$$

This law is suitable for modeling both primary and secondary creep. This model can be categorized as a combined stress-time dependent law. Other examples of this type are exponential law:

$$\dot{e}_c = Ae^{(B+C\sigma)} \tag{11}$$

or hyperbolic law:

$$\dot{e}_c = A[\sinh(B\sigma)]^C \tag{12}$$

Generally, in the case of metals, power law, (10) is more suitable for lower stresses, while exponential law (11) is more useful for higher stresses [6]. Hyperbolic sine law, (12) can be used for both lower and higher stresses.

Combined time-temperature-stress-dependent functions take the most complex form, for example:

$$\begin{aligned} e_c &= Ae^{-B/T}\sigma^C t^D \\ e_c &= Ae^{-B/T}[\sinh(C\sigma)]^D t^F \end{aligned} \tag{13}$$

Finally, it should be noted that the material parameters A, B, C, D, F in the above equations can be different for the tensile and compressive loading.

Multiaxial Model of Creep Strain Evolution

Upon definition of uniaxial models, these should be now extended to the multiaxial case. To keep the presentation as simple as possible, only isotropic models will be considered. Readers familiar with the theory of plasticity will find this subject more easily to understand.

For an isotropic body, the strain tensor and the stress tensor can be related through the Lévy-Mises equations [4, 14]. Basically, these equations state that principal axes of these two tensors coincide. The same assumption can be extended to the strain rate tensor:

$$\dot{e}_{ij} = S_{ij}\lambda \tag{14}$$

where S_{ij} represents the deviatoric part of stress tensor, i.e.:

$$S_{ij} = \sigma_{ij} - \frac{1}{3}\sigma_{kk}\delta_{ij} \tag{15}$$

and is δ_{ij} Kronecker delta. It is assumed that strain tensor can be additively separated into the elastic, the creep, and the thermal strain parts. Since the elastic and the thermal strain parts are not time dependent, there is:

$$e_{ij} = e^e_{ij} + e^c_{ij} + \alpha\delta_{ij}\Delta T \quad \Rightarrow \quad \dot{e}_{ij} = \dot{e}^c_{ij} \tag{16}$$

Furthermore, it should be noted that the creep strain tensor is isochoric, i.e., volume does not change during creep:

$$\mathrm{tr}e^c_{ij} = 0, \quad \mathrm{tr}\dot{e}^c_{ij} = 0 \tag{17}$$

Deviatoric part of the elastic strain tensor is calculated as:

$$e^{e,(d)}_{ij} = \frac{1}{2\mu}S_{ij} \tag{18}$$

where μ is the shear modulus. Because of (16) the creep strain rate tensor is defined by the flow rule:

$$\dot{e}^c_{ij} = S_{ij}\lambda \tag{19}$$

i.e., principal axes of the stress tensor and the creep strain tensor rate also coincide. Components of these tensors differ for a factor of proportionality λ. So, to complete determination of the stress–strain relationship, a factor λ must be calculated. In the line with that, effective stress:

$$\sigma^* = \sqrt{3J_2}, \quad J_2 = \frac{1}{2}S_{ij}S_{ij} \tag{20}$$

and effective creep strain rate:

$$\dot{e}^{*c} = \sqrt{\frac{4}{3}I_2}, \quad I_2 = \frac{1}{2}\dot{e}^c_{ij}\dot{e}^c_{ij} \tag{21}$$

are introduced. In (20) and (21) J_2, I_2 are second invariants of the stress and the creep strain rate tensors, respectively. Introduction of (19) into (21), together with (20), yields:

$$\begin{aligned} \dot{e}^{*c} &= \sqrt{\frac{2}{3}\dot{e}^c_{ij}\dot{e}^c_{ij}} = \sqrt{\frac{2}{3}S_{ij}\lambda S_{ij}\lambda} = \frac{2}{3}\lambda\sigma^* \\ \lambda &= \frac{3}{2}\frac{\dot{e}^{*c}}{\sigma^*} \end{aligned} \tag{22}$$

what now completes stress–creep strain rate constitutive law.

The above procedure must be valid in the uniaxial case as well. In that case, effective stress is equal to uniaxial stress and effective creep strain is equal to the uniaxial creep strain. Consequently, if now instead of effective creep strain a uniaxial model is used, say the Bailey-Norton law, (10):

$$\dot{e}^{*c} = \dot{e}_c = A(\sigma^*)^B C t^{C-1} \tag{23}$$

then the proportionality factor λ is:

$$\lambda = \frac{3}{2}\frac{\dot{e}^{*c}}{\sigma^*} = \frac{3}{2}A(\sigma^*)^{B-1}Ct^{C-1} \tag{24}$$

In this particular case, the constitutive law is:

$$\dot{e}^c_{ij} = S_{ij}\lambda = \frac{3}{2}A(\sigma^*)^{B-1}Ct^{C-1}S_{ij} \tag{25}$$

Other creep laws (e.g., any of (6)–(13)) can be easily employed in (23).

It should be emphasized that a more general theory of creep can be envisaged through the employment of the advanced continuum mechanics. Such considerations are beyond this entry and the interested reader should consult [4, 17] for an initial study.

Applications

The purpose of this section is to provide an insight into the above presented theory through simple applications that can be solved by hand. More details can be found in references cited in the text. If a more complex problem has to be solved, then perhaps some numerical procedure could be better suited. The most frequent choice is the finite element method [18, 19]. Better commercial finite element codes have the option for creep analysis readily available. However, the topic goes beyond the interest of this entry and the reader should consult appropriate literature for further information.

Application 1: Unixial Creep Relaxation in Bars

As a first application of the above presented theory, a creep relaxation of a bar is considered. Contrary to the classical creep problem in which the stresses are prescribed, in the creep relaxation strain is prescribed while stresses are allowed to vary. It is customary to assume that the same material data is valid for both creep and relaxation [14, 20]. Such assumption is frequently made since data about relaxation is scarce; therefore the reader is directed to verify if such an assumption can be made for the material in question. In this particular application, it will be assumed that creep and relaxation data are the same.

To visualize the problem at hand, consider a flange of pipe used to transport fluid at elevated temperature. Bolts are applied to connect two flanges. For the sake of simplicity, flanges will be treated as rigid. Therefore, total elongation of bolts ΔL must remain constant. Initially, bolts are tightened with stress in the elastic range. However, due to creep of the material, a part of elastic strain will be transformed into creep strain what will lead to the decrease in stresses (Fig. 2). This means that the total elongation of bolts ΔL in some time instant t will be:

$$\Delta L = \Delta L_e(t) + \Delta L_c(t) = \text{const} \tag{26}$$

where ΔL_e is elastic part of elongation and ΔL_c creep part of elongation. If initial stress in bolts is now denoted as σ_0, Young's modulus as E while initial strain is e_0, then it is:

$$e_0 = \frac{\sigma_0}{E} = \frac{\sigma(t)}{E} + e_c(t) \tag{27}$$

To obtain evolution of stresses, (27) should be differentiated with respect to time t:

$$0 = \frac{1}{E}\dot{\sigma} + \dot{e}_c \tag{28}$$

At this point, a suitable uniaxial law for creep strain rate should be used. Consider the Bailey-Norton creep law, (10), for example:

$$\dot{e}_c = A\sigma^B C t^{C-1} \tag{29}$$

A careful reader will notice that stress rate in the above creep strain rate equation is neglected. Such procedure has its stronghold in the fact that the Bailey-Norton law is almost exclusively obtained from the creep test – that is, with the constant load during the test. Therefore, it has an obvious shortcoming when processes that involve changes of stress are concerned. It basically limits the consideration to slower stress changes. Nevertheless, this is a standard procedure successfully applied in the series of problems [14, 20]. Another simplification is to consider only secondary creep where the creep strain rate is constant. In this case, the Bailey-Norton law (10) should be linear in time, that is $C = 1$. This transforms (28) to:

$$\frac{d\sigma}{\sigma^B} = -AE\,dt \tag{30}$$

Integration of (30) yields:

$$\sigma^{1-B}(t) = (B-1)(At \cdot E + C_1) \tag{31}$$

The constant of integration C_1 is evaluated from the initial conditions. Since in the time instant $t = 0$ bolts were tightened to stress $\sigma = \sigma_0$, then it is:

$$C_1 = \frac{\sigma_0^{1-B}}{B-1} \tag{32}$$

Therefore, creep relaxation of stresses in bolts is governed by the function:

$$\sigma(t) = \left[(B-1)At \cdot E + \sigma_0^{1-B}\right]^{1/(1-B)} \tag{33}$$

In the particular case when bolts are considered, additional effects, like bending of the flanges can increase the rate of the relaxation process. Such effects are not considered here and for further details the reader is directed to [20], for example.

Application 2: Mutliaxial Creep in Thin-Walled Tubes

To demonstrate an application of the multiaxial creep model, creep of a thin-walled tube with closed ends is considered. The tube radius is r, wall thickness h, and the constant inner pressure in the tube is p. Well-known formulas for stresses in radial, circumferential, and axial directions are [15]:

$$\sigma_{rr} = 0, \quad \sigma_{\theta\theta} = \frac{pr}{h}, \quad \sigma_{zz} = \frac{pr}{2h} \tag{34}$$

To evaluate effective stress, (20), deviatoric stresses should be known. Since hydrostatic stress is:

$$\sigma_0 = \frac{1}{3}\left(\frac{pr}{h} + \frac{pr}{2h}\right) = \frac{pr}{2h} \tag{35}$$

deviatoric stresses are:

$$S_{rr} = \sigma_{rr} - \sigma_0 = -\frac{pr}{2h}, \; S_{\theta\theta} = \sigma_{\theta\theta} - \sigma_0 = \frac{pr}{2h}, \; S_{zz} = \sigma_{zz} - \sigma_0 = 0 \tag{36}$$

Consequently, effective stress, (20), is:

$$\sigma^* = \sqrt{\frac{3}{2}S_{ij}S_{ij}} = \sqrt{\frac{3}{2}2\left(\frac{pr}{2h}\right)^2} = \sqrt{3}\frac{pr}{2h} \tag{37}$$

Now the effective stress should be related to the creep stain law. If the Bailey-Norton creep law is considered, the proportionality factor, (24), is:

$$\lambda = \frac{3}{2}\frac{\dot{e}^{*c}}{\sigma^*} = \frac{3}{2}A\left(\sqrt{3}\frac{pr}{2h}\right)^{B-1} C t^{C-1} \tag{38}$$

Therefore, creep strain rates are calculated using (25) as:

$$\begin{aligned}\dot{e}^c_{rr} &= \frac{3}{2}A\left(\sqrt{3}\frac{pr}{2h}\right)^{B-1}Ct^{C-1}\left(-\frac{pr}{2h}\right)\\ &= -\frac{\sqrt{3}}{2}AC\left(\frac{\sqrt{3}pr}{2h}\right)^{B}t^{C-1}\\ \dot{e}^c_{\theta\theta} &= \frac{3}{2}A\left(\sqrt{3}\frac{pr}{2h}\right)^{B-1}Ct^{C-1}\frac{pr}{2h}\\ &= \frac{\sqrt{3}}{2}AC\left(\frac{\sqrt{3}pr}{2h}\right)^{B}t^{C-1}\\ \dot{e}^c_{zz} &= 0\end{aligned} \tag{39}$$

Since $\dot{e}^c_{zz} = 0$ the pipe will not extend longitudinally. Radial displacement can be evaluated as a sum of initial elastic and creep displacement [15]:

$$\begin{aligned}u(t) = re_{\theta\theta}(t) &= u_0 + r\int_0^t \dot{e}^c_{rr}d\tau\\ &= u_0 + \frac{\sqrt{3}}{2}A\left(\frac{\sqrt{3}pr}{2h}\right)^{B}rt^{C},\end{aligned} \tag{40}$$

where initial elastic displacement is:

$$u_0 = \frac{pr^2}{Eh}\left(1-\frac{\nu}{2}\right) \tag{41}$$

Application 3: Creep Relaxation in Beams

In this case, creep relaxation of a beam is considered [3, 4]. In particular, stress redistribution due to creep is analyzed. Only stresses caused by the bending moment in a plane will be analyzed. The solution will be based on the small strain Euler-Bernoulli beam theory and the influence of shearing stresses will be neglected. Therefore, elaborations follow elementary steps from the beam theory. The longitudinal axis of a beam is denoted with x, while cross-section lies in the y-z plane. The bending moment vector is taken to be coaxial with y axis. The cross-section of the beam is arbitrary, where the height is defined with coordinates starting at $z_{\min}$ till $z_{\max}$ and the width is a function of height, $b = f(z)$.

It is assumed that strain in a point can be additively decomposed into the elastic and the creep parts:

$$e = e^e + e^c, \quad e^e = \frac{\sigma}{E} \tag{42}$$

Also, usual assumption of linear distribution of strain on the cross-section is accepted:

$$e = Kz \tag{43}$$

Combining (42) and (43) distribution of stresses $\sigma(z)$ can be evaluated as:

$$\sigma = E(e - e^c) = E(Kz - e^c) \tag{44}$$

Standard procedure from the equilibrium condition yields the bending moment:

$$M = \int_{z_{\min}}^{z_{\max}} \sigma bz\,\mathrm{d}z \tag{45}$$

If stress (44) is introduced into (45), it is:

$$\begin{aligned}M &= \int_{z\min}^{z\max} E(Kz - e^c)\,bz\mathrm{d}z\\ &= EK\int_{z\min}^{z\max} bz^2\mathrm{d}z - Ee\int_{z\min}^{z\max} e^c bz\mathrm{d}z\\ &= EKI_y - E\int_{z\min}^{z\max} e^c bz\mathrm{d}z\end{aligned} \tag{46}$$

Complete solution is obtained by differentiating (43), (44), (45):

$$\begin{aligned}\dot{e} &= \dot{K}z \quad \dot{\sigma} = E\left(\dot{K}z - \dot{e}^c\right)\\ \dot{M} &= E\dot{K}I_y - E\int_{z\min}^{z\max} \dot{e}^c bz\mathrm{d}z\end{aligned} \tag{47}$$

Model is completed by the selection of the suitable creep strain rate law $\dot{e}^c$ in (47) and exploiting condition that creep strain is not

present $e^c = 0$ at the $t = 0$. This condition also gives initial stress value and initial curvature value from (44) and (46), respectively:

$$\sigma(t=0) = \sigma_0 = EKz, \quad K(t=0) = K_0 = \frac{M}{EI_y} \tag{48}$$

Of special importance is the case when loading does not change, i.e., $M = \text{const}$. In that case $\dot{M} = 0$, so $(47)_3$ gives

$$\dot{K} = \frac{1}{I_y} \int_{z\min}^{z\max} \dot{e}^c b z \mathrm{d}z \tag{49}$$

so the stress rate, $(47)_2$ is now:

$$\dot{\sigma} = E\left(z\frac{1}{I_y} \int_{z\min}^{z\max} \dot{e}^c b z \mathrm{d}z - \dot{e}^c \right) \tag{50}$$

Finally, integration gives evolution of stresses as:

$$\begin{aligned} \sigma &= \int E\left(\dot{K}z - \dot{e}^c\right) dt + C_0 \\ &= \int E\left(z\frac{1}{I_y} \int_{z\min}^{z\max} \dot{e}^c b z \mathrm{d}z - \dot{e}^c \right) dt + C_0 \end{aligned} \tag{51}$$

where constant of integration is obtained from (48) as $C_0 = \sigma_0$. The model is completed by the selection of a suitable creep strain rate law $\dot{e}^c$ in (47). For example, if the hyperbolic law is adopted, (12), stresses can be calculated as:

$$\begin{aligned} \sigma = \sigma_0 + \int E\Bigg(& z\frac{1}{I_y} \int_{z\min}^{z\max} A[\sinh(B\sigma)]^C b z \, \mathrm{d}z \\ & - A[\sinh(B\sigma)]^C \Bigg) dt \end{aligned} \tag{52}$$

The analytical solution is not straightforward since stresses occur at both sides of (52), so an iterative solution sequence should be used to obtain the solution, see [3, 4] for more details.

Conclusions

A brief presentation of creep analysis was given, with an emphasis on analytical solutions. Procedures suitable for uniaxial and multiaxial cases were presented. They enable efficient solutions for both problems: one in which strains vary while stresses are kept constant and the other – stresses are relaxed while strains are kept fixed. An illustration of creep problems was provided through three typical applications. In order to provide a clear insight the focus was given to the simplicity. For other problems or extension of the applications given here, the interested reader is directed to [3, 4, 14] for a starting point.

References

1. Davis JR (1997) Heat-resistant materials. ASM International, Materials Park
2. Yagi K, Merckling G, Kern TU, Irie H, Warlimont H (eds) (2004) Landolt-Börnstein. Group VIII: advanced materials and technologies. In: Materials; subvolume B: creep properties of heat resistant steels and superalloys, vol 2. Springer, Berlin
3. Penny RK, Marriott DL (1995) Design for creep. Chapman & Hall, London
4. Hetnarski RB, Eslami MR (2009) Thermal stresses – advanced theory and applications. Springer, Berlin
5. Lanin A, Fedik I (2008) Thermal stress resistance of materials. Springer, Berlin
6. Garofalo F (1965) Fundamentals of creep and creep-rupture in metals. Macmillan, New York
7. Smith GV (1950) Properties of metals at elevated temperatures. McGraw-Hill, New York
8. Finnie I, Heller WR (1959) Creep of engineering materials. McGraw-Hill, New York
9. Kassner ME, Pérez-Prado MT (2004) Fundamentals of creep in metals and alloys. Elsevier, Amsterdam
10. Stouffer DC, Dame LT (1996) Inelastic deformation of metals. Wiley, New York
11. Ashby MF, Jones DRH (2002) Engineering materials 1. Butterworth-Heinemann, Oxford
12. Rösler J, Harders H, Bäker M (2007) Mechanical behaviour of engineering materials. Springer, Berlin
13. Menard KP (1999) Dynamic mechanical analysis. CRC, Boca Raton
14. Kraus H (1980) Creep analysis. Wiley, New York

15. Boresi AP, Schmidt RJ (2003) Advanced mechanics of materials. Wiley, New Jersey
16. Rusinko A, Rusinko K (2011) Plasticity and creep of metals. Springer, Berlin
17. Lemaitre J, Chaboche JL (1990) Mechanics of solid materials. Cambridge University Press, Cambridge
18. Bathe KJ (1996) Finite element procedures. Prentice Hall, Englewood Cliffs
19. Naumenko K, Altenbach H (2007) Modeling of creep for structural analysis. Springer, Berlin
20. Belyaev NM (1979) Strength of materials. Mir Publishers, Moscow

Creep Buckling

▶ Linear Aero-Thermo-Servo-Viscoelasticity, Part I: General Theory

Creep Crack Growth

Ching-Kong Chao
Department of Mechanical Engineering, National Taiwan University of Science and Technology, Taipei, Taiwan, Republic of China

Synonyms

Crack

Overview

Failure analysis of the Zircaloy cladding of spent fuel in interim storage is an important topic for the management of nuclear wastes. However, there have been few studies concerning the long-term behavior of the cladding, and its integrity, in dry storage conditions. Hydrides are usually dissolved into the material at high temperatures, and then, hydrogen in solid solution diffuses in the presence of concentration, temperature and stress gradients, and precipitates out as radial hydrides under the presence of the circumferential stress. In this study, the reorientation of hydrides and its effect on the creep life of the spent fuel Zircaloy cladding is also taken into account. A law of viscoplasticity for application to the cladding creep behavior during long-term dry storage has been established by Limon et al. [1]. The effects of hydride orientation on the cladding crack propagation have been studied by Daum et al. [2]. In this study, according to the latest version of ISG-11, we used the C^*-integral [3] and the strain energy density criteria [4] to analyze the creep effect for spent fuel cladding in interim dry storage, and discuss the effects of hydride embrittlement, the initial crack length and different storage temperature profiles on the cladding failure. The results obtained in this study can estimate what kind of environment and storage conditions are most likely to cause degradation leading to cladding failure during the interim dry storage.

Proposed Failure Criterion

Riedel [5] suggested that the stress intensity factor, K_I, and the path independent integral, C^*, are the appropriate parameters for linear elasticity. In the present study, the path independent integral, C^*, together with the strain energy density theory [4] is proposed to examine the effects of initial crack lengths and storage temperature profiles on cladding failure. Landes et al. [3] determined the energy rate line integral, C^*, to be defined as

$$C^* = \int_\Gamma \left(W^* dy - T_i \frac{\partial u_i}{\partial x} ds\right) \qquad (1)$$

where

$$W^* = \int_0^{\dot{\varepsilon}} \sigma_{ij} d\dot{\varepsilon}_{ij}$$

is the strain rate energy density associated with the point stresses, σ_{ij}, and the strain rate, $\dot{\varepsilon}_{ij}$. C^* is a modified J-integral in which the strain and the displacement vectors are replaced by their rates. Goldman et al. [6] described C^* as a single parameter characterizing the stress–strain rate in the near-tip field for a material governed by power laws for creep.

Sih [4] proposed the strain energy density theory, which states that the amount of incremental crack growth, $r_1, r_2 \ldots r_j$, is governed by

$$\left(\frac{dW}{dV}\right)_c = \frac{S_1}{r_1} = \frac{S_2}{r_2} = \ldots = \frac{S_j}{r_j} \tag{2}$$

where S_j represents the strain energy density factor, r_j is the crack growth increment, and $(dW/dV)_c$ is the critical strain energy density which is assumed to be a material dependent constant. Since the strain energy density factor, S, can be related to the energy rate line integral, C^*, by the equation

$$S = \lambda \int_0^t C^* dt \tag{3}$$

for a self-similar crack growth. The dimensionless constant λ is defined as

$$\lambda = \frac{1 - 2v}{2(1 - v)}$$

where v is the Poisson's ratio.

Substitution of (3) into (2) leads to

$$\frac{1}{\lambda}\left(\frac{dW}{dV}\right)_c = \frac{\int_0^{t_1} C_1^* dt}{r_1} = \frac{\int_{t_1}^{t_2} C_2^* dt}{r_2} = \ldots = \frac{\int_{t_{j-1}}^{t_j} C_j^* dt}{r_j} \tag{4}$$

If we further assume that the energy rate line integral, C^*, remains constant during each time interval Δt_j, (4) can then be replaced by

$$\frac{1}{\lambda}\left(\frac{dW}{dV}\right)_c = \frac{C_1^* \Delta t_1}{r_1} = \frac{C_2^* \Delta t_2}{r_2} = \ldots = \frac{C_j^* \Delta t_j}{r_j} \tag{5}$$

From (5), we now establish an important linear relationship between the creep crack growth rate, da/dt, and the energy rate line integral, C^*, by

$$\left(\frac{\Delta a}{\Delta t}\right)_j = \frac{\lambda C_j^*}{\left(\frac{dW}{dV}\right)_c} \tag{6}$$

where the crack growth increment, $r_j = \Delta a_j$.

This investigation determines the creep crack growth rate, da/dt, from the energy rate line integral, C^*, which can be evaluated from the numerical software simulation discussed in the next section. Note that the incremental crack growth for each time increment can be summed up over the entire computation for any specified crack size. A crack size with the total crack length exceeding the thickness of the cladding represents a through-wall crack.

Problem Description

In order to simplify the complex geometry with this irregular distribution of cracks, we adopted a symmetric distribution of eight double cracks embedded in the spent fuel Zircaloy cladding of dimensions, 9.5 mm OD, and 8.36 mm ID, as displayed in Fig. 1. Note that both the inner crack (Tip-A) and the outer crack (Tip-B) are considered to simulate the worst scenario of cladding failure (see Fig. 2). Three different initial crack lengths are considered in the present work, with a cladding thickness of $w = 0.57$ mm. To investigate the effects of hydride embrittlement on the creep life of cladding, radial hydrides with rectangular dimensions, 0.12 × 0.06 mm (see Fig. 2), are placed ahead of crack Tip-A and crack Tip-B. Material constants are listed in Table 1. A constant pressure of 90 MPa is applied to the inner boundary of the cladding, and a constant temperature of 400 °C is present at the outer boundary of the cladding. Meanwhile, the temperature ranges from 400 °C to 570 °C at the inner boundary of the cladding. Three different storage temperature profiles on the inner surface of the cladding are suggested in this work, and are shown in Fig. 3. The instantaneous response is purely elastic since creep deformation develops over a period of time. With the load held constant, subsequent creep deformation causes a relaxation of the crack-tip stresses until a steady-state stress distribution is reached. The material properties of the spent fuel Zircaloy cladding are listed in Table 2.

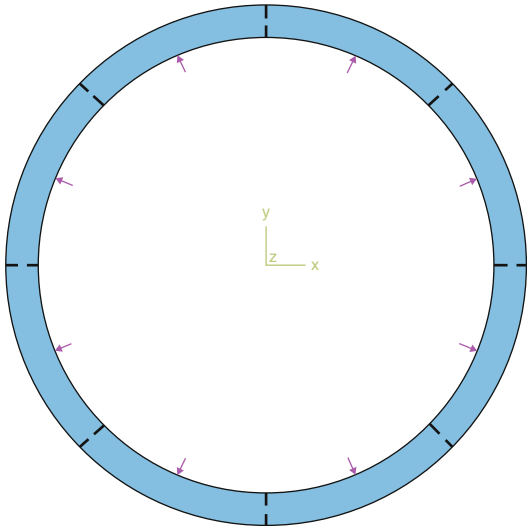

Creep Crack Growth, Fig. 1 The Zircaloy cladding model include inner and outer cracks

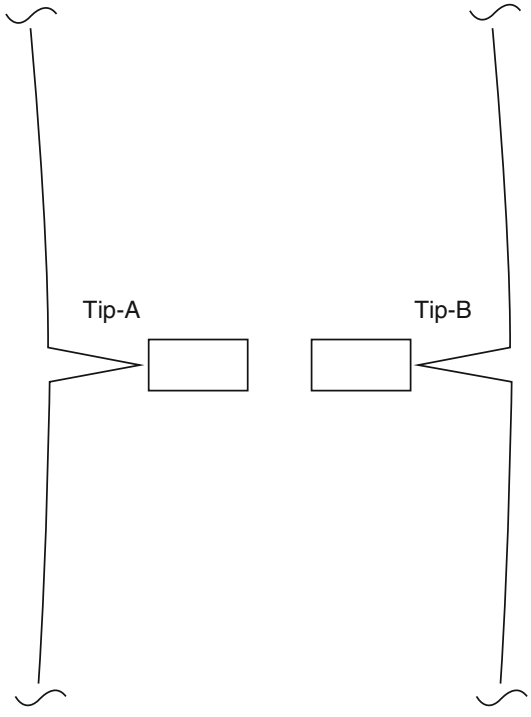

Creep Crack Growth, Fig. 2 Both the inner crack (Tip-A) and the outer crack (Tip-B)

Creep Crack Growth, Table 1 Material properties of the hydride

	Zr-2.5%Nb
Young's modulus, GPa	97.9
Poisson's ratio	0.33
Conduction coefficient, W/m·K	17.1
Expansion coefficient, 1/K	6.3×10^{-6}
Density, g/cc	6.44
Specific heat, J/g·K	0.285

Numerical Analysis

A finite element program which provides a high degree of accuracy for the crack tip element is now applied to perform the two-dimensional thermoviscoelastic analysis. The FEM program used in this study is ABAQUS™ v.6.5-1, which uses an embedded enriched eight-node biquadratic plane-stress quadratic reduced integration. Due to geometric symmetry, only one octant is needed to analyze the present study. Figure 4 represents the finite element mesh discretization where the elements are fine in the crack tip region and coarse in the region away from it. In order to calculate the energy rate line integral, C^*, we use Matsuo's creep model

$$\dot{\varepsilon} = A\left(\frac{E}{T}\right)\left(\sinh\left(\frac{a\sigma_\theta}{E}\right)\right)^n e^{-\frac{Q}{RT}} \qquad (7)$$

where A, n, and a are constant, T is the temperature, E is the Young's modulus, R is the universal gas constant, Q is the activation energy. These properties are listed in Table 2. Note that σ_θ represents the uniaxial equivalent deviatoric stress and the dependency of the Young's modulus (MPa) on the temperature (K) is assumed as

$$E = 9.93 \times 10^4 - 59.5 \times T$$

By interpreting the strain rate obtained from (7), the energy rate line integral C^* can be determined by using contour integral evaluation provided by ABAQUS™.

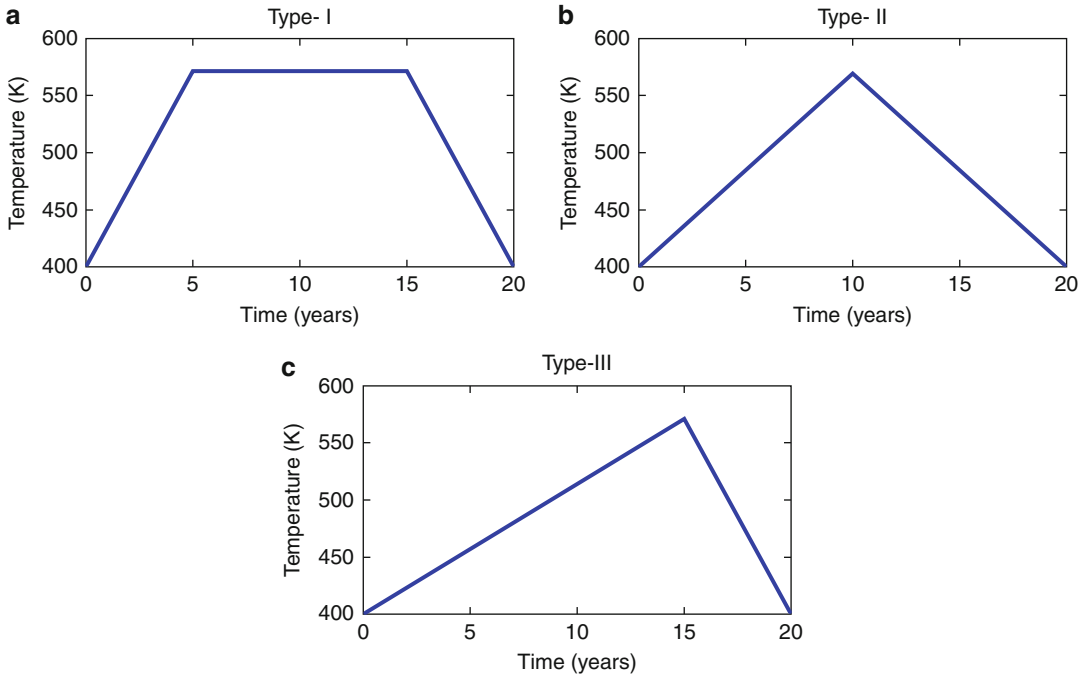

Creep Crack Growth, Fig. 3 Three different storage temperature profiles applied on the inner boundary of the cladding

Creep Crack Growth, Table 2 Material properties of the spent fuel Zircaloy cladding

	Zircaloy-2
Young's modulus, GPa	99.3
Poisson's ratio	0.37
Conduction coefficient, W/m·K	51.5
Expansion coefficient, 1/K	6×10^{-6}
Density, g/cc	6.56
Specific heat, J/g·K	0.285

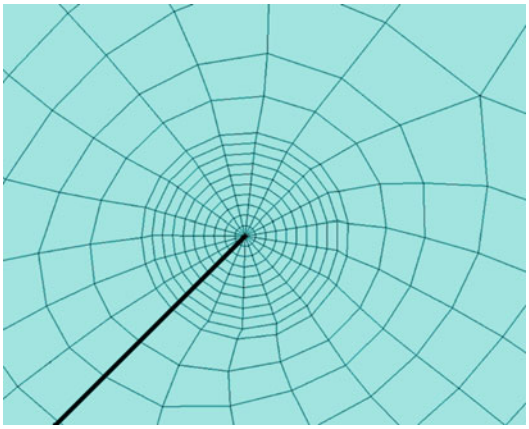

Creep Crack Growth, Fig. 4 The finite element mesh discretization where the elements are fine in the crack tip region

Results and Discussion

The three different temperature profiles: 0-5-15-20, 0-10-20, and 0-15-20, are defined as type I, II, and III, respectively, as shown in Fig. 3. These three types are all considered in the analyses. Referring to Fig. 3a, a storage temperature profile is applied at the inner boundary of cladding, while a constant pressure of 90 MPa is applied to the inner boundary of the cladding, and a constant temperature of 400 °C is present at the outer boundary of the cladding. The crack growth increment rate da/dt can be determined from our proposed criterion with the given material constant

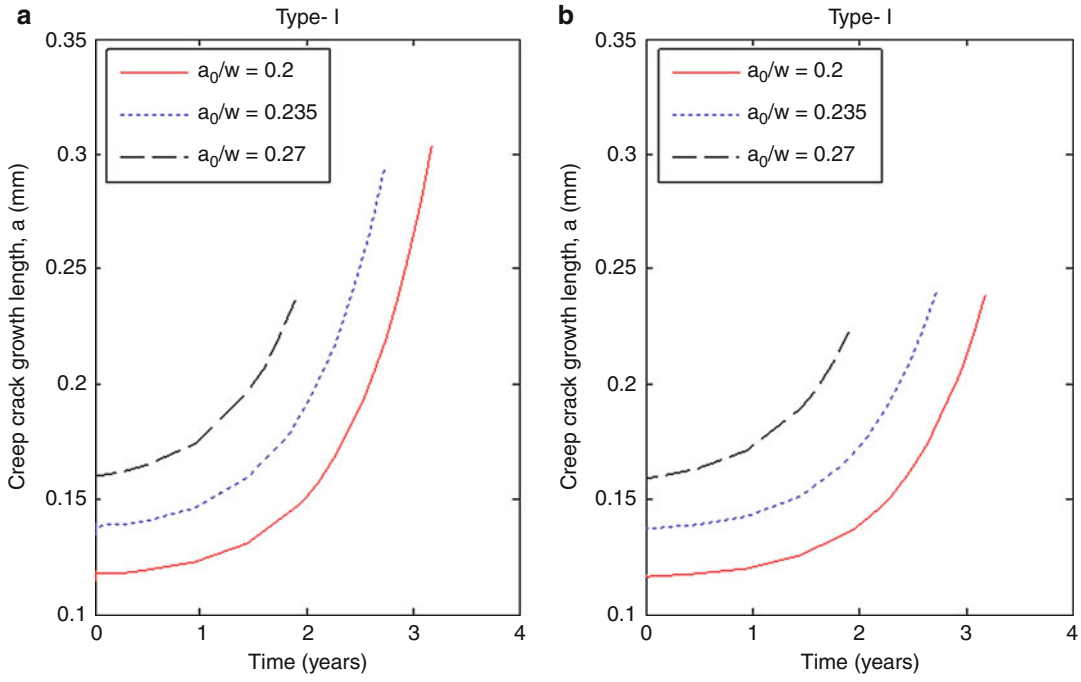

Creep Crack Growth, Fig. 5 The total crack growth for both Tip-A and Tip-B is shown in (**a**) and (**b**), respectively

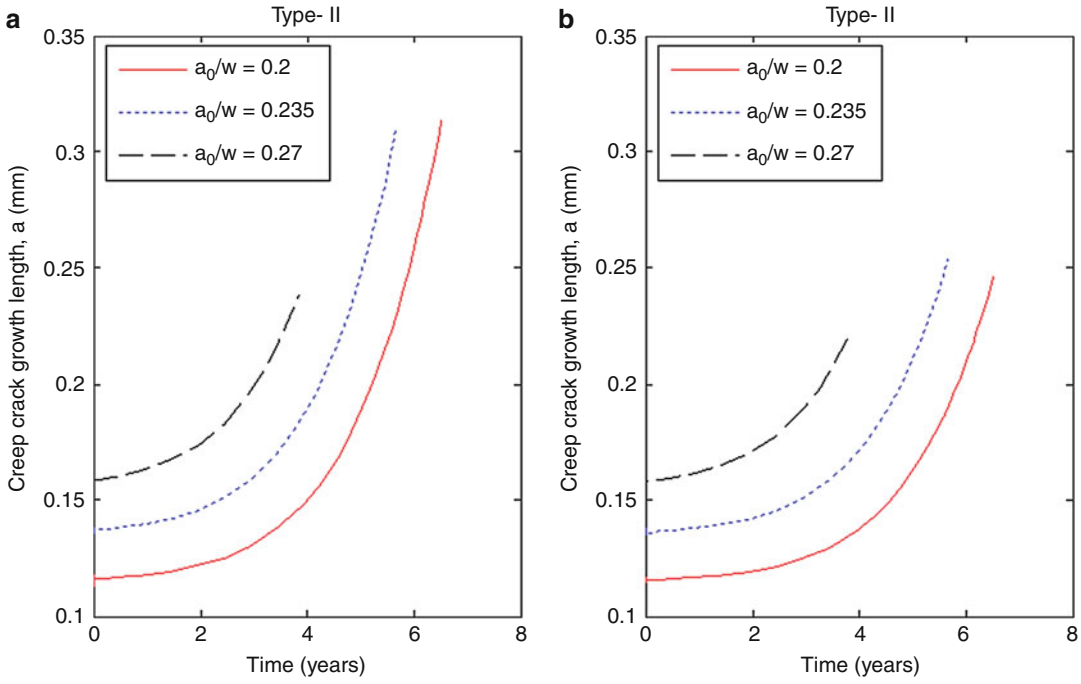

Creep Crack Growth, Fig. 6 The total crack growth for both Tip-A and Tip-B is shown in (**a**) and (**b**), respectively

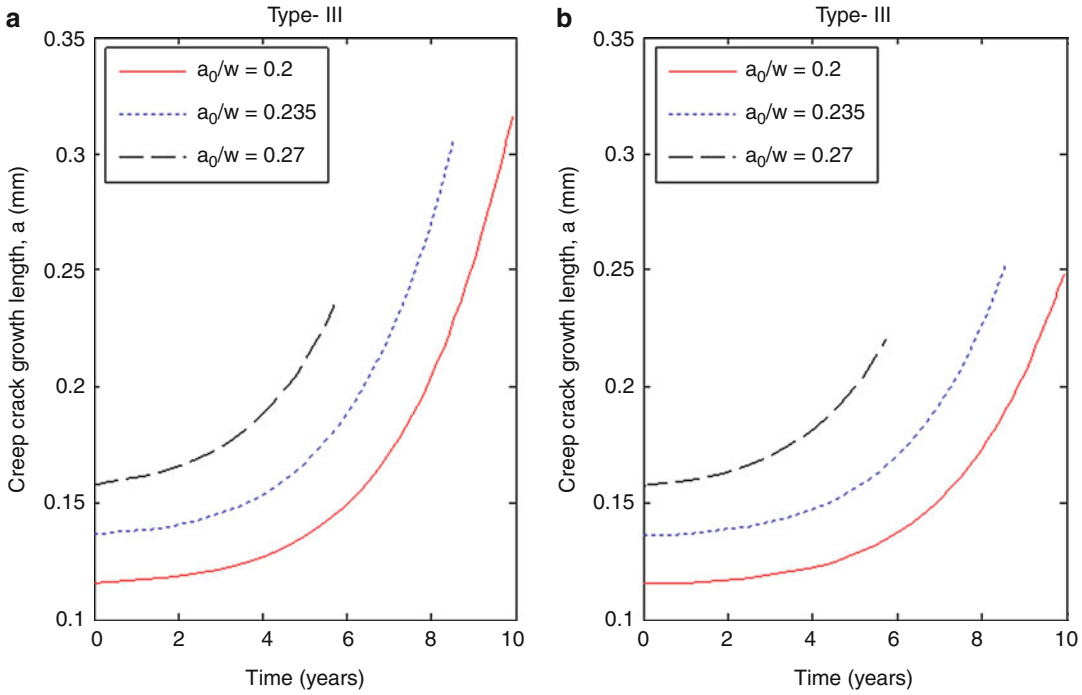

Creep Crack Growth, Fig. 7 The total crack growth for both Tip-A and Tip-B is shown in (**a**) and (**b**), respectively

$(dW/dV)_c = 0.32$ MPa. Note that the creep crack growth rate, da/dt, at Tip-A is larger than that at Tip-B since the circumferential stress along the inner boundary of cladding is greater than that along the outer boundary of cladding. The total crack growth for both Tip-A and Tip-B is obtained by directly integrating the crack growth increment rate. The total creep life can then be determined by setting conditions which represent the situation of through-wall crack, namely, when the sum of the total crack growth for both the inner and outer crack is equal to the thickness of the cladding. Here, it is understood that a larger initial crack length sustains a shorter creep life. The creep life for the different storage temperature profiles and different initial crack lengths is provided in Fig. 5. Referring to Fig. 3b, a storage temperature profile is applied at the inner boundary of cladding while a constant pressure of 90 MPa is applied to the inner boundary of the cladding, and a constant temperature of 400 °C is present at the outer boundary of the cladding. The C* value rises to its maximum value at $t = 10$ years with a maximum temperature of 570 °C and is then followed by a decrease from 570 °C to 400 °C for the last 10 years. The C^* value in the Type-II case rises less sharply than that seen in the Type-I, because the rate of increase of the storage temperature for the Type-II is just one half of that of the Type-I case. Consequently, both the crack growth increment rate, da/dt, and the total crack length, a, for the Type-II case are larger than those in the Type-I case. The results are displayed in Fig. 6. Referring to Fig. 3c, a storage temperature profile is applied at the inner boundary of cladding while a constant pressure of 90 MPa is applied to the inner boundary of the cladding, and a constant temperature of 400 °C is present at the outer boundary of the cladding. The trend of C^*, da/dt and the total crack length, a, is found to be similar to the trend presented by the Type-II case, except that both the crack growth increment rate, da/dt, and the total crack length, a, for the Type-III case are larger than those of the Type-II case, as indicated in Fig. 7. This is because the rate of increase of the storage temperature for Type-III is one half of that for Type-II, resulting in a higher creep life for the Type-III temperature profile.

Conclusions

Based on the energy rate line integral, C^*, and the strain energy density factor, S, a linear relationship between the energy rate line integral, C^*, and the creep crack growth rate, da/dt, is established theoretically. This criterion enables us to estimate the creep crack growth rate, da/dt, from the energy rate line integral, C^*, which is evaluated by using contour integral evaluation provided by the ABAQUS™ software. Three different storage temperature profiles and a constant storage temperature profile are used to simulate the loading conditions for spent fuel Zircaloy cladding in interim storage. The results show that the initial crack length and the storage temperature profile play an important role in the interim dry storage. We expect that a longer creep life can be predicted for claddings having a tougher material constant.

Acknowledgments The authors wish to acknowledge their appreciation to the National Science Council, Republic of China, through Grant No. NSC 93-2212-E011-001. Many thanks to G. A. Porter for his professional consultation services.

References

1. Limon R, Cappelaere C, Bredel T, Bouffioux P (2000) A formulation of the spent fuel cladding creep behaviour for long term storage. In: Proceedings of the 2000 international topical meeting on light water reactor fuel performance, Utah
2. Daum RS, Majumdar S, Liu Y, Billone MC (2005) Mechanical testing of high-burnup Zircaloy-4 fuel cladding under conditions relevant to drying operations and dry-cask storage. In: Proceedings of the 2005 water fuel performance meeting, Kyoto
3. Landes JD, Begley JA (1976) A fracture mechanics approach to creep crack growth. ASME STP, 590. American Society for Testing and Materials, Philadelphia
4. Sih GC (1973) Some basic problems in fracture mechanics and new concepts. J Energ Fract Mech 5:365–377
5. Riedel H (1981) Creep deformation at crack tips in elastic-viscoplasticitic solids. J Mech Phys Solids 29:35–50
6. Goldman NL, Hutchinson JW (1973) Fully plastic crack problems: the centre cracked strip under plane strain. Harvard University, Cambridge, MA

Creep Ratcheting

▶ Thermal Plastic Ratcheting

Creep Theory

▶ Thermo-creep Damage in Cu/Al-Alloys

Critical Flow Velocity

▶ Fluid-Thermal Structural Coupling in the Modeling of Carbon Nanotubes

Critical Speed

▶ Perturbation Methods in Thermoelastic Instability (TEI) with Finite Element Implementation

Critical Temperature Difference

▶ FGM Cones Surrounded by Pasternak-Type Elastic Medium Subjected to Thermal Load

Cryogenic Condition, Damage In

Błażej Skoczeń
Institute of Applied Mechanics, Faculty of Mechanical Engineering, Cracow University of Technology, Cracow, Poland

Synonyms

Cryogenic conditions, cryogenic temperatures; Discontinuous yielding, discontinuous plastic flow, serrated yielding; Evolution of micro-damage, damage in structures; Mechanisms of heat

transport, thermodynamic instability; Plastic strain-induced fcc-bcc phase transformation, γ - α phase transformation

Definition

The processes occurring in metals and alloys at very low temperatures are strictly related to their physical and mechanical properties, to the type of lattice and its imperfections, as well as to the mechanisms of heat transport. The basic mechanism of inelastic deformations remains the same and is based on the motion of dislocations. However, as the Peierls-Nabarro potential increases at low temperature, the dislocations are less mobile. Thus, the same load applied at the temperatures close to 0 K will produce much less inelastic deformation than at room temperature. Nevertheless, when approaching absolute zero several thermodynamic quantities like thermal conductivity, thermal contraction coefficient, specific heat at constant volume, or state functions like entropy also tend to 0. This fact results in the so-called thermodynamic instability at the temperatures close to absolute zero [1] and has fundamental meaning for the existence and triggering of coupled thermomechanical effects related to inelastic deformations.

Fcc (face-centered cubic) metals and alloys (such as Cu, Al, Cu-Al, stainless steels, etc.), frequently used in cryogenic applications, may undergo at low temperatures some or all of three distinct phenomena: *discontinuous plastic flow* related to dynamic strain ageing, *plastic strain–induced transformation* from the fcc parent phase to the bcc (body-centered cubic), and secondary phase and plastic strain–induced *evolution of micro-damage*. All three phenomena lead to irreversible degradation of lattice and can accelerate the process of material failure. Discontinuous plastic flow occurs below a temperature threshold, characteristic of given material [2], and is described by the mechanism of local catastrophic failure of Lomer-Cottrell (LC) locks under the stress fields related to the accumulating edge dislocations. Fcc-bcc phase transformation results from metastability of low stacking fault energy metals and alloys at very low temperatures. The phase transformation process leads to creation of two-phase continuum where the parent phase coexists with the inclusions of secondary phase. Evolution of micro-damage can be of brittle or ductile nature. In the case of brittle damage a micro-defect is initiated without a significant amount of plastic strain. Here, the intergranular damage mechanism plays fundamental role. It is related to nucleation and evolution of micro-cracks and micro-voids at the grain boundaries. In the case of ductile damage, the process of micro-decohesion is initiated as soon as the plastic strain threshold is reached. Ductile damage mechanism is often related to material instability that occurs within the slip-bands created in the favorably oriented crystal grains. The motion of dislocations is stopped by the micro-defects or the concentration of micro-stress on internal barriers (locks) as well as inclusions. Further increase of load leads to formation of micro-damage fields because of the increase of local shear stress beyond the cohesive strength. Thus, formation of micro-damage in cryogenic conditions appears to be strongly coupled to the mechanism of discontinuous plastic flow and to the phenomenon of phase transformation.

Overview

A broad class of fcc metals and alloys applied in cryogenic conditions is characterized by the low stacking fault energy. Such materials like austenitic stainless steels, strained at extremely low temperatures, undergo dynamic strain ageing (reflected by the plastic flow instability) and transformation from the parent phase (fcc) to the secondary phase (bcc). Each phenomenon can be classified as material instability associated on one hand with oscillatory mode of plastic flow (dynamic strain ageing) and, on the other hand, with a particular sensitivity to inelastic strain (fcc-bcc phase transformation). Thermodynamic conditions of plastic flow discontinuities and plastic strain–induced phase transformation are related to the so-called thermodynamic instability resulting from vanishing specific heat when

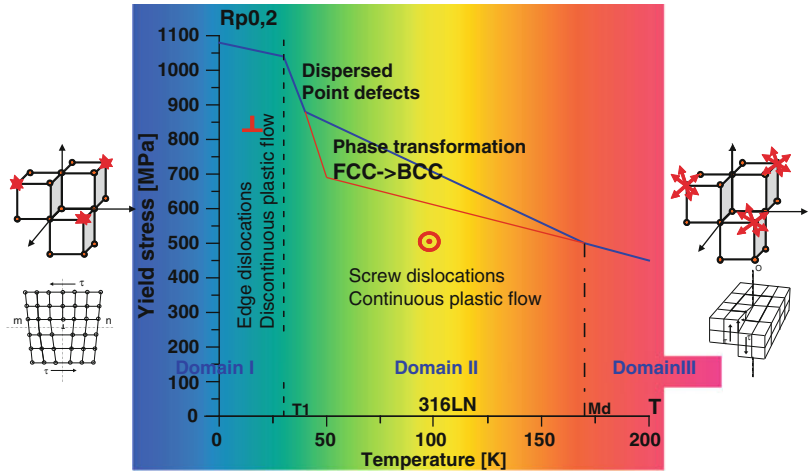

Cryogenic Condition, Damage In, Fig. 1 Three domains of response and prevailing dislocation modes in LSFE materials applied at low temperatures (316LN)

the temperature approaches absolute zero. While the dynamic strain ageing manifests itself at the macroscopic level by discontinuous plastic flow (serrated yielding), the phase transformation converts the material from homogeneous to a heterogeneous two-phase continuum. Both phenomena are accompanied by nucleation and evolution of micro-damage fields, driven by inelastic strains that develop at very low temperatures.

Three distinct phenomena (Fig. 1), associated with the evolution of plastic strains at very low temperatures, are characterized by the following features:

- Discontinuous (serrated) yielding is characteristic both of low (LSFE) and high stacking fault energy (HSFE) materials strained at very low temperatures. It represents oscillatory mode of plastic deformation and reflects discontinuous nature of plastic flow (discontinuous in terms of $d\sigma/d\varepsilon$). Serrated yielding occurs below a specific temperature: T_1 for LSFE materials and T_0 for HSFE materials. Each of them represents transition from screw to edge dislocations [2]. The transition temperature is material dependent and its maximum value known to date reaches some 35 K. Also, serrated yielding turns out to be a strain rate–sensitive phenomenon and occurs for plastic strain rate exceeding a critical – material-dependent – value [3, 4].
- During the plastic strain–induced phase transformation that occurs in LSFE materials at low temperatures the γ austenite (type fcc lattice) is transformed into α' martensite (type bcc lattice). The presence of lenticular martensite inclusions embedded in the austenitic matrix modifies the surrounding fcc lattice and implies local distortions. The plastic strain–induced phase transformation remains at the origin of considerable evolution of material properties (strong hardening). The main mechanism contributing to the onset of $\gamma \rightarrow \alpha'$ phase transformation in such materials like stainless steels is the intersection of shear bands [5]. These materials are often termed TRIP since they exhibit the so-called transformation-induced plasticity [6].
- The plastic strain driven evolution of ductile micro-damage at cryogenic temperatures [7] represents a dissipative and irreversible process that leads to creation of micro-cracks and micro-voids (micro-damage fields) and results in material "softening" (decrease of the effective unloading modulus). Formation of micro-damage fields is often related to material instabilities that occur when the motion of dislocations is stopped by the lattice defects, inclusions or the concentration of micro-stress on internal barriers (locks).

Three distinct domains of response of LSFE materials are indicated in Fig. 1 for one of the most frequently applied materials in cryogenic conditions – stainless steel 316LN. Domain I corresponds to the temperature range

below T_1 and to the plastic flow instability called discontinuous yielding. Domain II stretches between T_1 and M_d, the latter being the temperature above which the process of plastic strain–induced $\gamma \rightarrow \alpha'$ phase transformation does not take place. Inside this domain, the plastic flow is smooth and accompanied by the transformation from the parent γ phase to the secondary α' phase. The phase transformation leads to a significant increase of the yield stress. Finally, domain III above the temperature M_d is characterized by smooth plastic flow and no phase transformation. It is worth pointing out that the evolution of micro-damage occurs in all three domains and is driven by stable or unstable plastic flow.

Conditions of Plastic Flow and Damage Evolution

Domain I: Serrated yielding has been investigated – mostly experimentally – by many authors [8]. However, experimental evidence for the dislocation mechanism of serrated yielding was found in the 1990s [2, 9]. According to this explanation, the pile-ups of dislocations on the internal barriers in the lattice give rise to stress concentrations of the order of theoretical shear strength. The load drops observed in the stress–strain curves are due to catastrophic process consisting in the spontaneous generation of dislocations as soon as the internal barriers are broken. Thus, the origin of the plastic flow instability is of mechanical nature. A different point of view was developed earlier [10] and attributed the load drops to thermodynamic properties of materials at very low temperatures, such as the specific heat and the thermal conductivity tending to 0 with the temperature approaching 0 K. The so-called adiabatic heating hypothesis was based on the assumption that any sufficiently fast dissipative process at very low temperatures, where the plastic work is converted to heat, leads to increase of local temperature and to drastic decrease of flow stress (negative slope of flow stress against temperature). Two different theories: the mechanical and the thermodynamic originated from these two competing hypotheses. Both of them reflect complex nature of the flow instabilities that occur at very low temperatures.

Domain II: The classical model of plastic strain–induced $\gamma \rightarrow \alpha'$ phase transformation at low temperatures [5] attributes the onset of transformation to the intersection of shear bands. A three parameters model has been postulated for the so-called TRIP steels. It is capable of describing the experimentally verified sigmoidal curve that represents the volume fraction of martensite as a function of plastic strain. The sigmoidal curve is valid for a wide range of temperatures, including room temperature. However, at very low temperatures the rate of phase transformation for LSFE material becomes less temperature dependent and can be described by a simplified linearized model [11]. The $\gamma \rightarrow \alpha'$ phase transformation yields the initially homogeneous material strongly heterogeneous, as a result of the presence of α'-martensite platelets embedded in the γ-austenite matrix. Since the α'-martensite behaves in the flow range of austenite-martensite composite mostly elastically (yield point of α'-martensite is much higher that the yield point of γ-austenite), its presence in the lattice affects the plastic flow and the process of hardening [12]. As a result of the plastic strain–induced phase transformation at cryogenic temperatures, the material properties evolve in a considerable way and – in the critical cases – the parent γ-phase can be completely replaced by the brittle α'-phase leading to a premature failure of the material.

Domains I, II, and III: Ductile materials strained in cryogenic conditions develop micro-damage fields in a similar way like at room or enhanced temperatures. Evolution of damage fields (micro-cracks and micro-voids) is also driven by the plastic strains and similar kinetic laws can be used. The conjugate thermodynamic force associated to damage variable by means of the Helmholtz free energy is the strain energy density release rate. On the other hand, damage rate can be obtained directly from the potential of dissipation representing the irreversible process of damage evolution [13]. As at very low temperatures the yield stress of typical stainless steels is approximately doubled when compared to room temperature, the level of stress needed to obtain damage fields of similar intensity like at room temperature is much higher.

Basic Methodology

Thermodynamic Background of Low-Temperature Plasticity

A quantum representation of elastic vibrations of lattice (phonons) is adopted as one of the fundamental mechanisms of heat transport. Thus, it is assumed that the heat-induced vibrations of lattice are composed of phonons. The energy of lattice (sum of energy of all the "harmonic oscillators") is given by [14]:

$$E_{ph} = E_0 + \sum_{\mathbf{k}} N_{\mathbf{k}} \hbar \omega(\mathbf{k}) \tag{1}$$

where $N_{\mathbf{k}}$ denotes the sequence of quantum numbers, each representing the number of excited phonons, that corresponds to a given wave vector $\mathbf{k}$. Here, $\hbar$ denotes the Planck constant. Thus, the energy of lattice is expressed as a sum of two terms – the energy of zero vibrations and the energy of the phonon "gas." The main mechanism of heat transport at very low temperatures is based on the diffusion of phonon gas. The average free path of a phonon is determined by the mechanism of collisions either with the lattice imperfections or with other phonons. It is assumed that the reference (Debye) temperature, characteristic of the lattice, is defined as:

$$\Theta = \hbar \omega_{\max} \tag{2}$$

where $\omega_{\max}$ is the maximum frequency of acoustic phonons. The current temperature is considered low if the following inequality is satisfied:

$$T << \Theta \tag{3}$$

For the energy of lattice at low temperatures the following equation holds:

$$\Delta E_{ph} = E_{ph} - E_0 = \int_0^{\omega_{\max}} \psi(\omega) \nu(\omega) \hbar \omega d\omega \tag{4}$$

where $\psi(\omega)$ denotes the statistical distribution function (Bose-Einstein statistics) and $\nu(\omega)$ is the phonon density of states function. Given the assumption of linear dispersion law, the internal energy due to the phonon states takes the following form:

$$\Delta E_{ph} \sim N \left(\frac{T}{\Theta} \right)^3 T \tag{5}$$

where N denotes the number of atoms (cells) in the lattice. Based on the internal energy of lattice associated with phonon excitations, one can easily derive the specific heat under constant volume:

$$C_V = \left(\frac{\partial E_{ph}}{\partial T} \right)_V \sim N \left(\frac{T}{\Theta} \right)^3 \tag{6}$$

Thus, the specific heat is a nonlinear function of normalized temperature and tends to 0 when the temperature T approaches absolute zero. Specific heat under constant volume (strain) as a function of temperature normalized to Debye reference value is shown in Fig. 2a.

The thermal conductivity k_T in the lattice at low temperatures is defined (for uniaxial model) as:

$$\dot{q} = -k_T \frac{\partial T}{\partial x} \tag{7}$$

where $\dot{q}$ denotes the heat flux. Based on the kinetic theory of perfect gas the thermal conductivity can be written in the following form [15]:

$$k_T = \frac{C_V \upsilon l}{3} \tag{8}$$

where υ denotes the average velocity of gas particles and l is the average free path between the interactions. A similar reasoning can be applied to the phonon gas interactions in the lattice. At very low temperatures the free path of phonons between interactions is of the order of the size of sample or of the order of the distance between the lattice imperfections. In both cases the free path of phonons does not depend on temperature. The velocity of acoustic phonons is also constant and equal to the speed of sound in the lattice. Thus, the only function in (8) that depends on

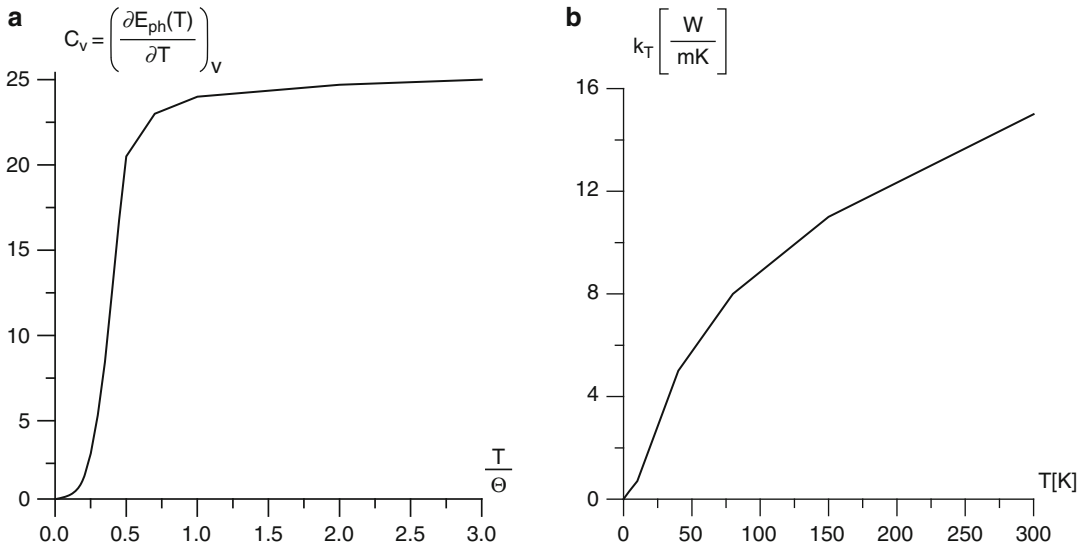

Cryogenic Condition, Damage In, Fig. 2 (**a**) Specific heat under constant volume as a function of temperature; (**b**) thermal conductivity as a function of temperature for 316L stainless steel

temperature is the specific heat. This leads to the following conclusion:

$$k_T \sim \frac{\upsilon_s L}{3} N \left(\frac{T}{\Theta}\right)^3 \tag{9}$$

where υ_s denotes the speed of sound and L is the size of sample. Thus, thermal conductivity is again a nonlinear function of temperature and tends to 0 when the temperature approaches absolute zero. Thermal conductivity as a function of temperature for stainless steel 316L is shown in Fig. 2b.

Thermodynamic Instability at Very Low Temperatures

The fact that the state functions tend to 0 when the temperature approaches absolute zero (which reflects the third law of thermodynamics) leads to the phenomenon of thermodynamic instability [1]. The heat increment is related to temperature by the following equation:

$$dQ = mC_V dT \tag{10}$$

where m is the mass of the sample. By transforming this equation to the form:

$$\frac{dT}{dQ} = \frac{1}{mC_V} \tag{11}$$

and knowing that $C_V \to 0$ when $T \to 0$ one obtains:

$$\frac{dT}{dQ} \to \infty \tag{12}$$

which means that close to absolute zero an arbitrary small dissipation of energy in the lattice will produce a significant increase of temperature. Such energy dissipation can be induced by plastic deformation (motion of dislocations in the lattice), accompanied by the plastic work partially converted to heat. Thus, thermodynamic instability is of fundamental importance for the plastic flow instabilities (discontinuous plastic flow) and determines their thermomechanical conditions.

Kinetics of the Plastic Strain–Induced Phenomena at Cryogenic Temperatures

Kinetics of Discontinuous (Serrated) Yielding (Domain I)

The main feature of serrated yielding consists in frequent abrupt drops of stress as a function of strain

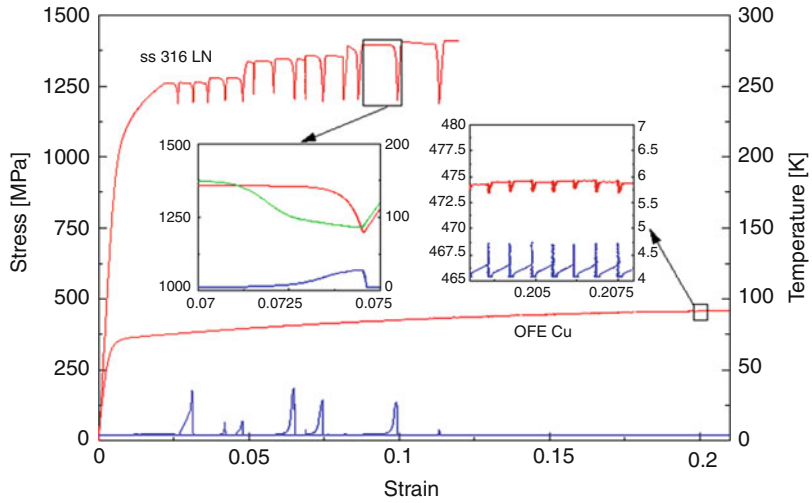

Cryogenic Condition, Damage In,
Fig. 3 Discontinuous plastic flow in fcc metals and alloys at cryogenic temperatures: 316LN stainless steel and OFE Copper

during monotonic loading. The mechanism of discontinuous yielding is related to formation of dislocation pile-ups at strong obstacles such as the Lomer-Cottrell locks during the strain hardening process. The back stresses of the piled-up groups block the motion of newly created dislocations. The local shear stress at the head of dislocation pile-up, proportional to the number of dislocations in the pile-up, reaches the level of cohesive strength and the Lomer-Cottrell lock collapses by becoming a glissile dislocation. This process takes place below the temperature T_1 (or T_0) where the dislocations have predominantly edge character and cannot leave the pile-up by cross-slip. Such a local catastrophic event can trigger similar effects in the other groups of dislocations. Thus, the final result is massive and has a collective character. At low temperatures, where very high stresses are expected, this avalanche-like process is followed by spontaneous generation of dislocations by rapidly increasing number of sources. This – in turn – leads to the load drops observed in the stress–strain curve. It is well known that the increasing intensity of plastic flow generates more barriers for the motion of dislocations. Therefore, the following kinetic law of evolution of density of the Lomer-Cottrell locks holds:

$$\dot{B} = F_{LC}(\rho, T, \sigma_{ij})\dot{p};$$
$$\dot{p} = \frac{dp}{dt} = \sqrt{\frac{2}{3}\dot{\varepsilon}^p_{ij}\dot{\varepsilon}^p_{ij}}; \quad p \geq p_{LC} \tag{13}$$

where F_{LC} is function of density of dislocations ρ, temperature T, and the level of stress σ_{ij}, whereas p_{LC} represents the plastic strain threshold above which the Lomer-Cottrell barriers massively develop. During tensile test at low temperature the avalanche-like barrier crossing by dislocation pile-ups is manifested by acoustic effects of "dry" sounds emitted by the specimen. Each serration is accompanied by a considerable increase of temperature, related to dissipation of plastic power and thermodynamic instability described in the previous section. Typical stress–strain curves for selected materials that exhibit discontinuous yielding (stainless steel 316LN and OFE Copper at 4.2 K) are illustrated in Fig. 3.

Kinetics of Phase Transformation (Domain II)

The plastic strain–induced $\gamma \rightarrow \alpha'$ phase transformation in metastable materials (like stainless steels) occurs in a wide range of temperatures below M_d (Fig. 4). For instance, it can be easily activated at 77 K, in liquid nitrogen. The process is represented by the transformation kinetics, reflected by the phase transformation curve. Kinetics of $\gamma \rightarrow \alpha'$ phase transformation [5] is described by typical sigmoidal curve defining the evolution of martensite content ξ as a function of plastic strain p. At very low temperatures the phase transformation process can be subdivided into three stages: low rate transformation below the plastic strain threshold p_ξ (stage I),

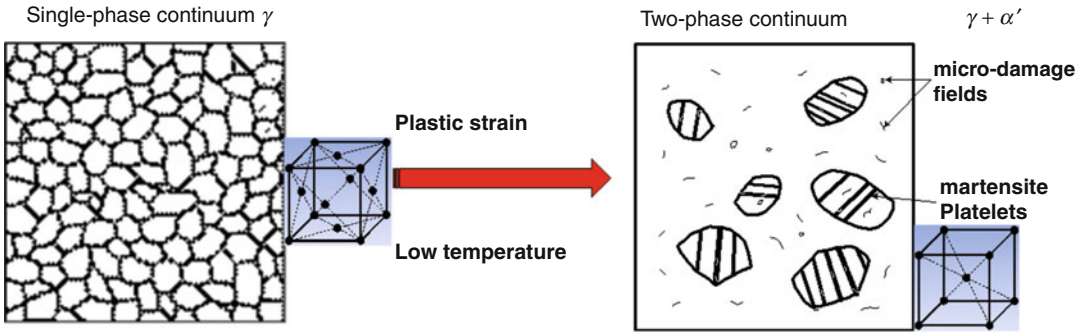

Cryogenic Condition, Damage In, Fig. 4 Plastic strain–induced $\gamma \rightarrow \alpha'$ phase transformation at cryogenic temperatures accompanied by evolution of micro-damage

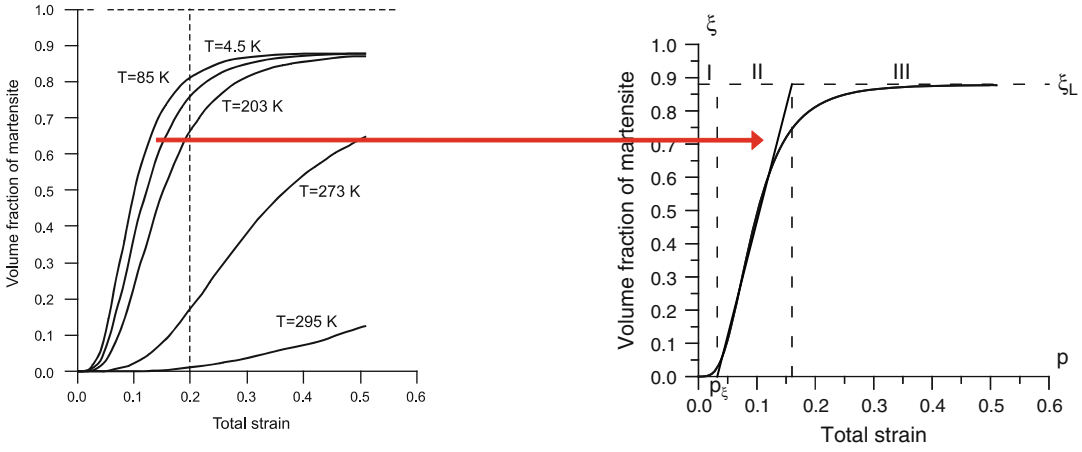

Cryogenic Condition, Damage In, Fig. 5 Kinetics of plastic strain–induced fcc-bcc phase transformation at cryogenic temperatures – sigmoidal curves

fast transformation with high and nearly constant transformation rate (stage II), and asymptotically vanishing transformation with the rate decreasing to 0 and the volume fraction of martensite reaching a maximum ξ_L (stage III). For the phase transformation that occurs at very low temperatures (typically in liquid helium 4.2 K or in liquid nitrogen 77 K), the steep part of the transformation curve (Fig. 5, stage II) remains in the domain of relatively small strains [7] and is expressed by the following equation:

$$\dot{\xi} = A\left(T, \sigma_{ij}, \dot{\varepsilon}^p_{ij}\right)\dot{p}; \quad p \geq p_\xi, \ \xi \leq \xi_L \qquad (14)$$

where A is a function of temperature T, stress state σ_{ij}, and strain rate $\dot{\varepsilon}^p_{ij}$.

Kinetics of Micro-damage Evolution (Domains I, II, and III)

Isotropic damage, represented by a scalar (damage parameter), is related to the plastic strain for monotonic loads and to the accumulated plastic strain for cyclic loads. The classical kinetic law of micro-damage evolution [16] for isotropic and ductile damage postulates linear relation between the damage rate and the plastic strain rate. The conjugate force associated to damage by means of the Helmholtz free energy is the strain energy density release rate. Kinetics of damage evolution can be obtained directly from the potential of dissipation that reflects the irreversible process of material degradation. As the materials applied at low temperatures are often characterized by texture, the scalar damage variable is replaced by

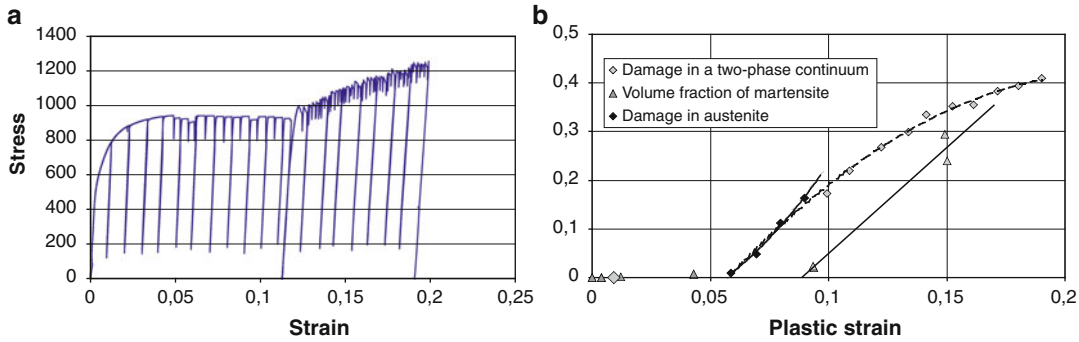

Cryogenic Condition, Damage In, Fig. 6 (**a**) Loading-unloading test for stainless steel 316L at 4.2 K; (**b**) evolution of micro-damage in two-phase continuum (316L transformed)

damage tensor [17] in order to allow for damage anisotropy. In the anisotropic case, the plastic strain remains the main driving force of ductile damage evolution [7]:

$$\dot{D}_{ij} = C_{ik} Y_{kl} C_{jl} \dot{p}; \quad p \geq p_D \tag{15}$$

where Y_{kl} stands for the strain energy density release rate tensor, C_{ij} defines the material properties in the principal directions of damage and p_D denotes the damage threshold. As the yield stress of typical stainless steels is approximately doubled at very low temperatures, the level of stress needed to obtain damage fields of similar intensity like at room temperature is much higher. The evolution of micro-damage at cryogenic temperatures starts as soon as the damage threshold, expressed in terms of plastic strain or accumulated plastic strain, is reached. In the simplest case, damage variable increases in the form of linear function of plastic strain. However, activation of the phase transformation process affects significantly the evolution of micro-damage, decreasing its rate (Fig. 6).

Damage in Structures Operating at Cryogenic Temperatures

Bellows expansion joints belong to thin-walled structures of high flexibility, commonly applied as compensation elements in complex cryogenic systems. They are used to compensate for the relative motion of two adjacent assemblies, subjected to thermal cycles or to service loads. Bellows are frequently used in extreme conditions, comprising various temperature ranges and load types, which makes them a class of highly engineered shell structures. Bellows expansion joints are crucial elements of systems working at cryogenic temperatures, where the adjacent structures contract significantly during the cool-down process and the emerging displacements of components need to be compensated. Among many systems working at cryogenic temperatures and using this type of thin-walled structures the modern particle accelerators comprising the superconducting magnets are eminent. The expansion bellows for low temperature applications are usually made of metastable stainless steels and – depending on the operational temperature – all or some of the above described phenomena may take place. In particular, the evolution of micro-damage accompanied by the phase transformation process is observed in the bellows wall. The bellows operating at extremely low temperatures (liquid helium) are subjected to plastic flow discontinuities and enhanced rate of micro-damage production. A profile of bellows segment (half wave) is illustrated in Fig. 7. Thin-walled bellows convolutions form a set of waves obtained from the hydroforming process, which induces an initial state of plastic deformation. The intensity of plastic strain fields depends on the ratio between the depth of convolutions and the pitch (the wave-length). Since the plastic strain intensity may locally reach high values after the forming process, an

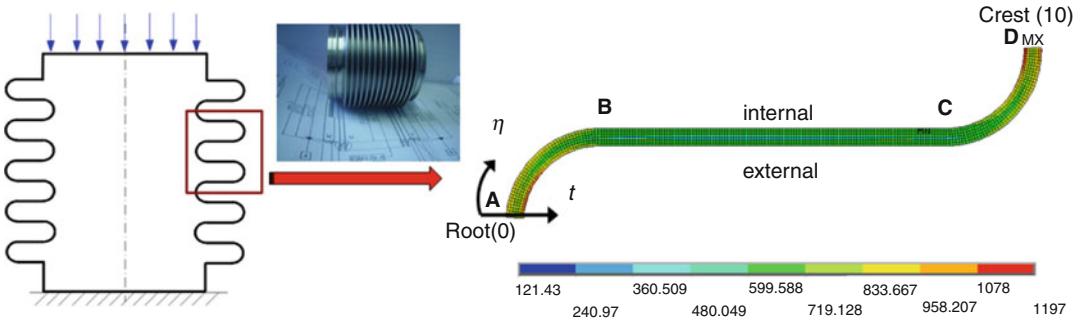

Cryogenic Condition, Damage In, Fig. 7 Half wave of expansion bellows operating at cryogenic temperatures

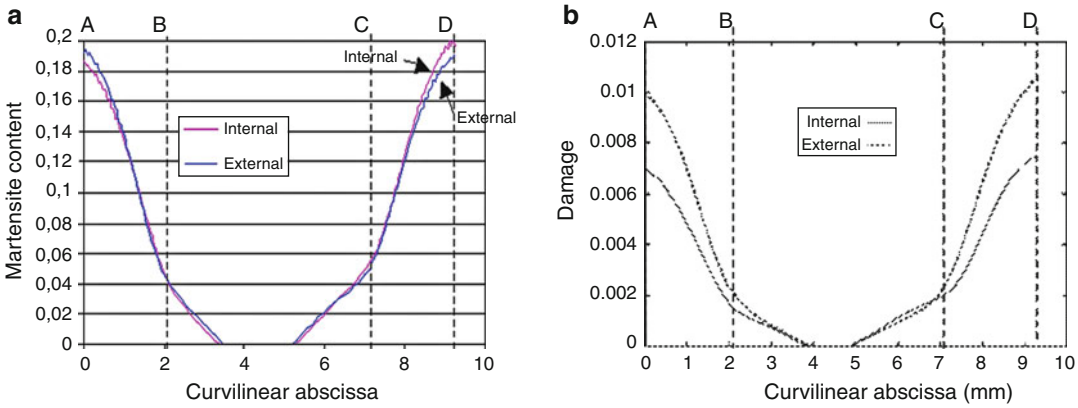

Cryogenic Condition, Damage In, Fig. 8 (**a**) Profile of volume fraction of martensite; (**b**) profile of micro-damage along the half wave of expansion bellows

initial state of damage exists even before the structure is loaded in cryogenic conditions. The bellows expansion joints are subjected to particularly severe conditions: thermomechanical cycles between room and operational temperature associated with axial deflections of the order of the bellows length and internal pressure up to 2 MPa. Such a severe loading conditions may cause fast evolution of micro-damage fields (Fig. 8) and lead to development of macro-crack and to fracture of the expansion joint (Fig. 9).

Key Research Findings

Three fundamental phenomena occur at extremely low temperatures in metals and alloys characterized by low stacking fault energy:

1. Dynamic strain ageing, reflected by *discontinuous plastic flow*
2. *Plastic strain–induced transformation* from the parent fcc phase to the secondary bcc phase, characteristic of metastable materials
3. *Evolution of micro-damage* fields (micro-voids and micro-cracks), reflected by decreasing unloading modulus in the course of deformation

The thermodynamic background is related to the mechanisms of heat transport in the weakly excited lattice at very low temperatures. In particular, the fact that the thermodynamic quantities (specific heat, thermal conductivity, thermal expansion coefficient) tend to 0 when the temperature approaches absolute zero, leads to the phenomenon of thermodynamic instability. It is of fundamental importance for the conditions of

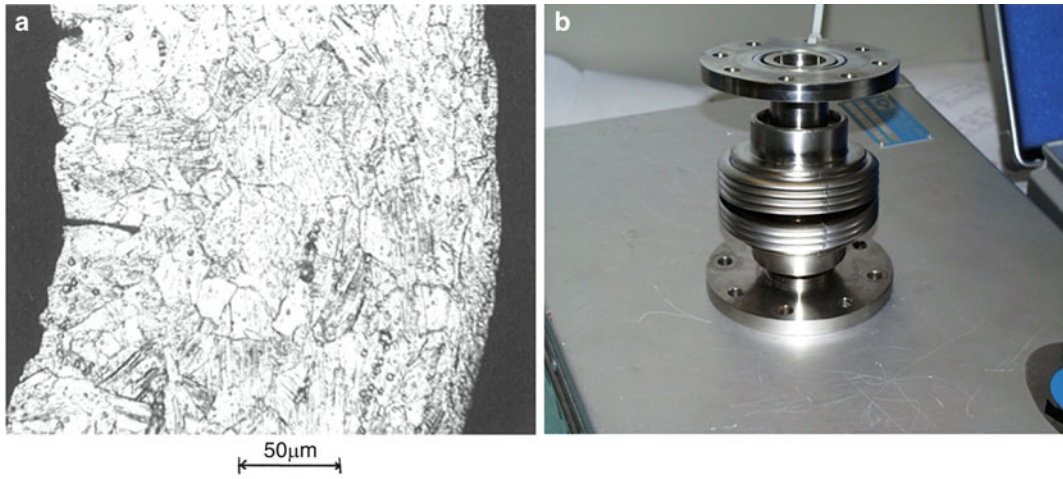

Cryogenic Condition, Damage In, Fig. 9 (**a**) Micrograph of typical zone containing damage at the root of bellows convolution; (**b**) fracture of bellows (macro-crack propagation)

plastic flow instabilities (discontinuous plastic flow) and provides the framework for thermomechanical coupling.

Discontinuous plastic flow may significantly intensify evolution of micro-damage, which leads to irreversible degradation of lattice and accelerates the process of material failure. On the other hand, plastic strain–induced phase transformation of small and moderate intensity essentially decelerates the evolution of micro-damage, which is beneficial for the lifetime of cryogenic installations. However, massive fcc-bcc phase transformation may cause embrittlement of structures and lead to premature fracture of the components. One of the cryogenic components loaded far beyond the yield point is called bellows expansion joint. Cryogenic expansion bellows are excellent examples of structures where all three phenomena may simultaneously occur. Integrity of expansion bellows is crucial for such applications like superconducting particle accelerators.

Cross-References

- ▶ Discontinuous Yielding at Cryogenic Temperatures
- ▶ Ductile Damage at Cryogenic Temperatures

References

1. Skoczeń B (2004) Compensation systems for low temperature applications. Springer, Berlin/Heidelberg/New York
2. Obst B, Nyilas A (1991) Experimental evidence on the dislocation mechanism of serrated yielding in f.c.c. metals and alloys at low temperatures. Mat Sci Eng A137:141–150
3. Reed RP, Walsh RP (1988) Tensile strain rate effect in liquid helium. Adv Cryogenic Eng Mater 34:199–208
4. Reed RP, Simon NJ (1988) Discontinuous yielding in austenitic steels at low temperatures. In: Proceedings of international cryogenic material conference, Boulder, vol 2, pp 851–863
5. Olson GB, Cohen M (1975) Kinetics of strain-induced martensitic nucleation. Metall Trans 6A:791–795
6. Cherkaoui M, Berveiller M, Lemoine X (2000) Couplings between plasticity and martensitic phase transformation: overall behavior of polycrystalline TRIP steels. Int J Plast 16:1215–1241
7. Garion C, Skoczeń B (2003) Combined model of strain induced phase transformation and orthotropic damage in ductile materials at cryogenic temperatures. Int J Damage Mech 12(4):331–356
8. Pustovalov VV (2008) Serrated deformation of metals and alloys at low temperatures. Low Temp Phys 34(9):683–723
9. Obst B, Nyilas A (1998) Time-resolved flow stress behavior of structural materials at low temperatures. In: Advances in cryogenic engineering (Materials), vol 44. Plenum, New York, pp 331–338
10. Basinski ZS (1957) The instability of plastic flow of metals at very low temperatures. Proc R Soc Lond Ser A 240:229–242

11. Garion C, Skoczeń B (2002) Modeling of plastic strain induced martensitic transformation for cryogenic applications. J Appl Mech 69(6):755–762
12. Garion C, Skoczeń B, Sgobba S (2006) Constitutive modelling and identification of parameters of the plastic strain induced martensitic transformation in 316L stainless steel at cryogenic temperatures. Int J Plast 22(7):1234–1264
13. Abu Al-Rub RK, Voyiadjis GZ (2003) On the coupling of anisotropic damage and plasticity models for ductile materials. Int J Solid Struct 40:2611–2643
14. Kosevich AM (1981) Fiziczeskaja mechanika realnych kristallov. Izdatielstvo Naukowa Dumka, Kijev (In Russian)
15. Kittel C (1996) Introduction to solid state physics. Wiley, New York
16. Lemaitre J (1992) A course on damage mechanics. Springer, Berlin/New York
17. Murakami S (1990) A continuum mechanics theory of anisotropic damage. In: Yielding, damage, and failure of anisotropic solids, Proceedings of the IUTAM/ICM symposium, Villard-de-Lans, EGF publication, 5, pp 465–482

Cryogenic Conditions, Cryogenic Temperatures

► Cryogenic Condition, Damage In

Curvilinear Cracks

Ching-Kong Chao[1] and M. H. Shen[2]
[1]Department of Mechanical Engineering, National Taiwan University of Science and Technology, Taipei, Taiwan, Republic of China
[2]Department of Automation Engineering, Nan Kai University of Technology, Tsao Tun, Nantou, Taiwan, Republic of China

Synonyms

Crack

Originally published in: Chao CK, Chen FM (2009) Heterogeneous Problems in Plane Thermoelasticity. Journal of Thermal Stresses Vol 32–6/7:623–655, reprinted by permission of © Taylor & Francis Group, LLC (http://tandfonline.com)

Overview

Problems of finding the stress distribution around circular-arc cracks in an infinite plate subjected to a uniform tensile load have been solved by using the complex variable theory [1]. The study was initiated by Muskhelishvili [2], and later, the formulae of the stress intensity factors were derived by Sih et al. [3]. Thereafter, a number of problems of various types of circular-arc cracks, including the inhomogeneous cases, have been published. The stress distribution in an infinite plate with a circular disk was investigated by Dundurs and Hctinyi [4]. The problems of curvilinear cracks in bonded dissimilar materials were studied by Perlman and Sih [5]. It was found that the stresses near the tips of a curved crack possess the same trig-log character of singularity as those obtained for a straight crack between dissimilar media. By using the boundary collocation method, Cheung et al. [6] obtained the stress intensity factors for a circular-arc crack in a finite width strip. In this entry, we focus on the determination of thermal stress distribution around circular-arc cracks embedded in an infinite elastic plate under a uniform heat flow. An exact solution is given for a semicircular insulated crack in an infinite plate subjected to a uniform heat flow at an arbitrary angle. Unlike the cases of straight cracks, the simultaneous existence of mode-I and mode-I1 stress intensity factors for curvilinear cracks in the thermoelastic body is found in this entry which will affect the pattern of initial crack propagation and failure instability.

Statement of the Problem

A homogeneous isotropic elastic body divided by two regions S^+, interior to the unit circle, $|r| = 1$, and S^-, exterior to the unit circle, is considered as shown in Fig. 1. If the bond between the two regions on the unit circle is imperfect, it can be represented as the sum of L and L^*, with L being the union of n circular-arc cracks $a_j b_j, j = 1, 2, \ldots, n,$ and L^* being the union of n circular-arc bond. Let the center of the unit circle be placed at the origin of the complex plane and $z = x + iy$ and $t = e^{i\varphi}$ be

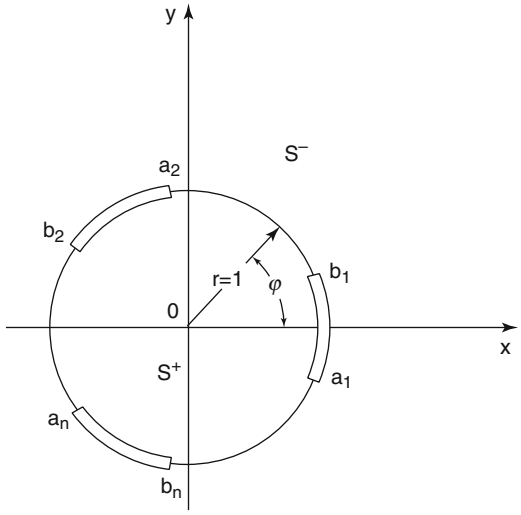

Curvilinear Cracks, Fig. 1 An infinite medium with curvilinear cracks along the interface of a unit disk

those of z on $|z| = 1$. For the problem of steady-state heat conduction, the temperature $T(x, y)$ can be related to the analytic function $\phi_0(z)$, i.e.,

$$T(x, y) = \mathrm{Re}[\phi_0(z)] \tag{1}$$

where Re stands for the real part of the complex function. By using the Cauchy-Riemann conditions, the temperature gradient is represented as:

$$\frac{\partial T}{\partial x} - i\frac{\partial T}{\partial y} = \phi_0'(z) = \Phi_0(z) \tag{2}$$

where the prime ($'$) denotes differentiation with respect to its argument. In order to specify the temperature gradient on L, the heat flux q_r is introduced in terms of the temperature gradient $\Phi_0(z)$ by the equation:

$$q_r = -\frac{k}{2}\left[\Phi_0(z) + \overline{\Phi_0(z)}\frac{\overline{z}}{z}\right]e^{i\varphi} \tag{3}$$

where the overbars denote the complex conjugates and k stands for the heat conductivity. By introducing a new function,

$$\Theta(z) = \frac{1}{z^2}\overline{\Phi_0}\left(\frac{1}{z}\right) \tag{4}$$

the heat flux q_r specified on L can be expressed as:

$$2{q_r}^+ e^{-i\varphi} = -k[{\Phi_0}^+(t) + \Theta^-(t)] \quad \text{on L} \tag{5}$$

$$2{q_r}^- e^{-i\varphi} = -k[{\Phi_0}^-(t) + \Theta^+(t)] \quad \text{on L} \tag{6}$$

where the superscripts + and − are used to denote the boundary values of the physical quantities as they are approached from S^+ and S^-, respectively. Equations (5) and (6) can be rewritten as the Hilbert problem:

$$[\Phi_0(t) - \Theta(t)]^+ - [\Phi_0(t) - \Theta(t)]^- = 2f(t) \quad \text{on L} \tag{7}$$

$$[\Phi_0(t) + \Theta(t)]^+ + [\Phi_0(t) + \Theta(t)]^- = 2g(t) \quad \text{on L} \tag{8}$$

where $f(t)$ and $g(t)$ are related to the heat flux q_r on L by

$$f(t) = -[{q_r}^+ - {q_r}^-]e^{-i\varphi}/k \tag{9}$$

$$g(t) = -[{q_r}^+ + {q_r}^-]e^{-i\varphi}/k \tag{10}$$

The solutions to the Hilbert problem can be found as:

$$\Phi_0(z) - \Theta(z) = \frac{1}{\pi i}\int_L \frac{f(t)}{t - z}dt + e_0 + \frac{e_1}{z} + \frac{e_2}{z^2} \tag{11}$$

$$\Phi_0(z) + \Theta(z) = \frac{1}{\pi i X_0(z)}\int_L \frac{X_0^+(t)g(t)}{t - z}dt + \frac{1}{X_0(z)}\left[Q_n(z) + \frac{E_1}{z} + \frac{E_2}{z^2}\right] \tag{12}$$

where the Plemelj function $X_0(z)$ is given by Muskhclishvili [2]

$$X_0(z) = \prod_{j=1}^{n}(z - a_j)^{1/2}(z - b_j)^{1/2} \tag{13}$$

and the polynomial $Q_n(z)$ is of degree not greater than n, i.e.,

$$Q_n(z) = \lambda_0 z^n + \lambda_1 z^{n-1} + \cdots + \lambda_n \tag{14}$$

The problem of finding the temperature field is now reduced to the determination of the $n + 6$ unknown constants $e_0, e_1, e_2, E_1, E_2, \lambda_j (j = 0, 1, \ldots, n)$ which may be solved by using the properties of the complex functions.

Thermal Stresses

For the two-dimensional theory of thermoelasticity, the components of the stress and displacement can be expressed in terms of the complex functions $\Phi(z)$ and $\psi(z)$. It follows [7]:

$$\sigma_r + \sigma_\theta = 4\,\mathrm{Re}\{\Phi(z)\} \tag{15}$$

$$\sigma_r + i\tau_{r\theta} = \Phi(z) + \overline{\Phi(z)} - \overline{z\Phi'(z)} - \left(\frac{\overline{z}}{z}\right)\overline{\Psi(z)} \tag{16}$$

$$2\mu(u + iv) = \kappa\phi(z) - z\overline{\phi'}(\overline{z}) - \overline{\psi}(\overline{z}) + 2\mu\beta g(z) \tag{17}$$

$$\phi'(z) = \Phi(z) \quad \psi'(z) = \psi(z) \quad g(z) = \int \phi_0(z)dz \tag{18}$$

where $\kappa = (3 - v)/(1 + v)$ for plane stress, $\kappa = 3 - 4v$ for plane strain, and $\beta = (1 + v)\alpha_0$, with v, μ, α_0, being Poisson's ratio, elastic modulus, and thermal expansion coefficient, respectively. By introducing a new function:

$$\Omega(z) = \overline{\Phi}\left(\frac{1}{z}\right) - \frac{1}{z}\overline{\Phi'}\left(\frac{1}{z}\right) - \frac{1}{z^2}\overline{\Psi}\left(\frac{1}{z}\right) \tag{19}$$

the traction force specified on L can be expressed in terms of two complex functions $\Phi(z)$ and $\Omega(z)$ as:

$$[\Phi(t) + \Omega(t)]^+ + [\Phi(t) + \Omega(t)]^- = 2p(t) \tag{20}$$

$$[\Phi(t) - \Omega(t)]^+ - [\Phi(t) - \Omega(t)]^- = 2q(t) \tag{21}$$

where

$$p(t) = \frac{1}{2}\left[\left(\sigma_r^+ + \sigma_r^-\right) + i\left(\tau_{r\theta}^+ + \tau_{r\theta}^-\right)\right]$$

$$q(t) = \frac{1}{2}\left[\left(\sigma_r^+ - \sigma_r^-\right) + i\left(\tau_{r\theta}^+ - \tau_{r\theta}^-\right)\right]$$

The general solution to the Hilbert problem can be ready to follow as:

$$\Phi(z) = \frac{1}{2\pi i}\int_L \frac{q(t)}{t - z}dt + \frac{1}{2\pi i \mathrm{X}(z)}\int_L \frac{\mathrm{X}^+(t)p(t)}{t - z}dt + \frac{d_0}{2} + \frac{d_1}{2z} + \frac{d_2}{2z^2} + \frac{1}{2\mathrm{X}(t)}\left[P_n(z) + \frac{D_1}{z} + \frac{D_2}{z^2}\right] \tag{22}$$

$$\Omega(z) = \frac{-1}{2\pi i}\int_L \frac{q(t)}{t - z}dt + \frac{1}{2\pi i \mathrm{X}(z)}\int_L \frac{\mathrm{X}^+(t)p(t)}{t - z}dt - \frac{d_0}{2} - \frac{d_1}{2z} - \frac{d_2}{2z^2} + \frac{1}{2\mathrm{X}(t)}\left[P_n(z) + \frac{D_1}{z} + \frac{D_2}{z^2}\right] \tag{23}$$

where the Plemelj function $X(z)$ is given by Muskhclishvili [5] as:

$$\mathrm{X}(z) = \prod_{j=1}^{n}\left(z - a_j\right)^{1/2}\left(z - b_j\right)^{1/2} \tag{24}$$

and the polynomial $P_n(z)$ is of degree not greater than n, i.e.,

$$\mathrm{P_n(z)} = \mathrm{c_0 z^n} + \mathrm{c_1 z^{n-1}} + \cdots + \mathrm{c}_n \tag{25}$$

The problem of finding the stress field is now reduced to the determination of the $n + 6$ unknown constants $d_0, d_1, d_2, D_1, D_2, c_j (j = 0, 1, \ldots, n)$ which may be solved by using the properties of the complex functions.

Semicircular Crack

Consider the problem of an infinite plate with a semicircular crack lying along the interface of a unit disk as shown in Fig. 2. The applied loads at infinity consist of uniform tension, p_0 directed at an angle α and uniform heat flux, q_0 directed at an angle γ, respectively, with respect to the x-axis. For an insulated crack free from surface tractions, all the functions $f(t), g(t), p(t), q(t)$ vanish. The ends of the crack L are located at $a = \exp(-i\pi/2)$ and $b = \exp(i\pi/2)$ on $|z| = 1$. Hence, the Plemelj functions in (13) and (24) yield:

$$\mathrm{X}_0(z) = \mathrm{X}(z) = \sqrt{z^2 + 1} \tag{26}$$

For the case of pure mechanical load, the stress functions in (22) and (23) can be obtained as:

$$\Phi(z) = \frac{p_0}{2\sqrt{z^2+1}}\left\{C_0 z - \frac{e^{2i\alpha}}{2z^2}\right\} + \frac{p_0}{4}\left\{1 - 2C_0 - \frac{e^{2i\alpha}}{z^2}\right\} \tag{27}$$

$$\Omega(z) = \frac{p_0}{2\sqrt{z^2+1}}\left\{C_0 z - \frac{e^{2i\alpha}}{2z^2}\right\} + \frac{p_0}{4}\left\{1 - 2C_0 - \frac{e^{2i\alpha}}{z^2}\right\} \tag{28}$$

where

$$C_0 = \frac{4 - \cos(2\alpha)}{12} + \frac{i\sin(2\alpha)}{4}$$

which is in agreement with the solution given by Muskhelishvili [5]. In order to examine the magnitude of the local stress field, the stress intensity factors are computed in the present study. With the usual definition, the stress intensity factors can be obtained as:

$$K_1 - iK_{11} = 2\sqrt{2\pi}\lim_{z\to z_1}(z - z_1)^{1/2}\Phi(z) \tag{29}$$

where $z_1 = a$ *or* b in the given problem. In order to treat the problem by making use of (29), the coordinate must be rotated such that the crack tip

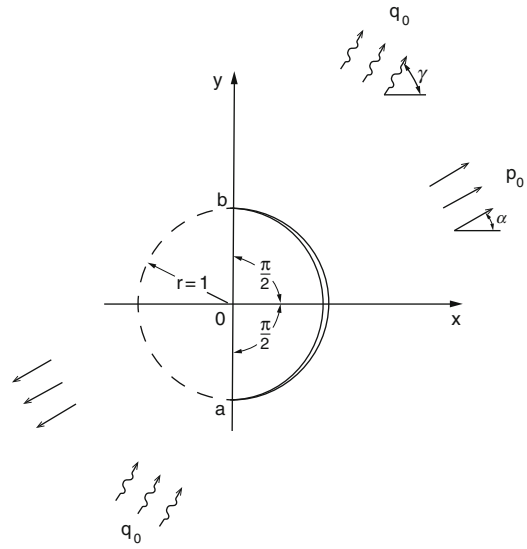

Curvilinear Cracks, Fig. 2 A semicircular crack under uniform heat flow or tensile load

is parallel to the x-axis. The convenient transformations for this purpose are:

$$z = -(z' - i) \tag{30}$$

at point b, and

$$z = -(z' + i) \tag{31}$$

at point a.

Substituting (30), (31), and (27) into (29), the stress intensity factors at point b are:

$$K_1 = \sqrt{\frac{\pi}{2}}p_0\left[\frac{4 - \cos(2\alpha)}{12} + \frac{3\sin(2\alpha)}{4} - \frac{\cos(2\alpha)}{2}\right]$$

$$K_{11} = \sqrt{\frac{\pi}{2}}p_0\left[\frac{4 - \cos(2\alpha)}{12} + \frac{\sin(2\alpha)}{4} + \frac{\cos(2\alpha)}{2}\right] \tag{32}$$

and the stress intensity factors at point a are:

$$K_1 = \sqrt{\frac{\pi}{2}}p_0\left[\frac{4 - \cos(2\alpha)}{12} - \frac{3\sin(2\alpha)}{4} - \frac{\cos(2\alpha)}{2}\right]$$

$$K_{11} = \sqrt{\frac{\pi}{2}} p_0 \left[\frac{4 - \cos(2\alpha)}{12} - \frac{\sin(2\alpha)}{4} + \frac{\cos(2\alpha)}{2} \right] \tag{33}$$

which is in agreement with the solution given by Sih [3].

For the case of thermal load, the stress functions in (22) and (23) become:

$$\Phi(z) = mq_0 \left\{ \frac{H_1(\gamma, z)}{\sqrt{z^2+1}} + H_2(\gamma, z) \right\} \tag{34}$$

$$\Omega(z) = mq_0 \left\{ \frac{H_1(\gamma, z)}{\sqrt{z^2+1}} - H_2(\gamma, z) \right\} \tag{35}$$

where

$$m = \frac{\mu\beta(\kappa+2)}{4(\kappa+1)k}$$

$$H_1(\gamma, z) = (-\cos\gamma + i\sin\gamma)z + 3\cos\gamma + i\sin\gamma - \frac{\kappa}{\kappa+2}(3\cos\gamma + i\sin\gamma)\frac{1}{z}$$

$$H_2(\gamma, z) = \cos\gamma - i\sin\gamma - \frac{\kappa}{\kappa+2}(3\cos\gamma + i\sin\gamma)\frac{1}{z}$$

Following the same procedures as aforementioned, the stress intensity factors at point b are:

$$K_1 = \sqrt{\frac{\pi}{2}} \frac{\mu\beta q_0}{2k(\kappa+1)} [(3\kappa+4)\sin\gamma - (\kappa+8)con\ \gamma]$$

$$K_{11} = \sqrt{\frac{\pi}{2}} \frac{\mu\beta q_0}{2k(\kappa+1)} [-\kappa\sin\gamma + (5\kappa+4)con\ \gamma] \tag{36}$$

and the stress intensity factors at point a are:

$$K_1 = \sqrt{\frac{\pi}{2}} \frac{\mu\beta q_0}{2k(\kappa+1)} [-(3\kappa+4)\sin\gamma - (\kappa+8)con\ \gamma]$$

$$K_{11} = \sqrt{\frac{\pi}{2}} \frac{\mu\beta q_0}{2k(\kappa+1)} [\kappa\sin\gamma + (5\kappa+4)con\ \gamma] \tag{37}$$

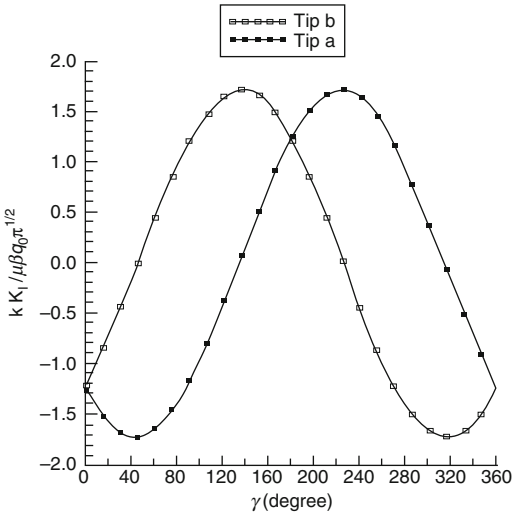

Curvilinear Cracks, Fig. 3 Dimensionless stress intensity factor K_I versus orientation of the heat flow for plane strain condition with $v = 0.3$

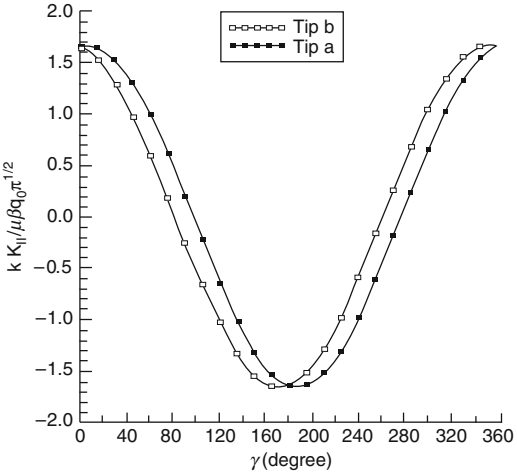

Curvilinear Cracks, Fig. 4 Dimensionless stress intensity factor K_{II} versus orientation of the heat flow for plane strain condition with $v = 0.3$

The dimensionless stress intensity factors versus the angle of heat flow are provided in graphical form as shown in Figs. 3, 4. Note that the mode-I stress intensity factor, K, is negative for $0 < \gamma < 133°$ and $314° < \gamma < 360°$ at the crack tip $z_1 = a$ and for $0 < \gamma < 46°$ and $227° < \gamma < 360°$ at the crack tip $z_1 = b$ which

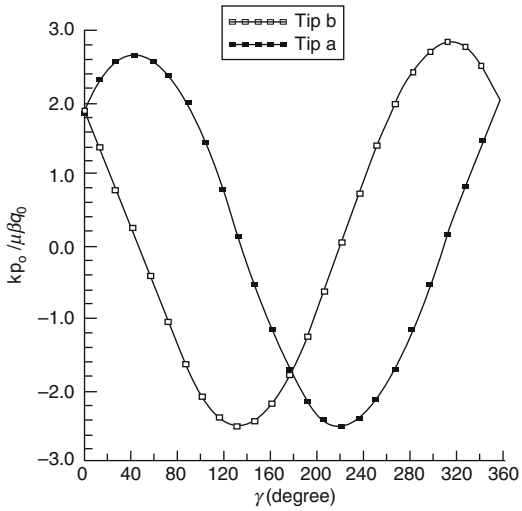

Curvilinear Cracks, Fig. 5 Values of $kp_0/\mu\beta q_0$ and γ for $\alpha = 90°$ to avoid crack closure

violates the assumption of fully open crack and hence the solution is invalid.

In order to avoid crack closure, a slight amount of mechanical load p_0 would have to be applied at an angle $\alpha = 90°$. The curve in Fig. 5 shows the minimum value of $kp_0/\mu\beta q_0$ as a function of the direction of the applied heat flow γ that must be maintained without having the crack surfaces come into contact.

Conclusions

The problem of finding the thermal stress field in an infinite region with circular-arc cracks has been reduced to the solutions of the Hilbert problem based on the method of complex variable. A closed form solution is given for an example with a semicircular crack. The stress intensity factors are obtained in terms of the heat flow (or tensile load), material geometry, and elastic and thermal isotropy.

References

1. England AH (1971) Complex variable methods in elasticity. Wiley-Interscience, New York
2. Muskhclishvili NI (1953) Some basic problems of the mathematical theory of elasticity. Noordhoff, Gronongcn
3. Sih GC, Paris PC, Erdogan F (1962) Crack-tip stress-intensity factors for plane extension and bending problem. J Appl Mech 29:306–312
4. Dundurs J, Hctinyi M (1961) The elastic plane with a circular insert loaded by a radial force. J Appl Mech 28:103–111
5. Perlman AB, Sih GC (1967) Elastostatic problem for curvilinear cracks in bonded dissimilar materials. J Eng Sci 5:845–867
6. Cheung YK, Woo CW, Wang YH (1989) Stress Intensity factors for a circular arc crack by collocation method. Eng Fract Mech 34:841–849
7. Bogdanoff JL (1954) Note on thermal stress. J Appl Mech 21:88

Cyclic Loading of Secondary Stresses

▶ Effect of Creep on Thermal Cyclic Loading of Rotating Disks
▶ Thermal Cyclic Loading of Beams Based on the Prager and Armstrong-Frederick Kinematic Hardening Models
▶ Thermal Cyclic Loading of Rotating Disks
▶ Thermal Cyclic Loading of Thick Cylindrical Vessels Based on the Prager and Armstrong-Frederick Kinematic Hardening Models
▶ Thermal Cyclic Loading of Thick Spherical Vessels Based on the Prager and Armstrong-Frederick Kinematic Hardening Models

Cyclic Loading of Strain-Controlled Stresses

▶ Thermal Cyclic Loading of Thick Spherical Vessels Based on the Prager and Armstrong-Frederick Kinematic Hardening Models

Cylinder

▶ Deterministic and Stochastic Coupled Thermoelasticity Analysis in Thick Hollow Cylinder Subjected to Thermal Shock Loading Using Green-Naghdi Theory

Cylindrical Elastic Bodies with Directors, Thermal Stresses

Mircea Bîrsan
Department of Mathematics, University "A.I. Cuza" of Iaşi, Iaşi, Romania
Faculty of Mathematics, University Duisburg–Essen, Essen, Germany

Synonyms

Cylindrical surface, Cosserat shell; Temperature distribution; Thermoelastic deformation of thin tubes

Overview

We consider the problem of thermal stresses in cylindrical elastic shells, modeled as Cosserat surfaces. In the theory of Cosserat shells, the thermal effects are described generally by means of two temperature fields. The problem consists in finding the equilibrium of the shell under the action of a given temperature distribution. For the case of a temperature distribution independent of the axial coordinate, we present the analytical solution in closed form. For the general case when the temperature fields are polynomial functions in the axial coordinate whose coefficients depend on the circumferential coordinate, we present a recurrence process with respect to the degree of the polynomials. Finally, we apply this method to solve a thermal stress problem for thin-walled circular tubes, when the temperature distribution is linear in the axial coordinate.

Introduction

The problem of thermal stresses in cylindrical bodies has been investigated in many works (see, e.g., [1–3]). In what follows we study the problem of thermal stresses in cylindrical elastic shells, using the Cosserat theory. The theory of Cosserat shells is an interesting approach to the mechanics of elastic shell-like bodies, in which the thin three-dimensional body is modeled as a two-dimensional continuum (i.e., a surface) endowed with a deformable director assigned to every point. For a detailed analysis of the theory of Cosserat surfaces and its relation with other (hierarchical) shell theories, we refer to the classical monograph of [4] and the more recent book of [5].

We employ the Cosserat theory for shells to solve the following problem: determine the static deformation of a cylindrical shell, due to a given temperature distribution in the body. We consider cylindrical shells made of isotropic and homogeneous materials. The cross sections of the cylindrical surfaces are curves of arbitrary shape. We assume that the temperature distribution is a general polynomial in the axial coordinate, which coefficients depend only on the circumferential coordinate. The mechanical loads are absent. We follow a procedure similar to that used in the corresponding problems for solid cylinders, from the three-dimensional thermoelasticity [1]. On the basis of some results concerning Saint-Venant's problem for cylindrical shells [6], we obtain a solution of the thermal stresses problem in the form of the displacement field. The result is expressed in terms of the solutions to some auxiliary boundary-value problems for ordinary differential equations. Finally, we apply these results to solve a special problem concerning the deformation of circular cylindrical shells.

Basic Equations and Formulation of the Problem

Let us present the equilibrium equations for thermoelastic Cosserat shells, specialized for cylindrical thin bodies. The general thermodynamic theory for Cosserat shells has been presented in the works [7–9].

Let $\mathcal{S}$ be the reference configuration of a cylindrical Cosserat surface and let (s, z) be the curvilinear material coordinate system on S such that z is the axial coordinate and s is the circumferential coordinate (i.e., s is the arc length

parameter along the cross-sectional curves of $\mathcal{S}$). The deformation of the thermoelastic Cosserat shell is defined by the functions

$$\begin{aligned} &\mathbf{r} = \mathbf{r}(s,z,t), \quad \mathbf{d} = \mathbf{d}(s,z,t) \\ &\theta = \theta(s,z,t), \quad \phi = \phi(s,z,t) \end{aligned} \tag{1}$$

where $\mathbf{r}$ and $\mathbf{d}$ represent the position vector and the director attached to each point at time t and the scalars θ and ϕ denote the two temperature fields which describe the thermal properties of Cosserat shells [9]: θ is regarded as representing the absolute temperature in the middle surface of the shell-like body, while ϕ accounts for the temperature variations along the thickness of the shell. Let $\mathbf{R}$, $\mathbf{D}$, $w(s) = \{\mathbf{f}(s), \mathbf{g}(s)\}$, and ϕ_0 designate, respectively, the reference values of the functions $\mathbf{r}$, $\mathbf{d}$, θ, and ϕ (on the reference surface $\mathcal{S}$).

Consider a rectangular Cartesian coordinate frame $Ox_1x_2x_3$ such that Ox_3 is parallel to the generators and S is situated between the planes $x_3 = 0$ and $x_3 = \bar{z}$. Denote by $\mathbf{e}_i$ the unit vectors along the Ox_i axes ($i = 1, 2, 3$). Then, the parametric equation of $\mathcal{S}$ can be written as

$$\begin{aligned} \mathbf{R} = \mathbf{R}(s,z) = x_1(s)\mathbf{e}_1 + x_2(s)\mathbf{e}_2 + z\mathbf{e}_3, \\ s \in [0, \bar{s}], \quad z \in [0, \bar{z}] \end{aligned} \tag{2}$$

where $x_\alpha(s)$ are known functions of class $C^3[0, \bar{s}]$ which determine the shape of the cross section. Let $\mathcal{C}_z$ be the cross-sectional curve of $\mathcal{S}$ lying in the plane $x_3 = z$. Subsequently, we deal with open cylindrical shells, but the same analysis can be adapted also for closed shells. The cross sections $\mathcal{C}_z$ are simple open curves of arbitrary shape ($0 \le z \le \bar{z}$). We designate by L_s the generator of $\mathcal{S}$ which points are characterized by the circumferential coordinate s. Clearly, the boundary $\partial\mathcal{S}$ of the surface S consists of the lateral edges L_0 and $L_{\bar{s}}$ and the end edges $\mathcal{C}_0$ and $\mathcal{C}_{\bar{z}}$.

In the linear theory, we introduce the infinitesimal displacement vector $\mathbf{u} = \mathbf{r}–\mathbf{R}$, the director displacement vector $\boldsymbol{\delta} = \mathbf{d} - \mathbf{D}$, and the variations in temperature fields $\tau = \theta - \theta_0$, $\sigma = \phi - \phi_0$. The displacement vectors can be decomposed in the vector bases $\{\mathbf{e}_i\}$ and $\{\mathbf{t}, \mathbf{n}, \mathbf{e}_3\}$ as

$$\begin{aligned} \mathbf{u} &= u_i\mathbf{e}_i = u_s\mathbf{t} + u_n\mathbf{n} + u_z\mathbf{e}_3 \\ \boldsymbol{\delta} &= \delta_i\mathbf{e}_i = \delta_s\mathbf{t} + \delta_n\mathbf{n} + \delta_z\mathbf{e}_3 \end{aligned}$$

where $\mathbf{t}$ and $\mathbf{n}$ are the unit tangent vector and normal vector to $\mathcal{C}_z$, given by

$$\begin{aligned} &\mathbf{t}(s) = x'_\alpha(s)\mathbf{e}_\alpha, \quad \mathbf{n}(s) = \varepsilon_{\alpha\beta}x'_\beta(s)\mathbf{e}_\alpha \\ &r(s) = \left[\varepsilon_{\alpha\beta}x'_\alpha(s)x''_\beta(s)\right]^{-1} \end{aligned}$$

Here, $\varepsilon_{\alpha\beta}$ is the two-dimensional alternator ($\varepsilon_{12} = -\varepsilon_{21} = 1$, $\varepsilon_{11} = \varepsilon_{22} = 0$) and $r(s)$ is the curvature radius of $\mathcal{C}_z$, and we use the notation $f' = \frac{df}{ds}$, for any field f.

We consider the following thermal stresses problem: *determine the equilibrium of a cylindrical Cosserat shell, under the action of a given temperature field*. As it is usual in the treatment of Saint-Venant's problem, we consider a relaxed formulation of the problem in which the pointwise assignment of mechanical loads on the end edges of cylindrical shells is replaced by prescribing the corresponding resultant forces and resultant moments acting on these boundaries.

The linear strain measures for cylindrical shells are [6]

$$\begin{aligned} &e_{ss} = \frac{\partial}{\partial s}u_s + u_n r^{-1}, \quad e_{sz} = e_{zs} = \frac{1}{2}\left(\frac{\partial}{\partial z}u_s + \frac{\partial}{\partial s}u_z\right) \\ &e_{zz} = \frac{\partial}{\partial z}u_z, \quad \gamma_s = \delta_s - u_s r^{-1} + \frac{\partial}{\partial s}u_n \\ &\gamma_z = \delta_z + \frac{\partial}{\partial z}u_n, \quad \gamma_n = \delta_n \\ &\rho_{ss} = \frac{\partial}{\partial s}\delta_s + r^{-1}\frac{\partial}{\partial s}u_s + u_n r^{-2}, \quad \rho_{zz} = \frac{\partial}{\partial z}\delta_z \\ &\rho_{sz} = \frac{\partial}{\partial z}\delta_s, \quad \rho_{zs} = \frac{\partial}{\partial s}\delta_z + r^{-1}\frac{\partial}{\partial z}u_s \\ &\rho_{ns} = \frac{\partial}{\partial s}\delta_n, \quad \rho_{nz} = \frac{\partial}{\partial z}\delta_n \end{aligned} \tag{3}$$

We designate by $\mathbf{N}$ the contact force vector and $\mathbf{M}$ the contact director couple acting per unit length of the curves c included in $\mathcal{S}$. For an arbitrary such curve c having the unit normal

$\boldsymbol{\nu} = v_s\mathbf{t} + v_z\mathbf{e}_3$ ($\boldsymbol{\nu}$ is tangent to the surface $\mathcal{S}$), these vectors admit Cauchy-type decompositions as follows: $\mathbf{N} = (N_{ss}\mathbf{t} + N_{sz}\mathbf{e}_3 + V_s\,\mathbf{n})v_s + (N_{zs}\mathbf{t} + N_{zz}\mathbf{e}_3 + V_z\,\mathbf{n})v_z$ and $\mathbf{M} = (M_{ss}\mathbf{t} + M_{sz}\mathbf{e}_3 + M_{sn}\mathbf{n})v_s + (M_{zs}\mathbf{t} + M_{zz}\mathbf{e}_3 + M_{zn}\mathbf{n})v_z$.

The constitutive equations of thermoelastic Cosserat shells, for isotropic and homogeneous materials, are given in the form [10]

$$\begin{aligned}
N_{ss} &= (\alpha_1 + 2\alpha_2)e_{ss} + \alpha_1 e_{zz} + \alpha_9\gamma_n \\
&\quad + \beta_1\tau + (\alpha_0\rho_{ss} + \alpha_5\rho_{zz} + \beta_4\sigma)r^{-1} \\
N_{zz} &= \alpha_1 e_{ss} + (\alpha_1 + 2\alpha_2)e_{zz} + \alpha_9\gamma_n + \beta_1\tau, \\
N_{sz} &= 2\alpha_2 e_{sz} \\
V_s &= \alpha_3\gamma_s, \quad V_z = \alpha_3\gamma_z \\
V_n &= \alpha_9(e_{ss} + e_{zz}) + \alpha_4\gamma_n + \beta_2\tau \\
M_{ss} &= \alpha_0\rho_{ss} + \alpha_5\rho_{zz} \\
M_{zz} &= \alpha_5\rho_{ss} + \alpha_0\rho_{zz} + \beta_4\sigma, \quad M_{sz} = \alpha_6\rho_{zs} + \alpha_7\rho_{sz} \\
M_{zs} &= \alpha_6\rho_{sz} + \alpha_7\rho_{zs}, \quad M_{sn} = \alpha_8\rho_{ns} \\
M_{zn} &= \alpha_8\rho_{nz}
\end{aligned} \tag{4}$$

where $\alpha_1, \ldots, \alpha_9$ and $\beta_1, \ldots, \beta_5$ are the constant constitutive coefficients of the shell and we denote by $\alpha_0 = \alpha_5 + \alpha_6 + \alpha_7$ and $\beta_0 = \alpha_5\alpha_0^{-1}$ for brevity.

The equilibrium equations in the absence of body loads can be written as

$$\begin{aligned}
&\frac{\partial}{\partial s}N_{ss} + \frac{\partial}{\partial z}N_{zs} + \frac{1}{r}V_s = 0 \qquad \frac{\partial}{\partial s}N_{sz} + \frac{\partial}{\partial z}N_{zz} = 0 \\
&\frac{\partial}{\partial s}V_s + \frac{\partial}{\partial z}V_z - \frac{1}{r}N_{ss} = 0 \qquad \frac{\partial}{\partial s}M_{ss} + \frac{\partial}{\partial z}M_{zs} - V_s = 0 \\
&\frac{\partial}{\partial s}M_{sz} + \frac{\partial}{\partial z}M_{zz} - V_z = 0 \qquad \frac{\partial}{\partial s}M_{sn} + \frac{\partial}{\partial z}M_{zn} - V_n = 0
\end{aligned} \tag{5}$$

Since the lateral edges are free of applied loads, we have the following boundary conditions on the lateral edges:

$$N_{ss} = N_{sz} = V_s = 0, \qquad M_{ss} = M_{sz} = M_{sn} = 0 \quad \text{on } L_0 \cup L_{\bar{s}} \tag{6}$$

We define the vector-valued linear functionals $\mathcal{R}(\cdot)$ and $\mathcal{M}(\cdot)$ by

$$\begin{aligned}
\mathcal{R}(v) &= \int_{\mathcal{C}_0}\mathbf{N}(v)\,\mathrm{d}l = -\int_{\mathcal{C}_0}\left[x'_\alpha N_{zs}(v) + \varepsilon_{\alpha\beta}x'_\beta V_z(v)\right]\mathrm{d}l\mathbf{e}_\alpha \\
&\quad - \int_{\mathcal{C}_0}N_{zz}(v)\,\mathrm{d}l\mathbf{e}_3, \\
\mathcal{M}(v) &= \int_{\mathcal{C}_0}[\mathbf{R}\times\mathbf{N}(v) + \mathbf{D}\times\mathbf{M}(v)]\mathrm{d}l \\
&= \int_{\mathcal{C}_0}\left[\varepsilon_{\beta\alpha}x_\beta N_{zz}(v) + x'_\alpha M_{zz}(v)\right]\mathrm{d}l\mathbf{e}_\alpha \\
&\quad + \int_{\mathcal{C}_0}\left[\varepsilon_{\alpha\beta}x'_\alpha x_\beta N_{zs}(v) + x_\alpha x'_\alpha V_z(v) - M_{zs}(v)\right]\mathrm{d}l\mathbf{e}_3
\end{aligned}$$

for any displacement field $v = \{\mathbf{u}, \boldsymbol{\delta}\} \in C^1(\bar{S})$. We mention that $\mathcal{R}(v)$ and $\mathcal{M}(v)$ represent the resultant force and the resultant moment about O of the contact forces and contact director couples acting on $\mathcal{C}_0$, corresponding to the field v.

We consider the following boundary conditions on the end edges:

$$\mathcal{R}(v) = \mathbf{0}, \qquad \mathcal{M}(v) = \mathbf{0} \tag{7}$$

which express that the resultant force and the resultant moment acting on the end edge $\mathcal{C}_0$ are zero. In view of (5)–(7), the resultant force and the resultant moment acting on the other end edge $\mathcal{C}_{\bar{s}}$ are also zero.

The problem of thermal stresses consists in finding the displacement field $\{\mathbf{u}, \boldsymbol{\delta}\}$ which satisfies equations (3)–(5) and the boundary conditions (6) and (7), assuming that the temperature fields τ and σ are given. We solve this problem in the case when the temperature distribution is a general polynomial in the axial coordinate z, i.e., we have

$$\begin{aligned}
\tau &= \tau(s, z) = \sum_{k=0}^{n}\tau_k(s)\,z^k \\
\sigma &= \sigma(s, z) = \sum_{k=0}^{n}\sigma_k(s)\,z^k
\end{aligned} \tag{8}$$

where τ_k and σ_k are given functions which depend only on s.

For any integer $m \in \{0, 1, \ldots, n\}$, let us denote by $P^{(m)}$ the problem of solving equations (3)–(5) together with the boundary conditions (6) and (7), when the temperature fields τ and σ have the forms

$$\tau = \tau_m(s)\, z^m, \qquad \sigma = \sigma_m(s)\, z^m \tag{9}$$

Obviously, by the linearity of the theory, if we know the solutions of the problems $P^{(m)}$ for $m \in \{0, 1, \ldots, n\}$, then we can find the solution of our initial thermal stresses problems (3)–(8), by additive superposition.

To solve the problem $P^{(m)}$, we proceed by mathematical induction: we solve first the problem $P^{(0)}$, and then we establish a method to find the solution of $P^{(m+1)}$ once the solution of $P^{(m)}$ is known. In this purpose, we notice that the problem of thermal stresses under consideration can be rewritten in the form of an elastostatic problem for cylindrical shells, where the mechanical loads are expressed in terms of the given temperature fields. We observe that if we separate the thermal terms (i.e., those involving τ and σ) from the elastic terms, then the constitutive equations (4) can be written as

$$\begin{aligned}
&N_{ss} = N^e_{ss} + \beta_1\tau + \beta_4\sigma r^{-1}, \quad N_{zz} = N^e_{zz} + \beta_1\tau\\
&N_{sz} = N^e_{sz}, \quad N_{zs} = N^e_{zs}, V_s = V^e_s, \quad V_z = V^e_z\\
&V_n = V^e_n + \beta_2\tau, \quad M_{ss} = M^e_{ss} + \beta_4\sigma, \quad M_{sz} = M^e_{sz}\\
&M_{zz} = M^e_{zz} + \beta_4\sigma, \quad M_{zs} = M^e_{zs}\\
&M_{sn} = M^e_{sn}, \quad M_{zn} = M^e_{zn}
\end{aligned} \tag{10}$$

where the superscript e is used to indicate the elastic terms. The expressions of the tensor components $N^e_{ss}, \ldots, M^e_{zn}$ follow readily from relations (4) and (10). Then, the equations of equilibrium (5) can be put in the form

$$\begin{aligned}
&\frac{\partial}{\partial s}N^e_{ss} + \frac{\partial}{\partial z}N^e_{zs} + \frac{1}{r}V^e_s = -\frac{\partial}{\partial s}(\beta_1\tau + \frac{1}{r}\beta_4\sigma)\\
&\frac{\partial}{\partial s}N^e_{sz} + \frac{\partial}{\partial z}N^e_{zz} = -\beta_1\frac{\partial\tau}{\partial z}\\
&\frac{\partial}{\partial s}V^e_s + \frac{\partial}{\partial z}V^e_z - \frac{1}{r}N^e_{ss} = \frac{1}{r}(\beta_1\tau + \frac{1}{r}\beta_4\sigma)\\
&\frac{\partial}{\partial s}M^e_{ss} + \frac{\partial}{\partial z}M^e_{zs} - V^e_s = -\beta_4\frac{\partial\sigma}{\partial s}\\
&\frac{\partial}{\partial s}M^e_{sz} + \frac{\partial}{\partial z}M^e_{zz} - V^e_z = -\beta_4\frac{\partial\sigma}{\partial z}\\
&\frac{\partial}{\partial s}M^e_{sn} + \frac{\partial}{\partial z}M^e_{zn} - V^e_n = \beta_2\tau
\end{aligned} \tag{11}$$

The boundary conditions on the lateral edges (6) reduce to

$$\begin{aligned}
&N^e_{ss} = -(\beta_1\tau + \frac{1}{r}\beta_4\sigma), \quad N^e_{sz} = 0, \quad V^e_s = 0,\\
&M^e_{ss} = -\beta_4\sigma, \quad M^e_{sz} = 0, \quad M^e_{sn} = 0, \quad \text{for} \quad s = 0,\ \bar{s}
\end{aligned} \tag{12}$$

On the other hand, the boundary conditions on the end edges (7) can be written as

$$\begin{aligned}
&\int_{\mathcal{C}_0}\left(x'_\alpha N^e_{zs} + \varepsilon_{\alpha\beta}x'_\beta V^e_z\right)\mathrm{d}l = 0, \quad \int_{\mathcal{C}_0} N^e_{zz}\mathrm{d}l = -\int_{\mathcal{C}_0}\beta_1\tau\mathrm{d}l,\\
&\int_{\mathcal{C}_0}\left(\varepsilon_{\beta\alpha}x_\beta N^e_{zz} + x'_\alpha M^e_{zz}\right)\mathrm{d}l = -\int_{\mathcal{C}_0}(\beta_4\sigma x'_\alpha + \beta_1\tau\varepsilon_{\beta\alpha}x_\beta)\mathrm{d}l,\\
&\int_{\mathcal{C}_0}\left(\varepsilon_{\alpha\beta}x'_\alpha x_\beta N^e_{zs} + x_\alpha x'_\alpha V^e_z - M^e_{zs}\right)\mathrm{d}l = 0
\end{aligned} \tag{13}$$

Our elastostatic problem (equivalent to the thermal stresses problem) consists in determining the displacement field $v = \{\mathbf{u}, \boldsymbol{\delta}\}$ which satisfies the equilibrium equations (11) and the boundary conditions (12) and (13).

The solution of this problem is based on certain results concerning Saint-Venant's problem for Cosserat shells [see 6], which have been presented in the section ▶ Saint-Venant's problem for Cosserat elastic shells of this Encyclopedia of Thermal Stresses. We introduce the displacement field $v[a_i, k]$ defined by relations (22) from the section ▶ Saint-Venant's problem for Cosserat elastic shells, depending on the arbitrary constants a_i and k. The displacement field $v[a_i, k]$ possesses the following properties:

(i) $\frac{\partial v[a_i,k]}{\partial x_3}$ is a rigid body displacement field of the Cosserat shell.

(ii) $v[a_i, k]$ satisfies the equations of equilibrium (4) for vanishing right-hand sides.

(iii) $v[a_i, k]$ verifies the following zero boundary conditions on the lateral edges

$$N^e_{ss} = N^e_{sz} = V^e_s = 0, \qquad M^e_{ss} = M^e_{sz} = M^e_{sn} = 0 \quad \text{on } L_0 \cup L_{\bar{s}} \tag{14}$$

(iv) The displacement field $v[a_i, k]$ corresponds to the resultant force and resultant moment on the end edge $\mathcal{C}_0$ given by

$$\mathcal{R}(v[a_i,k]) = I_{3i}a_i\mathbf{e}_3, \quad \mathcal{M}(v[a_i,k]) = I_{\alpha i}a_i\mathbf{e}_\alpha - k\bar{D}\mathbf{e}_3$$

i.e., $v[a_i,k]$ satisfies the end edges conditions

$$\int_{C_0}\left(x'_\alpha N^e_{zs} + \varepsilon_{\alpha\beta}x'_\beta V^e_z\right)\mathrm{d}l = 0, \quad \int_{C_0} N^e_{zz}\,\mathrm{d}l = -I_{3i}a_i,$$
$$\int_{C_0}\left(\varepsilon_{\beta\alpha}x_\beta N^e_{zz} + x'_\alpha M^e_{zz}\right)\mathrm{d}l = I_{\alpha i}a_i,$$
$$\int_{C_0}\left(\varepsilon_{\alpha\beta}x'_\alpha x_\beta N^e_{zs} + x_\alpha x'_\alpha V^e_z - M^e_{zs}\right)\mathrm{d}l = -k\bar{D} \tag{15}$$

The expressions of the constant coefficients I_{ji} and $\bar{D}$ appearing in (15) are given by the relations (26) from section ▶ Saint-Venant's problem for Cosserat elastic shells. In what follows, we use the field $v[a_i,k]$ to express the solution of our thermal stresses problem.

Solution of the Thermal Stresses Problem

Temperature Distribution Depending on the Circumferential Coordinate

Let us consider first the problem $P^{(0)}$ and assume that the temperature distribution is independent of the axial coordinate but depends only on the circumferential coordinate, i.e., it has the form

$$\tau = \tau_0(s), \qquad \sigma = \sigma_0(s) \tag{16}$$

where $\tau_0(s)$ and $\sigma_0(s)$ are given functions. Suggested by the corresponding results from the three-dimensional theory [1], we search for the solution v in the form

$$v = v[a_i,k] + w(s) \tag{17}$$

where a_i and k are constants and $w(s) = \{\mathbf{f}(s), \mathbf{g}(s)\}$ is a displacement field of class $C^2[0,\bar{s}]$ which depends only on s. In what follows, we determine the constants a_i and k and the functions $\mathbf{f}(s) = f_i(s)\mathbf{e}_i$ and $\mathbf{g}(s) = g_i(s)\mathbf{e}_i$ such that the displacement field v given by (16) represents a solution of problems (11)–(13). In this purpose, we denote by $Y(s)$ and $Z(s)$ the solution of the following boundary-value problem:

$$\alpha_8 Z''(s) - \alpha_4 Z(s) - \alpha_9 Y(s) = \beta_2\tau_0(s),$$
$$(\alpha_1 + 2\alpha_2)Y(s) + \alpha_9 Z(s) = -\beta_1\tau_0(s), \quad s\in[0,\bar{s}],$$
$$Z'(0) = Z'(\bar{s}) = 0 \tag{18}$$

We mention that the solution of the boundary-value problem (18) is unique and it can be calculated by the variation of constants method [see 11]. The following theorem [10] solves the problem $P^{(0)}$:

Theorem 1. *Let v be a displacement field of the form (17). Then, $v = \{\mathbf{u}, \boldsymbol{\delta}\}$ is a solution of the thermal stresses problems (3)–(7) with the temperature distribution (16) if and only if v is given by*

$$u_\alpha = -\frac{1}{2}a_\alpha x_3^2 + \beta_0\varepsilon_{\alpha\beta}\varepsilon_{\gamma\delta}a_\gamma\int_0^s x'_\beta x_\delta\,\mathrm{d}s + \int_0^s x'_\alpha\left(a_i y_{(i)} + Y\right)\mathrm{d}s + \int_0^s \varepsilon_{\alpha\beta}x'_\beta \times \int_0^s\left[\frac{1}{r}\left(a_i y_{(i)} + Y\right) + \frac{\beta_4}{\alpha_0}\sigma\right]\mathrm{d}s\,\mathrm{d}s,$$
$$\delta_\alpha = \beta_0\varepsilon_{\beta\gamma}a_\gamma x_\beta x'_\alpha + \varepsilon_{\alpha\beta}x'_\beta(a_i z_{(i)} + Z) - x'_\alpha\int_0^s\left[\frac{1}{r}\left(a_i y_{(i)} + Y\right) + \frac{\beta_4}{\alpha_0}\sigma\right]\mathrm{d}s,$$
$$u_3 = (a_\alpha x_\alpha + a_3)x_3, \qquad \delta_3 = \varepsilon_{\alpha\beta}a_\alpha x'_\beta x_3 \tag{19}$$

up to an additive rigid displacement field. The constants a_i in (19) are determined by the relations

$$I_{\alpha i}a_i = \int_0^{\bar{s}}\left[(1-\beta_0)\beta_4 x'_\alpha\sigma_0(s) + 2\alpha_2\varepsilon_{\beta\alpha}x_\beta Y(s)\right]\mathrm{d}s$$
$$I_{3i}a_i = \left[\beta_1(1 + y_{(3)}) + \beta_2 z_{(3)}\right]\int_0^{\bar{s}}\tau_0(s)\,\mathrm{d}s \tag{20}$$

Proof. In view of (17) and the properties (ii) and (iii) of the field $v[a_i,k]$, we see that v satisfies equations (5) and (6) if and only if

$w(s) = \{\mathbf{f}(s), \mathbf{g}(s)\}$ verifies (11) and (12). Using the constitutive relations, we find

$$
\begin{aligned}
&N^e_{ss}(w) = (\alpha_1 + 2\alpha_2 + \frac{\alpha_0}{r^2})\mathbf{f}' \cdot \mathbf{t} + \alpha_9\, \mathbf{g} \cdot \mathbf{n} + \frac{\alpha_0}{r}(\mathbf{g} \cdot \mathbf{t})',\\
&N^e_{zz}(w) = \alpha_1 \mathbf{f}' \cdot \mathbf{t} + \alpha_9 \mathbf{g} \cdot \mathbf{n}, \quad N^e_{sz}(w) = \alpha_2 f_3'(s),\\
&N^e_{zs}(w) = \alpha_2 f_3'(s) + \frac{\alpha_6}{r} g_3'(s), V^e_s(w) = \alpha_3(\mathbf{f}' \cdot \mathbf{n} + \mathbf{g} \cdot \mathbf{t}),\\
&V^e_z(w) = \alpha_3 g_3(s), \quad V^e_n(w) = \alpha_9 \mathbf{f}' \cdot \mathbf{t} + \alpha_4 \mathbf{g} \cdot \mathbf{n},\\
&M^e_{ss}(w) = \alpha_0[\frac{1}{r}\mathbf{f}' \cdot \mathbf{t} + (\mathbf{g} \cdot \mathbf{t})'],\\
&M^e_{zz}(w) = \alpha_5[\frac{1}{r}\mathbf{f}' \cdot \mathbf{t} + (\mathbf{g} \cdot \mathbf{t})'],\\
&M^e_{sz}(w) = \alpha_6 g_3'(s), \quad M^e_{zs}(w) = \alpha_7 g_3'(s),\\
&M^e_{sn}(w) = \alpha_8(\mathbf{g} \cdot \mathbf{n})', \quad M^e_{zn}(w) = 0
\end{aligned}
\tag{21}
$$

Using the equilibrium equations $(4)_{2,5}$ written for w and the lateral edge conditions $N^e_{sz}(w) = M^e_{sz}(w) = 0$ for $s = 0, \bar{s}$, we obtain that $f_3(s) = 0$ and $g_3(s) = 0$, for $s \in [0, \bar{s}]$.

On the other hand, if we write the equilibrium equations $(11)_{1,3,4,6}$ and the boundary conditions $(12)_{1,3,4,6}$ for the field w and use (21), then we deduce the following system of ordinary differential equations for the unknown functions $f_\alpha(s)$ and $g_\alpha(s)$:

$$
\begin{aligned}
&(\alpha_1 + 2\alpha_2)\mathbf{f}' \cdot \mathbf{t} + \alpha_9\, \mathbf{g} \cdot \mathbf{n} = -\beta_1 \tau_0,\\
&\alpha_8(\mathbf{g} \cdot \mathbf{n})'' - \alpha_4\, \mathbf{g} \cdot \mathbf{n} - \alpha_9 \mathbf{f}' \cdot \mathbf{t} = \beta_2 \tau_0,\\
&\frac{1}{r}\mathbf{f}' \cdot \mathbf{t} + (\mathbf{g} \cdot \mathbf{t})' = -\frac{\beta_4}{\alpha_0}\sigma_0,\\
&\mathbf{f}' \cdot \mathbf{n} + \mathbf{g} \cdot \mathbf{t} = 0, \qquad s \in [0, \bar{s}]
\end{aligned}
\tag{22}
$$

with the boundary conditions

$$
(\mathbf{g} \cdot \mathbf{n})'(0) = (\mathbf{g} \cdot \mathbf{n})'(\bar{s}) = 0 \tag{23}
$$

By virtue of (18), from the boundary-value problem $(22)_{1,2}$ and (23), we obtain

$$
\begin{aligned}
&(\mathbf{f}' \cdot \mathbf{t})(s) = Y(s), \qquad (\mathbf{g} \cdot \mathbf{n})(s) = Z(s),\\
&s \in [0, \bar{s}]
\end{aligned}
\tag{24}
$$

Finally, from relations $(22)_{3,4}$ and (24), we find that

$$
\begin{aligned}
&f_\alpha(s) = \int_0^s [x'_\alpha Y + \varepsilon_{\alpha\beta} x'_\beta \int_0^s (\frac{1}{r} Y + \frac{\beta_4}{\alpha_0}\sigma_0)\mathrm{d}s]\mathrm{d}s\\
&g_\alpha(s) = \varepsilon_{\alpha\beta} x'_\beta Z(s) - x'_\alpha \int_0^s (\frac{1}{r} Y + \frac{\beta_4}{\alpha_0}\sigma_0)\mathrm{d}s
\end{aligned}
\tag{25}
$$

If we substitute the expression of $v[a_i, k]$ and (25) into (17), then we deduce that v has the form (19). To determine the constants a_i and k, we impose the boundary conditions on the end edges (13). In view of (21) and the property (iv) of the displacement field $v[a_i, k]$, we see that v satisfies the conditions (13) if and only if we have

$$
\begin{aligned}
&I_{\alpha i} a_i + \int_{C_0} \left[\varepsilon_{\beta\alpha} x_\beta N_{zz}(w) + x'_\alpha M_{zz}(w)\right]\mathrm{d}l = 0,\\
&-I_{3i} a_i + \int_{C_0} N_{zz}(w)\, \mathrm{d}l = 0, \qquad k = 0
\end{aligned}
\tag{26}
$$

In view of (10), (21), (22), and (24), the relations $(26)_{1,2}$ reduce to equation (20). This completes the proof.

Thus, we have solved our thermal stresses problem in the case when the temperature distribution is independent of the axial coordinate.

Temperature Distribution Depending on the Axial Coordinate

Let us treat the thermal stresses problem in the case when temperature depends also on the axial coordinate. More precisely, we consider that the temperature distribution is a general polynomial in the axial coordinate, with coefficients being given functions of s, as it was written in relation (8).

In this context, we describe a method to solve the problem $P^{(m+1)}$, once a solution of the problem $P^{(m)}$ is known ($m \geq 0$). As we already mentioned, the problem $P^{(m)}$ consists in finding the displacement field which satisfies equations (3)–(7), when the temperature distribution is given by (9). Since the solution of problem $P^{(m)}$ is known for every function $\tau_m(s)$ and $\sigma_m(s)$, it means that we can also find the solution $v^* = \{\mathbf{u}^*, \boldsymbol{\delta}^*\}$ of the thermal stresses problem for the temperature distribution

$$\tau = \tau_{m+1}(s)\, z^m, \qquad \sigma = \sigma_{m+1}(s)\, z^m \tag{27}$$

In what follows, we show how to determine the solution $v = \{\mathbf{u}, \boldsymbol{\delta}\}$ of equations (3)–(7) with the thermal fields given by

$$\tau = \tau_{m+1}(s)\, z^{m+1}, \qquad \sigma = \sigma_{m+1}(s)\, z^{m+1} \tag{28}$$

in the hypothesis that we know the solution v^* of problems (3)–(7) corresponding to the temperature distribution (27). The next theorem [10] establishes the existence of such solution, and its proof describes the procedure to calculate it.

Theorem 2. *Let $v^* = \{\mathbf{u}^*, \boldsymbol{\delta}^*\}$ be a displacement field satisfying equations (3)–(7) corresponding to the thermal fields (27). Then, there exists a solution $v = \{\mathbf{u}, \boldsymbol{\delta}\}$ of the thermal stresses problems (3)–(7) with the temperature distribution (28), having the following form:*

$$v = (m+1)\Big(\int_0^{x_3} v^*\, \mathrm{d}x_3 + v[a_i, k] + w(s)\Big) \tag{29}$$

where a_i and k are constants and the field $w(s) = \{\mathbf{f}(s), \mathbf{g}(s)\}$ is a function of class $C^2[0, \bar{s}]$.

Proof. We determine the constants a_i and k and the functions $\mathbf{f}(s) = f_i(s)\mathbf{e}_i$ and $\mathbf{g}(s) = \mathrm{g}_i(s)\,\mathbf{e}_i$ such that the displacement field v given by (29) represents a solution of problems (3)–(7) and (28). First, we find the functions $f_i(s)$ and $g_i(s)$ from the boundary-value problems (11) and (6). To this aim, we use the constitutive equations (4), the induction hypothesis on v^*, and the properties (ii) and (iii) of the field $v[a_i, k]$. Thus, the equilibrium equation $(11)_2$ can be written as

$$f_3''(s) = -[\frac{\partial}{\partial s}\, u_s^* + \frac{1}{\alpha_2}\, N_{zz}^e(v^*)](s,0) - \frac{\beta_1}{\alpha_2}\, \tau_1(s)\delta_{0m}, \quad s \in [0, \bar{s}] \tag{30}$$

where δ_{0m} is the Kronecker symbol. The boundary conditions on the lateral edges $N_{sz}(v) = 0$ reduce to

$$f_3'(s) = -u_s^*(s,0) \qquad \text{for} \quad s = 0, \bar{s} \tag{31}$$

From the boundary-value problems (4) and (5), we find that

$$f_3(s) = -\int_0^s [u_s^*(s,0) + \frac{1}{\alpha_2} \times \int_0^s \big(N_{zz}^e(v^*)(s,0) + \beta_1 \tau_1(s)\delta_{0m}\big)\mathrm{d}s]\mathrm{d}s \tag{32}$$

In a similar way, the equilibrium equation $(11)_5$ and the conditions on the lateral edges $M_{sz}(v) = 0$ reduce to the following boundary-value problem for the unknown $g_3(s)$:

$$\begin{aligned} &\alpha_6 g_3''(s) - \alpha_3 g_3(s) = -[\frac{\partial}{\partial s}(\frac{\alpha_6}{r}\, u_s^* + \alpha_7 \delta_s^*) \\ &\qquad - \alpha_3 u_n^* + M_{zz}^e(v^*)](s,0) - \beta_4 \sigma_1(s)\delta_{0m} \\ &g_3'(0) = -\Big(\frac{1}{r}\, u_s^* + \frac{\alpha_7}{\alpha_6}\, \delta_s^*\Big)(0,0), \\ &g_3'(\bar{s}) = -\Big(\frac{1}{r}\, u_s^* + \frac{\alpha_7}{\alpha_6}\, \delta_s^*\Big)(\bar{s},0) \end{aligned} \tag{33}$$

The function $g_3(s)$ can be determined from the boundary-value problem (33).

In order to find $f_\alpha(s)$ and $g_\alpha(s)$, we write the equilibrium equations $(11)_{1,3,4,6}$ and the boundary conditions (6) for the field v given by (29). In this way, we obtain a system of four ordinary differential equations, together with appropriate boundary conditions in the endpoints $s = 0, \bar{s}$, which can be solved to determine $f_\alpha(s)$ and $g_\alpha(s)$. Thus, we consider that the field $w(s)$ has been determined.

Finally, we find the values of the constants a_i $(i = 1, 2, 3)$ and k by imposing that the field v given by (29) satisfies the end edge conditions (7). The proof is complete.

Remark. The expression of solution (29) has been suggested by the results of the three-dimensional thermoelastostatics [1] and those for loaded cylindrical Cosserat shells [8].

Using the above theorem and the method of induction, we obtain a solution of the thermal stresses problem when the temperature

distribution is a general polynomial (9) in the axial coordinate. We mention that the same approach can be adapted also for the case of *closed* cylindrical shells, i.e., for thin-walled tubes. We do not give the details about the thermal stresses problem for closed cylindrical shells in the general case, but we present the solution in a special situation: the case of closed circular cylindrical shells.

Thermal Stresses in Thin-Walled Tubes

Let us consider a thermal stresses problem for circular cylindrical closed shells, i.e., for thin-walled tubes. In the case of closed cylindrical shells, the boundary conditions on the lateral edges (6) are replaced by the following continuity conditions for $s = 0, \bar{s}$:

$$\left\{\mathbf{u}, \boldsymbol{\delta}, \frac{\partial^k \mathbf{u}}{\partial s^k}, \frac{\partial^k \boldsymbol{\delta}}{\partial s^k}\right\}(0, z) = \left\{\mathbf{u}, \boldsymbol{\delta}, \frac{\partial^k \mathbf{u}}{\partial s^k}, \frac{\partial^k \boldsymbol{\delta}}{\partial s^k}\right\}(\bar{s}, z)$$
$$\text{for} \quad z \in [0, \bar{z}], k = 1, 2 \tag{34}$$

Thus, the thermal stresses problem consists in finding the displacement field $v = \{\mathbf{u}, \boldsymbol{\delta}\}$ of the Cosserat shell which satisfies equations (3)–(5), the conditions on the end edges (7), and the continuity conditions (34), under a given temperature distribution.

Assume that the thermal fields τ and σ are linear functions of the axial coordinate, i.e., we have

$$\tau = \tau_0 + \tau_1 z, \qquad \sigma = \sigma_0 + \sigma_1 z \tag{35}$$

where τ_0, τ_1, σ_0 and σ_1 are known constants. Since τ is interpreted as the average temperature through the thickness of the shell and σ represents the average through-the-thickness temperature gradient [9], we see that the problem considered has practical significance for the situation when a thin elastic tube is subject to different temperatures applied at its end edges and also to a difference of temperature between the inner and outer regions. For the circular cylindrical surface S under consideration, the parametric equation is given by (2) with

$$x_1(s) = r_0 \cos\frac{s}{r_0}, \qquad x_2(s) = r_0 \sin\frac{s}{r_0}, \qquad s \in [0, 2\pi r_0] \tag{36}$$

where r_0 denotes the radius of the cylindrical surface. In accordance with the procedure established in the preceding sections, we divide our problem into two problems $P^{(0)}$ and $P^{(1)}$, described as

$$P^{(0)}: \text{ the thermal fields are } \tau = \tau_0, \ \sigma = \sigma_0;$$
$$P^{(1)}: \text{ the thermal fields are } \tau = \tau_1 z, \ \sigma = \sigma_1 z$$

Theorem 1 allows us to solve the problem $P^{(0)}$, while the solution of problem $P^{(1)}$ can be constructed by applying Theorem 2. After some calculations, we obtain the following solution for the thermal stresses problem corresponding to a temperature distribution linear in the axial coordinate [10]:

$$\begin{aligned}
u_\alpha &= -(bA_0 + A_2)x_\alpha x_3 - (aA_0 + A_1)x_\alpha, \\
u_3 &= \frac{1}{2} b x_3^2 + a x_3 \\
\delta_\alpha &= -\frac{1}{r_0}(bC_0 + C_2)x_\alpha x_3 - \frac{1}{r_0}(aC_0 + C_1)x_\alpha \\
\delta_3 &= \frac{1}{\alpha_3}\left[\beta_4\sigma_1 + \left(\alpha_3 r_0 - \frac{\alpha_5}{r_0}\right)(bA_0 + A_2)\right]
\end{aligned} \tag{37}$$

where the coefficients A_k and C_k $(k = 0, 1, 2)$ are given by

$$\begin{aligned}
&A_0 = (\alpha_9^2 - \alpha_1\alpha_4)d, \\
&C_0 = -\alpha_9(2\alpha_2 + \alpha_0 r_0^{-2})d, \\
&(\alpha_1 + 2\alpha_2 + \frac{\alpha_0}{r_0^2})A_1 + \alpha_9 C_1 = \beta_1\tau_0 + \frac{\beta_4}{r_0}\sigma_0, \\
&\alpha_9 A_1 + \alpha_4 C_1 = \beta_2\tau_0, \\
&(\alpha_1 + 2\alpha_2 + \frac{\alpha_0}{r_0^2})A_2 + \alpha_9 C_2 = \beta_1\tau_1 + \frac{\beta_4}{r_0}\sigma_1, \\
&\alpha_9 A_2 + \alpha_4 C_2 = \beta_2\tau_1
\end{aligned}$$

and the constants a, b, and d denote the expressions

$$a = -\frac{\alpha_1 A_1 + \alpha_9 C_1 - \beta_1 \tau_0}{\alpha_1 A_0 + \alpha_9 C_0 - (\alpha_1 + 2\alpha_2)},$$
$$b = -\frac{\alpha_1 A_2 + \alpha_9 C_2 - \beta_1 \tau_1}{\alpha_1 A_0 + \alpha_9 C_0 - (\alpha_1 + 2\alpha_2)},$$
$$d = [\alpha_9^2 - \alpha_4(\alpha_1 + 2\alpha_2 + \alpha_0 r_0^{-2})]^{-1}$$

Solution (37) gives the displacement and director displacement vector fields of the cylindrical Cosserat shell under the action of the thermal fields (35).

Finally, we mention that the results of the Cosserat theory for cylindrical shells are in accordance with those predicted by the three-dimensional thermoelasticity. The agreement between the two approaches has been shown in [10], where certain corresponding solutions have been compared using the identification of the constitutive coefficients for Cosserat shells in terms of the classical thermoelasticity constants [7, 9, 12].

Acknowledgments The author was supported by the German state grant: "Programm des Bundes und der Länder für bessere Studienbedingungen und mehr Qualität in der Lehre".

Cross-References

▶ Saint-Venant's Problem for Cosserat Elastic Shells

References

1. Ieşan D (2004) Thermoelastic models of continua. Kluwer, Dordrecht/Boston/London
2. Librescu L, Song O (2006) Thin-walled composite beams: theory and application. Springer, Dordrecht
3. Noda N, Hetnarski R, Tanigawa Y (2003) Thermal stresses, 2nd edn. Taylor & Francis, New York/London
4. Naghdi PM (1972) The theory of shells and plates. In: Flügge S (ed) Handbuch der Physik, vol VIa/2. Springer, Berlin/Heidelberg/New York, pp 425–640
5. Rubin MB (2000) Cosserat theories: shells, rods, and points. Kluwer, Dordrecht
6. Bîrsan M (2004) The solution of Saint-Venant's problem in the theory of Cosserat shells. J Elast 74:185–214
7. Bîrsan M (2006) On a thermodynamic theory of porous Cosserat elastic shells. J Therm Stress 29:879–900
8. Bîrsan M (2009) Linear Cosserat elastic shells: mathematical theory and applications. Matrix Rom, Bucharest
9. Green AE, Naghdi PM (1979) On thermal effects in the theory of shells. Proc R Soc Lond A365:161–190
10. Bîrsan M (2009) Thermal stresses in cylindrical Cosserat elastic shells. Eur J Mech Solids 28:94–101
11. Vrabie II (2004) Differential equations: an introduction to basic concepts, results and applications. World Scientific, Singapore
12. Rubin MB (2004) Restrictions on linear constitutive equations for a rigid heat conducting Cosserat shell. Int J Solids Struct 41:7009–7033

Cylindrical Orthotropic Thermoelastic Shells Modeled by Direct Approach

Mircea Bîrsan[1,3], Tomasz Sadowski[2] and Daniel Pietras[2]
[1]Department of Mathematics, University "A.I. Cuza" of Iaşi, Iaşi, Romania
[2]Faculty of Civil Engineering and Architecture, Lublin University of Technology, Lublin, Poland
[3]Faculty of Mathematics, University Duisburg–Essen, Essen, Germany

Synonyms

Coupling constitutive coefficients; Cylindrical thermoelastic shells; Layered shells

Overview

Using the direct approach to shell theory, we present a general set of constitutive equations which is able to describe thermoelastic orthotropic layered shells. By comparison of solutions to thermal stress problems in the shell theory and the three-dimensional theory, we determine the expression of the coupling thermoelastic coefficients for layered shells, in

terms of the three-dimensional material/geometrical parameters. We verify our theoretical analytical results by comparison with numerical (finite element) solutions for the thermal bending of layered shells.

Introduction

In the classical approach to shell theory, the shell-like body is described as a thin three-dimensional continuum [1]. The two-dimensional shell equations are then derived by integration over the thickness and certain simplifying assumptions. In some cases, the simplifying assumptions restrict the range of applicability of such theories.

An alternative to the classical approach is the direct approach to shell theory. In the direct approach, the shells are modeled as two-dimensional continua (i.e., deformable surfaces) endowed with a certain microstructure. This additional microstructure attached to each point of the surface accounts for the three-dimensional effects in the mechanical behavior of shells. The idea of the direct approach was first proposed by the Cosserat brothers and developed subsequently by many scientists like Truesdell, Ericksen, Green, Naghdi, and Antman. Following this original idea, Zhilin [2, 3] has developed a direct approach to shells in which the deformable surfaces are endowed with a triad of orthonormal vectors connected to each point. The three vectors (also called directors) are rigidly rotating during deformation, and they specify the orientation of the material points, which are thus viewed as infinitesimal rigid bodies.

In this theory, also called the theory of simple shells [4], Zhilin has supplemented the kinematical model proposed by Cosserat with specific constitutive equations, thus making the model useful for the treatment of practical shell problems [3]. The theory of simple shells describes thermal effects in thin shells by introducing two temperature fields assigned to the points of the deformable surface. The two thermal fields represent the temperature on the two major surfaces (top and bottom) of the shell. To formulate appropriate constitutive equations in the direct approach, one can use the effective stiffness concept. In this entry, we consider a general set of constitutive equations which can describe thermoelastic orthotropic layered shells. The components of the constitutive tensors represent the effective stiffness properties and the coupling thermoelastic coefficients of shells. We begin this entry with a short review of the governing equations for linear thermoelastic shells in the direct approach. Then, we present the structure of the constitutive tensors for orthotropic layered shells. In the next section, we turn our attention to cylindrical shells and investigate the equilibrium deformation under the action of given temperature fields. The analytical solution to the thermal stress problem allows us to determine the expression of the coupling thermoelastic coefficients. We present these expressions in closed form, in the case of three-layered shells. Finally, we consider the thermal deformation of two-layered plates and determine the coupling thermoelastic coefficients of such thin structures. The comparison between theoretical and numerical results shows a very good agreement, which indicates that the direct approach is an efficient model for the analysis of layered thermoelastic shells.

General Equations for Thermoelastic Shells

In the theory of simple elastic shells [2–4], the shell-like body is modeled as a directed surface, i.e., a two-dimensional continuum in which each material point is connected with an orthonormal triad of vectors (directors). These three vectors can undergo rigid rotations in the course of shell deformation. Thus, the directors describe the orientation of the material points, which are viewed as small rigid bodies.

Denote by $\mathcal{S}$ the actual configuration of the directed surface at time t, which is determined by the fields $\{\mathbf{R}(\mathbf{x}, t); \mathbf{D}_k(\mathbf{x}, t)\}$, $k = 1, 2, 3$, where $\mathbf{x} = (\mathrm{x}_1, \mathrm{x}_2)$ represents the material curvilinear coordinates on the surface, $\mathbf{R}$ is the position vector, and $\mathbf{D}_k$ are the directors associated to each

material point. In the reference configuration $\mathcal{S}_0$ (at time $t = 0$), we designate the corresponding fields by $\{\mathbf{r}(\mathbf{x}); \mathbf{d}_k(\mathbf{x})\}$. We have $\mathbf{d}_k \cdot \mathbf{d}_m = \delta_{km}$ (the Kronecker symbol), and we introduce the orthogonal *rotation tensor* $\mathbf{P}$ by $\mathbf{P}(\mathbf{x}, t) = \mathbf{D}_k(\mathbf{x}, t) \otimes \mathbf{d}_k(\mathbf{x})$. The Einstein summation convention is employed.

In the linear theory, we define the infinitesimal displacement vector $\mathbf{u}(\mathbf{x}, t) = \mathbf{R}(\mathbf{x}, t) - \mathbf{r}(\mathbf{x})$ and the infinitesimal rotation vector $\boldsymbol{\varphi}$ by the relations $\dot{\boldsymbol{\varphi}}(\mathbf{x}, t) = -\frac{1}{2}[\dot{\mathbf{P}} \cdot \mathbf{P}^T]_\times$ and $\partial_\alpha \boldsymbol{\varphi}(\mathbf{x}, t) = -\frac{1}{2}[\partial_\alpha \mathbf{P} \cdot \mathbf{P}^T]_\times$. Here, a superposed dot stands for the material time derivative; we designate by $[\cdot]_\times$ the vector invariant (or "Gibbsian cross") for any second-order tensor $[\cdot]$ and by $\partial_\alpha = \frac{\partial}{\partial x_\alpha}$. The Greek indices take the values $\{1, 2\}$, while the Latin indices range over the set $\{1, 2, 3\}$. We observe that $\dot{\boldsymbol{\varphi}}$ and $\partial_\alpha \boldsymbol{\varphi}$ are the axial vectors of the skew-symmetric tensors $\dot{\mathbf{P}} \cdot \mathbf{P}^T$ and $\partial_\alpha \mathbf{P} \cdot \mathbf{P}^T$, respectively.

Let us denote by $\mathbf{r}_\alpha(\mathbf{x}) = \partial_\alpha \mathbf{r}(\mathbf{x})$ the covariant base vectors in the tangent plane and by $\mathbf{n}(\mathbf{x})$ the unit normal to the surface $\mathcal{S}_0$ ($\mathbf{n} \cdot \mathbf{r}_\alpha = 0, \mathbf{n} \cdot \mathbf{n} = 1$). Consider also the vectors $\mathbf{r}^\alpha(\mathbf{x})$ given by $\mathbf{r}^\alpha \cdot \mathbf{r}_\beta = \delta^\alpha_\beta$. For simplicity, we chose the initial director $\mathbf{d}_3(\mathbf{x})$ to coincide with $\mathbf{n}(\mathbf{x})$. We may consider that $\boldsymbol{\varphi}(\mathbf{x}, t) \cdot \mathbf{n}(\mathbf{x}) = 0$, since the (drilling) rotations about the normal $\mathbf{n}$ do not intervene in the governing equations in the linear theory of simple shells [3]. The vector fields $\mathbf{u}$ and $\boldsymbol{\varphi}$ can be decomposed as $\mathbf{u} = u_\alpha \mathbf{r}^\alpha + u_3 \mathbf{n}$, $\boldsymbol{\varphi} = \boldsymbol{\varphi}_\alpha \mathbf{r}^\alpha$, which shows that we have five independent kinematical scalar fields (three displacements u_i and two rotations $\boldsymbol{\varphi}_\alpha$). Thus, the theory of simple shells is in this sense a Reissner-type theory for shells. The first and second fundamental tensors of $\mathcal{S}_0$ are $\mathbf{a} = \mathbf{r}^\alpha \otimes \mathbf{r}_\alpha$ and $\mathbf{b} = -\mathbf{r}^\alpha \otimes \partial_\alpha \mathbf{n}$, respectively. We also consider the skew-symmetric alternator tensor $\mathbf{c}$ given by $\mathbf{c} = -\mathbf{a} \times \mathbf{n} = -\mathbf{n} \times \mathbf{a}$.

In order to take into account the thermal effects in shells, we distinguish between the two sides of the directed surface, which will be labeled as faces 1 and 2, such that the unit normal $\mathbf{n}$ is taken from side 2 toward side 1. We denote by $T_1(\mathbf{x}, t)$ and $T_2(\mathbf{x}, t)$ the temperature fields on the sides 1 and 2, respectively, at time t. By means of these two temperature fields, one can describe the variation of temperature across the shell's thickness as $T_1 - T_2$ and the average temperature through the thickness as $\frac{1}{2}(T_1 + T_2)$. In the linear theory of thermoelastic simple shells, the infinitesimal temperature variations τ_1 and τ_2 are introduced by $\tau_1(\mathbf{x}, t) = T_1(\mathbf{x}, t) - T_0$, $\tau_2(\mathbf{x}, t) = T_2(\mathbf{x}, t) - T_0$, where T_0 is the constant temperature of the shell in the reference undeformed configuration $\mathcal{S}_0$. The linear strain tensors for simple shells are given by

$$\begin{aligned} \boldsymbol{\varepsilon} &= \frac{1}{2}\left(\mathbf{e} \cdot \mathbf{a} + \mathbf{a} \cdot \mathbf{e}^T\right) \\ \boldsymbol{\gamma} &= \mathbf{e} \cdot \mathbf{n} = (\nabla \mathbf{u}) \cdot \mathbf{n} + \mathbf{c} \cdot \boldsymbol{\varphi} \\ \mathbf{k} &= \boldsymbol{\kappa} \cdot \mathbf{a} + \frac{1}{2}(\mathbf{e} \cdot \cdot \mathbf{c})\mathbf{b} \end{aligned} \tag{1}$$

where we denote by $\mathbf{e} = \nabla \mathbf{u} + \mathbf{a} \times \boldsymbol{\varphi} = \mathbf{r}^\alpha \otimes \partial_\alpha \mathbf{u} + \mathbf{a} \times \boldsymbol{\varphi}$, $\boldsymbol{\kappa} = \nabla \boldsymbol{\varphi} = \mathbf{r}^\alpha \otimes \partial_\alpha \boldsymbol{\varphi}$. From (1) we see that ε is a symmetric tensor describing the extensional and in-plane shear strains of the shell, $\boldsymbol{\gamma}$ is a vector which accounts the transverse shear deformation, and $\mathbf{k}$ is a tensor of bending and twist strains [3].

In order to present the equilibrium equations, let us introduce the force tensor $\mathbf{T}$ and the moment tensor $\mathbf{M}$. For any subset $\mathcal{P}_0$ of the reference surface $\mathcal{S}_0$, we designate by $\boldsymbol{\nu}$ the external unit normal to the boundary curve $\partial \mathcal{P}_0$ which lies in the tangent plane and by $\mathbf{t}$ and $\mathbf{m}$ the vectors of external force and moment acting on the boundary $\partial \mathcal{P}_0$. Then, the force tensor $\mathbf{T}$ and the moment tensor $\mathbf{M}$ satisfy the relations of Cauchy type $\mathbf{t} = \boldsymbol{\nu} \cdot \mathbf{T}, \mathbf{m} = \boldsymbol{\nu} \cdot \mathbf{M}$. The equations of equilibrium have the form

$$\mathbf{r}^\alpha \cdot \partial_\alpha \mathbf{T} + \mathbf{F} = \mathbf{0}, \qquad \mathbf{r}^\alpha \cdot \partial_\alpha \mathbf{M} + \mathbf{T}_\times + \mathbf{L} = \mathbf{0} \tag{2}$$

Here the vectors $\mathbf{F}$ and $\mathbf{L}$ are the external forces and moments per unit area of $\mathcal{S}_0$.

Let us present next the constitutive equations for orthotropic nonhomogeneous thermoelastic simple shells. The Helmholtz free energy function Ψ is expressed in terms of the variables $(\boldsymbol{\varepsilon}, \boldsymbol{\gamma}, \mathbf{k}, \tau_1, \tau_2)$ by the relations [3, 8]

$$\begin{aligned}\Psi(\boldsymbol{\varepsilon},\boldsymbol{\gamma},\mathbf{k},\tau_1,\tau_2) &= \mathcal{U}(\boldsymbol{\varepsilon},\boldsymbol{\gamma},\mathbf{k}) + \Psi_T(\boldsymbol{\varepsilon},\mathbf{k},\tau_1,\tau_2),\\ \rho\mathcal{U} &= \frac{1}{2}\,\boldsymbol{\varepsilon}\cdot\cdot\mathbf{C}_1\cdot\cdot\boldsymbol{\varepsilon} + \boldsymbol{\varepsilon}\cdot\cdot\mathbf{C}_2\cdot\cdot\mathbf{k}\\ &\quad + \frac{1}{2}\,\mathbf{k}\cdot\cdot\mathbf{C}_3\cdot\cdot\mathbf{k} + \frac{1}{2}\,\boldsymbol{\gamma}\cdot\boldsymbol{\Gamma}\cdot\boldsymbol{\gamma},\\ \rho\Psi_T &= \boldsymbol{\varepsilon}\cdot\cdot(\mathbf{C}_4\,\tau_1 + \mathbf{C}_5\,\tau_2)\\ &\quad + \mathbf{k}\cdot\cdot(\mathbf{C}_6\,\tau_1 + \mathbf{C}_7\,\tau_2)\\ &\quad - \frac{1}{2}\,\tilde{\alpha}_1\tau_1^2 - \frac{1}{2}\,\tilde{\alpha}_2\tau_2^2\end{aligned} \tag{3}$$

Here ρ denotes the mass density in the reference configuration, while the tensors $\mathbf{C}_1$, $\mathbf{C}_2$, $\mathbf{C}_3$ (of fourth order), and the tensor $\boldsymbol{\Gamma}$ (of second order) represent the stiffness tensors which characterize the effective elastic properties of the simple shell. The second-order tensors $\mathbf{C}_k$ $(k = 4,\ldots,7)$ and the coefficients $\tilde{\alpha}_1$ and $\tilde{\alpha}_2$ express the material properties concerning the coupling between the thermal fields and the elastic deformations. These constitutive tensors satisfy the symmetry conditions $\boldsymbol{\Gamma} = \boldsymbol{\Gamma}^T$, $\mathbf{C}_4 = \mathbf{C}_4^T$, $\mathbf{C}_5 = \mathbf{C}_5^T$, $\mathbf{c}\cdot\cdot\mathbf{C}_\alpha = 0$ $(\alpha = 1,2)$, and $\mathbf{v}\cdot\cdot\mathbf{C}_k = \mathbf{C}_k\cdot\cdot\mathbf{v}$ $(k = 1,3)$ for any second-order tensor $\mathbf{v}$. Then, the constitutive equations for general orthotropic thermoelastic shells are [8]

$$\begin{aligned}\mathrm{sym}(\mathbf{T}\cdot\mathbf{a}) &\equiv \frac{1}{2}(\mathbf{T}\cdot\mathbf{a} + \mathbf{a}\cdot\mathbf{T}^T) = \mathbf{T}\cdot\mathbf{a}\\ &\quad + \frac{1}{2}\,(\mathbf{M}\cdot\cdot\mathbf{b})\mathbf{c} = \frac{\partial(\rho\Psi)}{\partial\boldsymbol{\varepsilon}}\\ &= \mathbf{C}_1\cdot\cdot\boldsymbol{\varepsilon} + \mathbf{C}_2\cdot\cdot\mathbf{k} + \mathbf{C}_4\,\tau_1 + \mathbf{C}_5\,\tau_2,\\ \mathbf{N} &\equiv \mathbf{T}\cdot\mathbf{n} = \frac{\partial(\rho\Psi)}{\partial\boldsymbol{\gamma}} = \boldsymbol{\Gamma}\cdot\boldsymbol{\gamma},\\ \mathbf{M} &= \frac{\partial(\rho\Psi)}{\partial\mathbf{k}}\\ &= (\boldsymbol{\varepsilon}\cdot\cdot\mathbf{C}_2 + \mathbf{C}_3\cdot\cdot\mathbf{k} + \mathbf{C}_6\,\tau_1 + \mathbf{C}_7\,\tau_2)^T\end{aligned} \tag{4}$$

together with the restrictions $\mathbf{M}^T\cdot\cdot\mathbf{b} + \mathbf{T}^T\cdot\cdot\mathbf{c} = 0$ and $\mathbf{M}\cdot\mathbf{n} = 0$, which follow from the fact that the (drilling) rotations about $\mathbf{n}$ are not taken into account [3].

This set of constitutive equations is quite general and can describe various types of composite shells, such as multilayered shells or reinforced shells. The system of governing field equations described above has been studied from a mathematical point of view in [5] in the isothermal theory and in [6] in the thermodynamical theory. In these papers, some important properties of solutions to the governing linear equations have been established, such as existence, uniqueness, continuous dependence on body loads and initial data, reciprocity, and variational characterization.

For orthotropic layered shells (with symmetric or nonsymmetric sequences of layers), the structure of the constitutive tensors in the isothermal theory has been derived in [3]. To obtain simpler forms of these expressions, we can assume that the basis $\{\mathbf{r}_1,\mathbf{r}_2\}$ is orthogonal. We denote by $\mathbf{a}_k$ $(k = 1,\ldots,4)$ the second-order tensors $\mathbf{a}_1 = \mathbf{a}, \mathbf{a}_2 = \mathbf{r}_1\otimes\mathbf{r}_1 - \mathbf{r}_2\otimes\mathbf{r}_2, \mathbf{a}_3 = \mathbf{c}, \mathbf{a}_4 = \mathbf{r}_1\otimes\mathbf{r}_2 + \mathbf{r}_2\otimes\mathbf{r}_1$. According to [3], the tensors $\mathbf{C}_1$, $\mathbf{C}_2$, $\mathbf{C}_3$, and $\boldsymbol{\Gamma}$ are expressed by

$$\begin{aligned}\mathbf{C}_1 &= A_{11}\mathbf{a}_1\otimes\mathbf{a}_1 + A_{12}(\mathbf{a}_1\otimes\mathbf{a}_2 + \mathbf{a}_2\otimes\mathbf{a}_1)\\ &\quad + A_{22}\mathbf{a}_2\otimes\mathbf{a}_2 + A_{44}\mathbf{a}_4\otimes\mathbf{a}_4\\ \mathbf{C}_2 &= B_{13}\mathbf{a}_1\otimes\mathbf{a}_3 + B_{14}\mathbf{a}_1\otimes\mathbf{a}_4 + B_{23}\mathbf{a}_2\otimes\mathbf{a}_3\\ &\quad + B_{24}\mathbf{a}_2\otimes\mathbf{a}_4 + B_{41}\mathbf{a}_4\otimes\mathbf{a}_1 + B_{42}\mathbf{a}_4\otimes\mathbf{a}_2\\ \mathbf{C}_3 &= C_{11}\mathbf{a}_1\otimes\mathbf{a}_1 + C_{12}(\mathbf{a}_1\otimes\mathbf{a}_2 + \mathbf{a}_2\otimes\mathbf{a}_1)\\ &\quad + C_{22}\mathbf{a}_2\otimes\mathbf{a}_2 + C_{33}\mathbf{a}_3\otimes\mathbf{a}_3\\ &\quad + C_{34}(\mathbf{a}_3\otimes\mathbf{a}_4 + \mathbf{a}_4\otimes\mathbf{a}_3)\\ &\quad + C_{44}\mathbf{a}_4\otimes\mathbf{a}_4, \qquad \boldsymbol{\Gamma} = \Gamma_1\,\mathbf{a}_1 + \Gamma_2\,\mathbf{a}_2\end{aligned} \tag{5}$$

where the coefficients A_{rs}, B_{rs}, C_{rs} and Γ_α are the effective stiffness moduli. Using the theory of tensor symmetry, we can deduce in the same way as in the structure of the thermoelastic coupling tensors $\mathbf{C}_4$, $\mathbf{C}_5$, $\mathbf{C}_6$, and $\mathbf{C}_7$.

In the general case of orthotropic shells with nonsymmetric arrangement of layers, the coupling thermoelastic tensors have the following representations [8]:

$$\begin{aligned}\mathbf{C}_4 &= C_4\mathbf{a}_1 + \widehat{C}_4\mathbf{a}_2, \qquad \mathbf{C}_5 = C_5\mathbf{a}_1 + \widehat{C}_5\mathbf{a}_2,\\ \mathbf{C}_6 &= C_6\mathbf{a}_3 + \widehat{C}_6\mathbf{a}_4, \qquad \mathbf{C}_7 = C_7\mathbf{a}_3 + \widehat{C}_7\mathbf{a}_4\end{aligned} \tag{6}$$

where C_k and $\widehat{C}_k$ are coupling coefficients. In the particular case when the shell is transversal isotropic, the relations (6) reduce to [8]

$$\begin{aligned} &\mathbf{C}_4 = C_4\mathbf{a}_1, \quad \mathbf{C}_5 = C_5\mathbf{a}_1, \\ &\mathbf{C}_6 = C_6\mathbf{a}_3, \quad \mathbf{C}_7 = C_7\mathbf{a}_3 \end{aligned} \tag{7}$$

In the case of transversal isotropic shells with symmetric distribution of layers, the structure of the thermoelastic constitutive tensors simplify [8]

$$\mathbf{C}_4 = \mathbf{C}_5 = C_4\mathbf{a}_1, \quad \mathbf{C}_6 = -\mathbf{C}_7 = C_6\mathbf{a}_3, \quad \tilde{\alpha}_1 = \tilde{\alpha}_2 \tag{8}$$

In what follows, we consider the general case of (nonsymmetric) layered shells having the constitutive tensors of the forms (5) and (6).

Deformation of Cylindrical Shells Under Given Temperature Fields

Let the reference configuration $\mathcal{S}_0$ be a cylindrical surface. We refer the surface to a Cartesian orthogonal frame $Ox_1x_2x_3$, such that the generators of $\mathcal{S}_0$ are parallel to the axis Ox_3. The material surface coordinates are denoted by $\mathrm{x}_1 = s$ and $\mathrm{x}_2 = z$, where the axial coordinate z is the distance to the plane x_1Ox_2, while the circumferential coordinate s is the arc length parameter along the cross-sectional curves $z = \text{const}$. If we designate by $\mathbf{e}_i$ the unit vectors along the axes Ox_i, then the parametric equation of the reference surface $\mathcal{S}_0$ can be written in the form

$$\begin{aligned} &\mathbf{r} = \mathbf{r}(s,z) = x_\alpha(s)\mathbf{e}_\alpha + z\ \mathbf{e}_3, \\ &s \in [0,\bar{s}], \quad z \in [0,\bar{z}] \end{aligned} \tag{9}$$

where $x_1(s)$ and $x_2(s)$ are given functions which describe the shape of the reference cylindrical surface. Let us designate by $\mathbf{s}$ the unit tangent vector to the cross-sectional curve, $\mathbf{n}$ the unit normal vector to the surface, and $r(s)$ the radius of curvature of the cross-sectional curve. For cylindrical shells, the following relations hold [8]:

$$\begin{aligned} &r_1 = s = x'_\alpha e_\alpha, \quad r_2 = e_3, \quad n = e_{\alpha\beta}x'_\beta e_\alpha, \\ &c = e_{\alpha\beta}r_\alpha \otimes r_\beta, \quad a = s\otimes s + e_3\otimes e_3, \\ &b = -\frac{1}{r(s)}\, s\otimes s, \quad r(s) = [e_{\alpha\beta}x'_\alpha(s)x''_\beta(s)]^{-1} \end{aligned} \tag{10}$$

where $(\,\cdot\,)' = \frac{\mathrm{d}(\cdot)}{\mathrm{d}s}$ and $e_{\alpha\beta}$ represent the two-dimensional alternator ($e_{12} = -e_{21} = 1$, $e_{11} = e_{22} = 0$). In view of $(10)_{1,2}$, we denote the components as follows [8, 9]:

$$\begin{aligned} &\mathbf{u} = u_1\mathbf{s} + u_2\mathbf{e}_3 + u_3\mathbf{n}, \quad \boldsymbol{\varphi} = -\varphi_2\mathbf{s} + \varphi_1\mathbf{e}_3, \\ &\boldsymbol{\gamma} = \gamma_1\mathbf{s} + \gamma_2\mathbf{e}_3, \\ &\boldsymbol{\varepsilon} = \varepsilon_1\mathbf{s}\otimes\mathbf{s} + \varepsilon_2\mathbf{e}_3\otimes\mathbf{e}_3 + \varepsilon_{12}\mathbf{s}\otimes\mathbf{e}_3 + \varepsilon_{21}\mathbf{e}_3\otimes\mathbf{s}, \\ &\mathbf{k} = -\delta_1\mathbf{s}\otimes\mathbf{s} + \delta_2\mathbf{e}_3\otimes\mathbf{e}_3 + \kappa_1\mathbf{s}\otimes\mathbf{e}_3 - \kappa_2\mathbf{e}_3\otimes\mathbf{s}, \\ &\mathbf{T} = T_1\mathbf{s}\otimes\mathbf{s} + T_2\mathbf{e}_3\otimes\mathbf{e}_3 + T_{12}\mathbf{s}\otimes\mathbf{e}_3 + T_{21}\mathbf{e}_3\otimes\mathbf{s} \\ &\quad + N_1\mathbf{s}\otimes\mathbf{n} + N_2\mathbf{e}_3\otimes\mathbf{n}, \\ &\mathbf{M} = -M_{12}\mathbf{s}\otimes\mathbf{s} + M_{21}\mathbf{e}_3\otimes\mathbf{e}_3 + M_1\mathbf{s}\otimes\mathbf{e}_3 \\ &\quad - M_2\mathbf{e}_3\otimes\mathbf{s} \end{aligned} \tag{11}$$

The strain tensor components are expressed by [9]

$$\begin{aligned} &\varepsilon_1 = u_{1,1} + \frac{1}{r}\,u_3, \quad \varepsilon_2 = u_{2,2} \\ &\varepsilon_{12} = \varepsilon_{21} = \frac{1}{2}(u_{1,2} + u_{2,1}) \\ &\gamma_1 = u_{3,1} - \frac{1}{r}\,u_1 + \varphi_1, \quad \gamma_2 = u_{3,2} + \varphi_2 \\ &\delta_1 = \varphi_{2,1} + \frac{1}{2r}(u_{1,2} - u_{2,1}), \quad \delta_2 = \varphi_{1,2} \\ &\kappa_1 = \varphi_{1,1}, \quad \kappa_2 = \varphi_{2,2} \end{aligned} \tag{12}$$

Here we designate the partial derivatives in the usual manner: $f_{,1} = \frac{\partial f}{\partial \mathrm{x}_1} = \frac{\partial f}{\partial s}$, $f_{,2} = \frac{\partial f}{\partial \mathrm{x}_2} = \frac{\partial f}{\partial z}$, for any function f. To write the constitutive equations (4) in component form, we decompose them in "elastic parts" T^e_α, M^e_α and "thermal parts" T^t_α, M^t_α [8]:

$$
\begin{aligned}
&T_1 = T_1^e + T_1^t, \quad T_2 = T_2^e + T_2^t,\\
&M_1 = M_1^e + M_1^t, \quad M_2 = M_2^e + M_2^t,\\
&T_1^t = f_1\tau_1 + f_2\tau_2, \quad T_2^t = f_3\tau_1 + f_4\tau_2,\\
&M_1^t = f_5\tau_1 + f_6\tau_2, \quad M_2^t = f_7\tau_1 + f_8\tau_2,\\
&T_1^e = a_1\varepsilon_1 + a_3\varepsilon_2 + b_1\kappa_1 + b_2\kappa_2,\\
&T_2^e = a_2\varepsilon_2 + a_3\varepsilon_1 + b_3\kappa_1 + b_4\kappa_2,\\
&M_1^e = b_1\varepsilon_1 + b_3\varepsilon_2 + c_1\kappa_1 + c_3\kappa_2,\\
&M_2^e = b_2\varepsilon_1 + b_4\varepsilon_2 + c_3\kappa_1 + c_2\kappa_2,\\
&T_{12} = \frac{1}{2}\left(b_5 - \frac{1}{r}\,c_4\right)\delta_1 + \frac{1}{2}\left(b_6 - \frac{1}{r}\,c_6\right)\delta_2\\
&\qquad + \frac{1}{2}\left(a_4 - \frac{1}{r}\,b_5\right)\varepsilon_{12}, \quad N_1 = d_1\gamma_1,\\
&T_{21} = \frac{1}{2}\left(b_5 + \frac{1}{r}\,c_4\right)\delta_1 + \frac{1}{2}\left(b_6 + \frac{1}{r}\,c_6\right)\delta_2\\
&\qquad + \frac{1}{2}\left(a_4 + \frac{1}{r}\,b_5\right)\varepsilon_{12}, \quad N_2 = d_2\gamma_2,\\
&M_{12} = b_5\varepsilon_{12} + c_4\delta_1 + c_6\delta_2,\\
&M_{21} = b_6\varepsilon_{12} + c_6\delta_1 + c_5\delta_2
\end{aligned}
\tag{13}
$$

The coefficients $f_1, \ldots, f_8$ entering in the thermal part of (13) are given by

$$
\begin{aligned}
&f_1 = C_4 + \widehat{C}_4, \quad f_2 = C_5 + \widehat{C}_5,\\
&f_3 = C_4 - \widehat{C}_4, \quad f_4 = C_5 - \widehat{C}_5,\\
&f_5 = -(C_6 + \widehat{C}_6), \quad f_6 = -(C_7 + \widehat{C}_7),\\
&f_7 = -(C_6 - \widehat{C}_6), \quad f_8 = -(C_7 - \widehat{C}_7)
\end{aligned}
\tag{14}
$$

The coefficients a_s, b_s, c_s, and d_γ appearing in the purely elastic terms of (13) are expressed in terms of the effective elastic moduli A_{rs}, B_{rs}, C_{rs} and Γ_α by

$$
\begin{aligned}
&a_1 = A_{11} + 2A_{12} + A_{22}, \quad a_2 = A_{11} - 2A_{12} + A_{22},\\
&a_3 = A_{11} - A_{22}, \quad a_4 = 4A_{44},\\
&b_1 = -B_{13} - B_{23} + B_{14} + B_{24},\\
&b_2 = -(B_{13} + B_{23} + B_{14} + B_{24}),\\
&b_3 = -B_{13} + B_{23} + B_{14} - B_{24},\\
&b_4 = -B_{13} + B_{23} - B_{14} + B_{24},\\
&b_5 = -2(B_{41} + B_{42}), \quad b_6 = 2(B_{41} - B_{42}),\\
&d_1 = \Gamma_1 + \Gamma_2, \quad d_2 = \Gamma_1 - \Gamma_2,\\
&c_1 = C_{33} - 2C_{34} + C_{44}, \quad c_2 = C_{33} + 2C_{34} + C_{44},\\
&c_3 = C_{33} - C_{44}, \quad c_4 = C_{11} + 2C_{12} + C_{22},\\
&c_5 = C_{11} - 2C_{12} + C_{22}, \quad c_6 = -C_{11} + C_{22}
\end{aligned}
\tag{15}
$$

The general form of the constitutive equations (13)–(15) is applicable for orthotropic layered thermoelastic shells. For any given material distribution in the layered cylindrical shell, one should make a suitable choice of the effective elastic moduli A_{rs}, B_{rs}, C_{rs} and Γ_α and the coupling coefficients C_k and $\widehat{C}_k$.

For the type of shells described above, we consider the following thermal stress problem: *find the equilibrium deformation of the layered orthotropic cylindrical shell under a given temperature field applied to the shell, in the absence of body loads*.

In our case, the equilibrium equations in component form are [8, 9]

$$
\begin{aligned}
&T_{1,1} + T_{21,2} + \frac{1}{r}\,N_1 = 0,\\
&T_{12,1} + T_{2,2} = 0,\\
&N_{1,1} + N_{2,2} - \frac{1}{r}\,T_1 = 0,\\
&M_{1,1} + M_{21,2} - N_1 = 0,\\
&M_{12,1} + M_{2,2} - N_2 = 0
\end{aligned}
\tag{16}
$$

As is usual in the treatment of the relaxed Saint-Venant's problem, the pointwise assignment of forces and couples on the end edges of the shell is replaced by prescribing the appropriate resultant forces and moments acting on these boundaries. We impose the condition that the resultant forces and resultant moments on the end edges of the shell are vanishing. The shells under consideration can be either *open* or *closed* cylindrical surfaces. In the case of open cylindrical shells, we impose that the lateral edges are traction free, i.e., we consider the boundary conditions $\mathbf{t} = \mathbf{0}$ and $\mathbf{m} = \mathbf{0}$ on the lateral edges. In the special case when the reference cylindrical surface $\mathcal{S}_0$ is open and *flat*, we deal with the deformation of *plates*. Thus, our solution procedure can be applied to cylindrical (open or closed) shells, as well as to plates, as we will show later on.

The cylindrical shell deforms under the action of the temperature fields τ_1 and τ_2, which are prescribed on the faces of the shell. In the case when the temperature fields τ_1 and τ_2 are

polynomials in the axial coordinate z, i.e., they have the form $\tau_\alpha(s,z)=\sum_{k=0}^{n}\tau_\alpha^{(k)}(s)\,z^k$ with $\tau_\alpha^{(k)}$ given functions of s, we can solve this thermal stress problem by an analytical solution procedure. First, we determine the solution for the case when τ_1 and τ_2 are independent of the axial coordinate. Then, we consider the more general case when the given temperature fields are polynomials in the axial coordinate (of degree n), and we obtain a solution of our thermoelastic equilibrium problem by the mathematical induction procedure with respect to the degree n.

This method is similar to a classical procedure from three-dimensional thermoelasticity theory (see, e.g., [7]). In the framework of the theory of Cosserat surfaces, this method is presented in the section ▶ Cylindrical Elastic Bodies with Directors, Thermal Stresses of this *Encyclopedia of Thermal Stresses*. Within the theory of simple thermoelastic shells, the solution procedure is described in details in the paper [8].

Identification of the Constitutive Coefficients

The analytical solution to the thermal stress problem allows us to determine the expression of the effective stiffness coefficients and of the coupling thermoelastic coefficients in terms of the three-dimensional material parameters. The idea is to compare the analytical solution obtained in the theory of shells with the three-dimensional solution of the same problem and to identify the corresponding quantities.

Layered Shells with Symmetrical Structure

For transversal isotropic shells with symmetric distribution of layers, the structure of thermoelastic constitutive tensors is given by $(8)_{1,2}$, so that they are expressed in terms of only two coefficients: C_4 and C_6. We present the expressions of the coefficients C_4 and C_6 in two particular situations: three-layered shells and homogeneous shells.

Let us consider first the simplest case, i.e., the case of isotropic and homogeneous shells. We denote by E the Young's modulus, ν the Poisson's ratio, μ the shear modulus, α the coefficient of linear expansion of the isotropic thermoelastic material, and by 2 h the constant thickness of the shell. The effective stiffness moduli appearing in the constitutive equations are given by [3, 9]

$$
\begin{aligned}
&A_{11}=\frac{E\,h}{1-\nu},\quad A_{12}=0,\quad A_{22}=A_{44}=\mu h,\\
&B_{13}=\frac{E\,h^3\nu}{3r(1-\nu)^2},\quad B_{14}=-\frac{E\,h^3}{3r(1-\nu)},\\
&B_{41}=\frac{E\,h^3}{6r(1+\nu)},\quad B_{23}=\frac{E\,h^3}{3r(1-\nu^2)},\\
&C_{11}=\frac{h^2}{12r^2}\;\frac{E\,h^3}{3(1+\nu)},\quad C_{33}=\frac{E\,h^3}{3(1-\nu)},\\
&C_{22}=C_{44}=\frac{E\,h^3}{3(1+\nu)},\\
&B_{24}=B_{42}=0,\quad C_{12}=C_{34}=0,\\
&\Gamma_1=\mu\,h\,\Gamma_0,\quad \Gamma_2=0
\end{aligned}
\tag{17}
$$

where $\Gamma_0=\frac{\pi^2}{12}$ stands for the shear correction factor. By comparison of exact shell solutions and three-dimensional solutions to thermal stress problems, the following expressions of thermoelastic coupling coefficients have been determined in [8]:

$$
C_4=\alpha\,\frac{E\,h}{\nu-1},\qquad C_6=\alpha\,\frac{E\,h^2}{3(1-\nu)}
\tag{18}
$$

Let us consider now the more complex case of three-layered shells with a symmetrical arrangement of layers: the two exterior layers have the same thickness h_2, and they are made of the same isotropic material, while the inner layer has the thickness $2h_1$ and is made from a different isotropic material. We denote by E_1, ν_1, μ_1, and α_1 the Young's modulus, Poisson's ratio, shear modulus, and coefficient of linear expansion of the interior layer, respectively, and use the analogous notations E_2, ν_2, μ_2, and α_2 for the exterior layers. In this case, the effective stiffness moduli have the form [3, 9]

$$
\begin{aligned}
&A_{11} = \frac{E_1 h_1}{1-\nu_1} + \frac{E_2 h_2}{1-\nu_2},\\
&A_{22} = A_{44} = \frac{E_1 h_1}{1+\nu_1} + \frac{E_2 h_2}{1+\nu_2}, \quad A_{12} = 0,\\
&C_{33} = \frac{E_1 h_1^3}{3(1-\nu_1)} + \frac{E_2(h^3 - h_1^3)}{3(1-\nu_2)},\\
&C_{22} = C_{44} = \frac{E_1 h_1^3}{3(1+\nu_1)} + \frac{E_2(h^3 - h_1^3)}{3(1+\nu_2)},\\
&\Gamma_2 = 0, \qquad C_{11} = C_{12} = C_{34} = 0,\\
&B_{kl} = 0 \quad (\forall k, l)
\end{aligned}
\tag{19}
$$

where $h = h_1 + h_2$. By comparison of solutions to various thermal stress problems in the two approaches (shell theory and three-dimensional), the thermoelastic coupling coefficients C_4 and C_6 are determined in the form [8]

$$
\begin{aligned}
C_4 &= \alpha_1 \frac{E_1 h_1}{\nu_1 - 1} + \alpha_2 \frac{E_2 h_2}{\nu_2 - 1}\\
C_6 &= \frac{1}{3h}\left(\alpha_1 \frac{E_1 h_1^3}{1-\nu_1} + \alpha_2 \frac{E_2(h^3 - h_1^3)}{1-\nu_2}\right)
\end{aligned}
\tag{20}
$$

The comparison between analytical solutions based on formulas (18) and (20) and numerical solutions obtained by finite element method shows a very good agreement [8].

Two-Layered Nonsymmetric Flat Shells

In this section, we investigate the case of two-layered thermoelastic flat shells and present in details the determination of all thermoelastic coupling coefficients.

Consider a flat shell (plate) with two layers of thicknesses h_1 and h_2, composed of different isotropic and homogeneous materials. We denote by $E_1, \nu_1, \mu_1, \alpha_1$ the thermoelastic material constants for the first layer and $E_2, \nu_2, \mu_2, \alpha_2$ for the second layer. Let us establish the appropriate form of the constitutive equations for two-layered thermoelastic plates. For the elastic part, the structure of the constitutive tensors is given by (5), where the effective stiffness moduli are

$$
\begin{aligned}
&A_{11} = \frac{1}{2}\bar{C}_\alpha(1+\nu_\alpha), \quad A_{22} = A_{44} = \frac{1}{2}\bar{C}_\alpha(1-\nu_\alpha),\\
&A_{12} = 0, \quad B_{14} = B_{23} = 0,\\
&B_{13} = \frac{1}{4}(h_1\bar{C}_1(1+\nu_1) - h_2\bar{C}_2(1+\nu_2)),\\
&B_{41} = B_{42} = 0, \quad C_{11} = C_{12} = 0,\\
&B_{24} = \frac{1}{4}(-h_1\bar{C}_1(1-\nu_1) + h_2\bar{C}_2(1-\nu_2)),\\
&C_{22} = C_{44} = \frac{1}{2}\bar{D}_\alpha(1-\nu_\alpha), \quad C_{34} = 0,\\
&C_{33} = \frac{1}{2}\bar{D}_\alpha(1+\nu_\alpha),\\
&\Gamma_1 = \frac{\lambda_0^2}{3\mu_\alpha h_\alpha}\left[\frac{1}{4}(\mu_1 h_1^2 - \mu_2 h_2^2)^2 + \mu_1\mu_2 h_1 h_2 h^2\right],\\
&\Gamma_2 = 0
\end{aligned}
\tag{21}
$$

In (21), we have used the notations

$$
\begin{aligned}
&\bar{C}_1 = \frac{E_1 h_1}{1-\nu_1^2}, \quad \bar{C}_2 = \frac{E_2 h_2}{1-\nu_2^2},\\
&\bar{D}_1 = \frac{E_1 h_1^3}{3(1-\nu_1^2)}, \quad \bar{D}_2 = \frac{E_2 h_2^3}{3(1-\nu_2^2)},\\
&h = h_1 + h_2
\end{aligned}
\tag{22}
$$

and λ_0 is the smallest positive solution of the equation $\mu_1 \tan(\lambda_0 h_1) + \mu_2 \tan(\lambda_0 h_2) = 0$.

The structure of the thermoelastic constitutive tensors is given by (7), so they are expressed in terms of four coupling coefficients C_4, C_5, C_6, and C_7. Then, the constitutive equations (13) reduce to the following form:

$$
\begin{aligned}
&T_1 = T_1^e + C_4\tau_1 + C_5\tau_2,\\
&T_2 = T_2^e + C_4\tau_1 + C_5\tau_2,\\
&T_1^e = (\bar{C}_1 + \bar{C}_2)\varepsilon_1 + (\bar{C}_\alpha\nu_\alpha)\varepsilon_2\\
&\qquad -\frac{1}{2}(\bar{C}_1 h_1 - \bar{C}_2 h_2)\kappa_1 - \frac{1}{2}(\bar{C}_1\nu_1 h_1 - \bar{C}_2\nu_2 h_2)\kappa_2,\\
&T_2^e = (\bar{C}_\alpha\nu_\alpha)\varepsilon_1 + (\bar{C}_1 + \bar{C}_2)\varepsilon_2\\
&\qquad -\frac{1}{2}(\bar{C}_1\nu_1 h_1 - \bar{C}_2\nu_2 h_2)\kappa_1 - \frac{1}{2}(\bar{C}_1 h_1 - \bar{C}_2 h_2)\kappa_2,\\
&M_1 = M_1^e - C_6\tau_1 - C_7\tau_2,\\
&M_2 = M_2^e - C_6\tau_1 - C_7\tau_2,\\
&M_1^e = (\bar{D}_1 + \bar{D}_2)\kappa_1 + (\bar{D}_\alpha\nu_\alpha)\kappa_2\\
&\qquad -\frac{1}{2}(\bar{C}_1 h_1 - \bar{C}_2 h_2)\varepsilon_1 - \frac{1}{2}(\bar{C}_1\nu_1 h_1 - \bar{C}_2\nu_2 h_2)\varepsilon_2,
\end{aligned}
$$

$$
\begin{aligned}
M_2^e &= (\bar{D}_\alpha \nu_\alpha)\kappa_1 + (\bar{D}_1 + \bar{D}_2)\kappa_2 \\
&\quad -\frac{1}{2}(\bar{C}_1 \nu_1 h_1 - \bar{C}_2 \nu_2 h_2)\varepsilon_1 - \frac{1}{2}(\bar{C}_1 h_1 - \bar{C}_2 h_2)\varepsilon_2, \\
T_{12} &= T_{21} = \bar{C}_\alpha (1 - \nu_\alpha)\varepsilon_{12} \\
M_{12} &= M_{21} = \frac{1}{2}\bar{D}_\alpha (1 - \nu_\alpha)(\delta_1 + \delta_2), \\
N_1 &= m\lambda_0^2 \gamma_1, \quad N_2 = m\lambda_0^2 \gamma_2, \\
m &= \frac{(\mu_1 h_1^2 - \mu_2 h_2^2)^2 + 4\mu_1 \mu_2 h_1 h_2 h^2}{12(\mu_1 h_1 + \mu_2 h_2)}
\end{aligned}
\tag{23}
$$

In order to make the equations (23) useful in applications, we need to express the coupling coefficients C_4, C_5, C_6, C_7 in terms of the three-dimensional parameters $h_1, h_2, E_1, E_2, \nu_1, \nu_2, \alpha_1, \alpha_2$. This identification of constitutive coefficients will be done by comparison of solutions for thermal stress problems.

The parametric equations of the plate are given by (9) with $x_1(s) = 0$, $x_2(s) = s - \frac{\bar{s}}{2}$, $s \in [0, \bar{s}]$. Thus, the flat surface of the plate occupies the region $\{(x_1, x_2, x_3) \,|\, x_1 = 0, x_2 \in (-\bar{s}/2, \bar{s}/2), x_3 \in (0, \bar{z})\}$. The equilibrium equations (16) can be written as

$$
\begin{aligned}
T_{1,1}^e + T_{21,2} &= -(C_4\tau_{1,1} + C_5\tau_{2,1}), \\
T_{12,1} + T_{2,2}^e &= -(C_4\tau_{1,2} + C_5\tau_{2,2}), \\
N_{1,1} + N_{2,2} &= 0, \\
M_{1,1}^e + M_{21,2} - N_1 &= C_6\tau_{1,1} + C_7\tau_{2,1}, \\
M_{12,1} + M_{2,2}^e - N_2 &= C_6\tau_{1,2} + C_7\tau_{2,2}
\end{aligned}
\tag{24}
$$

The conditions $\mathbf{t} = \mathbf{0}$ and $\mathbf{m} = \mathbf{0}$ on the lateral edges $s = 0, \bar{s}$ become

$$
\begin{aligned}
&T_1^e = -(C_4\tau_1 + C_5\tau_2), \quad T_{12} = 0, \quad N_1 = 0, \\
&M_{12} = 0, \quad M_1^e = C_6\tau_1 + C_7\tau_2
\end{aligned}
\tag{25}
$$

The condition that resultant forces and moments vanish on the end edges reduces to

$$
\begin{aligned}
&\int_{\mathcal{C}_0} T_{21}\,\mathrm{d}l = 0, \qquad \int_{\mathcal{C}_0} N_2\,\mathrm{d}l = 0, \\
&\int_{\mathcal{C}_0} T_2^e\,\mathrm{d}l = -\int_{\mathcal{C}_0} (C_4\tau_1 + C_5\tau_2)\mathrm{d}l, \\
&\int_{\mathcal{C}_0} M_2^e\,\mathrm{d}l = \int_{\mathcal{C}_0} (C_6\tau_1 + C_7\tau_2)\mathrm{d}l, \\
&\int_{\mathcal{C}_0} x_1 T_2^e\,\mathrm{d}l = -\int_{\mathcal{C}_0} x_1(C_4\tau_1 + C_5\tau_2)\mathrm{d}l, \\
&\int_{\mathcal{C}_0} (x_1 N_2 - M_{21})\mathrm{d}l = 0
\end{aligned}
\tag{26}
$$

Thus, the thermal stress problem for two-layered flat shells consists in the (23), (24) and the boundary conditions (25), (26).

Solution of Thermal Stress Problem

We present the closed-form solution in the case when the temperature fields are arbitrary given functions of the coordinate x_2, i.e.,

$$
\tau_1 = \tau_1(x_2), \qquad \tau_2 = \tau_2(x_2), \qquad x_2 \in \left(-\frac{\bar{s}}{2}, \frac{\bar{s}}{2}\right)
\tag{27}
$$

Using the general procedure [8], we find the following solution of the problem:

$$
\begin{aligned}
u_1 &= \frac{1}{2}\omega_2(A_1 x_2^2 - x_3^2) + (A_1\omega_3 + A_2\omega_1)x_2 \\
&\quad + \int_0^{x_2} (K_1\tau_1 + K_2\tau_2)\mathrm{d}x_2, \\
u_2 &= x_3(\omega_2 x_2 + \omega_3), \quad u_3 = -\frac{1}{6}B_1\omega_2 x_2^3 \\
&\quad -\frac{1}{2}[\omega_1 x_3^2 + (B_1\omega_3 + B_2\omega_1)x_2^2] \\
&\quad -\int_0^{x_2}\int_0^{x_2} (K_3\tau_1 + K_4\tau_2)\mathrm{d}x_2\mathrm{d}x_2, \\
\varphi_1 &= \frac{1}{2}B_1\omega_2 x_2^2 + (B_1\omega_3 + B_2\omega_1)x_2 \\
&\quad + \int_0^{x_2} (K_3\tau_1 + K_4\tau_2)\mathrm{d}x_2, \qquad \varphi_2 = \omega_1 x_3
\end{aligned}
\tag{28}
$$

where the constants A_1, B_1, A_2, B_2 are determined by the systems

$$
\begin{aligned}
&(\bar{C}_1+\bar{C}_2)A_1+\frac{1}{2}(-\bar{C}_1h_1+\bar{C}_2h_2)B_1\\
&\quad=-(\bar{C}_1\nu_1+\bar{C}_2\nu_2),\\
&\frac{1}{2}(-\bar{C}_1h_1+\bar{C}_2h_2)A_1+(\bar{D}_1+\bar{D}_2)B_1\\
&\quad=\frac{1}{2}(\bar{C}_1\nu_1h_1-\bar{C}_2\nu_2h_2)
\end{aligned}
\tag{29}
$$

$$
\begin{aligned}
&(\bar{C}_1+\bar{C}_2)A_2+\frac{1}{2}(-\bar{C}_1h_1+\bar{C}_2h_2)B_2\\
&\quad=\frac{1}{2}(\bar{C}_1\nu_1h_1-\bar{C}_2\nu_2h_2)\\
&\frac{1}{2}(-\bar{C}_1h_1+\bar{C}_2h_2)A_2+(\bar{D}_1+\bar{D}_2)B_2\\
&\quad=-(\bar{D}_1\nu_1+\bar{D}_2\nu_2)
\end{aligned}
\tag{30}
$$

and the coefficients $K_1,\dots,K_4$ are given by

$$
\begin{aligned}
K_1&=\frac{1}{\Delta}\left[\frac{C_6}{2}(\bar{C}_1h_1-\bar{C}_2h_2)-C_4(\bar{D}_1+\bar{D}_2)\right],\\
K_2&=\frac{1}{\Delta}\left[\frac{C_7}{2}(\bar{C}_1h_1-\bar{C}_2h_2)-C_5(\bar{D}_1+\bar{D}_2)\right],\\
K_3&=\frac{1}{\Delta}\left[C_6(\bar{C}_1+\bar{C}_2)-\frac{C_4}{2}(\bar{C}_1h_1-\bar{C}_2h_2)\right],\\
K_4&=\frac{1}{\Delta}\left[C_7(\bar{C}_1+\bar{C}_2)-\frac{C_5}{2}(\bar{C}_1h_1-\bar{C}_2h_2)\right],\\
\Delta&=(\bar{C}_1+\bar{C}_2)(\bar{D}_1+\bar{D}_2)-\frac{1}{4}(\bar{C}_1h_1-\bar{C}_2h_2)^2
\end{aligned}
$$

In (28), the constants ω_i are expressed in terms of the thermal loads by

$$
\begin{aligned}
D_{22}\,\omega_2&=[\bar{C}_1(1-\nu_1)+\bar{C}_2(1-\nu_2)]\\
&\quad\times\int_{-\bar{s}/2}^{\bar{s}/2}x_2(K_1\tau_1+K_2\tau_2)\mathrm{d}x_2\\
&\quad-\frac{1}{2}[\bar{C}_1h_1(1-\nu_1)-\bar{C}_2h_2(1-\nu_2)]\\
&\quad\times\int_{-\bar{s}/2}^{\bar{s}/2}x_2(K_3\tau_1+K_4\tau_2)\mathrm{d}x_2,\\
D_{11}\,\omega_1+D_{13}\,\omega_3&=[\bar{D}_1(1-\nu_1)+\bar{D}_2(1-\nu_2)]\\
&\quad\times\int_{-\bar{s}/2}^{\bar{s}/2}(K_3\tau_1+K_4\tau_2)\mathrm{d}x_2\\
&\quad-\frac{1}{2}[\bar{C}_1h_1(1-\nu_1)-\bar{C}_2h_2(1-\nu_2)]\\
&\quad\times\int_{-\bar{s}/2}^{\bar{s}/2}(K_1\tau_1+K_2\tau_2)\mathrm{d}x_2,\\
D_{31}\,\omega_1+D_{33}\,\omega_3&=[\bar{C}_1(1-\nu_1)+\bar{C}_2(1-\nu_2)]\\
&\quad\times\int_{-\bar{s}/2}^{\bar{s}/2}(K_1\tau_1+K_2\tau_2)\mathrm{d}x_2\\
&\quad-\frac{1}{2}[\bar{C}_1h_1(1-\nu_1)-\bar{C}_2h_2(1-\nu_2)]\\
&\quad\times\int_{-\bar{s}/2}^{\bar{s}/2}(K_3\tau_1+K_4\tau_2)\mathrm{d}x_2
\end{aligned}
\tag{31}
$$

where the coefficients D_{rk} for two-layered flat shells are

$$
\begin{aligned}
D_{11}&=\bar{s}\left[(\bar{D}_1+\bar{D}_2)+\frac{1}{2}(-\bar{C}_1\nu_1h_1+\bar{C}_2\nu_2h_2)A_2\right.\\
&\quad\left.+(\bar{D}_\alpha\nu_\alpha)B_2\right]\\
D_{22}&=\frac{\bar{s}^3}{12}\left[(\bar{C}_1+\bar{C}_2)+(\bar{C}_\alpha\nu_\alpha)A_1\right.\\
&\quad\left.+\frac{1}{2}(-\bar{C}_1\nu_1h_1+\bar{C}_2\nu_2h_2)B_1\right]\\
D_{33}&=\bar{s}\left[(\bar{C}_1+\bar{C}_2)+(\bar{C}_\alpha\nu_\alpha)A_1\right.\\
&\quad\left.+\frac{1}{2}(-\bar{C}_1\nu_1h_1+\bar{C}_2\nu_2h_2)B_1\right]\\
D_{13}&=\bar{s}\left[\frac{1}{2}(-\bar{C}_1h_1+\bar{C}_2h_2)\right.\\
&\quad\left.+\frac{1}{2}(-\bar{C}_1\nu_1h_1+\bar{C}_2\nu_2h_2)A_1+(\bar{D}_\alpha\nu_\alpha)B_1\right]\\
D_{31}&=\bar{s}\left[\frac{1}{2}(-\bar{C}_1h_1+\bar{C}_2h_2)+(\bar{C}_\alpha\nu_\alpha)A_2\right.\\
&\quad\left.+\frac{1}{2}(-\bar{C}_1\nu_1h_1+\bar{C}_2\nu_2h_2)B_2\right]
\end{aligned}
$$

The solution is determined up to a rigid body displacement–rotation field of the shell.

Let us consider also the special case when the given temperature fields τ_1 and τ_2 in (27) are constants. In this situation, the solution (28) reduces to

$$u_1 = \omega_3 x_2, \quad u_2 = \omega_3 x_3, \quad u_3 = -\frac{\omega_1}{2}(x_2^2 + x_3^2),$$
$$\varphi_1 = \omega_1 x_2, \quad \varphi_2 = \omega_1 x_3 \tag{32}$$

where ω_1 and ω_3 are specified by the system

$$\begin{aligned}
&[\bar{C}_1(1+\nu_1) + \bar{C}_2(1+\nu_2)]\omega_3 - \frac{1}{2}[\bar{C}_1 h_1(1+\nu_1) \\
&\quad - \bar{C}_2 h_2(1+\nu_2)]\omega_1 = -(C_4\tau_1 + C_5\tau_2), \\
&-\frac{1}{2}[\bar{C}_1 h_1(1+\nu_1) - \bar{C}_2 h_2(1+\nu_2)]\omega_3 \\
&\quad + [\bar{D}_1(1+\nu_1) + \bar{D}_2(1+\nu_2)]\omega_1 = C_6\tau_1 + C_7\tau_2
\end{aligned} \tag{33}$$

To identify the coupling constitutive coefficients $C_4, \ldots, C_7$, let us solve now the corresponding thermal stress problem for three-dimensional plates. Consider a layered plate which occupies the domain $\{(x_1^*, x_2^*, x_3^*); x_1^* \in (-h_1, h_2),\ x_2^* \in (-\bar{s}/2, \bar{s}/2),\ x_3^* \in (0, \bar{z})\}$, where the first layer corresponds to $x_1^* \in (-h_1, 0)$ and the second layer to $x_1^* \in (0, h_2)$. We determine the deformation of this plate under a temperature field T which varies linearly in the thickness direction, i.e., $T(x_1^*) = T_{(0)} + x_1^* T_{(1)}$ ($T_{(0)}, T_{(1)}$ const.).

This three-dimensional problem corresponds to the shell problem treated above and admits the following analytical solution:

$$u_2^* = (ax_1^* + b)\, x_2^*, \qquad u_3^* = (ax_1^* + b)\, x_3^*,$$
$$u_1^* = \begin{cases} -\dfrac{a}{2}(x_2^{*2} + x_3^{*2}) + \dfrac{1}{2} G_2 x_1^{*2} + g_2 x_1^* \\ \text{for } x_1^* \in (0, h_2) \\ -\dfrac{a}{2}(x_2^{*2} + x_3^{*2}) + \dfrac{1}{2} G_1 x_1^{*2} + g_1 x_1^* \\ \text{for } x_1^* \in (-h_1, 0) \end{cases} \tag{34}$$

where a, b, G_γ, and g_γ are constants given by

$$\begin{aligned}
&[\bar{C}_1(1+\nu_1) + \bar{C}_2(1+\nu_2)]b - \frac{1}{2}[\bar{C}_1 h_1(1+\nu_1) \\
&-\bar{C}_2 h_2(1+\nu_2)]a3 = [\alpha_1\bar{C}_1(1+\nu_1) + \alpha_2\bar{C}_2(1+\nu_2)]T_{(0)} \\
&-\frac{1}{2}[\alpha_1\bar{C}_1 h_1(1+\nu_1) - \alpha_2\bar{C}_2 h_2(1+\nu_2)]T_{(1)}, \\
&-\frac{1}{2}[\bar{C}_1 h_1(1+\nu_1) - \bar{C}_2 h_2(1+\nu_2)]b \\
&+[\bar{D}_1(1+\nu_1) + \bar{D}_2(1+\nu_2)]a \\
&= [\alpha_1\bar{D}_1(1+\nu_1) + \alpha_2\bar{D}_2(1+\nu_2)]T_{(1)} \\
&-\frac{1}{2}[\alpha_1\bar{C}_1 h_1(1+\nu_1) - \alpha_2\bar{C}_2 h_2(1+\nu_2)]T_{(0)}
\end{aligned} \tag{35}$$

and

$$G_\gamma = \alpha_\gamma \frac{1+\nu_\gamma}{1-\nu_\gamma} T_{(1)} - \frac{2\nu_\gamma}{1-\nu_\gamma} a,$$
$$g_\gamma = \alpha_\gamma \frac{1+\nu_\gamma}{1-\nu_\gamma} T_{(0)} - \frac{2\nu_\gamma}{1-\nu_\gamma} b, \quad \gamma = 1, 2 \tag{36}$$

To make the comparison between the three-dimensional solution $\mathbf{u}^* = u_i^* \mathbf{e}_i$ in (34)–(36) and the displacement–rotation field $(\mathbf{u}, \boldsymbol{\varphi})$ given by (32) and (33), we need to use the correspondence formulas

$$\begin{aligned}
\mathbf{u} &= \frac{1}{h}\left(1 + \frac{3(h_1 - h_2)^2}{h^2}\right) \int_{-h_1}^{h_2} \mathbf{u}^* \mathrm{d}x_1^* \\
&\quad + \frac{6(h_1 - h_2)}{h^3} \int_{-h_1}^{h_2} x_1^* \mathbf{u}^* \mathrm{d}x_1^*, \\
\boldsymbol{\varphi} &= \frac{12}{h^3} \int_{-h_1}^{h_2} x_1^* (u_2^* \mathbf{e}_3 - u_3^* \mathbf{e}_2) \mathrm{d}x_1^* \\
&\quad + \frac{6(h_1 - h_2)}{h^3} \int_{-h_1}^{h_2} (u_2^* \mathbf{e}_3 - u_3^* \mathbf{e}_2) \mathrm{d}x_1^*
\end{aligned} \tag{37}$$

The relations between the thermal fields τ_1 and τ_2 and the temperature T are given by

$$\tau_1 = T_{(0)} + h_2 T_{(1)}, \qquad \tau_2 = T_{(0)} - h_1 T_{(1)} \tag{38}$$

By virtue of relations (37) and (38), we obtain that the two solutions (32) and (34) coincide if

Cylindrical Orthotropic Thermoelastic Shells Modeled by Direct Approach, Table 1 Comparison of displacements for the points $P_1, \ldots, P_4$ of the shell, computed in the two approaches: analytical (Theor.) and numerical (FEM)

	Coordinates		u_1 (mm)		u_2 (mm)		u_3 (mm)	
Point	x_2 (mm)	x_3 (mm)	Theor.	FEM	Theor.	FEM	Theor.	FEM
P_1	47.5	0	0.0020	0.0020	0	0	0.41982	0.41982
P_2	23.75	100	0.0010	0.0010	0.00421	0.00421	1.96565	1.96565
P_3	0	150	0	0	0.00632	0.00632	4.18657	4.18657
P_4	47.5	210	0.0020	0.0020	0.00884	0.00884	8.62549	8.62549

and only if the constitutive coefficients are expressed by

$$C_4 = -\alpha_2 \frac{E_2 h_2}{1-\nu_2} - \frac{1}{2h}\left(\alpha_1 \frac{E_1 h_1^2}{1-\nu_1} - \alpha_2 \frac{E_2 h_2^2}{1-\nu_2}\right)$$
$$C_5 = -\alpha_1 \frac{E_1 h_1}{1-\nu_1} + \frac{1}{2h}\left(\alpha_1 \frac{E_1 h_1^2}{1-\nu_1} - \alpha_2 \frac{E_2 h_2^2}{1-\nu_2}\right)$$
$$C_6 = \alpha_2 \frac{E_2 h_2^2}{3(1-\nu_2)} - \frac{h_1}{6h}\left(\alpha_1 \frac{E_1 h_1^2}{1-\nu_1} - \alpha_2 \frac{E_2 h_2^2}{1-\nu_2}\right)$$
$$C_7 = -\alpha_1 \frac{E_1 h_1^2}{3(1-\nu_1)} - \frac{h_2}{6h}\left(\alpha_1 \frac{E_1 h_1^2}{1-\nu_1} - \alpha_2 \frac{E_2 h_2^2}{1-\nu_2}\right) \tag{39}$$

Thus, all thermoelastic constitutive coefficients have been determined.

Comparison Between Analytical and Numerical Solutions

In order to verify the formulas (39), we compare the theoretical solutions with numerical results obtained by the finite element method. Consider a rectangular two-layered flat shell as described in the previous section, whose surface occupies the region $\{(x_1, x_2, x_3) \,|\, x_1 = 0,\ x_2 \in (-\bar{s}/2, \bar{s}/2),\ x_3 \in (0, \bar{z})\}$. The dimensions of the rectangular plate are the length $\bar{z} = 210$ mm and the width $\bar{s} = 95$ mm. The first layer has thickness $h_1 = 2$ mm and is made of carbon steel 1 %, with material parameters $E_1 = 205$ GPa, $\nu_1 = 0.3$, and $\alpha_1 = 1.3 \cdot 10^{-5}$ K^{-1}. The second layer is a wrought aluminum alloy 1,060 of thickness $h_2 = 0.5$ mm and material parameters $E_2 = 69$ GPa, $\nu_2 = 0.33$, and $\alpha_2 = 2.35 \cdot 10^{-5}$ K^{-1}. The plate is deformed due to the difference of temperature applied to its surfaces: the temperature on the top surface

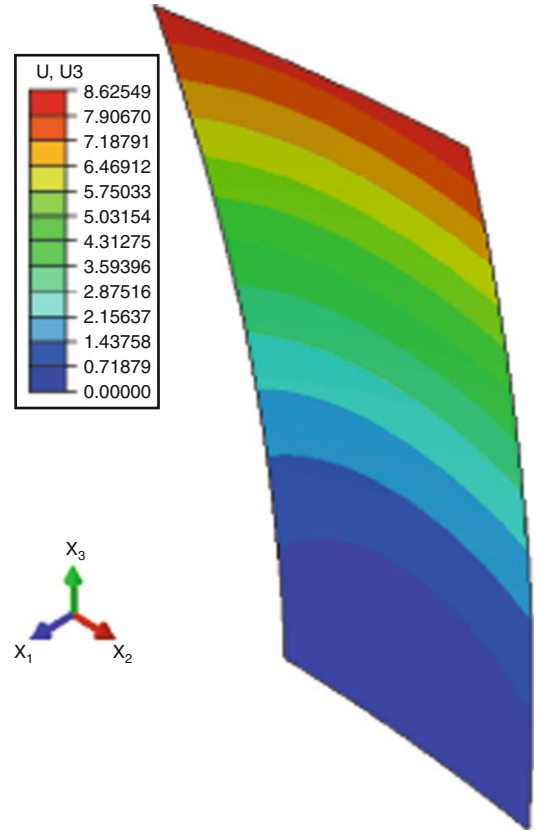

Cylindrical Orthotropic Thermoelastic Shells Modeled by Direct Approach, Fig. 1 The deformed shell and the distribution of transversal displacements (U3)

($x_1^* = h_2$) is $\tau_1 = -10°$ C, while the temperature on the bottom surface ($x_1^* = -h_1$) is $\tau_2 = 60°$ C.

The theoretical solution of the problem is given by relations (32), where the coupling coefficients $C_4, \ldots, C_7$ are expressed by (39). We observe that the displacements in thickness direction (i.e., the transversal displacements u_3) are of order 1 mm,

Cylindrical Orthotropic Thermoelastic Shells Modeled by Direct Approach,

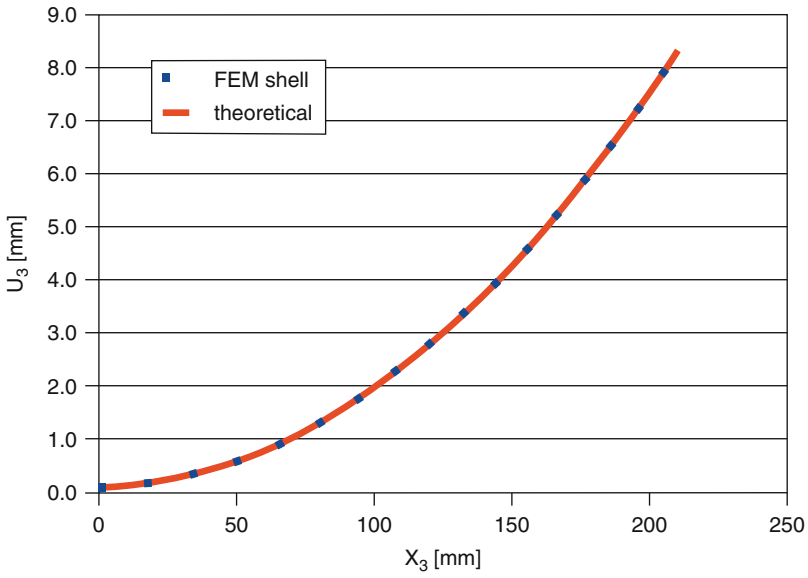

Fig. 2 Comparison of theoretical results and finite element solution (FEM) for transversal displacements (U_3) along the line ℓ

while the in-plane displacements u_1 (in width direction) and u_2 (in length direction) are of order 10^{-3} mm (see Table 1). We compare the values of u_i with the numerical results obtained by a finite element analysis with ABAQUS. We employ a shell model with elements of type S4T (a 4-node thermally coupled doubly curved general-purpose shell) and the section *Composite* from ABAQUS. The number of elements is 55,300. Since the analytical solution is determined up to a rigid body displacement field, we fix this rigid body field by considering in the numerical modeling some boundary conditions corresponding to the solution (32). The values of displacements u_i are recorded at the surface of separation between layers, in the numerical approach. The deformed shell and the distribution of transversal displacements u_3 are represented in Fig. 1.

For comparison of results, we choose four different points $P_1, \ldots, P_4$ distributed in the surface of the flat shell, whose coordinates (x_2, x_3) are presented in Table 1. We observe from Table 1 that the theoretical and numerical values for the displacements u_i *coincide*.

Figure 2 presents the comparison of the two solutions for u_3 along the straight line ℓ characterized by the constant coordinate $x_2 = 23.75$ mm and the variable coordinate x_3 from 0 to 210 mm. We can see that the agreement is very good all along the path ℓ. The very close agreement between analytical and numerical results indicates that the formulas for the coupling coefficients (39) are appropriate, and they can be used to treat thermoelastic shell problems.

Acknowledgments The research leading to these results has received funding from the European Union Seventh Framework Programme (FP7/2007 – 2013), FP7 - REGPOT – 2009 – 1, under grant agreement No: 245479; CEMCAST. This work was financially supported by Ministry of Science and Higher Education within the statutory research number S/20/2013. The first author (M.B.) was supported by the German state grant: "Programm des Bundes und der Länder für bessere Studienbedingungen und mehr Qualität in der Lehre".

References

1. Brischetto S, Carrera E (2009) Thermal stress analysis by refined multilayered composite shell theories. J Therm Stress 32:165–186
2. Zhilin PA (1976) Mechanics of deformable directed surfaces. Int J Solid Struct 12:635–648
3. Zhilin PA (2006) Applied mechanics – foundations of shell theory (in Russian). Politekhn. Univ. Publ, St. Petersburg
4. Altenbach H, Zhilin PA (2004) The theory of simple elastic shells In: Kienzler R, Altenbach H, Ott I (eds) Theories of shells and plates. Lecture notes in applied and computational mechanics, vol 16. Springer, Berlin, pp 1–12

5. Bîrsan M, Altenbach H (2010) A mathematical study of the linear theory for orthotropic elastic simple shells. Math Method Appl Sci 33:1399–1413
6. Bîrsan M, Altenbach H (2011) On the dynamical theory of thermoelastic simple shells. ZAMM 91:443–457
7. Ieşan D (2004) Thermoelastic models of continua. Kluwer Academic, Dordrecht/Boston/London
8. Bîrsan M, Sadowski T, Pietras D (2013) Thermoelastic deformations of cylindrical multi-layered shells using a direct approach. J Therm Stress (2013) DOI: 10.1080/01495739.2013.764802
9. Bîrsan M, Altenbach H (2011) Analysis of the deformation of multi-layered orthotropic cylindrical elastic shells using the direct approach. In: Altenbach H, Eremeyev VA (eds) Shell-like structures, vol 15, Advanced structured materials. Springer, Berlin/Heidelberg, pp 29–52

Cylindrical Shell

► Dynamic Stability of Electroconductive Cylindrical Shells in Magnetic Field
► Thermal Buckling and Dynamic Post-Buckling Analysis of Piezoelectric FGM Hybrid Cylindrical Shells
► Vibrations of Electroconductive Cylindrical Shells in a Magnetic Field

Cylindrical Surface, Cosserat Shell

► Cylindrical Elastic Bodies with Directors, Thermal Stresses

Cylindrical Thermoelastic Shells

► Cylindrical Orthotropic Thermoelastic Shells Modeled by Direct Approach